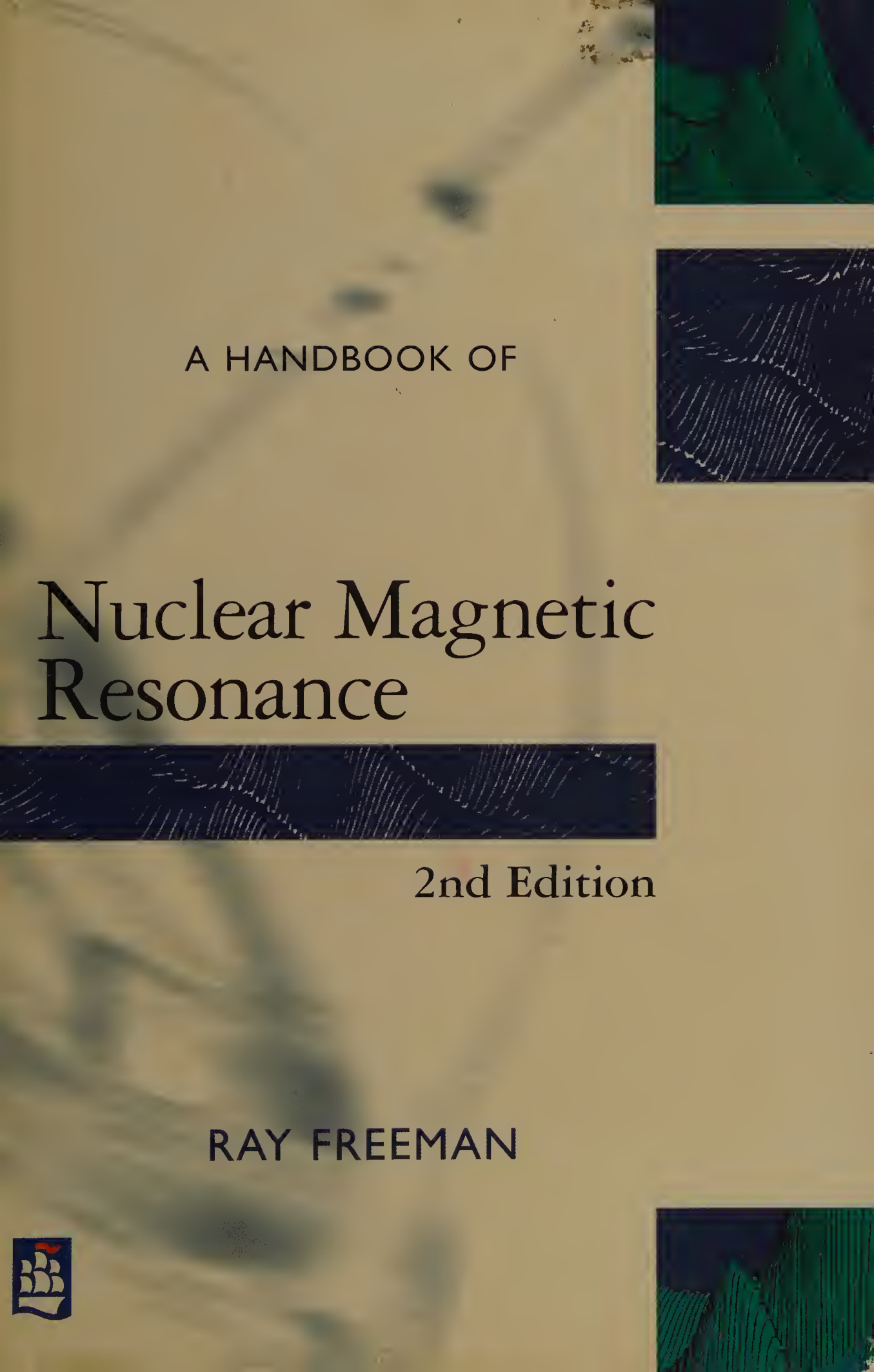

A HANDBOOK OF

Nuclear Magnetic Resonance

2nd Edition

RAY FREEMAN

A HANDBOOK OF NUCLEAR MAGNETIC RESONANCE

A Handbook of NUCLEAR MAGNETIC RESONANCE

Second Edition

Ray Freeman
Cambridge University

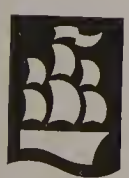

LONGMAN

Addison Wesley Longman
Addison Wesley Longman Limited,
Edinburgh Gate, Harlow,
Essex CM20 2JE, England
and associated companies throughout the world

First edition published 1987
This edition published 1997

British Library Cataloguing in Publication Data
A catalogue entry for this title is available from the British Library

ISBN 0-582-25184-2

Library of Congress Cataloging-in-Publication Data
A catalogue entry for this title is available from the Library of Congress

Produced by Longman Singapore Publishers (Pte) Ltd
Printed in Singapore

Dedicated to my wife Anne-Marie

Contents

Preface to the First Edition

Those of us who practise the art of high resolution NMR spectroscopy usually have a background in chemistry or biochemistry, yet the technique itself has a strong physical bias and its description is steeped in the vocabulary of quantum mechanics. Characteristically, the chemist's reaction has been to use NMR in a largely empirical fashion, interpreting the spectra according to familiar chemical principles, and avoiding too close a brush with the heavy physics. This approach has been remarkably successful and nowadays no self-respecting chemistry department can operate without an NMR spectrometer. However, in recent years a bewildering array of specialized NMR techniques has been introduced, each presenting an interesting problem in spin physics, and each requiring its own theoretical treatment. This leaves the hard-working spectroscopist struggling a little to keep pace with new ideas like multiple-quantum coherence and two-dimensional spectroscopy. Worse still, the new experiments come with their own protective armour of specialist terminology, discouraging to the beginner.

This book starts from the premise that it is possible to explain some of these new concepts (and some older ones) in a pictorial and largely non-mathematical manner, in the belief that this is the approach favoured by most practitioners of NMR. (After all, they have chemistry, biochemistry or even medicine as their prime concern, not the spin Hamiltonian.) It is not a treatise for the complete novice in the field – there are no entries under chemical shift or spin–spin coupling – but it is written for those who already have a grounding in practical NMR spectroscopy and who would like to understand it better. In order to focus on the difficult bits instead of embedding them in a bland matrix like a plum pudding, I have adopted an unusual format. There are about sixty separate entries arranged alphabetically, rather like a very specialized encyclopaedia. These sections are self-contained, but they are cross-referenced to related sections (indicated by an asterisk (*)) and there is also an index to help the reader to find topics that are nested within one of the main entries. This form owes a considerable debt to Peter Atkins' book *Quanta* (1) which I have always admired. It has the advantage that the busy spectroscopist can go directly to the subject in question without having to search through a lot of extraneous material. Indeed, the handbook will have achieved its aim if it sits on the spectrometer console next to the coffee, rather than on the library shelf. There are even a few cartoons to help while away the time during long signal accumulations.

The late Andy Warhol has taught us that in the future everyone will be famous for 15 minutes. Failing that, everyone can aspire to inventing a pulse sequence and bestowing on it a suitably outrageous acronym. My attempts to compile a catalogue of pulse sequences and their mnemonics proved to be a disaster and had to be abandoned. The entries were too numerous and perhaps too ephemeral. In the final version of the book, the use of acronyms has been kept to an absolute minimum; they are employed where a full description of the experiment would be cumbersome and repetitive.

In a certain sense, this is a specialist glossary or lexicon, one definition of which is a 'vocabulary characteristic of a particular group of people'. NMR spectroscopists certainly constitute such a group, constantly coining new terminology (not to say jargon) and protecting the exclusiveness of their club. Without wishing to perpetuate any of this, I have nevertheless tried to retain the most commonly used form of words, for example *solvent suppression* and *saturation transfer,* although these are really just codes for more complex ideas. The real danger with jargon lies in its very *familiarity*; this can lull us into a false sense of security about our understanding of the terms.

The scope of this book had to be restricted, and I have excluded solid-state NMR, nuclear quadrupole resonance, magnetic resonance imaging and most of the experiments performed by physicists – they have their own club anyway. If this leaves an incongruous collection of topics, this may well be unavoidable in anything remotely resembling a dictionary. This is a book for dipping into when there is nothing more exciting to do on the spectrometer. The desire to keep each entry reasonably self-contained has led to repetition of certain ideas; the alternative was a rather tedious cross-referencing scheme that made the sections hard to read. Controversy has been positively encouraged, hence the space devoted to subjects like *maximum entropy* and *zero filling* which are guaranteed to arouse the passions of most NMR spectroscopists with their hint of witchcraft and something-for-nothing.

For a work largely concerned with *explanations* of NMR phenomena, it seemed reasonable to adopt the viewpoint taken in Professor Abragam's excellent book (2) and refrain from quoting the literature simply to give credit for a particular piece of work. The references are intended more as a guide to further reading; many are to general articles and reviews. An exception had to be made when it came to acknowledging the source of spectra used as examples. Unfortunately, since I took the path of least resistance and used the spectra closest to hand, there is a discernible narcissistic tendency in these references. For both these reasons it seemed wiser not to compile a name index.

Where does the reader start in a book of this kind? Probably not with the index, nor with the list of contents, but more likely with one of the 'cartoons'. Actually, these are not mere cartoons; they are intended to highlight some of the anecdotes used in the text to illustrate NMR concepts. The drawings themselves are the work of a young Italian art student, Valeria Petrone, who is also a close family friend. They have given me a lot of pleasure, and I am most grateful to Valeria for her excellent work. Some connoisseurs may well want the book for the illustrations rather than the undoubtedly limited appeal of the magnetic resonance ideas.

In the early years of this battle with words and word processors I was greatly helped by the drive and enthusiasm of my co-author, Gareth Morris, but he was unfortunately forced to withdraw through ill-health. Several colleagues were kind enough to read the final manuscript and made many valuable comments – Geoffrey Bodenhausen, James Keeler, Peter Bloch, Simon Davies, Jan Friedrich, Sally Davenport and Patrick Cook – they have saved me much embarrassment and I am

greatly in their debt. Many of the spectra have been taken from the work of these and other Oxford students and I am grateful for their permission to use this material. My colleague Peter Hore was kind enough to perform several computer simulations specifically for illustrations in this book. Finally, I would also like to thank Bernhard Blümich, Andrew Derome and Tom Frenkiel for providing original spectra.

Magdalen College, Oxford. September 1986

REFERENCES

1. P. W. Atkins, *Quanta: A Handbook of Concepts.* Oxford University Press, 1974.
2. A. Abragam, *The Principles of Nuclear Magnetism.* Oxford University Press, 1961.

Preface to the Second Edition

In the ten years that have elapsed since the completion of the first edition of the *Handbook*, high-resolution NMR spectroscopy has made enormous strides – instrumentation has continuously improved, computers and software have changed out of all recognition, and, above all, multidimensional spectroscopy has become a generally accepted technique. It is now virtually impossible to cover the entire field of high-resolution NMR methodology in a single volume; there are just too many pulse sequences and variations. The guiding theme of the *Handbook* has always been the conviction that if we can understand a few *basic* experiments, the rest of this giant edifice can be constructed one building block at a time, and that there is no real need for a comprehensive catalogue that lists every possible NMR experiment.

This second edition has been updated by radically revising more than half of the original text, particularly those sections that touch on multidimensional spectroscopy, and by adding five new sections on topics that have come into prominence recently. The cross-referencing scheme is retained, but rather more importance has been attached to literature references, reflecting the enhanced activity in the field. The first edition suffered from a rather obsessive antipathy towards mathematical expressions; this has been noticeably relaxed in the present edition, but the reader should still find that the explanations are fundamentally physical rather than algebraic.

The goal is still the same. There is a comment in the Preface to the first edition to the effect that 'the handbook will have achieved its aim if it sits on the spectrometer console next to the coffee, rather than on the library shelf'. One anonymous reviewer remarked 'only if you attach it by a chain'. I take this as a rare compliment, rather than a sad commentary on the ethics of his research students.

My sincere thanks are due to Gareth Morris for pointing out where the first edition was most showing its age, and to Michael Woodley, Ēriks Kupče, Federico del Río-Portilla and Helmut Sengstschmid for spectra and simulations. I am indebted to Alex Seabrook of Addison Wesley Longman, for her enthusiasm, patience and long-standing support of this project.

Cambridge June 1996

Acknowledgements

I am grateful to the following for permission to reproduce diagrams:

Academic Press for Fig. 3 p. 28 (from Kupče & Freeman 1996); Fig. 5 p. 82 (from Bax & Freeman 1981); Fig. 1 p. 86 (from Freeman *et al.* 1981): Fig. 1 p. 111 (from Kupče & Freeman 1993); Fig. 1 p. 116 (from Levitt *et al.* 1983); Fig. 1 p. 119 (from Freeman & Hill 1975); Fig. 2 p. 120 (from Bodenhausen *et al.* 1977); Fig. 3 p. 121 (from Levitt & Freeman 1979); Fig. 5 p. 123 (from Woodley & Freeman 1996); Fig. 3 p. 130 (from Keeler & Neuhaus 1985); Fig. 4 p. 131 (from Bodenhausen *et al.* 1977); Fig. 1 p. 148 (from Freeman *et al.* 1981); Fig. 2 p. 149 (from Shaka & Freeman 1982); Fig. 1 p. 153 (from Freeman & Morris 1978); Fig. 3 p. 155 (from Pei & Freeman 1982); Fig. 1 p. 174 (from Bodenhausen *et al.* 1977); Fig. 1 p. 217 (from Bax & Freeman 1980); Fig. 2 p. 230 (from Morris & Freeman 1978); Fig. 2 p. 235 (from Kupče & Freeman 1993); Fig. 1 p. 238 and Fig. 3 p. 241 (from Bauer *et al.* 1984); Fig. 2 p. 239 (from Morris & Freeman 1978); Fig. 4 p. 273 (adapted from Pei & Freeman 1982); and Fig. 1 p. 304 (adapted from Blümich and Kaiser 1984); the American Chemical Society for Fig. 3 p. 49 (from Freeman *et al.* 1978) © 1978 American Chemical Society; The American Institute of Physics for Fig. 1 p. 286 (adapted from Freeman & Hill 1971) and Fig. 1 p. 316 (adapted from Ferretti & Freeman 1966); Elsevier for Fig. 2 p. 27 (from Kupče & Freeman 1996); Franklin Institute Press for Fig. 2 p. 154 (adapted from Freeman & Morris 1979); the Royal Society of London for Fig. 1 p. 126 (from Freeman 1980).

My thanks also to Carl Hanser Verlag, München, for the cartoon on p. 319 which is an adaptation of an illustration from '*Halbritters Waffenarsenal*', © Carl Hanser Verlag.

Adiabatic Rapid Passage

The usual way to invert nuclear magnetization is to apply a short, intense, 180° radiofrequency pulse, but there is an alternative approach known as *adiabatic rapid passage* (1). It involves sweeping the radiofrequency (or the applied field) from a point far below resonance to a point far above resonance so that the effective field in the rotating frame, initially aligned close to the +Z axis, moves through a semicircle in the XZ plane and terminates close to the –Z axis. Suppose that the nuclear magnetization vector is initially at equilibrium along the +Z axis, and that the sweep rate satisfies the inequality

$$d\theta/dt \ll |\gamma B_{eff}| \qquad [1]$$

where $B_{eff} = (\Delta B^2 + B_1^2)^{1/2}$ is the effective field, the resultant of the resonance offset ΔB and the radiofrequency field B_1, and $\theta = \arctan(\Delta B/B_1)$ is the inclination of B_{eff} with respect to the +X axis of the rotating reference frame. Under this *adiabatic condition* the magnetization vector follows the effective field, tracing out the same semicircular path from +Z to –Z. In this manner $+M_Z \rightarrow -M_Z$ and a population inversion is achieved. It is useful to define an adiabaticity factor,

$$Q = |\gamma B_{eff}/d\theta/dt|, \qquad [2]$$

which should be large compared with unity. In order to emphasize that the sweep may be implemented by ramping the frequency ($\Delta\omega = \gamma\Delta B$) or by varying the intensity ($\omega_1 = \gamma B_1$), or by changing both simultaneously, the adiabaticity factor may be expressed in the form

$$Q = \frac{(\omega_1^2 + \Delta\omega^2)^{3/2}}{|\omega_1(d\Delta\omega/dt) - \Delta\omega(d\omega_1/dt)|} . \qquad [3]$$

At first sight it may not be obvious that the adiabaticity requirement is a direct consequence of the Bloch equations, since they say nothing about the permissible rates of change of radiofrequencies or magnetic fields. However, the effect can be understood pictorially in terms of magnetization trajectories in the rotating frame*. Consider the case where the initial offset from resonance ΔB is large but finite. If the B_1 field is suddenly switched on at the beginning of the sweep, the effective field is slightly tilted out of alignment with the +Z axis. The Bloch equations indicate that the magnetization vector will then precess about B_{eff} at a rate γB_{eff} rad s^{-1}, the tip of the vector moving in a small circle that touches the +Z axis. When we start to

change the direction of B_{eff} by sweeping ΔB, this circular trajectory is converted into a cycloid, as the precessional motion alternatively accelerates and decelerates once every cycle (Fig. 1(a)). However, if the sweep rate is too high to satisfy eqn [1], there is no longer time to complete one cycle before B_{eff} has moved on; the prolate cycloid becomes curtate, and eventually the trajectory makes wild excursions, terminating far from the –Z axis (Fig. 1(b)). Note that the adiabatic condition first breaks down at resonance, where $B_{eff} = B_1$.

The process is called adiabatic *rapid* passage because the sweep is completed in a time short compared with the spin–lattice and spin–spin relaxation times, T_1 and T_2. This is to be contrasted with *slow* passage, where the time taken to sweep through a single resonance line is long in comparison with T_1 and T_2. (For slow passage the steady-state solutions of the Bloch equations are applicable and the B_1 field must be far less intense in order to avoid saturation.) Although adiabatic passage can be used to display the NMR response during the sweep by detecting the X component of magnetization as B_{eff} passes through the X axis, the full linewidth in this mode is 3.46 B_1, far too broad for high-resolution work. Since the sweep is completed before any significant relaxation losses occur, this method is sometimes used in the initial search for weak resonances with long spin–lattice relaxation times, for example those of silicon-29.

Half adiabatic passage can be used to excite a free induction decay, which may then be Fourier transformed to give the usual high-resolution spectrum. In this mode, B_1 is extinguished when the sweep reaches resonance, leaving the magnetization vectors free to precess in the XY plane, just as in conventional pulse

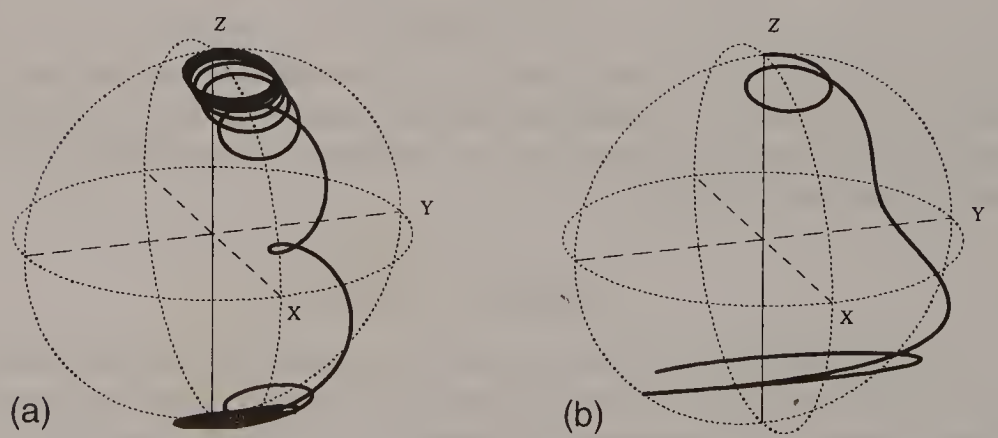

Fig. 1. Magnetization trajectories computed for adiabatic rapid passage with a constant amplitude, linear frequency sweep, starting with the effective field at a slight inclination with respect to the Z axis. (a) For a slow sweep, where the adiabaticity factor at resonance $Q_0 = 5$, the trajectory is a prolate cycloid and terminates close to the –Z axis. (b) For a faster sweep rate ($Q_0 = 1$) the precession can no longer keep pace with the frequency sweep, and the excursions become very large, terminating far from the –Z axis.

excitation. On the other hand, if the B_1 field is retained for a relatively long period after a half adiabatic passage, we have the situation known as *spin locking**. The magnetization vector is held fixed along the B_1 field direction, a situation sometimes called *forced precession* (2). Even if there is a slight misalignment of the magnetization vector with respect to the B_1 field, this eventually disappears as components perpendicular to B_1 are dispersed in the YZ plane by the effects of the spatial inhomogeneity of B_1. In the presence of B_1 the magnetization component M_X decays at a rate determined by the 'spin–lattice relaxation time in the rotating frame' essentially equal to the spin–spin relaxation time for a mobile liquid. This may be used as a method for determining T_2 without the complications that arise from J-modulation of spin echoes*.

There are several possible sweep modes for adiabatic passage. If the sweep rate conforms to a hyperbolic tangent function while the B_1 intensity follows the corresponding hyperbolic secant, the frequency-domain excitation profile has the desirable 'top-hat' shape (3–5). Since adiabaticity is easier to achieve the larger the resonance offset, this favours schemes that accelerate the sweep as a function of ΔB, such as the tangential sweep (5,6) or the constant adiabaticity pulse (5). When a wide range of chemical shifts has to be encompassed it is advantageous to maintain the sweep parameters (the sweep rate, B_1 intensity, and adiabaticity) essentially constant across the entire operating range, bringing the B_1 amplitude smoothly down to zero at the extremities of the sweep (7). This linear frequency-sweep mode, with an amplitude profile rounded at the edges, has proved extremely useful for broadband decoupling* since it provides good spin inversion with the minimum dissipation of radiofrequency power in the sample (8). In this application the decoupler field is kept as weak as possible (with the adiabaticity factor Q near unity), the residual imperfections being compensated by the appropriate phase cycling (9,10).

Wideband excitation can be achieved by a rapid frequency sweep across the entire spectrum, a technique sometimes called *chirp modulation* (11). However, the adiabatic condition is not always properly satisfied in this mode (7). The main problem with this method is the strong induced frequency dependence of the signal phase, a quadratic function of the frequency offset. This phase distortion can be largely compensated by the application of a second chirp pulse with the sweep rate doubled (12). Wideband excitation of double-quantum coherence can also be implemented with a suitable combination of chirp pulses (7,13).

One of the principal advantages of adiabatic passage is that it operates over a wide frequency band, in this respect using the B_1 field more efficiently than a hard radiofrequency pulse. A second useful property is that the performance is rather insensitive to the B_1 intensity, provided that B_1 is strong enough to satisfy the adiabatic condition. This means that it is possible to tolerate even gross spatial inhomogeneities in the B_1 field, such as those that occur when surface coils are used for spatial localization experiments (14).

REFERENCES

1. A. Abragam, *The Principles of Nuclear Magnetism.* Oxford University Press, 1961.
2. I. Solomon, *CR Acad. Sci. Paris* **248**, 92 (1959).
3. S. L. McCall and E. L. Hahn, *Phys. Rev.* **183**, 457 (1969).
4. M. S. Silver, R. J. Joseph and D. I. Hoult, *Phys. Rev. A* **31**, 2753 (1985).
5. J. Baum, R. Tycko and A. Pines, *Phys. Rev. A* **32**, 3435 (1985).
6. C. J. Hardy, W. A. Edelstein and D. Vatis, *J. Magn. Reson.* **66**, 470 (1986).
7. J. M. Böhlen and G. Bodenhausen, *J. Magn. Reson. A* **102**, 293 (1993).
8. E. Kupče and R. Freeman, *J. Magn. Reson. A* **115**, 273 (1995).
9. M. H. Levitt and R. Freeman, *J. Magn. Reson.* **43**, 502 (1981).
10. R. Tycko, A. Pines and R. Gluckenheimer, *J. Chem. Phys.* **83**, 2775 (1985).
11. J. Delayre, unpublished work.
12. V. I. Ermakov, J. M. Böhlen and G. Bodenhausen, *J. Magn. Reson. A* **103**, 226 (1993).
13. I. Burghardt, J. M. Böhlen and G. Bodenhausen, *J. Chem. Phys.* **93**, 7687 (1990).
14. K. Uğurbil, M. Garwood and A. R. Rath, *J. Magn. Reson.* **80**, 448 (1988).

Cross-references

Broadband decoupling
Rotating frame
Spin echoes
Spin locking

Apodization

Apodization is a term borrowed from infrared Fourier transform spectroscopy, with the literal meaning 'removing the feet'. The feet in question are the set of small sidelobes which appear on each side of the resonances in the frequency domain; they are derived from the sinc function character imposed on the lineshape by truncation of the time-domain signal before it has completely decayed.

Although an ideal free induction signal* in Fourier transform NMR would decay smoothly to zero, in practice the process of acquisition is usually terminated before the decay is complete, introducing a step function at the end. Often the data table is then completed by zero filling*. The signal fed into the Fourier transformation* program may thus be regarded as the 'ideal' free induction decay multiplied by a step function. The convolution* theorem tells us that this corresponds to the convolution of the ideal frequency-domain lineshape with a sinc function; the more severe the discontinuity in the time-domain signal, the more marked are the sinc function 'wiggles'.

The effect may be removed by the application of a suitably chosen sensitivity enhancement* weighting function to the free induction signal, but this sacrifices resolution. Apodization is used to describe attempts to remove the sinc function 'wiggles' without significantly altering the resolution or signal-to-noise ratio. The idea is to apply a particular type of weighting function to the last 20–30% of the time-domain signal in order to bring it smoothly to zero at the end of the acquisition period. A widely used apodization function is made up from a half cycle of a cosine wave, $\frac{1}{2}(1 + \cos x)$. In fact, this only alleviates the problem and does not eliminate the wiggles (Fig. 1). Only a weighting function which operates on the entire time-domain signal can eradicate the sinc function artefacts entirely.

The frequency-domain spectrum obtained by digital Fourier transformation is of course discrete. It turns out that a step function at the very end of the free induction decay (with no zero filling) leads to a spectrum where the data points fall at the crossing points of the sinc function, disguising the effect. The transform of the corresponding zero-filled signal interpolates data points and reveals the underlying oscillatory structure.

Apodization is particularly important when a strong resolution enhancement* function has been used to emphasize the later parts of the free induction signal. Although many computer programs incorporate a mild apodization routine, it is preferable in these cases to include a component in the time-domain weighting function which brings the signal smoothly to zero at the end of acquisition. The

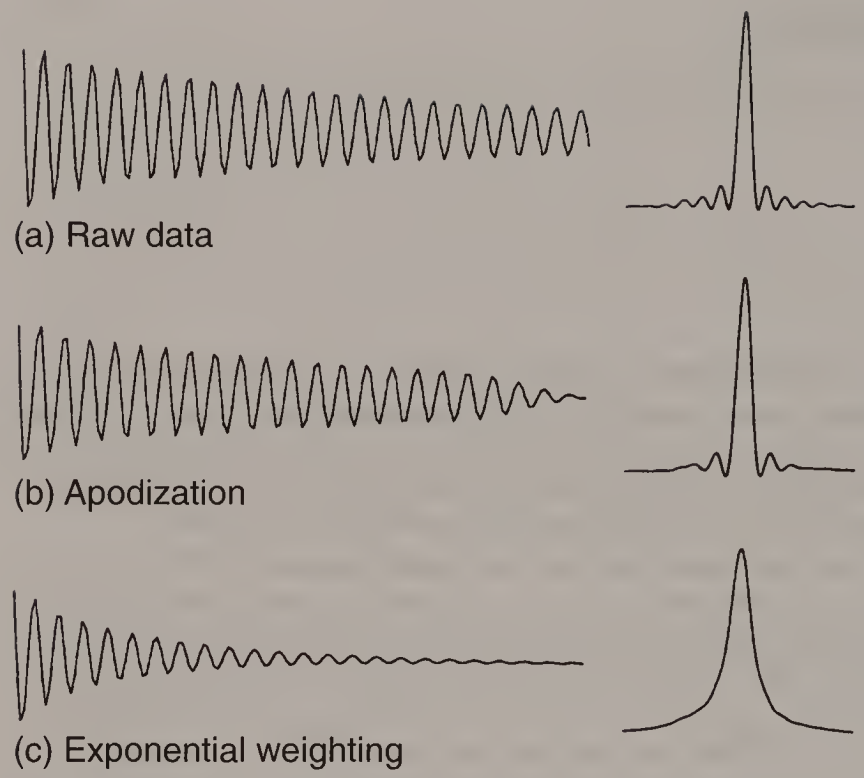

Fig. 1. (a) A free induction signal that is truncated (and zero filled) corresponds to a line in the frequency domain that has sinc function wiggles. (b) Apodization with the $0.5(1 + \cos \theta)$ function on the last 25% of the data attenuates but does not eliminate these wiggles. (c) An exponentially decaying weighting function removes the wiggles but broadens the line significantly.

Lorentzian-to-Gaussian function accomplishes this quite effectively. In two-dimensional spectroscopy*, apodization functions may be required in both the t_1 and t_2 dimensions.

In many types of two-dimensional Fourier transform experiment, early truncation of the signal in the t_1 time domain is unavoidable if the total experimental time is to be kept within reasonable limits. There are also some related 'interferogram' experiments where echo-modulation patterns are used to distinguish CH_3, CH_2, CH and quaternary carbon sites, and where the total experiment time must be limited. In such cases, some rather more sophisticated methods may be used to eliminate the sinc function artefacts (1). Parametric fitting of the time-domain signal is one approach, allowing for the fact that the signal is truncated. Alternatively, the maximum entropy method* (2) may be applied; it is particularly effective for removing known artefacts of this kind (3).

REFERENCES

1. J. Keeler, *J. Magn. Reson.* **56**, 463 (1984).
2. S. F. Gull and G. J. Daniell, *Nature* **272**, 686 (1978).
3. P. J. Hore, *J. Magn. Reson.* **62**, 561 (1985).

Cross-references

Convolution
Fourier transformation
Free induction decay
Maximum entropy method
Resolution enhancement
Sensitivity enhancement
Two-dimensional spectroscopy
Zero filling

Baseline Correction

Quantitative measurements in high-resolution NMR spectroscopy demand accurate integration of the area under each peak of interest, and such integrals are quite sensitive to small changes in the baseline of the spectrum. Any offset, tilt, hump or oscillatory contribution to the baseline can introduce gross errors into the integral. The effect is compounded for two-dimensional spectroscopy, for example when estimating the intensity of NOESY cross-peaks, because we need to measure the volume under the peak.

INSTRUMENTAL EFFECTS

Baseline problems can arise from several sources, some purely instrumental, others with an NMR origin. Perhaps the most common of all is the effect of 'transmitter breakthrough', the fact that the receiver takes a short time to recover from the effect of the radiofrequency pulse, despite being gated off while the pulse is applied. This can falsify the first few points of the free induction decay, particularly the first point. An incorrect first point transforms into a d.c. offset of the baseline of the spectrum; when the first two points are falsified, there is also a bowing of the baseline (Fig. 1). If several ordinates are corrupted at the beginning of the free induction decay, higher-frequency components are introduced – the so-called 'rolling baseline'. One remedy is to restore the fidelity of these early data points by a linear prediction algorithm (1) which is very efficient for such short extrapolations.

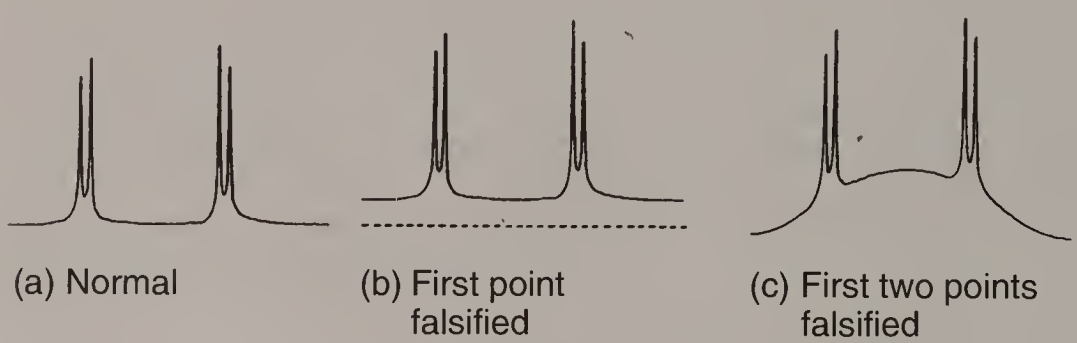

Fig. 1. The effect on the spectrum of falsifying the first data point or the first two data points of the free induction decay. (b) A baseline offset. (c) A bowed baseline.

The discrete Fourier transform has a slight idiosyncrasy, first noted by Otting *et al.* (2), that can easily be overlooked. It is a question of the first data point at time t = 0. The program treats the incoming time-domain signal as if it were a periodically repeated function, so the ordinate at t = 0 should then represent the algebraic mean of the first and last data points. For most free induction decays the last data point is very near zero, so the actual first point should strictly be halved before being fed into the Fourier transform algorithm (3). We can view this in another way. A continuous analogue signal has to be divided into discrete time slices prior to digitization. In effect, we approximate the slice by a narrow vertical trapezium and evaluate its area, converting this into a number. If τ is the dwell time (the width of the slice) this number should stand for the digitized signal at time $\tau/2$, not at time zero. If it *is* represented as the ordinate at time zero, it should be halved in amplitude. Failure to take this precaution results in a positive offset of the baseline of the Fourier transform. While this will probably pass unnoticed in a plot of the spectrum, it will falsify integrals and can give rise to ridges in two-dimensional spectroscopy (see t_1 noise*).

If signal acquisition is not initiated at exactly the right instant, a linear phase gradient is induced across the spectrum, usually corrected through a computer algorithm just before plotting. Stejskal and Schaefer (4) showed that under these conditions, the long dispersive tails of a Lorentzian line were aliased from outside the spectral window and thus contributed to the baseline distortion.

There is another artefact generated by such a frequency-dependent phase correction routine, and it is particularly important for any broad lines in the spectrum. Each resonance line should strictly be associated with a unique phase angle, not one that varies across the width of the line. Plateau *et al.* (5) showed that a frequency-dependent phase correction leads to a distortion of the baseline in the immediate vicinity of the broad line; essentially the tails contain dispersion contributions if the centre is adjusted for pure absorption.

To avoid aliasing of noise from outside the spectral window, audiofrequency cut-off filters are commonly employed (see Digitization*). The leading edge of the transient free induction signal is distorted by such a filter (6) introducing another source of baseline distortion. Although this problem could be alleviated by more rapid sampling and a higher filter cut-off frequency, this is counterproductive in terms of sensitivity. The newer digital filtration schemes are to be preferred.

NMR RESPONSES

The baseline of a high-resolution spectrum may be distorted simply by the presence of broad resonance lines, for example from chemically exchanging species, macromolecules, solid substrates, polymers, heterogeneous samples, liquid crystals, paramagnetic species, etc. A very common problem is the residual broad hump left behind after suppression of an intense water peak. Very small samples, which are particularly affected by discontinuities in magnetic susceptibility at the

walls of the container, or materials that are inherently heterogeneous, can often be studied in a high-resolution magic-angle spinning probe (7), where these field gradients are averaged at quite modest spinning rates (typically 2 kHz).

Probe construction techniques usually require small amounts of adhesive, and although this is kept to an absolute minimum in the immediate vicinity of the receiver coil, it eventually contributes a broad background NMR signal that becomes evident when very weak samples are being investigated. High-resolution *in vivo* spectroscopy of animals, for example phosphorus-31 studies, almost inevitably contain a broad background hump, for example from immobile phosphorus atoms in bone. The spatial localization technique itself may induce broad signal components if it employs magnetic field shaping to define a homogeneous volume surrounded by regions with steep gradients.

CORRECTION ROUTINES

Although some of these 'distortions' represent genuine NMR responses, it is often necessary to suppress broad background signals to obtain more quantitative measurements of the well-resolved resonances. A simple remedy is to delay acquisition for a small number of initial data points to allow these undesirable signal components to decay by spin–spin relaxation. The main consequence is the introduction of an appreciable linear phase gradient into the spectrum, which can then be corrected at the display stage. The danger is that any residual broad components are distorted through the effect described above. Spin-echo methods can also be used.

A rather more elegant solution is to employ a time-domain resolution enhancement function that de-emphasizes the first few data points. A procedure that seems particularly appropriate in this context is the 'convolution-difference' method (8). This applies a severe sensitivity enhancement function to broaden all the lines; this is then scaled down by a suitable factor and subtracted from the unprocessed free induction decay. The operation is most easily visualized in the frequency domain. The spectrum contains both narrow and broad lines; the former are appreciably altered by the sensitivity enhancement broadening function, while the latter are scarcely affected. If the relative scaling is carefully judged, the broad resonances cancel, leaving only the narrow lines, with a reasonably flat baseline.

Baseline correction can also be carried out in the frequency domain. Offset and tilt are readily compensated by a simple algorithm; the only problem is to indicate suitable regions of the spectrum (usually the low- and high-field edges) which are known to contain no genuine signals. More complicated distortions can be handled by fitting the baseline to a polynomial, which is then subtracted out. This requires that the operator indicate several points throughout the spectral width that may be used to define the baseline. In two-dimensional spectroscopy, a flat baseplane can prove even more important because of the need to integrate weak cross-peaks, for example those observed in NOESY spectra. Then the efficient deconvolution of

solvent peaks (9) and iterative baseline fitting algorithms (10) take on a particular importance.

REFERENCES

1. D. Marion and A. Bax, *J. Magn. Reson.* **83**, 205 (1989).
2. G. Otting, G. Widmer, G. Wagner and K. Wüthrich, *J. Magn. Reson.* **66**, 187 (1986).
3. C. Tang, *J. Magn. Reson. A* **109**, 232 (1994).
4. E. Stejskal and J. Schaefer, *J. Magn. Reson.* **14**, 160 (1974).
5. P. Plateau, C. Dumas and M. Guéron, *J. Magn. Reson.* **54**, 46 (1983).
6. D. I. Hoult, C.-N. Chen, H. Eden and M. Eden, *J. Magn. Reson.* **51**, 110 (1983).
7. P. A. Keifer, L. Baltusis, D. M. Rice, A. A. Tymiak and J. N. Shoolery, *J. Magn. Reson. A* **119**, 65 (1996).
8. I. D. Campbell, C. M. Dobson, R. J. P. Williams and A. V. Xavier, *J. Magn. Reson.* **11**, 172 (1973).
9. D. Marion, M. Ikura and A. Bax, *J. Magn. Reson.* **84**, 425 (1989).
10. C. Bartels, P. Güntert and K. Wüthrich, *J. Magn. Reson. A* **117**, 330 (1995).

Cross-references

Convolution
Digitization
Fourier transformation
Sample spinning
t_1 noise
Two-dimensional spectroscopy

Bilinear Rotation Decoupling

Echo modulation through spin–spin coupling has proved a very powerful tool in high-resolution NMR spectroscopy. One widely used application is *bilinear rotation decoupling* (BIRD) introduced by Garbow *et al.* (1) to discriminate protons directly attached to carbon-13 from all other types of protons. This latter category of 'remote' protons comprises those coupled through long-range interactions and those that are not coupled at all. The beauty of the method is that it can be used as a compact module that can be inserted into an existing pulse sequence to select one or other of these two types of protons. It is convenient to distinguish two forms of the BIRD module that have opposite effects.

BIRD-CP

This is derived from the Carr–Purcell spin-echo sequence (2) in which all the radiofrequency pulses applied to the I spins (protons) have the same phase. We consider a heteronuclear two-spin system IS and write the pulse sequence:

I spins: $90°\ (+X) - \tau - 180°\ (+X) - \tau - 90°\ (+X)$

S spins: $180°$. [1]

The chemical shift evolution of the two I-spin vectors (α and β) during the τ intervals is refocused by the 180°(+X) pulse, but the divergence due to spin–spin coupling persists, and when $\tau = 1/(2J_{IS})$ this divergence reaches 180° (Fig. 1(b)). This discriminates against long-range couplings, which are too small to generate any appreciable divergence on this time scale. The 180°(+X) refocusing pulse rotates the α and β vectors into mirror image positions with respect to the XZ plane (Fig. 1(c)). At this point the 180° pulse applied simultaneously to the S spins interchanges the I-spin labels ($\alpha \leftrightarrow \beta$), placing them in such a configuration (Fig. 1(d)) that further free precession carries them into alignment along the +Y axis. For the remote I spins (which have negligible coupling to the S spins) the sequence merely generates a 270° rotation about the +X axis, leaving them aligned along –Y. Directly bound and remote I spins are thus separable. Normally the sequence is followed by a 90°(+X) pulse so that coupled spins are rotated to –Z, thus suffering a population inversion, whereas the remote spins are returned to Boltzmann equilibrium along +Z.

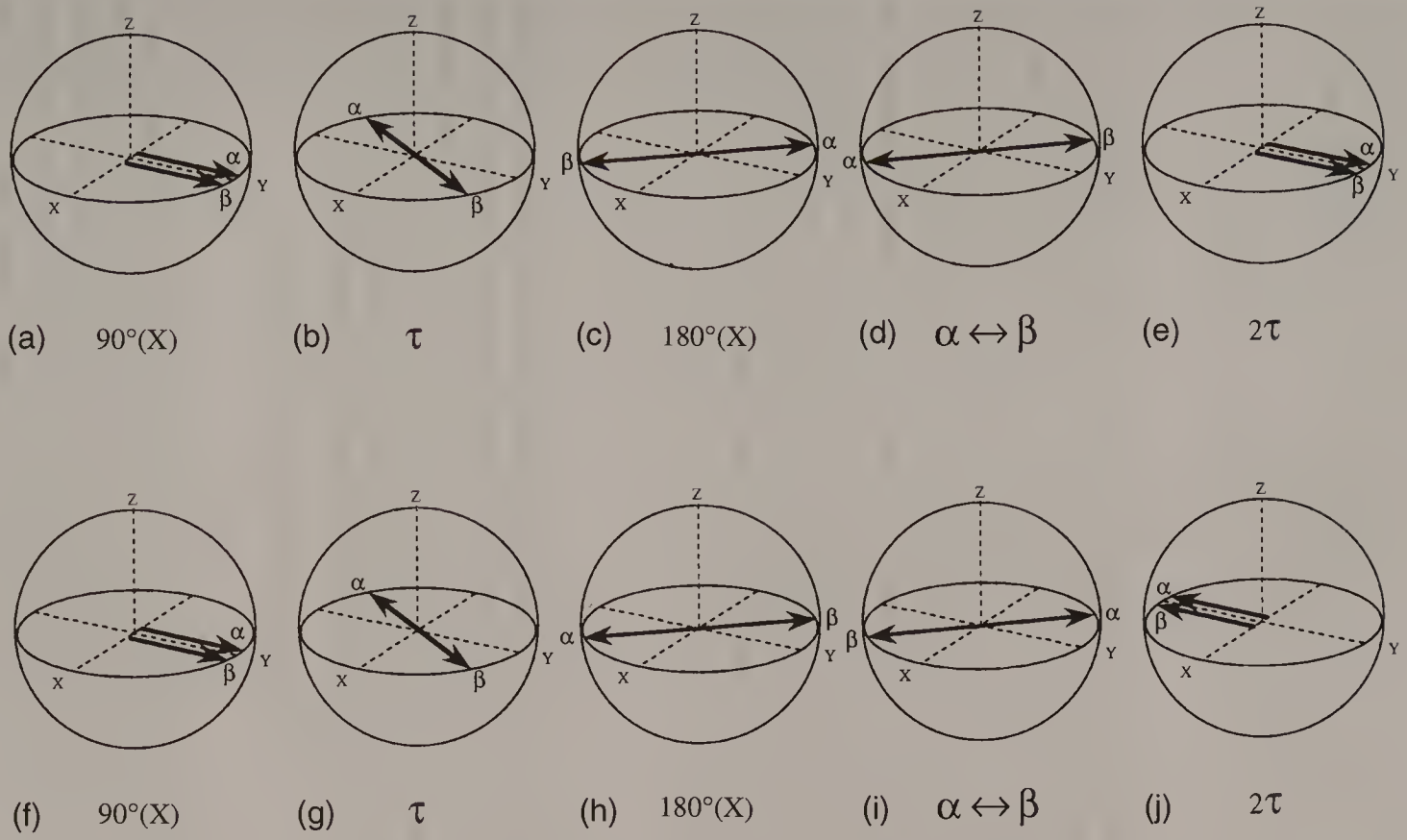

Fig. 1. (Top) Evolution of magnetization vectors α and β from directly bound protons in the BIRD-CP scheme, which parallels the Carr–Purcell spin-echo sequence and culminates in excitation along the +Y axis. Remote protons (not shown) do not diverge significantly during the τ intervals and are returned to –Y. (Bottom) Comparable evolution in the BIRD-MG scheme, which parallels the Meiboom–Gill experiment where the 180° refocusing pulse is applied along the +Y axis instead of the +X axis. The result is to align directly bound protons along –Y and remote protons along +Y.

BIRD-MG

This is a vivid demonstration of how a very minor change in a pulse sequence (a 90° phase shift) completely reverses the behaviour of the spins. The change is the Meiboom–Gill modification (3) where the refocusing pulse now rotates the vectors about the +Y axis instead of the +X axis:

I spins: $90°\ (+X) - \tau - 180°\ (+Y) - \tau - 90°\ (+X)$ [2]

S spins: $180°$.

The corresponding vector description is shown in Fig. 1 (bottom). The key difference is the configuration shown in Fig. 1(h) where the α and β vectors are reversed with respect to their positions in Fig. 1(c). As a result, the final orientation (Fig. 1(j)) has the I-spin vectors aligned along the –Y axis. Remote I spins accomplish only an overall 90° rotation about the +X axis and terminate along +Y. As before, the sequence is normally followed by a 90°(+X) pulse which rotates the coupled I-spin vectors to the +Z axis (corresponding to Boltzmann equilibrium) but creating a population inversion for the remote I spins. This type of preparation is often used as the first stage of a heteronuclear single-quantum correlation (HSQC) experiment (4), where the inverted spins are allowed a period ($T_1 \ln 2$) of spin–lattice relaxation so that they just reach the null condition when the main sequence is started.

TANGO

There is an analogue of bilinear rotation decoupling that leads directly to excitation of the chosen category of protons (directly bound or remote). It has been called TANGO (Testing for Adjacent Nuclei with a Gyration Operator) (5). Unlike most other pulse sequences it utilizes 45° and 135° pulses, and all free precession takes place on the surface of a 45° cone. To excite the directly bound protons we use the version derived from the Carr–Purcell echo sequence (TANGO-CP):

I spins: $135°\ (+X) - \tau - 180°\ (+X) - \tau - 45°\ (+X)$ [3]

S spins: $180°$.

where $\tau = 1/(2J_{IS})$. The evolution is set out in Fig. 2. The initial 135° pulse rotates the α and β vectors onto the lower part of the 45° cone, and during τ they precess according to the chemical shift and diverge by 180° (Fig. 2(b)). The 180°(+X) pulse rotates them into symmetrically related positions on the upper cone (Fig. 2(c)) and the 180° pulse on the S spins interchanges the α and β labels (Fig. 2(d)). Free precession for a further period τ brings the two vectors into alignment (Fig. 2(e)) and the final 45°(+X) pulse rotates them onto the +Y axis where they induce an absorption-mode signal (Fig. 2(f)). Remote protons exhibit negligible divergence

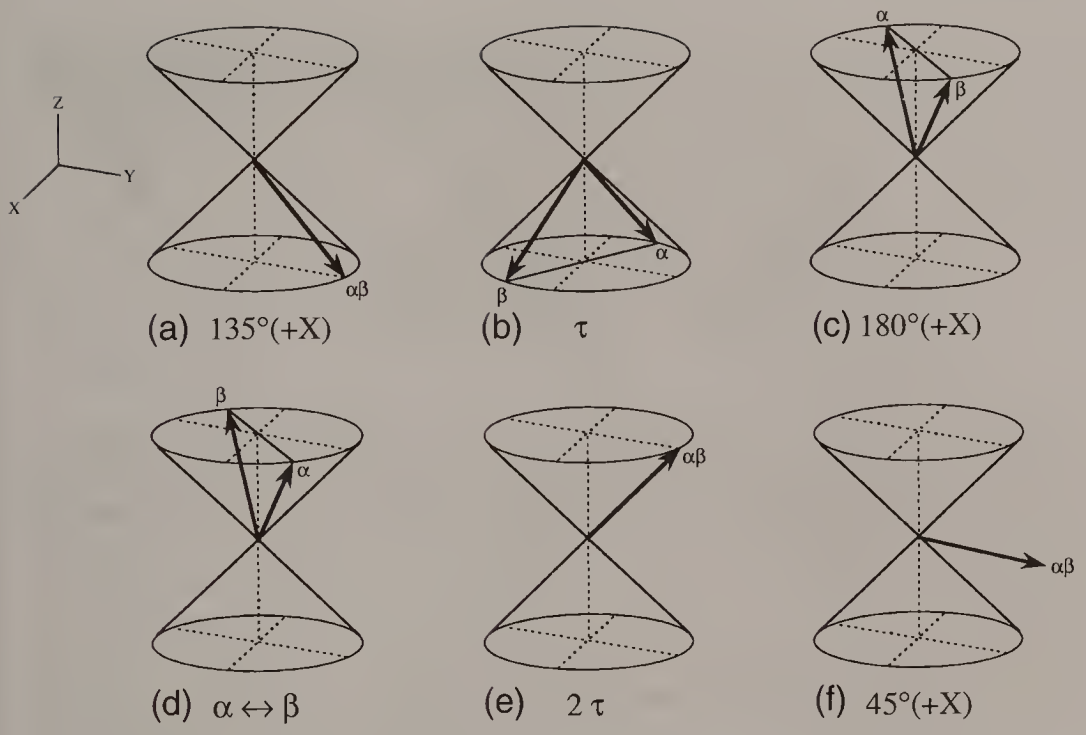

Fig. 2. Evolution of directly-bound proton magnetization vectors α and β on the surface of a 45° cone according to the TANGO-CP scheme. During the τ intervals the α and β vectors diverge through 180°. The interchange α ↔ β is achieved by a 180° pulse on the coupled S spins (carbon-13). The result is to leave these vectors along the +Y axis (absorption). Remote proton vectors (not shown) do not diverge significantly during the τ intervals and are therefore returned to the +Z axis.

during the short τ intervals, merely executing a 360° overall rotation back to the +Z axis (equivalent to Boltzmann equilibrium). This is an important advantage over the BIRD technique which can only discriminate the two categories of protons through selective population inversion.

There is an analogous TANGO-MG sequence that excites remote protons but leaves the directly bound protons at equilibrium. The only change is the Meiboom–Gill (3) shift of the phase of the 180° refocusing pulse:

I spins: $135°\ (+X) - \tau - 180°\ (+Y) - \tau - 45°\ (+X)$ [4]

S spins: $180°$.

The corresponding evolution of proton vectors is illustrated in Fig. 3. The key difference is the configuration after the 180°(+Y) pulse (Fig. 3(c)). Note that the α and β vectors are interchanged with respect to Fig. 2(c). The final result (Fig. 3(f)) has the directly bound proton vectors aligned along the +Z axis. Remote protons exhibit negligible divergence during the τ intervals and experience an overall 90°(+X) rotation, generating an absorption-mode signal. There are several other possible modifications of the TANGO sequence but the results all fall into these two categories.

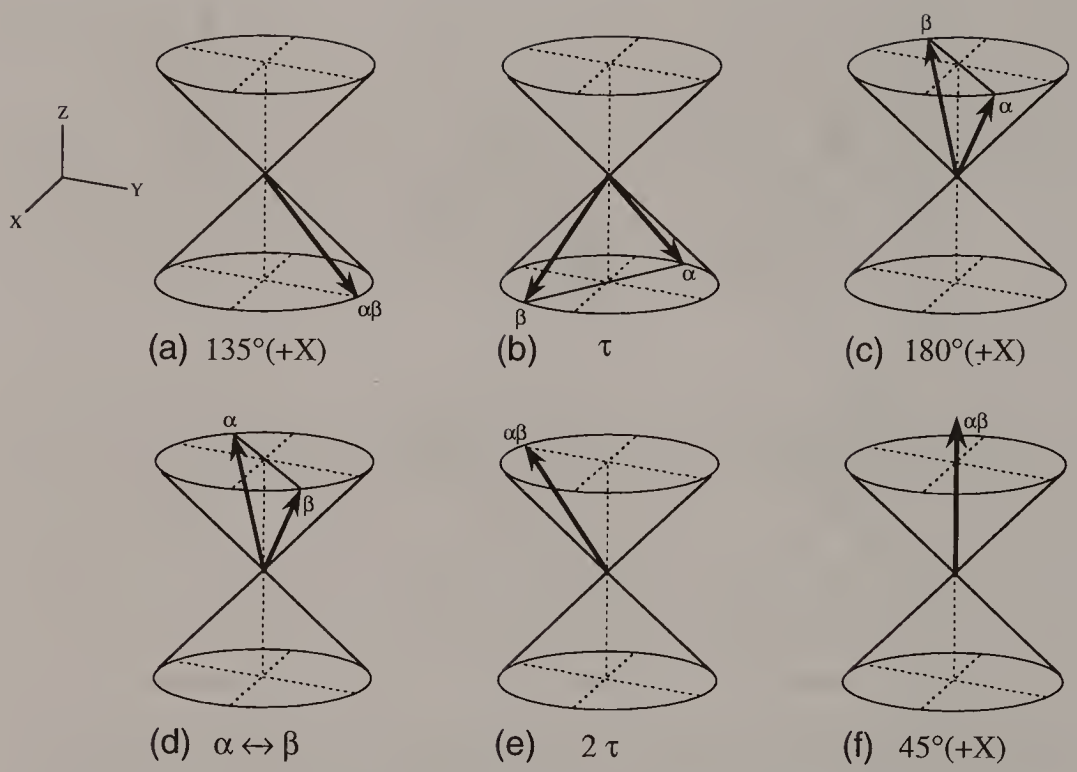

Fig. 3. Evolution of directly-bound proton magnetization vectors α and β on the surface of a 45° cone according to the TANGO-MG scheme. During the τ intervals the α and β vectors diverge through 180°. The interchange α ↔ β is achieved by a 180° pulse on the coupled S spins (carbon-13). The key difference is the 180° rotation about the +Y axis rather than the +X axis (c). The result is to leave these vectors along the +Z axis (absorption). Remote proton vectors (not shown) do not diverge significantly during the τ intervals and are therefore rotated to the +Y axis.

REFERENCES

1. J. R. Garbow, D. P. Weitekamp and A. Pines, *Chem. Phys. Lett.* **93**, 514 (1982).
2. H. Y. Carr and E. M. Purcell, *Phys. Rev.* **94**, 630 (1954).
3. S. Meiboom and D. Gill, *Rev. Sci. Instrum.* **29**, 688 (1958).
4. A. Bax, M. Ikura, L. E. Kay, D. E. Torchia and R. Tschudin, *J. Magn. Reson.* **86**, 304 (1990).
5. S. Wimperis and R. Freeman, *J. Magn. Reson.* **58**, 348 (1984).

Cross-references

Polarization transfer
Rotating frame
Spin echoes
Spin–lattice relaxation
Vector model

Bloch–Siegert Effect

Almost all NMR experiments use an excitation which is a linearly oscillating radiofrequency field. This can be thought of as the superposition of two counter-rotating fields of the same frequency (Fig. 1), and the nuclear spins are principally affected by the component which rotates in the same sense as their precession. Thus protons would be sensitive to (say) the clockwise component, whereas nitrogen-15, which has a negative gyromagnetic ratio, would react to the counterclockwise component of radiation at the appropriate frequency. Bloch and Siegert (1) calculated the influence of the other 'unused' rotating component and found that its main effect was a very slight shift of the observed resonance line. To a good approximation, this *Bloch–Siegert shift* is given by

$$\Delta f = \tfrac{1}{2}(\gamma B_1/2\pi)^2/2F \qquad [1]$$

where B_1 is the intensity of one rotating component of the transmitter field and F is the Larmor precession frequency, making a resonant offset of 2F Hz for the unused rotating component of the field. The shift is in a direction *away* from the offending non-resonant rotating component. In most practical high-resolution cases, where $\gamma B_1/2\pi$ would seldom exceed 10 kHz, and 2F might be as high as 1000 MHz, the Bloch–Siegert shift is very small (in this example only 0.05 Hz). The shift

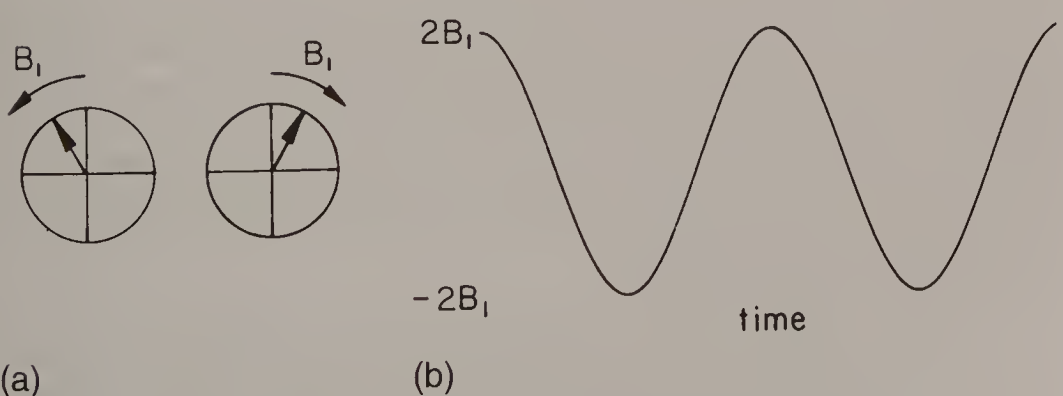

Fig. 1. NMR experiments are normally performed with a linearly oscillating field (b) which can be decomposed into two equal counter-rotating fields (a). Only the component that rotates in the same sense as the nuclear precession gives rise to resonance, but the other component causes the Bloch–Siegert effect.

disappears as soon as B_1 is extinguished, so that in pulsed NMR we are seldom concerned with this type of Bloch–Siegert effect.

An equivalent effect occurs whenever there is another radiofrequency field B_2 applied away from resonance for the nuclear spins. It was first described by Ramsey (2) but is still universally known as the Bloch–Siegert effect. It can be visualized using the vector model for nuclear magnetism in the rotating reference frame*. In the coordinate frame rotating in synchronism with the appropriate rotating component of this *second* radiofrequency field B_2, the spins 'see' an effective field which is the resultant of B_2 and the resonant offset ΔB. Their precession frequency is thus increased slightly, by an amount $\gamma(B_{eff} - \Delta B)2\pi$. For the usual cases where $\Delta B \gg B_2$ this gives a Bloch–Siegert shift of approximately

$$\Delta f = \tfrac{1}{2}(\gamma B_2/2\pi)^2/(\gamma \Delta B/2\pi) \qquad [2]$$

in analogy with eqn [1]. Since B_2 fields employed for decoupling are usually quite intense, and since ΔB can now be very much smaller than the Larmor frequency, this type of Bloch–Siegert shift can be appreciable. For example, in the determination of nuclear Overhauser effects*, where B_2 is applied during the observation of the free induction decay, these shifts can be an undesirable complication if difference spectroscopy* is employed. Much better difference spectra are obtained if B_2 is switched off during the acquisition of the free induction decay.

The ΔB term in the denominator of eqn [2] suggests that significant Bloch–Siegert shifts will normally only appear in *homonuclear* double-resonance experiments. However, the effect cannot be entirely ruled out in certain heteronuclear experiments where the B_2 field is applied to another nuclear species. One example is the case of broadband decoupling of carbon-13 (proton observation), where a strong irradiation field B_2 can give rise to an appreciable Bloch–Siegert shift of the deuterium resonance at a distance of several tens of MHz. The process of switching the decoupler on or off may then seriously interfere with the operation of the field/frequency regulation*.

The Bloch–Siegert effect is quite general. The expression for the shift, eqn [2], can be used to predict coherent decoupling* and spin-tickling* effects in double resonance by transforming the energy-level diagram into the rotating frame of reference and then calculating the Bloch–Siegert shifts of the energy levels due to the presence of the effective field B_{eff}, the resultant of B_2 and the resonance offset of the X spins. This accounts for the coalescence of spin multiplet structure on the A-spin resonance, the appearance of weak satellite lines or (under the appropriate conditions) the spin-tickling effect.

In situations where there is an appreciable spatial inhomogeneity in the radiofrequency field B_2, the Bloch–Siegert effect can give rise to line broadening as well as a shift. Different volume elements of the sample experience different Bloch–Siegert shifts; the consequent broadening is usually accompanied by a marked distortion of the lineshape.

When homonuclear decoupling experiments are used for determining chemical shifts, accurate measurements require correction for the Bloch–Siegert shifts. There is also a second correction to be applied which is twice as large and in the opposite sense. It arises because the optimum decoupling condition requires the quantization axes of the observed and irradiated spins to be orthogonal (3). Optimum decoupling occurs when B_2 is slightly displaced from exact resonance in a direction towards the observed resonance by an amount

$$\Delta f \approx (\gamma B_2/2\pi)^2/(\delta_A - \delta_X), \qquad [3]$$

where $\delta_A - \delta_X$ is the chemical shift difference.

REFERENCES

1. F. Bloch and A. Siegert, *Phys. Rev.* **57**, 522 (1940).
2. N. F. Ramsey, *Phys. Rev.* **100**, 1191 (1955).
3. W. A. Anderson and R. Freeman, *J. Chem. Phys.* **37**, 85 (1962).

Cross-references

Coherent decoupling
Difference spectroscopy
Field/frequency regulation
Nuclear Overhauser effect
Rotating frame
Spin tickling

Broadband Decoupling

Carbon-13 spectra with proton–carbon splittings are in general too complicated for easy interpretation, and they are of low sensitivity because each resonance is split into several multiplet components. Broadband decoupling is a technique that provides intense irradiation over the entire range of proton chemical shifts in order to decouple all the CH spin–spin interactions. This irradiation also saturates the proton spins and enhances the carbon-13 signals through the nuclear Overhauser effect*. More recently, a family of multidimensional experiments has emerged involving $H \rightarrow X \rightarrow H$ coherence transfer, where the X nucleus may be carbon-13 or nitrogen-15. These experiments require decoupling over a much wider frequency range, aggravated by the fact that it is more difficult to generate suitable radiofrequency levels when the gyromagnetic ratio is low.

The first effective scheme for decoupling over a band of proton frequencies was 'noise decoupling' (1). We can get some insight into how this works by considering the related case of chemical exchange. If two nuclei I and S are coupled, and if the atom carrying the I nucleus exchanges with another chemical site, then I changes its spin state ($\alpha \leftrightarrow \beta$) at random intervals. Provided that the exchange rate is fast compared with J_{IS}, the S resonance coalesces to a singlet. Noise decoupling may be regarded as an attempt to introduce a similar scrambling of the α and β spin states by radiation that has an incoherent character. The radiofrequency phase of the decoupler is inverted by a pseudo-random sequence generated by a shift register. Although the sequence repeats itself periodically, it is a simple matter to make the number of steps in the period very large, so that the behaviour is almost indistinguishable from purely random modulation.

Decoupling methods work better if the decoupler level B_2 is increased, but only at the cost of some radiofrequency heating of the sample. The problem can be quite serious for aqueous samples, and is particularly acute if ions are present. For any sample that might be altered or damaged by heating, the operator should always check the cooling system and the decoupler power dissipation before embarking on a lengthy experiment. In extreme situations the decoupler may be switched on only during signal acquisition but left off during the preparation period, thus sacrificing the nuclear Overhauser enhancement but reducing the mean power dissipation.

These difficulties led to the search for more efficient decoupling schemes. Several frequency-modulation procedures were suggested, on the premise that they would spread the decoupler power over a set of modulation sidebands covering a wide

frequency range, but this 'frequency-domain' picture is not really helpful because it takes no account of interference between adjacent sidebands. The problem is better viewed in the time domain. If we can invert the I spins at a rate that is fast compared with J_{IS}, then the splitting on the S spins vanishes. Simple 180° inversion pulses are too sensitive to off-resonance effects, but composite 180° pulses (2) allow a wide range of I-spin frequencies to be covered. There is no need for 'windows' of free precession between the composite inversion pulses, and there is no requirement that the S-spin data acquisition be synchronized with the decoupler pulses. This approach has led to the discovery of an entire family of *deterministic* decoupling schemes (3–8) that have now completely replaced noise decoupling.

THEORY OF BROADBAND DECOUPLING

We abandon the frequency-domain picture entirely, examining the behaviour of the I spins in the time domain under the influence of some spin inversion sequence, represented by R, which may be a composite 180° pulse or, as we shall see later, an adiabatic pulse. Relaxation effects are neglected. After two consecutive inversions RR, the I spins are returned almost to their initial state; we say that this sequence is approximately *cyclic* (6). The importance of cyclicity can be appreciated from the following argument. The coupled IS spin system can be represented by the energy-level diagram in Fig. 1.

There are four transitions, with frequencies f_1 through f_4, and they necessarily obey a frequency sum rule

$$f_1 + f_4 = f_2 + f_3 \qquad [1]$$

which requires that

$$f_1 - f_2 = f_3 - f_4 \qquad [2]$$

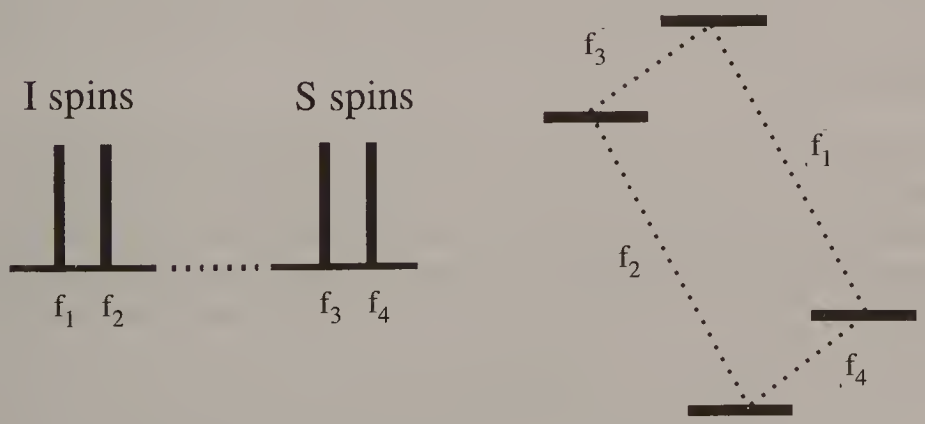

Fig. 1. Energy-level diagram appropriate to a weakly coupled two-spin IS system illustrating the frequency sum rule, $f_1 + f_4 = f_2 + f_3$.

even in the presence of radiofrequency perturbations. Now, suppose we observe the system *stroboscopically*, that is to say, in synchronism with the end of the decoupler period RR. Just as a disco dancer viewed in a suitable strobe light might appear motionless although actually performing quite complex gyrations, so the I spins would appear almost stationary when observed at these specific points in time. In actual practice the I-spin motion is not quite cyclic, leaving an apparent slow rotation. If $\gamma B_2/2\pi >> J_{IS}$, both I-spin vectors rotate at almost the same frequency. Under such conditions of *forced precession*, the splitting $f_1 - f_2$ is very small indeed, and consequently, from eqn [2], the S-spin splitting, $f_3 - f_4$, is equally small. Thus, by forcing the I spins to perform a nearly cyclic motion, we ensure that the residual splitting of the S spins is very much less than the instrumental linewidth; the S spins are effectively decoupled.

The degree of cyclicity is considerably improved by combining RR with its phase-inverted counterpart $\bar{R}\bar{R}$. This 'magic cycle' $RR\bar{R}\bar{R}$ was first proposed by Levitt (3), using the composite inversion pulse:

$$R = 90°(X)\ 180°(Y)\ 90°(X). \qquad [3]$$

The decoupling is therefore improved (a smaller residual splitting) if the sampling is synchronized with the end of each magic cycle. In practice this is inconvenient; the sampling rate normally needs to be faster than this, and it is often not synchronous with the decoupling period at all. The result is the introduction of a weak spurious modulation of the S-spin signal; after Fourier transformation this modulation manifests itself as a set of cycling sidebands (9). Reduction in the height of these cycling sidebands can be achieved by deliberately introducing small variations in the decoupling parameters from one cycle to the next, but there is then a danger that they will resemble baseline noise and obscure very weak signal components. We see that although magic cycles improve decoupling performance by compensating residual imperfections in the spin inversion, this is at the cost of introducing cycling sidebands, which may eventually limit the sensitivity of the method.

SUPERCYCLES

Using intuitive arguments, Levitt *et al.* (10,11) showed that magic cycles could be extended into supercycles that achieve a higher degree of compensation for imperfections of the spin inversion. The theoretical analysis of Waugh (6) demonstrated the rationale behind such expansion procedures. He showed that the performance of a given decoupling cycle is unaffected by phase inversion, for example

$$RR\bar{R}\bar{R} \rightarrow \bar{R}\bar{R}RR, \qquad [4]$$

and it is also unaffected by cyclic permutation of some part of the cycle, for example

$$RR\bar{R}\bar{R} \rightarrow \bar{R}RR\bar{R}. \qquad [5]$$

However, the residual rotation of a phase-inverted or permuted cycle is not the same as that of the original cycle, often having the opposite sense of rotation. Thus an appropriate combination of magic cycles gives a supercycle with superior compensation. For example, the MLEV-4 sequence, $R\bar{R}\bar{R}R$, has a residual rotation about an axis near +Z, whereas the permuted cycle, $\bar{R}R\bar{R}R$, has a residual rotation of similar amplitude about an axis near –Z. Together they form the MLEV-8 supercycle, which has a residual rotation about an axis in the XY plane. This can be largely cancelled by combination with the phase-inverted counterpart, giving the MLEV-16 decoupling sequence:

$$R\bar{R}\bar{R}R\ \bar{R}R\bar{R}R\ \bar{R}\bar{R}RR\ R\bar{R}\bar{R}R. \qquad [6]$$

The MLEV-16 sequence achieves an effective decoupling bandwidth $\Delta F^* = 1.5 \times (\gamma B_2/2\pi)$ kHz, roughly five times that of noise decoupling under similar conditions.

The cyclic permutation rule can be formulated more precisely (6): if a pulse (or combination of pulses) representing a rotation $\theta(+X)$ is cyclically permuted, then the axis of residual rotation of the original sequence is itself rotated about the +X axis through an angle θ. We therefore seek to permute 180° pulses in an attempt to reverse the sense of the residual rotation. However, if the permuted element is not well behaved as a function of resonance offset, the compensation deteriorates at large offsets.

One of the best single elements in this regard is the 90° pulse, because it is largely self-compensating with respect to resonance offset, rotating Z magnetization from the Z axis to the XY plane, albeit with an increasing phase shift with increasing offset (12). This has been made the basis of an alternative expansion procedure (7,8). Suppose we discover a magic cycle whose residual rotation is about an axis close to +Z. Permutation of a 90° pulse rotates this axis so that it lies close to the XY plane. If this permuted cycle is represented by P, then its phase-inverted counterpart $\bar{P}$ has a residual rotation axis similarly placed with respect to the XY plane except that the X and Y coordinates are reversed. The combination $P\bar{P}$ has its residual imperfections largely compensated at all offsets within the effective decoupling bandwidth, in spite of the phase dispersion created by the 90° pulse elements.

WALTZ DECOUPLING

It turns out that any composite inversion pulse that requires rotations about two orthogonal axes, for example R = 90°(X) 180°(Y) 90°(X), is quite sensitive to small errors in the 90° phase shift, whereas composite pulses that employ only 180° shifts are remarkably insensitive, tolerating errors as high as 10° with little penalty. This is the main drawback of the MLEV decoupling scheme. It led to the introduction of WALTZ decoupling (7,8) where the new inversion element is

$$R = 90°(+X)\ 180°(-X)\ 270°(+X) = 1\ \bar{2}\ 3 \qquad [7]$$

where, in a convenient shorthand notation introduced by Waugh (6), a 90° pulse is represented by '1', a 180° pulse by '2', and a 270° pulse by '3' (hence the acronym WALTZ). The primitive sequence is WALTZ-4 which may be written

$$\mathrm{R\bar{R}\bar{R}R} = 1\bar{2}3\ 1\bar{2}3\ \bar{1}2\bar{3}\ \bar{1}2\bar{3}. \qquad [8]$$

This has a residual rotation axis near +Z, so we permute a 90° pulse from left to right and combine the result with the phase-inverted counterpart to give WALTZ-8:

$$\mathrm{K\bar{K}\bar{K}K} = \bar{2}4\bar{2}3\bar{1}\ 2\bar{4}2\bar{3}1\ 2\bar{4}2\bar{3}1\ \bar{2}4\bar{2}3\bar{1}. \qquad [9]$$

Here we have combined adjacent elements when they have the same phase, for example 3 + 1 = 4. The next stage of expansion permutes a 90° pulse element from right to left and combines the result with its phase-inverted counterpart, giving the widely used WALTZ-16 supercycle:

$$\mathrm{Q\bar{Q}\bar{Q}\,Q} = \bar{3}4\bar{2}3\bar{1}2\bar{4}2\bar{3}\ 3\bar{4}2\bar{3}1\bar{2}4\bar{2}3\ 3\bar{4}2\bar{3}1\bar{2}4\bar{2}3\ \bar{3}4\bar{2}3\bar{1}2\bar{4}2\bar{3}. \qquad [10]$$

WALTZ-16 covers an effective decoupling bandwidth $\Delta F^* = 1.8(\gamma B_2/2\pi)$ with very small residual splittings. With suitable precautions, decoupled carbon-13 linewidths as narrow as 0.02 Hz can be recorded (13). There is little point in continuing the expansion procedure, and, in practice, no particular benefit ensues because other sources of imperfection intervene, and they cannot be compensated by this kind of expansion procedure. These adverse influences include spatial inhomogeneity of the decoupler field, imbalance between the 0° and 180° channels, and miscalibration of the 90° pulse length.

EXTENDED BANDWIDTHS

The extremely small residual splittings achieved by WALTZ-16 decoupling are not usually necessary for routine carbon-13 spectroscopy, or for studies of larger molecules where the natural linewidths are appreciable. By relaxing this requirement, and by accepting pulse flip angles other than multiples of 90°, it is possible to improve on the effective decoupling bandwidth for a given radiofrequency level. Computer optimization schemes may be employed. One result is the GARP scheme (14) which includes the requirement that the performance be relatively insensitive to spatial inhomogeneity of the decoupler field. Although the residual splittings are appreciably larger that those obtained with WALTZ-16, they are normally obscured by the instrumental or natural linewidths. GARP attains an effective bandwidth $\Delta F^* = 4.8(\gamma B_2/2\pi)$ kHz.

ADIABATIC PULSES

Many present-day correlation experiments involve a double transfer of magnetization of the type H → C → H, designed to exploit the large proton

Boltzmann factors and the inherently high sensitivity of proton detection. These 'inverse detection' experiments usually entail broadband decoupling of carbon-13 while observing the proton signals, a task that is much more demanding than conventional proton decoupling. For a given spectrometer field, the range of carbon-13 shifts (in kHz) is about five times wider than that of protons, and the radiofrequency power required to reach the same decoupler field ($\gamma_C B_2/2\pi$) is increased 16-fold. Furthermore, there has been an unrelenting drive towards higher and higher magnetic fields, so that chemical shift ranges are all increased. Radiofrequency heating can be very serious for biological samples in aqueous solution, particularly when there are ions present. On the other hand, biochemical applications do not usually demand the very highest resolution, so the decoupling need not be quite so efficient in terms of the residual splittings.

Radiofrequency power can be used more effectively if the spin inversion is achieved through adiabatic rapid passage* through resonance (15–18). For effective decoupling, the sweep rate must be high in comparison with J_{IS}; a typical duration for the adiabatic sweep would be 1 millisecond. These adiabatic 'pulses' are used in place of the composite spin inversion pulses employed in the MLEV and WALTZ schemes. Imperfections in spin inversion are compensated by incorporating the adiabatic pulses into a supercycle. This is not without its drawbacks, since it inevitably introduces cycling sidebands into the decoupled spectrum (9). One useful supercycle is the five-step sequence (0°, 150°, 60°, 150°, 0°) of Tycko *et al.* (19) nested within the (0°, 0°, 180°, 180°) MLEV sequence (3).

We define an effective field, $B_{eff} = (\Delta B^2 + B_2^2)^{1/2}$, inclined with respect to the X axis at an angle $\theta = \arctan(\Delta B/B_2)$. As ΔB is swept from a large negative value to a large positive value, θ varies from approximately +90° to approximately –90°. The nuclear magnetization vector follows the direction of the effective field provided that the adiabatic condition is satisfied:

$$d\theta/dt << |\gamma B_{eff}|, \qquad [11]$$

that is to say, the effective field must change direction slowly in comparison with the rate at which nuclear magnetization precesses about B_{eff}. It is useful to define an adiabaticity factor (17)

$$Q = |\gamma B_{eff}/d\theta/dt|. \qquad [12]$$

For broadband decoupling the aim is to treat all the dccoupled resonances essentially equally, and it seems logical to employ a constant amplitude, linear frequency sweep. In this manner there is the same adiabaticity factor for all the chemically shifted sites. We can write the adiabaticity factor at resonance ($\Delta B = 0$) as (17)

$$Q_0 = \frac{(\gamma B_2)^2}{d\Delta\omega/dt} \qquad [13]$$

where $\Delta\omega = \gamma\Delta B$. Conventional wisdom has always maintained that Q_0 should be large compared with unity, but in practice $Q_0 = 1$ can be used if the imperfections are compensated by a suitable supercycle (20). For a linear frequency sweep of

duration T seconds we may write

$$d\Delta\omega/dt = 2\pi\Delta F/T \qquad [14]$$

where ΔF is the total sweep range, related to the effective decoupling bandwidth ΔF^* through the coefficient

$$\xi = \Delta F^*/\Delta F \qquad [15]$$

where ξ is a number less than, but close to, unity. From eqns [13], [14] and [15] we derive an expression for the effective decoupler bandwidth:

$$\Delta F^* = 2\pi\xi\left(\frac{\gamma B_2}{2\pi}\right)^2 \frac{T}{Q_0} \quad . \qquad [16]$$

This dependence on the *square* of the radiofrequency intensity is to be contrasted with composite pulse decoupling, where the effective bandwidth ΔF^* is *linearly* proportional to the decoupler level. This accounts for the high efficiency of adiabatic decoupling schemes. Note that the bandwidth increases as the adiabaticity factor Q_0 is reduced; eventually this violates the adiabatic condition to the extent that the spin inversion is too inefficient for effective decoupling. Slow sweep rates also increase the decoupling bandwidth, but unless the sweep rate is sufficiently high in comparison with J_{IS}, the cycling sidebands become too obtrusive. A reasonable compromise would be a sweep rate determined by

$$1/T \geq 4\left|J_{IS}\right| . \qquad [17]$$

This accounts for the fact that it is easier to cover a wide range of I-spin chemical shifts when the magnitude $\left|J_{IS}\right|$ is small.

Adiabatic pulses are therefore very efficient, covering a wide frequency band ΔF^* at a relatively low radiofrequency level, and outperforming composite pulse decoupling in most practical situations. Several adiabatic decoupling sequences (20–28) have been proposed; we concentrate here on one representative scheme that embraces a wide range of experimental requirements – extremely wide effective bandwidths at one extreme, very low cycling sidebands at the other. The experimental parameters (Q_0, T, n, B_2) can be tailored to suit the particular application in hand.

In practice the frequency sweep must be terminated at some finite offset, leaving B_{eff} slightly inclined with respect to the Z axis. To correct this edge effect, the B_2 amplitude is brought smoothly down to zero at the extremities of the sweep (29). Several possible 'apodization' functions could be used; one that has proved effective in practice is the sausage-shaped amplitude profile defined by

$$A = \pm A_0\left(1 - \left|\sin\theta\right|^n\right) \qquad [18]$$

where the exponent n is usually large, say 20 or 40. This leaves a wide central region with a constant B_2 level, preserving the adiabaticity and giving an effective decoupling bandwidth that is a large fraction (ξ) of the total range of the adiabatic sweep (20). These sequences are called 'WURST' to emphasize the key properties

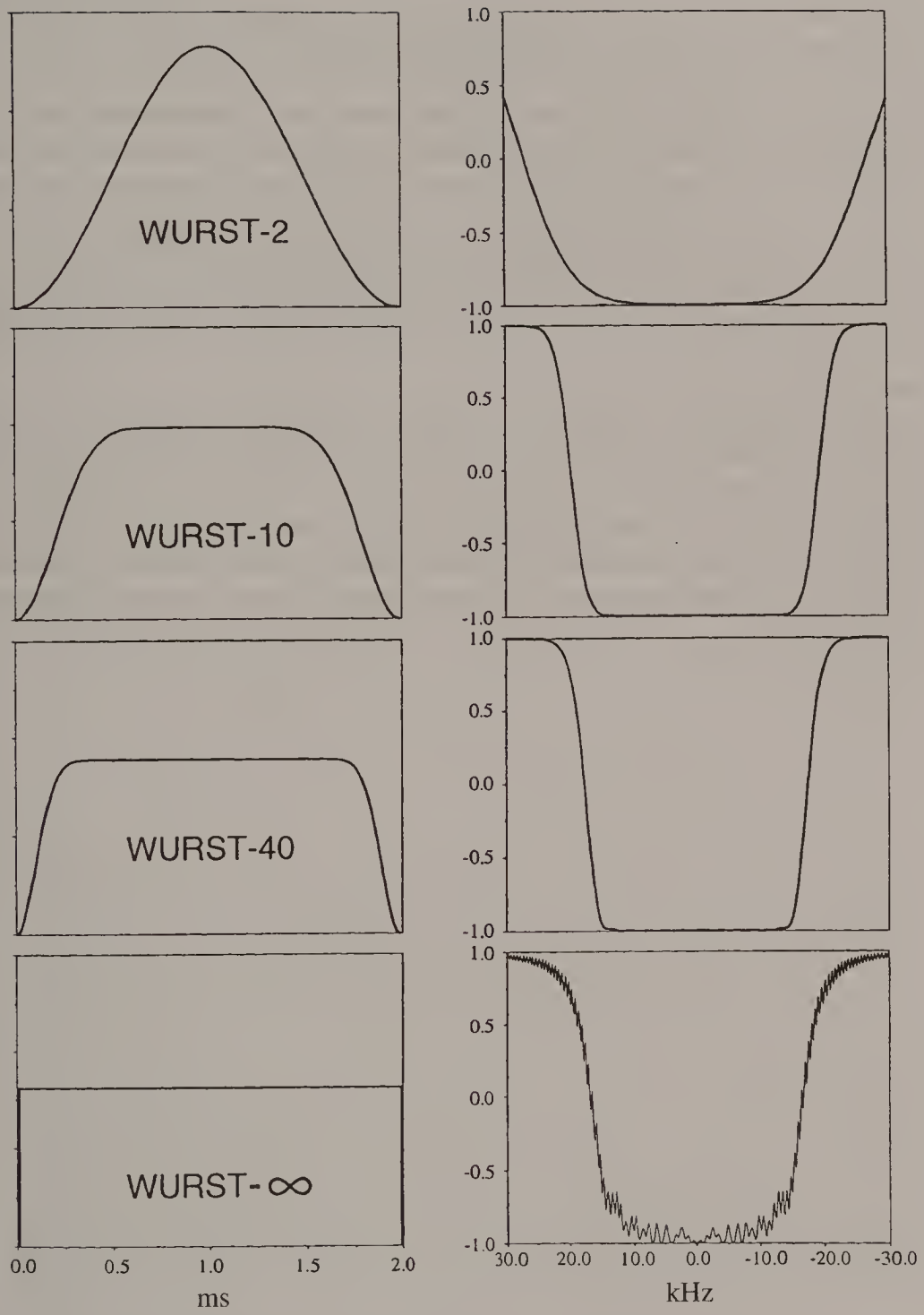

Fig. 2. Amplitude envelopes for various WURST-n pulses plotted as a function of time (left), and the corresponding spin inversion profiles plotted as a function of offset (right). The index n determines the severity of the round-off function (eqn [18]). Note the oscillations that appear in the spin inversion profile when the amplitude profile is rectangular (bottom).

– wideband, uniform-rate smooth truncation. They represent an entire family of decoupling schemes defined principally by the shape index n (Fig. 2). If n is extremely large, giving negligible apodization of the edge effects, WURST approaches the CHIRP-95 scheme (25,26), but the sharp discontinuities at the leading and trailing edges of the pulse violate the adiabatic condition and give rise to oscillatory components in the spin inversion profile (Fig. 2). At the other extreme where n = 2, the amplitude profile is a cosine-squared function, and if the frequency-sweep function is then optimized (27) the performance is close to that of the hyperbolic secant pulse (22,23). This mode might be used where it is essential to minimize the intensity of the cycling sidebands, but where a wide decoupling bandwidth is not the prime concern. Sidebands can be kept below the 0.2% level in practice (30).

Figure 3 illustrates WURST-240 adiabatic decoupling of carbon-13 while observing protons, demonstrating an effective bandwidth of 290 kHz with the relatively low radiofrequency level $\gamma B_2(\text{r.m.s.})/2\pi = 5.6$ kHz (27). Here $B_2(\text{r.m.s.})$ represents the constant radiofrequency level that would have the same power dissipation as the actual amplitude-modulated field B_2. Cycling sidebands (9) are in evidence, but if necessary they can be reduced by only a modest increase in decoupler level.

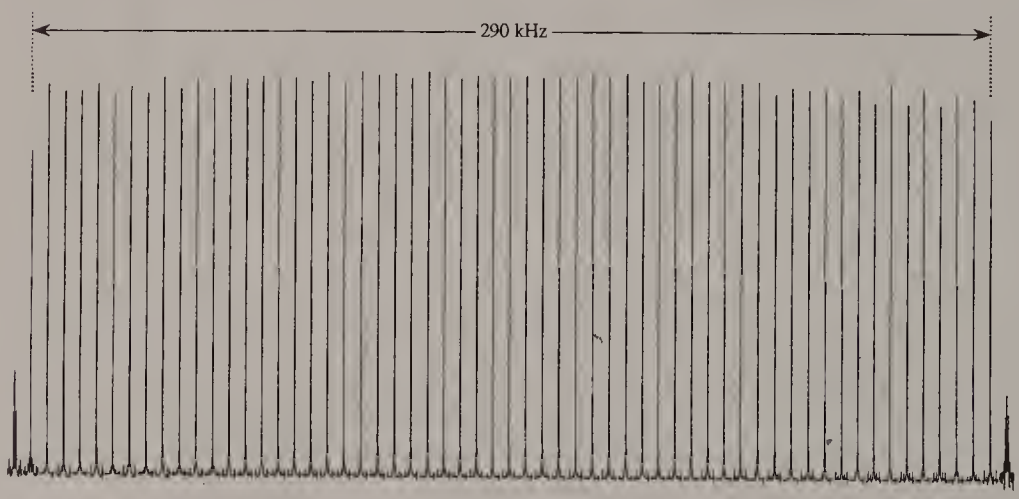

Fig. 3. Broadband decoupling of carbon-13 in methyl iodide with proton detection at 400 MHz using the adiabatic pulse sequence WURST-240 in a 20-step phase cycle. The decoupler offset was incremented in 5 kHz steps over a total range of 300 kHz. The decoupler level was set at $\gamma B_2/2\pi = 5.8$ kHz, corresponding to the same power dissipation as a constant level $\gamma B_2/2\pi = 5.6$ kHz.

REFERENCES

1. R. R. Ernst, *J. Chem. Phys.* **45**, 3845 (1966).
2. M. H. Levitt and R. Freeman, *J. Magn. Reson.* **33**, 473 (1979).
3. M. H. Levitt and R. Freeman, *J. Magn. Reson.* **43**, 502 (1981).
4. M. H. Levitt, R. Freeman and T. Frenkiel, *Advances in Magnetic Resonance*, ed. J. S. Waugh. Academic Press: New York, Vol. 11, 1983.
5. A. J. Shaka and J. Keeler, *Progress in NMR Spectroscopy*, ed. J. W. Emsley, J. Feeney and J. Sutcliffe. Pergamon Press: Oxford, Vol. 19, 1987.
6. J. S. Waugh, *J. Magn. Reson.* **50**, 30 (1982).
7. A. J. Shaka, J. Keeler, T. Frenkiel and R. Freeman, *J. Magn. Reson.* **52**, 335 (1983).
8. A. J. Shaka, J. Keeler and R. Freeman, *J. Magn. Reson.* **53**, 313 (1983).
9. A. J. Shaka, P. B. Barker, C. J. Bauer and R. Freeman, *J. Magn. Reson.* **67**, 396 (1986).
10. M. H. Levitt, R. Freeman and T. Frenkiel, *J. Magn. Reson.* **47**, 328 (1982).
11. M. H. Levitt, R. Freeman and T. Frenkiel, *J. Magn. Reson.* **50**, 157 (1982).
12. R. Freeman and H. D. W. Hill, *J. Chem. Phys.* **54**, 3367 (1971).
13. A. Allerhand, R. E. Addleman, D. Osman and M. Dohrenwend, *J. Magn. Reson.* **65**, 361 (1985).
14. A. J. Shaka, P. B. Barker and R. Freeman, *J. Magn. Reson.* **64**, 547 (1985).
15. S. L. McCall and E. L. Hahn, *Phys. Rev.* **183**, 457 (1969).
16. M. S. Silver, R. J. Joseph and D. I. Hoult, *Phys. Rev. A* **31**, 2753 (1985).
17. J. Baum, R. Tycko and A. Pines, *Phys. Rev. A* **32**, 3435 (1985).
18. C. J. Hardy, W. A. Edelstein and D. Vatis, *J. Magn. Reson.* **66**, 470 (1986).
19. R. Tycko, A. Pines and R. Gluckenheimer, *J. Chem. Phys.* **83**, 2775 (1985).
20. Ē. Kupče and R. Freeman, *J. Magn. Reson. A* **115**, 273 (1995).
21. T. Fujiwara, T. Anai, N. Kurihara and K. Nagayama, *J. Magn. Reson. A* **104**, 103 (1993).
22. Z. Starčuk, Jr, K. Bartušek and Z. Starčuk, *J. Magn. Reson. A* **107**, 24 (1994).
23. M. R. Bendall, *J. Magn. Reson. A* **112**, 126 (1995).
24. Ē. Kupče and R. Freeman, *J. Magn. Reson. A* **117**, 246 (1995).
25. R. Fu and G. Bodenhausen, *J. Magn. Reson. A* **117**, 324 (1995).
26. R. Fu and G. Bodenhausen, *Chem. Phys. Lett.* **245**, 415 (1995).
27. Ē. Kupče and R. Freeman, *J. Magn. Reson. A* **118**, 299 (1996).
28. Ē. Kupče and R. Freeman, *Chem. Phys. Lett.* **250,** 523 (1996).
29. J. M. Böhlen and G. Bodenhausen, *J. Magn. Reson. A* **102**, 293 (1993).
30. Ē. Kupče, R. Freeman, G. Wider and K. Wüthrich, *J. Magn. Reson. A* **120**, 264 (1996).

Cross-references

Adiabatic rapid passage
Coherent decoupling
Composite pulses
Nuclear Overhauser effect

Chemical Exchange

Historically, the first substance to show a high-resolution proton spectrum with several distinct lines (ethanol) also showed clear evidence that the hydroxyl proton was undergoing chemical exchange, and the physics of this process was analysed in a classic paper by Arnold (1). In effect, the nuclear spin acts as a label that allows us to monitor the movement of an atom or group of atoms from one chemical site to another. They may be sites in different molecules or in different conformers of the same molecule. Whereas almost all other methods for following rate processes involve a displacement from equilibrium, the NMR method applies to systems actually in an equilibrium state.

The manner in which chemical exchange affects the NMR spectrum depends very much on the rate of chemical exchange in comparison with the chemical shift difference between the two sites, and there are two regimes that are important – slow and fast exchange.

SLOW EXCHANGE

When the rate of exchange between two sites I and S is slow in comparison with the chemical shift difference $|\delta_I - \delta_S|$, we observe a slight additional broadening of the I and S lines. Viewed in the time domain, this represents a reduction in the phase memory time (T_2) because the free precession of the spins at (say) site S is interrupted owing to the replacement by spins transferred from site I with an arbitrary precession phase. Suppose we apply a hard excitation pulse at time zero, initiating the precession of a typical I spin and a typical S spin with the same phase (Fig. 1). For simplicity we may neglect the other spin–spin relaxation processes and focus only on the loss of phase coherence due to exchange. At some random time later, the I and S spins exchange, carrying with them their individual precession phases. We see that this creates a phase jump at each site; they are equal in magnitude but opposite in sign. If the average interval τ between exchange events is long in comparison with the time it normally takes for the S spins to precess 360° further than the I spins, then the perturbation of the precession phase is small; this is the slow exchange limit,

$$(\tau)^{-1} << |\delta_I - \delta_S|. \qquad [1]$$

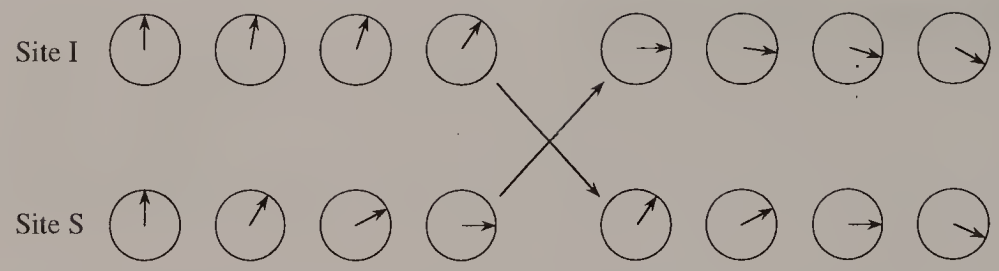

Fig. 1. Slow chemical exchange between two sites introduces a small phase jump in the precession, reducing the phase memory time at each site, and slightly broadening the two resonance lines.

We may write

$$(T_2')^{-1} = (T_2)^{-1} + (\tau)^{-1} \qquad [2]$$

where T_2 is the spin–spin relaxation time in the absence of exchange, and T_2' is the phase memory time taking exchange into account. In many practical high-resolution situations we do not observe the natural linewidth $(T_2)^{-1}$ but the broader instrumental linewidth $(T_2^*)^{-1}$, so in the slow exchange limit the effect only becomes observable when τ is shorter than T_2^*. Slower rates of exchange can be monitored by their effect on a spin-echo experiment where T_2' can be observed directly.

TWO-DIMENSIONAL SPECTROSCOPY

One alternative method for the study of slow exchange is the saturation transfer experiment (2), where the movement of an atom between two sites is monitored by the transfer of saturated spins (or spins suffering a population inversion). This topic is covered separately under Saturation transfer*. The same concept is the basis of exchange studies by two-dimensional spectroscopy* (3). During an initial evolution period, the spins precess freely and are essentially 'labelled' by their chemical shift frequencies. The magnetization is then returned to the Z axis and a short interval τ_m is allowed for chemical exchange to occur. A hard pulse then recreates transverse magnetization, and if any spins have moved from site I to site S they will have a different precession frequency during the detection period. This generates a cross-peak in the two-dimensional spectrum at the coordinates (δ_I, δ_S) and a corresponding cross-peak at (δ_S, δ_I) representing transfer from site S to site I. The rate of exchange can be measured directly by following the build-up of cross-peak intensity as τ_m is increased. More commonly, the relative cross-peak intensities are used to compare exchange rates involving different paths. This is a very powerful method for investigating multisite exchange.

FAST EXCHANGE

The opposite extreme is the case where the rate of exchange is fast in comparison with the chemical shift difference, the fast exchange limit:

$$(\tau)^{-1} >> |\delta_I - \delta_S|. \qquad [3]$$

The observed behaviour is now quite different. First of all, we must take into account the populations at the two sites p_I and p_S. Then we fix our attention on a given spin and note that it hops rapidly between sites I and S, spending so little time at each site that the phase jump $\Delta\phi = 2\pi|\delta_I - \delta_S|\tau$ is always much less than 1 radian. The precession of the chosen spin is a very jerky motion, made up of short segments at δ_I Hz alternating with segments at δ_S Hz, and with many such segments per revolution. We may think of this as a 'pure' precession at the weighted mean frequency

$$\delta_{mean} = \frac{\delta_I p_I + \delta_S p_S}{p_I + p_S} \qquad [4]$$

with a weak superimposed random modulation which depends on the average value of $\Delta\phi$. Figure 2 illustrates this case schematically; the mean position of the I and S vectors shows a progressive rotation with a slight superimposed random forward-and-backward perturbation. Consequently, instead of the expected resonances at δ_I and δ_S, we observe only a single coalesced line at the weighted mean frequency δ_{mean}. As the exchange rate increases, the phase jumps $\Delta\phi$ become smaller, making the precessional motion less jerky, and the coalesced line becomes narrower. Note that this is the opposite behaviour to that observed in the slow exchange limit where increasing the exchange rate *broadens* the resonances.

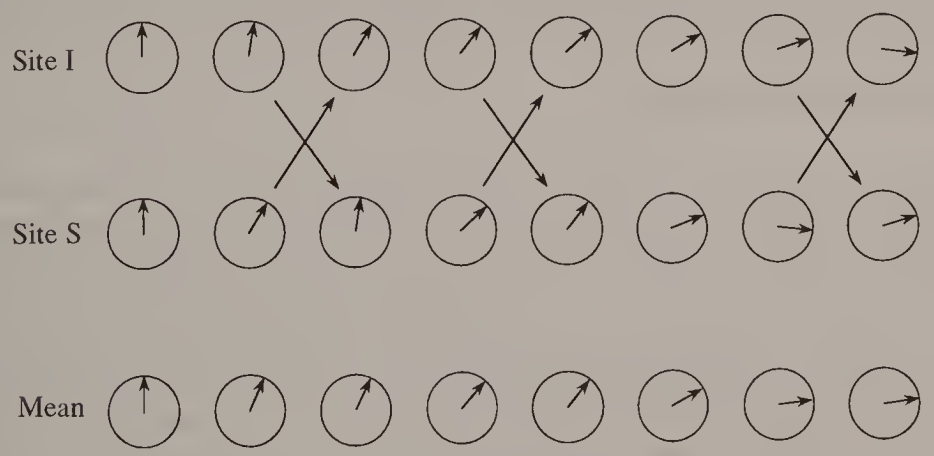

Fig. 2. Fast chemical exchange between two sites causes many random phase jumps in the free precession. This is equivalent to the motion of a 'mean' vector that precesses at the weighted mean chemical shift frequency, slightly perturbed by the small phase jumps. Only a single coalesced resonance is observed.

In the more general case of several exchanging sites, the width of the coalesced resonance line may be written (4)

$$(T_2')^{-1} = (T_2)^{-1} + M_2\tau \qquad [5]$$

where M_2 is the second moment of the lines in the absence of exchange, defined by

$$M_2 = \sum_j p_j[2\pi(\delta_j - \delta_{mean})]^2. \qquad [6]$$

The frequencies are all measured with respect to the mean frequency δ_{mean} for which

$$\sum_j 2\pi p_j(\delta_j - \delta_{mean}) = 0. \qquad [7]$$

For the simplest case of two exchanging sites, equally populated, eqn [5] reduces to

$$(T_2')^{-1} = (T_2)^{-1} + [\pi(\delta_I - \delta_S)]^2\tau. \qquad [8]$$

For very fast exchange the last term becomes negligible in comparison with $(T_2)^{-1}$ and the coalesced line eventually reaches the natural linewidth again. There is then no direct evidence of chemical exchange.

In many rapidly exchanging systems, the relative populations can also change, causing the coalesced line to shift dramatically across the spectrum, as the mean frequency δ_{mean} is shifted. A good example is provided by the proton spectrum of ethanol, where the hydroxyl proton is normally in fast exchange between hydrogen-bonded and 'free' sites. Inert solvents like carbon tetrachloride discourage hydrogen bonding and the hydroxyl resonance shifts to high field (between the methylene and methyl resonances). On the other hand, neat ethanol, which favours hydrogen bonding, generates a spectrum with the hydroxyl resonance at low field. Whenever a resonance line changes its position over a wide frequency range as a result of solvent or temperature effects, this is often evidence for hydrogen bonding.

SPIN-ECHO METHODS

In order to circumvent the effects of instrumental broadening, investigations of chemical exchange often employ the Carr–Purcell multiple-spin-echo technique (5). These are usually studies of simple systems in the fast exchange limit, where the decay rate of the spin-echo envelope yields the modified relaxation time T_2'. A rather unexpected phenomenon occurs if the repetition rate of the refocusing pulses is increased (6). The apparent relaxation time T_2' (usually significantly shorter than the 'true' spin–spin relaxation time T_2) begins to increase, and eventually approaches T_2 as the repetition rate becomes high in comparison with the exchange rate. The nuclei appear to behave as if no chemical exchange were taking place. This can be understood when it is realized that the reduction in phase memory time in the fast exchange limit depends on the magnitude of the average phase jump. For the simple two-site exchange case represented by eqn [8], the relevant term is

$[\pi(\delta_I - \delta_S)]^2\tau$ when the pulse repetition rate is low. However, the echo peak intensity is only affected by phase jumps which build up in the interval since the last refocusing pulse, so at high pulse repetition rates the effective phase errors are reduced, and in the limit the echo envelope decays at a rate determined only by T_2. This experimental approach allows both T_2 and T_2' to be evaluated.

INTERMEDIATE EXCHANGE RATES

When the exchange rate is comparable with the chemical shift difference between the sites, this simple picture breaks down. For two-site exchange, increasing the exchange rate first broadens the individual lines, then draws them together so that they eventually coalesce to a single peak, which then gets narrower as the exchange rate is further increased. A proper analysis of the line profiles in the intermediate case for several chemical sites requires numerical methods. However, this is just the situation where the NMR spectrum is most strongly affected by exchange, so reliable values of the exchange rates can usually be extracted.

Chemical exchange can also influence spin multiplet structure. If a resonance S exhibits a spin multiplet pattern due to coupling to another spin I, then if I undergoes chemical exchange at a rate that is fast in comparison with $|J_{IS}|$, the S multiplet coalesces to a singlet at the chemical shift frequency. This is why the hydroxyl resonance of ethanol is normally a singlet and why the nearby methylene group shows no doublet structure attributable to coupling the hydroxyl group. However, if the sample is purified, cutting down the rate of chemical exchange, the hydroxyl resonance becomes a 1:2:1 triplet and the methylene resonance acquires an additional doublet splitting (1).

The possibility of chemical exchange can inhibit the use of NMR spectroscopy for certain types of investigation. Suppose we suspect that a molecule exists as two distinct conformers. The fact that only a simple spectrum is observed does not necessarily imply that only one conformer exists; it may merely indicate that the two forms are interchanging at a rate that is fast compared with the relevant chemical shift difference, which is usually not known *a priori*.

REFERENCES

1. J. T. Arnold, *Phys. Rev.* **102**, 136 (1956).
2. S. Forsén and R. A. Hoffman, *J. Chem. Phys.* **39**, 2892 (1963).
3. J. Jeener, B. H. Meier, P. Bachmann and R. R. Ernst, *J. Chem. Phys.* **71**, 4546 (1979).
4. L. H. Piette and W. A. Anderson, *J. Chem. Phys.* **30**, 899 (1959).
5. H. Y. Carr and E. L. Purcell, *Phys. Rev.* **94**, 630 (1954).
6. Z. Luz and S. Meiboom, *J. Chem. Phys.* **39**, 366 (1963).

Cross-references

Saturation transfer
Spin echoes
Spin–spin relaxation
Two-dimensional spectroscopy

Chemically Induced Nuclear Polarization

An NMR spectrum measures the absorption of radiofrequency energy, and net emission only occurs in very special circumstances, for example if some kind of pumping of spin populations occurs, as in selective population transfer or some kinds of Overhauser experiments (see Nuclear Overhauser effect*). It was therefore quite a surprise when it was discovered that certain free radical reactions yielded products with strong (transient) emission and absorption lines. These 'anomalous' lines decayed to near-zero intensity by spin–lattice relaxation*, suggesting that they were the result of a non-Boltzmann population distribution. The presence of unpaired electron spins in the free radical stage led the initial investigators to the erroneous conclusion that this must be some kind of electron–nucleus Overhauser or dynamic polarization effect and hence used the name *chemically induced dynamic nuclear polarization* (CIDNP).

The actual mechanism (1–3) is quite remarkable, for it proposes that the nuclear spin can influence the course of a chemical reaction despite the fact that the energy gap between nuclear spin states in a magnetic field is tiny by comparison with bond dissociation energies. Consider the simplest possible case of a molecule ABH. In order to keep the model simple, only one nuclear spin (H) has been assumed, but more complicated extensions follow the same principles. Ultraviolet irradiation raises this to an excited singlet state ABH* which usually undergoes rapid intersystem crossing to the triplet state and then dissociates into radicals.

$$\text{ABH} \rightarrow \text{ABH*}\ (\text{singlet}) \rightarrow \text{ABH*}\ (\text{triplet}) \rightarrow \text{A}\bullet + \bullet\text{BH}.$$

Thus the two electrons in the radical pair have *parallel* spins, a triplet state. The reaction takes place in solution, usually in a deuterated solvent, so the nascent radical pair is trapped in a solvent cage for a time that is sufficiently long that many recollisions occur between the two radicals. As long as the two radicals remain within interaction range of each other they are referred to as a *geminate pair* and if they recombine to form a molecule this process is called *geminate recombination.* Although the two radicals may collide many times inside the solvent cage, they cannot recombine as long as the electron spins remain in a triplet configuration, for this represents antibonding. Bond formation can only occur if there is some triplet-to-singlet conversion before one of the radicals escapes from the cage.

There are three triplet states of different energy in a magnetic field (Fig. 1) called

the T_0, T_+ and T_- states. All that is required for interconversion between the T_0 and S states is that one electron precess faster than the other for a sufficiently long period that a 180° phase difference builds up. This differential precession occurs because of the presence of the nuclear spin (H) operating through its hyperfine coupling to the electron on the •BH radical.

We might visualize this process by sketching the hypothetical electron spin resonance spectra of the two radicals (Fig. 2(a)). This is a single line at the g value for the A radical, but is a doublet of splitting equal to the hyperfine coupling a_H for the B radical. For any given radical pair *only* the α nuclear spin state *or* the β nuclear spin state is applicable; somewhere else in the solution there will be another radical pair with the opposite label. Suppose it is in fact an α state; then for this radical pair the two electron precession frequencies are very close and there is only a low probability of triplet–singlet conversion. The two radicals may not form a chemical bond and the most likely fate is escape from the solvent cage followed by eventual reaction with the solvent (deuteron extraction). Note that escape of an A• radical and subsequent reaction with some distant •BH radical is *not* the same as geminate recombination: all phase memory is lost when one of the radicals escapes from its partner. By contrast, if we had considered a different radical pair where the proton was in a β state, then the two electrons would have had appreciably different precession frequencies, there would have been a high probability of triplet–singlet conversion, and the two radicals would be quite likely to form a bond (geminate recombination).

Geminate recombination thus leads to an ABH molecule with an enormous preponderance of protons in the β state, far in excess of the usual Boltzmann population. The corresponding proton resonance is therefore in emission and is extremely intense considering the small number of such product molecules (the free radical concentration is never very high). This is not a stable situation and at a rate

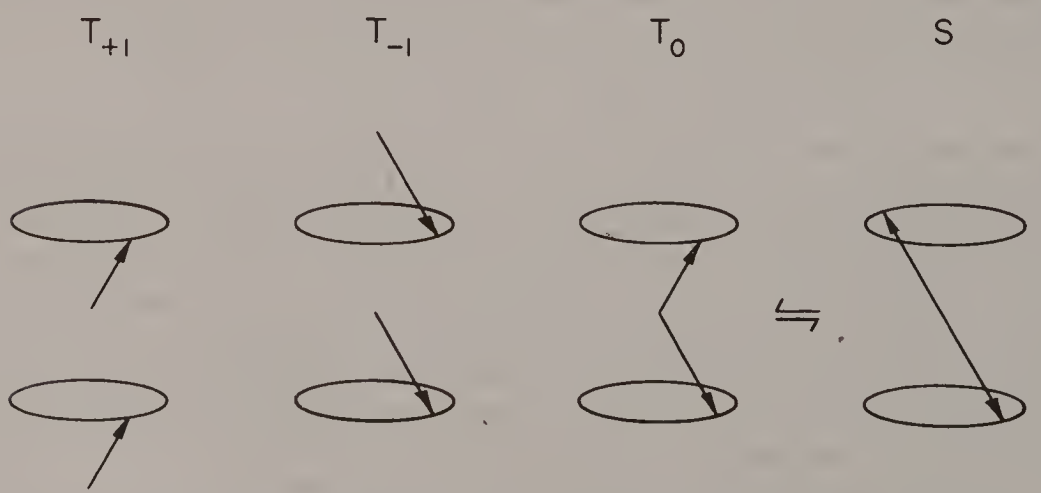

Fig. 1. Representation of the triplet and singlet states of a radical pair trapped in a solvent cage. In a magnetic field the T_0 and S states may interchange if one of the unpaired electron spins precesses faster than the other.

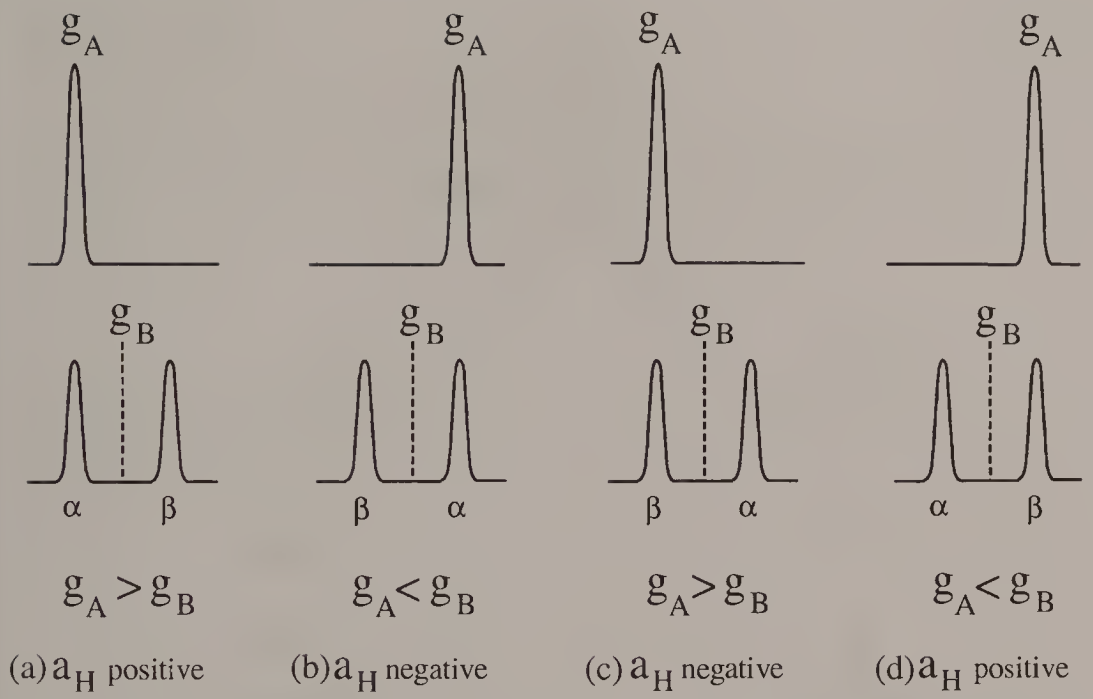

Fig. 2. Hypothetical ESR spectra of a radical A• and a radical •BH in a magnetic field. The important parameters are the sign of the difference in g values and the sign of the hyperfine coupling a_H. Cases (a) and (b) favour triplet-to-singlet conversion for radical pairs with a β proton, whereas cases (c) and (d) favour conversion for radical pairs with an α proton.

determined by the spin–lattice relaxation* time this excess population relaxes by dropping down to the α level. The corresponding equilibrium NMR signal is very weak indeed and is often undetectable.

An escape product, perhaps a DBH molecule, has a large excess of protons in the α state, giving a very intense line in *absorption*. Since its resonance will in general be at a different frequency from the ABH molecule cited above, the two signals do not overlap and cancel. Spin–lattice relaxation causes a decay of this signal as proton spins move up to the β state (Fig. 3).

The sorting of the chemical reaction path is not of course as complete as inferred in this argument; it is possible that the radical pair makes two conversions, triplet–singlet–triplet, but usually the lifetime for trapping in the solvent cage is short compared with the inverse frequency difference for electron precession.

By now the reader will be objecting that some quite *ad hoc* assumptions were made in sketching the hypothetical electron spin resonance spectra used in this treatment. Indeed, it was assumed that $g_A > g_B$ and that the hyperfine coupling constant a_H was positive (otherwise the α and β labels would need to be interchanged). Reversal of one of these assumptions would have reversed the argument: geminate recombination generating an absorption spectrum and escape products an emission spectrum. Reversal of *both* assumptions brings us back to the result of Fig. 3. The four different cases are set out in Fig. 2. These sign reversals for the CIDNP effect are embodied in Kaptein's rules (3).

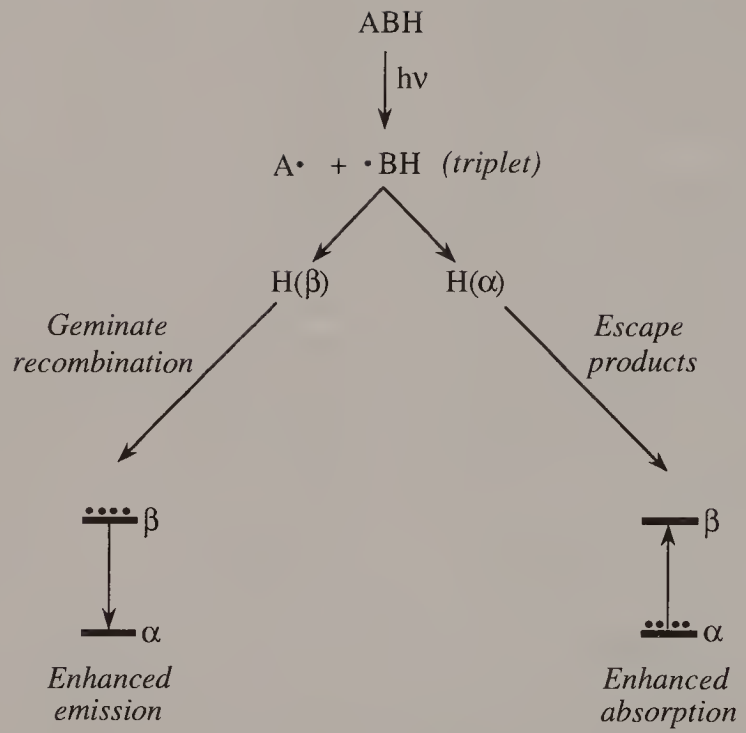

Fig. 3. Sorting into two possible reaction paths after a radical pair has been generated. If radical pairs with a β proton undergo triplet-to-singlet conversion, they are more likely to recombine within the solvent cage, producing ABH molecules with enhanced NMR emission. Radical pairs with an α proton are unlikely to recombine; they eventually escape from the cage, attacking the solvent and giving enhanced NMR absorption.

The beauty of this experiment is that it provides good evidence for a free radical mechanism in the reaction under investigation, and the form of the enhanced NMR spectrum gives information about the structure of the radicals involved. The presence of two or more nuclei in a given radical gives rise to a new phenomenon – the *multiplet effect* – in which the relative intensities are perturbed within the spin multiplet. The mechanism for this follows along similar lines.

Historically, the discovery of chemically induced nuclear polarization provides a cautionary tale. It appears that several spectroscopists had noticed occasional inverted resonance lines long before the effect was reported and characterized. They had dismissed them as instrumental artefacts because when they tried to repeat the experiment (a second scan through the spectrum, for this was in the days of continuous-wave spectroscopy*) the anomalies disappeared. What they did not realize was that a free radical reaction was involved, initiated by ultraviolet irradiation (sunlight). To repeat the experiment properly would have required taking the sample out of the probe and re-exposing it to sunlight; then the emission lines would have been reproducible. They were not simply things that went bump in the night.

REFERENCES

1. G. L. Closs, *J. Am. Chem. Soc.* **91**, 4552 (1969).
2. G. L. Closs and A. D. Trifunac, *J. Am. Chem. Soc.* **91**, 4554 (1969).
3. R. Kaptein and L. J. Oosterhoff, *Chem. Phys. Lett.* **4**, 195, 214 (1969).

Cross-references

Continuous-wave spectroscopy
Nuclear Overhauser effect
Polarization transfer
Spin–lattice relaxation

Coherence

At Boltzmann equilibrium there is a small excess of nuclear spins aligned along the direction of the applied magnetic field (the +Z axis). Although the individual spins all precess in the applied field, their phases are random, and there is no resultant magnetization in the transverse (XY) plane. However, if we apply a radiofrequency pulse, these excess spins precess in phase and create macroscopic nuclear magnetization. This induces a radiofrequency current in the receiver coil – the well-known free induction decay. We say that there is now *coherence* between the phases of the spins as they precess. If we think of the individual spins as tiny precessing vectors, they now move in step and have an appreciable resultant that can be detected.

Properties that represent an ensemble average over all the spins in the sample can be characterized by a *density matrix* σ (1). Couched in terms of this density matrix, coherence of this kind would be represented by an off-diagonal element connecting states separated by $\Delta m = \pm 1$, whereas the spin populations correspond to the diagonal elements. Figure 1 illustrates such a density matrix for the simple case of two coupled spin-$\frac{1}{2}$ nuclei. The cross-hatched elements characterize coherences that are directly observable in the spectrometer. In terms of an energy-level diagram they would correspond to the four *allowed transitions,* and in the vocabulary of product operators* they are represented by terms like I_X and I_Y . These coherences die away with time as interactions between spins upset the time keeping, destroying the phase relationship between individual spins. The quiescent condition of the density matrix has only diagonal elements (Fig. 1(a)).

On the other hand, if we apply a suitable sequence of hard pulses, or a cascade of soft (frequency-selective) pulses, coherences can be excited that correspond to off-diagonal elements of the density matrix connecting eigenstates with $\Delta m = 0$ or $\Delta m = \pm 2$ (Fig. 1(c)). They do *not* represent macroscopic precessing magnetization and they do *not* induce radiofrequency current in the receiver coil. In terms of an energy-level diagram, they correspond to the formally forbidden zero-quantum and multiple-quantum transitions. The product operator formalism represents them as terms of the form $(2I_XS_X + 2I_YS_Y)$ or $(2I_XS_X - 2I_YS_Y)$. This concerted motion of the I and S spins is not amenable to the simple vector representation. Nevertheless these coherences can be shown to evolve with time, to be affected by radiofrequency pulses and to decay by relaxation processes. Their presence is inferred indirectly, by reconversion into observable precessing nuclear magnetization at some later time.

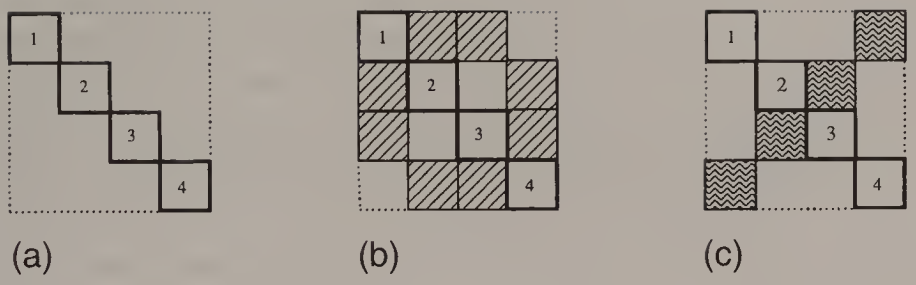

Fig. 1. Schematic representation of the density matrix for a system of two coupled spin-$\frac{1}{2}$ nuclei. (a) The diagonal elements correspond to spin populations on the energy levels 1–4. (b) The cross-hatched off-diagonal elements ($\Delta m = \pm 1$) give rise to observable transverse magnetization. (c) The shaded off-diagonal elements ($\Delta m = 0$, $\Delta m = \pm 2$) represent the unobservable multiple-quantum coherences.

COHERENCE ORDER

This *coherent superposition of eigenstates* has come to be called simply a *coherence*. We use radiofrequency pulses to bring the precession of individual spins into phase (single-spin coherence) or to create a concerted motion of two or more different types of spin (multiple-quantum coherence). In addition to this distinction between observable and 'invisible' coherences, it is useful to define the *order of coherence*. Thus double-quantum coherence has order 2, triple-quantum coherence has order 3, etc. The sense of precession imposes a sign on the coherence order. The properties of zero-quantum coherence and longitudinal magnetization are difficult to distinguish, and both are categorized as coherence order 0.

The utility of this notation becomes clear when it is applied to experiments involving complex pulse sequences, where it is important to select one type of NMR response but reject another. Take, for example, the case of double-quantum filtration, where the signals of interest might be those from coupled pairs of carbon-13 nuclei in the INADEQUATE technique (2). Only one molecule in 8100 contains the coupled spin pairs of interest, whereas one molecule in 90 has isolated carbon-13 spins. The key to this separation is to chart the orders of coherence (p) through the sequence of manipulations. This is called the *coherence transfer pathway* (3). Free precession maintains a constant order of coherence, but radiofrequency pulses cause 'jumps' between orders. Most experiments start at Boltzmann equilibrium with $p = 0$. If the receiver is to detect an observable response, it requires either $p = +1$ or $p = -1$, the two possible senses of precession in the rotating frame. The accepted convention is to select $p = -1$ in the quadrature phase detector, rejecting the counter-rotating component $p = +1$. To keep the picture simple, coherence pathways that do not terminate at $p = -1$ are not shown on the diagram.

The different orders of coherence have different properties, which may be exploited in separation experiments; for example, they evolve at different rates in the chosen frame of reference. Thus, while single-quantum coherence precesses at an angular rate $\Delta\omega$, where $\Delta\omega$ is the offset from the transmitter frequency, double-quantum coherence precesses at $(\Delta\omega_I + \Delta\omega_S)$ rad s^{-1}. By extension, we see that any spatial inhomogeneity of the magnetic field (or any field gradient that is applied) must affect the various coherences in proportion to their orders p. Matched pulsed field gradients are widely used to separate various orders of coherence (4).

One important property is the effect of a radiofrequency phase shift. If a pulse changes the coherence order by Δp, and if we shift the pulse phase by ϕ, the coherence in question suffers a phase shift of $\phi\Delta p$. This provides a recipe for designing a phase cycle to accept signals that follow the prescribed coherence pathway while rejecting the rest. For the example of double-quantum filtered carbon–carbon correlation spectroscopy (3), double-quantum coherence is excited only for the short interval Δ (a few microseconds) and then the final radiofrequency pulse reconverts this into coherence order –1. The change in coherence order is $\Delta p = +1$ or –3 (Fig. 2). We take four scans, with the phase of the final pulse advanced in steps of +90° and with the receiver phase advanced in steps of +90° (or –270°) so as to follow the signal of interest. The intense signals from isolated carbon-13 spins are in the form of longitudinal magnetization ($p = 0$) during the interval Δ and therefore suffer a change $\Delta p = -1$ as a result of the final pulse. Since the receiver phase rotates in the opposite sense, these undesirable signals are suppressed after four scans.

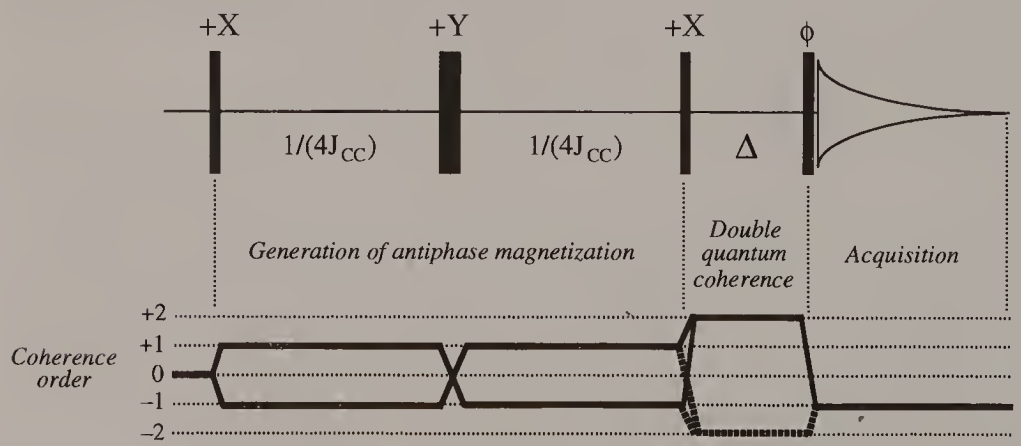

Fig. 2. Coherence transfer pathways in double-quantum-filtered carbon–carbon correlation spectroscopy (INADEQUATE). Double-quantum coherence from coupled spin pairs exists only in the Δ interval, and is reconverted into observable precessing magnetization by the final pulse, which causes a change in coherence order $\Delta p = +1$ or –3. The undesirable signal from the isolated carbon-13 spins suffers a change $\Delta p = -1$. The weak signal can therefore be filtered from the strong signal by cycling the pulse phase ϕ with a matching rotation of the receiver phase.

REFERENCES

1. K. Blum, *Density Matrix Theory and Applications.* Plenum: New York, 1981.
2. A. Bax, R. Freeman and S. P. Kempsell, *J. Am. Chem. Soc.* **102**, 4849 (1980).
3. G. Bodenhausen, H. Kogler and R. R. Ernst, *J. Magn. Reson.* **58**, 370 (1984).
4. A. Bax, P. G. de Jong, A. F. Mehlkopf and J. Smidt, *Chem. Phys. Lett.* **69**, 567 (1980).

Cross-references

Phase cycling
Product operator formalism

Coherent Decoupling

One of the first indications that NMR might provide scope for sophisticated new techniques was the early introduction of double-resonance methods (1). Many of the new laser experiments involving double irradiation have their counterparts in some of these early NMR experiments. Included under this heading are the related fields of broadband decoupling*, off-resonance decoupling, the nuclear Overhauser effect*, spin tickling*, polarization transfer*, the Hartmann–Hahn experiment*, saturation transfer*, and selective decoupling*. The simplest of all these techniques is coherent decoupling (2,3).

Coherent decoupling involves the irradiation of one group of nuclear spins X with a monochromatic source of intensity B_2, such that γB_2 is of the same order as $2\pi J_{AX}$, so as to modify the spin multiplet structure of any group of coupled spins A. In a Fourier transform spectrometer decoupling effects are only observed if the B_2 field is applied while the free induction signal is being acquired. If the B_2 irradiation is centred on the chemical shift frequency of X, and is sufficiently far away from the A resonance, then the A multiplet coalesces to a single line. On the other hand, if the irradiation is offset somewhat from this condition then the A-spin multiplet splitting is scaled down, the apparent splitting increasing with decoupler offset and decreasing with the intensity B_2. Some new lines also make their appearance in each flank of the A-spin multiplet; they are generally weak and their positions are quite sensitive to the intensity of B_2, so they are severely broadened by B_2 inhomogeneity. These *satellite lines* are accounted for in terms of multiple-quantum effects where at least one quantum comes from the irradiation field B_2.

Coherent decoupling is mainly used to establish which resonances are coupled together in spectra too complicated for this to be decided by inspection. The irradiation field B_2 can also be used to search for resonances that are hidden by overlapping lines (in homonuclear systems) or resonances that are not directly observable in the spectrometer (in heteronuclear systems). When it is necessary to eliminate all CH splittings from a carbon-13 spectrum, broadband decoupling methods are used.

The form of a decoupled spectrum can be calculated from a relatively simple theory (3). For convenience, we may neglect all population disturbances and concentrate our attention on the line positions and their intrinsic intensities. In fact, in a Fourier transform spectrometer this simplification is readily achieved if B_2 is only applied during acquisition of the free induction signal. Consider the simple

case of a homonuclear AX spin system where the X region is irradiated with the B_2 field while the A region of the spectrum is investigated. First-order coupling is assumed. Figure 1 shows the energy-level diagram appropriate to this system. In order to calculate the effect of introducing the radiofrequency field B_2, the energy-level diagram is transformed into a rotating frame* synchronized with f_2, the frequency of the B_2 irradiation. This transformation allows B_2 to be represented as a *static* field in this frame. Energies and magnetic fields are both expressed in frequency units (hertz). The new energies after the transformation are easily calculated since all the allowed transitions are diminished in frequency by f_2 Hz. Some energy levels become nearly degenerate in this frame (1 and 2, for example) and are particularly sensitive to the introduction of the static field B_2 because a non-crossing rule comes into play, which holds these levels apart.

The amount of this perturbation is calculated according to the effective magnetic fields E_1 and E_2 acting on the X spins in the rotating frame, the resultants of their offset from resonance D_1 and D_2 and the perturbing field expressed in frequency units $\gamma B_2/2\pi$:

$$E_1 = [D_1^2 + (\gamma B_2/2\pi)^2]^{1/2} \qquad E_2 = [D_2^2 + (\gamma B_2/2\pi)^2]^{1/2} \qquad [1]$$

$$D_1 = \delta_X + \tfrac{1}{2}J - f_2 \qquad D_2 = \delta_X - 53$$

$\frac{1}{2}J - f_2$. [2]

Energy levels 1 and 2 are forced apart from D_1 to E_1, while levels 3 and 4 are forced apart from D_2 to E_2 (Fig. 1(c)). As a direct consequence, the A lines are shifted in

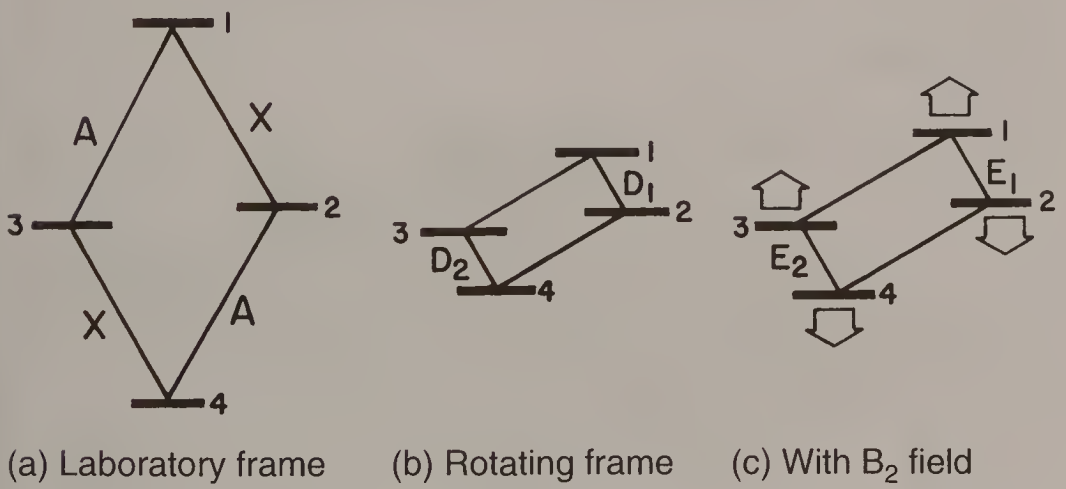

Fig. 1. Transformation from the laboratory frame (a) into the rotating frame (b) reduces all transition frequencies by the rotation frequency of the frame; consequently, it lowers energy level 1 and raises energy level 4 by the same amount (not to scale). The introduction (c) of the decoupling field B_2 near to resonance for the X spins increases the separation of levels 1 and 2 ($D_1 \rightarrow E_1$) and the separation of levels 3 and 4 ($D_2 \rightarrow E_2$). This diagram may then be used to predict the spectrum observed for the A spins.

frequency by an amount which depends on the decoupler offset. They remain symmetrically disposed about the chemical shift δ_A but move inwards to give a splitting $E_1 - E_2$ rather than J. This is illustrated for several different offsets in Fig. 2. Note that for irradiation at exact resonance, $f_2 = \delta_X$, the two lines coalesce into a single line at δ_A. The behaviour is symmetrical for positive and negative offsets.

The relative intensities of the lines are also a function of the decoupler offset. The intrinsic intensity is given by $\frac{1}{2}(1 + \cos\theta)$, where θ is the angle between the two effective field vectors E_1 and E_2. Note that if $\gamma B_2/2\pi > |J|$, then θ is never a very large angle and the intensities remain not far below unity. But where does the remaining intensity go? It reappears in weak satellite lines symmetrically placed outside the A multiplet with a separation $E_1 + E_2$. They can be considered as the two previously forbidden transitions, the zero-quantum line 2–3 and the double-quantum line 1–4, the selection rules being broken because of the perturbation by the B_2 irradiation. They are most prominent when B_2 is at exact resonance (Fig. 2), while for large decoupler offsets they move apart and lose intensity.

Analogous results apply to AX_2 and AX_3 spin systems where the X resonance is irradiated. The decoupled A spectrum remains a triplet or quartet with a reduced splitting given by $E_1 - E_2$, although a more complicated set of satellite lines can be observed. The AX_2 case has the interesting feature that one-half of the intensity of the centre line of the A triplet is quite unaffected by irradiation of the X spins – it represents a transition between antisymmetric A-spin energy levels not shared by any X transitions. Thus the 1:2:1 intensity ratio is not strictly maintained. In the

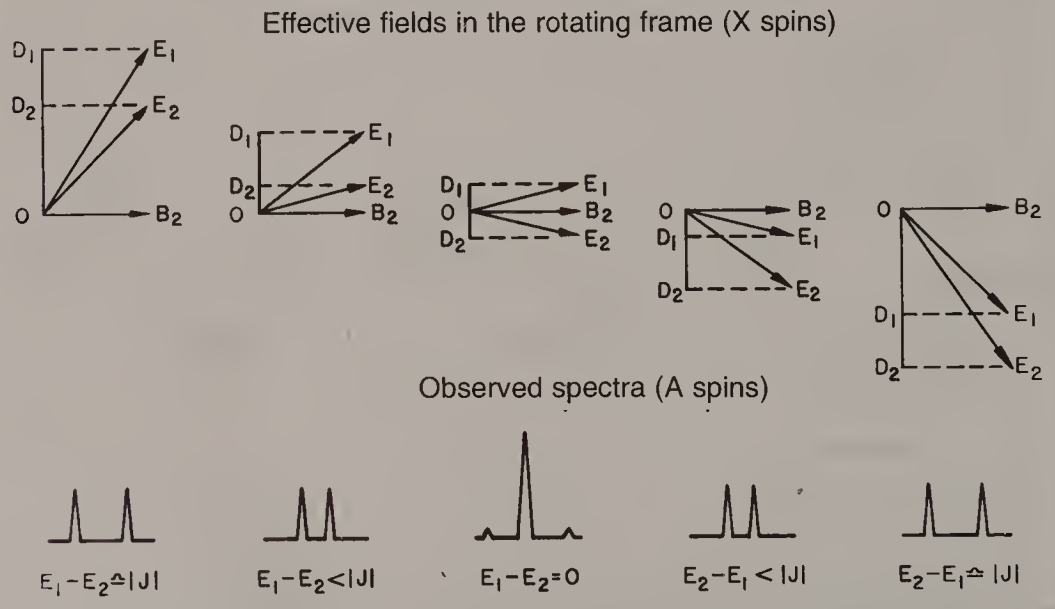

Fig. 2. Decoupling in an AX system with the B_2 field applied to the X spins. The A-spin resonance frequencies show a splitting $|E_1 - E_2|$ that is close to $|J|$ when B_2 is far from the X resonance but reduces to zero at exact X resonance. The weak satellite lines have a separation $|E_1 + E_2|$ and lose intensity as the decoupler goes off resonance.

AX_3 case the quartet intensity ratio remains 1:3:3:1 throughout. The positions of the outer lines, however, are three times as sensitive to the strength of B_2 as the inner lines, so that in a spatially inhomogeneous irradiation field these lines are preferentially broadened. Where off-resonance proton decoupling is used to determine multiplicities of carbon-13 resonances, this has occasionally led to the misassignment of a quartet as a doublet. Figure 3 shows the dependence of a carbon-13 quartet from a methyl group as a function of proton resonance offset, taking into account the broadening due to the spatial inhomogeneity of B_2, and shows this preferential broadening of the outer lines (4).

When the sense of decoupling experiment is reversed, so that we are observing the A resonance of an A_2X or A_3X system while irradiating the X spins, the behaviour is different. It is no longer possible to find an irradiation frequency f_2 which causes complete coalescence of the A spectrum into a single line. Consider the A_3X case. It is now necessary to define four effective fields acting on the X spin, E_1, E_2, E_3 and E_4, corresponding to the four possible combinations of the A-spin states. Part of the A doublet intensity coalesces when $E_1 = E_2$, another part when $E_2 = E_3$, and yet another part when $E_3 = E_4$. There is said to be a *residual splitting* whatever the offset $f_2 - \delta_X$. However, by increasing the intensity $\gamma B_2/2\pi$ compared with J, this residual splitting can be reduced to any desired extent.

Coherent decoupling can be used to locate hidden resonance lines in homonuclear systems by searching for the frequency f_2 which gives optimum coalescence of an observed multiplet. In most cases it is perfectly permissible to take this as a measure of the chemical shift of the hidden resonance. However, the treatment given above makes the assumption that the A spins are not directly influenced by the irradiation field B_2, that is to say $|f_2 - \delta_A| \gg \gamma B_2/2\pi$. For

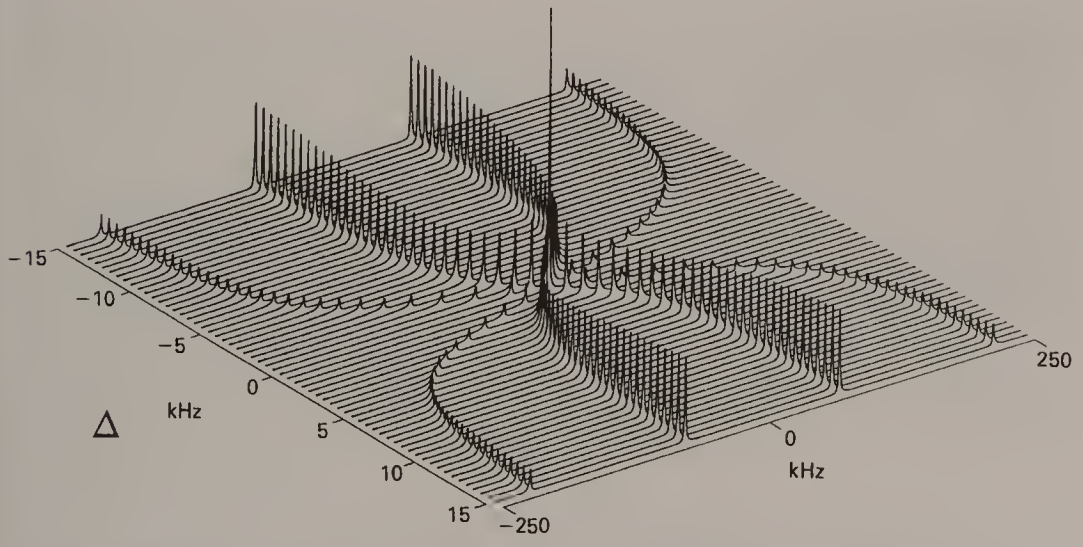

Fig. 3. Simulated A-spin spectra of an AX_3 system with the decoupler applied to the X spins, as a function of decoupler resonance offset Δ. This simulation takes into account the spatial inhomogeneity of the B_2 field which broadens the lines and distorts the lineshapes.

relatively small chemical shift differences this condition may not be satisfied, and a small correction must then be applied. For the purpose of evaluating this correction we may neglect the small differences in resonance frequencies caused by J-coupling and define an average effective field E_A acting on the A spins and an average effective field E_X acting on the X spins. The condition for exact decoupling is that E_A and E_X should be orthogonal. Since E_A is not quite aligned along the Z axis, f_2 must be moved slightly away from δ_X towards the A resonance in order to achieve this condition. The correction is therefore approximately given by

$$C = (\gamma B_2/2\pi)^2/(\delta_A - f_2) \text{ Hz.} \quad [3]$$

This effect thus slightly underestimates the chemical shift difference; on top of this, there is a Bloch–Siegert shift* of the observed A resonance due to the B_2 field; it acts in the opposite sense to the correction above and has half the magnitude.

REFERENCES

1. V. Royden, *Phys. Rev.* **96**, 543 (1954).
2. A. L. Bloom and J. N. Shoolery, *Phys. Rev.* **97**, 1261 (1955).
3. R. Freeman and W. A. Anderson, *J. Chem. Phys.* **37**, 85 (1962).
4. R. Freeman, J. B. Grutzner, G. A. Morris and D. L. Turner, *J. Am. Chem. Soc.* **100**, 5637 (1978).

Cross-references

Bloch–Siegert effect
Broadband decoupling
Hartmann–Hahn experiment
Nuclear Overhauser effect
Polarization transfer
Rotating frame
Saturation transfer
Selective decoupling
Spin tickling

Composite Pulses

The pendulum is an excellent time keeper because the period of the swing is virtually independent of its amplitude, and in any case, when it is used in a clock the amplitude of swing remains constant. The period is, however, dependent on the length, and small changes in length due to thermal expansion have a significant effect on the time keeping. Hence the invention of the compensated pendulum in which the thermal expansion of one metal is arranged to counteract the different thermal expansion of another metal.

A similar principle has been applied to radiofrequency pulses*. When a single pulse does not achieve the desired effect, a composite 'sandwich' of pulses may often be devised to produce a better result. The possible applications of this idea cover a wide field, from solvent suppression* (1) to new methods of broadband decoupling*. Only two examples are discussed here – compensation for the effects of B_1 inhomogeneity and resonance offset errors. These are the two most serious pulse imperfections in high-resolution work with liquids.

COMPOSITE 90° PULSES

Suppose it is required to convert Z magnetization into transverse magnetization. Certain spin–lattice relaxation* methods, for example, demand an initial condition where there is no Z component from any part of the sample (not merely that residual Z components cancel). A simple 90°(X) pulse subject to spatial inhomogeneity in the B_1 field would not accomplish this, since magnetization from some volume elements of the sample would either undershoot or overshoot the equatorial plane. A composite 90°(X) 90°(Y) pulse helps considerably, by converting the spread in the ZY plane to a corresponding spread in the XY plane (Fig. 1). For certain relaxation applications this would suffice, but it does introduce phase errors, which in extreme cases could give rise to a serious loss in total transverse signal.

There is a more complicated composite sequence which takes a magnetization vector from the Z axis to the Y axis with good compensation for pulse length errors (2). This is the sequence

$$45°(-Y)\ 90°(X)\ 90°(Y)\ 45°(X). \qquad [1]$$

Figure 2 illustrates this sequence of four rotations. Note first that trajectories b and c are of equal length and are opposed tangentially, so that an increase in b is compensated by an equal increase in c. More subtly, an increase in trajectory a is

converted by the changes in b and c into a situation in which it is compensated by an equal increase in the length of trajectory d. Such a composite pulse sequence might be used to initiate a spin–spin relaxation experiment in which it is important to have the magnetization accurately aligned along the Y axis of the rotating frame* (as in spin locking*).

When resonance offset effects have to be taken into account, the situation becomes more complicated because rotations are now about an axis tilted in the XZ plane through an angle θ, where

$$\tan \theta = \Delta B/B_1 \qquad [2]$$

and the flip angle is increased from $\gamma B_1 t$ to $\gamma B_{eff} t$, where

$$B_{eff} = (\Delta B^2 + B_1^2)^{1/2}. \qquad [3]$$

An interesting self-compensation occurs for a 90° pulse because these two effects cancel to a large extent (3) and magnetization vectors initially along the Z axis are

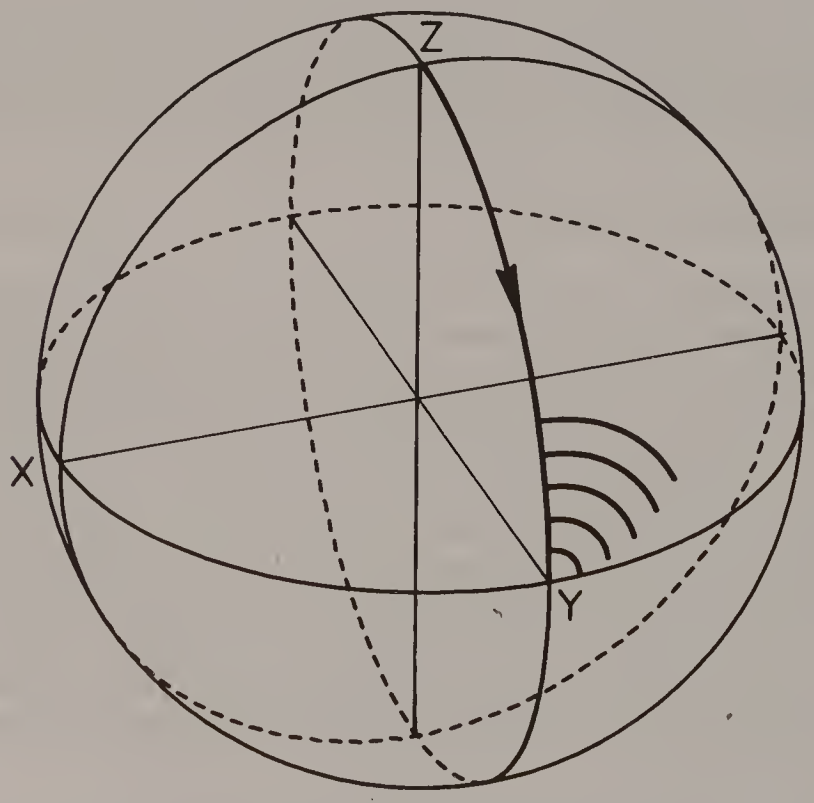

Fig. 1. A composite 90° pulse sequence 90°(X) 90°(Y) which compensates for small errors in the pulse length due to miscalibration or spatial inhomogeneity. The trajectories end close to the XY plane, but a significant phase error is introduced. Pulse length errors of 0°, 5°, 10°, 15°, 20° and 25° are shown.

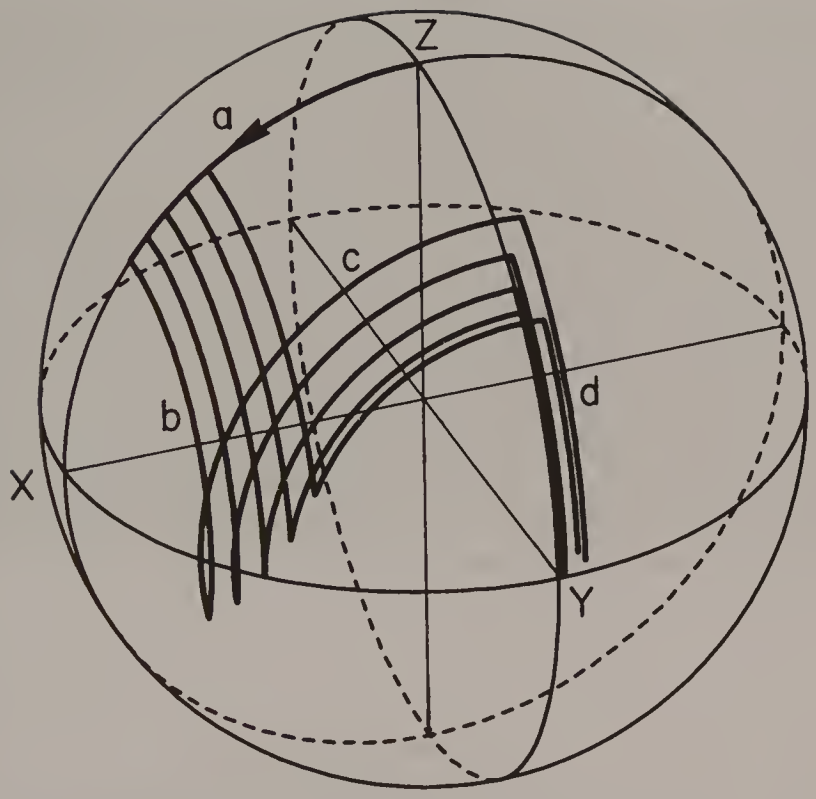

Fig. 2. A composite 90° pulse sequence 45° (–Y) 90°(+X) 90°(+Y) 45°(+X) designed to compensate pulse length errors. A family of five trajectories is shown for initial pulse lengths of 35°, 40°, 45°, 50° and 55° with the other pulses increased in proportion. The compensation relies on the approximate 'antitangential' condition of the curves b and c. All five trajectories terminate close to the +Y axis.

taken very close to the XY plane over a wide range of resonance offsets. Furthermore, the phase errors introduced by this single 90° pulse are essentially linearly dependent on offset and are hence easily corrected by a simple phase adjustment. Such self-compensation appears to be a relatively rare event.

It is important to note that this type of compensation is not particularly demanding: there are some applications in which it would be necessary to take all Z magnetization vectors to the Y axis rather than simply disperse them in the XY plane. More difficult still is the general problem of constructing a compensated pulse which effects a pure 90° rotation *whatever the initial conditions* of the magnetization vectors.

COMPOSITE 180° PULSES

Population inversion pulses, which are widely used in spin–lattice relaxation measurements, may also be replaced by a composite sequence in order to compensate B_1 inhomogeneity or miscalibration. A simple and effective sequence is

$$90°(X)\ 180°(Y)\ 90°(X). \qquad [4]$$

It is rather easy to see that if the first pulse is short, leaving the magnetization vector above the equatorial plane, the 180°(Y) pulse translates it to a point an equal distance below the equatorial plane, so that the last pulse carries the vector down to the –Z axis. Small errors in the 180°(Y) pulse have only very small second-order effects because the corresponding trajectory is so short (4).

The same sequence, or the slightly modified sequence 90°(X) 240°(Y) 90°(X), can also compensate for the effects of finite offset from resonance, although the two types of compensation do not mix – at significant offsets, pulse length errors are not corrected. Symmetry arguments are no longer useful, and the manner in which the compensation arises is best appreciated from the magnetization trajectories (Fig. 3). A family of such trajectories is shown covering the offset range where $\Delta B/B_1$ goes from 0.4 to 0.6. Figure 4 shows the corresponding trajectories for a simple 180° pulse. Spin–lattice relaxation measurements by inversion recovery would benefit considerably from this type of offset compensation. Sequences of this type have been used for broadband decoupling, allowing effective decoupling to be achieved at significantly lower radiofrequency powers (5).

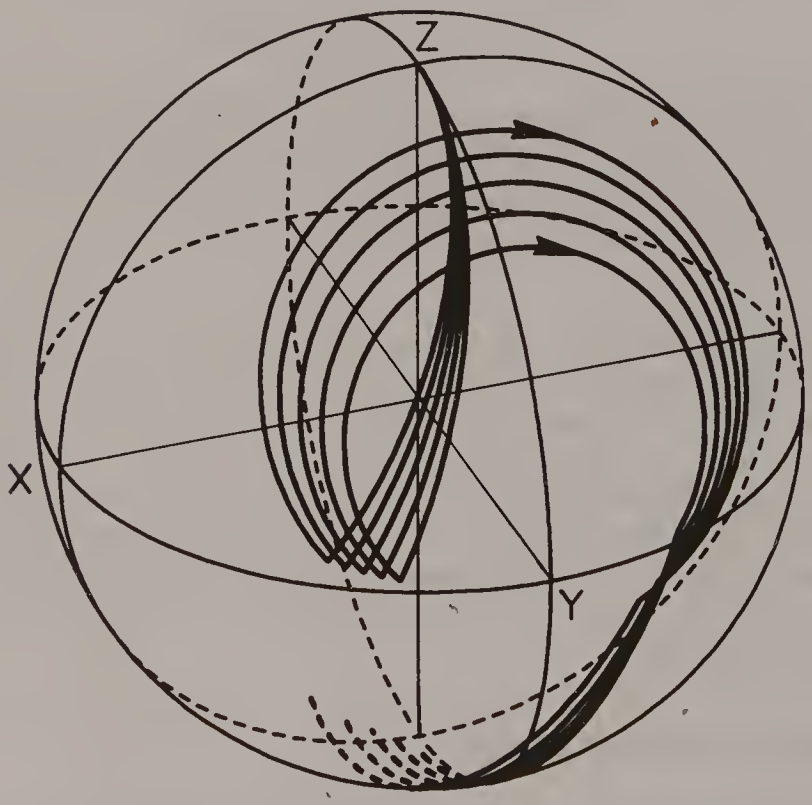

Fig. 3. A composite 180° pulse sequence 90°(X) 240°(Y) 90°(X) which compensates either for resonance offset (shown) or for pulse length error (not shown). Five trajectories are illustrated corresponding to resonance offsets between $\Delta B/B_1 = 0.4$ and 0.6. All five trajectories terminate near the –Z axis.

A pulse which inverts longitudinal magnetization effectively must necessarily rotate XY magnetization back into the XY plane, that is to say it must behave as a 180° rotation about some axis in the XY plane. Any residual errors due to resonance offset effects are translated into phase shifts of the rotation axis rather than into any tilting of this axis out of the equatorial plane. For this reason, the 90°(X) 240°(Y) 90°(X) sequence acts as an efficient refocusing pulse in spin-echo* experiments. Although pulse imperfections introduce a phase error on odd-numbered echoes, these are cancelled on the even-numbered echoes, and the compensation is not affected by echo-modulation effects (6). Once again, a distinction can be drawn between different classes of compensation (7). Full compensation would take vectors through essentially the same angle as the corresponding ideal pulse, irrespective of initial conditions, provided we remain within the compensation range. Partial compensation achieves a similar result except for the introduction of a phase shift which depends on the extent of the imperfections.

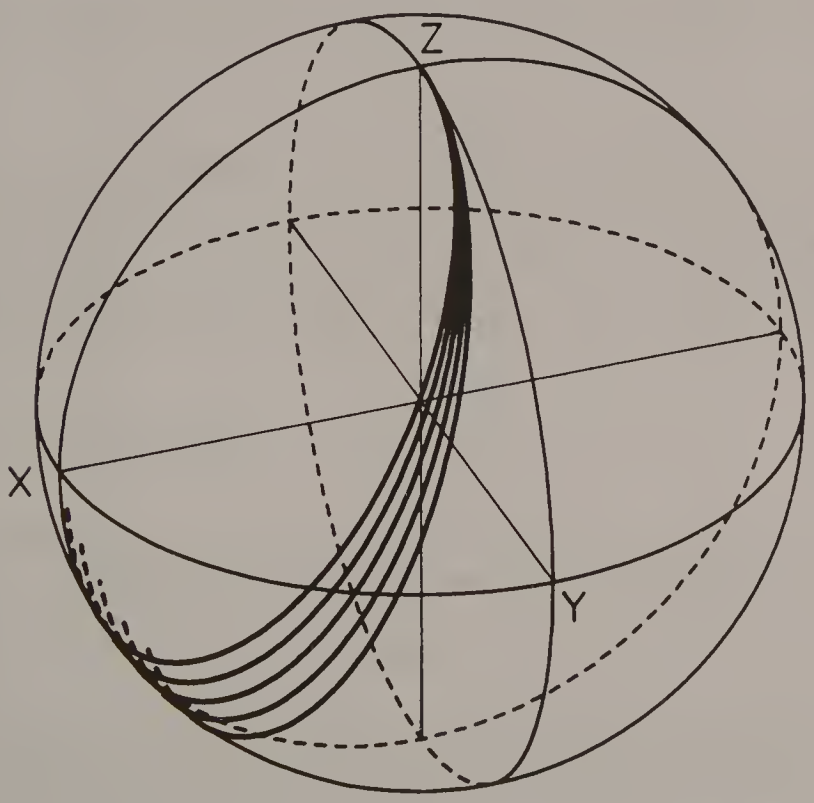

Fig. 4. The five trajectories of Fig. 3 for a simple 180°(X) pulse, indicating that resonance offset effects carry the magnetization vectors far from the –Z axis.

EFFICIENCY OF COMPOSITE PULSES

The effectiveness of a given pulse for spin inversion may be measured in terms of the magnetization along the –Z axis compared with M_0. An ideal pulse would therefore give –1. This allows the assessment of simultaneous imperfections due to pulse length error and resonance offset effects in the form of a contour diagram. Figure 5 shows such a diagram for the sequence 90°(X) 240°(Y) 90°(X), emphasizing that resonance offset effects can be compensated, provided there are not appreciable pulse length errors, or that compensation can be achieved for short pulses (not long pulses) provided there are no appreciable resonance offset effects.

Simultaneous compensation for both kinds of pulse imperfection is more difficult to achieve although there are many situations where both are likely to occur, for example with phosphorus-31 *in vivo* high-resolution spectroscopy using a surface coil. Good compensation for pulse length error and resonance offset at the same time infers a contour diagram with an approximately rectangular region in which there are only contours near –1. The GROPE-16 sequence (8) makes a valuable contribution here. It was constructed by employing an important general principle

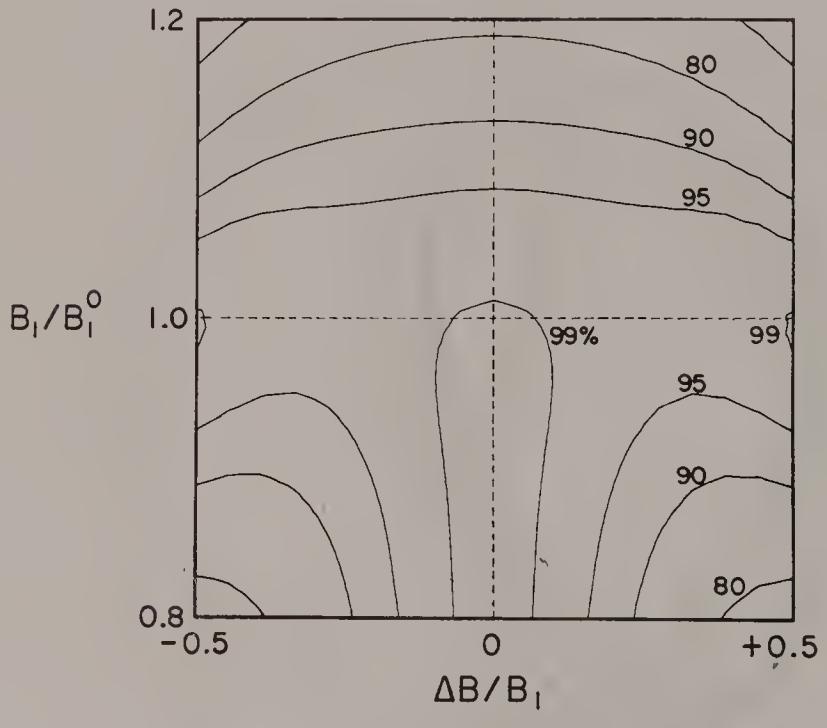

Fig. 5. Contour diagram plotting the efficiency for spin inversion for the 90°(X) 240°(Y) 90°(X) composite pulse as a function of resonance offset $\Delta B/B_1$ and mis-set of the radiofrequency field intensity $B_1/B_1°$. The sequence compensates for low values of B_1 near exact resonance, or for offset effects when B_1 is correctly set, but does not compensate for both types of error simultaneously.

known as *inverse rotation*. For a given nuclear species, the sign of the gyromagnetic ratio determines the sense of the rotation about the B_1 field. An inverse rotation is one which would turn magnetization vectors in the opposite sense. When resonance offset effects can be neglected, the inverse sequence can be constructed by reversing the chronological order of the pulses and inverting all the radiofrequency phases. In the more general case of appreciable resonance offsets, it is not possible to form the inverse sequence exactly, but a good approximation can be achieved by starting with a sequence which is a *cycle*. A cycle (9) is a set of rotations that has the overall effect of a rotation angle very close to zero. Now, if a sequence S has an inverse S^{-1}, then SS^{-1} must be a cycle. Consequently, if a broadband cycle has been found with a 90°(X) pulse at the beginning or at the end, then the remainder of the cycle (minus the 90°(X) pulse) is a good approximation to the inverse of a 90°(X) pulse. Because a 90° pulse takes magnetization efficiently from +Z to the XY plane, the combination 90°(X) $90°(-X)^{-1}$ behaves like a 180° pulse with good compensation. An inverse rotation pulse based on these principles was used to construct the GROPE-16 sequence.

PHASE SHIFTS

Suppose we take a pulse sequence S which has the overall effect of a rotation through an angle β about the –Y axis of the rotating frame, and sandwich it between two ideal 90° pulses

$$90°(X)\ \beta(-Y)\ 90°(-X). \qquad [5]$$

The result is an equal rotation β about the +Z axis of the rotating frame. That is to say, the bracketing pulses 90°(X) and 90°(–X) have had the effect of rotating the rotation axis through +90° (from –Y to +Z) without altering β. This is known as a *similarity transformation*. The method can be used in order to achieve the effect of an arbitrary radiofrequency phase shift in equipment that has only hardware for 90° phase shifts (10).

PHASE DISTORTION

A given 90° pulse may provide good compensation for pulse imperfections when judged by its ability to take magnetization from the Z axis into the XY plane, but it still may not be an *ideal* 90° pulse. Often the imperfections appear in the form of a phase shift of the signal which varies as a function of resonance offset or pulse length error. Similar considerations apply to composite 180° pulses, limiting certain applications, for example refocusing in spin-echo experiments. This is known as *phase distortion* (11). All the composite pulses mentioned so far suffer from this problem.

One important consequence of phase distortion is that it is not normally feasible to 'clean up' a complicated pulse sequence merely by replacing each pulse with its composite pulse equivalent, since the phase errors are likely to be cumulative. Levitt and Ernst (12) have demonstrated that by careful analysis of the effect of pulse imperfections in the 'INADEQUATE' experiment it is possible to incorporate composite pulses in such a manner that phase distortions are essentially self-compensating, whereas the indiscriminate substitution of composite pulses leads to disaster. Tycko *et al.* (11) have shown that a method based on the Magnus expansion can lead to the discovery of composite pulses that do not cause any significant phase distortion. Such pulse clusters can be substituted directly into a complex pulse sequence without fear of further complications due to cumulative phase errors. They are also useful where it is necessary to compensate for a *distribution* of values of some pulse parameter, for example gross spatial inhomogeneity of the radiofrequency field. If we wished to employ a surface coil to observe the *in vivo* NMR signal from an extensive sample volume, phase distortion caused by the distribution of B_1 values could lead to considerable signal cancellation.

HOW ARE COMPOSITE PULSES DEVISED?

The discovery of the first composite 180° pulse by Levitt and Freeman (4) seems to have been inspired principally by intuition guided by visualization of the magnetization trajectories on the unit sphere (the vector model*). Sometimes, an analytical solution is possible, based on trigonometrical requirements or symmetry considerations. It helps enormously to have the trajectories drawn out by computer simulation as in Figs 1–4. These calculations are usually carried out using rotation operators, a powerful method for analysing the effect of a composite pulse (13). Geometrical methods remain the simplest and possibly the most satisfying approach, and have been used extensively in this section. Nevertheless, the field of composite pulses has grown enormously (even into laser spectroscopy) and many different methods of analysis have been used. Mention has already been made of the concept of *inverse rotation* where magnetization vectors rotate about an effective field in the opposite sense to that predicted by the sign of the gyromagnetic ratio.

Spin inversion can be achieved through adiabatic rapid passage*, including versions where the radiofrequency amplitude or the sweep rate varies during passage through resonance. Composite pulses have been devised by approximating these frequency-sweep experiments by a limited number of radiofrequency pulses of the appropriate phases (14).

While tinkering with someone else's composite pulse sequence is frowned upon, it is often possible to take an existing composite pulse and to improve it by an iterative expansion procedure (15), in which better compensation is achieved at the expense of a more complicated sequence. Numerical optimization by computer can

be a very powerful technique for this purpose (16). Finally, as mentioned above, Tycko *et al.* (11) have demonstrated the utility of a theoretical approach based on the Magnus expansion, which allows phase distortion to be compensated at the same time as the other imperfections.

We have certainly not heard the last word on composite pulses (17).

REFERENCES

1. A. G. Redfield, S. D, Kunz and E. K. Ralph, *J. Magn. Reson.* **19**, 114 (1975).
2. M. H. Levitt, *J. Magn. Reson.* **48**, 234 (1982).
3. R. Freeman and H. D. W. Hill, *J. Chem. Phys.* **54**, 3367 (1971).
4. M. H. Levitt and R. Freeman, *J. Magn. Reson.* **33**, 473 (1979).
5. A. J. Shaka, J. Keeler and R. Freeman, *J. Magn. Reson.* **53**, 313 (1983).
6. M. H. Levitt and R. Freeman, *J. Magn. Reson.* **43**, 65 (1981).
7. M. H. Levitt, *Prog. NMR Spectrosc.* **18**, 61 (1986).
8. A. J. Shaka and R. Freeman, *J. Magn. Reson.* **55**, 487 (1983).
9. J. S. Waugh, *J. Magn. Reson.* **50**, 30 (1982).
10. R. Freeman, T. Frenkiel and M. H. Levitt, *J. Magn. Reson.* **44**, 409 (1981).
11. R. Tycko, H. M. Cho, E. Schneider and A. Pines, *J. Magn. Reson.* **61**, 90 (1985).
12. M. H. Levitt and R. R. Ernst, *Mol. Phys.* **50**, 1109 (1983).
13. M. H. Levitt, *J. Magn. Reson.* **50**, 95 (1982).
14. J. Baum, R. Tycko and A. Pines, *J. Chem. Phys.* **79**, 4643 (1983).
15. M. H. Levitt and R. R. Ernst, *J. Magn. Reson.* **55**, 247 (1983).
16. A. J. Shaka, *Chem. Phys. Lett.* **120**, 201 (1985).
17. M. H. Levitt, *Prog. NMR Spectrosc.* **18**, 61 (1986).

Cross-references

Adiabatic rapid passage
Broadband decoupling
Radiofrequency pulses
Rotating frame
Solvent suppression
Spin echoes
Spin–lattice relaxation
Spin locking
Vector model

Continuous-wave Spectroscopy

Almost all high-resolution NMR spectrometers before about 1970 employed continuous-wave irradiation and swept either the applied field or the radiofrequency. This mode of operation seemed natural to the early NMR workers since it represented a direct parallel with the familiar optical spectroscopy techniques. Although it had been realized for a long time that the transient response to a radiofrequency pulse gave the Fourier transform of the slow-passage spectrum, it was not until the pioneering work of Ernst and Anderson (1) that the enormous sensitivity advantage of the Fourier transform mode was properly appreciated. Implementation of this principle on commercial spectrometers was further delayed until inexpensive digital minicomputers were readily available and the Cooley–Tukey algorithm* was introduced (2).

The Fourier transform revolution was soon complete. It is now difficult to find any definite advantage of the continuous-wave method for high-resolution work, except the absence of dynamic range problems and the doubtful economic argument that a digital computer is not strictly necessary (although time averaging* would require one). A Fourier transform spectrometer can perform all the same functions and at the same time delivers one or two orders of magnitude better sensitivity and provides access to time-dependent phenomena such as relaxation and chemical exchange. Continuous-wave spectroscopy has never been satisfactory for low-sensitivity nuclei such as carbon-13 or nitrogen-15. Nevertheless it is still used, particularly for simple proton spectrometers of moderate cost.

Continuous-wave spectrometers sweep the irradiation frequency (or field) sufficiently slowly that the slow-passage condition is approached. This requires that the sweep rate be reduced to the point that the time taken to sweep through a resonance line is of the order of the spin–spin relaxation time T_2, if the line has its natural width $(\pi T_2)^{-1}$ Hz. In practice, linewidths are more usually determined by instrumental effects $(\pi T_2^*)^{-1}$ and the sweep rate may be increased to the point where the time taken to traverse resonance is of the order of T_2^*. Violation of the slow-passage criterion broadens and distorts the observed resonance, introducing the familiar ringing pattern on the trailing edge of the line, the 'wiggles' (Fig. 1). Most spectra obtained by continuous-wave methods show some trace of wiggles, and this may thus be used to distinguish such spectra from those obtained by Fourier transformation* where sweep artefacts are absent. Rapid-scan correlation spectroscopy seeks to occupy the middle ground, sweeping rapidly through

resonance in order to improve sensitivity* but later removing the intense wiggle–beat pattern by cross-correlation with the response from a single, isolated resonance line.

STEADY-STATE SOLUTIONS TO THE BLOCH EQUATIONS

A slow-passage continuous-wave spectrometer excites an NMR response which can be calculated from the steady-state solutions to the Bloch equations (3,4) in the rotating frame*. It is assumed that the radiofrequency field B_1 is at a low level and has been applied for a sufficiently long time that any transient effects have all died away. The steady-state signal may then be represented by a vector M (see Vector model*) having three components, each of which is a function of Δf, the offset from resonance:

$$M_X = M_0 2\pi\Delta f\gamma B_1 T_2^2/[1 + (2\pi\Delta f T_2)^2 + \gamma^2 B_1^2 T_1 T_2] \qquad [1]$$

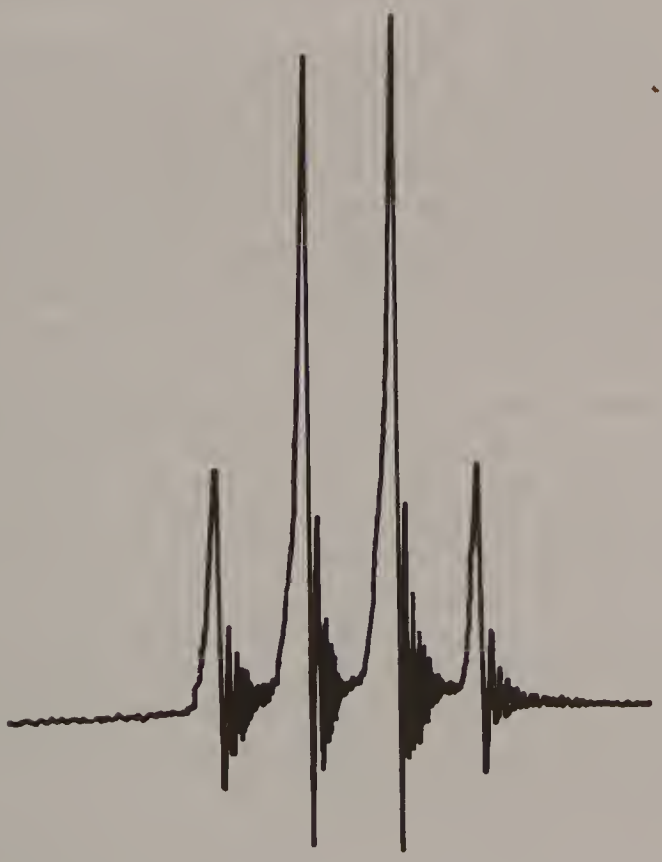

Fig. 1. Typical continuous-wave NMR spectrum (quartet of acetaldehyde) showing the wiggles on the trailing edge of the lines. This is a result of failure to meet the slow-passage condition.

$$M_Y = M_0\gamma B_1 T_2/[1 + (2\pi\Delta f T_2)^2 + \gamma^2 B_1^2 T_1 T_2] \quad [2]$$

$$M_Z = M_0[1 + (2\pi\Delta f T_2)^2]/[1 + (2\pi\Delta f T_2)^2 + \gamma^2 B_1^2 T_1 T_2]. \quad [3]$$

The signal is thus always proportional to M_0, the initial polarization at Boltzmann equilibrium. In order to gain more insight into the meaning of these equations it is convenient to make the simplification that $T_1 = T_2$, and to rewrite with the substitutions $a = 2\pi\Delta f T_2$ and $b^2 = \gamma^2 B_1^2 T_1 T_2$. Thus a is the resonance offset parameter expressed in multiples of the natural linewidth, and b^2 is the saturation parameter.

$$M_X = M_0 ab/(1 + a^2 + b^2) \quad \text{(dispersion mode)} \quad [4]$$

$$M_Y = M_0 b/(1 + a^2 + b^2) \quad \text{(absorption mode)} \quad [5]$$

$$M_Z = M_0(1 + a^2)/(1 + a^2 + b^2) \quad \text{(population difference).} \quad [6]$$

The general vector M is constrained by these equations to move so that its tip is always on the surface of a hemisphere centred at a point $+\frac{1}{2}M_0$ on the Z axis, with a radius $\frac{1}{2}M_0$ and allowing only positive values of M_Y. This is readily proved by some straightforward trigonometry.

A passage through resonance corresponds to the motion of the vector M over the surface of this hemisphere (Fig. 2) starting and finishing at the point Z where a is $\pm\infty$. In the process, an absorption-mode component is induced in the receiver coil proportional to M_Y and a dispersion-mode component is detected which is proportional to M_X. In the laboratory frame both components are oscillating at the frequency of the rotating frame, which is the frequency f_1 of the irradiation field B_1. In a continuous-wave spectrometer this frequency f_1 may be swept slowly through resonance at constant B_0 intensity, or the static field B_0 may be swept slowly while the frequency f_1 is held constant. Figure 2 shows a family of possible trajectories of M during slow passage through resonance for various different choices of the saturation parameter b^2. Each trajectory is a circular loop starting from Z and finishing at Z, the rate at which the vector M moves being greatest as it passes through the exact resonance condition.

Several useful deductions can be made from the pictorial description of the steady-state Bloch equations shown in Fig. 2. First, both the dispersion-mode and absorption-mode signals are very weak far from resonance when $a^2 \gg 1 + b^2$, and only reach a significant level reasonably close to resonance. It is also clear that the tails of the dispersion-mode signal M_X fall off more slowly with offset (as M_0/a) than the absorption-mode signal M_Y, which falls off as M_0/a^2. This is the reason for using the absorption mode for high-resolution work.

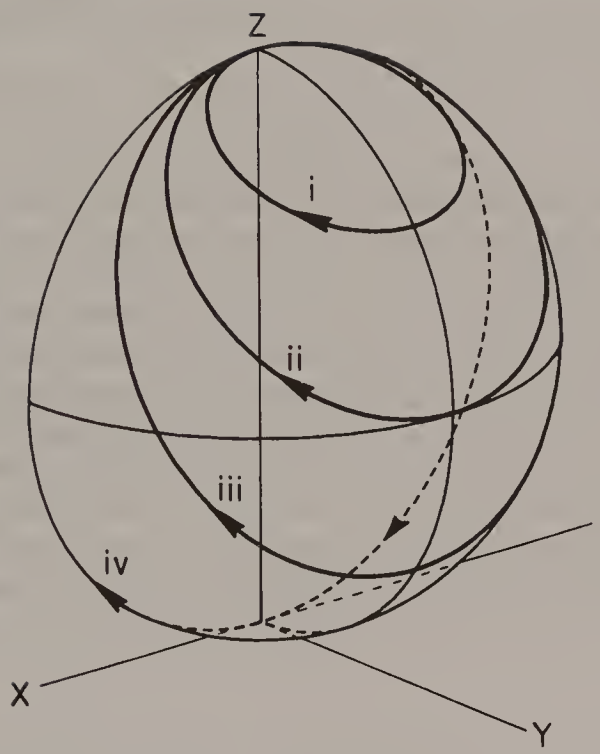

Fig. 2. The steady-state solutions of the Bloch equations (for $T_1 = T_2$) constrain the magnetization vector to follow a circular trajectory on the surface of a hemisphere centred at $Z = 0.5M_0$ on the Z axis. All trajectories start at Z far from resonance and induce a maximum Y component (absorption mode) as they pass through exact resonance, returning to Z as the sweep carries them far from resonance again. Trajectory i is for negligible saturation ($b^2 = 0.5$), while trajectory ii corresponds to $b^2 = 1$ (maximum absorption signal), trajectory iii is for appreciable saturation ($b^2 = 2$), and trajectory iv for complete saturation ($b^2 = \infty$). The dispersion-mode signal is represented by the X component of magnetization.

ABSORPTION-MODE SIGNALS

For negligible saturation, where B_1 has been reduced to a sufficiently low level that $b^2 \ll 1$, the absorption-mode response has the form of a pure Lorentzian line

$$M_Y = M_0 b/(1 + a^2). \qquad [7]$$

The half width at half height occurs when $a = \pm 1$, that is to say, $2\pi\Delta f = \pm 1/T_2$. The inverse of the linewidth is thus a measure of the spin–spin relaxation time provided there are no additional broadening influences such as B_0 inhomogeneity. A typical trajectory for M in this case of negligible saturation makes a small circular excursion near the top of the hemisphere close to point Z (Fig. 2). The induced signal is small compared with $\frac{1}{2}M_0$ but increases linearly with B_1 intensity until the

onset of saturation. The optimum peak absorption-mode signal occurs for the condition b = 1, that is to say

$$\gamma^2 B_1^2 T_1 T_2 = 1. \qquad [8]$$

Slow passage through resonance then corresponds to trajectory ii of Fig. 2 which just touches the equatorial plane of the hemisphere for a = 0, giving a peak signal of $M_Y = \frac{1}{2}M_0$. The linewidth is increased by a factor $2^{1/2}$, indicating that the price for optimum signal strength is a loss in resolution. This broadening occurs because saturation is most effective at exact resonance and is least effective in the tails. For strongly saturating B_1 fields, a typical trajectory iii loops down below the bulge of the hemisphere, inducing a smaller-than-optimum peak absorption-mode signal and broadening the line by a factor $(1 + b^2)^{1/2}$. This situation is thus to be avoided on both sensitivity and resolution grounds. In the limit of extreme saturation, the vector M follows the great circle trajectory iv and the absorption-mode signal vanishes. The behaviour of the absorption-mode signals is shown in Fig. 3(a).

(a) Absorption mode

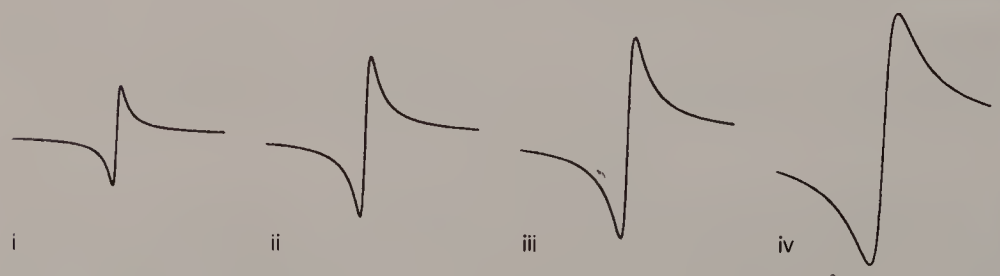

(b) Dispersion mode

Fig. 3. (a) Absorption- and (b) dispersion-mode signals predicted by the steady-state solutions of the Bloch equations corresponding to the four trajectories of Fig. 2. The absorption-mode signal passes through a maximum for $b^2 = 1$ (trajectory ii) but the dispersion-mode signal approaches an asymptotic value when $b^2 = \infty$ (trajectory iv).

DISPERSION-MODE SIGNALS

The dispersion-mode signal has a different form and behaves differently under saturation. As the radiofrequency f_1 is swept through resonance, the dispersion-mode signal passes through a minimum, goes through zero at exact resonance ($a = 0$) and passes through a maximum before falling asymptotically to zero in the tail. It is thus an odd rather than even function of offset. The maximum and minimum coincide with the points of maximum slope on the absorption-mode signal, and can thus be used to measure the linewidth. For negligible saturation, these extrema occur when $a = \pm 1$. In this limit, the strength of the dispersion-mode signal increases with the strength of the radiofrequency field B_1, but unlike the absorption-mode signal, it does not reach a maximum for $b^2 = 1$ but continues to increase with the degree of saturation until it reaches $\pm\frac{1}{2}M_0$ asymptotically for trajectory iv of Fig. 2. For this reason, a search for a completely unknown resonance is often carried out with a strong B_1 field and with the receiver adjusted to the dispersion mode, since this requires no estimate of the relaxation times T_1 and T_2. The linewidth, measured between the points of maximum and minimum signal, increases as $(1 + b^2)^{1/2}$. These signals are illustrated in Fig. 3(b).

POPULATIONS

The component M_Z is a measure of the difference in spin populations between the two energy levels involved in the NMR transition. For negligible saturation, the difference from the Boltzmann population difference depends on the saturation parameter only to second order. For the optimum absorption-mode signal ($a = 0$, $b = 1$) this population difference is reduced to one-half as f_1 sweeps through the resonance peak. For very strong saturation ($b^2 \gg 1$) there is no population difference.

The above description assumed $T_1 = T_2$. For the general case where $T_2 < T_1$, the picture is modified, the locus for the tip of the vector M becoming an ellipsoid with major axis in the Z direction unchanged at $\frac{1}{2}M_0$ but with the two minor axes reduced by the factor $(T_2/T_1)^{1/2}$. This has the effect that the expressions for signal intensity are reduced by $(T_2/T_1)^{1/2}$, giving an optimum peak absorption mode of $\frac{1}{2}M_0(T_2/T_1)^{1/2}$ and an asymptotic dispersion mode of $\pm\frac{1}{2}M_0(T_2/T_1)^{1/2}$. For large molecules which are tumbling relatively slowly in solution this can mean a significant loss in sensitivity.

Many practical cases of high-resolution spectroscopy involve a significant broadening of the line by B_0 inhomogeneity, often discussed in terms of an instrumental linewidth $1/T_2^*$ corresponding to a fast decay of the free induction signal with time constant T_2^*. In the steady-state solutions of the Bloch equations discussed above it is not correct to substitute T_2^* in place of the spin–spin relaxation time T_2. In particular, the saturation behaviour of an inhomogeneously broadened line is quite different: it is possible to burn a hole in the line profile by selective

saturation. The linewidth does not change with degree of saturation until the broadening of the natural linewidth by saturation becomes comparable with the inhomogeneity broadening. The peak height of the absorption-mode signal does not pass through the usual maximum at $b = 1$ but continues to increase until the saturated natural linewidth $(1 + b^2)^{1/2}/T_2$ approaches the inhomogeneous linewidth $1/T_2^*$.

In the absence of selective saturation effects, the observed resonance response should be thought of as the natural linewidth convoluted with the distribution function representing the inhomogeneity of the applied B_0 field. Since the area under the line remains constant (representing the intensity), broadening by field inhomogeneity severely reduces the peak height and hence the sensitivity. Optimum absorption-mode signals are then considerably weaker than $\frac{1}{2} M_0(T_2/T_1)^{1/2}$. This loss can be redeemed by reducing T_1 and T_2 by the addition of a relaxation reagent ('doping') until the linewidth is again determined by T_2 rather than by T_2^* and the optimum absorption-mode signal again approaches $\frac{1}{2} M_0$. Too much doping causes an unnecessary broadening of the lines, so a high-resolution spectroscopist uses this method with circumspection. Dissolved oxygen from the air is a rather mild paramagnetic relaxation reagent and a significant shortening of very long relaxation times can be achieved by bubbling pure oxygen through the sample solution and capping the sample tube.

REFERENCES

1. R. R. Ernst and W. A. Anderson, *Rev. Sci. Instrum.* **37**, 93 (1966).
2. J. W. Cooley and J. W. Tukey, *Math. Comput.* **19**, 297 (1965).
3. F. Bloch, *Phys. Rev.* **102**, 104 (1956).
4. A. Abragam, *The Principles of Nuclear Magnetism.* Oxford University Press, 1961.

Cross-references

Cooley–Tukey algorithm
Fourier transformation
Rotating frame
Sensitivity
Time averaging
Vector model

Convolution

The problem of distinguishing between a true signal and random noise has proved a real challenge to spectroscopists, and in the wider world, random phenomena are often a source of fascination. In the stock market, the price of a given stock fluctuates with time, and it would be useful and profitable to discover which part of this fluctuation is a 'real' movement and which is just meaningless erratic behaviour. On the assumption that the longer-term fluctuations are 'real', a 30 day moving average is calculated; this is 30 times less sensitive to day-to-day variations, but shows up the longer-term trends. This smoothing process is actually a convolution of the raw data with a rectangular function spanning 30 days.

Similar problems are posed by noisy NMR data. Suppose that we have a spectrum described by a function g(f) and we wish to improve the signal-to-noise ratio by convolution with a smoothing function h(f) which might be (for example) a Gaussian or Lorentzian curve. If we use the symbol $\otimes$ to denote convolution, this is described by the integral,

$$g(f) \otimes h(f) = \int_{-\infty}^{+\infty} g(f')\, h(f - f')\, df'. \qquad [1]$$

In practice g(f) is normally a digitized spectrum, and the integral is replaced by the appropriate summation between finite limits. Equation [1] indicates that the smoothing function h(f) is reversed left to right, but since in many cases of interest it is a symmetric function, this 'folding' is usually irrelevant. The convolution operation is performed at each ordinate of the experimental spectrum in turn. Consider a typical ordinate $g(f_k)$. The smoothing function h(f) is moved so as to be centred on the frequency f_k, and then each and every ordinate of g(f) is multiplied by the corresponding ordinate of h(f), the normalized sum being replaced at the frequency f_k. In this way, the new ordinate at f_k comprises information about the intensities of neighbouring points, weighted inversely as their distance from f_k (Fig. 1). The smoothing function is then moved along to f_{k+1} and the whole process repeated. Clearly the broader the function h(f), the more severe the smoothing process. If h(f) is too broad, then the signal itself is broadened and reduced in height, and there is no further improvement in the signal-to-noise ratio.

The key concept here is the convolution theorem, which states that the convolution of two functions g(f) $\otimes$ h(f) is the same as the Fourier transform of the product G(t)H(t), where G(t) and H(t) are the inverse Fourier transforms of g(f) and h(f). Consequently the smoothing process in the frequency domain is equivalent to

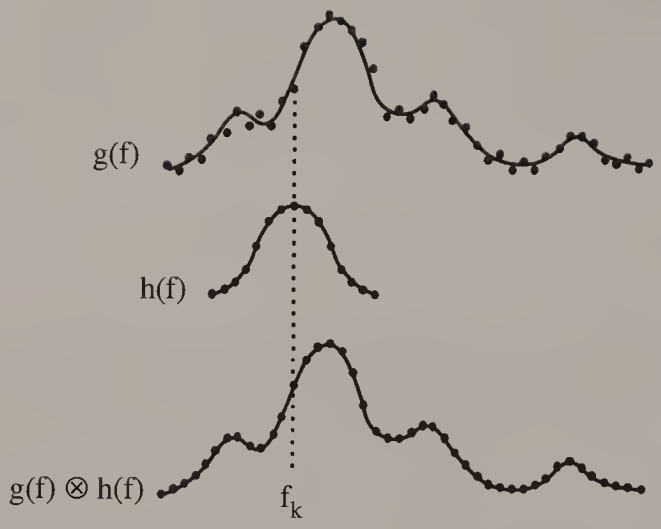

Fig. 1. Convolution of a spectrum g(f) with a smoothing function h(f) in order to improve the signal-to-noise ratio. At each frequency step f_k, corresponding points on g(f) and h(f) are multiplied and then summed over the entire curve. The normalized result is then used to construct the smoothed spectrum, one step at a time. This takes out the more rapid fluctuations in g(f).

multiplication of a free induction decay G(t) by a 'sensitivity enhancement function' H(t). If H(t) is a decaying exponential exp(–t/T), then absorption lines in the spectrum are convoluted with a Lorentz curve

$$h(f) = \frac{T}{1 + (2\pi\Delta f)^2 T^2} . \qquad [2]$$

This time-domain processing is easy to implement and is widely employed. The optimum enhancement of sensitivity is achieved with a 'matched filter' (1), where H(t) has the same decay constant as the experimental free induction signal G(t). Note that we sacrifice resolution when we employ sensitivity enhancement*. Severe weighting functions smooth out both signals and noise, yielding diminishing returns.

There seems to be no recognized formal definition of *deconvolution,* but it is easy to imagine a process that is the reverse of the smoothing operation described above. Indeed, we can take experimental data that has been broadened by an instrumental effect (B_0 inhomogeneity) and process it so as to *deconvolve* the undesirable blurring. Since broadening corresponds to an acceleration of the decay rate of the time-domain NMR signal, it is clear that multiplication by a function that *increases* with time will lead to resolution enhancement* (and a concomitant loss of sensitivity). The only problem is that this process accentuates any step at the end of the experimental free induction decay, so some form of rounding off (*apodization*) may be required, otherwise sinc function wiggles appear on all the lines in the

spectrum. The practical limit on resolution enhancement is set by the fact that noise and certain artefacts are also sharpened and enhanced.

Biochemists who were concerned with emphasizing narrow features of an NMR spectrum at the expense of broad underlying resonances introduced the idea of *convolution difference* (2). A relatively severe weighting function is applied to the free induction decay, calculated to affect the slowly decaying components much more than those with a fast decay; this is then subtracted from the unperturbed experimental time-domain signal. The resulting spectrum shows each narrow line sitting in a broad, shallow depression (note that the integral across the entire spectrum is zero because the first point of the time-domain signal is zero). A milder form of resolution enhancement is achieved by subtraction of a scaled-down version of the weighted free induction decay.

REFERENCE DECONVOLUTION

If we wish to deconvolve the instrumental broadening effect, it seems logical to make use of the lineshape information provided by a known singlet in the same experimental spectrum; we may then hope to narrow all the lines and impose some desirable lineshape, such as a Gaussian (3). In fact this process of *reference deconvolution* (4–7) has wider-ranging applications once we realize that many different types of instrumental shortcomings affect all the lines of the spectrum in exactly the same manner. The effects of instabilities in the phase or amplitude of the radiofrequency pulses, changes in spatial inhomogeneity of the applied field, drifts of the field/frequency ratio, spinning sidebands, and many other imperfections can be compensated in this manner. However, perturbations that influence different lines to different extents, for example temperature-dependent chemical shifts, cannot be corrected by this technique.

The first step is to isolate a known singlet reference line R(f) from an uncluttered region of the spectrum. It should have extensive wings for both the absorption and dispersion modes, so that there are no significant steps at the edges of the frequency window. If truncation of the broad tails of the dispersion-mode signal is unavoidable, it is preferable to derive this component from the absorption signal by a Hilbert transform (8). Inverse Fourier transformation of the (complex) reference line R(f) gives the time-domain reference signal R(t). We then define an ideal (complex) lineshape T(f) (which might, for example, be a Gaussian) and derive the corresponding ideal time-domain function T(t) by inverse transformation. Then the ratio T(t)/R(t) is a (complex) correction function that can be applied to the experimental free induction signal, removing the effects of instrumental imperfections by slightly altering the amplitude and phase at each data point. This not only improves resolution but also corrects the jitter and distortions introduced by spectrometer shortcomings. In two-dimensional spectroscopy, reference deconvolution can be applied in both dimensions, reducing the effects of both short-term and long-term instabilities (9) and providing an effective antidote to the

ubiquitous t_1 noise*. It is particularly useful in difference spectroscopy* where the signals of interest are themselves relatively weak, for example in two-dimensional correlation spectroscopy involving low-abundance isotopes like carbon-13 or nitrogen-15.

REFERENCES

1. R. R. Ernst, Sensitivity Enhancement in Magnetic Resonance. In *Advances in Magnetic Resonance*, ed. J. S. Waugh. Academic Press: New York, 1966.
2. I. D. Campbell, C. M. Dobson, R. J. P. Williams and A. V. Xavier, *J. Magn. Reson.* **11**, 172 (1973).
3. R. R. Ernst, R. Freeman, B. Gestblom and T. R. Lusebrink, *Mol. Phys.* **13**, 283 (1967).
4. J. Taquin, *CR Acad. Sci. Paris* **280 B**, 485 (1975).
5. J. Taquin, *CR Acad. Sci. Paris* **283 B**, 257 (1976).
6. J. M. Wouters and G. A. Petersson, *J. Magn. Reson.* **28**, 81, 93 (1977).
7. G. A. Morris, *J. Magn. Reson.* **80**, 547 (1988).
8. A. Gibbs and G. A. Morris, *J. Magn. Reson.* **91**, 77 (1991).
9. A. Gibbs, G. A. Morris, A. G. Swanson and D. Cowburn, *J. Magn. Reson. A* **101**, 351 (1993).

Cross-references

Difference spectroscopy
Fourier transformation
Resolution enhancement
Sensitivity enhancement
t_1 noise

Cooley–Tukey Algorithm

The time-domain free induction decay* can always be represented by a superposition of several different sine and cosine waves of appropriate amplitudes, which mutually interfere. This is the principle of Fourier analysis. In the section on Fourier transformation* a spectrum analyser was employed to seek out these components one at a time. It accomplishes this by choosing a monochromatic frequency (the reference frequency f_r), multiplying it by the free induction signal and integrating the result from time zero to infinity. Only the components at or near the reference frequency give a finite integral; the rest quickly get out of phase with the reference frequency and give near zero integrals. The procedure is then repeated for different values of the reference frequency until all the appropriate frequencies have been explored.

Transformation in the computer requires that the free induction signal be sampled in the time domain at discrete intervals, and hence the transformation process is necessarily discrete, and the integration is replaced by a summation. Suppose that the free induction decay is represented by an array of values X, with a typical value X_k, where k runs from 0 to N – 1. The frequency-domain spectrum is an array A with typical value A_r, where r runs from 0 to N – 1. The elements of the array X are simply multiplied by the appropriate values of a sine wave and a cosine wave, and the products summed over all values of the index k. This may be written

$$A_r = \sum_{k=0}^{N-1} X_k W^{rk} \qquad r = 0, 1, \ldots, N-1 \qquad k = 0, 1, \ldots, N-1, \qquad [1]$$

where $W^{rk} = \exp(-2\pi irk/j)$. In some computer programs a table of values of sines is calculated beforehand and used as a look-up table instead of computing the sine or cosine (via a Taylor series) at each stage of the calculation. Because of the periodicity of the expression for W, there are some useful relationships between certain powers of W. For example

$$W^{rk+N} = \exp(-2\pi irk/N)\exp(-2\pi i) = \exp(-2\pi irk/N) = W^{rk} \qquad [2]$$

$$W^{rk+N/2} = \exp(-2\pi irk/N)\exp(-\pi i) = -\exp(-2\pi irk/N) = -W^{rk}. \qquad [3]$$

Thus for N = 4, $W^6 = W^2$ and $W^3 = -W^1$. Note also that $W^2 \times W^3 = W^5$, etc.

The first computer programs for Fourier transformation operated on exactly this principle, multiplying the elements as in eqn [1] and summing the result. Unfortunately, multiplication is a very time-consuming operation in a computer and the transformation times by this method were measured in tens of minutes. The

operation of addition is much faster, and in what follows this time will be neglected, only the slow multiplication steps being considered. There are N^2 complex multiplication steps required to evaluate all the N values.

A breakthrough in the speed of computation was achieved by the *fast Fourier transform* algorithm of Cooley and Tukey (1) as modified by Bergland (2). It happened at just the opportune moment for the development of Fourier transform NMR (1965), for it would be hard for today's spectroscopist to have to wait 20 minutes for his high-resolution spectrum to be computed.

The way in which this time saving comes about has been presented in some detail by Oran Brigham (3). His treatment is followed here by considering the simple case of N = 4 and then generalizing the result. For N = 4 the summation of eqn [1] can be written

$$\begin{aligned} A_0 &= X_0W^0 + X_1W^0 + X_2W^0 + X_3W^0 \\ A_1 &= X_0W^0 + X_1W^1 + X_2W^2 + X_3W^3 \\ A_2 &= X_0W^0 + X_1W^2 + X_2W^4 + X_3W^6 \\ A_3 &= X_0W^0 + X_1W^3 + X_2W^6 + X_3W^9 \end{aligned} \qquad [4]$$

Using the relationship between the different powers of W,

$$\begin{pmatrix} A_0 \\ A_1 \\ A_2 \\ A_3 \end{pmatrix} = \begin{pmatrix} W^0 & W^0 & W^0 & W^0 \\ W^0 & W^1 & W^2 & W^3 \\ W^0 & W^2 & W^0 & W^2 \\ W^0 & W^3 & W^2 & W^1 \end{pmatrix} \begin{pmatrix} X_0 \\ X_1 \\ X_2 \\ X_3 \end{pmatrix}. \qquad [5]$$

Now suppose that we reorder the column vector A_r and the matrix W^{rk}:

$$\begin{pmatrix} A_0 \\ A_2 \\ A_1 \\ A_3 \end{pmatrix} = \begin{pmatrix} 1 & 1 & 1 & 1 \\ 1 & W^2 & W^0 & W^2 \\ 1 & W^1 & W^2 & W^3 \\ 1 & W^3 & W^2 & W^1 \end{pmatrix} \begin{pmatrix} X_0 \\ X_1 \\ X_2 \\ X_3 \end{pmatrix}. \qquad [6]$$

Here we have interchanged the second and third rows and replaced W^0 by 1 except in one location where it is retained in order to be consistent with the more general results. This matrix can be factorized into two:

$$M = \begin{pmatrix} 1 & W^0 & 0 & 0 \\ 1 & W^2 & 0 & 0 \\ 0 & 0 & 1 & W^1 \\ 0 & 0 & 1 & W^3 \end{pmatrix} \begin{pmatrix} 1 & 0 & W^0 & 0 \\ 0 & 1 & 0 & W^0 \\ 1 & 0 & W^2 & 0 \\ 0 & 1 & 0 & W^2 \end{pmatrix}. \qquad [7]$$

The frequency-domain values A_r may now be evaluated by taking two matrix multiplications separately. First define an intermediate column vector

$$\begin{pmatrix} x_0 \\ x_1 \\ x_2 \\ x_3 \end{pmatrix} = \begin{pmatrix} 1 & 0 & W^0 & 0 \\ 0 & 1 & 0 & W^0 \\ 1 & 0 & W^2 & 0 \\ 0 & 1 & 0 & W^2 \end{pmatrix} \begin{pmatrix} X_0 \\ X_1 \\ X_2 \\ X_3 \end{pmatrix}. \qquad [8]$$

Suppose we choose to calculate x_0 and x_2, remembering that $W^0 = -W^2$:

$$x_0 = X_0 + W^0X_2 \qquad x_2 = X_0 - W^0X_2.$$

Thus in calculating this pair of values only one complex multiplication is involved instead of two. Moreover, X_0 and X_2 are never needed again in the calculation so that x_0 and x_2 may be stored in their locations. Exactly the same reasoning applies to the pair of values x_1 and x_3, and these may be stored in the locations previously used for X_1 and X_3. Hence the calculation can be performed 'in place' without increasing the size of the data table. This first 'pass' through the calculation is usually represented diagrammatically as in Fig. 1. The connecting lines with a W attached involve multiplication, but only two independent multiplications occur.

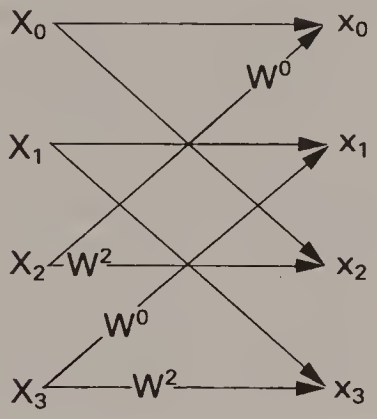

Fig. 1.

The next 'pass' multiplies the intermediate column vector x_k by the left-hand matrix of eqn [7]:

$$\begin{pmatrix} A_0 \\ A_2 \\ A_1 \\ A_3 \end{pmatrix} = \begin{pmatrix} 1 & W^0 & 0 & 0 \\ 1 & W^2 & 0 & 0 \\ 0 & 0 & 1 & W^1 \\ 0 & 0 & 1 & W^3 \end{pmatrix} \begin{pmatrix} x_0 \\ x_1 \\ x_2 \\ x_3 \end{pmatrix}. \qquad [9]$$

An exactly analogous reasoning indicates that again only two complex multiplications are involved, provided the calculations are carried out on the appropriate pairs of intermediate values (x_0, x_1) and (x_2, x_3). The 'flow diagram' can thus be extended as in Fig. 2.

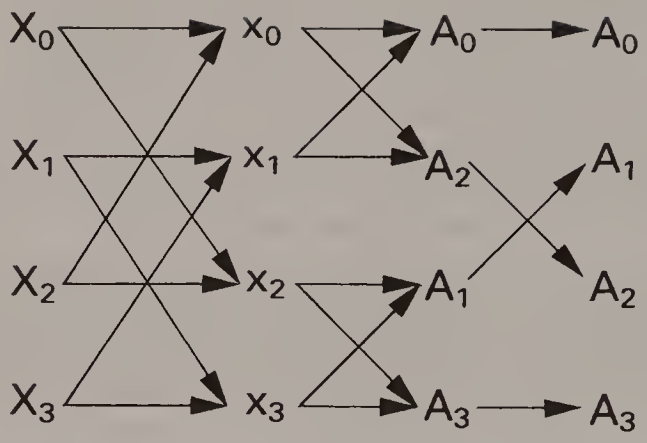

Fig. 2.

This factorization procedure and the pairing of the calculations have thus reduced the total of complex multiplications from 16 to four. If the argument is generalized for $N = 2^p$ the fast Fourier transform algorithm factorizes the $N \times N$ matrix into p matrices of size $N \times N$, each containing many zeros, and p passes are required in the calculation. Instead of N^2 complex multiplications, only $\frac{1}{2}Np$ complex multiplications are required, giving a reduction in overall computing time of approximately 2N/p, which for N = 8000 words is roughly an advantage of 1300.

Because of the reordering that was employed in eqn [6] the values for the frequency-domain points A_r are in a scrambled order and must be unscrambled before the spectrum is displayed. In the case considered, where N = 4, this simply involves interchanging A_1 with A_2, as indicated in the last step of the flow diagram. The recipe for reordering the general case is quite interesting. It requires that the index r be expressed in binary digits and then be reversed. This 'bit-reversed order' is illustrated for the slightly less trivial case of N = 8:

$$
\begin{array}{lll}
A_0 & 000 \rightarrow 000 & A_0 \\
A_1 & 001 \rightarrow 100 & A_4 \\
A_2 & 010 \rightarrow 010 & A_2 \\
A_3 & 011 \rightarrow 110 & A_6 \\
A_4 & 100 \rightarrow 001 & A_1 \\
A_5 & 101 \rightarrow 101 & A_5 \\
A_6 & 110 \rightarrow 011 & A_3 \\
A_7 & 111 \rightarrow 111 & A_7 .
\end{array}
$$

Reordering could equally well be accomplished before the transformation by an operation on the matrix X_k.

Note that the flow diagrams shown above suggest that Fourier transformation could be further speeded up by parallel processing of the data in contrast to the serial processing discussed here. Array processors are now being used increasingly

in high-resolution spectrometers as data tables become larger and larger, and particularly in the growing field of two-dimensional spectroscopy*, where two-dimensional arrays are involved, and transformation times for serial processing are appreciable.

REFERENCES

1 J. W. Cooley and J. W. Tukey, *Math. Comput.* **19**, 297 (1965).

2. G. D. Bergland, *Commun. ACM* **11**, 703 (1968).

3 E. Oran Brigham, *The Fast Fourier Transform.* Prentice Hall: Englewood Cliffs, New Jersey, 1974.

Cross-references

Fourier transformation
Free induction decay
Two-dimensional spectroscopy

Correlation Spectroscopy

When NMR spectroscopy is used to elucidate molecular structure, the assignment of the resonances is often the weakest link in the chain of evidence. Comparison with the spectra of similar molecules, and the organic chemist's knowledge of the trends in chemical shielding, usually provide the required information, but where these methods fail, recourse must be made to further NMR experiments such as double-resonance or cross-relaxation studies. Two-dimensional spectroscopy* (1) has now taken over from double-resonance methods, and a particularly useful form for assignment purposes is called *correlation spectroscopy*. (An earlier use of the same term to mean high-resolution spectroscopy examined by rapid-passage methods has now fallen into disuse.) Correlation is now taken to mean the identification of chemical sites that are related by a resolvable spin–spin coupling.

HETERONUCLEAR CORRELATION SPECTROSCOPY

Consider the simple case of correlation of proton and carbon-13 chemical shifts. We might employ polarization transfer* in the directions H $\rightarrow$ C or C $\rightarrow$ H, or we might exploit the inherently higher sensitivity of 'round-trip' transfer H $\rightarrow$ C $\rightarrow$ H. Since direct (single-bond) CH couplings are very much larger than long-range couplings, the experiment can be set up so that essentially all the polarization transfer occurs via the direct route (2). For simplicity, the H $\rightarrow$ C correlation technique is analysed here (3). Basically the experiment labels the proton frequencies by allowing free proton precession during the evolution period t_1 and identifies the directly coupled carbon-13 sites by detecting these resonances during the acquisition period t_2. The key is the transfer step when polarization is passed from each proton to a *specific* carbon site, just as runners in a relay race pass on the baton to a *designated* team-mate. A peak in the resulting two-dimensional spectrum has an F_1 frequency equal to the proton chemical shift and an F_2 frequency equal to the correlated carbon-13 chemical shift. Such a response is known as a *cross-peak* (4). This spectrum is conveniently displayed as an intensity contour map, since we are rather more interested in the frequencies than the relative intensities.

The observed carbon-13 signal is restricted to the transferred polarization; any 'natural' carbon-13 signal is suppressed by difference spectroscopy, since it serves no useful purpose in correlation experiments. The proton polarization is inherently

four times stronger than the natural carbon-13 polarization ($\gamma_H = 4\gamma_C$) and, because protons relax rather faster than carbon-13 nuclei, the cycle time for repeating the measurement can be quite short, further improving the sensitivity. For the case of $C \rightarrow H$ or $H \rightarrow C \rightarrow H$ correlation, the intense signal from protons attached to carbon-12 nuclei must be suppressed. Bilinear rotation decoupling* is useful in this regard (5).

The simplest way to visualize the mechanism of correlation spectroscopy is in terms of spin population effects, based on the fact that coupled proton and carbon spins share the same energy levels. Perturbation of proton populations necessarily affects the carbon-13 populations, and this can be detected by a final carbon-13 'read' pulse. In this sense the method is related to 'selective population transfer' experiments which apply a soft 180° pulse to one of the carbon-13 satellites of the proton spectrum.

A pulse sequence suitable for $H \rightarrow C$ correlation spectroscopy is set out in Fig. 1. An initial 90° pulse excites proton magnetization along the +Y axis, represented by two vectors α and β which precess during the first part of the evolution period at frequencies $2\pi(\delta_H + \frac{1}{2}J_{IS})$ and $2\pi(\delta_H - \frac{1}{2}J_{IS})$ rad s^{-1} respectively (Fig. 2(a)). At the mid-point of the evolution period, a 180° pulse applied to carbon-13 reverses the α and β labels of these vectors so that they now precess at $2\pi(\delta_H - \frac{1}{2}J_{IS})$ and $2\pi(\delta_H + \frac{1}{2}J_{IS})$ rad s^{-1} respectively (Fig. 2(b)). The net precession angle at the end of the evolution period is therefore $\theta = 2\pi\delta_H t_1$ radians; the spin–spin coupling term has been removed (Fig. 2(c)). As a result, CH splittings do not appear in the F_1 dimension of the correlation spectrum. The fixed interval $\Delta_1 = 1/(2J_{CH})$ allows these parallel vectors to diverge into the antiparallel orientation in preparation for the actual polarization transfer (Fig. 2(d)).

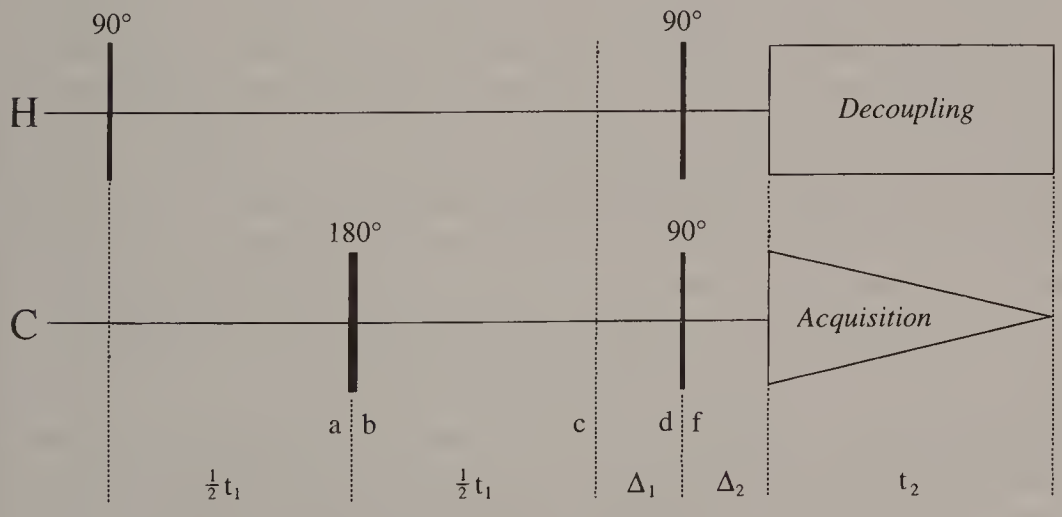

Fig. 1. Pulse sequence for heteronuclear correlation spectroscopy employing polarization transfer from protons to carbon-13. The timing markers a through f refer to the vector diagram of Fig. 2. The CH splittings are removed in both frequency dimensions.

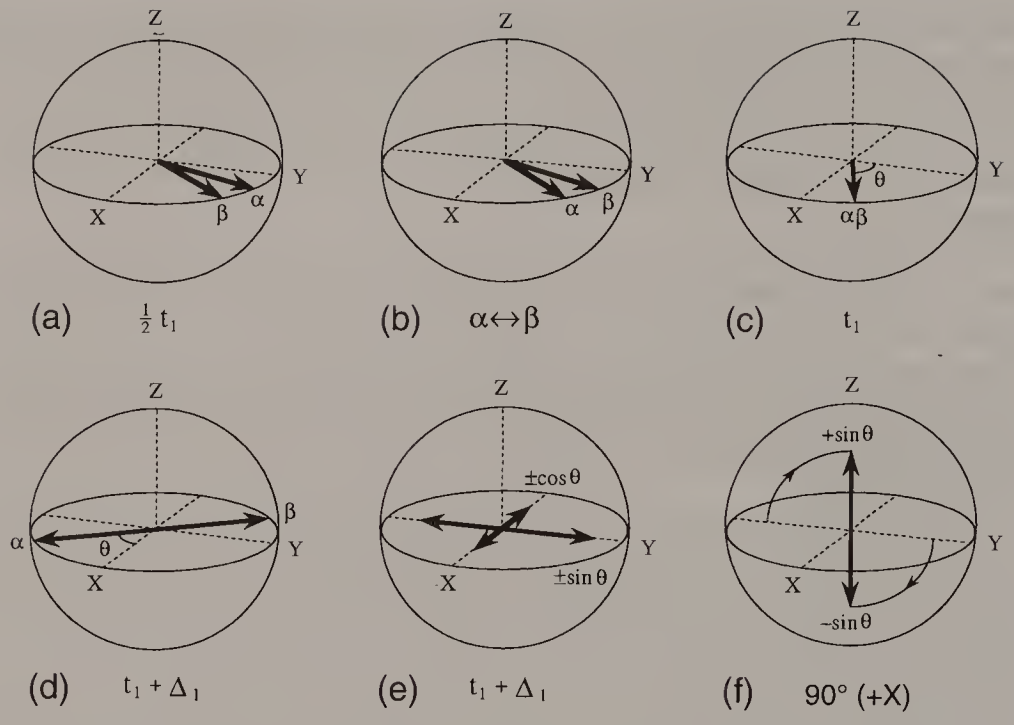

Fig. 2. Schematic diagram illustrating the motion of the proton vectors during a heteronuclear polarization transfer. (a) After a period $\frac{1}{2}t_1$ of free precession. (b) The effect of the 180° pulse on carbon-13. (c) Refocusing after a further period $\frac{1}{2}t_1$ of free precession. (d) Evolution into an antiphase configuration. (e) Vectors resolved into components along ±X and ±Y. (f) The Y components converted into longitudinal magnetization.

We now resolve these two vectors into their components ±M cos θ along the ±X axis, and ±M sin θ along the ±Y axis (Fig. 2(e)). The 90° pulse applied about the +X axis rotates the latter components into the ±Z axes (a population disturbance), but converts the former component into unobservable multiple-quantum coherence* which is never heard from again. These non-equilibrium spin populations are similar to those that would be created by a line-selective 180° pulse, but the amplitude of the disturbance is modulated by sin θ; this is how the proton chemical shift information is coded into the final two-dimensional spectrum. Because the carbon-13 spins share energy levels with the protons, the population disturbance also affects carbon-13 (Fig. 3(b)). If we express the *changes* in populations as a ratio of the equilibrium populations, they are +2a sin θ for one carbon-13 transition and –2a sin θ for the other, compared with the equilibrium population differences 2b, where the ratio $a/b = \gamma_H/\gamma_C = 4$. These population disturbances are converted into observable carbon-13 signals by the 90° 'read' pulse, giving an antiphase absorption-mode signal. Note that the last two 'simultaneous' 90° pulses can be taken in either order; it is convenient to consider the proton 90° pulse first, since then the mechanism can be described in terms of a disturbance of the spin populations. Had we made the other choice, we would have had to embark on a short excursion into multiple-quantum coherence.

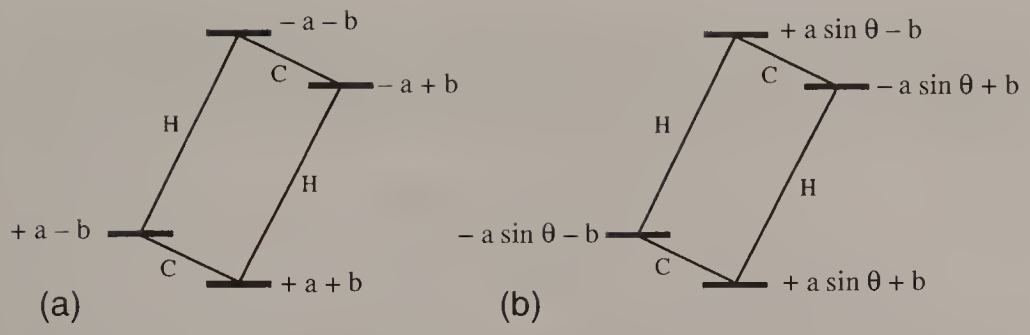

Fig. 3. Spin populations on the energy-level diagram for a proton (H) coupled to a carbon-13 spin (C). (a) At Boltzmann equilibrium the proton population differences are 2a, and the carbon-13 population differences are 2b, where a/b = 4. (b) After partial inversion of the proton populations, the carbon-13 population differences change by ±2a sin θ.

The second fixed delay Δ_2 allows the antiphase carbon-13 vectors to precess into alignment so that broadband proton decoupling can be imposed without fear of signal cancellation. For a CH group, Δ_2 is set equal to $1/(2J_{CH})$, but in general there may be CH_2 and CH_3 groups, and a compromise setting must be found, for example $\Delta_2 = 1/(3.3J_{CH})$. In this manner, the CH splitting has now been removed from *both* frequency dimensions, giving a particularly simple correlation spectrum. The only caveat is to beware of strong coupling effects between protons, remembering that this means between *carbon-13 satellites,* not between the main proton resonances.

HOMONUCLEAR CORRELATION SPECTROSCOPY

Proton–proton correlation spectroscopy was in fact the very first two-dimensional experiment (1) and it pioneered this new field of research. Homonuclear correlation spectroscopy, usually called COSY, exhibits some important differences with respect to the heteronuclear case treated above. There is no scope for 'decoupling' the active splitting J_{IS} because a 180° pulse would now affect both I and S. The coupling constants lie in a smaller, continuous range, and the rates of polarization transfer depend on the magnitudes of the active coupling constants. The contour map (6) is basically square in shape rather than rectangular; both axes span the same range of chemical shifts.

The COSY pulse sequence is deceptively simple:

$$90° - t_1 - 90° \text{ acquisition } (t_2). \qquad [1]$$

Normally the mechanism is described as coherence transfer, and is analysed by the density matrix or product operator formalisms (4), but it can be treated more simply in terms of population disturbances, just as in the heteronuclear case above.

We consider a weakly coupled two-spin (IS) system. Since the problem is symmetrical with respect to the I and S spins, we can concentrate simply on the $I \rightarrow S$ transfer which generates a cross-peak centred at (δ_I, δ_S). The corresponding

S → I transfer gives a symmetrically related cross-peak centred at (δ_S, δ_I).

The I-spin magnetization is represented by two equal vectors (M_0). After excitation by the first 90° pulse, they are initially aligned along the +Y axis and precess in the XY plane through angles

$$\theta_1 = (2\pi\delta_H + \pi J_{IS})t_1 \qquad [2]$$

$$\theta_2 = (2\pi\delta_H - \pi J_{IS})t_1. \qquad [3]$$

We resolve these vectors into $M_0 \sin\theta_1$ and $M_0 \sin\theta_2$ along the X axis, and $M_0 \cos\theta_1$ and $M_0 \cos\theta_2$ along the Y axis. The second 90° pulse is treated as a cascade of two 90° pulses, the first applied to the I spins and the second (a read pulse) applied to the S spins. The 90° pulse on the I spins rotates the Y components into the –Z axis but leaves the X components unchanged. Now a vector M_0 aligned along the –Z axis corresponds to a complete population inversion. We can represent this as a disturbance of the spin populations on a four-level diagram (Fig. 4). If $t_1 = 0$, $\cos\theta_1 = \cos\theta_2 = 1$, and there is complete population inversion across both I-spin transitions, but this leaves the population differences across the S-spin transitions unchanged. Only if the two I-spin transitions suffer *differential* population inversions ($\theta_1 \neq \theta_2$) does this affect the S-spin populations. The effect is of the same magnitude for the two S-spin transitions, but in opposite senses, giving the differential population disturbance:

$$\Delta p = \pm a(\cos\theta_2 - \cos\theta_1). \qquad [4]$$

Through a standard trigonometrical identity this can be rewritten as

$$\pm 2a \sin[\tfrac{1}{2}(\theta_1 + \theta_2)] \sin[\tfrac{1}{2}(\theta_1 - \theta_2)] = \pm 2a \sin(2\pi\delta_I t_1) \sin(\pi J_{IS} t_1). \qquad [5]$$

This tells us that the polarization transfer to the S spins builds up quite slowly, as a function of $\sin(\pi J_{IS} t_1)$, so if the maximum evolution time is too short, or if the I-spin signal decays too rapidly (broad lines compared with J_{IS}), then the transfer is negligible. The expression in eqn [5] also indicates that the cross-peak will be

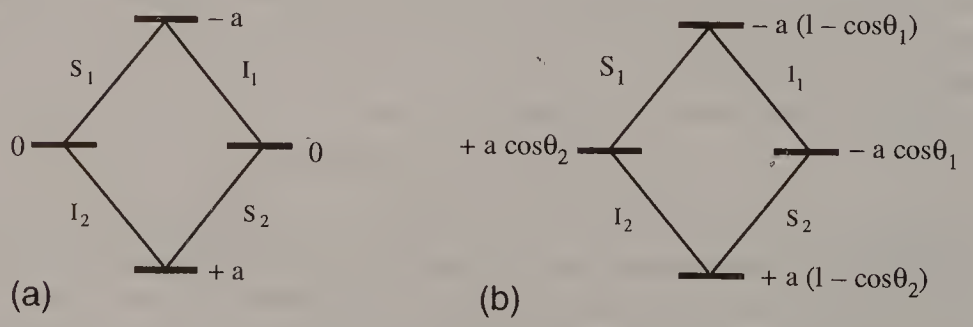

Fig. 4. Spin populations for a weakly coupled homonuclear two-spin (IS) system. (a) At Boltzmann equilibrium. (b) After partial spin inversions across the I-spin transitions. Only a differential disturbance ($\theta_1 \neq \theta_2$) affects the S-spin population differences.

centred at δ_I in the F_1 dimension and will have an antiphase doublet structure, the Fourier transform of the term $\sin(\pi J_{IS} t_1)$. The signal is detected at the S-spin frequency so the cross-peak is centred at δ_S in the F_2 dimension, and because the two S-spin transitions are affected in opposite senses, it will also have an antiphase doublet structure.

The characteristic shape of a COSY cross-peak is therefore an antiphase square pattern. Normally the spectrometer phase is adjusted so that cross-peaks appear in the absorption mode. We can draw the conclusion (mentioned above) that if the linewidth exceeds the splitting J_{IS}, there is mutual cancellation between positive and negative lines. In the limit the cross-peak vanishes.

It is convenient to designate I and S as 'active' spins, and the coupling J_{IS} as the 'active' coupling. When there are other spins coupled to I and S, they are called 'passive' spins and they introduce new splittings into the IS cross-peak. That is to say, a passive spin R converts δ_I and δ_S into effective chemical shifts, $(\delta_I \pm \frac{1}{2}J_{IR})$ and $(\delta_S \pm \frac{1}{2}J_{SR})$, each acting as a centre for the basic antiphase square patterns of lines. The cross-peak would therefore consist of 16 lines. We can easily pick out such patterns in the COSY spectrum of 2,3-dibromopropanoic acid (6) illustrated in Fig. 5(a).

This form of cross-peak is the most common but it only occurs when the second pulse of the COSY sequence is a 90° pulse. If a much smaller flip angle is chosen (45° is often used) the passive spins do not change their spin states during the experiment, but remain mere spectators. If the effective chemical shift in one dimension is $(\delta_I + \frac{1}{2}J_{IR})$ then the effective shift in the other dimension is $(\delta_S + \frac{1}{2}J_{SR})$, not $(\delta_S - \frac{1}{2}J_{SR})$. Instead of four basic square patterns, just two predominate, connected by a 'displacement vector' which is the resultant of J_{IR} and J_{SR}, taking account of their signs (Fig. 6). The sign of the slope of the displacement vector gives the relative signs of J_{IR} and J_{SR}. Thus a COSY spectrum with a 45° flip angle (Fig. 5(b)) shows examples of both like and opposite signs of the passive couplings.

So far we have neglected the components $M_0 \sin\theta_I$ and $M_0 \sin\theta_2$, which represent magnetization that remains at the I-spin site during the acquisition period. We might have expected that these two resonances would maintain their individual identities throughout t_1 and t_2 and thus give responses at the coordinates

$$\begin{aligned}&(\delta_I + \tfrac{1}{2}J_{IS},\ \delta_I + \tfrac{1}{2}J_{IS})\\&(\delta_I - \tfrac{1}{2}J_{IS},\ \delta_I - \tfrac{1}{2}J_{IS})\end{aligned} \qquad [6]$$

which lie exactly on the principal diagonal $F_1 = F_2$. This is to forget the influence of the second 90° pulse applied to the S spins. Had this been a 180° pulse, it would have interchanged the frequencies of the I-spin resonances, generating lines at the coordinates

$$\begin{aligned}&(\delta_I + \tfrac{1}{2}J_{IS},\ \delta_I - \tfrac{1}{2}J_{IS})\\&(\delta_I - \tfrac{1}{2}J_{IS},\ \delta_I + \tfrac{1}{2}J_{IS})\end{aligned} \qquad [7]$$

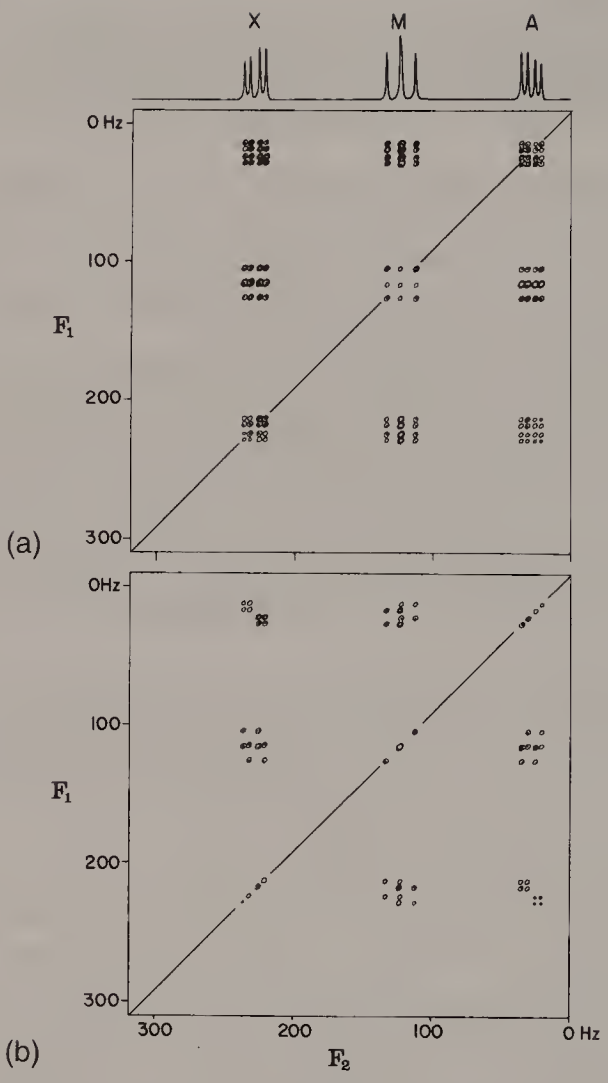

Fig. 5. COSY spectra of a three-spin system (a) with a 90° final pulse and (b) with a 45° final pulse. In spectrum (a) cross-peaks and diagonal peaks are 4×4 rectangular patterns. In spectrum (b) the cross-peaks consist of only two square patterns, and the slope of the displacement vector gives the relative signs of the two passive couplings; the diagonal peaks fall exactly on the diagonal (see text).

which lie just off the principal diagonal. On the other hand if the flip angle had been small, the S spins would have remained in the same state, and these lines would have fallen exactly on the principal diagonal (Fig. 5(b)). The actual 90° pulse has an intermediate effect, flipping the S spins in 50% of the cases, creating a square pattern of side J_{IS} straddling the diagonal. With the normal spectrometer phase setting, these diagonal peaks are in dispersion; there is no sign alternation.

Often we are interested in searching for weak cross-peaks close to the diagonal. Then it is a considerable advantage to employ double-quantum filtration in conjunction with the COSY experiment (7). The diagonal peaks (like the cross-peaks) are now principally in absorption and their tails are therefore less likely to

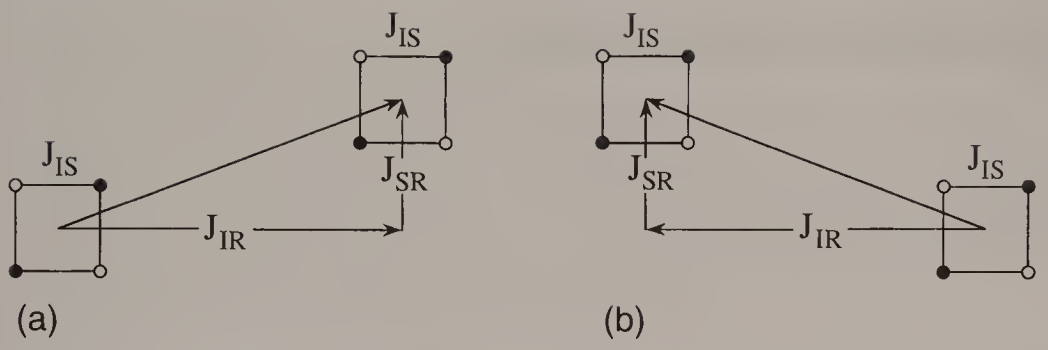

Fig. 6. Schematic diagram of a COSY cross-peak when the second pulse has a flip angle of 45° rather than 90°. (a) For like signs of the passive couplings J_{IR} and J_{SR}, giving a displacement vector with a positive slope. (b) For opposite signs, giving a displacement vector with a negative slope. Compare the experimental cross-peaks in Fig. 5(b).

obscure nearby cross-peaks. Furthermore, resonances from isolated spins, in particular intense solvent peaks, are suppressed since they cannot support double-quantum coherence.

REFERENCES

1. J. Jeener, Ampère International Summer School, Basko Polje, Yugoslavia, 1971, reported in *NMR and More. In Honour of Anatole Abragam,* ed. M. Goldman and M. Porneuf. Les Editions de Physique: Les Ulis, France, 1994.
2. A. A. Maudsley and R. R. Ernst, *Chem. Phys. Lett.* **50**, 368 (1977).
3. G. Bodenhausen and R. Freeman, *J. Magn. Reson.* **28**, 471 (1977).
4. W. P. Aue, E. Bartholdi and R. R. Ernst, *J. Chem. Phys.* **64**, 2229 (1976).
5. J. R. Garbow, D. P. Weitekamp and A. Pines, *Chem. Phys. Lett.* **93**, 514 (1982).
6. A. Bax and R. Freeman, *J. Magn. Reson.* **44**, 542 (1981).
7. U. Piantini, O. W. Sørensen and R. R. Ernst, *J. Am. Chem. Soc.* **104**, 6800 (1982).

Cross-references

Bilinear rotation decoupling
Coherence
Multiple-quantum coherence
Polarization transfer
Product operator formalism
Two-dimensional spectroscopy
Vector model

Difference Spectroscopy

Overcrowded spectra are the bane of the NMR spectroscopist's life, and considerable efforts have been devoted to methods of spectral simplification. One general method is to impose some kind of selective perturbation and then to record the difference between the perturbed and the unperturbed spectrum (1). Although difference spectra can be obtained by chemical modification of the sample, for example by adding a relaxation reagent, the best results are obtained by physical perturbations such as double irradiation. In principle, the milder the perturbation, the cleaner the difference spectrum. A good example is a proton spin-echo* experiment with and without a 180° spin-flip pulse applied to a coupled carbon-13 or nitrogen-15 site. If perturbations of the field/frequency regulation* can be avoided, nothing changes in the proton spectrum except that the echoes become modulated. If the delay between excitation and acquisition of the echo is chosen to be a half cycle of the modulation, a clean difference spectrum is obtained showing the carbon-13 or nitrogen-15 satellites.

It should be remembered that difference spectroscopy merely alters the display mode without introducing any new information. It *highlights* the features that change in the spectrum and forces them upon our attention but does not in itself improve the accuracy of the measurement. For example, it has become common to record proton–proton Overhauser spectra in a difference mode on the grounds that the intensity variations are usually very small, as little as 1% of the unperturbed proton line intensities. Difference spectroscopy ensures that we do not overlook any of these small changes, but the accuracy of the measurement of the Overhauser enhancement is not improved.

One source of frequency displacement between the original spectrum and the double-resonance spectrum is the Bloch–Siegert effect*. For determinations of the nuclear Overhauser enhancement this can be avoided by switching off the second irradiation field B_2 just before acquisition of the free induction decay, since coherence effects (the Bloch–Siegert shift) are removed instantaneously, whereas population disturbances (the Overhauser effect) persist for times comparable with the spin–lattice relaxation time. Otherwise, the Bloch–Siegert shifts interfere with the subtraction process and spurious difference-mode responses appear, looking rather like dispersion-mode signals. Similar artefacts appear in the difference spectrum if there is a shift caused by improper operation of the field/frequency control. Carried over into two-dimensional spectroscopy*, this becomes the

problem of 't_1 noise', spurious baseline fluctuations wherever there is a strong signal in the two-dimensional spectrum (2).

Since Fourier transformation is a linear operation, a difference spectrum can be obtained by subtraction either in the time domain or in the frequency domain. Subtraction of free induction decays before transformation is sometimes preferable since it reduces the dynamic range of the signal to be transformed. The unperturbed free induction decay should not, however, be discarded since it contains potentially useful information not present in the difference mode.

APPLICATIONS OF DIFFERENCE SPECTROSCOPY

Difference spectroscopy is often used in measurements of the nuclear Overhauser effect. For this purpose, it is important to *interleave* the 'control' and 'perturbed' measurements rather than time-average a large number of the former and then a similar number of the latter. This tends to reduce the effects of slow drifts in the gain or resolution of the spectrometer.

Networks of spin–spin coupling are nowadays best investigated by homo-nuclear correlation spectroscopy* (COSY). An alternative is decoupling difference spectroscopy. This allows a well-separated multiplet to be irradiated by the B_2 field and all coupled groups to be identified as responses in the difference spectrum even though they are normally hidden in a crowded region of the spectrum. Indeed, the experiment can be performed 'blind' when even the irradiated group is obscured by other overlapping resonances, and it may be advantageous to conduct a computer-controlled search where the frequency of B_2 is incremented in small steps through the appropriate chemical shift range. Similar heteronuclear double-resonance difference experiments can be performed. In this context, when high decoupling fields are employed, the possibility of a heteronuclear Bloch–Siegert shift cannot be dismissed. A decoupling field strength $\gamma B_2/2\pi = 10$ kHz applied to carbon-13 resonance would, for example, shift a deuterium internal field/frequency signal 20 MHz distant by 2.5 Hz.

One of the most demanding applications of difference spectroscopy is the 'isotope filter' experiment mentioned above, involving the detection of the very weak satellite resonances which appear in proton spectra due to a low-abundance nucleus such as carbon-13, nitrogen-15 or silicon-29 (3). It puts severe demands on spectrometer stability since it involves the observation of very small differences in a very intense proton signal. It may be advisable to employ a polarization transfer* technique here, rather than spin-echo difference spectroscopy, since this permits presaturation of the proton signal, the detected signal being excited by transfer from the low-abundance nuclei. Figure 1 illustrates the application of the reverse 'INEPT' experiment (3) to the direction of the carbon-13 satellites in the proton spectrum of the methyl group of acetaldehyde. Two experiments are performed; in

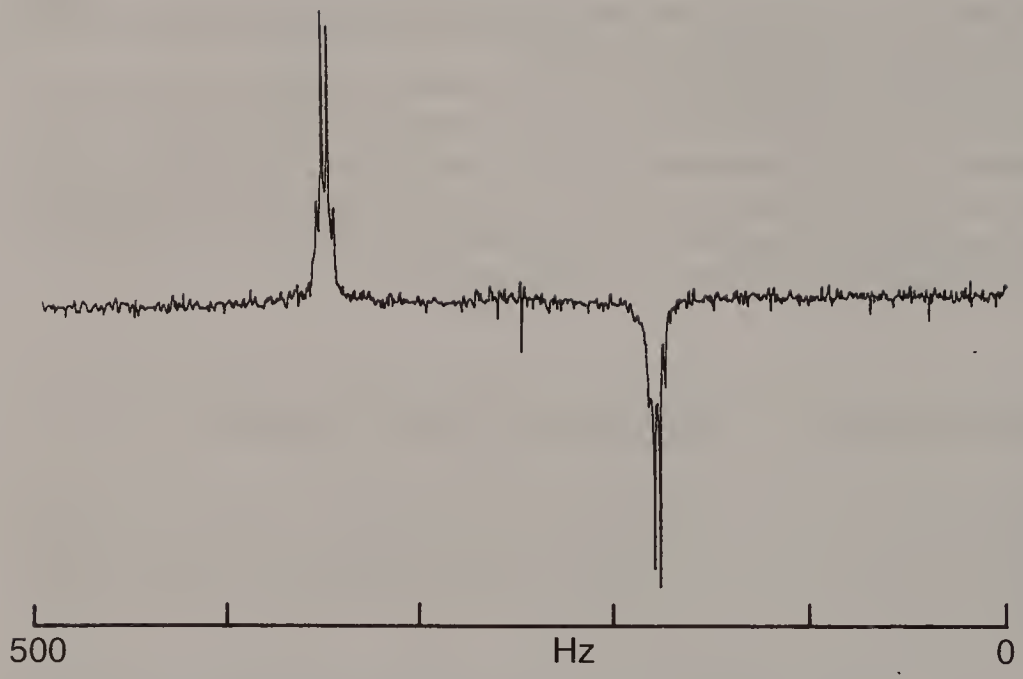

Fig. 1. The carbon-13 satellites in the proton spectrum of the methyl group of acetaldehyde with the parent proton line (centre) suppressed by difference spectroscopy. Polarization transfer from carbon-13 to protons was carried out by the 'reverse INEPT' experiment, first to give 'up–down' multiplets and then 'down–up' multiplets. When the difference spectrum is calculated the strong parent proton signal is eliminated.

the second, the sense of the polarization transfer is inverted. When the difference signal is displayed the strong parent proton peak is almost entirely suppressed.

The full power of difference spectroscopy is demonstrated when it is used to eliminate spurious instrumental artefacts. For example, if the genuine magnetic resonance response can be reversed in sense by changing the phase of a radiofrequency pulse, while an undesirable instrumental effect persists in the same sense, then difference spectroscopy eliminates the latter but retains the 'true' magnetic resonance signal. This is the basis of several phase-cycling techniques used in two-dimensional spectroscopy and in studies of multiple-quantum coherence*.

REFERENCES

1. J. K. M. Sanders and J. D. Mersh, *Prog. NMR Spectrosc.* **15**, 353 (1982).
2. A. F. Mehlkopf, D. Korbee, T. A. Tiggelman and R. Freeman, *J. Magn. Reson.* **58**, 315 (1984).
3. T. H. Mareci and R. Freeman, *J. Magn. Reson.* **44**, 572 (1981).

Cross-references

Bloch–Siegert effect
Correlation spectroscopy
Field/frequency regulation
Multiple-quantum coherence
Phase cycling
Polarization transfer
Spin echoes
t_1 noise
Two-dimensional spectroscopy

Digitization

Fourier transformation is almost invariably carried out on a digital computer, and therefore an essential step in the data processing is to convert the analogue free induction signal from the spectrometer into digital form. There are two aspects to this process: sampling as a function of time and the conversion of each analogue ordinate into digital form.

THE SAMPLING THEOREM

A jazz musician may *understate* the theme by playing rather fewer notes than are strictly necessary to define the musical phrases exactly. We might pose the same question in the NMR context – what is the minimum number of discrete samples required to define a given monochromatic frequency unambiguously? The answer is provided by the sampling theorem, which states that there must be at least two samples per cycle. Now, since a free induction decay contains many frequency components, this demands a rate of at least two samples per cycle of the *highest frequency component*. If this *Nyquist condition* is violated, the corresponding frequency is decreased by an integral multiple of the sampling rate; the frequency is said to be *aliased*. The maximum frequency which is faithfully reproduced is called the Nyquist frequency.

This phenomenon is not so surprising. It is related to the stroboscopic effect well known to Western movie buffs, where stagecoach wheels appear to slow down and even turn backwards, as a subharmonic of the rotation frequency (related to the number of spokes) interacts with the frame speed of the camera. Clearly, if this subharmonic exactly matches the frame speed, there can be no evidence on the screen that the wheels are moving at all; any slight difference in frequency translates into a slow apparent rotation, either forwards or backwards.

The phenomenon of aliasing may be appreciated diagrammatically by considering the sampling operation on a frequency F which has exactly two samples per cycle, and also on a slightly higher frequency $F + \Delta F$. From Fig. 1 we see that, for a cosine wave, the sampling ordinates for $F + \Delta F$ are identical with those for $F - \Delta F$, whereas for a sine wave they are identical but inverted, equivalent to changing the sign of the frequency ($-\sin\theta = \sin(-\theta)$). By sampling too slowly, we

have converted F + ΔF into –F + ΔF. That is to say, we have *subtracted the sampling frequency* (2F) from the true frequency.

Consider a practical case where the customary quadrature phase-sensitive detection is employed so that positive and negative frequencies are properly discriminated, with zero (the transmitter frequency) in the centre of the spectral range under investigation (Fig. 2(a)). Suppose that all the chemical shifts are encompassed within the range –10 kHz to +10 kHz. The required sampling rate would be 20 kHz, each sampling operation involving one real and one imaginary data point, as required for quadrature detection. Now let us imagine one chemical species with a resonance just outside this range, say at +11 kHz. Aliasing converts this to a frequency of –9 kHz, just inside the left-hand edge of the spectral width. Resonances outside our 'window' of frequencies are always aliased (perhaps by a *multiple* of the sampling rate) so that they appear within the window; they are never 'lost' unless suppressed by a low-pass filter. In the stagecoach analogy, filming at too low a frame speed always makes the wheels appear to turn more slowly so that they remain within the frequency window of the camera.

In a spectrometer with only single-channel phase detection the story is slightly different – resonances appear to 'fold over' at the edges of the spectral width (Fig. 2(b)). With the same constraints as above, the spectral range under investigation

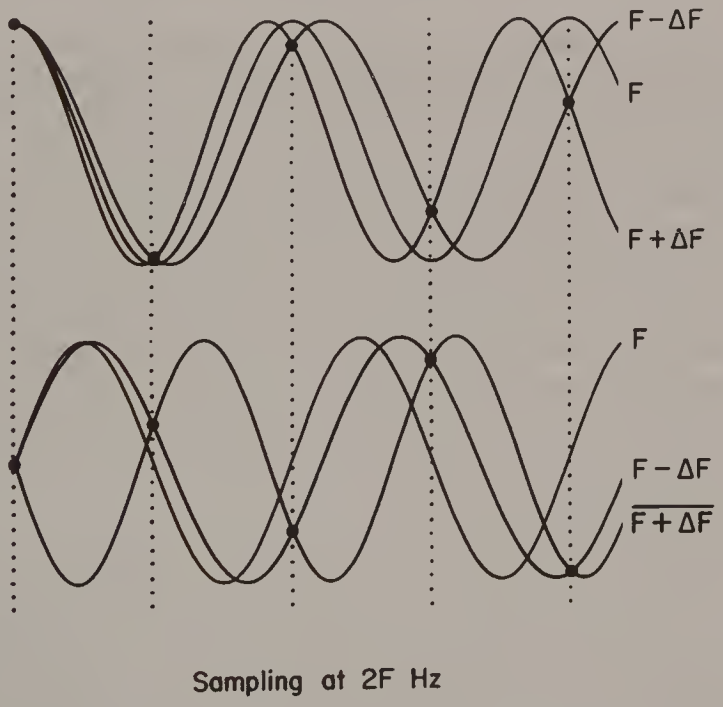

Fig. 1. Aliasing of frequencies above the Nyquist frequency (F). For a cosine wave (top) the sampled ordinates are identical for the frequencies F + ΔF and F – ΔF. For a sine wave (bottom) these ordinates are again identical except that they are inverted for the frequency F + ΔF, indicated by an overbar. The result is to subtract the sampling frequency 2F from the actual frequency.

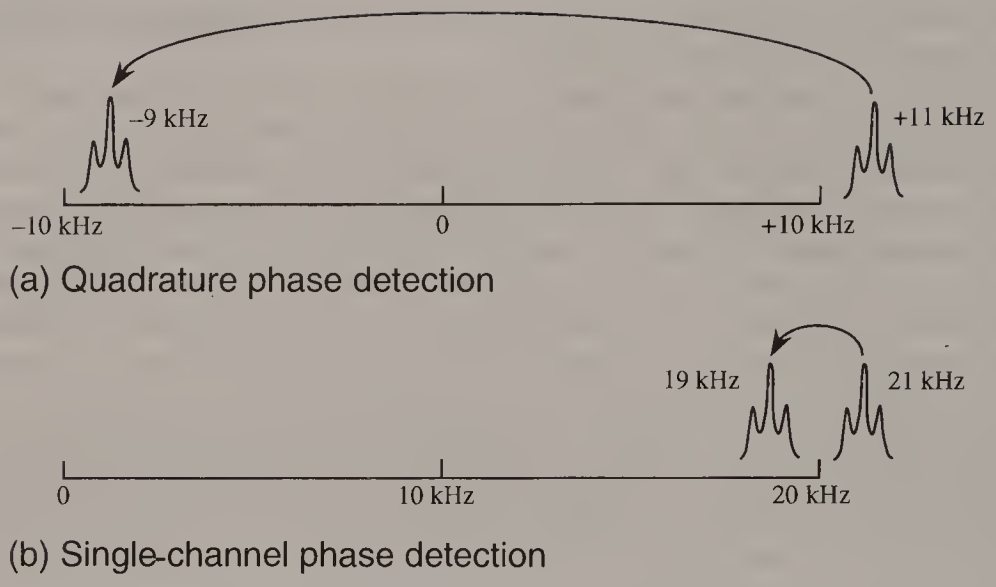

Fig. 2. Aliasing of a resonance with a frequency above the Nyquist frequency. (a) With quadrature phase detection, the apparent frequency is the actual frequency reduced by an integral multiple of the sampling rate (20 kHz). (b) With single-channel phase detection, the frequency is reduced by a multiple of the sampling rate (40 kHz) but the sign information is lost, giving the effect of 'foldover' about the Nyquist frequency.

would have to run from 0 to + 20 kHz and the sampling rate would need to be 40 kHz, with only one data point collected per sample. Folding about zero frequency is a natural consequence of our inability to distinguish the sign of a frequency with this technique, but a 'rogue' species just above this range, at 21 kHz, will be folded and will appear at 19 kHz. First, we imagine that true aliasing takes place, so that +21 kHz is converted into −19 kHz; then the sign ambiguity causes this to appear at +19 kHz. Some Fourier spectrometers, those that employ the 'pseudo-quadrature' detection scheme of Redfield and Kunz (1), exhibit a similar foldover effect instead of true aliasing. They sample the real and imaginary signal components, not simultaneously, but interleaved in time, using a sampling rate that is now *four* times the Nyquist frequency. There is therefore a fixed time shift between the acquisition of the real and the imaginary data sets (2) and this results in a situation represented by Fig. 2(b) rather than by Fig. 2(a).

This concept of a 'spectral window' is important. We cannot afford to be too profligate with our sampling rate, or the data storage requirement becomes excessive. On the other hand, we cannot usually tolerate aliasing in spectra of unknown compounds. The spectral window must be carefully chosen so as to encompass all the chemically shifted resonances. It is of course feasible to filter out any signals that lie outside our chosen window but that destroys information that might have been useful. In two-dimensional spectroscopy, aliasing can occur in both frequency dimensions; sometimes this can be tolerated because we know that there are 'empty' regions of frequency space.

ALIASING OF NOISE

By satisfying the Nyquist condition, we keep the entire NMR spectrum within the frequency window defined by the sampling rate, but unless we avoid aliasing noise from outside this window, sensitivity is seriously degraded. The usual remedy is to design a low-pass filter to cut out the majority of these noise components without significantly affecting the amplitudes or phases of signals in the NMR spectrum. Originally quite sophisticated analogue filters were used, but more recently digital filters have been introduced. They sample the incoming time-domain data much faster than the requirement of the Nyquist condition ('oversampling') and then perform a suitable smoothing operation in the time domain before reconversion to a lower sampling rate, a process sometimes called 'decimation'. The frequency-domain amplitude profile can then approach the ideal 'top-hat' shape, with uniform intensity and minimum phase distortion within the spectral width, and there is much greater flexibility in setting the bandwidth. In situations where the Fourier transform program can handle a very large data table, oversampling can be used *without* explicit digital filtration; information in regions of frequency space outside the spectral window is simply discarded.

ANALOGUE-TO-DIGITAL CONVERSION

Future NMR spectrometers may well treat all signals digitally, but at the time of writing we still need to convert analogue signals into digital form for processing. A typical analogue-to-digital converter (ADC) works by successive approximations, and it requires a finite time (microseconds) to accomplish a conversion (3). In order to avoid errors caused by variation of the input signal during the conversion period, the first step is to store the incoming signal on a sample-and-hold device which 'freezes' the voltage. Suppose that the ADC has been designed to accommodate a full-scale analogue signal of 10 volts. The first step is to set the spectrometer gain so that the extreme excursions of the free induction signal almost fill this 10 volt range. The signal must not of course exceed this range, for that would lead to clipping and the consequent introduction of artefacts in the Fourier transform spectrum.

The ADC employs a digital-to-analogue converter (DAC) to generate an analogue signal of 5 volts. It compares this with the incoming signal on the sample-and-hold device, and if the latter is higher than 5 volts, the most-significant bit of the ADC is set. The next stage takes account of the information gleaned from this first test and now resets the DAC to generate an analogue signal of 7.5 volts, knowing that the incoming signal must lie between 5 and 10 volts. When it has decided whether the raw signal is above or below the 7.5 volt level, it sets the next-most-significant bit. These stages are repeated until the least-significant bit has been set.

Clearly this leaves the final digitized signal in error by as much as half the least-significant bit; we have reached the limit of *resolution* of the ADC. It follows as a

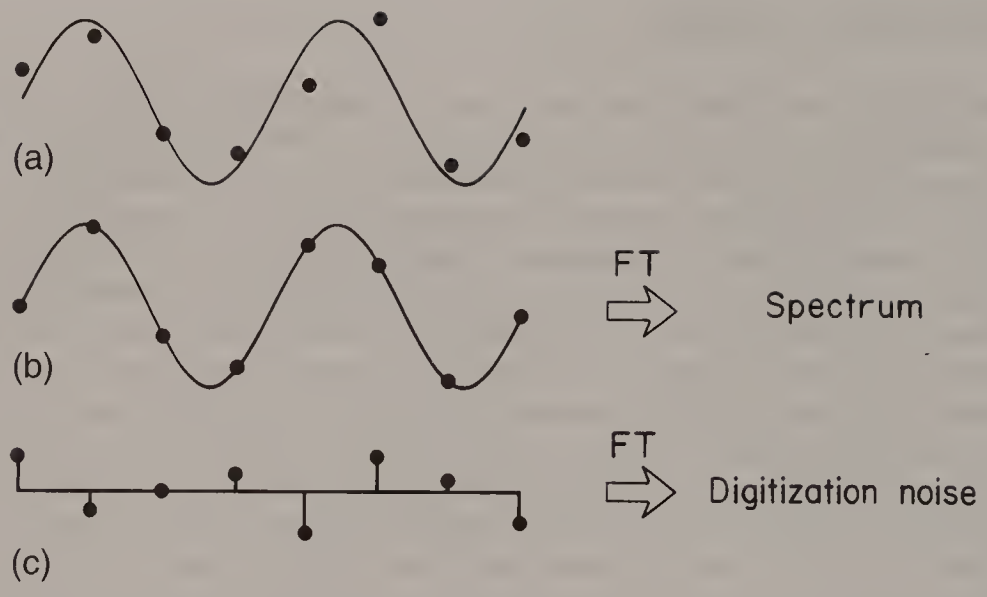

Fig. 3. Digitization errors in the analogue-to-digital converter (grossly exaggerated). The incoming signal (a) may be represented as the sum of a perfectly digitized signal (b) and the digitization errors (c). Because Fourier transformation is a linear operation, (b) and (c) can be transformed separately, giving an ideal spectrum and superimposed digitization noise.

general rule that the higher the resolution (the more stages used in the conversion) the lower the maximum sampling rate.

The free induction decay is now represented as a sequence of numbers, each of which can be thought of as being made up of a 'true' signal ordinate and a digitization error (Fig. 3). Because Fourier transformation is a linear operation, we can imagine the two components to be transformed separately and then recombined. The former constitutes the 'true' NMR spectrum while the latter is the added *digitization noise*. This can seriously compromise the sensitivity of the method if the free induction signal contains both strong and weak signal components. This is called the *dynamic range* problem; it is most serious in proton spectra where there is a strong signal from the solvent, for example water. The spectrometer gain cannot be increased without running into overflow in the ADC, but the solute signals are so weak that (after Fourier transformation) they may be swamped by the digitization noise. The available ADC resolution does not match the dynamic range of the NMR signals. This serious problem has persisted for about three decades and has spawned a whole family of techniques designed to cancel the strong water resonance from aqueous solutions. (See Solvent suppression*.)

We might have been tempted to visualize the problem in a much simpler form, arguing that an NMR signal weaker than the least-significant bit of the ADC would be lost for ever and could not appear in the transformed spectrum at all. This is not

the case (3). Noise can 'carry' weak signal components so that they influence the least-significant bit on some fraction of the conversions, thus contributing to the time-averaged free induction decay. In the absence of an appreciable level of noise, spectrometer instabilities achieve a similar effect. Even in a one-shot experiment, the presence of a strong signal component permits a very weak component to trigger the least-significant bit in some of the conversions.

There have been attempts to circumvent the limitations imposed by the restricted ADC resolution by operating in a differential mode with the water signal near zero frequency where its derivative with respect to time is very small (4). Another approach deliberately samples at a rate much higher than the Nyquist frequency ('oversampling') thereby improving the effective resolution of the ADC and attenuating the digitization noise (5). However, we have not yet seen any general solution to the dynamic range problem inherent in Fourier transform spectrometers.

REFERENCES

1. A. G. Redfield and S. D. Kunz, *J. Magn. Reson.* **19**, 250 (1975).
2. C. J. Turner and H. D. W. Hill, *J. Magn. Reson.* **66**, 410 (1986).
3. J. C. Lindon and A. G. Ferrige, *Prog. NMR Spectrosc.* **14**, 27 (1980).
4. S. J. Davies, C. J. Bauer, P. B. Barker and R. Freeman, *J. Magn. Reson.* **64**, 155 (1985).
5. M. A. Delsuc and J. Y. Lallemand, *J. Magn. Reson.* **69**, 504 (1986).

Cross-references

Fourier transformation
Free induction decay
Quadrature detection
Solvent suppression

Field/Frequency Regulation

NMR enjoys an advantage over many forms of spectroscopy by virtue of the narrow width of the resonance lines, holding out the promise of very high resolving power. In order to benefit from this, the applied magnetic field must be homogeneous in space to the extent of about 1 part in 10^9 (taking into account the beneficial averaging effect of sample spinning). We might also anticipate that it should be stable in time to the same degree, and for experiments which involve the coherent addition of many free induction decays, this high stability needs to be maintained for several hours. Fortunately the critical requirement is rather less rigorous – it is sufficient to hold the *ratio* of applied field to frequency within these stability limits, since a proportional change in both field and frequency, if small enough, has a negligible effect on the spectra. (The only perturbations arise from changes in strong coupling effects, and from any non-linear dependence of the chemical shielding on the magnetic field.)

The magnetic field generated in an iron magnet is inherently rather unstable because the geometry and the magnetic permeability both have a relatively strong temperature dependence. Fortunately, modern superconducting solenoids are much more stable; the current is constant and the dimensional stability of the coils is high, since they are in a constant temperature bath. When there is particular concern about stability, it is advisable to operate with a reasonably high level of liquid helium in the dewar vessel in order to avoid any distortion of the coil geometry. Disturbances due to mechanical vibrations or pressure oscillations in the helium gas give rise to modulation sidebands in the spectra.

Stability is further improved by a servo loop driven by an error signal derived from the internal reference material (1). This is usually the deuterium resonance of the deuterated solvent. Pulse excitation is used, but since only a singlet resonance is involved, Fourier transformation is not required. The dispersion-mode component of this signal constitutes an ideal discriminator curve. At the desired magnetic field strength, the dispersion-mode signal is zero, but if the field drifts, an error voltage is generated – positive for one sense of field drift and negative for the other. The field and frequency are said to be 'locked'. Changing the sample unlocks the system, but the basic stability of the superconducting solenoid holds the field close to the desired intensity, and the regulator easily recaptures the lock condition when a new sample is inserted.

While the dispersion-mode reference signal is being used for regulation, it is customary to display the corresponding absorption-mode signal on a meter or similar display device. The peak height of the absorption-mode signal provides a very convenient method of monitoring the resolution, provided that the system is locked. When the linewidth is narrowed by adjustment of the field correction coils (a task usually known as 'shimming' the magnet), the peak signal increases accordingly. This proves to be a surprisingly effective procedure, even though in principle a reduction in width at half height does not necessarily go hand-in-hand with an increase in peak height. Gradients that are predominantly along the Z axis are adjusted with the sample spinning, whereas the transverse gradients are optimized with a stationary sample. Most automatic 'shimming' programs also monitor the peak height of the reference line.

Since any noise on the reference line is necessarily converted into instability of the field/frequency ratio, it is preferable to choose a solvent with a strong deuterium signal and an inherently narrow line. (Heavy water is unsuitable since it has an appreciable temperature-dependent chemical shift.) Fortunately the quadrupole moment of deuterium is very small, and the spin–spin relaxation* times of the commonly used deuterium solvents are sufficiently long for the purpose (the natural linewidths are very narrow). However, at very high applied fields we must be aware of the possibility of a slight splitting of the reference line through the interaction of the deuterium quadrupole moment with the electric field gradient in the molecule (2). At high magnetic field there is a slight degree of molecular alignment and the quadrupole interaction is not quite averaged to zero as it would be in a truly isotropic liquid.

Occasionally some spectrometer operations can perturb the field/frequency lock condition. For example, field gradient pulses may also interfere with the deuterium reference signal, particularly if eddy currents are induced in the surrounding conductors. Under such circumstances it may be necessary to inhibit the regulator loop momentarily while the gradients are applied, using a sample-and-hold circuit. During certain heteronuclear double-resonance experiments with intense B_2 fields, the Bloch–Siegert effect* may be large enough to disturb the deuterium resonance condition and upset the field/frequency regulation. For example, a decoupler field $\gamma B_2/2\pi = 6$ kHz applied to carbon-13 (at 100 MHz) shifts the deuterium resonance (at 61 MHz) by almost 0.5 Hz.

There is another significant perturbation from a source that is widely overlooked. The bulk nuclear susceptibility effect of a sample of high proton density (e.g. water) cannot be neglected at present magnetic field strengths (3). Unlike the electronic bulk susceptibility which can be ignored because it remains constant, the nuclear susceptibility is destroyed by saturation or reversed in sign by spin inversion. For a cylindrical sample, inversion of the water signal suddenly shifts the field by as much as 2.7 parts in 10^9. This can cause a transient perturbation of the regulation circuit, but once the deuterium lock has settled, the field/frequency ratio is unaffected.

REFERENCES

1. H. Primas, *Fifth European Congress on Molecular Spectroscopy*, Amsterdam, 1961.
2. A. A. Bothner-By, C. Gayathri, P. C. M. van Zijl and C. MacLean, *J. Magn. Reson.* **56**, 456 (1984).
3. H. T. Edzes, *J. Magn. Reson.* **86**, 293 (1990).

Cross-references

Bloch–Siegert effect
Nuclear susceptibility
Sample spinning
Spin–spin relaxation

Fourier Transformation

Some years ago it was considered something of an art-form to demolish a grand piano with a sledgehammer. In the vocabulary of NMR this would be known as the impulse response, while the more usual note-by-note excitation would be the equivalent of slow-passage (digitized) frequency sweep. Unlike the piano, the nuclear spins recover from a pulse in a few seconds and may then be excited again. Ernst and Anderson (1) showed that this gives an enormous improvement in the sensitivity of the NMR method, and opens up a wealth of new transient experiments, so that now essentially all NMR spectrometers operate in the pulse-excited mode.

The sensitivity advantage arises because the sweep method excites only one resonance line at a time, whereas the pulse method excites all resonances simultaneously. This can be appreciated by consideration of the motion of the nuclear magnetization vectors in the presence of a strong radiofrequency pulse

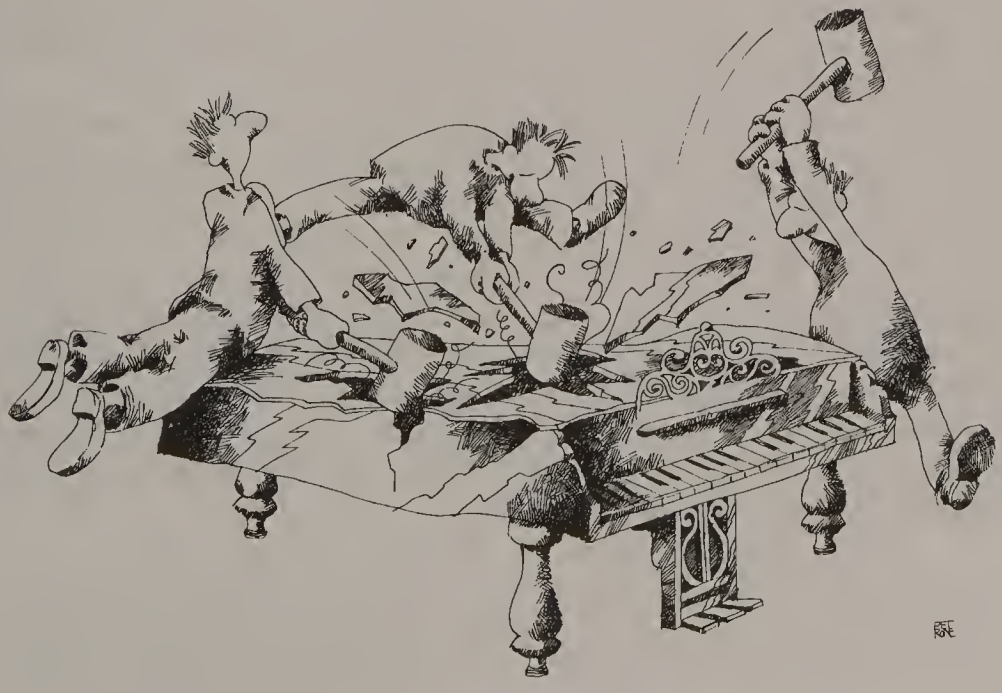

acting in the rotating frame*. The resulting sensitivity gain, known to infrared spectroscopists as the 'Fellgett advantage' (2), can be predicted approximately using the principle that signal-to-noise increases as the square root of the number of independent signals that are added together.

Suppose that a typical line in the spectrum has a width Δ given by $1/(\pi T_2^*)$ Hz, where T_2^* is the decay time constant due to instrumental effects. Consider first the case where the slow passage condition is satisfied, the sweep rate being adjusted so that a time nT_2^* is taken to sweep through a single resonance line (n being a small number, say 2 or 3). If the total sweep width to be covered is F Hz then this experiment requires a total time of nT_2^*F/Δ seconds. In order to achieve comparable resolution in the pulse mode, it is necessary to sample each transient for a time long compared with T_2^*, say nT_2^* s, where n is again 2 or 3. However, in the long time taken by the sweep experiment it is possible to repeat the pulse experiment N times and to add the N transient signals together in registration. Thus, by equating the total times required by the two experiments,

$$nT_2^*F/\Delta = NnT_2^*$$

$$N = F/\Delta.$$

The repeated pulse experiment consequently shows a sensitivity improvement of $N^{1/2} = (F/\Delta)^{1/2}$. For a typical carbon-13 spectrum F could be as large as 40 kHz and Δ might be 1 Hz, giving more than two orders of magnitude sensitivity advantage for the pulse mode.

In practice, the proper digitization of such a spectrum would require well over 40 000 words of data storage, which is not always available. Moreover, there is a significant improvement in sensitivity to be gained in the sweep experiment by violating the slow-passage condition to some extent, thus sacrificing some resolving power. These factors make the 'Fellgett advantage' rather lower than calculated above, although the order of magnitude is still correct.

A piano certainly sounds more pleasant played in the 'continuous-wave' mode and NMR spectroscopists find that the interpretation of a frequency-domain spectrum is far easier than attempting to disentangle all the component frequencies of the transient free induction decay* after a radiofrequency pulse; yet the information content is the same. Indeed, the time-domain signal is related to the slow-passage frequency-domain spectrum by the process of Fourier transformation.

High-resolution pulse spectrometers are therefore known as Fourier transform spectrometers, this transformation facility being essential. This necessarily involves temporary storage of the time-averaged free induction signal; hence the process of digitization*. Two methods are available for Fourier transformation: the *spectrum analyser* and the discrete Fourier transform.

THE SPECTRUM ANALYSER

While this method is now hardly ever used in practice, it is important in that it provides some insight into the process of Fourier transformation. The spectrum analyser (or wave analyser) is a device which accepts a complex waveform S(t), examines the intensities of the various sine waves that may be said to make up the input waveform and presents the result in the form of a graph of intensity against frequency S(f). S(f) is the Fourier transform of S(t).

One implementation of this method is illustrated in Fig. 1. The waveform S(t) is stored digitally and read repetitively into a synchronous detector, basically an amplifier with significant gain only near the reference frequency f_r. This device measures the content of S(t) carried at or near the frequency f_r, and represents the result as a point on the frequency-domain spectrum S(f). Then f_r is incremented and the waveform S(t) is again read into the synchronous detector, giving the next point in the spectrum S(f). The method is thus intrinsically discrete, but carries the advantage that the frequency steps may be made arbitrarily small, giving very fine digitization. The first computer programs used for Fourier transformation used a similar step-by-step examination of the waveform S(t) to find one frequency component at a time. These programs could take as long as 20 minutes to perform the Fourier transformation and were soon superseded by the Cooley–Tukey algorithm* (3).

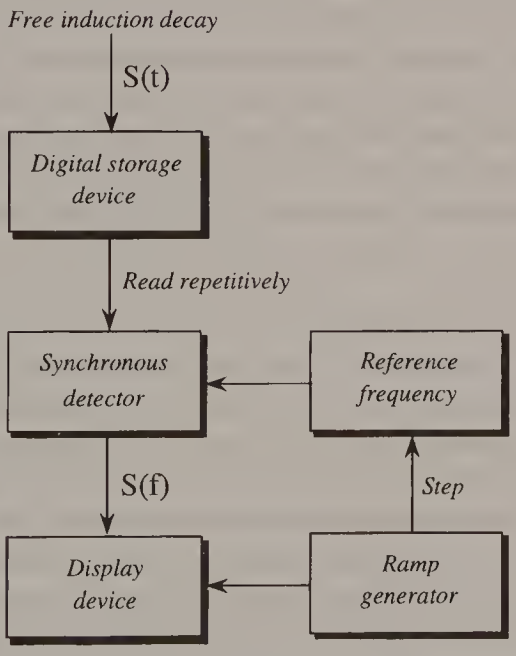

Fig. 1. Discrete Fourier transformation as implemented in a spectrum analyser or wave analyser. Digitization in the frequency domain may be as fine as desired, but each point involves a separate operation of reading the free induction decay into the synchronous detector.

Since the spectrum analyser method of Fourier transformation requires a multichannel storage device essentially equivalent to a minicomputer, it turns out to be quicker and more convenient to calculate the transforms in a computer; essentially all the commercial Fourier transform spectrometers have adopted this method.

ARTEFACTS IN THE TRANSFORMED SPECTRUM

It is important for the NMR user to be aware of the possible artefacts which may appear in the final frequency-domain spectrum. Most of these may be attributed to improper handling of the free induction signal before the transformation, and some of these are treated in more detail in the section 'Digitization'.

Both the analogue-to-digital converter and the computer storage word have finite dynamic range, leading to the possibility of clipping the free induction signal. The principal result of this non-linear process is to introduce harmonics and sums and differences of NMR frequencies into the spectrum, together with some baseline distortion (see below). If the incoming free induction decay is scaled down to avoid clipping, then the digitization errors of the analogue-to-digital converter introduce *digitization noise* into the spectrum and this may obscure the very weak signals.

The sampling theorem requires that there should be at least two sampling points per period of the highest frequency component of the free induction signal. If this condition is violated, then some high-frequency resonances are aliased. The sampling rate may be said to define a spectral window which should encompass all the NMR lines of the spectrum. Continuous-wave spectroscopy* with an insufficiently wide sweep runs the risk of losing certain resonances; in Fourier transform spectroscopy these resonances are aliased into the spectral window and appear at the wrong frequencies. This is an ever-present danger in the interpretation of spectra from unknown compounds. High-frequency noise may also be aliased in this way and it is important to remove it with a suitable low-pass filter *before* the free induction signal is sampled, otherwise the sensitivity is unnecessarily impaired.

Because of instrumental shortcomings, the free induction signal entering the analogue-to-digital converter is not always exactly balanced about zero volts. After Fourier transformation, this d.c. offset gives rise to a spurious spike in the frequency-domain spectrum at zero frequency, a particularly unfortunate artefact when quadrature detection* is employed. If such an unbalanced free induction decay is multiplied by a sensitivity enhancement weighting function, the spike is broadened and affects several data points near zero frequency. In order to remedy this effect, many computer programs calculate the mean value of the free induction signal (or the last section of it) and subtract it from all the data points before any weighting function is applied.

A sensitive NMR receiver requires a finite time to recover from the effects of a strong radiofrequency pulse, although, like a radar receiver, it is gated off at the

time of the pulse. The practical result is that the receiver gain may vary somewhat during the acquisition of the first few points of the free induction decay. This has come to be called *pulse breakthrough.* If only the very first data point is falsified, this displaces the baseline of the frequency-domain spectrum, a relatively trivial matter, even when the spectrum is to be integrated. However, if the next data points are significantly affected, this distortion transforms into a rolling baseline corresponding to the introduction of spurious low-frequency sine waves. One solution is to delay acquisition until the receiver has recovered, but this introduces a frequency-dependent phase shift into the spectrum which must be corrected by the phasing routine. An alternative remedy is to apply a baseline correction to the frequency-domain spectrum. The third possible approach is to apply a 180° pulse in order to generate a spin echo*, all frequency components being brought back into phase at a time when the receiver has recovered from the two pulses. This method has serious complications for proton spectroscopy where there are homonuclear spin–spin couplings which modulate the echo, but is satisfactory for carbon-13 spectroscopy where homonuclear coupling can be neglected. Note that none of these solutions is really suitable when there are very broad NMR lines in the spectrum.

NMR pulse experiments should be repeated as rapidly as possible if high sensitivity is required. This often entails a compromise with resolution requirements, such that the free induction signal is truncated before the decay is complete. When the technique of zero filling* is used, this gives a step function discontinuity in the envelope of the free induction decay. Resolution enhancement* shaping functions may exaggerate this discontinuity. Since the Fourier transform of a step function is a sin x/x function, this introduces some sin x/x character into the frequency-domain lineshape, the degree depending upon the severity of the time-domain discontinuity. It is therefore important to 'round off' this step in the envelope by means of an apodization* function which affects only a section of the data table just before the discontinuity, or more effectively, by a sensitivity enhancement* weighting function modifying the entire data table.

A digital computer necessarily introduces round-off errors in the calculation, which are aggravated when there is a cascade of operations as in Fourier transformation. Normally, these errors are outweighed by the noise present on the NMR signals and no harm is done. However, if time averaging is continued to the point where dynamic range is beginning to be limited by the computer word length (the noise level being reduced to the level of one bit) then these round-off errors in the transformation program become significant. Furthermore, these errors cannot be treated as noise and reduced by time averaging several frequency-domain spectra, since under these conditions the round-off errors are coherent from one Fourier transform to the next. This is most probably the reason why very protracted time-averaging experiments sometimes fail to yield the expected $N^{1/2}$ improvement in signal-to-noise ratio. The remedy is to use double-precision arithmetic or a floating-point Fourier transform program.

REFERENCES

1. R. R. Ernst and W. A. Anderson, *Rev. Sci. Instrum.* **37**, 93 (1966).
2. P. Fellgett, Ph.D. Thesis, Cambridge University (1951).
3. J. W. Cooley and J. W. Tukey, *Math. Comput.* **19**, 297 (1965).

Cross-references

Apodization
Continuous-wave spectroscopy
Cooley–Tukey algorithm
Digitization
Free induction decay
Quadrature detection
Resolution enhancement
Rotating frame
Sensitivity enhancement
Spin echoes
Zero filling

Free Induction Decay

The response of a nuclear spin system to a radiofrequency impulse is known as the 'free precession signal' or the 'free induction decay' and is of fundamental importance because its Fourier transform is the frequency-domain high-resolution spectrum. It is here that the Bloch vector model* is useful. Instead of considering individual nuclear spins obeying the laws of quantum mechanics, Bloch (1) showed that it is sufficient to focus attention on the net macroscopic nuclear magnetization obtained by taking the ensemble average over all the spins. This macroscopic magnetization obeys the laws of classical mechanics in its interaction with the applied static and radiofrequency fields, while the effects of spin–spin and spin–lattice relaxation may be accounted for phenomenologically by the introduction of simple damping terms into the Bloch equations (1). For the pulse excitation used in Fourier transform spectrometers, the transient solutions of the Bloch equations are used. For the older continuous-wave spectrometers, the more complicated steady-state solutions are required. The Bloch equations take on a particularly simple form when described in a reference frame* rotating in synchronism with the radiofrequency field B_1.

The high-resolution NMR spectroscopist tends to generalize this picture to the case of systems with many different chemical shifts, and with spin–spin couplings. Most of the observed NMR phenomena can be accounted for on the assumption that each individual resonance in the high-resolution spectrum can be represented by a vector M with a characteristic intensity and a characteristic precession frequency. Each such vector M is assumed to obey the Bloch equations. Difficulties can arise when the spins are subjected to more than one radiofrequency pulse, for example when multiple-quantum coherence is involved.

For a spin system that has been allowed to reach Boltzmann equilibrium, all these vectors are aligned along the Z axis of the rotating frame, and a 90° radiofrequency pulse rotates them about the X axis, leaving them along the Y axis. For the purposes of this section it is convenient to assume that the pulse is 'perfect' in that it affects all parts of the effective sample volume uniformly, and that its action is independent of the offset of a given line from the transmitter frequency. The reference phase of the receiver is usually taken to be such as to detect the Y magnetization in phase. Thus the signal intensity immediately after the pulse is at its maximum value. In fact, this first ordinate of the free induction decay represents the integral of the total intensity in the absorption spectrum.

The individual magnetization vectors are then free to precess at their characteristic frequencies, generating an interference pattern. (This has led some spectroscopists to refer to free induction decays as interferograms by analogy with the infrared experiment.) In a very simple case, such as the familiar 1:3:3:1 quartet, the beat pattern itself may be recognized (see Fig. 1) and the frequency difference measured directly, but in the general case the pattern is not decipherable by inspection and a Fourier transform must be computed. When there are both strong and weak components present in the free induction decay the dynamic range of the detection equipment must be sufficiently high to handle both adequately. This contrasts with continuous-wave spectroscopy where the strong and weak signals are not usually riding on top of each other, so the weak signal can be examined while the strong signal is being truncated.

The envelope of the free precession signal decays with time, in many cases falling to a negligible level before acquisition is stopped. This is a result of spin–spin relaxation* and the mutual interference between macroscopic signals from different regions of the sample due to the inhomogeneity of the field B_0. Residual instabilities in the field/frequency regulation may also contribute to this decay, particularly if several sequential free induction signals are being summed together. For a single line, the Fourier transform of this envelope determines the frequency-domain lineshape. For example, an exponentially decaying envelope gives a Lorentzian lineshape. The common practice of imposing an exponential envelope on the free induction signal for the purposes of sensitivity enhancement*

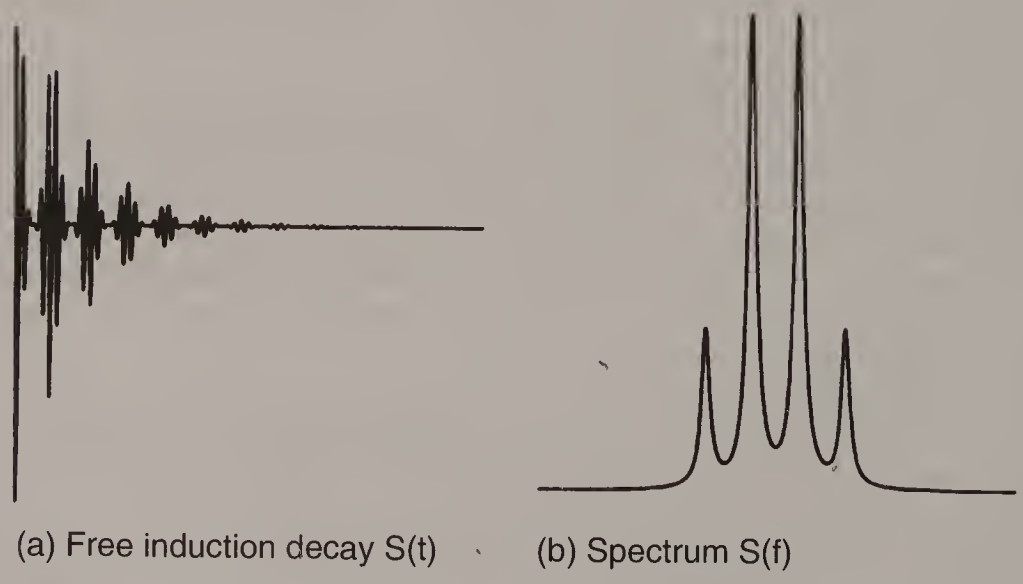

Fig. 1. (a) A free induction decay S(t), and (b) its Fourier transform S(f). In practice, S(t) was extended to four times its length by zero filling in order to improve the digitization of S(f).

introduces a strong Lorentzian character on the spectral lines. For the purposes of high resolution in spectra of many overlapping lines, a Gaussian shape might be preferable since it falls off more rapidly in the skirts of the line. Because of this Fourier transform relationship between the envelope of the free induction decay and the lineshape in the frequency domain, a slowly decaying free precession signal gives a narrow line. High resolution therefore requires a long acquisition time; early termination of the free induction decay will broaden and distort the lines. Thus by setting a lower limit on the interval between excitation pulses, high resolution competes with the requirements of high sensitivity. Artificial techniques for slowing down the decay come under the heading of resolution enhancement*.

Most modern NMR spectrometers acquire two free induction signals simultaneously by having two synchronous detectors operators in quadrature. This makes it possible to determine the signs of the precession frequencies in the rotating frame, thus removing any ambiguity about whether a given resonance is at a higher or lower frequency than the transmitter. (See Quadrature detection*.) Sensitivity is increased by a factor $2^{1/2}$ by this techniques, and it allows the transmitter frequency to be set in the centre of the spectrum, thus using the pulse intensity more effectively.

ABNORMALITIES IN THE FREE INDUCTION SIGNAL

Some distortions of the free induction decay may be ascribed to shortcomings of the detection scheme, for example receiver dead time or improper sampling; these are treated under Fourier transformation* and Digitization*. Quite another type of problem can arise because of the physics of the excitation process, and this is treated below.

Under ideal operating conditions, the interval between successive pulse excitations would be long compared with all relaxation times. In practice, sensitivity considerations rule out such an extravagant mode of operation, the normal practice being to excite the spins again as soon as a free induction decay of sufficient length has been acquired. This gives rise to the possibility of steady-state effects* which may be divided into those concerned with longitudinal magnetization (pulse interval comparable with T_1), and those concerned with transverse magnetization (pulse interval comparable with T_2). Needless to say, both types of steady-state effects tend to occur together since T_1 and T_2 tend to be closely related in liquid samples used for high-resolution work.

Repetition of the pulse excitation at a rate comparable with the rate of spin–lattice relaxation sets up a steady-state Z magnetization which is weaker than the equilibrium magnetization M_0; this is the equivalent of saturation in continuous-wave spectroscopy. It causes both loss of overall intensity and variations in relative intensities within a given spectrum if the individual spin–lattice relaxation times differ. In fact, this technique can be made the basis of a method for determining the spin–lattice relaxation times (2). As a consequence,

considerable care should be exercised when using relative intensities for quantitative measurements if the free induction decays were obtained under steady-state conditions. Usually, a second experiment at a different repetition rate will resolve any doubts about the reliability of the relative intensity measurements.

Steady-state effects on transverse magnetization are more complex. A free precession signal which has started to decay owing to field inhomogeneity may be seen to refocus again into a spin echo*. This can be seen in terms of spin *isochromats* (signals from small volume elements of the sample), each isochromat having a slightly different precession frequency because that volume element sits in a slightly different applied field B_0. In the steady-state regime, a vector representing a given ischromat is not aligned along the Z axis at the time of the pulse but has a significant X–Y component. The pulse rotates this vector about the X axis, maintaining the same X component and changing the Y component in the same way as for all other isochromats. Since the individual vectors have a particular phase relationship immediately after the pulse, they must also have a very similar phase relationship just before the pulse. Free precession trajectories are thus constrained by the steady-state requirements so that refocusing occurs. Since the actual trajectory depends quite strongly on offset from the transmitter, the lines in the final spectrum exhibit anomalies in phase and intensity which themselves depend on offset (3). These anomalies can be avoided by introducing a small random variation in the interpulse interval, or by a suitable phase-cycling* technique.

WHAT IS A FREE INDUCTION DECAY?

There are difficulties in attempting to apply the spectroscopic concepts of stimulated absorption, stimulated emission or spontaneous emission to the free precession signal following a radiofrequency pulse. Spontaneous emission probabilities are known to depend on the cube of the radiation frequency, and for NMR are known to be quite negligibly small (one event in 10^{23} seconds for a typical example). Continuous-wave spectroscopy may be discussed in terms of stimulated absorption of energy by the nuclei, but during a free induction decay there is no applied radiation field to stimulate either absorption or emission. Furthermore, this signal is detected in many cases while the populations of upper and lower energy levels are equal. Hence the importance of Bloch's concept of *nuclear induction* – a concerted motion of the individual nuclear spins, generating a current in the receiver coil according to the well-known laws of electromagnetic induction. Immediately before the excitation pulse there is a very small excess spin population Δ in the lower energy level, but no phase coherence between the precession of individual spins. There is thus a very small longitudinal magnetization M_0 which can induce no signal in the receiver coil. Now a radiofrequency pulse acts on each spin independently, rotating it about the X axis

of the rotating frame. When we consider the ensemble of spins in the sample, the net effect is to rotate the macroscopic magnetization M_0 away from the Z axis towards the Y axis. The existence of a macroscopic magnetization M_Y can be rationalized by saying that the pulse has induced a small degree of phase coherence into the previously random motion of the individual precessing spins.

Viewed in the laboratory frame, M_Y is precessing at the Larmor frequency and cuts the turns of the receiver coil, inducing a voltage at this frequency. Under most high-resolution conditions the induced signal is very weak, but at high fields and with strong samples, this induced signal generates a rotating magnetic field strong enough to affect the motion of the nuclei, as in a continuous-wave experiment. This radiation damping* effect broadens the lines involved.

It is important to bear in mind that in many high-resolution situations, the concerted precession of the nuclear spins usually persists for considerably longer than the observed free induction decay. This is because the 'phase memory time' or spin–spin relaxation time may well be of the order of 10 seconds, while the decay time constant due to field inhomogeneity T_2^* would normally be of the order of 1 second. Certain NMR techniques involve the application of B_0 field gradients which are often said to 'destroy' transverse nuclear magnetization. Actually, they only disperse the isochromats from different sample regions, and the possibility always remains that these isochromats may be refocused into a spin echo, if the spin–spin relaxation time is long. This is the origin of one of the steady-state effects described above.

REFERENCES

1. F. Bloch, *Phys. Rev.* **102**, 104 (1956).
2. R. Freeman and H. D. W. Hill, *J. Chem. Phys.* **54**, 3367 (1971).
3. R. Freeman and H. D. W. Hill, *J. Magn. Reson.* **4**, 366 (1971).

Cross-references

Digitization
Fourier transformation
Phase cycling
Quadrature detection
Radiation damping
Resolution enhancement
Rotating frame
Sensitivity enhancement
Spin echoes
Spin–spin relaxation
Steady-state effects
Vector model

Hartmann–Hahn Experiment

The nuclear spin has been likened to a spy insinuated into a molecule to report information about the local electronic structure, using a radio transmitter at the Larmor frequency. In a given organic molecule there are several such spies, all capable of communicating with the outside world but unable to talk to each other because their transmitters operate on different frequencies. The Hartmann–Hahn experiment is designed to circumvent this problem by providing several nuclei with a common communication frequency.

The original Hartmann–Hahn experiment (1) is a solid-state technique for sensitivity enhancement of a nuclear species S of low natural abundance, by cross-polarization with a much more abundant species I. The I nuclei are strongly interacting, having a short spin–spin relaxation time and a long spin–lattice relaxation time; it is therefore permissible to describe them by a 'spin temperature' which may differ from the temperature T_0 of the lattice. When they are spin locked along a radiofrequency field B_1 they have a very low spin temperature T_0B_1/B_0, since they possess an intense polarization in a relatively weak field $B_1 << B_0$. On the other hand, the S spins are very 'hot' because they are deliberately saturated. Thermodynamic contact is made between I and S by applying radiofrequency fields B_1 and B_2 with intensities that satisfy the Hartmann–Hahn condition

$$\gamma_I B_1 = \gamma_S B_2 \qquad [1]$$

where the I-spin precession is considered in a frame synchronized with the B_1 field, and the S-spin motion in a frame synchronized with the B_2 field. This provision of a common 'communication frequency' allows energy-conserving 'flip-flop' processes to take place through the mutual dipole–dipole interaction. The 'cold' I spins interact with the 'hot' S spins, cooling them down (increasing their polarization). This transfer may be detected either as a slight loss of I-spin polarization or as a slight gain in S-spin polarization. Because the I spins are far more abundant, they act as a thermal reservoir, only slightly affected by the modest amounts of polarization transferred to the rare S spins. Consequently, the detected signals can be enhanced by performing multiple Hartmann–Hahn contacts. This technique is now widely employed in high-resolution solid-state NMR for sensitivity enhancement, often in combination with magic-angle spinning.

HETERONUCLEAR CROSS-POLARIZATION IN LIQUIDS

A short section of the original Hartmann–Hahn paper (1) describes a related *liquid-phase* experiment that has important implications for coherence transfer in high-resolution spectroscopy. However, the mechanism is rather different. In the liquid-phase experiment there is no I-spin thermal reservoir, the interaction between I and S is the scalar spin–spin coupling J_{IS} rather than the dipole–dipole interaction, and it is no longer correct to use the concept of spin temperature because the spin–spin and spin–lattice relaxation times are comparable. Nevertheless, the key is still the Hartmann–Hahn matching condition, where there are equal rates of precession in the respective rotating frames. Note that the matching condition can be degraded by spatial inhomogeneity in the B_1 and B_2 fields, since they are generated in different transmitter coils. For this heteronuclear case, liquid-phase cross-polarization can exploit a population advantage to improve the sensitivity of the low-abundance species (2). For example, polarization transfer* from protons to carbon-13 enjoys a leverage of $\gamma_H/\gamma_C = 4$. The efficiency of transfer falls off unless any mismatch of the Hartmann–Hahn condition is kept small compared with the spin–spin coupling $|J_{IS}|$; thus polarization is rather easily transferred through one-bond C–H couplings but less effectively through long-range couplings. Cross-polarization by this method has about the same efficiency as the INEPT scheme (3).

HOMONUCLEAR CROSS-POLARIZATION IN LIQUIDS

In practice the technique has found much wider use, not as a sensitivity enhancement scheme, but as a correlation method in *homonuclear* spin systems in the guise of the well-known TOCSY (4) or HOHAHA (5) experiment. Consider the simplest case of two protons I and S coupled by a spin–spin interaction J_{IS}. The usual weak-coupling Hamiltonian is written

$$\mathcal{H} = \omega_I I_Z + \omega_S S_Z + 2\pi J_{IS} I_Z S_Z. \qquad [2]$$

Spin locking of both I and S while satisfying the Hartmann–Hahn condition corresponds to a mixing Hamiltonian of the form

$$\mathcal{H}_m = 2\pi J_{IS} (I_X S_X + I_Y S_Y + I_Z S_Z). \qquad [3]$$

The Zeeman terms have been removed but the coupling terms are now 'isotropic'. Under these conditions the spin system evolves in *collective spin modes* such as

$$\Sigma = (I_Y + S_Y)/2 \quad \text{and} \quad \Delta = (I_Y - S_Y)/2 \qquad [4]$$

instead of the more usual single spin modes. These resemble the collective motions (the 'normal modes') of a set of coupled mechanical oscillators. The sum term Σ remains invariant, but the difference term Δ evolves into antiphase terms of the form $(I_Z S_X - I_X S_Z)$ which are reconverted into $-\Delta$ after a half cycle of the oscillation.

If both I and S are prepared in exactly the same way before spin locking, for example if both magnetizations are aligned along the +Y axis, then no coherence transfer is observed, but if the system is unbalanced in some manner, for example by aligning the I spins along +Y but the S spins along –Y, then there is an oscillatory transfer of coherence between I and S which persists until damped by relaxation effects. Both spin–spin and spin–lattice relaxation mechanisms are involved.

One mode of operation employs a relatively intense spin-lock field B_1 that encompasses both the I and S resonances. In this case the coupling terms are isotropic, and one coherence transfer cycle is completed in a time $\tau = 1/J_{IS}$. In the general case there are appreciable offsets ΔB_I and ΔB_S and the Hartmann–Hahn condition should be written in terms of the two effective fields

$$\gamma(B_1^2 + \Delta B_I^2)^{1/2} = \gamma(B_1^2 + \Delta B_S^2)^{1/2}. \quad [5]$$

Note that the signs of ΔB_I and ΔB_S are irrelevant. Since there is a practical limit to the maximum B_1 field, it is difficult to avoid Hartmann–Hahn mismatch caused by off-resonance effects when a continuous spin-lock field is used. Fortunately the effective bandwidth can be considerably increased by using multipulse spin-locking sequences related to the well-known broadband decoupling* schemes (5–10). A comprehensive analysis of the various modulated spin-locking procedures has been presented by Ernst *et al.* (11).

If this isotropic mixing scheme is incorporated into a two-dimensional experiment, the unbalancing of the difference term Δ is achieved through differential precession of the I and S spins during the evolution period. Isotropic mixing then takes place for a period τ, which can no longer be optimized since a range of coupling constants is involved. Fourier transformation of the subsequent free induction decay generates a spectrum similar to conventional correlation spectroscopy (COSY) apart from two important features. First of all, the cross-peaks are all in phase and so there is no mutual cancellation when the coupling constant is comparable with the linewidth; this ensures better sensitivity in this situation. Second, coherence transferred from I to S may be passed on to further coupled spins R, Q, etc., in a sequence of steps, eventually involving all the spins in the coupled system; hence the name *total* correlation spectroscopy (4). At short spin-locking times τ, the transfer is essentially restricted to directly coupled spins as in the classic COSY technique (12), but for longer spin-locking periods the coherence spreads throughout the system; hence the term 'spin diffusion'. Multistep transfer necessarily reduces the intensities of the direct correlation peaks compared with those in the corresponding COSY spectrum, dissipating the coherence among more distant spins. A careful analysis of the evolution of TOCSY cross-peaks as a function of the spin-locking time gives useful information about the number of individual steps involved (13).

CONCATENATED COHERENCE TRANSFERS

An alternative mode of operation applies *selective* spin-lock fields B_1 and B_2 to I and S respectively. In this situation the equations of motion resemble those for the heteronuclear case; the coupling terms are no longer isotropic because the transverse components of I- and S-spin coherence go rapidly in and out of phase, halving the extent of the interaction, and doubling the period of the oscillation to $\tau' = 2/J_{IS}$.

Figure 1 illustrates the cyclic polarization transfer between protons in uracil. The I protons are spin locked along the field B_1 but the S protons are first prepared along the –Y axis before being spin locked in opposition to the field B_2. Acquisition of the free induction decay after spin locking for a time equal to the half period of the oscillation ($1/J_{IS}$ = 140 ms) shows a complete interchange between the two sites – the I signal is now inverted and the S signal is upright; both are in pure absorption. (For intermediate spin-locking times the detected signal contains an admixture of antiphase magnetization components.) After one complete cycle ($\tau' = 2/J_{IS}$) the inverted signal returns to site S and the upright signal to site I.

It is usually convenient to employ a one-way coherence transfer I $\rightarrow$ S by exciting only the I spins with a selective 90° pulse, followed by the application of separate spin-locking fields at the I and S sites. With a suitable phase cycle, this

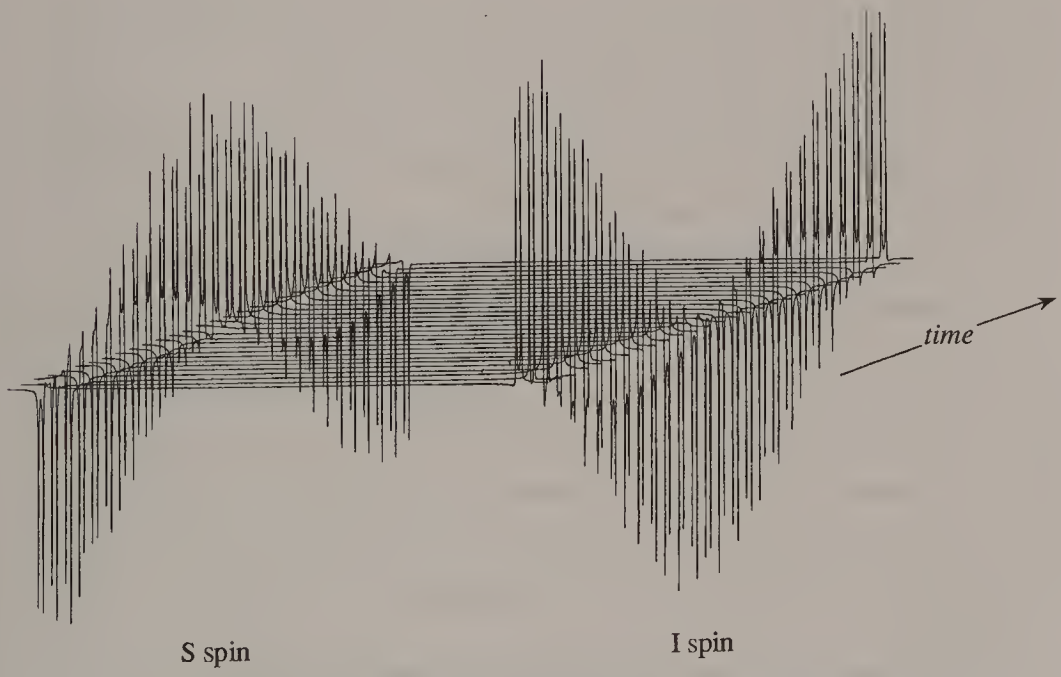

Fig. 1. Hartmann–Hahn coherence transfer between two protons in uracil (J_{IS} = 7.5 Hz). The S-spin response was initially aligned along the –Y axis with a selective 90° pulse and then separate spin-locking fields were applied at the two proton sites for a time τ ranging from 0 to 270 ms in 10 ms steps. The maximum transfer S $\rightarrow$ I and I $\rightarrow$ S occurs near τ = 140 ms.

doubly selective experiment gives very clean spectra, suppressing all responses save those arising from coherence transfer I → S. If the spin-locking period is set close to the condition $\tau' = 1/J_{IS}$ then essentially 100% of the coherence arrives at the S-spin site, provided that relaxation losses can be neglected. The stage is then set for a further coherence transfer S → R by applying spin-locking fields at sites S and R for a period $1/J_{SR}$, and the process can be concatenated for as many steps as relaxation losses allow (14–16). No coherence is 'wasted' in extraneous pathways or in back-transfer. Experimentally, as many as six consecutive Hartmann–Hahn transfers have been strung together along a chain of seven protons in sucrose octa-acetate (16). This can be a powerful test for discriminating between alternative candidates for a particular molecular structure. By adding a non-selective heteronuclear polarization transfer stage at the end of the chain, this can be used to identify the directly bound carbon-13 sites and thus trace the connectivity of the carbon atoms making up the backbone of the molecule (17).

REFERENCES

1. S. R. Hartmann and E. L. Hahn, *Phys. Rev.* **128**, 2042 (1962).
2. G. C. Chingas, A. N. Garroway, R. D. Bertrand and W. B. Moniz, *J. Chem. Phys.* **74**, 127 (1981).
3. G. A. Morris and R. Freeman, *J. Am. Chem. Soc.* **101**, 760 (1979).
4. L. Braunschweiler and R. R. Ernst, *J. Magn. Reson.* **53**, 521 (1983).
5. A. Bax and D. G. Davis, *J. Magn. Reson.* **65**, 355 (1985).
6. M. H. Levitt, R. Freeman and T. Frenkiel, *J. Magn. Reson.* **47**, 328 (1982).
7. A. J. Shaka, J. Keeler and R. Freeman, *J. Magn. Reson.* **53**, 313 (1983).
8. M. Rance, *J. Magn. Reson.* **74**, 557 (1987).
9. A. J. Shaka, C. J. Lee and A. Pines, *J. Magn. Reson.* **77**, 274 (1988).
10. M. Kadkhodaie, O. Rivas, M. Tan, A. Mohebbi and A. J. Shaka, *J. Magn. Reson.* **91**, 437 (1991).
11. M. Ernst, C. Griesinger, R. R. Ernst and W. Bermel, *Mol. Phys.* **74**, 219 (1991).
12. W. P. Aue, E. Bartholdi and R. R. Ernst, *J. Chem. Phys.* **64**, 2229 (1976).
13. C.-W. Chung, J. Keeler and S. Wimperis, *J. Magn. Reson. A* **114**, 188 (1995).
14. S. J. Glaser and G. P. Drobny, *Chem. Phys. Lett.* **184**, 553 (1991).
15. R. Konrat, I. Burghardt and G. Bodenhausen, *J. Am. Chem. Soc.* **113**, 9135 (1991).
16. Ē. Kupče and R. Freeman, *J. Magn. Reson.* **100**, 208 (1992).
17. Ē. Kupče and R. Freeman, *Chem. Phys. Lett.* **204**, 524 (1993).

Cross-references

Broadband decoupling
Polarization transfer
Rotating frame
Spin locking
Two-dimensional spectroscopy

Intensities

High-resolution NMR possesses the very valuable property that the intensity of a given line is proportional to the number of nuclei contributing to that line, provided that certain instrumental precautions are taken. This allows a quantitative determination of the relative amounts of two substances present in the sample, and the measurement can be made effectively absolute by adding a carefully measured concentration of one of these substances followed by a second recording of the spectrum. This property may also be used as an assignment technique by counting the number of equivalent protons giving rise to a given resonance line and thereby identifying, for example, a methyl group.

Intensity is measured by the area under the line. In situations where all the lines in the spectrum have the same width and shape, peak heights may be used as a simpler measure of intensity, but in general it is safer to measure the area by means of integration (see below). In the case of only partially resolved lines, some method of decomposition into the individual constituents is required, which may involve curve fitting through a computer program.

The precautions necessary in order to ensure reliable intensity measurements are listed below.

(1) A slow-passage spectrum is recorded, as otherwise the lines are distorted and the intensities become functions of the relaxation times. Fortunately, Fourier transform spectra are equivalent to slow-passage spectra except in very unusual circumstances.

(2) No significant saturation is allowed to occur. For slow-passage continuous-wave spectrometers (see Continuous-wave spectroscopy*) this means ensuring that $\gamma^2 B_1^2 T_1 T_2 \ll 1$ for all lines in the spectrum; for Fourier spectrometers this requires a long waiting time between 90° pulses (T of the order of $5T_1$). (See Steady-state effects*.)

(3) In pulse Fourier transform spectrometers, no appreciable steady-state transverse magnetization is set up, since this leads to anomalies in phase and intensity which vary in a cyclic fashion across the spectrum. This can be a problem if the interval between pulses is shorter than, or comparable with, T_2, the spin–spin relaxation* time. One remedy is to introduce a short random timing delay between excitation pulses (1).

(4) If pulse excitation is used, then the excitation is uniform across the entire spectrum. This requires that the intensity of the pulse be high enough that

$B_1 >> |\Delta B|$, the offset of the resonance line furthest from the transmitter frequency. Quadrature phase detection* helps somewhat in that it allows the transmitter frequency to be set near the centre of the spectrum.

(5) The low-pass filters used in Fourier spectrometers in order to avoid aliasing of noise should have a flat response over the frequency range of interest. These filters sometimes encroach at the ends of the spectrum, reducing the intensities there. Digital filters are much better in this respect.

(6) For the observation of nuclei such as carbon-13 where there may be differential nuclear Overhauser enhancements, the effect is quenched by adding suitable relaxation reagents (2), or is suppressed by gating the proton decoupler off in the period immediately before the carbon excitation pulse.

(7) The entire spectrum is correctly phased for the absorption-mode signal. This is a routine adjustment in a Fourier transform spectrometer, but it is particularly important when measuring integrals.

(8) Nothing must be allowed to falsify the early part of the free induction decay. Thus pulse breakthrough must be prevented. Only well-behaved weighting functions should be used – those which do not alter the initial value of the free induction decay. *Convolution-difference* or *pseudo-echo* weighting functions (3) should be avoided in this context.

(9) The spectrometer response must be linear. Problems arise when the signals span a large dynamic range, giving difficulties with amplification and analogue-to-digital conversion.

(10) Sampling in the frequency domain should be sufficiently fine in comparison with the linewidths and there should be adequate digitization* of the intensity ordinates. Sometimes an interpolation routine may be required.

(11) For carbon-13 spectroscopy, or for any nuclear species that requires broadband heteronuclear decoupling, the decoupling efficiency should be essentially uniform over the appropriate frequency range. This suggests the use of the new broadband decoupling* methods.

It should be emphasized that these precautions are suggested for applications which demand accurate intensity comparisons; they are difficult to reconcile with sensitivity* considerations and some are therefore ignored in routine high-resolution spectroscopy. For example, carbon-13 spectra are often run under conditions where lines with long spin–lattice relaxation times are partially saturated. Indeed, the resulting low intensity is often used to recognize a quaternary carbon site. Similarly, it is not usual to sacrifice the advantage of the nuclear Overhauser effect in carbon-13 spectroscopy. The remaining precautions, however, incur very little penalty in routine operations.

Figure 1 shows the carbon-13 spectrum of p-ethoxybenzaldehyde obtained under conditions where the intensities are essentially uniform across the entire spectrum, allowing for the fact that there are two pairs of equivalent carbon sites (4).

INTEGRATION

There are several methods of measuring the area under a resonance line. The more primitive methods of counting squares on graph paper or electronic integration based on the charging of a capacitor have given way to summation of the digitized signal in the spectrometer computer. This is essentially adding together the ordinates of a histogram representing the spectrum.

The practical difficulties arise not from the process of integration itself but in eliminating sources of systematic error. The most serious of these is the difficulty in defining the baseline level of the spectrum. The integral is extremely sensitive to small changes in the baseline. The total integral of the entire spectrum is determined by the value of the first data point of the free induction decay; if this is falsified by 'pulse breakthrough' this introduees a spurious contribution to the mean baseline level of the resulting spectrum. The spectrometer computer can be instructed to examine regions of signal-free baseline near the ends of the spectrum and thus perform a baseline correction* to remove offset and tilt. More sophisticated programs can correct the low-frequency 'baseline roll' which sometimes occurs when the first few points of the free induction signal are in error. Integration errors arising from such baseline problems are reduced if the frequency range of the integration is carefully limited to the resonance line of interest. Accurate integration presupposes that the resonance lines are adequately sampled and digitized.

Some spectrometer computer programs incorporate these features and automatically print out integrals along with the line frequencies. Others give intensities in the form of peak heights, using some form of peak-finding routine (with a minimum threshold); this is clearly less satisfactory unless all lines have been broadened to the same linewidth. For measurements that are sensitive to

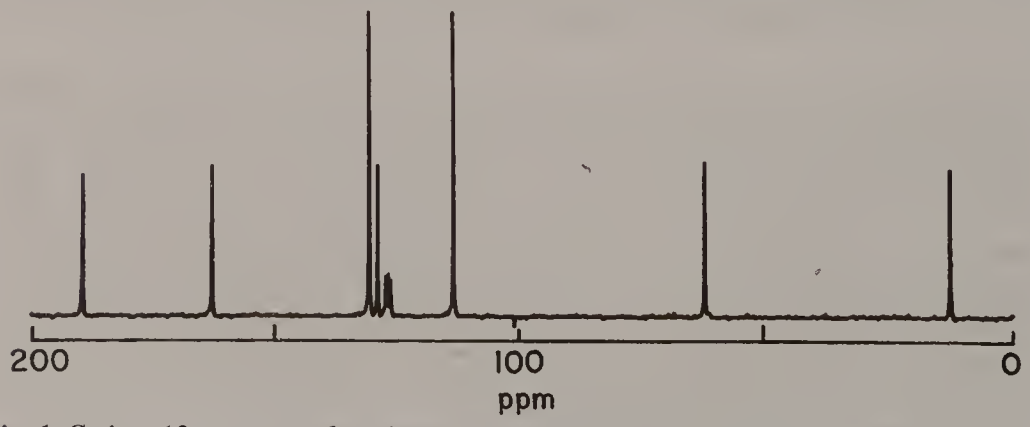

Fig. 1. Carbon-13 spectrum of p-ethoxybenzaldehyde after precautions have been taken to avoid all factors which perturb the intensities. Apart from the signal from the solvent $CDCl_3$, all the resonance lines have essentially equal intensities (two lines are doubly degenerate).

systematic error, in particular weak nuclear Overhauser enhancements or spin–lattice relaxation* studies based on a small number of measurements, a check should be made on exactly how the program handles intensity measurements.

Integration of peaks in two-dimensional spectroscopy* presents special difficulties. Data storage limitations for the two-dimensional array may impose quite coarse digitization in the two frequency dimensions and this reduces the accuracy of the integrals. Perhaps more serious is the problem of deciding just where to truncate the integration, since a relatively high proportion of the total intensity resides in the skirts of the line. In one-dimensional spectra the truncated portion is a small *area*, but in two-dimensional spectroscopy it is a *volume* encircling the peak, falling off only quite slowly with offset. Measurements of the nuclear Overhauser effect* (5) would appear to be particularly susceptible to this problem.

REFERENCES

1. R. Freeman and H. D. W. Hill, *J. Magn. Reson.* **4**, 366 (1971).
2. R. Freeman, K. G. R. Pachler and G. N. La Mar, *J. Chem. Phys.* **55**, 4586 (1971).
3. J. C. Lindon and A. G. Ferrige, *Prog. NMR Spectrosc.* **14**, 27 (1980).
4. M. H. Levitt, R. Freeman and T. Frenkiel, *Adv. Magn. Reson.* **11**, 47 (1983).
5. J. Jeener, B. H. Meier, P. Bachmann and R. R. Ernst, *J. Chem. Phys.* **71**, 4546 (1979).

Cross-references

Baseline correction
Broadband decoupling
Continuous-wave spectroscopy
Digitization
Nuclear Overhauser effect
Quadrature detection
Sensitivity
Spin–lattice relaxation
Spin–spin relaxation
Steady-state effects
Two-dimensional spectroscopy

J -spectroscopy

It would be a great simplification to be able to separate chemical shifts from spin–spin coupling effects. Spin echoes* offer the key to such a separation, because chemical shift effects are refocused by a 180° pulse, whereas spin–spin interactions, involving the bilinear term $J_{IS}I_ZS_Z$, are unaffected if the 180° pulse acts on both the I and S spins. Consider a spin-echo pulse sequence applied to a system of two weakly coupled spins, I and S. If the time evolution of the peak of the spin echo is monitored, it is found to carry an amplitude modulation $\cos(\pi J_{IS}t)$. In the more general case of several couplings there is a superposition of several such modulation terms and it is convenient to call the corresponding time-domain signal an *interferogram* in order to distinguish it from a free induction decay. Fourier transformation of this interferogram generates a new kind of spectrum which contains no chemical shift information but only spin–spin multiplets. We call this a 'J-spectrum'. It may be thought of as being derived from the conventional high-resolution spectrum by collapsing all the chemical shifts (but nevertheless retaining the weak-coupling approximation) so that the centres of all the spin multiplets converge at zero frequency. This point is a true zero frequency, not related to any chemical shift reference frequency. In principle the effects of magnetic field inhomogeneity are also refocused, and we might anticipate enhanced resolution within the J-spectrum, even approaching the limit set by the natural linewidths if molecular diffusion and spectrometer instabilities can be neglected. An example is provided by the proton J-spectrum of $CH_2Cl.CHCl_2$ (Fig. 1) where the highest-frequency line (from the CH group) is only 0.08 Hz wide (1). This is much narrower than the normal instrumental linewidth.

HETERONUCLEAR J-SPECTROSCOPY

One-dimensional J-spectra rapidly become too complex for general use, but the concept comes into its own with two-dimensional spectroscopy (2,3). Spin-echo modulation takes place during the evolution period t_1, and the detection period t_2 monitors the second half of the spin echo, which has essentially the same form as a conventional free induction decay. The pulse sequence may be written as

$$\begin{array}{lcl} \text{S spins:} & 90° - \tfrac{1}{2}t_1 - 180° - \tfrac{1}{2}t_1 - \text{acquire } (t_2) \\ \text{I spins:} & 180° \quad \text{decouple} \end{array} \qquad [1]$$

Note that the 180° pulse on the I spins is essential for echo modulation.

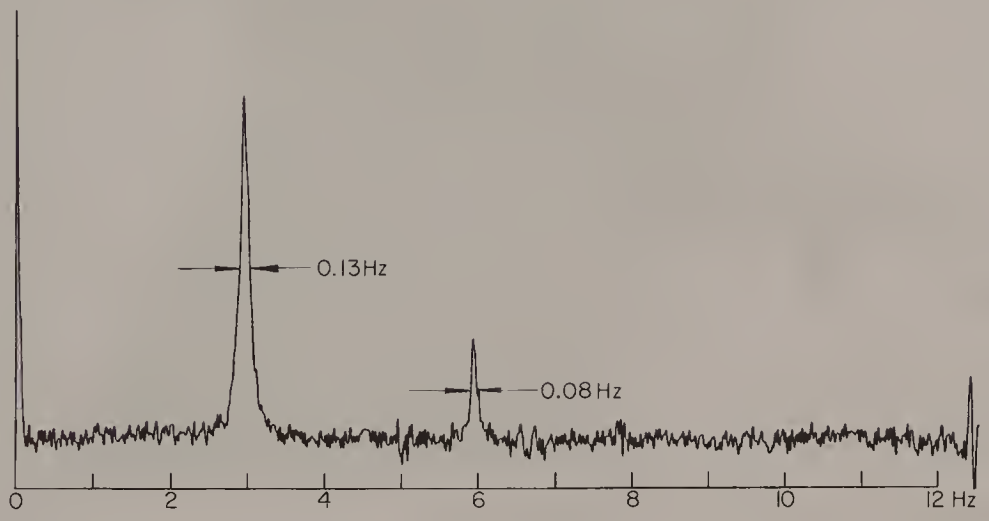

Fig. 1. One-dimensional J-spectrum of protons in 1,1,2-trichloroethane obtained by Fourier transformation of the spin-echo modulation. The spectrum is the superposition of a 1:1 doublet and a 1:2:1 triplet, but only positive frequencies are displayed. The coupling constant is 5.95 Hz.

Consider, as an example, the case where the I spins are protons and the S spins carbon-13. For each increment of the evolution time t_1, the second half of the carbon-13 spin echo is acquired, building up a two-dimensional time-domain matrix $S(t_1, t_2)$. Fourier transformation with respect to t_2 generates a series of carbon-13 spectra $S(t_1, F_2)$ that are amplitude modulated as a function of the evolution time. Figure 2 illustrates the simple case of signals from a methyl group, where the modulation function is $3\cos(\pi J_{IS} t_1) + \cos(3\pi J_{IS} t_1)$. Corresponding points are then extracted from each spectrum. If there is a signal present it appears as an interferogram carrying the modulation terms given above. Repeated Fourier transformation as a function of t_1 generates a two-dimensional spectrum $S(F_1, F_2)$. A typical result is the J-spectrum of carbon-13 in 2-(1-methylcyclohexyl) 4,6-dimethylphenol illustrated in Fig. 3. The spin multiplets are arrayed in the F_1 dimension, but separated in the F_2 dimension according to their respective chemical shifts. In this example fine digitization has been employed in the F_1 dimension so that long-range CH couplings are resolved. Alternatively, coarse digitization may be used, giving information about the number of directly attached protons, a form of multiplicity determination*.

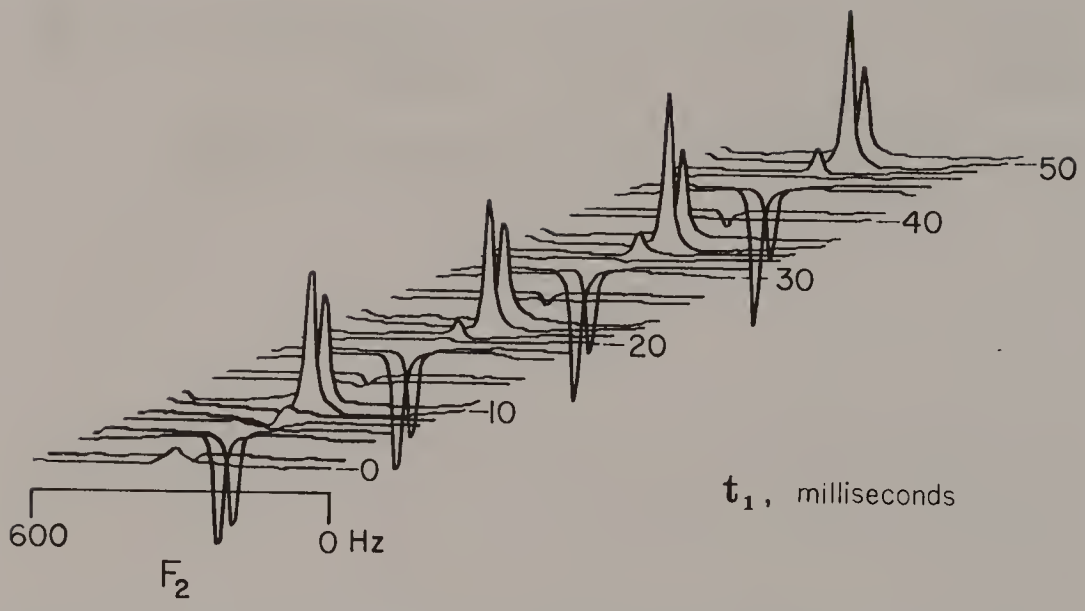

Fig. 2. J-modulation obtained by Fourier transformation of carbon-13 spin echoes from a methyl group. The spectra are displayed as a function of the evolution period t_1.

HOMONUCLEAR J-SPECTROSCOPY

When this scheme is applied to homonuclear coupled spin systems, the pulse sequence would be written as

I and S spins: $\quad 90° - \frac{1}{2}t_1 - 180° - \frac{1}{2}t_1 - \text{acquire } (t_2).$ [2]

The crucial difference is that no broadband decoupling is available during acquisition, so the F_2 dimension contains both shifts *and* couplings. Consequently the spin multiplets run along 45° diagonals rather like a half-open Venetian blind. An example is shown in Fig. 4 for the protons of a tricyclodecanone derivative. In principle this still offers a method of separation of chemical shifts from spin–spin splittings (4). Projections of the two-dimensional spectrum at 45° onto the F_2 axis would catch the multiplets in *enfilade*, leaving singlets at the chemical shift frequencies. The appropriate sections through the spectrum at 45° would give the spin multiplet structure for each chemically distinct site.

In practice this procedure is fraught with many difficulties. The most serious problem arises from the form of the two-dimensional response – the superposition of a two-dimensional absorption line on a (negative) two-dimensional dispersion line. This unusual 'phase-twist' lineshape is described in more detail in the section Lineshapes in two-dimensional spectra*. One curious property of a phase-twist response is that its 45° projection vanishes (5). This is surprising when one realizes that it implies that the 45° projections of a (positive) two-dimensional dispersion response and a two-dimensional absorption response must therefore be identical. There is a related problem when we attempt to record individual spin multiplets by taking 45° slices through the two-dimensional spectrum. Each line profile consists

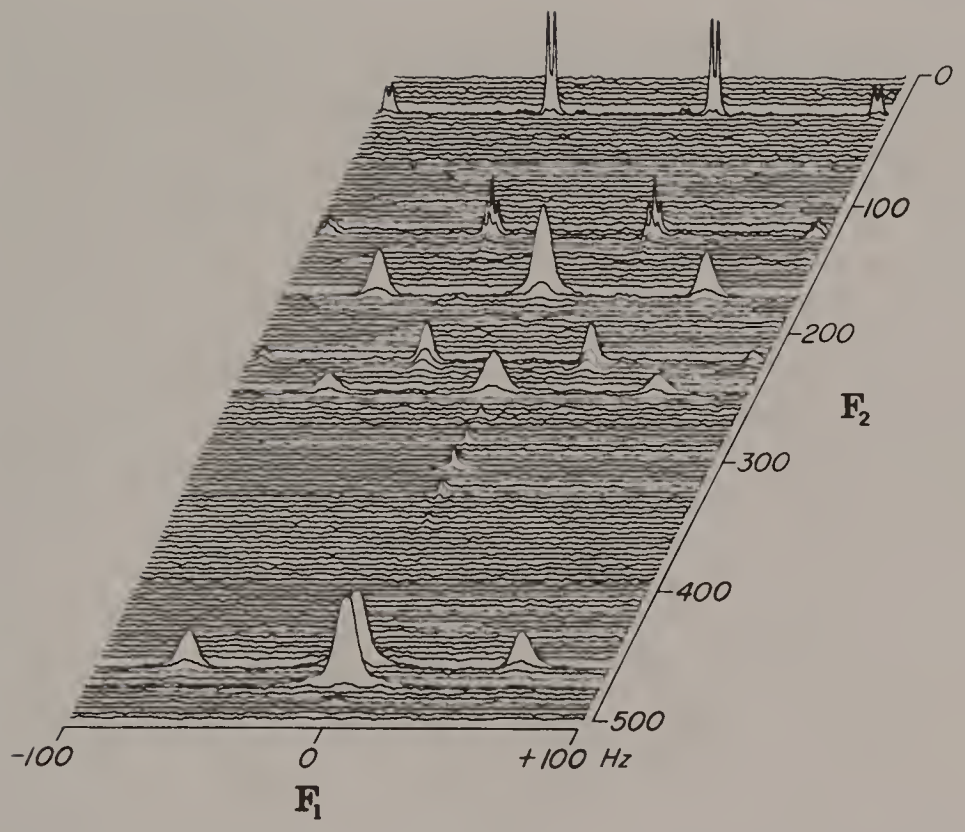

Fig. 3. Two-dimensional J-spectrum of carbon-13 in 2(1-methylcyclohexyl) 4,6-dimethylphenol. The three methyl resonances are clearly distinguished by the different fine structure patterns due to long-range CH coupling.

of a central positive peak flanked on both sides by negative dispersion tails (which interfere with adjacent lines). Clearly the phase-twist lineshape is quite unsuitable for our purposes.

Many remedies have been tried, with mixed success. 'Skyline projection' takes the maximum ordinate along the line of projection instead of the integral (6). This gives a decoupled proton spectrum but the intensities are grossly distorted. Similar criticisms may be levelled at the 'constant time' method (7) and pseudo-echo weighting of the detected free induction decay (8) because the projected intensities are affected by the magnitudes of the coupling constants, and by the differences in spin–spin relaxation times. A peak-finding routine used in radioastronomy has also been adapted to the problem (9). Once the two-dimensional phase-twist response has been located it may be replaced by a pure absorption peak, but there are difficulties with this algorithm in severely crowded or very noisy spectra. Another approach imposes a particular form of symmetry (C_4) on the J-spectrum and then uses a symmetry filter to pick out the individual peaks one at a time, thus sidestepping the overlap problem (10–12). Perhaps the simplest method of all is to perform a two-dimensional lineshape transformation in the frequency domain aimed at suppressing the broad dispersion-mode components (13).

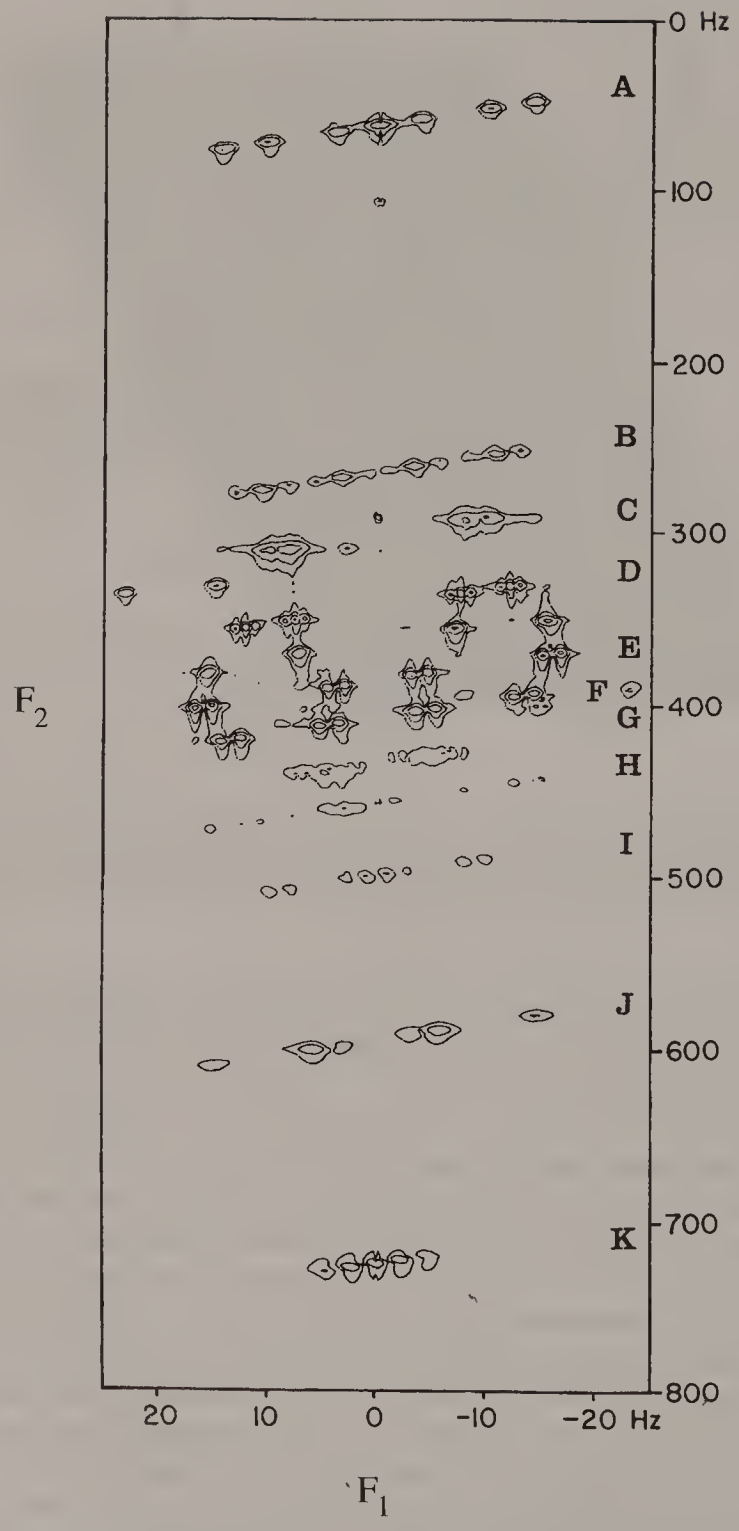

Fig. 4. Two-dimensional J-spectrum of protons in a tricyclodecanone derivative. When allowance is made for the different frequency scales in the two dimensions, we see that the spin multiplets actually lie on 45° diagonals. A chemical shift spectrum would be derived by projection along these 45° diagonals onto the F_2 axis.

The principal application of this 'broadband proton decoupling' scheme is as a first step in assignment of crowded spectra. This is particularly important in two-dimensional correlation spectroscopy (1,2) when there are severely overlapping cross-peaks. Not only does this confuse the determination of the pattern of connectivity but it can also make it very difficult to extract reliable values of coupling constants. Correlation spectra are now so widely used that assignment of cross-peaks by hand can be excessively tedious, and there is an urgent need for automated procedures. Basically these are pattern recognition methods based on the known symmetry of the cross-peaks. They can be speeded up considerably by using the information from the projected J-spectrum to construct a two-dimensional 'chemical shift grid' that we can superimpose on the correlation spectrum (14). Each genuine cross-peak must be centred on an intersection of this grid (although of course not all intersections are occupied). The pattern recognition search is then

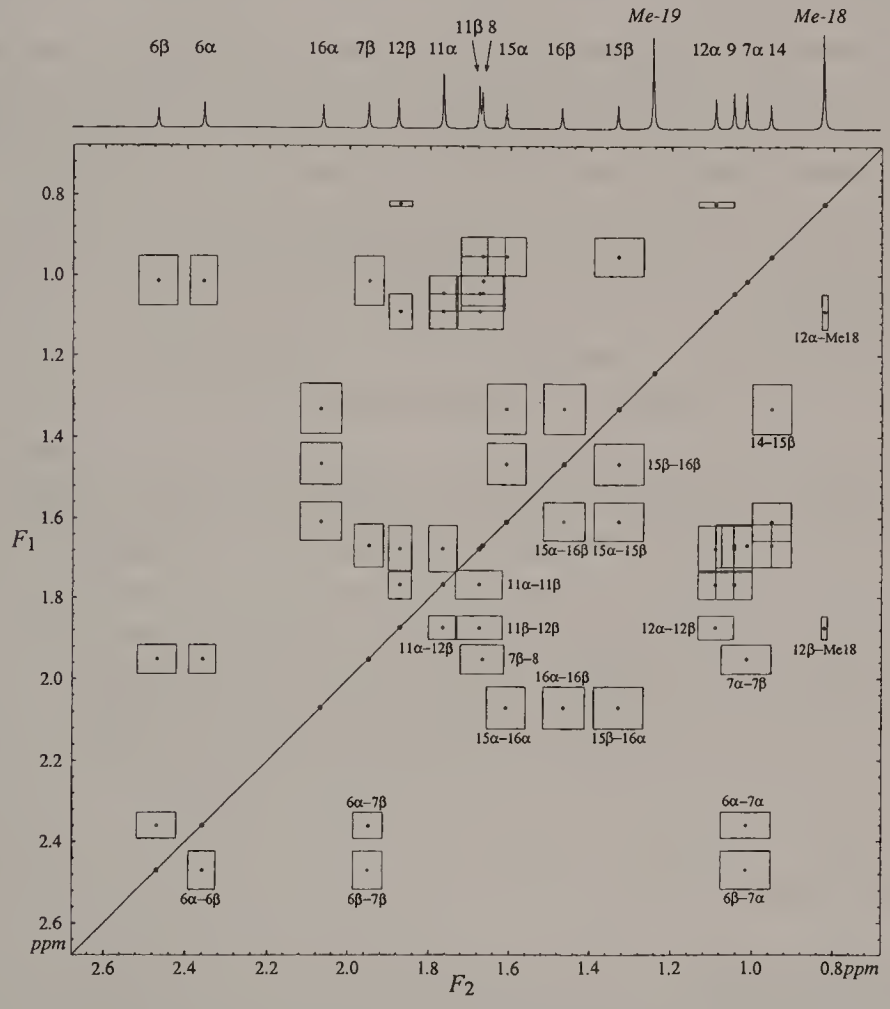

Fig. 5. The 400 MHz two-dimensional correlation spectrum of 1-dehydrotestosterone, processed by examining the local antisymmetry at all intersections of a 'chemical shift grid' derived from the proton J-spectrum. The boundary of each cross-peak is indicated by a rectangle and its centre by a dot. Note the eight severely overlapping cross-peaks in the region between 0.90 and 1.15 ppm.

restricted to these centres instead of having to examine every single location on the two-dimensional data matrix. Figure 5 shows such a 'reduced' two-dimensional correlation spectrum of a sample of 1-dehydrotestosterone in which a congested region (between 0.90 and 1.15 ppm) has been separated into eight overlapping cross-peaks (15). The end result of this type of data processing is a simple table of chemical shifts and their correlations; the two-dimensional spectrum may never need to be displayed.

REFERENCES

1. R. Freeman and H. D. W. Hill, *Dynamic Nuclear Magnetic Resonance Spectroscopy,* ed. L. M. Jackman and F. A. Cotton. Academic Press: New York, Ch. 5, 1975.
2. J. Jeener, *Ampère International Summer School*, Basko Polje, Yugoslavia, 1971, reported in *NMR and More. In Honour of Anatole Abragam,* ed. M. Goldman and M. Porneuf. Les Editions de Physique: Les Ulis, France, 1994.
3. W. P. Aue, E. Bartholdi and R. R. Ernst, *J. Chem. Phys.* **64**, 2229 (1976).
4. W. P. Aue, J. Karhan and R. R. Ernst, *J. Chem. Phys.* **64**, 4226 (1976).
5. K. Nagayama, P. Bachmann, K. Wüthrich and R. R. Ernst, *J. Magn. Reson.* **31**, 133 (1978).
6. B. Blümich and D. Ziessow, *J. Magn. Reson.* **49**, 151 (1982).
7. A. Bax and R. Freeman, *J. Magn. Reson.* **44**, 542 (1981).
8. A. Bax, R. Freeman and G. A. Morris, *J. Magn. Reson.* **43**, 333 (1981).
9. A. J. Shaka, J. Keeler and R. Freeman, *J. Magn. Reson.* **56**, 294 (1984).
10. P. Xu, X. L. Wu and R. Freeman, *J. Magn. Reson.* **95**, 132 (1991).
11. P. Xu, X. L. Wu and R. Freeman, *J. Am. Chem. Soc.* **113**, 3596 (1991).
12. M. Woodley and R. Freeman, *J. Magn. Reson. A* **109**, 103 (1994).
13. M. Woodley and R. Freeman, *J. Magn. Reson. A* **111**, 225 (1994).
14. M. Woodley and R. Freeman, *J. Am. Chem. Soc.* **117,** 6150 (1995).
15. M. Woodley and R. Freeman, *J. Magn. Reson. A* **118,** 39 (1996).

Cross-references

Broadband decoupling
Correlation spectroscopy
Lineshapes in two-dimensional spectra
Multiplicity determination
Spin echoes
Two-dimensional spectroscopy

Lineshapes in Two-dimensional Spectra

Many two-dimensional experiments, for example correlation spectroscopy (COSY) and nuclear Overhauser enhancement spectroscopy (NOESY) (see Nuclear Overhauser effect*), involve polarization transfer* from one group of spins to another. It is characteristic of these experiments that the observed signal is *amplitude* modulated as a function of the evolution time t_1; this can be represented as two equal counter-rotating phase modulations. Consequently, the sense of the precession during t_1 remains ambiguous; if there is a response in the two-dimensional spectrum at $(+\Omega_1, \Omega_2)$ there is always a mirror image response at $(-\Omega_1, \Omega_2)$. The section of the spectrum lying above the transmitter frequency is folded over into the remainder of the spectrum (and vice versa) causing considerable confusion. In early two-dimensional experiments (see Two-dimensional spectroscopy*), this could only be avoided by shifting the transmitter frequency to one extreme end of the spectrum so that all resonances had offsets of the same sign. Only the positive frequencies are then displayed, but a great deal of data storage is wasted.

One way out of this dilemma involves relating the sense of precession during t_1 with the sense of precession during t_2. For opposite senses of rotation, the observed response is called a *coherence transfer echo* (1,2) because static field inhomogeneity effects are refocused. When the senses of precession are the same, the response can be called an antiecho; field inhomogeneity effects are not refocused. Selection of the coherence transfer echo is achieved by a phase-cycling* scheme; on successive transients the receiver reference phase is shifted in 90° steps while the phases of all radiofrequency pulses prior to the evolution period are shifted by 90° in the opposite sense (for multiple-quantum coherence of order n, the phase shifts of the pulses should be 90°/n). This is equivalent to imposing a phase modulation during the evolution period rather than an amplitude modulation. There are some other forms of two-dimensional spectroscopy where phase modulation is inherent; these include J-spectroscopy*.

Spectra obtained by Fourier transformation of a phase-modulated signal exhibit a very characteristic two-dimensional lineshape known as the *phase twist,* illustrated in Fig. 1. Sections parallel to the F_1 or F_2 axes through the exact centre of this response show a pure absorption lineshape, but all other sections have dispersion-mode contributions which increase as the offset from exact resonance increases. If

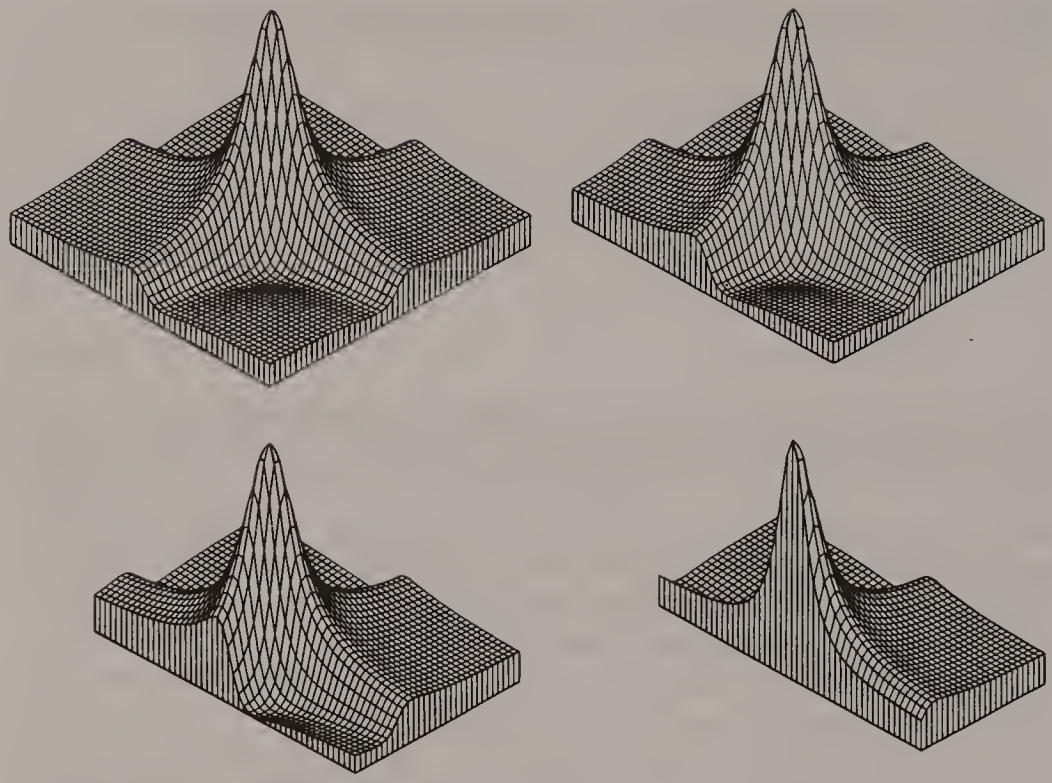

Fig. 1. The 'phase-twist' lineshape showing various sections at different offsets from exact resonance. Far from resonance the section is predominantly dispersion mode, but closer to resonance there is an increasing absorption-mode character and at exact resonance it is pure absorption.

several parallel sections are examined sequentially, the phase of the NMR signal appears to rotate from pure dispersion through pure absorption to dispersion in the other sense; hence the term phase twist.

The phase twist lineshape has several undesirable properties. The tails of the line (mainly dispersion mode) extend out a long way from the centre and interfere with adjacent lines in a complicated manner. A more serious problem occurs with projections of a phase-twist line. In two-dimensional proton J-spectroscopy, where the F_1 axis displays J-couplings and the F_2 axis displays chemical shifts and J-couplings, it would be possible to obtain a spectrum devoid of all H–H couplings if a 45° projection could be made, since this would catch all the spin multiplets in *enfilade*. Unfortunately, a projection in this direction vanishes because the negative lobes of this lineshape exactly cancel the positive central peak.

In many early two-dimensional experiments, the awkward nature of the phase-twist lineshape was sidestepped by plotting the absolute-value mode, the square root of the sum of the squares of the absorptive and dispersive components. This allows projections of two-dimensional spectra at any angle and incidentally removes the necessity of spectrometer phase adjustment in two dimensions. The problem of overlapping lines is still serious of course. It can be alleviated by

multiplying the time-domain signals (in both dimensions) by suitable weighting functions, such as the *sine bell* and *pseudo-echo.* These reshape the time-domain envelopes so that they peak at their mid-points and decay approximately symmetrically on either side. Now, the Fourier transform of a symmetric function is itself symmetric and therefore contains no dispersive part. The absolute-value mode must still be used but now it contains only the absorption-mode component. Unfortunately, this procedure carries a severe sensitivity penalty since these are quite drastic resolution enhancement* functions.

For these reasons it is important to be able to achieve sign discrimination in the F_1 dimension while retaining the pure two-dimensional absorption-mode lineshape. Procedures for accomplishing this were developed by States *et al.* (3) and Marion and Wüthrich (4). The treatment outlined here is based on the analysis of Keeler and Neuhaus (5). Since these techniques offer an important advantage in resolving power and a small increase in sensitivity, they have been widely adopted in two-dimensional spectroscopy.

Consider a signal which is amplitude modulated as a function of t_1, represented by a cosine wave

$$C(t_1, t_2) = \cos(\Omega_1 t_1)[\cos(\Omega_2 t_2) + i \sin(\Omega_2 t_2)]E_1E_2 \qquad [1]$$

where $E_1 = \exp(-t_1/T_2)$ and $E_2 = \exp(-t_2/T_2)$ are the decay terms in the two time dimensions. The form of this equation indicates that the sense of rotation during t_2 is determined, but not the sense during t_1. The amplitude modulation can be viewed as two counter-rotating phase modulations $\cos(\Omega_1 t_1) + i \sin(\Omega_1 t_1)$ and $\cos(\Omega_1 t_1) - i \sin(\Omega_1 t_1)$.

The usual complex Fourier transformation is performed with respect to t_2 (quadrature detection*). The absorption-mode spectrum is

$$C_a(t_1, F_2) = \cos(\Omega_1 t_1)A_2E_1. \qquad [2]$$

Here A_2 represents a Lorentzian absorption-mode signal

$$A_2 = T_2/(1 + \Delta\omega^2 T_2^2) \qquad [3]$$

where $\Delta\omega$ is the offset from the centre of the line. (The Lorentzian shape is a result of transforming an exponentially decaying time-domain function.) The dispersion-mode spectrum is

$$C_d(t_1, F_2) = \cos(\Omega_1 t_1)D_2E_1 \qquad [4]$$

where D_2 represents a Lorentzian dispersion-mode signal

$$D_2 = \Delta\omega T_2^2/(1 + \Delta\omega^2 T_2^2). \qquad [5]$$

These are the normal results obtained by quadrature detection; the problems arise when the second transformation is performed. We can now define a cosine transform (for a continuous function) by

$$C^{\cos}(F_1, F_2) = \int C(t_1, F_2) \cos(2\pi F_1 t_1)\, dt_1. \qquad [6]$$

We assume for simplicity that the spectrometer phase has been properly adjusted in both frequency dimensions. The cosine transform of eqn [2] represents a response that has no sign discrimination of its frequency in the F_1 dimension. We choose to write this as

$$C_a^{cos}(F_1, F_2) = A_1^+ A_2 + A_1^- A_2, \qquad [7]$$

which corresponds to a peak A_1^+ in the $+F_1$ dimension and a symmetrically related peak A_1^- in the $-F_1$ dimension. This is equivalent to regarding the amplitude modulation of eqn [2] as two counter-rotating phase modulations. Both peaks have the two-dimensional absorption-mode lineshape illustrated in Fig. 2(d).

We may also calculate the sine transform defined by

$$C_a^{sin}(F_1, F_2) = \int C(t_1, F_2) \sin(2\pi F_1 t_1)\, dt_1. \qquad [8]$$

This gives

$$C_a^{sin}(F_1, F_2) = D_1^+ A_2 + D_1^- A_2. \qquad [9]$$

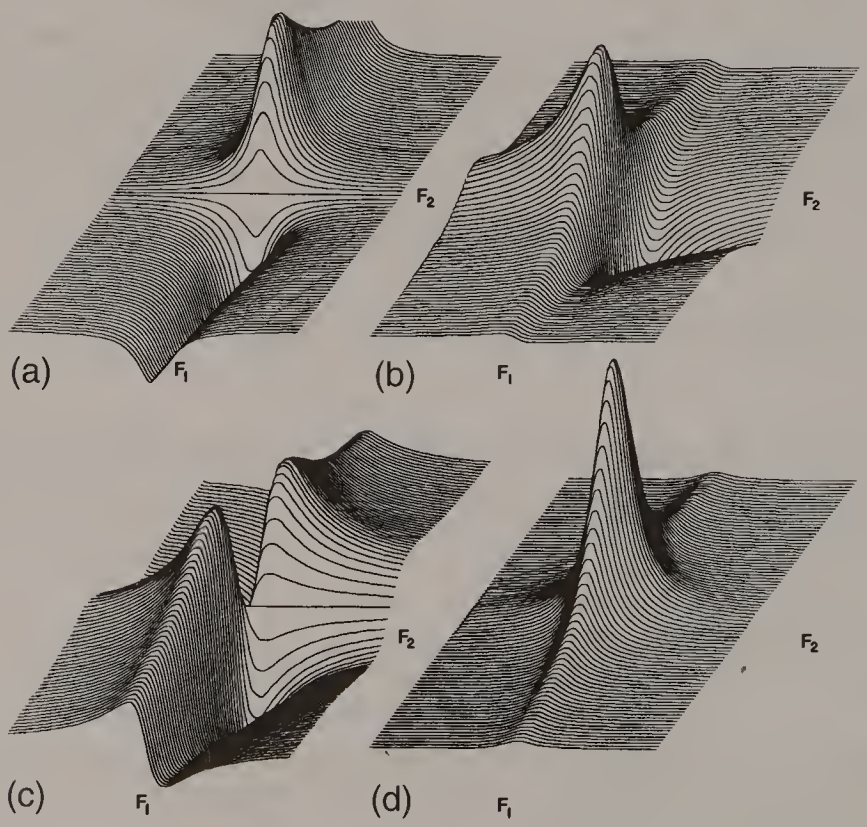

Fig. 2. Four types of two-dimensional lineshape: (a) absorption mode in F_1 and dispersion mode in F_2; (b) dispersion mode in F_1 and absorption mode in F_2; (c) dispersion mode in both dimensions; and (d) absorption mode in both dimensions.

This represents two lines that have dispersion-mode profiles in the F_1 dimension but absorption-mode profiles in the F_2 dimension (Fig. 2(b)). Alternatively, we could transform the dispersion-mode spectrum, eqn [4], to give

$$C_d^{cos}(F_1, F_2) = A_1^+ D_2 + A_1^- D_2. \qquad [10]$$

These two lines have absorption-mode profiles in F_1 and dispersion profiles in F_2 (Fig. 2(a)), while the sine transform of eqn [4] gives

$$C_d^{sin}(F_1, F_2) = D_1^+ D_2 + D_1^- D_2. \qquad [11]$$

These two lines have dispersion-mode profiles in both dimensions (Fig. 2(c)).

Clearly, additional information is required to determine the sense of precession during t_1. The basic problem is to determine, without ambiguity, the phase angle β of a vector evolving in t_1. If we knew that $x = \sin \beta$, then we could say that $\beta = \arcsin x$ or $\beta = \arcsin x - \pi$. If we knew that $y = \cos \beta$, then we could say that $\beta = \pm \arccos y$. Only if we know $\sin \beta$ and $\cos \beta$ simultaneously can we be sure about the angle β. This additional information is provided by a second experiment in which the modulation during t_1 follows a sine rather than a cosine wave:

$$S(t_1, t_2) = \sin(\Omega_1 t_1)[\cos(\Omega_2 t_2) + i \sin(\Omega_2 t_2)]E_1 E_2. \qquad [12]$$

For example, in a homonuclear chemical shift correlation experiment (COSY) this would involve a 90° phase shift in the coherence that evolves during t_1, which is achieved by shifting the phase of the initial pulse by 90°. For multiple-quantum coherence of order n, all the pulses which precede the evolution period would need to be shifted in phase by 90°/n. This function $S(t_1, t_2)$ is always kept separate from the function $C(t_1, t_2)$.

As above, we perform quadrature detection in the t_2 dimension and compute the absorption spectrum

$$S_a(t_1, F_2) = \sin(\Omega_1 t_1)A_2 E_1, \qquad [13]$$

and the dispersion spectrum

$$S_d(t_1, F_2) = \sin(\Omega_1 t_1)D_2 E_1. \qquad [14]$$

If we were to proceed as with the first experiment, the result would again be a pair of lines at $(+\Omega_1, \Omega_2)$ and $(-\Omega_1, \Omega_2)$. The method of States *et al.* (3) avoids this by zeroing the dispersion-mode spectrum, eqn [14], before the next stage of complex Fourier transformation. The absorption part corresponds to a line with no sign discrimination of its F_1 frequency, which we choose to write

$$S_a^{sin}(F_1, F_2) = A_1^+ A_2 - A_1^- A_2. \qquad [15]$$

Only the sine transform is retained, S_a^{cos} being discarded. The negative sign in eqn [15] is important; it reflects the fact that $\sin(\Omega_1 t_1)$ reverses its sign for negative frequencies (A_1^-). Combination with the results from the first experiment, eqn [7], gives

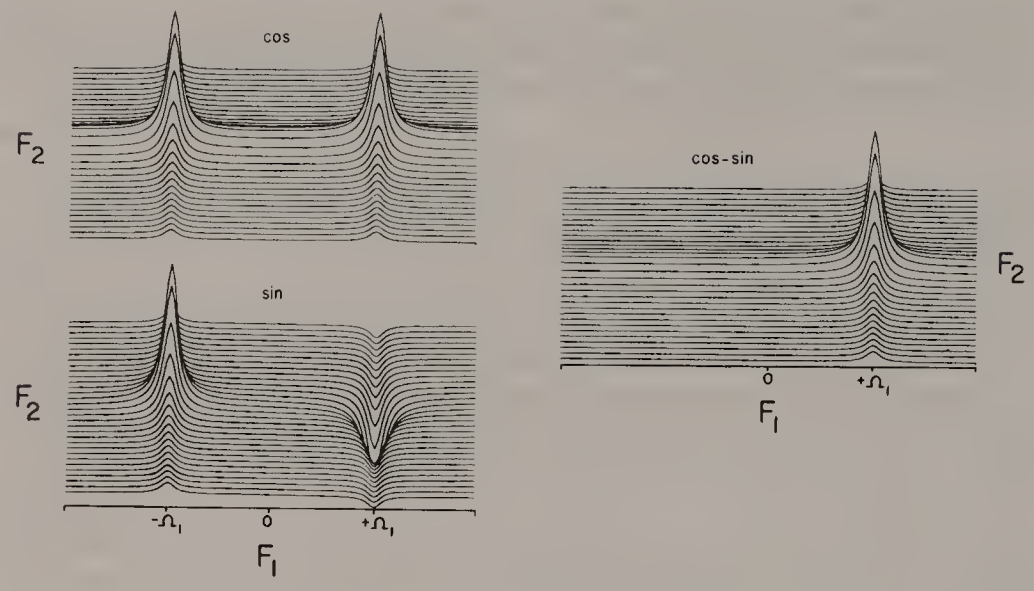

Fig. 3. Discrimination of the sign of the frequency for pure absorption-mode spectra. By subtraction of the spectra obtained by transformation of the cosine-modulated signal and the sine-modulated signal, a single peak is obtained at a positive frequency.

$$C_a^{cos}(F_1, F_2) + S_a^{sin}(F_1, F_2) = 2A_1^{+}A_2. \qquad [16]$$

This is a two-dimensional absorption-mode line at a positive frequency in the F_1 dimension. The component at a negative frequency has been cancelled as indicated schematically in Fig. 3.

The alternative method proposed by Marion and Wüthrich was developed for spectrometers which do not have a complex Fourier transform program. It is based on Redfield's method (6) for obtaining the equivalent of quadrature detection with only a single phase-sensitive detector. This involves doubling the sampling rate and shifting the receiver phase in 90° steps at each new sampling operation. Translated into the t_1 dimension this method is usually known as TPPI (time-proportional phase incrementation) (7). It has the effect of increasing the apparent frequencies in the F_1 dimension by a frequency Ω_c equal to half the spectral width in this dimension, just as if the reference frame were rotating at $\Omega_0 - \Omega_c$ rather than at the Larmor frequency Ω_0. This keeps all precession frequencies positive and avoids aliasing problems. Real Fourier transforms are used in this method rather than complex transforms, but otherwise the principles are the same as in the method of States *et al.* Both techniques use the same amount of data storage, but the method of Marion and Wüthrich is particularly easy to program. The concept of *coherence transfer pathways* (8) provides a clear description of both methods for obtaining pure absorption-mode lineshapes.

There are several practical advantages of the pure absorption-mode display and it has been widely adopted. It avoids the difficulties of the *phase twist* or absolute-value lineshapes without the complications associated with the *pseudo-echo* or

sine-bell weighting functions. It achieves high resolution of the multiplet components within a given cross-peak and does not obscure the 'up–down' pattern of their intensities. These considerations are important when pattern recognition techniques (9) are employed to characterize cross-peaks in two-dimensional spectra.

LORENTZIANS AND GAUSSIANS

When exponential weighting functions are imposed in both time dimensions of a two-dimensional experiment, pure absorption-mode responses have lineshapes that are two-dimensional Lorentzians (Fig. 4(a)). This can be an undesirable shape because it has ridges that run parallel to the F_1 and F_2 axes, and they can cause misleading effects in the case of overlap with adjacent lines. Looked at in another way, the line has intensity contours that are not circular (or elliptical) but the shape of a starfish with only four legs. A more suitable time-domain weighting function is the Gaussian, for this gives a Gaussian lineshape in the frequency domain (Fig. 4(b)), with circular (or elliptical) intensity contours.

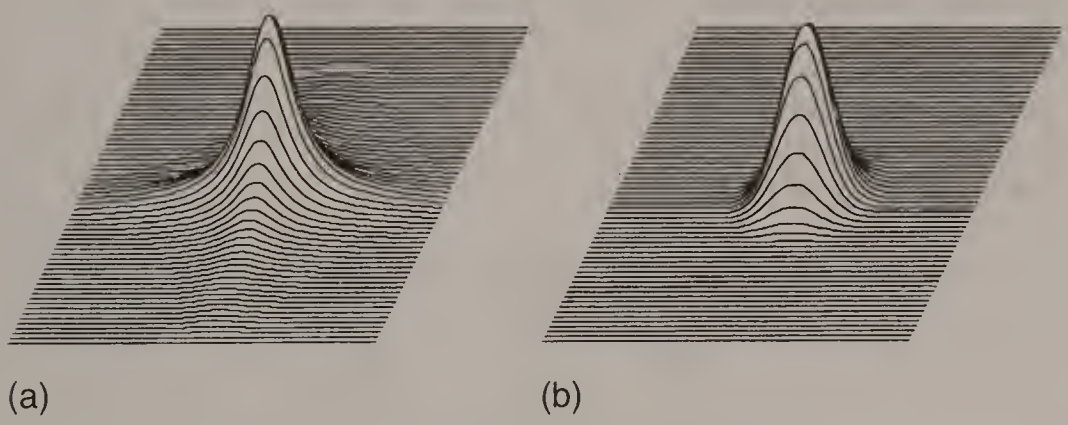

Fig. 4. (a) A two-dimensional Lorentzian lineshape. (b) A two-dimensional Gaussian lineshape.

REFERENCES

1. K. Nagayama, K. Wüthrich and R. R. Ernst, *Biochem. Biophys. Res. Commun.* **90**, 305 (1979).
2. A. Bax, R. Freeman and G. A. Morris, *J. Magn. Reson.* **42**, 164 (1981).
3. D. J. States, R. A. Haberkorn and D. J. Ruben, *J. Magn. Reson.* **48**, 286 (1982).
4. D. Marion and K. Wüthrich, *Biochem. Biophys. Res. Commun.* **113**, 967 (1983).
5. J. Keeler and D. Neuhaus, *J. Magn. Reson.* **63**, 454 (1985).
6. A. G. Redfield and S. D. Kunz, *J. Magn. Reson.* **19**, 250 (1975).
7. G. Drobny, A. Pines, S. Sinton, D. Weitekamp and D. Wemmer, *Faraday Div. Chem. Soc. Symp.* **13**, 49 (1979).
8. G. Bodenhausen, H. Kogler and R. R. Ernst, *J. Magn. Reson.* **58**, 370 (1984).
9. B. U. Meier, G. Bodenhausen and R. R. Ernst, *J. Magn. Reson.* **60**, 161 (1984).

Cross-references

J-spectroscopy
Nuclear Overhauser effect
Phase cycling
Polarization transfer
Quadrature detection
Resolution enhancement
Two-dimensional spectroscopy

Maximum Entropy Method

Imagine the following scenario. A man who witnessed a serious crime is describing the suspect so that a police artist can make an identification sketch of the wanted person, a notoriously difficult operation. Influenced by his revulsion at the details of the crime, the witness lets his own impressions influence his recollections, for example by imagining the villain to be scowling and unshaven. This situation would be improved if half a dozen eyewitnesses could be found. Assuming that they were all reliable observers and that the artist was competent, this should produce a set of sketches, all of which are *compatible* with the raw data, although they will obviously differ in detail. The policeman in charge of the case is presented with six

'How did they catch you then?'
'Dunno, something to do with maximum entropy.'

drawings – which one should be choose? To be of the most use for identification purposes, the chosen sketch should obviously contain the least amount of *extraneous* information, but since there is no criterion for judging what is extraneous the only safe solution is to choose the drawing with the lowest information content. In the (inelegant) language of information theory this is said to be the 'maximally non-committal' solution. On the grounds that entropy is the negative of information content, it is also called the *maximum entropy solution*. This data processing technique (1–7) is now being applied to problems of magnetic resonance where it has been successful in suppressing undesirable artefacts in the spectra.

Present-day NMR spectrometers yield their information in the form of a free induction decay* and the conversion into the frequency domain is almost always carried out by Fourier transformation*. There are some possible alternatives. The free induction decay could be fitted to a superposition of decaying oscillations with suitable frequencies, phases and intensities, using a least-squares procedure. The result could then be displayed in the form of a frequency-domain spectrum with the appropriate linewidths and lineshapes, without any need for Fourier transformation. Computational time would be saved by terminating the iterations before the program began to fit the noise components in the raw data. This is where the danger lies, since the final spectrum would then appear to be noise-free, but since the search program would also miss signal components comparable in intensity with the noise, no sensitivity advantage would ensue.

The real advantages of this method are more subtle. Often an experimental free induction signal has to be truncated before it has decayed to a negligible level, in order to minimize the time spent on acquisition. After zero filling* and Fourier transformation, this step function introduces a degree of sinc function character to the spectral lineshapes, which is undesirable. A direct computer fitting of the free induction decay can take into account the fact that the experimental data set had been truncated in this manner, thus avoiding sinc function artefacts. Similarly, the distortions which often appear on the first one or two sample points of the free induction decay due to receiver dead time need not be carried over into the final spectrum.

The maximum entropy method represents a rather more sophisticated approach to this type of problem, and one that need not incorporate a model for the spectrum. In the application of this method to NMR spectroscopy, we might imagine a number of possible 'trial spectra' which, by inverse Fourier transformation, give free induction decays compatible with the experimental one. This inability to settle on a single 'correct' spectrum arises out of the uncertainty associated with the presence of noise in the experimental data. None of the free induction decays obtained by back-transformation of the trial spectra corresponds exactly with the experimental time-domain signal because each sample point carries a component of noise.

The choice between several 'acceptable' spectra is made on the basis of the maximum entropy criterion. This chosen spectrum is no more likely to be 'correct'

than any of the other acceptable spectra, since there is just no hard evidence available to make a meaningful distinction. It nevertheless represents the safest choice simply because it has the lowest information content.

In this context, entropy represents the negative of the information content

$$S = -\sum_{k}^{N} p_k \log p_k \qquad [1]$$

where the p_k values represent the intensity ordinates which define the trial spectrum and N is the total number of ordinates. These intensities must be suitably normalized in order to prevent the algorithm from simply raising the level of the baseline in order to increase S. The aim is to choose the trial spectrum that has the largest value of S subject to the constraint that it is consistent with the experimental data. It can be shown that there is normally a unique maximum entropy solution to a given problem. The spectrum chosen according to the maximum entropy principle has the important property that it contains no more 'structure' than is strictly justified by the experimental evidence. No unnecessary artefacts are introduced, in contrast to the much more common Fourier transform method.

Since it would be incorrect to attempt to fit the experimental free induction decay exactly (because of the presence of noise) we only use those trial spectra that have a suitable chi-squared statistic

$$\chi^2 = \sum_{a}^{M} (I_a - I_a')^2/\sigma^2_a \qquad [2]$$

where I represents an actual signal intensity in the time-domain free induction decay and I' the corresponding time-domain intensity derived from the trial spectrum, while σ is the r.m.s. noise. The parameter χ^2 should be of the order of M, the number of measurements made on the free induction signal (M is less than or equal to N). This means that the error in fitting a given point on the free induction decay is of the order of the r.m.s. noise.

The entropy function is non-linear and its maximization entails an iterative procedure, but the starting point for this iteration is not critical. It is possible to assume an initial trial spectrum that is merely a flat baseline, and this has the advantage of avoiding prejudice on the part of the spectroscopist. In other circumstances it can be advantageous to incorporate prior knowledge about the spectrum, measuring the entropy with respect to that of an initial model spectrum m rather than with respect to a completely featureless flat baseline:

$$S = -\sum_{k}^{N} p_k(\log p_k - \log m_k)/m_k. \qquad [3]$$

Of course, if some aspect of this model spectrum is erroneous, the maximum entropy algorithm can do nothing to correct it, so the procedure must be used with caution.

The maximum entropy method is used in a wide variety of applications including radioastronomy, tomographic reconstruction, the deconvolution of blurred photographic images, and X-ray crystallography. Sometimes the experimental data may be incomplete; some pixels may be missing from an image or a free induction decay may be prematurely truncated. The maximum entropy method handles this

kind of data corruption very effectively, rejecting trial images or spectra that contain artefacts attributable to defective input data. Thus sinc function artefacts are suppressed very efficiently. The maximum entropy method can also be used for resolution enhancement* as an alternative to manipulating the decay rate of the free induction signal. As an example, Fig. 1 shows one of the proton resonances (H_5) of 3-bromonitrobenzene with and without resolution enhancement by the maximum entropy method. The central triplet (doublet of doublets) now appears well resolved, whereas in the unprocessed spectrum it had only a hint of shoulders on the line profile.

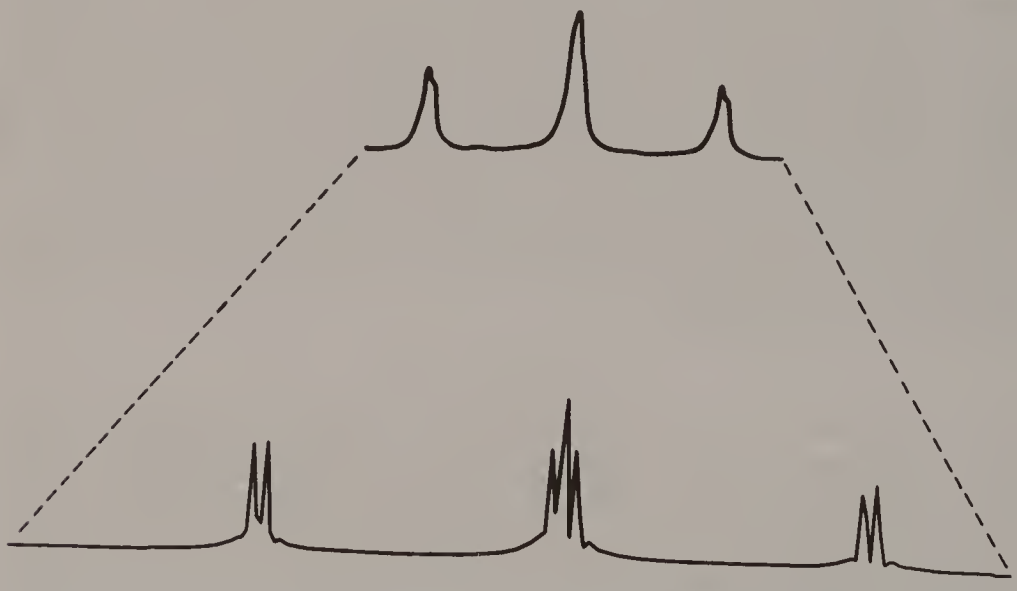

Fig. 1. Resolution enhancement by the maximum entropy method. The multiplet from H_5 in 3-bromonitrobenzene is shown before and after processing by the maximum entropy method. The width of the spectrum is 22.4 Hz.

SENSITIVITY ENHANCEMENT*?

NMR spectroscopists are accustomed to working with linear systems and to processing the data with linear operations such as Fourier transformation. They may therefore be forgiven for using the terms *sensitivity* and *signal-to-noise ratio* essentially interchangeably. If a test sample with a concentration C mol dm^{-3} gives a signal-to-noise ratio of, say, 10, then in a linear system, we can estimate the minimum concentration that would just give a detectable signal, something near C/4 or C/5 mol dm^{-3}. This is a measure of the sensitivity of the spectrometer.

With non-linear operations (maximum entropy is one of these) we must be careful to distinguish the two terms, since an improvement in signal-to-noise ratio is no longer equivalent to an improvement in sensitivity. For signals significantly more intense than the noise, the signal-to-noise ratio can be increased by very large

factors by non-linear amplification, by plotting on a recorder with an appreciable dead band, or by many possible data processing tricks. None of these serves any really useful purpose, because for the case that matters – signals comparable with noise – they fail to enhance the signal-to-noise ratio and may even degrade it. They *do not* improve sensitivity.

Noise should not be thought of as an 'artefact' that can be separated from true signals and discarded. High-frequency components of the noise can be filtered out, and it is common practice to do this with the optimum matched filter when sensitivity is crucial. Since noise is uncorrelated between one experiment and the next, it can be reduced by time averaging*. Beyond that, there are no obvious properties that distinguish signal from noise and we should not expect any miraculous new data processing technique to be able to enhance sensitivity. Indeed, the very crux of the maximum entropy principle is not to introduce any feature into the final spectrum for which there is no clear evidence in the experimental data. Weak signals hidden in the noise remain unobservable. There is then no strong incentive to use these non-linear operations to 'clean up' the spectrum by reducing baseline noise; if we do so, it is important to remember that some very weak signals have been similarly suppressed.

Noise in a spectrum actually serves a useful purpose provided that we are dealing with a linear system. If the baseline noise has an amplitude equal to (say) 10% of a given NMR signal, then the operator recognizes that the peak height of this signal is unreliable to the same degree. On the other hand, if the noise is suppressed by a non-linear data processing method (such as maximum entropy) the intensity of this line is clearly no more reliable than before, although the operator might be misled into thinking that it is.

REFERENCES

1. C. E. Shannon, *Bell Syst. Tech. J.* **27**, 623 (1948).
2. S. F. Gull and G. J. Daniell, *Nature* **272**, 686 (1978).
3. S. Sibisi, *Nature* **301**, 134 (1983).
4. J. Skilling, *Nature* **309**, 748 (1984).
5. S. Sibisi, J. Skilling, R. G. Brereton, E. D. Laue and J. Staunton, *Nature* **311**, 446 (1984).
6. E. D. Laue, J. Skilling, J. Staunton, S. Sibisi and R. G. Brereton, *J. Magn. Reson.* **62**, 437 (1985).
7. P. J. Hore, *J. Magn. Reson.* **62**, 561 (1985).

Cross-references

Fourier transformation
Free induction decay
Resolution enhancement
Sensitivity enhancement
Time averaging
Zero filling

Measurement of Coupling Constants

If all spin multiplets were well resolved, properly digitized and had a good signal-to-noise ratio, there would be no need for specialized techniques for their determination; we would simply set cursors on two of the multiplet lines and have a standard computer algorithm evaluate the splitting. The trouble begins with incompletely resolved splittings. For simplicity we restrict the discussion to doublets, since more complicated multiplets can be regarded as being derived by repeated doubling. If the two component lines of a doublet are in phase and poorly resolved, a direct measurement of the splitting underestimates the coupling constant; in the limit the two lines merge and no splitting can be observed. If the two component lines are antiphase, as in many two-dimensional experiments, the direct measurement of a poorly resolved splitting *over*estimates the coupling constant owing to mutual cancellation of signals in the region of overlap. Instead of losing the splitting we lose signal intensity by cancellation and soon reach the detection limit set by the noise level.

A great many methods have been proposed to solve this problem, for coupling constants provide unique information about the conformation of molecules, based principally on a theoretical relation derived by Karplus (1) for vicinal couplings

$$^3J_{VIC} = A + B \cos \phi + C \cos 2\phi. \qquad [1]$$

This relates $^3J_{VIC}$ to the dihedral angle ϕ between the terminal bonds. Often the couplings of interest are in macromolecules, where the natural linewidths can be quite large and where the fineness of digitization in the frequency domain may leave something to be desired.

The simplest approach to the measurement of a poorly resolved splitting is to apply some resolution enhancement (2) if the signal-to-noise ratio is high enough to support such a manipulation of the data. Comparable results can be achieved by fitting procedures applied in the time or frequency domains. This may involve the assumption of an idealized lineshape function such as a Lorentzian, or it might exploit the measurement of an experimental lineshape of a known singlet in the same spectrum (2).

Quite often the spectroscopist first suspects the possibility of a weak unresolved splitting by noting a perceptible broadening of a given resonance compared with others in the same spectrum. Then a selective decoupling* experiment can be

performed, a slight line narrowing being taken as confirmation that there is indeed a coupling between those spins. Its magnitude can then be evaluated by reconvolution of the decoupled line with a trial splitting J*, followed by a least-squares optimization routine (3).

Maximum entropy* reconstruction has also been used for this purpose. Although the key tenet of this technique is that it never suggests features for which there is no good evidence in the raw data, we have to remember that in the case of an unresolved doublet, the evidence *is* there – it takes the form of a distortion of the observed lineshape in a predictable manner. Because it is an inverse process, the maximum entropy method is quite effective in the deconvolution of a given splitting if the coupling constant is known beforehand (4). The splitting is imposed on the trial spectrum and, after Fourier transformation, the result is compared with the experimental time-domain data, maximizing the entropy subject to the usual χ^2 constraint. The procedure is less reliable for the determination of an unknown splitting, where there is the complication of a new search dimension (5).

The J-modulation of spin echoes seems to offer an attractive approach to the determination of poorly resolved splittings since, in principle, the limiting factor should be the natural linewidth rather than the instrumental linewidth. Selective excitation* and selective spin inversion experiments can be used in the context, deriving one echo decay curve that is modulated by the desired coupling and a second decay curve that is unmodulated (6). The raw modulation frequency is extracted by division of the two decay curves point by point. Equivalent results can be obtained by two-dimensional J-spectroscopy*.

The 'zero-crossing' technique enjoys the advantage that it is completely independent of the instrumental lineshape because the crossing point in the time domain is unaffected by the shape of the decay envelope (7). It operates, not on the normal free induction decay, but on a time-domain signal obtained by back-transformation of the isolated multiplet that has been carefully centred in the frequency window so that there is no interfering modulation from the chemical shift. It searches for the first zero crossing of this signal due to the (heavily damped) J-modulation. In the presence of noise and a rapid decay of the time-domain signal, a quite sophisticated search algorithm is required to locate the zero crossing with sufficient accuracy.

J-EXTENSION

In two-dimensional spectroscopy and related coherence transfer experiments, it is often possible to derive two forms of the poorly resolved doublet – an in-phase pattern and an antiphase pattern. Then there are several possible procedures for extracting the coupling constant. We limit the discussion to just one of these, called J-extension (8). The in-phase form of the doublet can be represented by the time-domain signal modulated by a cosine term

$$S(\uparrow\uparrow) = A \cos(2\pi\delta_S t) \cos(\pi J_{IS} t) \exp(-t/T_2^*) \quad [2]$$

while the antiphase form involves modulation by a sine term

$$S(\uparrow\downarrow) = B \cos(2\pi\delta_S t) \sin(\pi J_{IS} t) \exp(-t/T_2^*), \quad [3]$$

where δ_S is the chemical shift, J_{IS} is the coupling constant and $1/(\pi T_2^*)$ is the instrumental linewidth.

The first step is to scale the relative intensities of the two signals; we may then put A = B. The idea is to add a large dummy splitting J_0 to the poorly resolved splitting, thus rendering it amenable to direct measurement. We multiply eqn [2] by $\cos(\pi J_0 t)$ and eqn [3] by $\sin(\pi J_0 t)$ and then subtract the results:

$$\begin{aligned} S(\uparrow\uparrow) \cos(\pi J_0 t) - S(\uparrow\downarrow) \sin(\pi J_0 t) &= A \cos(2\pi\delta_S t) \cos(\pi J_{IS} t) \cos(\pi J_0 t) \exp(-t/T_2^*) \\ &\quad - A \cos(2\pi\delta_S t) \sin(\pi J_{IS} t) \sin(\pi J_0 t) \exp(-t/T_2^*) \\ &= A \cos(2\pi\delta_S t) \exp(-t/T_2^*) \cos[\pi(J_{IS} + J_0)t]. \quad [4] \end{aligned}$$

This represents an in-phase doublet of splitting $|J_{IS} + J_0|$, and since J_0 is known, an accurate value of J_{IS} is obtained.

J-DOUBLING

More commonly, only one form of the poorly resolved doublet is available and then a procedure that repeatedly doubles the splitting appears to be the most promising (9). Consider the case of an in-phase splitting. As a first step we isolate the doublet in question and by back-transformation generate the corresponding time-domain signal. We multiply this by $\sin(\pi J^* t)$ where J* is a trial splitting:

$$S(\uparrow\uparrow)\sin(\pi J^* t) = A \cos(2\pi\delta_S t) \cos(\pi J_{IS} t) \sin(\pi J^* t) \exp(-t/T_2^*). \quad [5]$$

Through a standard identity this can be written

$$S(\uparrow\uparrow) \sin(\pi J^* t) = \tfrac{1}{2} A \cos(2\pi\delta_S t) \exp(-t/T_2^*)\{\sin[\pi(J_{IS} + J^*)t] - \sin[\pi(J_{IS} - J^*)t]\}. \quad [6]$$

We Fourier transform this processed time-domain signal to give a 'test spectrum'. It comprises a wide antiphase doublet $|J_{IS} + J^*|$ and a narrow antiphase doublet $|J_{IS} - J^*|$. If J* is now varied until it reaches the value J_{IS}, the narrow antiphase doublet disappears through mutual cancellation of signals and we are left with a splitting $2J_{IS}$. As J* is varied in suitably small steps, we monitor Σ, the sum of the magnitudes of all the ordinates in the test spectrum. It goes through a minimum when $J^* = J_{IS}$ as the cancellation takes place. This marks the value of J_{IS}. Often better results can be achieved by further doubling of the experimental splitting, now using $\cos(2n\pi J^* t)$ as multiplier, with n = 1, 2, 4, ... Analogous procedures can be applied to the determination of a poorly resolved antiphase splitting.

The reader will have noticed that most of these processing methods involve

jumping back and forth between time and frequency domains. Although the Fourier transformation is a rapid algorithm, it can be time consuming when used repeatedly in an iterative loop. A faster version of J-doubling (10) operates directly on frequency-domain data, multiplying an in-phase doublet J_{IS} by an antiphase stick spectrum of splitting J*. The processing then proceeds as outlined above.

J-DECONVOLUTION

Bothner-By and Dadok (11) took the direct approach of dividing an experimental time-domain signal $S(\uparrow\uparrow)$ by $\cos(\pi J^*t)$, with the intention of deconvolving that particular splitting:

$$\frac{S(\uparrow\uparrow)}{\cos(\pi J^*t)} = \frac{A\cos(2\pi\delta_S t)\cos(\pi J_{IS}t)\exp(-t/T_2^*)}{\cos(\pi J^*t)}. \qquad [7]$$

When $J^* = J_{IS}$ that splitting disappears. Unfortunately a serious problem arises with numerical division by zero or near-zero values when the numerator is an experimental signal containing noise. It can be circumvented by judicious sampling of the cosine wave so as to avoid the vicinity of the zero crossings (12) but then the subsequent data processing begins to resemble that of the J-doubling method described above, and yields comparable results.

Deconvolution has another practical application. Once the coupling constants have been measured, it can be useful to remove the corresponding splittings from the spectrum. For example, we could reduce each cross-peak in a two-dimensional correlation spectrum to a singlet response at the chemical shift coordinates by taking out the splittings one after another. There is a simple frequency-domain algorithm that accomplishes this task (13).

REFERENCES

1. M. Karplus, *J. Chem. Phys.* **30**, 11 (1959).
2. R. R. Ernst, R. Freeman, B. Gestblom and T. R. Lusebrink, *Mol. Phys.* **13**, 283 (1967).
3. F. del Rio-Portilla and R. Freeman, *J. Magn. Reson. A* **104**, 358 (1993).
4. M. A. Delsuc and G. C. Levy, *J. Magn. Reson.* **76**, 306 (1988).
5. J. A. Jones, D. S. Grainger, P. J. Hore and G. J. Daniell, *J. Magn. Reson. A* **101**, 162 (1993).
6. R. Freeman and H. D. W. Hill, *J. Chem. Phys.* **54**, 301 (1971).
7. J. Stonehouse and J. Keeler, *J. Magn. Reson. A* **112**, 43 (1995).
8. R. Freeman and L. M. McIntyre, *Isr. J. Chem.* **32**, 231 (1992).
9. L. M. McIntyre and R. Freeman, *J. Magn. Reson.* **96**, 425 (1992).
10. F. del Rio-Portilla, V. Blechta and R. Freeman, *J. Magn. Reson. A* **111**, 132 (1994).
11. A. A. Bothner-By and J. Dadok, *J. Magn. Reson.* **72**, 540 (1987).
12. J. M. Le Parco, L. M. McIntyre and R. Freeman, *J. Magn. Reson.* **97**, 553 (1992).
13. F. del Rio-Portilla and R. Freeman, *J. Magn. Reson. A* **108**, 124 (1994).

Cross-references

Correlation spectroscopy
J-spectroscopy
Maximum entropy method
Selective decoupling
Selective excitation
Two-dimensional spectroscopy

Multiple-quantum Coherence

The selection rule for NMR transitions is $\Delta m = \pm 1$. A transition that obeys this selection rule can be excited by weak continuous-wave irradiation or by a single hard radiofrequency pulse. It generates a macroscopic transverse magnetization which induces a signal in the receiver coil. All other transitions are strictly forbidden. Nevertheless, p-quantum transitions ($p > 1$) can be observed in a continuous-wave spectrometer by the simple expedient of increasing the radiofrequency level beyond its usual setting, although zero-quantum transitions remain forbidden. For example, an intense radiofrequency field 'forces' a double-quantum transition by simultaneously exciting the extreme tails of two progressively connected single quantum transitions f_1 and f_2 at the mean frequency $\frac{1}{2}(f_1 + f_2)$. The observation of such a double-quantum transition may be used to establish connectivities of normal transitions within the energy-level diagram (1) or to determine the relative signs of coupling constants (2). However, since the same information can be obtained by double-resonance methods, interest in multiple-quantum effects waned for more than a decade until the new two-dimensional techniques for excitation and indirect detection were devised (3).

One way of describing the effect of a hard radiofrequency pulse is to say that it creates *coherence** between two states of the spin system differing in quantum number by one unit. If two or more pulses are used, they may act in cascade, exciting multiple-quantum coherence, including zero-quantum coherence. The interesting difference is that these types of coherence do not induce any voltage in the receiver coil; they can only be detected indirectly by allowing them to evolve in a two-dimensional experiment, followed by reconversion into observable transverse magnetization.

EXCITATION BY PULSES

The standard technique for excitation of even orders of multiple-quantum coherence employs the hard-pulse sequence

$$90°(X) - \tau - 180°(X) - \tau - 90°(X) \qquad [1]$$

with the delay adjusted to the condition $\tau = 1/(4J)$. In the vocabulary of product operators, double-quantum coherence would be excited in a homonuclear IS spin system according to the scheme

$$+I_Z + S_Z \xrightarrow{I_X} \xrightarrow{S_X} -I_Y - S_Y \xrightarrow{2I_ZS_Z} + 2I_XS_Z + 2I_ZS_X$$
$$\xrightarrow{I_X} \xrightarrow{S_X} +2I_XS_Y + 2I_YS_X \qquad [2]$$

where, for simplicity, the 180° pulse has been omitted since it has no effect on the terms $+ 2I_XS_Z$ and $+ 2I_ZS_X$ but merely refocuses the chemical shift evolution. Single-quantum coherence is returned to the +Z axis by the same sequence:

$$+I_Z \xrightarrow{I_X} -I_Y \xrightarrow{(\pi)\, I_X} +I_Y \xrightarrow{I_X} +I_Z. \qquad [3]$$

To excite odd orders of multiple-quantum coherence it is sufficient to shift the phase of the last two pulses:

$$90°(X) - \tau - 180°(Y) - \tau - 90°(Y). \qquad [4]$$

For example, triple-quantum coherence can be excited in a three-spin ISR system. If we assume for simplicity that $J_{IS} = J_{SR} = J_{IR}$, so that the intervals τ can be optimized for all three coupling constants, then we may write

$$+I_Z \xrightarrow{I_X} -I_Y \xrightarrow{2I_ZS_Z} +2I_XS_Z \xrightarrow{2I_ZR_Z} +4I_YS_ZR_Z \xrightarrow{S_Y} \xrightarrow{R_Y} +4I_YS_XR_X. \qquad [5]$$

Similar expressions, starting with $+S_Z$ and $+R_Z$, generate the terms $+4I_XS_YR_X$ and $+4I_XS_XR_Y$ respectively. Together these three terms represent triple-quantum coherence and three-spin single-quantum coherence (sometimes called *combination lines*). Note that p-quantum coherence can only be excited in an n-spin system if p is less than or equal to n.

SPECIAL PROPERTIES OF MULTIPLE-QUANTUM COHERENCE

If we regard a multiple-quantum transition as a cascade of single-quantum transitions (not necessarily all in the same sense) then we might well anticipate special properties determined by p, the order of the coherence. Indeed, multiple-quantum coherence exhibits a heightened sensitivity to certain instrumental parameters, whereas zero-quantum coherence is virtually unaffected by the same variables. Consider, first of all, the evolution of double-quantum coherence in an IS-spin system due to the chemical shifts δ_I and δ_S (measured with respect to the transmitter frequency). Intuition would suggest that a shift of the transmitter frequency should have a two-fold effect on double-quantum coherence. Formally, we treat the chemical shift evolution as a cascade of two consecutive rotations about

the Z axis, taken in either order. Double-quantum coherence can be represented by $2I_XS_X - 2I_YS_Y$; we consider the evolution of the two terms separately:

$$2I_XS_X \xrightarrow{(2\pi\delta_I t)\, I_Z} \xrightarrow{(2\pi\delta_S t)\, S_Z}$$

$$2[I_X \cos(2\pi\delta_I t) + I_Y \sin(2\pi\delta_I t)]\,[S_X \cos(2\pi\delta_S t) + S_Y \sin(2\pi\delta_S t)] \qquad [6]$$

$$2I_YS_Y \xrightarrow{(2\pi\delta_I t)\, I_Z} \xrightarrow{(2\pi\delta_S t)\, S_Z}$$

$$2[I_Y \cos(2\pi\delta_I t) - I_X \sin(2\pi\delta_I t)]\,[S_Y \cos(2\pi\delta_S t) - S_X \sin(2\pi\delta_S t)]. \qquad [7]$$

Subtraction of eqn [7] from eqn [6] and the application of standard trigonometrical identities gives

$$\sigma_{DQC} = (2I_XS_X - 2I_YS_Y) \cos[2\pi(\delta_I + \delta_S)t]. \qquad [8]$$

This demonstrates that double-quantum coherence evolves at the sum of the chemical shift frequencies. Furthermore, a shift of the transmitter frequency translates into a two-fold frequency shift of the double-quantum coherence.

Now zero-quantum coherence is represented by the term $(2I_XS_X + 2I_YS_Y)$ and its chemical shift evolution can be evaluated by adding eqn [6] to eqn [7], and invoking standard trigonometrical identities:

$$\sigma_{ZQC} = (2I_XS_X + 2I_YS_Y) \cos[2\pi(\delta_I - \delta_S)t]. \qquad [9]$$

This confirms the intuitive expectation that homonuclear zero-quantum coherence is insensitive to chemical shift effects or to displacement of the transmitter frequency. The general conclusion is that p-quantum coherence evolves as the sum of p different chemical shifts, and exhibits a p-fold dependence on offset from the transmitter frequency. This latter property serves as a useful method for separating spectra from different orders of multiple-quantum coherence.

Since the chemical shift is determined by the applied magnetic field intensity, a field gradient imposes a distribution of the chemical shift terms in eqns [6] and [7], resulting in a dispersion of multiple-quantum isochromats in proportion to the order (p) of the coherence, leaving zero-quantum coherence unaffected. This is a powerful method for separation of the different coherence orders, using a pulsed field gradient of duration t_p during evolution, and a refocusing gradient of duration pt_p after reconversion into observable transverse magnetization (4–6). This 'matched gradient' method has the marked advantage over phase-cycling methods that it can be implemented in a single scan and does not rely on difference spectroscopy. Similar considerations apply to the natural inhomogeneity of the applied magnetic field, rendering p-quantum coherences p times as sensitive to instrumental broadening as conventional single-quantum signals.

We normally view the precession of multiple-quantum coherence in a reference frame rotating in synchronism with the radiofrequency transmitter. Then a phase

shift ϕ of the transmitter corresponds to a rotation of a single-quantum magnetization vector through ϕ radians about the +Z axis:

$$I_Y \cos(2\pi\delta_S t) \xrightarrow{(+\phi)\, I_z} I_Y \cos(2\pi\delta_S t) \cos\phi - I_X \sin(2\pi\delta_S t) \sin\phi = I_Y \cos(2\pi\delta_S t + \phi). \quad [10]$$

It follows that homonuclear double-quantum coherence must be twice as sensitive to such phase shifts since, using identities for $\cos 2\phi$ and $\sin 2\phi$, we may write

$$\begin{aligned}(2I_XS_X - 2I_YS_Y) &\xrightarrow{(+\phi)\, I_z} (2I_XS_X - 2I_YS_Y)\cos\phi + (2I_YS_X + 2I_XS_Y)\sin\phi \\ &\xrightarrow{(+\phi)\, S_z} (2I_XS_X - 2I_YS_Y)\cos 2\phi + (2I_XS_Y + 2I_YS_X)\sin 2\phi \end{aligned} \quad [11]$$

which represents a *doubling* of the phase shift. On the other hand, a similar derivation applied to homonuclear zero-quantum coherence yields the simpler result

$$\begin{aligned}(2I_XS_X + 2I_YS_Y) &\xrightarrow{(+\phi)\, I_z} (2I_XS_X + 2I_YS_Y)\cos\phi + (2I_YS_X - 2I_XS_Y)\sin\phi \\ &\xrightarrow{(+\phi)\, S_z} (2I_XS_X + 2I_YS_Y). \end{aligned} \quad [12]$$

That is to say, there is no phase shift at all. Generalization of these results suggests that a radiofrequency phase shift of ϕ radians for all pulses in the excitation sequence translates into a phase shift $p\phi$ in the p-quantum coherence. This is the basis of the phase-cycling methods used for separation of coherence orders. The receiver phase is programmed to rotate (usually in 90° steps) so as to follow the desired coherence order, while signals from the remaining orders rotate at different rates and cancel after a complete cycle. These phase cycles are at the basis of the well-known filtration experiments – INADEQUATE (7–9) or double-quantum filtered COSY (10).

Multiple-quantum spectra are normally recorded by allowing the various coherences to precess during the evolution period of a two-dimensional experiment, detecting them indirectly by reconversion to observable transverse magnetization just before signal acquisition. An illustration of the p-fold sensitivity to radiofrequency phase shifts is provided by the multiple-quantum spectrum of the three-spin system in acrylic acid (9), obtained by projection of the two-dimensional spectrum onto the F_1 frequency axis (Fig. 1). We consider the motion in a frame of reference rotating in synchronism with the transmitter, normally identical to the receiver frequency. However, we may contrive to make the receiver reference frame appear to rotate at a different frequency if we introduce a progressive shift of the receiver phase as each acquisition step. An incremental shift of ϕ radians at each of k steps over a total acquisition time of T seconds induces an apparent frequency shift of $k\phi/(2\pi T)$ Hz. This is known as the 'time-proportional phase incrementation (TPPI)' technique (11) and it may be implemented in the evolution period t_1, or in the detection period t_2.

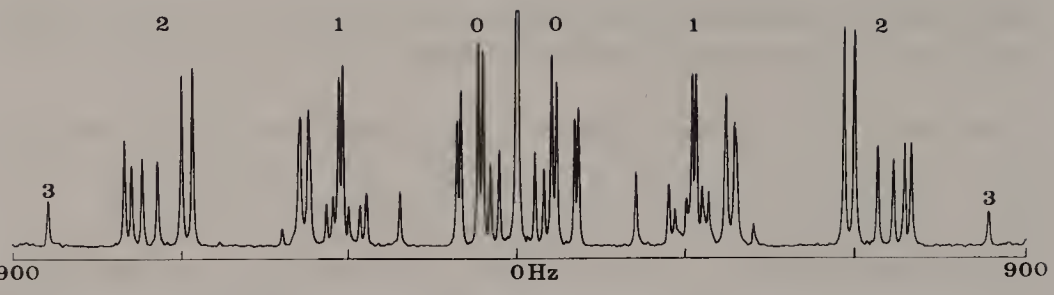

Fig. 1. Multiple-quantum spectrum of the three-spin system of protons in acrylic acid obtained by projection of the two-dimensional spectrum onto the F_1 axis. The orders of coherence (0, 1, 2, 3) were separated by advancing the receiver phase by $\pi/3$ radians at each increment of t_1. The single-quantum spectrum (1) consists of 15 lines, three of which are three-spin single-quantum transitions ('combination lines'). There is only one triple-quantum transition (shown aliased from above 900 Hz).

In the acrylic acid experiment (Fig. 1) the radiofrequency phase was increased through an angle of $\pi/3$ radians at each time increment in the evolution period (12). This leaves zero-quantum transitions unaffected, but shifts single-quantum transitions by one-third of the F_1 spectral width, double-quantum transitions by two-thirds of this spectral width, and the triple-quantum transition by the full spectral width. There are six zero-quantum and six double-quantum lines, as expected. The single-quantum spectrum contains 15 lines, of which three are three-spin single-quantum transitions (combination lines). There is just one triple-quantum transition (shown aliased).

APPLICATIONS OF MULTIPLE-QUANTUM COHERENCE

The insensitivity of zero-quantum coherence to spatial inhomogeneity of the B_0 field suggests that it could be used to extract high-resolution chemical shift or spin–spin coupling information from samples that are in a very non-uniform magnetic field, where the conventional NMR spectrum would be hopelessly broad. Some biological and medical applications of NMR are forced to deal with samples that are magnetically inhomogeneous, and zero-quantum experiments can be useful here, for example for lactate editing (13). Only the relative chemical shift ($\delta_I - \delta_S$) between the two nuclei of a coupled IS-spin system is accessible by this method. In principle the linewidths of zero-quantum transitions may be used as a measure of spin–spin relaxation rates.

In a multispin system, multiple-quantum spectra (particularly the spectra derived from higher-order coherences) contain fewer lines than the conventional single-quantum spectrum. This is an important method of simplification and it has been exploited for high-resolution spectra of isotropic liquids (14) as well as for spectra derived from partially ordered samples in liquid-crystal matrices (15).

Perhaps the most practically useful application to date has been the separation of spectra from different spin systems by exploiting the special properties of multiple-quantum coherence. The ubiquitous double-quantum filtered COSY technique (10) gives much better access to cross-peaks close to the diagonal and suppresses singlet signals which carry no useful correlation information and which often interfere with the signals of interest. Another example is the detection of the weak carbon-13 satellite lines that appear in the flanks of the 'parent' carbon-13 resonances in natural abundance material. These satellites carry the interesting carbon–carbon coupling information while the parent lines are an embarrassment because they tend to obscure the satellites. Correlation information is derived from the satellite subspectra from AB or AX coupled spin systems in which double-quantum coherence can be generated, whereas the parent lines arise from isolated carbon-13 spins and cannot sustain multiple-quantum coherence under any circumstances. By monitoring the evolution of double-quantum coherence during the evolution period of a two-dimensional experiment, we may separate the satellite subspectra at different levels in the F_1 (double-quantum) dimension. Filtration is achieved by the appropriate phase cycle or by the application of matched field gradients. Each subspectrum straddles the skew diagonal of slope 2, since its centre lies at $\frac{1}{2}(\delta_I + \delta_S)$ and the corresponding double-quantum frequency is $(\delta_I + \delta_S)$. The result is a particularly simple correlation diagram that allows the carbon skeleton of the

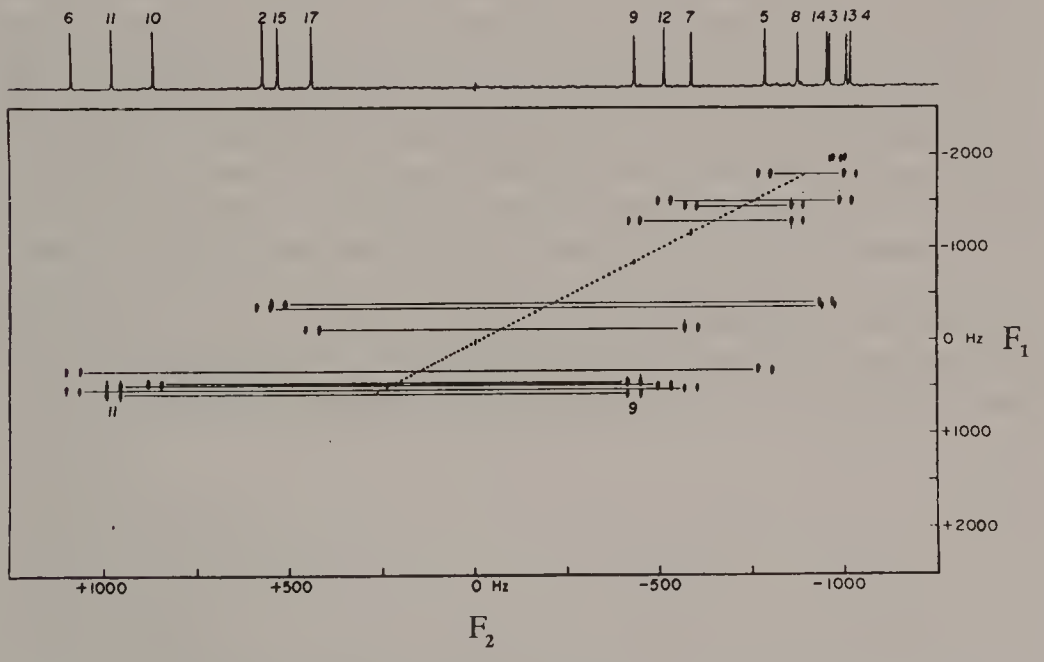

Fig. 2. Two-dimensional INADEQUATE spectrum showing the connectivities between carbon-13 sites in sparteine in natural abundance material. Each pair of directly coupled carbon-13 spins gives rise to a four-line pattern in the F_2 dimension, displaced according to the double-quantum frequency in the F_1 dimension. The centres of these subspectra must all lie on the diagonal of slope 2 (the dotted line).

molecule to be built up, one linkage at a time. Figure 2 shows the two-dimensional INADEQUATE spectrum of sparteine recorded at 100 MHz; proton decoupling is used throughout (9).

HETERONUCLEAR MULTIPLE-QUANTUM CORRELATION

There is now a wide range of multidimensional experiments designed to simplify high-resolution spectra of biological macromolecules by recording the proton subspectra from samples artificially enriched in carbon-13 or nitrogen-15. One of the techniques used to achieve this separation is called the heteronuclear multiple-quantum correlation (HMQC) experiment (16). The method was first described in an early paper by Müller (17) and is an example of 'round-trip' coherence transfer $I \rightarrow S \rightarrow I$.

Stripped to its bare essentials, the pulse scheme may be written as

I spins:	$90° - \tau -$	$\vert$	$180°$	$\vert$	$- \tau$	– acquire
S spins:		$90° - \frac{1}{2}t_1 -$	$\vert$	$- \frac{1}{2}t_1 - 90°$		decouple.

Proton (I-spin) magnetization is prepared in an antiphase state ($+2I_XS_Z$) through the operation of the $2I_ZS_Z$ product operator during the interval $\tau = 1/(2J_{IS})$. The second 90° pulse, acting on the S spins, creates heteronuclear two-spin coherence ($-2I_XS_Y$). This evolves during the t_1 period of the multidimensional experiment. Normally the S-spin chemical shift information would be encoded into the multiple-quantum frequencies ($\delta_I + \delta_S$) and ($\delta_I - \delta_S$), but it would be more convenient to eliminate the I-spin chemical shift contribution in this dimension. This is achieved by the 180° pulse on the I spins at the mid-point of the evolution period, which interchanges zero- and double-quantum coherence (17) leaving the S-spin evolution determined only by δ_S. The final 90° pulse converts the two-spin coherence ($+2I_XS_Y$) into antiphase I-spin magnetization ($+2I_XS_Z$) which then evolves during the second τ period into in-phase magnetization ($+I_Y$). This ensures a high sensitivity for detection, similar to that obtained in the related heteronuclear single-quantum correlation (HSQC) experiment (18). The S-spin chemical shift intervenes only to separate the proton subspectra in the F_1 frequency domain. Often these are themselves two-dimensional spectra, for example NOESY or TOCSY.

REFERENCES

1. W. A. Anderson, R. Freeman and C. A. Reilly, *J. Chem. Phys.* **39**, 1518 (1963).
2. A. D. Cohen, R. Freeman, K. A. McLauchlan and D. H. Whiffen, *Mol. Phys.* **7**, 45 (1963).
3. W. P. Aue, E. Bartholdi and R. R. Ernst, *J. Chem. Phys.* **64**, 2229 (1976).
4. A. Bax, P. G. de Jong, A. F. Mehlkopf and J. Smidt, *Chem. Phys. Lett.* **69**, 567 (1980).
5. P. Barker and R. Freeman, *J. Magn. Reson.* **64**, 334 (1985).
6. R. E. Hurd, *J. Magn. Reson.* **87**, 442 (1990).
7. A. Bax, R. Freeman, T. A. Frenkiel and M. H. Levitt, *J. Magn. Reson.* **43**, 478 (1981).
8. A. Bax, R. Freeman and T. A. Frenkiel, *J. Am. Chem. Soc.* **103**, 2102 (1981).
9. A. J. Shaka and R. Freeman, *J. Magn. Reson.* **50,** 502 (1982).
10. U. Piantini, O. W. Sørensen and R. R. Ernst, *J. Am. Chem. Soc.* **104**, 6800 (1982).
11. A. Pines, D. E. Wemmer, J. Tang and S. Sinton, *Bull. Am. Phys. Soc.* **23**, 21 (1978).
12. R. Freeman, T. A. Frenkiel and M. H. Levitt, *J. Magn. Reson.* **44**, 409 (1981).
13. D. M. Freeman and R. E. Hurd, *NMR Basic Princ. & Prog.* **27**, 200 (1992).
14. X. L. Wu and P. Xu, *J. Magn. Reson.* **88**, 417 (1990).
15. G. Bodenhausen, R. L. Vold and R. R. Vold, *J. Magn. Reson.* **37**, 93 (1980).
16. A. Bax, R. H. Griffey and D. L. Hawkins, *J. Magn. Reson.* **55**, 301 (1983).
17. L. Müller, *J. Am. Chem. Soc.* **101**, 4481 (1979).
18. A. Bax, M. Ikura, L. E. Kay, D. E. Torchia and R. Tschudin, *J. Magn. Reson.* **86**, 304 (1990).

Cross-references

Coherence
Phase cycling
Polarization transfer
Product operator formalism
Pulsed field gradients
Rotating frame
Two-dimensional spectroscopy

Multiplicity Determination

Nowadays, the recording of a decoupled high-resolution carbon-13 spectrum is a straightforward matter, but the assignment of the resonances to individual carbon sites still presents a considerable challenge. Fortunately there is now quite an armoury of techniques available to assist in the assignment. Apart from deductions based on chemical shifts, relaxation properties, double resonance or chemical shift correlation, there are several methods designed to identify the number of attached protons, relying on the fact that the direct interaction $^1J_{CH}$ is very much larger than the long-range couplings $^nJ_{CH}$.

J-SCALING

In the very early days of carbon-13 spectroscopy, multiplicity was determined by off-resonance decoupling with a monochromatic radiofrequency field B_2. The idea was to shrink the CH splittings so that adjacent multiplets no longer overlapped, while still leaving the multiplet structure resolved (1). Since these residual splittings are very variable, depending on the decoupler offset, this is an inconvenient and time-consuming method. It has been replaced by 'J-scaling' techniques which retain the same ratio of observed splitting to coupling constant throughout the carbon-13 spectrum, independent of the proton chemical shifts.

Figure 1 illustrates the application to the carbon-13 spectrum of camphor, which gives a J-scaled spectrum in which there is a doublet and triplet at almost the same carbon-13 chemical shift. These interpenetrating multiplets are readily recognized by running the J-scaled spectrum twice, with different scaling factors. These spectra were actually recorded by a time-consuming 'interferogram' method where the scaling was implemented during an evolution period of a two-dimensional experiment (2). There is now a 'real-time' analogue of this technique that is simpler and much faster. The idea is to apply a broadband decoupling* scheme (such as WALTZ-16) in a time-shared mode, in which a period t_w of decoupling is followed by a shorter period t_p of free precession when the carbon-13 spins are coupled to protons. The apparent multiplet splitting is then scaled down from $^1J_{CH}$ by a factor $t_p/(t_p + t_w)$, independent of proton chemical shift within the effective decoupling

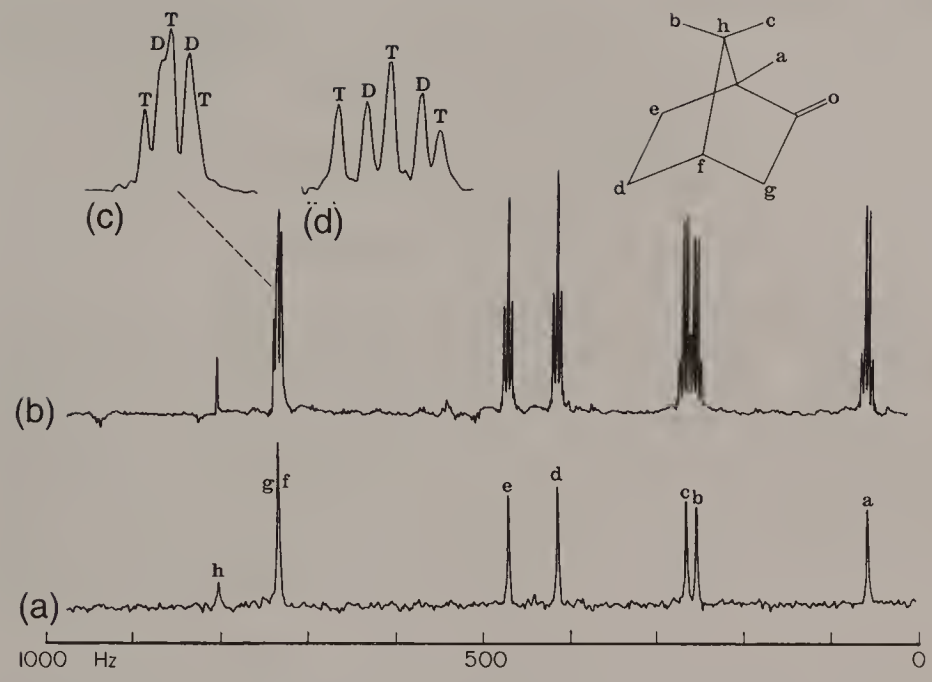

Fig. 1. (a) The conventional decoupled carbon-13 spectrum of camphor. (b) The spectrum after J-scaling. The multiplicities indicate the numbers of directly bound protons. The overlapping multiplets g and f have been recorded with different scaling factors in (c) and (d).

bandwidth. The scaling factor is normally adjusted to some suitable fraction (e.g. 1/20) in order to display well-resolved carbon-13 multiplets that are still clearly separated from their nearest neighbours (3).

TWO-DIMENSIONAL J-SPECTRA

Carbon-13 spin echoes* are modulated by the heteronuclear spin–spin coupling J_{CH} if the proton spins are inverted in synchronism with the carbon-13 refocusing pulses. A two-dimensional experiment can be devised in which echo modulation takes place during the evolution period while carbon-13 shifts are refocused; the carbon-13 signal is then acquired in the decoupled mode. The result is a two-dimensional spectrum that has only carbon-13 chemical shifts in the F_2 dimension and only CH splittings on the F_1 dimension. Figure 2 illustrates the carbon-13 spectrum of sucrose recorded by this method, indicating the multiplicities of the various sites. At the cost of a fairly protracted experiment, the F_1 dimension may be finely digitized, displaying both direct and long-range CH splittings. Where multiplicity is the only requirement, it is advantageous to strip down the measurements to the bare minimum of t_1 increments, so that singlets, doublets, triplets and quartets are just well enough resolved to be distinguishable. Nishida *et*

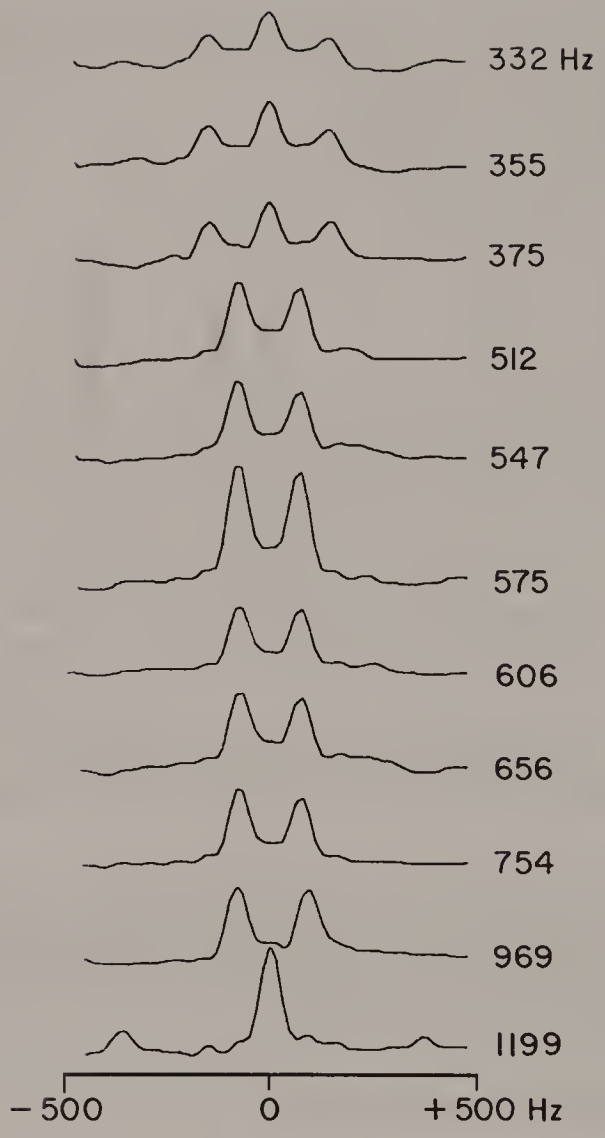

Fig. 2. Traces extracted from the carbon-13 two-dimensional J-spectrum of sucrose corresponding to the carbon-13 chemical shifts indicated on the right.

al. (4) have demonstrated that as few as five t_1 increments suffice to provide unambiguous multiplicity information. This makes the technique competitive with other methods of multiplicity determination.

SPECTRAL EDITING

The decomposition of decoupled carbon-13 spectra into subspectra from the quaternary, CH, CH_2 and CH_3 groups has come to be known as spectral editing. One early experiment exploits the echo-modulation effect outlined above. The time

evolution of spin echoes from the different sites can be represented by the cosine modulations

$$\text{CH groups: } S = S_0 \cos(\pi J_{CH} t) \quad [1]$$

$$\text{CH}_2 \text{ groups: } S = S_0 \cos^2(\pi J_{CH} t) \quad [2]$$

$$\text{CH}_3 \text{ groups: } S = S_0 \cos^3(\pi J_{CH} t) \quad [3]$$

while the quaternary sites are modulated at such a low frequency that the changes can be neglected on this time scale. If the interval t is set equal to $1/J_{CH}$ then the signals from the CH and CH_3 groups are inverted while the signals from the quaternary and CH_2 groups remain upright. This can be regarded as a first step, establishing the 'parity' of the carbon sites, as illustrated by the 100 MHz edited carbon-13 spectrum of estrone methyl ether (Fig. 3) recorded by Fourier transformation of spin echoes observed after a delay t = 7 ms (5). Elaboration of the method allows all four cases to be identified.

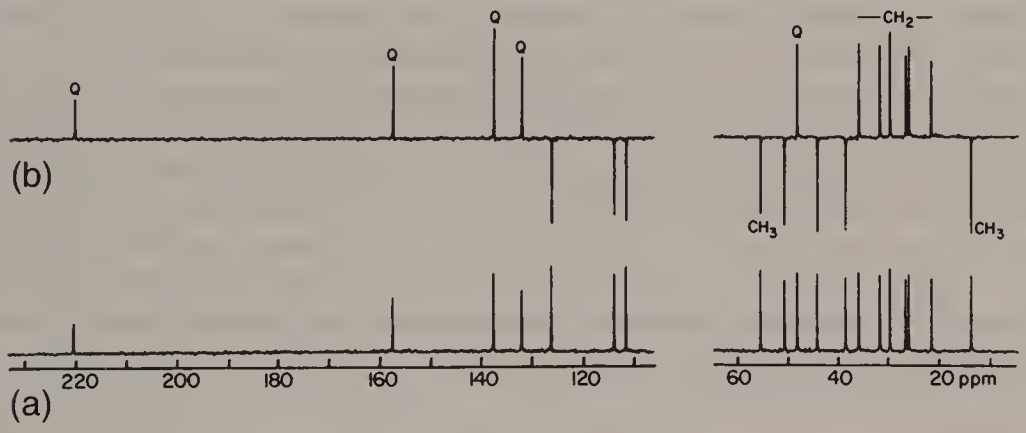

Fig. 3. Carbon-13 spectra of estrone methyl ether. (a) Conventional decoupled spectrum. (b) Spectrum edited according to parity; quaternary (Q) and CH_2 sites give upright signals while CH and CH_3 sites give inverted signals. The CH signals are not labelled.

A more practically convenient method is the widely employed DEPT (distortionless enhancement by polarization transfer) technique which relies on multiple-quantum coherence effects (6). The sequence is set out in Fig. 4 with the key time points numbered for easy reference. At first sight, the mechanism of the DEPT experiment may appear somewhat obscure. This is partly because the sequence has been condensed from a more elaborate scheme with four 180° pulses, but since the proton chemical shift evolution is only effective during the interval 1–4, while the carbon-13 chemical shift evolution is only effective during the interval 3–6, just two refocusing pulses suffice.

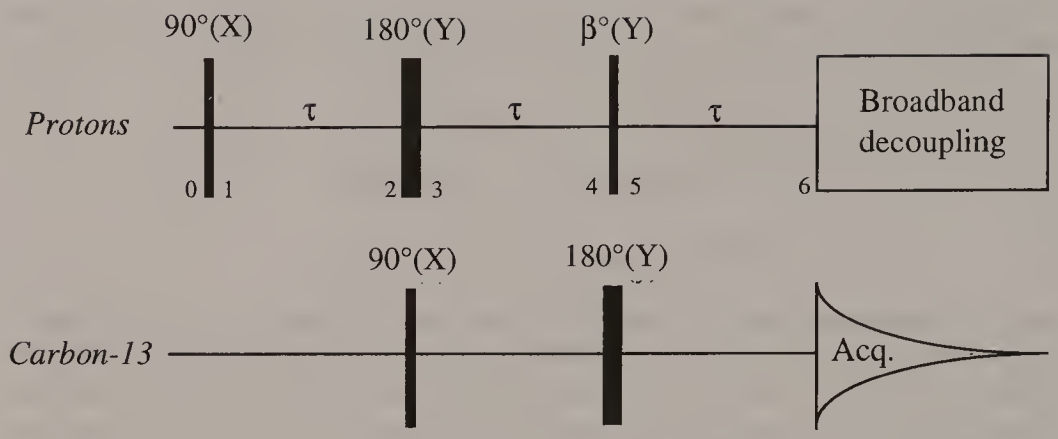

Fig. 4. Pulse sequence for the DEPT experiment. The product operator terms are discussed in the text with reference to the timing points 1 through 6.

The first step is to generate heteronuclear two-spin coherence (zero- and double-quantum coherence) by setting the τ intervals to the condition $\tau = 1/(2J_{CH})$. At point 4 in the sequence, three types of two-spin coherence have been generated, $+2I_XS_Y$ from the CH groups, $-(4I_XI_ZS_X + 4I_ZI_XS_X)$ from the CH_2 groups, and $-(8I_XI_ZI_ZS_Y + 8I_ZI_XI_ZS_Y + 8I_ZI_ZI_XS_Y)$ from the CH_3 groups. (The second 180° pulse inverts the sign of the $-(4I_XI_ZS_X + 4I_ZI_XS_X)$ terms.) The crucial step is the application of the variable flip angle pulse (β) to the protons between time points 4 and 5. Because it acts on only one proton in a CH group, two in a CH_2 group, and three in a CH_3 group, it can distinguish these three cases. We can think of it as a cascade of one, two or three consecutive operations. In the formalism of product operators* with I = protons and S = carbon-13, we may write

CH group: $$+2I_XS_Y \xrightarrow{(\beta)I_Y} -2I_ZS_Y \sin\beta \qquad [4]$$

CH_2 group: $$+4I_XI_ZS_X + 4I_ZI_XS_X \xrightarrow{(\beta)I_Y} \xrightarrow{(\beta)I_Y} -4I_ZI_ZS_X\, 2\sin\beta\cos\beta \qquad [5]$$

CH_3 group: $$-8I_XI_ZI_ZS_Y - 8I_ZI_XI_ZS_Y - 8I_ZI_ZI_XS_Y \xrightarrow{(\beta)I_Y} \xrightarrow{(\beta)I_Y} \xrightarrow{(\beta)I_Y}$$

$$+ 8I_ZI_ZI_ZS_Y\, 3\sin\beta\cos^2\beta. \qquad [6]$$

The last stage is a period τ of free precession to allow the antiphase components to come back into phase under the action of the spin–spin coupling operator $2I_ZS_Z$:

CH group: $$-2I_ZS_Y \sin\beta \xrightarrow{2I_ZS_Z} +S_X \sin\beta \qquad [7]$$

CH_2 group: $$-4I_ZI_ZS_X\, 2\sin\beta\cos\beta \xrightarrow{2I_ZS_Z} +2S_X \sin\beta\cos\beta \qquad [8]$$

CH_3 group: $+8I_ZI_ZI_ZS_Y\ 3 \sin\beta \cos^2\beta \xrightarrow{2I_ZS_Z} +3S_X \sin\beta \cos^2\beta$ [9]

Editing consists in exploiting the differences between these trigonometrical expressions so as to extract the three kinds of subspectra (quaternary sites remain unmodulated on this time scale). By carefully choosing the settings of the flip angle β we can separate the subspectra. If $\beta = 45°$, all three types of subspectra give positive signals. With $\beta = 135°$, signals from the CH and CH_3 groups are upright but the signals from the CH_2 group are inverted. Consequently, a pure methylene subspectrum can be obtained by subtraction of these results. When $\beta = 90°$ the CH subspectrum is isolated. Thus, by taking the appropriate linear combinations, a complete separation of the subspectra should be feasible. However, some allowance must be made for the fact that there is a range of magnitudes for the CH coupling constants. A refinement called 'SEMUT' is more tolerant of this natural variation of $^1J_{CH}$ values (7).

REFERENCES

1. H. J. Reich, M. Jautelat, F. J. Weigert and J. D. Roberts, *J. Am. Chem. Soc.* **91**, 7445 (1969).
2. R. Freeman and G. A. Morris, *J. Magn. Reson.* **29**, 173 (1978).
3. G. A. Morris, G. L. Nayler, A. J. Shaka, J. Keeler and R. Freeman, *J. Magn. Reson.* **58**, 155 (1984).
4. T. Nishida, C. Enzell and J. Keeler, *J. Chem. Soc. (London) Chem. Commun.* 1489 (1985).
5. F. K. Pei and R. Freeman, *J. Magn. Reson.* **48**, 318 (1982).
6. D. M. Doddrell, D. T. Pegg and M. R. Bendall, *J. Magn. Reson.* **48**, 323 (1982).
7. O. W. Sørensen, D. Dønstrup, H. Bildsøe and H. J. Jakobsen, *J. Magn. Reson.* **55**, 347 (1983).

Cross-references

Broadband decoupling
J-spectroscopy
Multiple-quantum coherence
Product operator formalism
Spin echoes
Two-dimensional spectroscopy

Nuclear Overhauser Effect

A. W. Overhauser (1) suggested a novel experiment whereby the intensity of an NMR signal could be greatly enhanced by saturating the electron spin resonance signal from unpaired electrons in the sample. In effect, it confers on the nuclear spins the benefits of the large spin population differences that normally exist across electron spin resonance transitions. A prerequisite for this *cross-relaxation* experiment is that the spin–lattice relaxation of the nuclei is dominated by dipole–dipole interactions with the unpaired electron spins. Enhancements of two to three orders of magnitude are observed in practice (2–4). No widespread use has been made of this *electron–nuclear* Overhauser effect for enhancement of NMR spectra, since it involves rather complex arrangements for simultaneous microwave and radiofrequency irradiation, and requires the addition of free radicals to the NMR sample. Furthermore, the enhancements measured in practice depend on the nature of the sample in a complicated fashion. We concentrate here on the analogous *nuclear–nuclear* Overhauser effect (5,6) which has turned out to be of widespread importance for structural studies of macromolecules. It is also used as a routine method for enhancing carbon-13 spectra by saturating the proton resonances.

Let us suppose (7) that there are two Alpine villages A and B, each with a ski lift to the top of their respective slopes, A* and B* (Fig. 1). Both ski runs have the same length, but since the village A is slightly higher up the mountain than B, the top of the ski lift A* is similarly higher than B*. Imagine that we are interested in the relative popularities of the two ski villages, and that we attempt to measure this in terms of the ratio of the numbers of skiers at each village. There might well be a small preponderance at B since it is the first village on the approach road. This 'natural' population ratio could also be measured between A* and B* since the two lifts are assumed to have the same passenger-carrying capacity, and the ratio would not be affected by the normal flow of skiers down the slopes (relaxation). We might, however, suppose that towards the end of the day many 'gung-ho' skiers at A* might choose to make their last run on the longer *piste* from A* to B, having no particular preference for the *après ski* activities at the two villages (Fig. 1(a)). A head count would then indicate an appreciably enhanced ratio in favour of B, a consequence of the asymmetry introduced into the problem by the 'cross-relaxation' path A*–B. Alternatively, we could take the opposite view (Fig. 1(b))

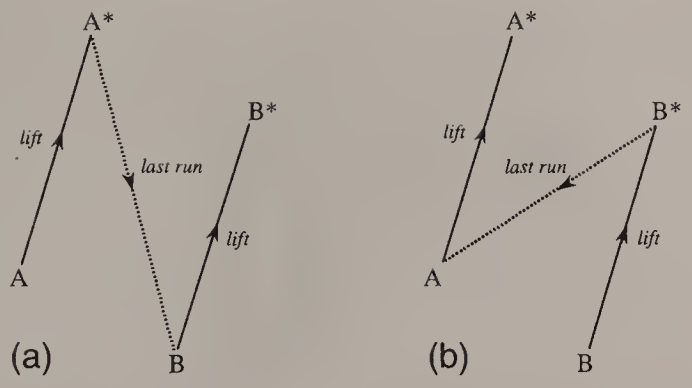

Fig. 1. Schematic diagram for the ski analogy. Energetic skiers (a) take the 'double-quantum' path for their final run, whereas the tired skiers (b) choose the 'zero-quantum' path.

that tired skiers would choose the shorter path B*–A for the last run. This would have the effect of reversing the relative 'popularities' of the two ski villages.

This is the essence of the nuclear Overhauser effect, in which the pumping of two I-spin transitions by radiofrequency fields (the ski lifts), combined with strong cross-relaxation of the S spins by the I spins, has the effect of transferring the strong I-spin polarization to the weak S spins. Two kinds of cross-relaxation are possible, depending on whether the molecular reorientation is fast (Fig. 1(a)) or slow (Fig. 1(b)). For the former, the Overhauser enhancement is positive, whereas for the latter it is negative.

THE TWO-SPIN SYSTEM

We consider the simplest case, a four-level system where I and S may have different gyromagnetic ratios γ_I and γ_S (Fig. 2). The efficiencies with which relaxation occurs are represented by the relaxation transition probabilities, W_I, W_S W_0 and W_2. The 'natural' transition probabilities W_I and W_S correspond to a single spin flipping, for example the I-spin transitions $\alpha\beta \rightarrow \beta\beta$ and $\alpha\alpha \rightarrow \beta\alpha$:

$$W_I = \frac{3}{20}\left(\frac{\mu_0}{4\pi}\right)^2 \gamma_I^2\gamma_S^2\left(\frac{h}{2\pi}\right)^2 r^{-6}\,\frac{\tau_c}{1+(\omega_I)^2\tau_c^2} \qquad [1]$$

where $\mu_0/4\pi$ is the conversion factor into SI units, h is Planck's constant, r is the internuclear distance, and τ_c is the correlation time for molecular reorientation (see below). The corresponding S-spin transitions $\alpha\alpha \rightarrow \alpha\beta$ and $\beta\alpha \rightarrow \beta\beta$ have the probability

$$W_S = \frac{3}{20}\left(\frac{\mu_0}{4\pi}\right)^2 \gamma_I^2\gamma_S^2\left(\frac{h}{2\pi}\right)^2 r^{-6}\,\frac{\tau_c}{1+(\omega_S)^2\tau_c^2}. \qquad [2]$$

The cross-relaxation terms involve two spins flipping simultaneously, for example the zero-quantum transition $\alpha\beta \rightarrow \beta\alpha$

$$W_0 = \frac{1}{10}\left(\frac{\mu_0}{4\pi}\right)^2 \gamma_I{}^2\gamma_S{}^2\left(\frac{h}{2\pi}\right)^2 r^{-6} \frac{\tau_c}{1+(\omega_1-\omega_S)^2\tau_c{}^2} \qquad [3]$$

and the double-quantum transition probability involving a concerted flip of both spins in the same sense, $\alpha\alpha \rightarrow \beta\beta$,

$$W_2 = \frac{3}{5}\left(\frac{\mu_0}{4\pi}\right)^2 \gamma_I{}^2\gamma_S{}^2\left(\frac{h}{2\pi}\right)^2 r^{-6} \frac{\tau_c}{1+(\omega_I+\omega_S)^2\tau_c{}^2}. \qquad [4]$$

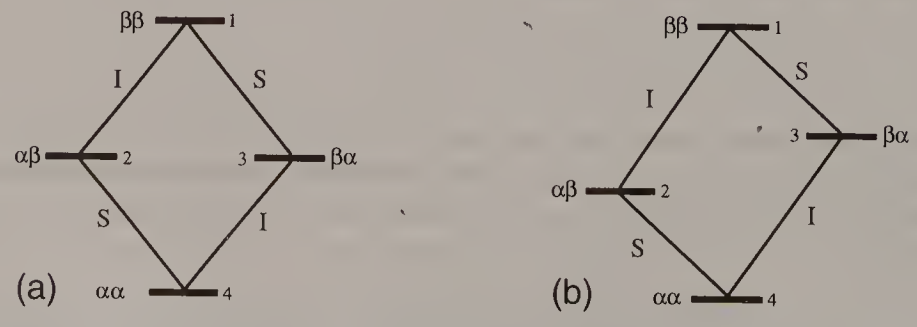

Fig. 2. Energy-level diagram for (a) a homonuclear two-spin system and (b) a heteronuclear two-spin system with γ_I larger than γ_S.

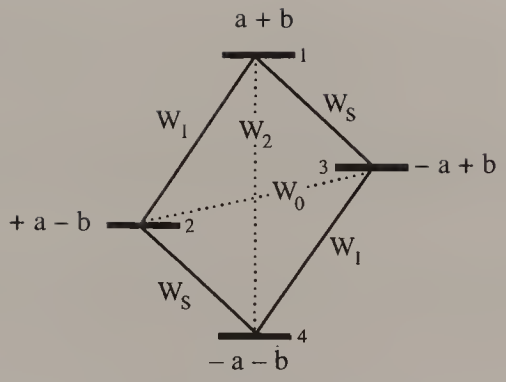

Fig. 3. Energy-level diagram for the heteronuclear IS system showing the relaxation transition probabilities W_I, W_S, W_0 and W_2. The numbers a and b are proportional to the deviations of the populations from equilibrium.

It is these cross-relaxation transition probabilities W_0 and W_2 (Fig. 3) that cause the Overhauser effect; W_0 is dominant for large, sluggish molecules, while W_2 is dominant for small, agile molecules.

POPULATION DYNAMICS

The signal intensities are proportional to the spin population differences across the appropriate energy levels. For simplicity of notation we write the deviations of the spin populations from equilibrium in terms of two numbers a and b:

$$2a = S_Z - S_0 \qquad [5]$$

$$2b = I_Z - I_0 \qquad [6]$$

where S_0 and I_0 are the intensities at Boltzmann equilibrium, related by

$$\frac{I_0}{S_0} = \frac{\gamma_I}{\gamma_S}. \qquad [7]$$

When the spin population of a given level deviates from equilibrium, there is a resulting flux of spins tending to restore equilibrium, and this flux is proportional to the product of the relevant population differences and the associated relaxation transition probabilities. Thus we may write for levels 1 and 2:

$$-\frac{dn_1}{dt} = +2aW_S + 2bW_1 + 2(a+b)W_2 \qquad [8]$$

$$-\frac{dn_2}{dt} = -2aW_S + 2bW_1 - 2(a-b)W_0. \qquad [9]$$

Consequently,

$$-\frac{d(n_1 - n_2)}{dt} = 2a(2W_S + W_2 + W_0) + 2b(W_2 - W_0). \quad [10]$$

The term $(W_2 - W_0)$ represents cross-relaxation and is given the symbol σ in the famous Solomon equations (8), while the term $(2W_S + W_2 + W_0)$ is given the symbol ρ.

A steady-state nuclear Overhauser effect is observed if the I spins are held in a continuous state of saturation ($I_Z = 0$) and the system is allowed time to reach a dynamic balance between the competing effects. Thus $d(n_1 - n_2)/dt = 0$ and

$$-\frac{a}{b} = \frac{W_2 - W_0}{2W_S + W_2 + W_0}. \quad [11]$$

Substitution of eqn [7] gives an expression for the steady-state enhancement factor:

$$\eta = \frac{S_Z - S_0}{S_0} = \frac{W_2 - W_0}{2W_S + W_2 + W_0}\frac{\gamma_I}{\gamma_S}. \quad [12]$$

In order to be able to evaluate this, we need to learn more about the relaxation transition probabilities W_I, W_S, W_2 and W_0, although we can see at once that there can be no enhancement if the cross-relaxation term $W_2 - W_0$ is zero.

MOLECULAR REORIENTATION

The details of the nuclear Overhauser effect depend on the rate at which molecules reorient in the liquid phase, since cross-relaxation results from fluctuations of the local magnetic field at the zero- or double-quantum frequencies. Because vibrations are far too rapid compared with these frequencies, and because translational motion involves large internuclear distances, only reorientation ('tumbling') is important. Actually we know rather little about the details of molecular reorientation, but we dress up this ignorance by defining a rotational correlation function,

$$g(\tau) = \langle R(t)R(t+\tau)\rangle, \quad [13]$$

which represents an ensemble average over all the molecules. R(t) is the molecular orientation at some time t, and $R(t + \tau)$ is the orientation at some later time $t + \tau$. The correlation function $g(\tau)$ is assumed to decay exponentially with time constant τ_c, the rotational correlation time, that is to say the time taken for a typical molecule to rotate through 1 radian. The Fourier transform of $g(\tau)$,

$$J(\omega) = \int_{-\infty}^{+\infty} g(\tau)\exp(-i\omega\tau)\,d\tau, \quad [14]$$

is called the spectral density function. If $g(\tau)$ decays exponentially then the spectral density adopts a Lorentzian form:

$$J(\omega) = \frac{2\tau_c}{1 + \omega^2\tau_c^2}. \quad [15]$$

It is usually plotted on a logarithmic frequency scale which gives the impression that the curve is essentially flat over a broad range of frequencies before cutting off on a sigmoid curve.

Spectral density curves are the key to understanding the influence of molecular reorientation. The small molecules of interest to organic chemists, dissolved in a mobile liquid solvent, have a $J(\omega)$ curve that extends well beyond the nuclear frequencies of interest. Since the area under the curve is constant, the components at the required frequencies are all essentially the same and relatively small (Fig. 4). This is called the 'extreme narrowing' condition (9). For the opposite extreme of macromolecules, we restrict the discussion to the proton–proton case, where the zero-quantum frequency $|\omega_I - \omega_S|$ is very small compared with ω_I or ω_S. These molecules tumble relatively slowly and $J(\omega)$ cuts off well below ω_I, ω_S and $(\omega_I + \omega_S)$, leaving an appreciable component only at the zero-quantum frequency. We treat these two cases in turn.

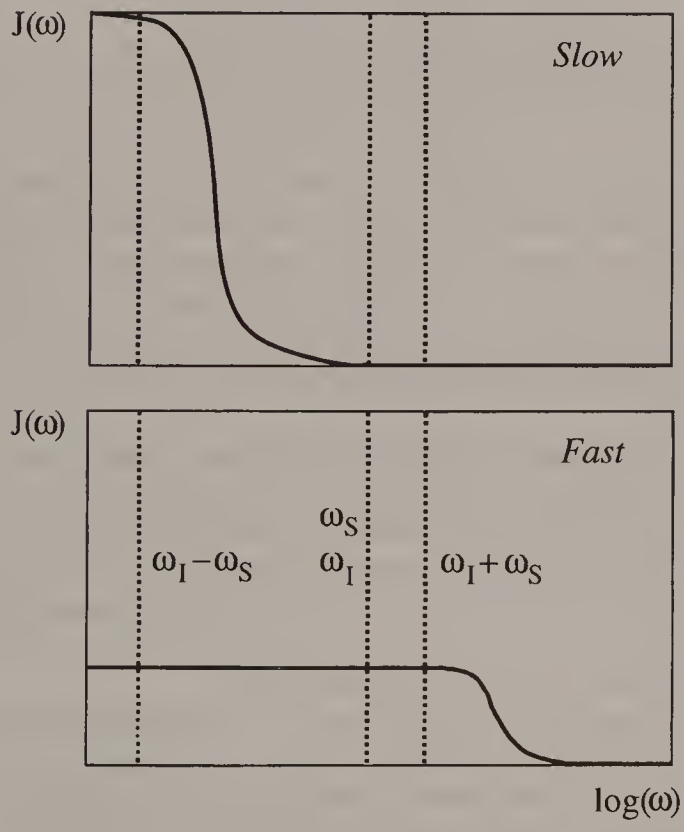

Fig. 4. Schematic spectral density functions for slow and fast molecular tumbling in a homonuclear IS spin system, showing the components at the I- and S-spin Larmor frequencies and at the zero- and double-quantum frequencies.

FAST MOLECULAR TUMBLING

Consider the case of relatively small molecules dissolved in a mobile liquid where the reorientation is fast compared with all the relevant nuclear precession frequencies:

$$\begin{aligned} |\omega_I - \omega_S|\tau_c &<< 1 \\ \omega_I\tau_c &<< 1 \\ \omega_S\tau_c &<< 1 \\ (\omega_I + \omega_S)\tau_c &<< 1. \end{aligned} \qquad [16]$$

The appropriate components of the spectral density function are then essentially the same and eqns [1]–[4] are considerably simplified, giving the ratios

$$W_2 : W_S : W_I : W_0 \quad :: \quad 12 : 3 : 3 : 2. \qquad [17]$$

In this case the double-quantum transition probability W_2 has the dominant effect. Whenever an I spin relaxes it carries with it an S spin in the same sense. When we substitute eqn [17] into eqn [12] we find the steady-state enhancement is

$$\eta = \frac{S_Z - S_0}{S_0} = \frac{1}{2}\frac{\gamma_I}{\gamma_S} \qquad [18]$$

The fraction by which the S-spin signal is increased is given by

$$1 + \eta = \frac{S_Z}{S_0} = 1 + \frac{1}{2}\frac{\gamma_I}{\gamma_S}. \qquad [19]$$

Thus if I represents protons and S represents carbon-13, the steady-state signal is increased three-fold, since for this case $\gamma_I = 4\gamma_S$. Almost all carbon-13 spectra are recorded with broadband proton decoupling, which saturates the protons and enhances the carbon-13 signals. For the case when protons are saturated and nitrogen-15 spins are observed, the signal is increased four-fold, but inverted, since $\gamma_H/\gamma_N = -10$. Homonuclear Overhauser experiments offer an increase of only 50% of the natural signal.

Note that these are the *maximum* obtainable Overhauser enhancements; they are only realized if the dipole–dipole mechanism is dominant and all other ('leakage') relaxation paths are negligible. This is a good approximation for proton decoupled carbon-13 spectroscopy, at least for protonated sites. But it is clearly a poor approximation for proton–proton Overhauser experiments because usually only two proton sites are involved in the cross-relaxation measurement, so all the other proton–proton dipolar interactions act as leakage paths.

Competition from other relaxation mechanisms can have unfortunate results when one of the gyromagnetic ratios is negative. The negative enhancement predicted for nitrogen-15 may vanish altogether if the leakage term just compensates. Sometimes it may be useful to quench the Overhauser effect completely, by adding a relaxation reagent (10).

INTERNUCLEAR DISTANCES

It is possible to use the determination of the steady-state Overhauser enhancement to measure internuclear distances, usually proton–proton distances. In its crudest form, this technique is exploited simply to distinguish two possible candidates for the molecular structure, for example *cis/trans* isomers, by comparing the relative magnitudes of two proton–proton Overhauser enhancements. More quantitative studies must take into account the complication presented by the leakage terms, which are usually of unknown magnitude.

One approach is to resign ourselves to the determination of *relative* distances. Suppose we have a three-spin system ISR, in which we can neglect the dipolar interaction between I and R because this internuclear distance is relatively large. We also assume that these spins are in a rigid part of the molecule so that the rotational correlation times are the same. Then we can perform two separate experiments, first saturating the I spins and measuring the S-spin Overhauser enhancement $\eta_S\{I\}$, then saturating the R spins and observing the new S-spin enhancement $\eta_S\{R\}$. Now, since the leakage term is the same in both experiments, it cancels, and it is possible to write

$$\frac{\eta_S\{I\}}{\eta_S\{R\}} = \frac{(W_2 - W_0)_{IS}}{(W_2 - W_0)_{SR}} = \left(\frac{r_{SR}}{r_{IS}}\right)^6 \qquad [20]$$

since the cross-relaxation terms are inversely proportional to the sixth powers of the respective internuclear distances. This very rapid fall-off with distance is one of the great assets of the nuclear Overhauser technique; it means that a 6% error in determining the enhancement ratio translates into just a 1% error in the distance ratio.

In general, nuclear Overhauser measurements in systems of more than two interacting spins can become quite complex, a problem that is usually formulated in terms of the 'three-spin effect'. In the ISR system, saturation of the I spins enhances the intensity of the S spins, and this very enhancement *decreases* the intensity of the R spins through the S–R dipolar interaction. If, in addition, there is a *direct* dipolar interaction between I and R, then this is a competing effect that enhances the R-spin signal. The important conclusion is that the observed enhancement of the R-spin signal is not simply a function of the internuclear distance r_{IR}; indeed the enhancement could be positive or negative, depending on the relative geometry.

SLOW MOLECULAR TUMBLING

Molecular tumbling of macromolecules (or smaller molecules in a very viscous medium) falls in the slow reorientation regime (the tired skier syndrome). We restrict the discussion to the most common case of proton–proton Overhauser

measurements where the spectral density function $J(\omega)$ has a significant component only at the zero-quantum frequency (Fig. 4):

$$\omega_I \tau_c >> 1 \quad [21]$$

$$\omega_S \tau_c >> 1 \quad [22]$$

$$(\omega_I + \omega_S)\tau_c >> 1 \quad [23]$$

$$|\omega_I - \omega_S|\tau_c << 1. \quad [24]$$

Then only eqn [3] is important, and the dominant cross-relaxation term is $-W_0$ which gives $\eta = -1.0$ for predominantly dipolar relaxation (eqn [12]). Since the vast majority of applications are on biomolecules that contain large numbers of protons, these Overhauser measurements are almost always carried out by two-dimensional spectroscopy (NOESY) which measures all the interactions in a single experiment (11). The evolution period t_1 serves to label the various proton sites according to their chemical shifts, a subsequent mixing period τ_m allows cross-relaxation to build up, and the detection period t_2 monitors the transfer of intensity to the new chemical sites. The useful information lies in the relative intensities of the NOESY cross-peaks. These have the same sense as the diagonal peaks because the enhancement is now negative.

A new complication now arises owing to the large number of proton–proton interactions. The transferred magnetization can propagate to more distant spins in multiple transfer steps, dissipating the Overhauser enhancement over a very large number of sites. This has been given the misleading name 'spin diffusion'. However, since the multistep transfers build up more slowly than direct transfer, the effects of spin diffusion can be minimized by operating with a short mixing period:

$$|W_0 \tau_m| << 1. \quad [25]$$

This also helps to reduce the influence of non-dipolar leakage mechanisms.

Two-dimensional nuclear Overhauser spectroscopy has enjoyed enormous success in the study of protein structure in solution (12). Some NOESY spectra have literally thousands of cross-peaks. Any initial concerns we might have had about the lack of rigidity of the macromolecules in question, possible variations in the rotational correlation times, spin diffusion, or competing relaxation mechanisms, have all been dispelled by the practical results. No attempt is usually made to extract accurate interproton distances; the results are expressed simply as 'distance constraints'. In the limit this reduces to a simple 'yes/no' decision – do the two protons in question give a NOESY cross-peak? If they do, they must lie within (say) 0.6 nm. Such evidence may be used for amino acid sequencing or to establish that an amino acid chain loops back on itself.

Between the fast and slow tumbling regimes lies a region where the steady-state Overhauser enhancement passes through zero. There is then a danger that a proximity determination might turn up a 'false negative' result. The remedy is to

employ rotating-frame Overhauser effect spectroscopy (ROESY) (13,14). This involves the use of a spin-locking field B_1 so that the nuclei behave as if they were relaxing in a very weak field B_1 instead of in the intense spectrometer field B_0. Dipolar relaxation is now effective if a much milder requirement is fulfilled:

$$\gamma B_1 \tau_c << 1, \qquad [26]$$

so in this situation we are almost always in the fast tumbling regime and the Overhauser enhancement is always positive, never approaching zero.

REFERENCES

1. A. W. Overhauser, *Phys. Rev.* **92**, 411 (1953).
2. T. R. Carver and C. P. Slichter, *Phys. Rev.* **92**, 212 (1953).
3. A. Abragam, J. Combrisson and I. Solomon, *CR Acad. Sci. Paris* **247**, 2237 (1958).
4. C. D. Jeffries, ed. *Dynamic Nuclear Orientation.* Interscience: New York, 1963.
5. J. H. Noggle and R. E. Schirmer, *The Nuclear Overhauser Effect.* Academic Press: New York, 1971.
6. D. Neuhaus and M. P. Williamson, *The Nuclear Overhauser Effect in Structural and Conformational Analysis*. VCH Publishers: New York, 1989.
7. Adapted from a story in A. Abragam, *Réflexions d'un Physicien.* Hermann: Paris, 1983.
8. I. Solomon, *Phys. Rev.* **99**, 559 (1955).
9. A. Abragam, *The Principles of Nuclear Magnetism*. Clarendon Press: Oxford, 1961.
10. R. Freeman, K. G. R. Pachler and G. N. LaMar, *J. Chem. Phys.* **55**, 4586 (1971).
11. A. Kumar, R. R. Ernst and K. Wüthrich, *Biochem. Biophys. Res. Commun.* **95**, 1 (1980).
12. K. Wüthrich, *NMR of Proteins and Nucleic Acids* John Wiley: New York, 1986.
13. A. A. Bothner-By, R. L. Stephens, J.-M. Lee, C. D. Warren and R. W. Jeanloz, *J. Am. Chem. Soc.* **106**, 811 (1984).
14. A. Bax and D. G. Davis, *J. Magn. Reson.* **63**, 207 (1985).

Cross-references

Sensitivity enhancement
Spin–lattice relaxation
Two-dimensional spectroscopy

Nuclear Susceptibility

Materials can be generally divided into two classes – diamagnetic and paramagnetic. When placed in a magnetic field, the former materials slightly exclude the magnetic lines of force and experience an internal field slightly lower than the applied field, whereas the latter tend to concentrate the lines of force and have a slightly higher internal field. The main bulk susceptibility effect stems from the magnetic moments of the electrons, and although it shifts NMR signals slightly (proportional to the applied field), it is a constant shift and affects all the nuclear species uniformly, so it is normally neglected in spectroscopic studies, because all the resonance frequencies are related to an internal reference standard, usually the deuterium signal of the solvent. A very small additional contribution to the applied magnetic field is then irrelevant.

There is also a *nuclear* susceptibility effect arising from the nuclear magnetic moments. Nuclear magnetic moments are small, and because there are almost equal numbers of spins in the α and β states at room temperature, the nuclear susceptibility effect is normally very weak indeed unless we examine a sample of high spin density containing nuclei of high gyromagnetic ratio. The effect has been measured in solid hydrogen at 4 K (1) and for lithium nuclei strongly polarized by the solid effect (2). Using an extremely sensitive quartz fibre torsion balance, Evans (3) was able to detect the change in nuclear susceptibility of protons at room temperature in solid hexaethylbenzene upon saturation of the proton signal. In principle, any lump of material, suddenly placed in a magnetic field, acquires a macroscopic nuclear susceptibility at a rate determined by the spin–lattice relaxation time T_1. If the spins are then saturated or inverted, the field due to this nuclear susceptibility changes.

The magnitude of the nuclear paramagnetic effect depends on the shape of the sample: for an ellipsoid the induced field is uniform within the sample, and for a sphere it vanishes. In high-resolution studies the sample is normally an infinite cylinder aligned along the main field direction, approximating an ellipsoid of very high eccentricity. In 1951, Dickinson calculated that the nuclear susceptibility effect could be safely neglected at the magnetic field intensities of contemporary high-resolution spectrometers (4). However, in the very high magnetic fields used in modern NMR, and for a sample of water (which has a proton concentration of 110 molar), the effect amounts to an (upfield) shift of 0.0027 ppm upon spin inversion, that is to say, 2 Hz in a 750 MHz spectrometer (5). This displacement is halved for

saturation rather than population inversion. Normally this shift is masked by the compensating effect of the internal field/frequency lock, because the deuterium signal experiences the same magnetic field displacement (generated by the change in *proton* susceptibility). Several workers have reported a disturbance of the lock signal upon saturation of the water resonance. In the unlocked mode, the shift is quite evident (Fig. 1) and could be a significant perturbation in many modern NMR experiments involving water suppression techniques. Because spin–lattice relaxation changes the longitudinal magnetization during acquisition of the free induction decay, the nuclear susceptibility effect can also distort the lineshape, but this rather mild effect is usually masked by the gross distortion occasioned by radiation damping* which usually occurs at the same time as the susceptibility effect, being similarly favoured by high spin densities and high gyromagnetic ratios. Experimental investigations of the nuclear susceptibility effect are best performed by first eliminating radiation damping by using a very small sample, by detuning the receiver coil, or by electronic negative feedback to the coil.

Perhaps the most alarming aspect of bulk nuclear paramagnetism is the introduction of spurious cross-peaks in two-dimensional correlation spectra (6). Consider the case of the widely used COSY experiment, in which proton spins experience the effect of two 90° pulses separated by a variable evolution period t_1.

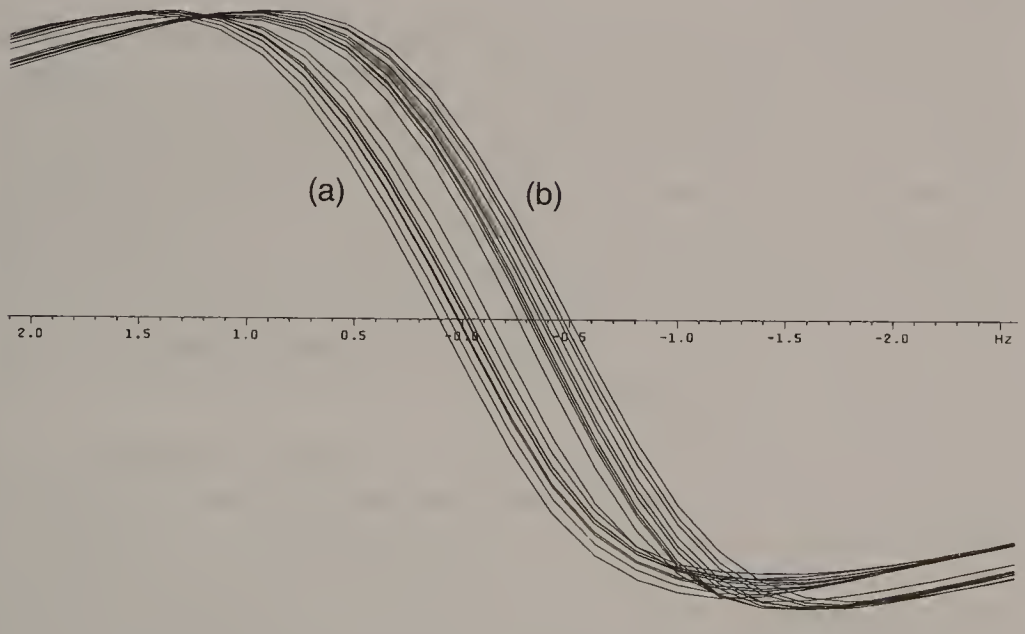

Fig. 1. A dispersion-mode proton resonance from the CH_3 protons of methanol dissolved in water (90%), excited by a soft radiofrequency pulse and repeatedly scanned in an unlocked 400 MHz spectrometer (a) with the water signal at equilibrium, and (b) after pre-saturation of the water resonance with a 4 second, low-intensity radiofrequency pulse. The change in bulk nuclear susceptibility accounts for the observed upfield shift of 0.40 ± 0.09 Hz. The theoretical value is 0.48 Hz. Spectra courtesy of Helmut Sengstschmid.

After the first 90° pulse, proton magnetization from water precesses through an angle $\Delta\omega t_1$, where $\Delta\omega$ is the offset of the water signal from the transmitter frequency. After the second 90° pulse, the Y component of magnetization $M_0 \cos(\Delta\omega t_1)$ is rotated into the –Z direction, leading to a modulation of the bulk nuclear susceptibility and a consequent 'anomalous' modulation of the magnetic field. This gives rise to the spurious cross-peaks in the F_1 frequency dimension, which are easily mistaken for signals resulting from multiple-quantum coherence. These anomalies, which challenge the widely held belief that a cross-peak is unequivocal evidence for a correlation, fortunately disappear if the transmitter is set exactly at the water frequency.

An *apparently* different explanation of the spurious cross-peaks has been advanced by Warren *et al.* (7). It is based on the proposition that dipole–dipole interactions over large macroscopic distances might not, after all, be negligible because of imperfect motional averaging and the fact that the number of such interactions at large distances is also very large (the effect vanishes for a perfectly spherical sample). These long-range interactions lead to 'correlation' peaks that mimic the frequencies and phase-cycling behaviour of genuine multiple-quantum coherences. This collective effect of all the spins in the sample challenges important simplifying assumptions that are usually made in NMR, namely that it is justifiable to restrict our attention to interactions within a given molecule, and that a quantum-mechanical treatment embracing all the spins in the sample is unnecessary and impossibly complex.

The pragmatic chemist might well consider this a good case for the application of Occam's razor – accepting the bulk nuclear susceptibility explanation because it is simple and certainly explains the observed behaviour, while rejecting the 'dipolar field' theory as too complex and involving unfamiliar new concepts. However, we must not assume that the latter theory is incorrect (6). A new formulation by Jeener and coworkers (8,9) incorporates the coupling of each spin with a classical average dipolar field into the Bloch–Redfield equations, which are traditionally employed to describe the equations of motion of the reduced density operator for the spins in a single molecule. This destroys the linearity of these equations and can therefore lead to apparently spurious modulation effects when there is a substance of very high spin density in the sample.

A rather more esoteric manifestation of the bulk nuclear susceptibility effect arises when a Hahn spin-echo experiment is performed in a strong magnetic field gradient applied along the Z axis (10–12). Normally the $90° - \tau - 90°$ sequence excites only a single Hahn echo, but in this situation, if the proton density is high enough, multiple echoes are observed. Just as in the case of the COSY experiment described above, the $90° - \tau - 90°$ sequence alters the Z magnetization in a periodic fashion. As a consequence, the additional magnetic field arising from the nuclear susceptibility is modulated along the gradient direction and can oppose or even cancel the applied gradient at certain regularly spaced zones within the sample. Signals from these homogeneous regions of the field are then repeatedly refocused, giving rise to multiple Hahn echoes.

REFERENCES

1. B. Lasarew and L. Schubnikow, *Phys. Z. Sowjet.* **11**, 445 (1937).
2. Ch. Richter, *Phys. Rev. Lett.* **5**, 10 (1960).
3. D. F. Evans, *Philos. Mag. R. Soc.* **1**, 370 (1956).
4. W. C. Dickinson, *Phys. Rev.* **81**, 717 (1951).
5. H. T. Edzes, *J. Magn. Reson.* **86**, 293 (1990).
6. M. H. Levitt, *Concepts Magn. Reson.* **8**, 77 (1996).
7. W. S. Warren, W. Richter, A. H. Andreotti and B. T. Farmer, *Science* **262**, 2005 (1993).
8. J. Jeener, A. Vlassenbroek and P. Broekaert, *J. Chem. Phys.* **103**, 1309 (1995).
9. P. Broekaert, A. Vlassenbroek, J. Jeener, G. Lippens and J. M. Wieruszeski, *J. Magn. Reson. A* **120**, 97 (1996).
10. G. Deville, M. Bernier and J. M. Delrieux, *Phys. Rev. B* **19**, 5666 (1979).
11. R. Bowtell, R. M. Bowley and P. Glover, *J. Magn. Reson.* **88**, 643 (1990).
12. R. P. O. Jones, G. A. Morris and J. C. Waterton, *J. Magn. Reson.* **98**, 115 (1992).

Cross-references

Correlation spectroscopy
Field/frequency regulation
Multiple-quantum coherence
Radiation damping
Spin echoes

Phase Cycling

Most of modern NMR spectroscopy employing multiple-pulse sequences involves some kind of phase-cycling routine to separate the useful signals from undesirable artefacts. The phase of the appropriate radiofrequency pulse is incremented in N steps in such a manner that the artefacts acquire a systematic phase shift $\phi = 360°/N$, distributing the corresponding vectors uniformly around a circle so that they cancel, whereas the signal of interest is always accumulated with the same phase (this may require changes on the receiver reference phase). The case $N = 2$ is usually called difference spectroscopy. Although $N = 3$ and $N = 5$ have been used, the majority of phase cycles use $N = 4$, since 90° phase shifts are readily available on most spectrometers.

The first phase cycle to be introduced addressed a rather specific problem – the imperfections of quadrature phase detectors (see Quadrature detection*). Two phase-sensitive detectors are used, driven by the same reference frequency, but with a 90° phase shift. They allow us to determine the *sense* of the nuclear precession and thus permit operation with the transmitter frequency set in the centre of the NMR spectrum. They have three basic problems. The first is a slight amplitude imbalance between the two 'channels', the second is an inaccuracy in the 90° phase shift. These imperfections introduce a weak version of the true spectrum reflected about the transmitter frequency – the *quadrature image.* This is readily understood, because either imperfection, taken to the limit, reduces the system to single-channel phase detection where the sense of precession is not discriminated, and the NMR spectrum is always superimposed on its own reflection. The third problem is a small d.c. offset in the incoming free induction decay which gives rise to a weak spurious response at the transmitter frequency – the *quadrature glitch.*

Hoult and Richards (1) found that the effects of amplitude imbalance and lack of orthogonality could be compensated by continually interchanging the roles of the two phase detectors so that the errors were shared equally between the two channels. Some second-order errors remain if both types of imperfection occur simultaneously. Strictly only two acquisitions are required for this type of compensation, but Hoult and Richards extended this to a four-step cycle by incrementing the phase progressively in 90° steps. This is the full cyclically ordered phase sequence (CYCLOPS). If the two phase detector channels are labelled a and b the signal routing scheme may be written in the form

Pulse	'Absorption'	'Dispersion'
90°(+X)	+a	+b
90°(–Y)	+b	–a
90°(–X)	–a	–b
90°(+Y)	–b	+a

where, for convenience, we have labelled the two NMR signal components 'absorption' and 'dispersion'. Because the last two steps are the same as the first two, but inverted, any baseline error (which is independent of the phase of the pulse) is cancelled. Consequently the full cycle removes the quadrature glitch. In some spectrometers this is actually the dominant imperfection.

The first application of phase cycling to remove artefacts created by the radiofrequency pulses themselves was the EXORCYCLE sequence (2). It was initially introduced to suppress some spurious responses in heteronuclear two-dimensional J-spectroscopy, but has since proved useful in a wide variety of pulse sequences. Spectra obtained by two-dimensional Fourier transformation of carbon-13 spin echoes were found to contain not only the expected spin multiplets arising from the CH couplings, but also some weak replicas of these multiplets displaced as indicated in Fig. 1(a). These 'ghost' and 'phantom' signals could be traced to the influence of imperfections in the radiofrequency pulses. Ghost signals arise from imperfections of the 180° pulse; a small part of the transverse magnetization escapes the refocusing effect. Consequently, it is possible to shift the phase of these pulses without affecting the ghost signals, and since it is well known that a 90° phase shift of the refocusing pulse inverts the sense of a spin echo (3), ghost responses can be eliminated by difference spectroscopy. Phantom responses originate in imperfections of both the 90° and 180° pulses, as residual Z magnetization after the 90° pulse is converted by the imperfect 180° pulse into XY magnetization. Phase inversion of the 180° pulse reverses the sense of this signal but not that of the spin echo; hence addition of the signals from two scans eliminates the phantom signals. Both ghosts and phantoms are 'exorcised' by the four-step cycle

90°(+X)	$\frac{1}{2}t_1$	180°(+X)	$\frac{1}{2}t_1$	Acquisition (+)
90°(+X)	$\frac{1}{2}t_1$	180°(–Y)	$\frac{1}{2}t_1$	Acquisition (–)
90°(+X)	$\frac{1}{2}t_1$	180°(–X)	$\frac{1}{2}t_1$	Acquisition (+)
90°(+X)	$\frac{1}{2}t_1$	180°(+Y)	$\frac{1}{2}t_1$	Acquisition (–)

Figure 1 illustrates the operation of the EXORCYCLE scheme in an experiment

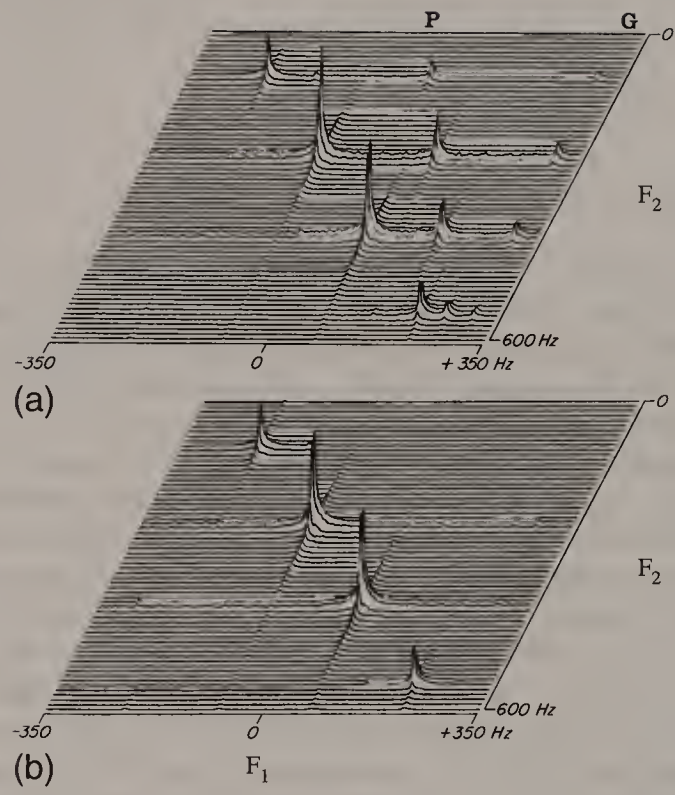

Fig. 1. Two-dimensional J-spectrum of carbon-13 in methyl iodide obtained by Fourier transformation of the modulated carbon-13 spin echoes. (a) Spurious ghost (G) and phantom (P) responses observed when the pulse lengths were deliberately mis-set. (b) Elimination of the ghosts and phantoms through the EXORCYCLE scheme.

where the pulse flip angles had been deliberately mis-set in order to emphasize the spurious responses. EXORCYCLE has proved to be the precursor of an entire family of phase cycles designed to suppress undesirable responses, even when the latter are far more intense than the signal of interest. When one phase cycle is nested within another, the overall scheme can become quite complex, and careful thought should be given to the appropriate ordering of the steps if steady-state effects* are involved (4).

Although the four-step phase cycle is most widely used, other schemes are quite feasible. The N = 3 cycle is the simplest in which a sense of rotation is defined, and it has been employed by Bodenhausen *et al.* (5). Cycles with an arbitrary number N have been proposed as a method for phase encoding experiments in which several selective radiofrequency pulses are employed at the same time (6). This exploits an idea related to Hadamard spectroscopy (7). The multiple-excitation experiment is repeated N times with a systematic phase-encoding scheme that shifts the radiofrequency pulse phases in steps of $2\pi/N$ radians. For example, if N = 5 we could use the following encoding scheme for simultaneous excitation of five chemical sites, A through E:

	A	B	C	D	E
Scan 1	0	0	0	0	0
Scan 2	0	$2\pi/5$	$4\pi/5$	$6\pi/5$	$8\pi/5$
Scan 3	0	$4\pi/5$	$8\pi/5$	$2\pi/5$	$6\pi/5$
Scan 4	0	$6\pi/5$	$2\pi/5$	$8\pi/5$	$4\pi/5$
Scan 5	0	$8\pi/5$	$6\pi/5$	$4\pi/5$	$2\pi/5$

Note that aliasing makes $12\pi/5$ radians (for example) equivalent to $2\pi/5$ radians.

The stored responses are then interrogated five separate times, and decoded with the appropriate combinations of the receiver phase. For example, the combination (0, $2\pi/5$, $4\pi/5$, $6\pi/5$, $8\pi/5$) singles out the response from chemical site B only; all other responses cancel because they correspond to five vectors equally distributed around a circle. The result is equivalent to five *simple* selective excitation experiments, except that the sensitivity is increased by the square root of five because new information (and noise) was accumulated in all five measurements. In general the enhancement factor is the square root of N.

MULTIPLE-QUANTUM COHERENCE

When we apply a phase shift ϕ to the radiofrequency pulses used to excite multiple-quantum coherence, this shifts the phase of that coherence through an angle $p\phi$ where p is the order of the coherence. Thus zero-quantum coherence is unaffected, whereas double-quantum coherence experiences a two-fold phase shift. We can rationalize this by saying that the pulse acts in a cascade of operations affecting the relevant single-quantum transitions one at a time, and therefore the phase shifts accumulate (algebraically). We see that this offers a powerful method for separating the various orders of coherence, because we can program the receiver phase to follow signals derived from the desired coherence order while the other signals accumulate a progressive phase error and eventually cancel.

The key to the design of a suitable phase cycle is to analyse the time development of the coherence order – that is to say, to map out the so-called coherence transfer pathway (5). This concept has been examined in detail in the section on Coherence* in relation to the two-dimensional carbon–carbon correlation experiment (INADEQUATE). Double-quantum filtration is employed to suppress the intense signals from isolated carbon-13 spins while retaining the much weaker signals from coupled pairs of carbon-13 spins (8).

Broadband decoupling* schemes also make extensive use of phase cycling. The residual imperfections of the spin inversion pulses are largely compensated by assembling groups of pulses into a suitable magic cycle, of which the simplest is the MLEV-4 (9) sequence 0°, 0°, 180°, 180°. Using intuitive arguments, Levitt showed how this could be expanded into more efficient 'supercycles' (10) by the

operations of cyclic permutation and phase inversion, and Waugh (11) justified these procedures theoretically. More recently decoupling cycles based on odd numbers of steps have been introduced by Tycko *et al.* (12), for example the five-step cycle 0°, 150°, 60°, 150°, 0°. Often one type of phase cycle is nested within another for broadband decoupling purposes.

Although a properly constructed phase cycle accumulates signal intensity in the same manner as normal time averaging, it does prolong the experiment, often well beyond the point where the signal-to-noise ratio has reached the required level. More importantly, phase cycling relies on cancelling the undesirable responses in successive scans, and this renders the method sensitive to all manner of medium-term spectrometer instabilities. For these reasons, phase cycling is gradually being replaced by techniques based on pulsed field gradients* (13,14) which achieve the same suppression in a single scan.

REFERENCES

1. D. I. Hoult and R. E. Richards, *Proc. R. Soc. A* **344**, 311 (1975).
2. G. Bodenhausen, R. Freeman and D. L. Turner, *J. Magn. Reson.* **27**, 511 (1977).
3. S. Meiboom and D. Gill, *Rev. Sci. Instrum.* **29**, 688 (1958).
4. C. J. Turner, *J. Magn. Reson.* **96**, 551 (1992).
5. G. Bodenhausen, H. Kogler and R. R. Ernst, *J. Magn. Reson.* **58**, 370 (1984).
6. Ē. Kupče and R. Freeman, *J. Magn. Reson. A* **105**, 310 (1993).
7. J. Hadamard, *Bull. Sci. Math.* **17,** 240 (1893).
8. A. Bax, R. Freeman and T. Frenkiel, *J. Am. Chem. Soc.* **103**, 2102 (1981).
9. M. H. Levitt and R. Freeman, *J. Magn. Reson.* **43**, 502 (1981).
10. M. H. Levitt, R. Freeman and T. Frenkiel, *J. Magn. Reson.* **47**, 328 (1982).
11. J. S. Waugh, *J. Magn. Reson.* **50**, 30 (1982).
12. R. Tycko, A. Pines and R. Gluckenheimer, *J. Chem. Phys.* **83**, 2775 (1985).
13. W. P. Aue, E. Bartholdi and R. R. Ernst, *J. Chem. Phys.* **64**, 2229 (1976).
14. R. E. Hurd, *J. Magn. Reson.* **87**, 422 (1990).

Cross-references

Broadband decoupling
Coherence
Difference spectroscopy
Multiple-quantum coherence
Pulsed field gradients
Quadrature detection
Selective excitation
Steady-state effects

Polarization Transfer

Many interesting nuclei suffer from poor inherent sensitivity as a result of low natural isotopic abundance or their low gyromagnetic ratio. Notable among these are the nuclei carbon-13 and nitrogen-15, now extensively used for the simplification of proton spectra of biologically important macromolecules. Since the magnetic moment, the Boltzmann populations, and the nuclear precession frequency (which determines the induced NMR voltage), all increase in proportion to the gyromagnetic ratio γ, the signal intensity increases as γ^3, give or take some minor corrections for radiofrequency losses in the probe. As noise increases as the square root of the frequency, sensitivity is roughly proportional to $\gamma^{5/2}$. Thus, apart from the special case of radioactive tritium, protons have by far the highest intrinsic sensitivity of all nuclear species.

From the earliest days of NMR it was realized that considerable improvements in sensitivity could be achieved by artificially increasing the Boltzmann factors. The possible techniques include prepolarization in a very intense magnetic field, the electron–nuclear Overhauser effect (1), Hartmann–Hahn cross-polarization (2), optical pumping experiments, chemically induced nuclear polarization, and the exploitation of the special properties of parahydrogen (3). However, for the most part, these methods are insufficiently general to be important for high-resolution liquid-phase spectroscopy.

The nuclear Overhauser effect* provides a signal enhancement given by

$$E = 1 + \frac{1}{2}\left(\frac{\gamma_I}{\gamma_S}\right) \qquad [1]$$

in situations where the spin–lattice relaxation of the low-sensitivity nuclei (the S spins) is dominated by their dipole–dipole interaction with the protons (the I spins). Consequently, carbon-13 spectra can benefit from a signal-to-noise improvement as high as three-fold when the attached protons are saturated. Unfortunately, since the gyromagnetic ratio of nitrogen-15 is negative, the maximum enhancement $E = -4$, and if the dipolar relaxation has to compete with other mechanisms (leakage), the observed nitrogen-15 signal can be near zero.

Polarization transfer experiments offer a bigger sensitivity advantage for two reasons. First, by transferring the benefits of proton polarization to the S spins, they augment the signal-to-noise by the population factor (γ_I/γ_S) which is larger than E in eqn [1]. Second, they permit multiple acquisitions of the S-spin signal at a rate limited only by the spin–lattice relaxation of the protons, which is usually more

efficient than that of the S spins. No penalty is incurred by a negative gyromagnetic ratio. Thus nitrogen-15 signals are enhanced by a factor of ten.

THE 'INEPT' TECHNIQUE

Insensitive nuclei enhanced by polarization transfer (INEPT) is now used as a module in a large number of pulse sequences designed to improve sensitivity. First it is helpful to consider an earlier experiment called selective population transfer (4) in which a selective 180° spin inversion pulse is applied to one proton line of the doublet generated by the heteronuclear coupling J_{IS}. The appropriate energy-level

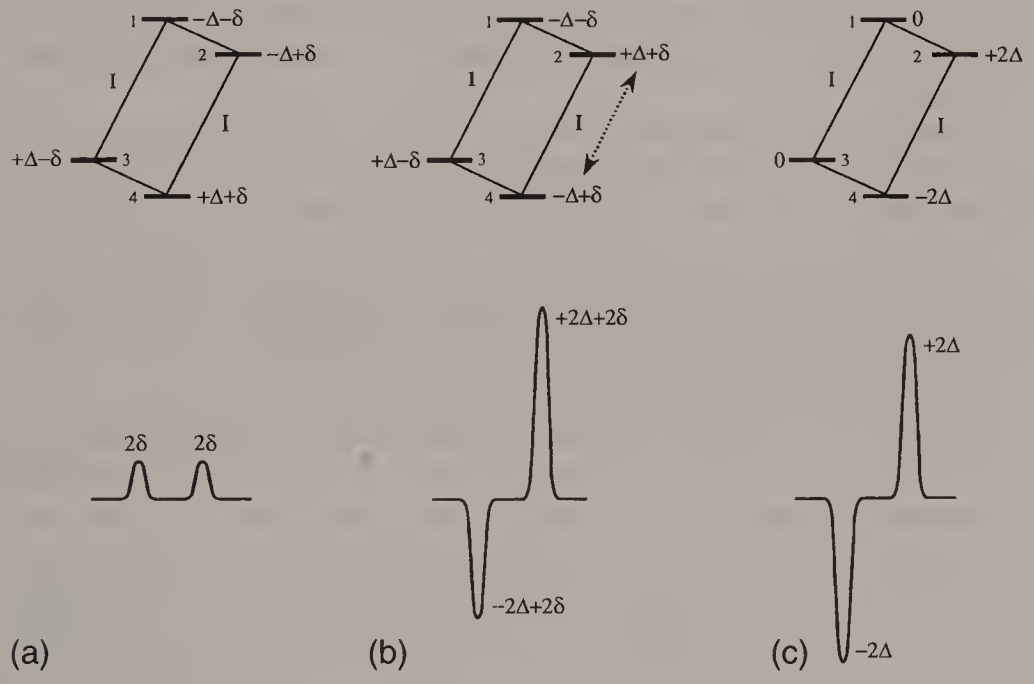

Fig. 1. Energy-level diagram for a two-spin IS system illustrating how a selective 180° pulse inverts the populations across one of the I-spin transitions (2–4). (a) Boltzmann populations and intensities. (b) Perturbed populations and intensities. (c) Changes from Boltzmann populations, indicating a sensitivity advantage of $\Delta/\delta = \gamma_I/\gamma_S$.

diagram is set out in Fig. 1. At Boltzmann equilibrium the spin populations on these levels can be written as

(1) $-\Delta - \delta$
(2) $-\Delta + \delta$
(3) $+\Delta - \delta$
(4) $+\Delta + \delta$

where 2Δ represents the equilibrium population difference across the proton (I) transitions and 2δ corresponds to the population difference across the S-spin transitions; thus $\Delta/\delta = \gamma_I/\gamma_S$. Selective inversion of (say) the (2–4) proton transition, leaving the (1–3) transition unaffected, rearranges the spin populations into a non-equilibrium distribution:

$$\begin{aligned}(1)\ &-\Delta - \delta\\ (2)\ &+\Delta + \delta\\ (3)\ &+\Delta - \delta\\ (4)\ &-\Delta + \delta\end{aligned}$$

If we now evaluate the population differences across the S-spin transitions (1–2) and (3–4), we see that they are increased to $+2\Delta + 2\delta$ and $-2\Delta + 2\delta$, instead of their normal values 2δ. The *changes* are therefore $\pm 2\Delta$, one line being increased in a positive sense and the other inverted (Fig. 1). We shall see below that this 'up–down' pattern of intensities is characteristic of many polarization transfer experiments.

Although selective population transfer is hardly a general method of signal enhancement, because the appropriate proton transition has to be located by a tedious trial-and-error search (it is one of the weak satellites of the main proton resonance) it anticipates the mechanism of the INEPT experiment. Here the effect of selective population inversion is achieved by a hard-pulse technique that is effective over the entire band of proton chemical shifts. It may be analysed either by the vector model* or by the product operator formalism*.

After the initial 90° excitation pulse, we represent the proton (I-spin) transverse magnetization by two vectors, α and β, precessing freely at frequencies $(\nu_I + \frac{1}{2}J_{IS})$ and $(\nu_I - \frac{1}{2}J_{IS})$ in the XY plane. After an interval $\tau_1 = 1/(4J)$ they will have precessed to positions that depend on both ν_I and J_{IS}, but the angle between the two vectors will be just 90° (Fig. 2(b)). Then we apply simultaneous hard 180° pulses to both spin species. The I-spin inversion pulse flips these vectors into mirror image positions with respect to the XZ plane of the rotating frame (Fig. 2(c)). This serves to refocus the I-spin chemical shift after a further period τ_1 of free precession, but the 180° pulse applied to S spins (Fig. 2(d)) interchanges the I-spin labels α and β, so that the I-spin vector that initially precessed at a frequency $(\nu_I + \frac{1}{2}J_{IS})$ now precesses at $(\nu_I - \frac{1}{2}J_{IS})$, and vice versa. Consequently the divergence due to J-coupling persists, and the two vectors reach the $\pm X$ axes at time $2\tau_I$ (Fig. 2(e)). At this point a 90° pulse applied about the +Y axis (that is to say, a phase-shifted pulse) turns the two vectors into the $\pm Z$ axes (Fig. 2(f)). One of the two proton transitions has suffered a population inversion while the other is at Boltzmann equilibrium. This is just the configuration that would have been reached by a selective population transfer experiment, but it has been achieved for all the I spins, irrespective of chemical shift. A final 90° read pulse applied to the S spins generates 'up–down' doublets for all the S-spin sites. Usually the natural (unenhanced) signals from the S spins are cancelled by difference spectroscopy by applying alternating $90°(\pm Y)$ pulses on the I spins at the stage shown in Fig. 2(f).

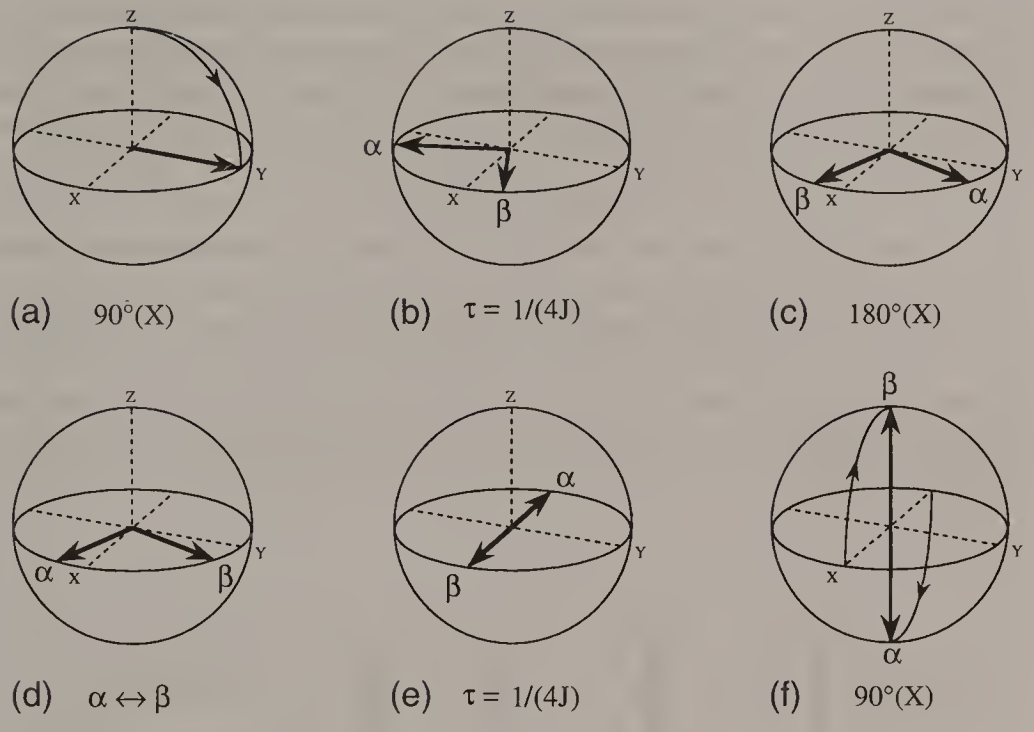

Fig. 2. The INEPT preparation of the I spins according to the vector model. (b) The vectors α and β are allowed to evolve for a time $\tau = 1/(4J_{IS})$ until they subtend an angle of 90°. (c) A 180°(X) pulse applied to the I spins flips these vectors into mirror image positions with respect to the XZ plane. (d) A 180° pulse on the S spins interchanges the I-spin labels ($\alpha \leftrightarrow \beta$). (e) Free precession for a further period τ brings the I-spin vectors into opposition along the ±X axes. (f) A 90°(Y) pulse realigns them along the ±Z axes, a condition equivalent to the selective population inversion of Fig. 1(c).

This leaves just the polarization transfer components, enhanced over their normal intensities by a factor $\pm(\gamma_I/\gamma_S)$.

In the product operator formalism these spin manipulations would be written as

$$\begin{aligned} &I_Z \xrightarrow{I_X} -I_Y \xrightarrow{(\pi/4)\,2I_ZS_Z} -I_Y\cos(\pi/4) + 2I_XS_Z\sin(\pi/4) \xrightarrow{\pi I_X} \\ &+I_Y\cos(\pi/4) + 2I_XS_Z\sin(\pi/4) \xrightarrow{\pi S_X} +I_Y\cos(\pi/4) - 2I_XS_Z\sin(\pi/4) \\ &\xrightarrow{(\pi/4)\,2I_ZS_Z} +2I_XS_Z \xrightarrow{I_Y} -2I_ZS_Z \xrightarrow{S_X} +2I_ZS_Y. \end{aligned} \qquad [2]$$

For simplicity we have neglected the chemical shift evolution of the I spins on the grounds that it is refocused at time $2\tau_1$. Note that an important simplification of the trigonometrical terms has resulted from the condition $\tau_1 = 1/(4J)$, ensuring that the evolution under the $2I_ZS_Z$ operator amounts to π/4 radians, where the sine and cosine are equal. The final term $2I_ZS_Y$ represents an S-spin absorption-mode doublet with the 'up–down' pattern of intensities. The signal enhancement factor (γ_I/γ_S) usually remains only implicit in the product operator treatment.

If we plan to record the enhanced S-spin spectrum in the coupled mode, the 'up–down' pattern causes little difficulty, but if we intend to decouple the I spins this would result in mutual signal cancellation. The remedy is to introduce a further interval $2\tau_2$ to allow the S-spin antiphase vectors to come back into alignment (5):

$$+2I_ZS_Y \xrightarrow{2I_ZS_Z} -S_X. \qquad [3]$$

Then the decoupler can be safely switched on. To avoid any phase shifts that would build up from S-spin chemical shift precession during the $2\tau_2$ interval, it is usual to introduce refocusing and spin inversion 180° pulses at the mid-point of this interval (Fig. 3). Where there is only a single I spin attached to the S-spin site, then the optimum setting of the interval is $\tau_2 = 1/(4J)$, but if some of the S-spin sites have two or three directly attached I spins, then a compromise setting must be employed, usually $\tau_2 = 1/(6J)$.

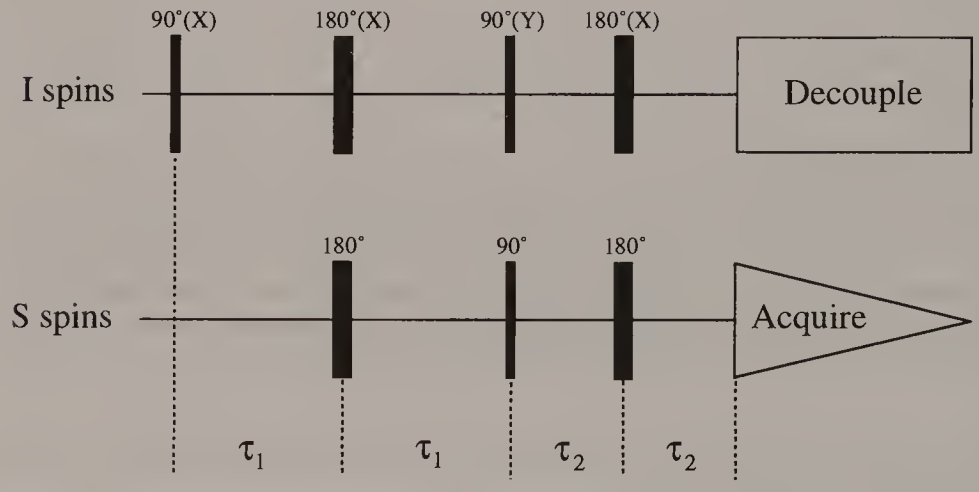

Fig. 3. The pulse sequence for the refocused INEPT experiment. The actual polarization transfer is effected by the simultaneous 90° pulses on the I and S spins. The ensuing evolution during $2\tau_2$ allows antiphase S-spin vectors to come to a focus along the –X axis so that I-spin decoupling can be used.

RELAXATION EFFECTS

The actual sensitivity improvement by the INEPT scheme can be significantly higher than γ_I/γ_S in practice. This is because most experiments involve time averaging, and the rate at which the scans can be repeated is a critical factor. The nitrogen-15 nucleus can have quite long spin–lattice relaxation times compared with protons in the same material, so the direct observation of nitrogen-15 signals would involve long recycling intervals. In the INEPT experiment the natural nitrogen-15 signal is cancelled, all the intensity being obtained through the

polarization transfer. The experiment may therefore be cycled quite fast, limited only by proton spin–lattice relaxation. A clear demonstration of the importance of this relaxation factor is provided by an INEPT experiment performed by Rinaldi and Baldwin (6) using deuterium as the source (I spins). Even though deuterium has far less favourable Boltzmann populations than protons ($\gamma_H = 6.5\gamma_D$), the faster spin–lattice relaxation of this quadrupolar nucleus more than compensates for the population disadvantage.

'ROUND-TRIP' POLARIZATION TRANSFER

It was soon realized that even greater improvements in sensitivity could be achieved if we could return the S-spin polarization to protons before detection, making use of their high detection efficiency. We might describe this as 'round-trip' polarization transfer, I → S → I. The S-spin signal is only detected indirectly and the gyromagnetic ratio of the S spins does not enter into the expression for the sensitivity. Compared with the direct detection of the S-spin spectrum, this round-trip transfer scheme would be expected to enjoy a sensitivity advantage of approximately $(\gamma_I/\gamma_S)^{5/2}$ which is a factor of 32 if S is carbon-13, and 300 if S is nitrogen-15.

Bodenhausen and Ruben (7) were the first to exploit this idea in a technique now known as heteronuclear single-quantum correlation (HSQC). An initial INEPT sequence implements the polarization transfer I → S, and the S spins are allowed to precess for an evolution period t_1 (decoupled from the I spins by a 180°

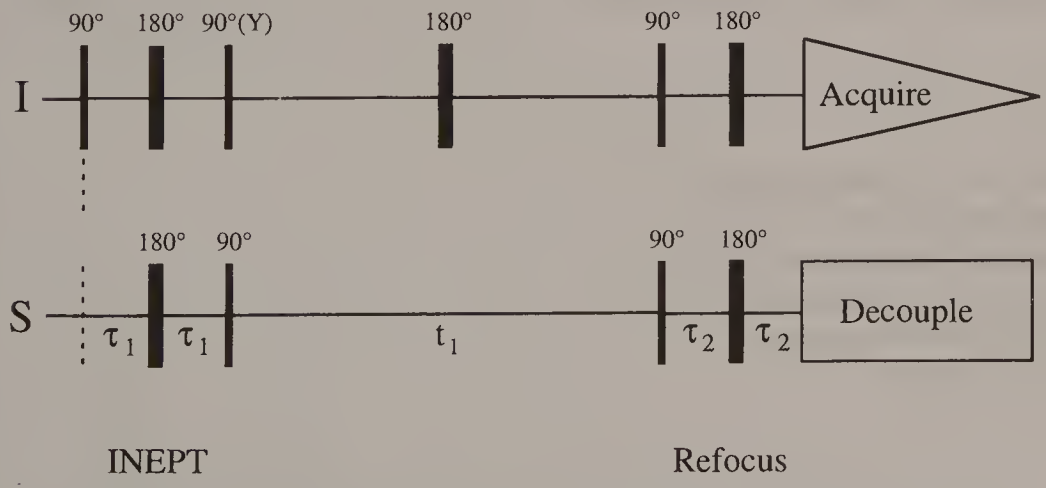

Fig. 4. Pulse sequence for heteronuclear single-quantum correlation (HSQC). All pulses are applied along the X axis except for the one marked 90°(Y). The evolution period t_1 allows the S spins to evolve according to their chemical shifts, while the 180° pulse at the mid-point removes the J_{IS} splittings. The second delay τ_2 has a compromise setting since there may be one, two or three I spins at a given S-spin site.

refocusing pulse). At this point the S-spin signal is an antiphase multiplet, so the reverse transfer S → I is achieved by the application of simultaneous 90° pulses on both the I and S spins (Fig. 4). If the decoupled I-spin spectrum is required, the usual refocusing stage is tacked on to the end of the sequence.

This analysis has ignored an important complication – the intense signal from the I spins (protons) not coupled to carbon-13 or to nitrogen-15. It is not permissible to presaturate the I spins because their polarization is required to initiate the HSQC transfer. The usual strategy is to start the experiment with the 'BIRD' module (see Bilinear rotation decoupling*) which has the property that it leaves the coupled I spins unchanged, but inverts the spin populations of all the I spins not directly attached to the S spins (8). The inverted I-spin signal then recovers through spin–lattice relaxation, passing through the null condition after an interval $T_1 \ln 2$. At this point the HSQC experiment is started, and the only appreciable signals in the final spectrum are those that participate in the round-trip polarization transfer.

REFERENCES

1. A. W. Overhauser, *Phys. Rev.* **92**, 411 (1953).
2. S. R. Hartmann and E. L. Hahn, *Phys. Rev.* **128**, 2042 (1962).
3. C. R. Bowers and D. P. Weitekamp, *Phys. Rev. Lett.* **57**, 2645 (1986).
4. K. G. R. Pachler and P. L. Wessels, *J. Magn. Reson.* **12**, 337 (1973).
5. D. P. Burum and R. R. Ernst, *J. Magn. Reson.* **39**, 163 (1980).
6. P. L. Rinaldi and N. J. Baldwin, *J. Am. Chem. Soc.* **104**, 5791 (1982).
7. G. Bodenhausen and D. J. Ruben, *Chem. Phys. Lett.* **69**, 185 (1980).
8. J. R. Garbow, D. P. Weitekamp and A. Pines, *Chem. Phys. Lett.* **93**, 514 (1982).

Cross-references

Bilinear rotation decoupling
Multiple-quantum coherence
Nuclear Overhauser effect
Product operator formalism
Sensitivity enhancement
Vector model

Product Operator Formalism

Wherever possible in this book, the simplest, non-mathematical treatment has been adopted. The majority of pulsed NMR experiments have been described in terms of extensions of the vector model* first introduced by Bloch. In a few applications, notably those involving multiple-quantum coherence*, this model breaks down, or at least has to be extended in an *ad hoc* manner. The general theory to describe the response to an arbitrary pulse sequence is the *density matrix* or *density operator* treatment (1,2). Unfortunately, this becomes very unwieldy for systems of several coupled spins, and very quickly gets out of touch with physical intuition which has been our principal guide in this book.

Fortunately, there is a more pictorial approach, championed by Sørensen *et al.* (3), which allows the new spin gymnastics to be treated formally without losing sight of the physical interpretation so important for our sanity. It is based on the decomposition of the density operator into a linear combination of products of spin angular momentum operators (4). It is applicable to weakly coupled spin systems. With this shorthand algebra, the fate of the various operators can be followed throughout a complex sequence of pulses and free precessions, throwing light on the details of the time evolution of the particular experiment. Lallemand (5) has suggested a tree-like pictorial representation to aid this kind of visualization.

For simplicity, we restrict ourselves here to the weakly coupled two-spin system IS, writing down the 16 product operators,

E/2	(where E is the unity operator)
I_X	X component of I-spin magnetization
I_Y	Y component of I-spin magnetization
I_Z	Z component of I-spin magnetization (populations)
S_X	X component of S-spin magnetization
S_Y	Y component of S-spin magnetization
S_Z	Z component of S-spin magnetization (populations)
$2I_XS_Z$	Antiphase I-spin magnetization
$2I_YS_Z$	Antiphase I-spin magnetization
$2I_ZS_X$	Antiphase S-spin magnetization
$2I_ZS_Y$	Antiphase S-spin magnetization
$2I_ZS_Z$	Longitudinal two-spin order
$2I_XS_X$	Two-spin coherence
$2I_YS_Y$	Two-spin coherence
$2I_XS_Y$	Two-spin coherence
$2I_YS_X$	Two-spin coherence.

The term $2I_XS_Z$ represents the X component of the I-spin magnetization split into two antiphase components corresponding to the two possible spin states of S. Such operators can be represented by the vector model but the last five product operators cannot be easily represented by vectors.

Longitudinal two-spin order $2I_ZS_Z$ is a specific disturbance of the populations of the four energy levels, having no net polarization. If the normal Boltzmann populations are represented as in Fig. 1(a), with population differences of 2Δ across each transition, then this *J-ordered state* has the populations indicated in Fig. 1(b). Both the I-spin doublet and the S-spin doublet have population disturbances such that a small flip angle read pulse would indicate an 'up–down' pattern of intensities. This is a common occurrence in certain polarization transfer* experiments.

Two-spin coherence $2I_XS_X$ is a concerted motion of the I and S spins that induces no signal in the NMR receiver coil, but can only be detected indirectly by two-dimensional spectroscopy*. It is a superposition of zero-quantum coherence (simultaneous I and S spin flips in opposite senses) and double-quantum coherence (flips in the same sense). Pure zero-quantum coherence corresponds to linear combinations of these product operators

$$2I_XS_X + 2I_YS_Y \text{ or } 2I_YS_X - 2I_XS_Y.$$

Pure double-quantum coherence corresponds to the alternative linear combinations

$$2I_XS_X - 2I_YS_Y \text{ or } 2I_XS_Y + 2I_YS_X.$$

We shall see below that one of the great strengths of the product operator formalism is its ability to account for experiments which involve multiple-quantum coherence.

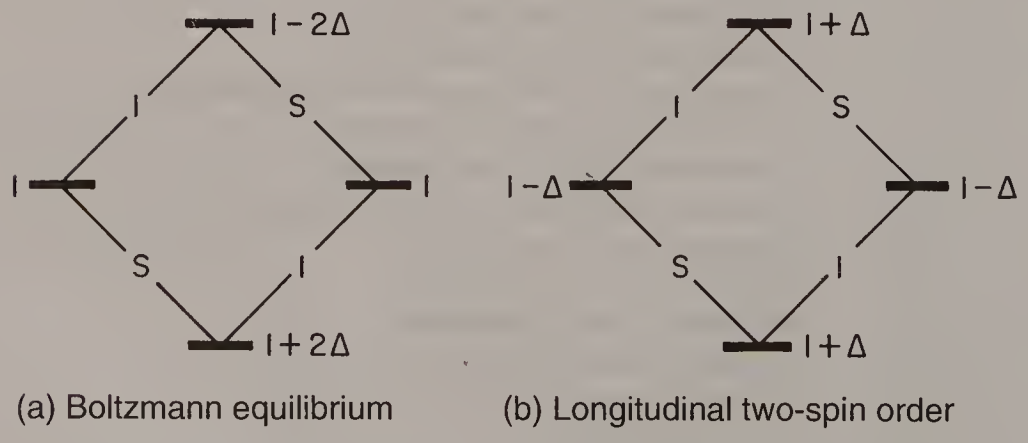

Fig. 1. (a) Energy-level populations appropriate to a homonuclear IS spin system at Boltzmann equilibrium ($\Delta << 1$). (b) Populations corresponding to longitudinal two-spin order represented by the product operator term $2I_ZS_Z$.

SIGN CONVENTIONS FOR ROTATIONS

For the vast majority of NMR experiments, the outcome is independent of the choice of the direction of precession of spins about magnetic fields. When using the vector model we adopted the widely used convention that (for a positive gyromagnetic ratio) a vector M rotates about a field in the rotating frame* as in Fig. 2. Thus for a radiofrequency field B_1 applied along the +X axis, a 90° pulse rotates $+M_Z$ to $+M_Y$

$$+M_Z \xrightarrow{90°(+X)} +M_Y. \qquad [1]$$

Similarly, we chose to take the sense of free precession to be clockwise looking down on the XY plane

$$+M_Y \rightarrow +M_X \rightarrow -M_Y \rightarrow -M_X \qquad [2]$$

for a Larmor frequency higher than the frequency of the rotating frame (ΔB positive). This convention simplifies diagrams of magnetization trajectories by concentrating on the front quadrant of the unit sphere.

When it comes to mathematical treatments using density operators or product operators, the sense of rotation is rather less of an academic point, and two opposite

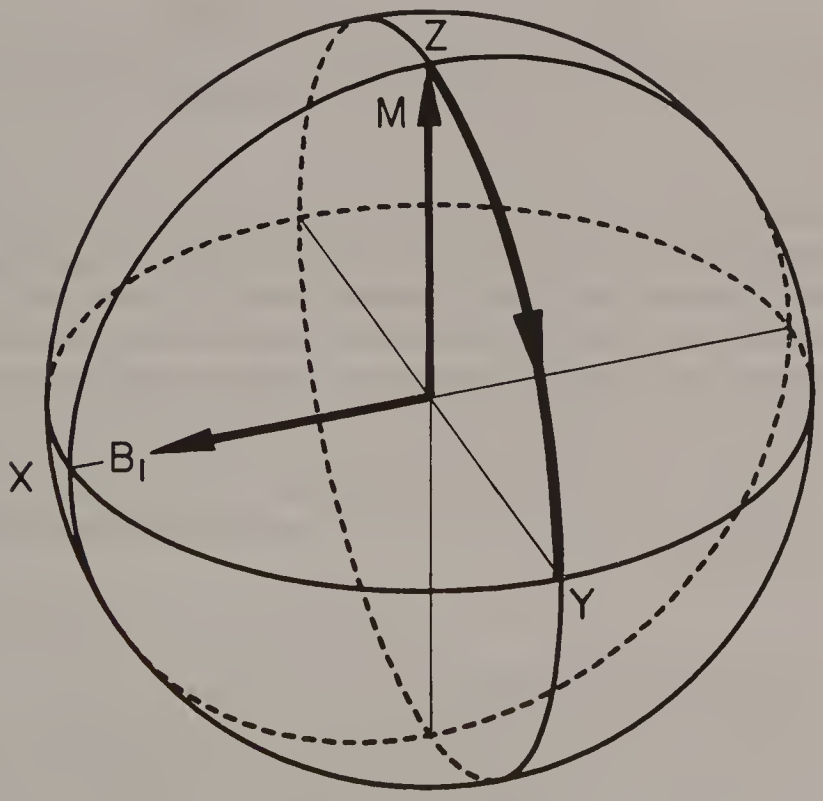

Fig. 2. Convention adopted for the sense of rotation of a magnetization vector M about a radiofrequency field B_1.

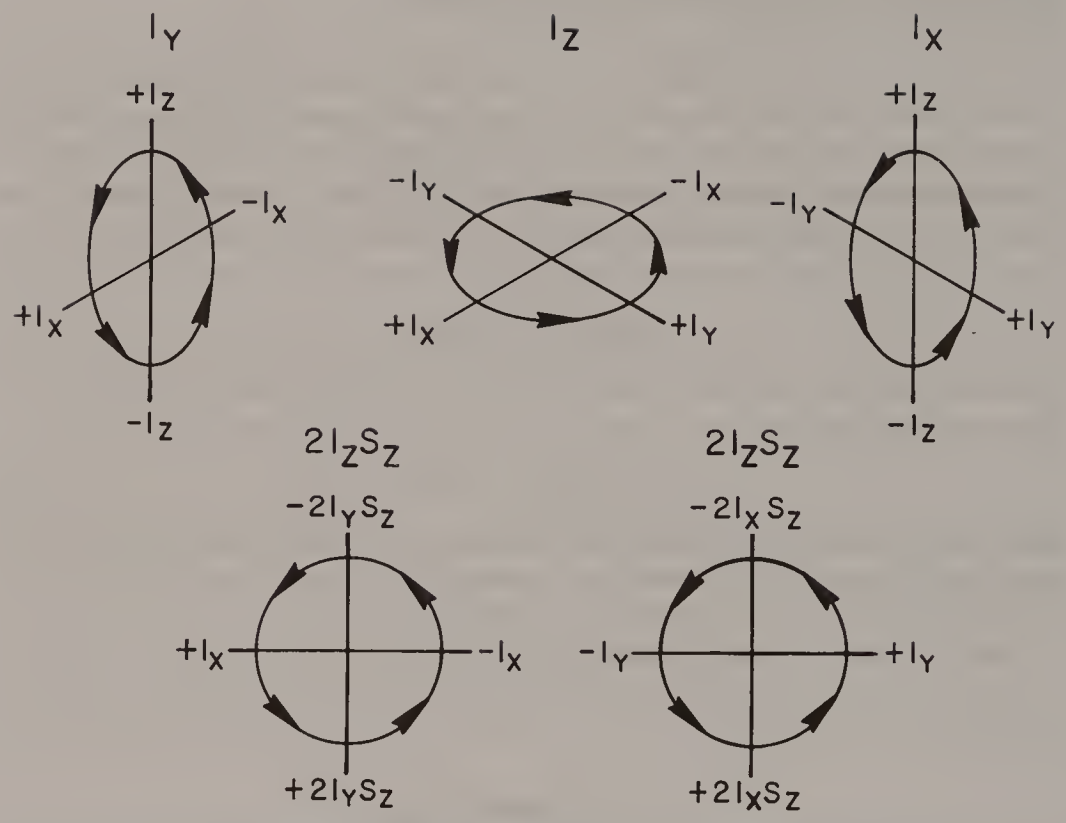

Fig. 3. Sign conventions for the evolution operators I_Y, I_Z, I_X and $2I_ZS_Z$ acting on the product operators I_X, I_Y, I_Z, $2I_XS_Z$ and $2I_YS_Z$. This schematic diagram is equivalent to Table 1.

schools of thought persist. Since the treatise of Sørensen *et al.* has become the standard article on the use of product operators in NMR pulse experiments, we adopt their sign convention, which is opposite to that of several other authors (2,5,6). In the product operator nomenclature, an operator (I_Z) is acted on by another operator I_X and the sign convention is *opposite* to that used above for magnetization vectors and fields (Fig. 3)

$$+I_Z \xrightarrow{+I_X} -I_Y. \qquad [3]$$

Similarly, a resonance offset effect causes a counter-clockwise rotation looking down on the XY plane

$$+I_Y \xrightarrow{+I_Z} -I_X \xrightarrow{+I_Z} -I_Y \xrightarrow{+I_Z} +I_X.$$

Finally, an operator $2I_ZS_Z$ has a specific sense of rotation

$$+I_X \xrightarrow{+2I_ZS_Z} +2I_YS_Z$$
$$+I_Y \xrightarrow{+2I_ZS_Z} -2I_XS_Z \qquad [4]$$

These conventions are illustrated pictorially in Fig. 3 and embodied in Table 1.

Table 1. The effect of one of the evolution operators (top row) acting on one of the operators describing the state of the spin system (left-hand column).

	I_X	I_Y	I_Z	S_X	S_Y	S_Z	$2I_ZS_Z$
I_X	E/2	$-I_Z$	I_Y	E/2	E/2	E/2	$2I_YS_Z$
I_Y	I_Z	E/2	$-I_X$	E/2	E/2	E/2	$-2I_XS_Z$
I_Z	$-I_Y$	I_X	E/2	E/2	E/2	E/2	E/2
S_X	E/2	E/2	E/2	E/2	$-S_Z$	S_Y	$2I_ZS_Y$
S_Y	E/2	E/2	E/2	S_Z	E/2	$-S_X$	$-2I_ZS_X$
S_Z	E/2	E/2	E/2	$-S_Y$	S_X	E/2	E/2
$2I_ZS_Z$	$-2I_YS_Z$	$2I_XS_Z$	E/2	$-2I_ZS_Y$	$2I_ZS_X$	E/2	E/2
$2I_XS_Z$	E/2	$-2I_ZS_Z$	$2I_YS_Z$	$-2I_XS_Y$	$2I_XS_X$	E/2	I_Y
$2I_YS_Z$	$2I_ZS_Z$	E/2	$-2I_XS_Z$	$-2I_YS_Y$	$2I_YS_X$	E/2	$-I_X$
$2I_ZS_X$	$-2I_YS_X$	$2I_XS_X$	E/2	E/2	$-2I_ZS_Z$	$2I_ZS_Y$	S_Y
$2I_ZS_Y$	$-2I_YS_Y$	$2I_XS_Y$	E/2	$2I_ZS_Z$	E/2	$-2I_ZS_X$	$-S_X$
$2I_XS_X$	E/2	$-2I_ZS_X$	$2I_YS_X$	E/2	$-2I_XS_Z$	$2I_XS_Y$	E/2
$2I_XS_Y$	E/2	$-2I_ZS_Y$	$2I_YS_Y$	$2I_XS_Z$	E/2	$-2I_XS_X$	E/2
$2I_YS_X$	$2I_ZS_X$	E/2	$-2I_XS_X$	E/2	$-2I_YS_Z$	$2I_YS_Y$	E/2
$2I_YS_Y$	$2I_ZS_Y$	E/2	$-2I_XS_Y$	$2I_YS_Z$	E/2	$-2I_YS_X$	E/2

MANIPULATION OF PRODUCT OPERATORS

For the majority of pulsed NMR experiments in liquids, we are concerned with three main types of evolution – rotation by a radiofrequency pulse, rotation due to chemical shift, and rotation due to spin–spin coupling. Although the operation of a given pulse sequence clearly depends on the time ordering of the pulses and the intervening periods of free precession, during these latter periods we are at liberty to change the ordering of chemical shift and spin coupling evolutions, provided that the spin system is weakly coupled. The corresponding terms in the Hamiltonian are said to *commute*. We may speak of a *cascade* (7) of chemical shift or spin coupling terms where the time ordering is immaterial. Furthermore, a non-selective radiofrequency pulse acting on both the I and S spins may be broken down into a cascade of two pulses acting selectively on the I spins and the S spins, and the relative ordering does not matter.

RADIOFREQUENCY PULSES

During a radiofrequency pulse, the chemical shifts and spin–spin coupling constants can be imagined to be 'switched off' and the rotation is about an axis in the XY plane, normally the X axis. If necessary, we can consider rotation about a

tilted radiofrequency field B_{eff}. Consider, first of all, an excitation pulse $\beta(X)$ acting on the Z magnetization of the I spins, represented by I_Z. Thus

$$I_Z \xrightarrow{\beta I_X} I_Z \cos\beta - I_Y \sin\beta. \qquad [5]$$

In the common example of a 90° pulse, this generates pure –Y magnetization; if it is a 180° pulse, there is a population inversion ($-I_Z$). Analogous expressions apply to pulses applied to the S spins, and for a non-selective pulse we would cascade the two rotations

$$+I_Z \xrightarrow{(\pi/2) I_X} -I_Y \qquad [6]$$

$$+S_Z \xrightarrow{(\pi/2) S_X} -S_Y \qquad [7]$$

A more complicated example occurs in the INEPT (8) experiment for polarization transfer in a heteronuclear IS system, commonly used to enhance the sensitivity of carbon-13 or nitrogen-15 spectra. In the key step of this sequence, I-spin magnetization vectors are prepared in an antiphase alignment along the ±X axes of the rotating frame and a $\pi/2$ pulse is applied to the I spins about the +Y axis. This rotation can be written as

$$2I_X S_Z \xrightarrow{(\pi/2) I_Y} -2I_Z S_Z \qquad [8]$$

This creates longitudinal two-spin order, usually represented by I-spin vectors aligned along the ±Z axes. These population disturbances affect the S spins through the common energy levels, and these perturbations can be 'read' by a $\pi/2$ pulse applied to the S spins

$$-2I_Z S_Z \xrightarrow{(\pi/2) S_X} 2I_Z S_Y \qquad [9]$$

We observe that the S-spin doublet has one line inverted and one line in the usual sense; in the case where the I spins are protons and the S spins are carbon-13, the 4:1 population advantage is transferred from protons to carbon-13, improving the sensitivity.

CHEMICAL SHIFTS

The evolution due to chemical shift effects may be represented by the operator equation

$$I_Y \xrightarrow{(2\pi\delta_I t) I_Z} I_Y \cos(2\pi\delta_I t) - I_X \sin(2\pi\delta_I t) \qquad [10]$$

where δ_I is the shift of the I-spin resonance measured from the transmitter frequency. Note the sense of rotation is opposite to that used in the vector model.

Chemical shifts of the S spins are handled in analogous fashion. For heteronuclear systems a separate rotating reference frame is assumed for each spin, the chemical shifts being measured with respect to the appropriate transmitter frequencies in their respective frames.

SPIN–SPIN COUPLING

According to the vector model, spin–spin coupling causes a divergence of I-spin vectors at rates $\pm\frac{1}{2}J_{IS}$ with respect to a hypothetical vector precessing at the chemical shift frequency. In the product operator formalism coupling is represented by

$$I_Y \xrightarrow{(\pi J_{IS}\tau)\,2I_ZS_Z} I_Y\cos(\pi J_{IS}\tau) - 2I_XS_Z\sin(\pi J_{IS}\tau). \qquad [11]$$

If the interval τ is chosen such that $\tau = 1/(2J_{IS})$ then the cosine term is zero and we are left with

$$I_Y \xrightarrow{(\pi/2)\,2I_ZS_Z} -2I_XS_Z; \qquad [12]$$

that is to say, two I-spin magnetization vectors aligned in opposition along the $\pm X$ axes. We may then consider another period of free precession:

$$-2I_XS_Z \xrightarrow{(\pi J_{IS}\tau)\,2I_ZS_Z} -2I_XS_Z\cos(\pi J_{IS}\tau) - I_Y\sin(\pi J_{IS}\tau). \qquad [13]$$

If we make this second interval $\tau = 1/(2J_{IS})$ then we find that the two vectors are realigned along the –Y axis

$$-2I_XS_Z \xrightarrow{(\pi/2)\,2I_ZS_Z} -I_Y. \qquad [14]$$

With these simple rules the evolution of spin systems under the influence of a pulse sequence can be followed by evaluating the effect of the seven evolution operators I_X, I_Y, I_Z, S_X, S_Y, S_Z and $2I_ZS_Z$ on the operators describing the state of the spin system (15 in all). Table 1 shows the results. Then an 'evolution tree' can be constructed (5) where by convention each left-hand branch represents the cosine term of the evolution equations [5], [10], [11] or [13], while the right-hand side represents the sine term (evaluated from Table 1). When the two operators commute (E/2 in Table 1) then there is no change in that term. Note that the unaffected term is always associated with cosine; the affected term is associated with sine.

CORRELATION SPECTROSCOPY (COSY)

For the worked example we take the homonuclear correlation spectroscopy (COSY) for a system of two coupled spins I and S. This simple system illustrates the essential points; additional spins merely make the spectrum more complicated by increasing the number of resonances and by splitting the IS peaks through 'passive' couplings J_{IQ} and J_{SQ}, etc. A second important simplification is to drop S_Z from the initial density matrix, concentrating our attention on what happens to I_Z, since the problem is symmetrical with respect to the two spin systems.

The pulse sequence is deceptively simple:

$$90^\circ(+X) - t_1 - 90^\circ(+X) - \text{acquisition}\,(t_2). \qquad [15]$$

For the present purposes we may ignore the phase cycling* that is normally employed.

Chemical shift (I_Z) and spin coupling operators ($2I_ZS_Z$) may be applied in any order; in the acquisition period t_2 precession of the S spins is also considered, since by then there has been some transfer of coherence from the I spins. The evolution tree is set out in Fig. 4 showing the four stages of branching, leading to 13 terms in the final density operator. Of these, nine represent unobservable quantities – longitudinal magnetization (Z), multiple-quantum coherence (M) and antiphase magnetizations (A). It is the remaining four terms that are important; they can be grouped in pairs

$$D = \sin(2\pi\delta_I t_1)\cos(\pi J_{IS} t_I)\cos(\pi J_{IS} t_2)[I_X \cos(2\pi\delta_I t_2) + I_Y \sin(2\pi\delta_I t_2)] \quad [16]$$

$$C = \sin(2\pi\delta_I t_1)\sin(\pi J_{IS} t_1)\sin(\pi J_{IS} t_2)[S_X \cos(2\pi\delta_S t_2) + S_Y \sin(2\pi\delta_S t_2)]. \quad [17]$$

It is clear that D represents coherence that has precessed at frequencies close to the chemical shift δ_I in both t_1 and t_2. These are the *diagonal* peaks. The term in square brackets indicates that there is phase modulation in the t_2 interval. The significance

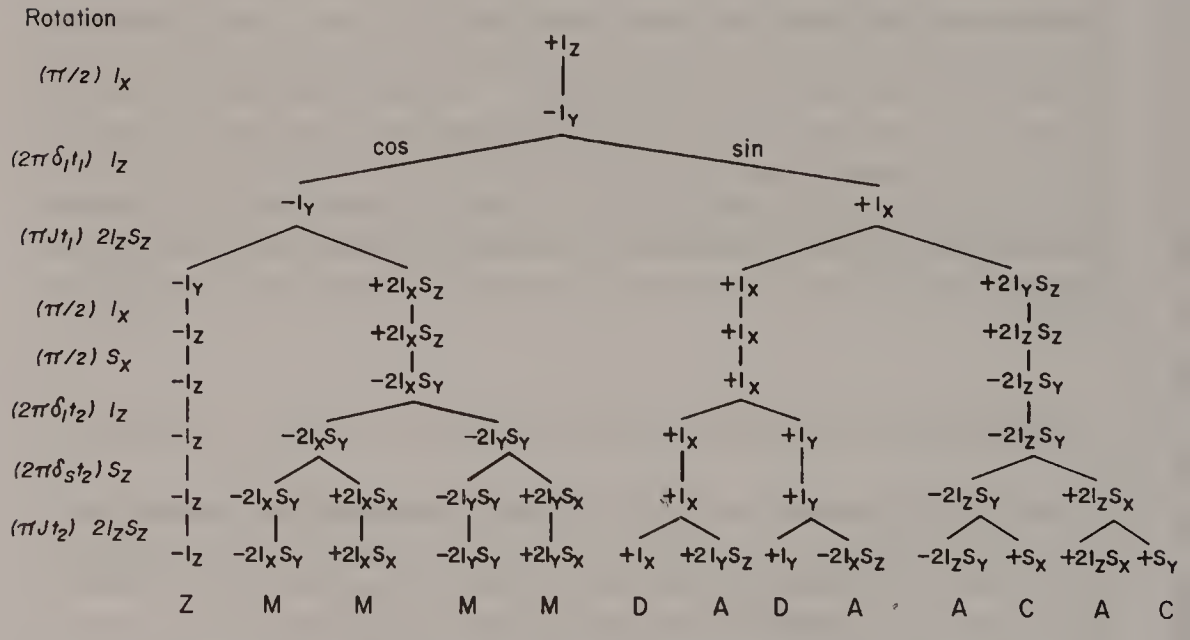

Fig. 4. Evolution of product operators appropriate to the homonuclear shift correlation experiment 'COSY'. For simplicity, the evolution of S_Z is omitted; it may be deduced from considerations of symmetry. Each left-hand branch implies multiplication by the cosine of the argument shown in the left-hand column, for example $-I_Y \cos(2\pi\delta_I t_1)$, while each right-hand branch implies multiplication by the corresponding sine term. The final 13 product operators are identified as Z magnetization (Z), multiple-quantum coherence (M), antiphase magnetization (A), diagonal peaks (D) or cross-peaks (C).

of the two J-modulation terms, $\cos(\pi J_{IS} t_1)$ and $\cos(\pi J_{IS} t_2)$, may not be immediately apparent. They may be converted by means of trigonometrical identities

$$\sin(2\pi\delta_I t_1) \cos(\pi J_{IS} t_1) = 0.5[\sin(2\pi\delta_I + \pi J_{IS})t_1 + \sin(2\pi\delta_I - \pi J_{IS})t_1]. \quad [18]$$

This represents a response in the F_1 dimension, centred at δ_I and split into a doublet (J_{IS}), both lines having the same phase. Similarly, the terms in t_2 may be combined to show that there is an in-phase doublet in the F_2 dimension. This is the familiar square pattern of lines straddling the principal diagonal.

By contrast, eqn [17] represents coherence that originated at frequencies near the chemical shift δ_I but which was detected at frequencies near δ_S, and thus describes one of the *cross-peaks*. (The other cross-peak would have been predicted by following the fate of S_Z, neglected in our calculation.) In this case the trigonometrical identity is

$$\sin(2\pi\delta_I t_1) \sin(\pi J_{IS} t_1) = 0.5[\cos(2\pi\delta_I - \pi J_{IS})t_1 - \cos(2\pi\delta_I + \pi J_{IS})t_I]. \quad [19]$$

This represents a response, centred at δ_I in the F_1 dimension, which is an antiphase doublet (J_{IS}). A similar identity shows that it is also an antiphase doublet in the F_2 dimension, centred at δ_S. The cross-peak is therefore a square pattern with the familiar intensity alternation. Normally we adjust the spectrometer phase so that the cross-peaks are in the absorption mode; then the diagonal peaks are in dispersion (sine modulation).

The presence of the terms $\sin(\pi J_{IS} t_1) \sin(\pi J_{IS} t_2)$ has another interesting consequence. It predicts that cross-peaks will have low relative intensities unless both t_1 and t_2 are permitted to evolve for times comparable with $(\pi J_{IS})^{-1}$, whereas the diagonal peaks will be relatively strong. This is important when searching for correlations based on very small coupling constants. Sometimes, a fixed delay is introduced into the evolution period in order to emphasize the effects of very small couplings (9).

Since this has been an illustrative exercise, all the evolutions have been worked out explicitly. Once familiarity with product operator algebra has been acquired, it is not normally necessary to carry through the calculation to the bitter end. For example, we could choose to stop the COSY calculation immediately after the second pulse ($t_2 = 0$), recognizing that the I_X term will give an in-phase doublet in the F_2 dimension and that the $-2I_Z S_Y$ term will evolve to give an antiphase doublet in F_2.

REFERENCES

1. A. Abragam, *The Principles of Nuclear Magnetism.* Oxford University Press, 1961.
2. C. P. Slichter, *The Principles of Magnetic Resonance.* Springer: Berlin, 1978.
3. O. W. Sørensen, G. W. Eich, M. H. Levitt, G. Bodenhausen and R. R. Ernst, *Prog. NMR Spectrosc.* **16**, 163 (1983).
4. U. Fano, *Rev. Mod. Phys.* **29**, 74 (1957).
5. J. Y. Lallemand, *École d'Été sur la Spectroscopie en Deux Dimensions,* Orléans, France, 1984.
6. U. Haeberlen, *High Resolution NMR in Solids, Selective Averaging.* Academic Press: New York, 1976.
7. G. Bodenhausen and R. Freeman, *J. Magn. Reson.* **36**, 221 (1979).
8. G. A. Morris and R. Freeman, *J. Am. Chem. Soc.* **101**, 760 (1979).
9. A. Bax and R. Freeman, *J. Magn. Reson.* **44**, 542 (1981).

Cross-references

Correlation spectroscopy
Multiple-quantum coherence
Phase cycling
Polarization transfer
Rotating frame
Two-dimensional spectroscopy
Vector model

Pulsed Field Gradients

Pulsed magnetic field gradients are gradually replacing phase cycling* as a method for removing undesirable signal components from high-resolution NMR spectra. There are basically two modes of operation: purging schemes and matched field gradients.

PURGING SCHEMES

A purging gradient can be used to disperse transverse components of magnetization but retain longitudinal components. Because the early experiments achieved this by grossly mis-setting the current in one of the homogeneity correction coils, this is still sometimes called a 'homospoil' pulse. One early application was to remove the undesirable transverse magnetization created by a slightly imperfect 180° population inversion pulse used to initiate an inversion-recovery spin–lattice relaxation experiment (1). In a more recent implementation where a two-dimensional nuclear Overhauser technique (NOESY) stores the magnetization of interest along the Z axis for a short mixing period τ_m, a pulsed field gradient is employed to disperse any undesirable XY magnetization.

These 'spoiler' gradients do not of course destroy magnetization but distribute the tips of the isochromatic vectors along a helix whose axis is the direction of the applied gradient (often the Z axis). We must therefore be careful to check whether subsequent radiofrequency pulses might not bring these vectors back to a focus at some later time through the action of naturally occurring gradients of the magnetic field. Accidental refocusing is less likely if spoiler gradients are applied in three orthogonal directions, creating a more isotropic distribution in space. Where repeated homospoil pulses are used, they should be randomized in length or intensity to avoid possible refocusing.

The spatial inhomogeneity of the radiofrequency field B_1 can also be used to purge undesirable signal components. This is usually implemented as a short spin-lock pulse with the phase set so that B_1 lies along the signal component to be retained, signals at right angles fanning out in all directions around a circle. One example is the removal of dispersion-mode components excited by a half-Gaussian selective radiofrequency pulse (2). This is an important improvement because the

dispersion components would otherwise spread across a much wider band of frequencies than the absorption mode.

MATCHED FIELD GRADIENTS

Phase cycling* distributes various signal components in phase space, and then rotates the receiver reference phase to recover the signal of interest. The analogous pulsed field gradient scheme spreads the isochromats in physical space and recovers the one of interest by application of a 'recall' gradient. The preparation and recall gradients are not necessarily equal in intensity and duration; indeed many of the interesting applications require that they be applied in some fixed ratio and with appropriate signs. This is the 'matched gradient' scheme.

To understand the need for matched pairs of field gradients, we need to invoke the concept of *coherence order*. We saw in the section on Multiple-quantum coherence* that homonuclear double-quantum coherence evolves in time as a cascade of evolutions with respect to the I-spin and S-spin chemical shifts (measured as offsets from the transmitter frequency):

$$2I_XS_X - 2I_YS_Y \xrightarrow{(2\pi\delta_I t)\,I_Z} \xrightarrow{(2\pi\delta_S t)\,S_Z} (2I_XS_X - 2I_YS_Y)\cos\left[2\pi(\delta_I + \delta_S)t\right]. \quad [1]$$

Consequently, any increment ΔB in the applied magnetic field has a two-fold effect on the evolution of double-quantum coherence (and a negligible effect on homonuclear zero-quantum coherence). In general, an additional field ΔB behaves as a shift $p\Delta B$ for p-quantum coherence, and a pulsed field gradient disperses the isochromats of p-quantum coherence p times as far as it spreads those of single-quantum coherence (3). Bax *et al.* (4) demonstrated that pulsed gradients of carefully matched durations were the most convenient way to separate the various orders of coherence. The matching condition is given by

$$G_1\tau_1p_1\gamma_1 = -G_2\tau_2p_2\gamma_2 \quad [2]$$

where G represents the gradient intensity (usually held constant) and τ its duration, p is the coherence order and γ the gyromagnetic ratio (which may change in coherence transfer experiments). Note that G, p and γ carry intrinsic signs.

Analysis of the appropriate coherence transfer pathway (5) is the key to the design of a suitable pair of matched field gradients, since we need to know p_1 and p_2 in order to set τ_1 and τ_2 in eqn [2]. Suppose we create p-quantum coherence during an evolution period and then convert it into transverse magnetization ($p = -1$) during a subsequent acquisition period, and suppose we wish to select only those signals originating from the p-quantum coherence. A pulsed gradient of duration τ in the evolution period spreads out the p-quantum isochromats at an accelerated rate so that they are only refocused if a second gradient of duration $p\tau$ is applied after the conversion; signals arising from other orders of coherence are

not refocused. If the two coherence orders have the same sign, then the second gradient must be reversed in sense.

The practical advantages of pulsed gradients compared with phase cycling (6) can scarcely be overestimated. Suppression of undesirable responses takes place within a single scan. Because we do not need to rely on taking the difference between two consecutive scans, medium-term spectrometer instabilities are far less important and a much higher degree of suppression can be achieved. This is particularly important in water suppression sequences, because even a slight instability generates appreciable artefacts reminiscent of t_1 noise*. Furthermore, an N-step phase cycle reverts to a single scan, drastically reducing the overall duration of the pulsed gradient experiment if the signal-to-noise ratio is already adequate. As pulse sequences for multidimensional spectroscopy become more and more complex, nested phase cycling tends to be an unaffordable luxury.

Phase cycling has been successfully replaced by pulsed field gradients in two-dimensional correlation (COSY) spectroscopy (3,6). Multiple-quantum filters can be constructed in a similar manner; they have been exploited, for example, in double-quantum filtered (7) and four-quantum filtered (8) correlation spectroscopy. The general availability of pulsed gradient technology in the 1990s led to a burst of activity in 'gradient enhanced spectroscopy' triggered by the excellent suppression of water t_1 noise* obtained by Hurd (9) for a double-quantum filtered COSY spectrum of an aqueous solution of angiotensin II. Here the macroscopic diffusion of water molecules in the intense field gradient probably improves the degree of suppression.

A matched gradient scheme may involve only a change in the sign of the coherence order. A very useful water suppression module, called 'WATERGATE' (10), employs two equal gradient pulses of the same polarity acting on transverse magnetization. A hard 180° pulse and a selective 180° pulse are applied between the two gradients. The selective pulse is tuned to the water frequency and negates the effect of the hard pulse for the water signal, which is therefore dispersed by the successive gradients acting in the same sense. On the other hand, the remaining lines of the spectrum experience only the hard 180° pulse, and the divergence of isochromats caused by the first gradient is brought to a focus by the second.

The technology for the implementation of pulsed field gradient experiments has been driven by the urgent needs of magnetic resonance imaging, where a field gradient is an essential ingredient of the method (11). Initially there were serious difficulties created by the eddy currents induced in nearby metallic conductors, but this has been solved by 'active shielding', where an outer coil is fed with a current of opposite polarity, trapping the return path of the magnetic flux between the two coils. A gradient coil placed in the intense static magnetic field B_0 acts rather like a loudspeaker and vibrates quite strongly; it is therefore embedded in a suitable insulator such as epoxy resin.

REFERENCES

1. R. L. Vold, J. S. Waugh, M. P. Klein and D. E. Phelps, *J. Chem. Phys.* **48**, 3831 (1968).
2. H. Kessler, U. Anders, G. Gemmecker and S. Steuernagel, *J. Magn. Reson.* **85**, 1 (1989).
3. A. Wokaun and R. R. Ernst, *Chem. Phys. Lett.* **52**, 407 (1977).
4. A. Bax, P. G. de Jong, A. F. Mehlkopf and J. Smidt, *Chem. Phys. Lett.* **69**, 567 (1980).
5. G. Bodenhausen, H. Kogler and R. R. Ernst, *J. Magn. Reson.* **58,** 370 (1984).
6. P. Barker and R. Freeman, *J. Magn. Reson.* **64**, 334 (1985).
7. U. Piantini, O. W. Sørensen and R. R. Ernst, *J. Am. Chem. Soc.* **104**, 6800 (1982).
8. A. J. Shaka and R. Freeman, *J. Magn. Reson.* **50,** 502 (1982).
9. R. E. Hurd, *J. Magn. Reson.* **87**, 422 (1990).
10. M. Piotto, V. Saudek and V. Sklénar, *J. Biomed. NMR* **2**, 661 (1992).
11. P. C. Lauterbur, *Nature* **242**, 190 (1973).

Cross-references

Multiple-quantum coherence
Nuclear Overhauser effect
Phase cycling
Spin–lattice relaxation
t_1 noise
Two-dimensional spectroscopy

Quadrature Detection

Suppose we represent precessing transverse nuclear magnetization by a vector M which rotates (say) clockwise in the rotating reference frame*. A phase-sensitive detector that measures the Y component would pick up a signal M cos ωt and, although it could measure the frequency ω, it would be unable to determine the *sense* of the rotation. Indeed the observation would be quite compatible with the case of two equal counter-rotating vectors each of amplitude $\frac{1}{2}$ M. In order to find the sense of rotation we need a second phase-sensitive detector to measure the X component, described by M sin ωt. The two detectors are therefore fed with the same reference frequency, but one is shifted in phase by 90°; the method is therefore called quadrature detection (1).

For reasons of simplicity, the very early Fourier transform spectrometers used only a single phase-sensitive detector, and were unable to determine the sense of rotation (the sign of the nuclear precession frequency). Consequently, the transmitter frequency had to be set at one extreme edge of the NMR spectrum, otherwise both positive and negative frequencies were aliased and superimposed on one another, leading to unacceptable confusion. Placing the transmitter outside the range of NMR frequencies had two serious disadvantages. First, the transmitter power was not used to the best advantage; for a given permissible tilt angle of the effective field, the B_1 field had to be doubled. Second, noise components were accepted from both sides of the carrier frequency, whereas signals were gathered from only one side; thus, for a given filter bandwidth, the noise was doubled and the sensitivity decreased by the square root of two.

Quadrature detection can be achieved with only a *single* phase-sensitive detector by means of the 'Redfield trick' (2) where the sampling rate is doubled and the real and imaginary signal components are sampled alternately by switching the detector phase by ±90°. One might object that this interleaving of real and imaginary data sets would complicate the subsequent processing stage, but if the signs are also inverted for every third and fourth acquisition, this becomes a phase cycle (0°, 90°, 180°, 270°) and the data can be processed just like any normal free induction decay (3). This progressive stepwise rotation of the phase behaves exactly like a smooth rotation of the 'receiver reference frame' with respect to the 'transmitter reference frame', at a frequency of one-half of the spectral width (4). This foreshadows the 'time-proportional phase incrementation (TPPI)' technique which has proved so important in two-dimensional spectroscopy (5). There are important practical advantages in having the freedom to set the transmitter frequency at a particular

point in the spectrum, for example for certain solvent suppression* experiments.

Modern Fourier transform spectrometers invariably employ quadrature detection with two carefully matched phase-sensitive detectors. Each sampling operation involves two orthogonal measurements and the signal is usually represented by a complex number, $S_a + iS_b$. The transmitter frequency is set in (or near) the centre of the spectrum and the sampling rate is made equal to the spectral width SW, so that all NMR responses with frequencies within the range $-\frac{1}{2}$SW to $+\frac{1}{2}$SW are properly digitized according to the Nyquist criterion (see Digitization*). Noise is only accepted from regions of frequency space also occupied by NMR signals, while noise outside the spectral width is removed by analogue or digital filtration.

CHANNEL IMBALANCE

Early quadrature detection schemes experienced some difficulty in accurately matching the two phase-sensitive detectors (the real and imaginary 'channels'). This could be simply an amplitude imbalance, or a small error in the 90° phase shift, leading to a slight admixture of the real component in the imaginary channel and vice versa. After complex Fourier transformation this generates *quadrature images*, weak replicas of the true spectrum reversed with respect to zero frequency (the transmitter frequency). We can understand how this comes about because, if either imperfection reaches the extreme limit, the system reverts to single-channel phase-sensitive detection where the parent and image signals are of equal intensity. There is a further potential problem associated with any d.c. offset of the incoming NMR signal: it generates a spurious response at the centre of the spectrum (zero frequency) called the *quadrature glitch.* The scheme for compensating these imperfections, introduced by Hoult and Richards (6), is described in detail in the section on Phase cycling*.

TWO-DIMENSIONAL SPECTROSCOPY

In a two-dimensional experiment there is no actual signal detection during the evolution period (t_1) so quadrature detection cannot be implemented in the normal way. Nevertheless, for the majority of cases (e.g. COSY, NOESY, or INADEQUATE) the signals of interest are amplitude modulated in the t_1 dimension. Amplitude modulation can be represented as two equal counter-rotating magnetization vectors and we would like to select just one of these; in other words, we need to discriminate positive and negative frequencies in the F_1 dimension. In doing so, we would wish to avoid methods that lead to lineshapes that are admixtures of two-dimensional absorption- and dispersion-mode responses – the 'phase-twist' lineshape (7). Only two-dimensional pure absorption-mode signals are suitable for high-resolution studies.

A data processing scheme to retain pure absorption signals and also achieve sign

discrimination in the evolution dimension was first suggested by States *et al.* (8) and is sometimes called the hypercomplex Fourier transform technique. By analogy with quadrature detection in one-dimensional spectroscopy, we see that we need to acquire two separate time-domain signals, one with cosine modulation and the other with sine modulation in the t_1 dimension:

$$S_C(t_1, t_2) = \cos(\Omega_1 t_1) \exp(-\lambda_1 t_1) \exp(i\Omega_2 t_2) \exp(-\lambda_2 t_2) \quad [1]$$

$$S_S(t_1, t_2) = \sin(\Omega_1 t_1) \exp(-\lambda_1 t_1) \exp(i\Omega_2 t_2) \exp(-\lambda_2 t_2) \quad [2]$$

where λ_1 and λ_2 are lineshape functions in the respective frequency dimensions. Because the cosine is an even function and the sine an odd function, Fourier transformation of eqn [1] gives positive absorption lines at $-\Omega_1$ and $+\Omega_1$, whereas eqn [2] gives a *negative* absorption signal at $-\Omega_1$ and a positive absorption signal at $+\Omega_1$. If these two spectra are combined, only the response at $+\Omega_1$ remains; we have achieved sign discrimination in the evolution (F_1) dimension. Normal quadrature detection is employed in the F_2 dimension; this has been recognized by writing the frequency as $\exp(i\Omega_2 t_2)$ rather than $\cos(\Omega_2 t_2)$.

Alternatively, the requisite sign discrimination in the F_1 dimension can be achieved with the transmitter in the centre of the spectrum but with the receiver reference frame effectively displaced by half the spectral width so that none of the lines are aliased about the carrier frequency. This TPPI scheme (5) advances the signal phase by 90° for each increment in the t_1 dimension. If the signal of interest represents p-quantum coherence, this 90° phase shift of the signal is achieved by 90°/p phase shift of all the radiofrequency pulses prior to the evolution period. This technique has been employed by Marion and Wüthrich (9) in the context of spectrometers that employ only real Fourier transforms; the underlying principles can be shown (10) to be the same as those governing the method of States *et al.* (8).

REFERENCES

1. A. G. Redfield and R. K. Gupta, *Adv. Magn. Reson.* **5**, 81 (1971).
2. A. G. Redfield and R. K. Gupta, *J. Chem. Phys.* **54**, 1418 (1971).
3. A. G. Redfield and S. D. Kunz, *J. Magn. Reson.* **19**, 250 (1975).
4. G. Bodenhausen, R. Freeman, G. A. Morris, R. Niedermeyer and D. L. Turner, *J. Magn. Reson.* **25**, 559 (1977).
5. G. Drobny, A. Pines, S. Sinton, D. P. Weitekamp and D. Wemmer, *Faraday Symp. Chem. Soc.* **13**, 49 (1978).
6. D. I. Hoult and R. E. Richards, *Proc. R. Soc. A* **344**, 311 (1975).
7. G. Bodenhausen, R. Freeman, R. Niedermeyer and D. L. Turner, *J. Magn. Reson.* **26**, 133 (1977).
8. D. J. States, R. A. Haberkorn and D. J. Ruben, *J. Magn. Reson.* **48**, 286 (1982).
9. D. Marion and K. Wüthrich, *Biochem. Biophys. Res. Commun.* **113**, 967 (1983).
10. J. Keeler and D. Neuhaus, *J. Magn. Reson.* **63**, 454 (1985).

Cross-references

Digitization
Fourier transformation
Lineshapes in two-dimensional spectra
Phase cycling
Rotating frame
Solvent suppression

Radiation Damping

This is a phenomenon that is easily overlooked, although it can have quite a profound effect under certain circumstances. The radiofrequency energy associated with a free induction signal is usually understood to be tiny in relation to the energy of the driving radiofrequency pulse, but in fact a sample of high spin density in a high magnetic field induces a significant current in the receiver coil, creating a new continuous-wave radiofrequency field that reacts on the nuclear spins. The precession is no longer 'free'. The induced radiofrequency field is at right angles to the precessing transverse nuclear magnetization, and in such a sense as to rotate the magnetization vector back to the +Z axis. Consequently the NMR signal decays faster than normal. This is sometimes described as a *damping* process; hence the name radiation damping (1). We shall see below that this is not an entirely suitable description.

Radiation damping is significant for samples of high spin density, nuclei with a high gyromagnetic ratio, and at high applied magnetic fields. It therefore often goes hand in hand with an appreciable nuclear susceptibility* effect, although the two phenomena are separable (see below). The most notorious candidate is water, which is 110 M in protons, and which, for many cases of practical importance, cannot be used in its deuterated form. The resulting extensive tails of the water signal cause havoc with spectral baselines.

The radiation damping phenomenon is quantified in terms of a decay time constant given by

$$T_{RD} = (2\pi\eta Q\gamma M_{XY})^{-1} \qquad [1]$$

where η is the receiver coil filling factor (of the order unity), Q is the coil quality factor (typically 250), γ is the gyromagnetic ratio, and M_{XY} is the transverse magnetization (maximum value M_0). The larger these parameters, the more rapid the decay of the free precession signal and the broader the observed resonance. High levels of prepolarization also increase M_{XY} in eqn [1] and aggravate the radiation damping. As a consequence, Earth's field proton magnetometers generate free induction signals with decay rates largely dominated by this phenomenon. The quality factor Q enters eqn [1] because it enhances the current induced in the receiver coil. Consequently the radiation damping can be considerably reduced by detuning the coil, moving right down into the tail of the resonance curve of the tuned circuit. This is a simple and effective test for radiation damping. It

distinguishes it from the nuclear susceptibility effect which is quite independent of the coil tuning.

In a high-resolution spectrum consisting of one intense resonance and a weak neighbour, the broadening effect is mainly restricted to the intense line, because the radiation damping effect falls off quite rapidly with offset from resonance. Instead of a radiation damping field B_{RD}, the adjacent spin experiences an effective field B_{eff}, the resultant of B_{RD} and the offset ΔB, tilted towards the +Z axis through an appreciable angle $\arctan(\Delta B/B_{RD})$. The principal effect is then a dephasing of the adjacent (weak) resonance rather than an acceleration of its decay. A good example is provided by the inner carbon-13 satellites of an intense proton signal subject to radiation damping. Although the parent proton signal is appreciably broadened, the weak satellites remain sharp but are phase shifted (in opposite senses) towards the dispersion mode (2).

A common manifestation of radiation damping in high-resolution spectra is a distortion of the relative peak heights of spin multiplets that would normally appear as 1:2:1 triplets or 1:3:3:1 quartets (3). Because the stronger lines are preferentially broadened by radiation damping, their peak heights are reduced. This effect is evident in the 500 MHz spectrum of ethanol (Fig. 1(a)) but disappears when the receiver coil is grossly detuned (Fig. 1(b)). The peak height distortion is also absent in the carbon-13 satellite spectrum, which has signals 180 times weaker than in the parent spectrum and is therefore far less susceptible to radiation damping.

The most striking effects are observed after a 180° inversion pulse (4). If the pulse is perfect (leaving no residual transverse magnetization) then no current is induced in the coil by radiation damping, but even a very slight deviation from

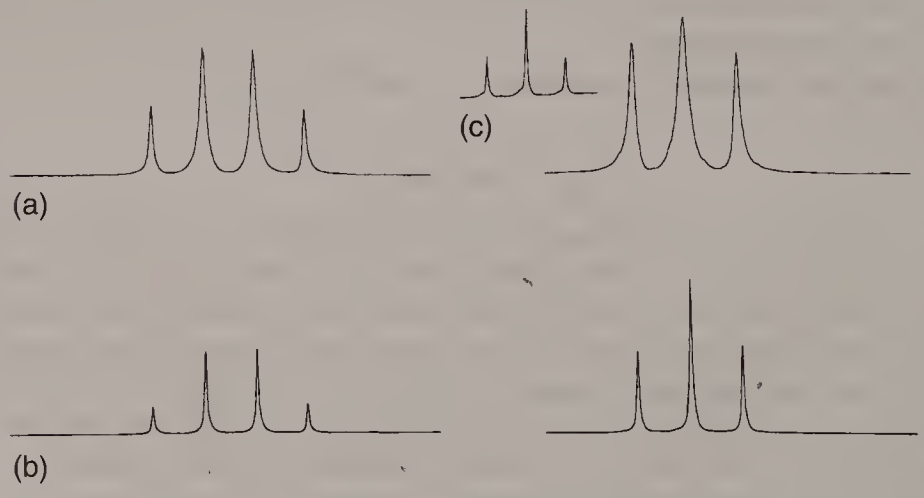

Fig. 1. Multiplets from the 500 MHz proton spectrum of ethanol, showing severe line broadening by radiation damping, most marked on the strongest lines. The expected 1:3:3:1 peak height pattern of the quartet and the 1:2:1 pattern of the triplet are grossly distorted (a), but return to normal when the receiver coil is detuned (b) and for the weak carbon-13 satellites (c). Spectra courtesy of Dr Tom Frenkiel.

ideality induces a tiny current which turns the magnetization vector further away from the –Z axis in an escalating process in which the observed signal grows rapidly with time until the magnetization swings through the XY plane on its way to the +Z axis. (This is why the description in terms of a damping process is inadequate.) Fourier transformation of such a time-domain signal produces a severely distorted lineshape. We can readily appreciate how this effect could interfere with the proper determination of spin–lattice relaxation* times by the inversion-recovery method (5) and we may anticipate analogous perturbations of spin-echo* experiments, as isochromats come into phase and induce an increasing radiation damping current in the coil.

There are now many complex pulse sequences used to manipulate nuclear spins in high-resolution NMR, particularly in two-dimensional spectroscopy*. In such experiments, radiation damping can have an insidious effect because intervals of 'free' precession can actually become intervals of forced precession through the introduction of the radiation damping field. Take, for example, the widely used 'jump-and-return' water suppression sequence (6) which rotates the intense water vector into the XY plane for a period τ and then rotates it back to the +Z axis. Successful elimination of the water resonance presupposes that its magnetization vector does not leave the XY plane during the τ interval, but the additional torque caused by radiation damping ensures that it does. The situation is further complicated if phase cycling* is employed.

Practical techniques have been introduced to suppress the radiation damping during such manipulations, by electronic negative feedback to the coil (7) or by rapid Q switching (8). Radiation damping is generally considered to be an undesirable artefact to be eliminated wherever possible. However, it can occasionally be put to good use. An example is the detection of subspectra from proton sites that exchange chemically with water (9). In an experiment consisting of two consecutive scans, a selective 180° pulse inverts the water signal and the signals are collected in the difference mode. In the first scan the water vector is returned rapidly to the +Z axis by augmenting the radiation damping through positive feedback; in the second scan the radiation damping is inhibited by negative feedback and the water vector remains inverted. Thus the signals transferred by chemical exchange change sign between the first scan and the second, and they are thus separated from all other proton signals in the difference spectrum.

Even more subtle effects of radiation damping have been reported. Barjat *et al.* (10) have analysed the interactions that occur between two lines of a J-doublet, where two equal radiation damping fields, $B_{RD}(1)$ and $B_{RD}(2)$, are at work. First of all, the two lines broaden asymmetrically since $B_{RD}(1)$ and $B_{RD}(2)$ act in opposition between the two lines but reinforce each other outside the doublet. Perhaps more surprisingly, weak satellite lines appear at multiples of the doublet splitting. We may think of these as arising from the resultant of $B_{RD}(1)$ and $B_{RD}(2)$, which contains an oscillatory component that gives rise to a slight wiggling of the magnetization trajectories.

REFERENCES

1. N. V. Bloembergen and R. V. Pound, *Phys. Rev.* **95**, 8 (1954).
2. R. Freeman and W. A. Anderson, *J. Chem. Phys.* **42**, 1199 (1965).
3. T. Frenkiel, private communication.
4. A. Szöke and S. Meiboom, *Phys. Rev.* **113**, 585 (1959).
5. X. A. Mao, J. X. Guo and C. H. Ye, *Chem. Phys. Lett.* **222**, 417 (1994).
6. P. Plateau and M. Guéron, *J. Am. Chem. Soc.* **104**, 7310 (1982).
7. P. Broekaert and J. Jeener, *J. Magn. Reson. A* **113**, 60 (1995).
8. C. Anklin, M. Rindlisbacher, G. Otting and F. H. Laukien, *J. Magn. Reson. B* **106**, 199 (1995).
9. J.Y. Lallemand, A. Louis-Joseph and D. Abergel, *La RMN, un Outil pour la Biologie,* Institut Pasteur, Paris (February 1996).
10. H. Barjat, G. P. Chadwick, G. A. Morris and A. G. Swanson, *J. Magn. Reson. A* **117**, 109 (1995).

Cross-references

Difference spectroscopy
Free induction decay
Nuclear susceptibility
Phase cycling
Solvent suppression
Spin echoes
Spin–lattice relaxation
Two-dimensional spectroscopy

Radiofrequency Pulses

According to the vector model* of the magnetic resonance phenomenon, pulse excitation is represented as a rotation of a macroscopic magnetization vector M about the X axis of the rotating frame through a 'flip angle' α radians. If resonance offsets (ΔB) can be neglected, $\alpha = \gamma B_1 t_p$, where B_1 is the radiofrequency field intensity and t_p the pulse duration. This requires that $B_1 >> \Delta B$ for all lines in the spectrum of interest, the 'hard-pulse' condition. For proton spectroscopy, a radiofrequency intensity such that $\gamma B_1/2\pi \sim 25$ kHz might be typical; this necessarily entails a short duration of 10 μs for a 90° pulse. For carbon-13 spectroscopy the range of chemical shifts is such that the condition $B_1 >> \Delta B$ is not so well satisfied, leaving lines distant from the transmitter frequency not properly excited. Hence the importance of quadrature phase detection* which allows the transmitter to be set in the centre of the spectrum.

For the best sensitivity it is customary to pulse and acquire free induction decays as fast as permitted by the constraints of spin–lattice relaxation*. The most common mode of operation sets the flip angle to 90° and allows a suitable waiting period t_d between the end of acquisition and the next radiofrequency pulse, adjusting t_d according to some estimate of the spin–lattice relaxation times. There may be a significant range of relaxation times involved, and in routine operations no actual relaxation measurements are normally available, so a suitable guess is made. Fortunately sensitivity is not critically dependent on this choice. An alternative mode of operation sets t_d to zero and adjusts the flip angle to some value less than 90° so that a favourable steady state is established for longitudinal magnetization. The more efficient the spin–lattice relaxation, the closer the flip angle should be set to 90°. A quantitative treatment of these effects is given under Steady-state effects*.

Proper adjustment of the pulse flip angle is much more important for relaxation studies and modern multipulse experiments. It must be set to 90° for progressive saturation or saturation-recovery measurements, and to 180° for spin inversion or spin-echo refocusing experiments. Particular care is required in repetitive experiments where pulse length errors could be cumulative.

PULSE IMPERFECTIONS

Several instrumental shortcomings conspire to make radiofrequency pulses behave imperfectly. Apart from simple miscalibration of the flip angle, this may also come about through the effects of spatial inhomogeneity of the radiofrequency field B_1, so that different regions of the sample experience different pulse flip angles. This inhomogeneity must be considered over the effective volume of the sample, restricted radially because the sample is contained within a cylindrical tube, and longitudinally by the decreased coupling of the spins to the receiver coil as a function of distance from the coil. Where the effects of the spatial inhomogeneity of the B_1 field could be critical, a small spherical sample may be used.

A second source of imperfection arises from resonance offset effects. In the general case the nuclei experience an effective field B_{eff} which is the resultant of B_1 and the offset from resonance ΔB. The flip angle is increased and the axis of rotation is tilted away from the X axis through an angle θ towards the $\pm Z$ axis (Fig. 1). A significant tilt prevents proper inversion of M_Z whatever the flip angle, a fact of key importance in broadband decoupling* techniques. If the nominal flip angle is 90° there is a relatively uniform conversion of M_Z into transverse magnetization

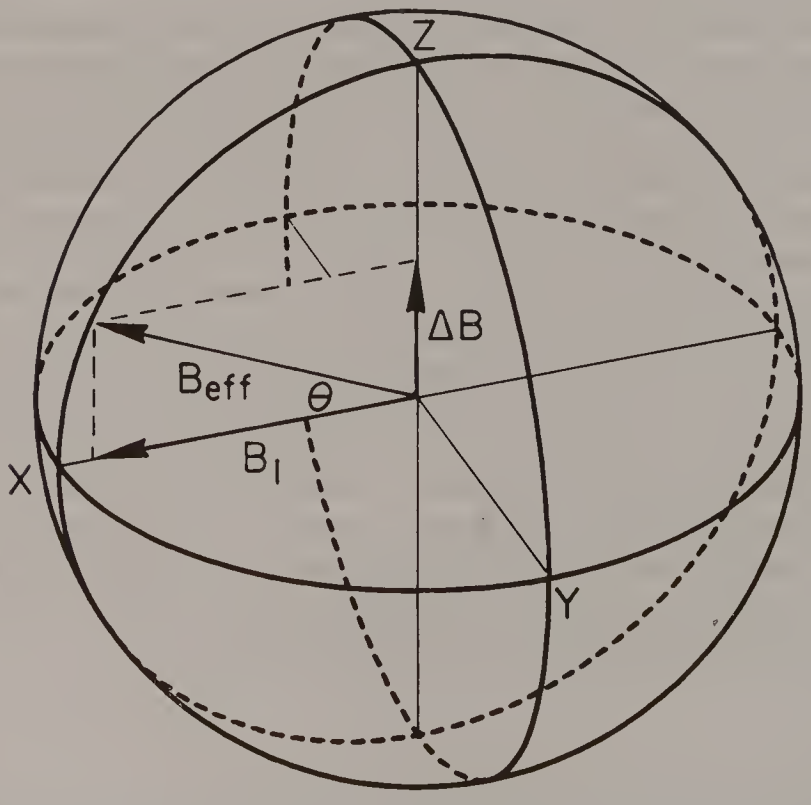

Fig. 1. In the rotating reference frame, a radiofrequency field of intensity B_1 at an offset ΔB acts as an effective field B_{eff} tilted through an angle θ with respect to the X axis.

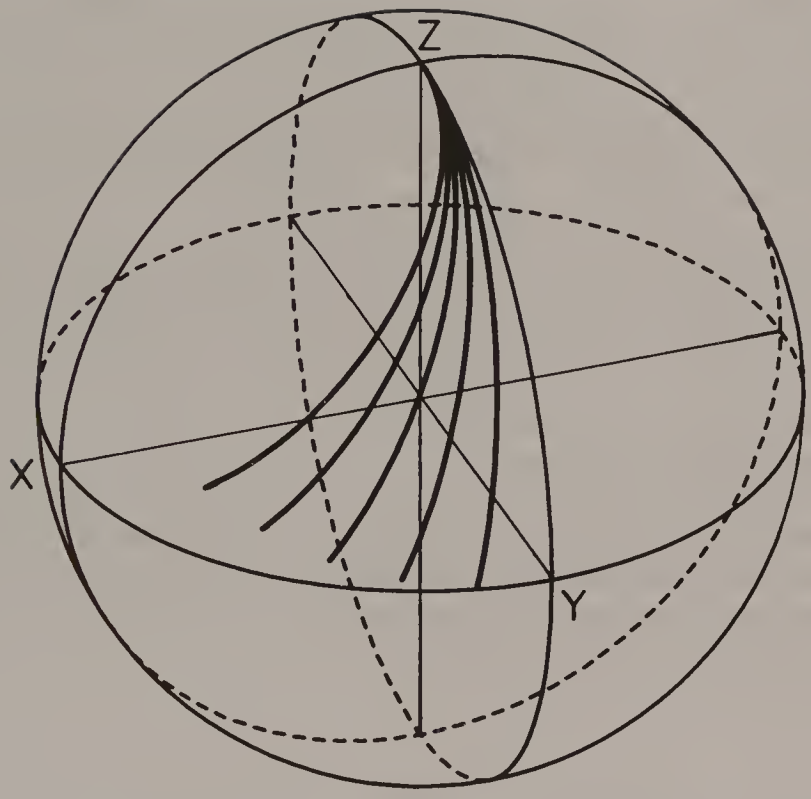

Fig. 2. The self-compensating property of a 90° pulse with respect to resonance offset. The influence of the tilt of the effective field is partially compensated by the increase in flip angle. Magnetization trajectories are shown for $\Delta B/B_1 = 0.1, 0.2, 0.3, 0.4$ and 0.5. The intensity of the excited signal (the XY projection) is approximately constant but it is appreciably shifted in phase.

M_{XY} because the tilt effect is largely compensated by the increase in the flip angle as B_{eff} increases. Figure 2 shows a family of magnetization trajectories calculated according to the Bloch equations for various values of $\Delta B/B_1$. All terminate close to the XY plane but there is a strong induced phase gradient, giving increasing dispersion mode as the offset increases. This gradient is an approximately linear function of ΔB, so it can be compensated by a linear phase correction routine in the standard data processing software.

PULSE WIDTH CALIBRATION

Calibration of the radiofrequency pulse width is normally carried out by searching for the null signal corresponding to a 180° or 360° pulse flip angle for a resonance close to the transmitter frequency (negligible ΔB). Searching for the maximum signal after a 90° pulse is not a sufficiently sensitive test because the signal intensity is at a turning point. In practice the required null condition is often

partially obscured by an effect that depends on an interaction between the B_0 and B_1 spatial distributions, which cannot be regarded as independent in this context.

We might anticipate a relatively uniform B_1 field near the centre of the radiofrequency coil with simultaneously good B_0 homogeneity, since this major contribution to the signal is monitored when shimming the magnetic field. On the other hand, sample regions above or below the coil would be expected to lie in abnormally low B_1 fields and could well have inferior B_0 homogeneity. The corresponding null conditions would then occur at different values of the pulse width. In general the null is ill defined, but can be interpolated from the signal intensities just before and just after the zero crossing. We can judge this effect from the calibration plots of Fig. 3(a), carried out with a conventional long cylindrical sample, and Fig. 3(b), performed with a smaller spherical sample for which the B_1 field is necessarily far more uniform.

The radiofrequency field intensity B_2 used for heteronuclear decoupling may be calibrated by recording the residual splitting in an off-resonance decoupling experiment. In the section on Selective decoupling* an expression is derived for the residual splitting for an offset Δ Hz large compared with J:

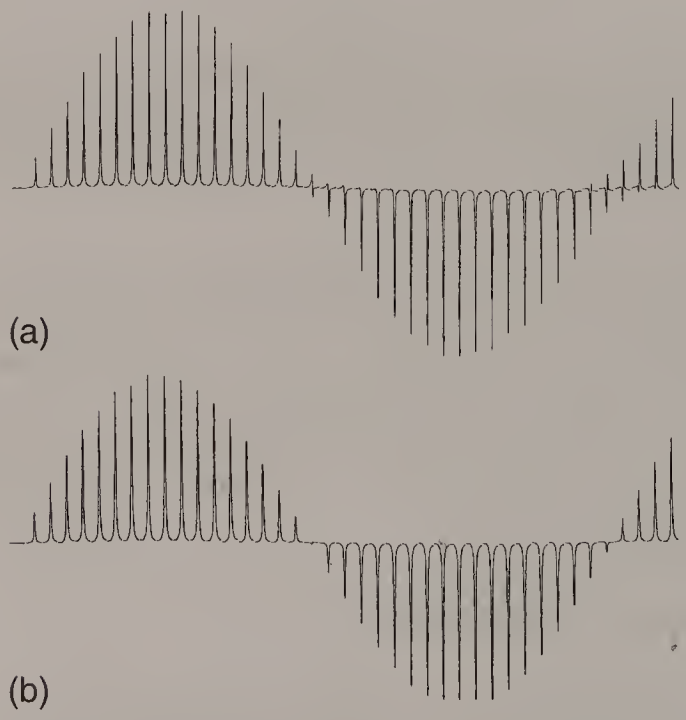

Fig. 3. Pulse calibration by recording the signal as a function of pulse flip angle (10° to 400° in 10° steps). Note that the usual 5 mm cylindrical sample (a) shows no clear null at the 180° or 360° condition, owing to a spatial correlation between the inhomogeneities of the B_0 and B_1 fields. The effect disappears (b) when a spherical microcell is used. Spectra courtesy of H. Sengstschmid.

$$S_{resid} = \frac{J\Delta}{\left[\Delta^2 + (\gamma B_2 / 2\pi)^2\right]^{1/2}}. \quad [1]$$

If the offset is nevertheless small compared with $\gamma B_2/2\pi$, then this simplifies to

$$\gamma B_2/2\pi = J\Delta/S_{resid}. \quad [2]$$

The residual splitting gives a calibration of B_2 if Δ and J are known. Alternatively, we can use the expression for the splitting (S_t) observed in a spin-tickling* double-resonance experiment (1) at the exact resonance condition where

$$\gamma B_2/2\pi = S_t. \quad [3]$$

This method is applicable to both homonuclear and heteronuclear experiments.

Pulses often need to be recalibrated when the sample is changed, particularly when the dielectric properties are different. Careful pulse calibration can be particularly important in two-dimensional experiments where quite small imperfections can give rise to spurious resonance peaks. The calibration of shaped soft radiofrequency pulses may require comparison with the calibration of a hard radiofrequency pulse, using previously determined proportionality (Q) factors (2).

COMPENSATION OF PULSE IMPERFECTIONS

It was Meiboom and Gill (3) who first showed the way to compensate the cumulative effects of pulse length error. When a long train of spin echoes* is excited by a repetitive sequence of 180° pulses, the magnetization vectors are progressively forced out of the XY plane if the 180° pulses are too long or too short. However, the introduction of a 90° phase shift between the initial 90° excitation pulse and all the subsequent 180° pulses alters the symmetry of the problem in such a way that the errors are compensated for all even-numbered echoes, and the cumulative effect disappears. We can appreciate that the same kind of compensation occurs if no 90° phase shift is used but the 180° pulses are alternated in phase (4). A similar compensatory effect can be achieved in spin–lattice relaxation studies by alternating the phase of the initial spin inversion pulse (5).

Many multidimensional experiments remove the artefacts created by radiofrequency pulse imperfections by phase cycling* (6) or by the application of pulsed field gradients* (7). A more satisfactory approach to the problem is provided by the concept of composite pulses* – sandwiches of two or more pulses grouped closely together, usually with no intervals between them (8). An example is the sequence 90°(X) 180° (Y) 90°(X) which acts as a 180° pulse compensated for pulse length error or resonance offset effects.

CLASSIFICATION OF RADIOFREQUENCY PULSES

The explosive growth of experiments in pulse sequencing (sometimes called *spin gymnastics*) merits consideration of some form of classification of radiofrequency pulses. We have already drawn a distinction between *hard pulses* that affect the entire range of chemical shifts, and s*oft pulses* that selectively excite or invert a spin multiplet or even a single transition. See Selective excitation*.

Most sequences start with an *excitation pulse* which converts equilibrium Z magnetization into transverse magnetization; often this is a 90°(X) pulse. A pulse which converts $+M_Z$ into $-M_Z$ is a 180° *inversion pulse*. It may be the first step in an inversion-recovery sequence to measure spin–lattice relaxation times, or it can be used to interchange the spin states (α and β) of a neighbour nucleus, an important trick for generating spin-echo modulation (4). A 180° inversion pulse should be clearly distinguished from a 180° *refocusing pulse* that is designed to carry a vector in the XY plane into a mirror image position with respect to a vertical plane through the pulse axis. Such a pulse is virtually indispensable for spin-echo experiments. If the operation of an excitation or refocusing pulse is independent of the initial state, it is called a *universal* pulse (9). A hard pulse that affects two or more different spins is often represented as a *cascade* of selective pulses applied to the various spin species in turn, the ordering being irrelevant.

Not all radiofrequency pulse effects can be represented according to the vector model*. The most common exception is a *conversion pulse* that operates on antiphase transverse magnetization to create multiple-quantum coherence*. This can sometimes be a useful device for suppressing unwanted antiphase magnetization components by conversion into unobservable multiple-quantum coherence (10). It is then known as a *purging pulse*. A pulse whose only purpose is to convert unobservable coherences or population effects into a detectable precessing magnetization is usually called a *read pulse*.

REFERENCES

1. R. Freeman and W. A. Anderson, *J. Chem. Phys.* **37**, 2053 (1962).
2. Ē. Kupče and R. Freeman, *J. Magn. Reson. A* **102**, 364 (1993).
3. S. Meiboom and D. Gill, *Rev. Sci. Instrum.* **29**, 688 (1958).
4. R. Freeman and H. D. W. Hill, *J. Chem. Phys.* **54**, 301 (1971).
5. D. E. Demco, P. van Hecke and J. S. Waugh, *J. Magn. Reson.* **16**, 467 (1974).
6. G. Bodenhausen, R. Freeman and D. L. Turner, *J. Magn. Reson.* **27**, 511 (1977).
7. R. E. Hurd, *J. Magn. Reson.* **87**, 422 (1990).
8. M. H. Levitt and R. Freeman, *J. Magn. Reson.* **33**, 473 (1979).
9. H. Geen and R. Freeman, *J. Magn. Reson.* **93**, 93 (1991).
10. O. W. Sørensen and R. R. Ernst, *J. Magn. Reson.* **51**, 477 (1983).

Cross-references

Broadband decoupling
Composite pulses
Multiple-quantum coherence
Phase cycling
Pulsed field gradients
Quadrature detection
Selective decoupling
Selective excitation
Spin echoes
Spin–lattice relaxation
Spin tickling
Steady-state effects
Vector model

Resolution Enhancement

It is a considerable technological feat to achieve magnetic field uniformity approaching parts in 10^9 over volumes of the order of 1 cm^3, as in present-day high-resolution NMR spectrometers. This is accomplished only by very careful design of the magnet or solenoid, the use of a complex array of current shims, and by spinning the sample to average out transverse field gradients. For high-resolution work on small molecules, it would be attractive to go beyond these 'instrumental' linewidths and observe natural linewidths, for then much more fine structure would be discernible. The observed lineshape may be considered to be the natural lineshape convoluted* with the magnet field distribution function. Attempts to reverse this broadening effect are sometimes referred to as *deconvolution*. In fact, this process is not limited to the removal of field inhomogeneity broadening but is a general data manipulation technique known as resolution enhancement.

The convolution theorem states that the process of convoluting a curve A with another curve B in the frequency domain is equivalent to a multiplication of the Fourier transform of A by the Fourier transform of B in the time domain. It is therefore not surprising that most procedures for resolution enhancement operate on the transient free induction signal, multiplying it with a time-domain 'shaping function', a simpler operation than deconvolution in the frequency domain. When the linewidth is determined by field inhomogeneity, the free induction signal decays because of mutual interference between signals from different regions of the sample. In order to counteract this decay the free induction signal may be multiplied by a shaping function that increases with time, emphasizing the tail. This is therefore the converse of a sensitivity enhancement* function.

A shaping function that increases with time introduces two practical problems. It emphasizes any step function discontinuity at the end of the free induction decay* (if zero filling* is used). Since the Fourier transform of a step function is a sinc function, this process introduces some sinc function character into the frequency-domain lineshape, which is undesirable in many-line spectra. The shaping function should therefore rise with time but fall quite rapidly towards the end of the free induction decay in order to round off any discontinuity (see Apodization*). The second problem is that the shaping function emphasizes the noise in the tail of the free induction decay. Resolution can therefore only be improved at the expense of sensitivity. This is the practical limit on the extent of resolution enhancement which can be imposed in a given case; at some point the procedure enhances the high-

frequency components of the noise, introducing spurious splittings or shoulders on the lines and false peaks elsewhere.

Many different shaping functions have been used for resolution enhancement. Possibly the simplest and most common is the rising exponential $\exp(at/T_2^*)$ followed by a suitable apodization function. An elegant alternative is the Lorentzian-to-Gaussian conversion which uses a time-domain shaping function of the form

$$\exp[at/T_2^* - b(t/T_2^*)^2].$$

Here T_2^* is the time constant of the unprocessed free induction decay, and a and b are variable parameters. If the original decay approximates to an exponential (which would give a Lorentzian lineshape) it can be counteracted by the first term of this expression through a suitable choice of the parameter a. The second term then imposes a Gaussian decay, and since the Fourier transform of this is another Gaussian, the lineshapes in the frequency domain are converted from Lorentzian into Gaussian. The smaller the choice of b, the narrower the resulting linewidth. An interesting extension of this procedure employs such a large value of a that the first term greatly overcompensates the raw decay, giving a free induction signal which rises very rapidly with time; the second term once again imposes a Gaussian shape, but now the maximum has moved from $t = 0$ to some point further along the time axis. There is particular interest in the case where the peak of the Gaussian envelope is set at the centre of the acquisition period. The free induction signal then resembles a spin echo in several respects, having an envelope which falls off essentially symmetrically on either side of the centre, and is therefore known as a *pseudo-echo* (1). Since the Fourier transform of an even function is also an even function, the resulting spectrum has no dispersion-mode components. However, unlike a true spin echo, a pseudo-echo does not have its constituent frequencies in phase at the centre, but at $t = 0$, and this introduces a strong frequency-dependent phase shift into the spectrum. It is nevertheless easy to sidestep this difficulty by computing the absolute-value mode spectrum which has lineshapes identical to pure absorption once the dispersion-mode components have been eliminated. Similar results can be achieved by any shaping function that forces the free induction signal to have approximate symmetry about its centre, for example the *sine bell* (2). The price that has to be paid (in either case) is a rather severe loss in sensitivity.

A more pragmatic approach to resolution enhancement is offered by the technique of 'convolution difference' (3). This simply imposes a sensitivity enhancement function on the free induction decay, for example $\exp(-at/T_2^*)$, and subtracts the result from the unprocessed free induction signal. This is particularly useful for the elimination of very broad lines from a spectrum which contains broad and narrow lines, since any broad component that is essentially unaffected by the sensitivity enhancement shaping function is simply cancelled by this process. The technique does, however, illustrate one drawback of certain resolution enhancement functions, in that the resulting spectra can no longer be properly

integrated, and quite often the component lines have negative-going wings; this is a result of falsifying the initial ordinate of the free induction decay. In situations where linewidths vary within the unprocessed spectrum, resolution enhancement may affect the relative peak heights, rendering quantitative analysis unreliable.

There are certain special techniques for improving resolution which do not rely on data manipulation. In principle, a very small sample would be insensitive to the inhomogeneity of the applied magnetic field; in practice there are discontinuities in magnetic susceptibility at the walls of the sample container which introduce field gradients which broaden the line. It is, however, possible to limit the *effective* volume of the sample by borrowing the technology of NMR imaging. For example, a signal may be excited by a frequency-selective pulse in a deliberately imposed field gradient, the free induction signal being acquired after this gradient is removed. Usually, the most critical gradient would be used; this is the Z gradient for a superconducting solenoid. In this way only a thin disc-shaped volume of the sample is excited, and when the transient signal evolves in the absence of the imposed gradient, it is insensitive to the residual Z gradients (4). Figure 1 shows an example of this method of resolution enhancement.

Certain phenomena based on spin–spin coupling can be used to circumvent the effect of magnetic field inhomogeneity since, by acting within a given molecule, they are not sensitive to field gradients. This effect can be seen in the spin-tickling* experiment where the doublets can be better resolved than the B_0 inhomogeneity would suggest. Similarly, a second radiofrequency field B_2 can be made to 'burn a hole' in a chosen resonance line, affecting only a limited region of the sample, and the resulting population disturbance may be observed on another line which shares a common energy level (the *regressive* case). A hole then appears in the second line and it may be much narrower than the instrumental linewidth. Spin echoes* provide another method of counteracting the effects of non-uniform magnetic fields, the signals from different volume elements of the sample getting out of phase with one another and then being refocused by a 180° radiofrequency pulse. Chemical shift effects are also refocused, but spin–spin coupling modulates the echo envelope, and if this modulation information is Fourier transformed, the lines of the resulting spectrum can approach their natural linewidths. Thus through J-spectroscopy* the spin multiplet structure can be resolved even though the conventional spectrum has broad lines.

In a similar way, the excitation of homonuclear zero-quantum coherence may be used to defeat the effects of magnetic field inhomogeneity. This requires a system of at least two coupled spins and a pulse sequence which excites a coherence between energy states which have the same magnetic quantum number. If the process is thought of as the absorption of one quantum of energy at frequency f_1 and simultaneous emission of another quantum at frequency f_2 then it is clear that homonuclear zero-quantum coherence is almost completely insensitive to field inhomogeneity, since this will only shift f_1 and f_2 together by the same amount.

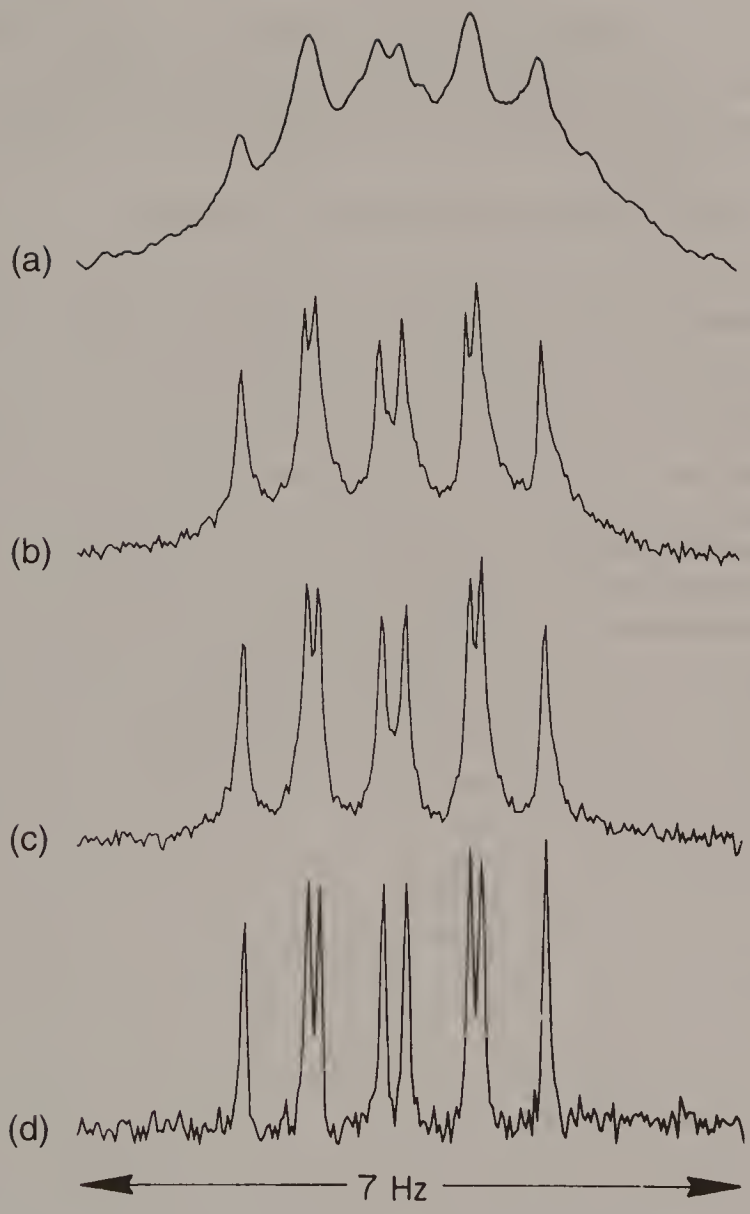

Fig. 1. Resolution enhancement by restricting the active sample volume. A selective pulse in an applied Z gradient excites a flat disc-shaped volume of the sample. The free induction decay is acquired with this gradient switched off. The intensity of the applied gradient is increased in the series (a) to (d), reducing the active sample volume and thus increasing the resolution.

For large molecules or very viscous solutions, linewidths are usually determined by spin–spin relaxation rather than field inhomogeneity, so these last-mentioned methods are not applicable.

REFERENCES

1. A. Bax, R. Freeman and G. A. Morris, *J. Magn. Reson.* **43**, 333 (1981).
2. A. de Marco and K. Wüthrich, *J. Magn. Reson.* **24**, 201 (1976).
3. I. D. Campbell, C. M. Dobson, R. J. P. Williams and A. V. Xavier, *J. Magn. Reson.* **11**, 172 (1973).
4. A. Bax and R. Freeman, *J. Magn. Reson.* **37**, 177 (1980).

Cross-references

Apodization
Convolution
Free induction decay
J-spectroscopy
Multiple-quantum coherence
Selective excitation
Sensitivity enhancement
Spin echoes
Spin tickling
Zero filling

Rotating Frame

In a magnetic resonance experiment we need to be able to predict the combined effect of immersing the sample in a static magnetic field B_0 and a radiofrequency field B_1. In practice, the radiofrequency is applied in the form of a linearly oscillating field $2B_1 \cos \omega t$, but this can be regarded as two counter-rotating fields of strength B_1 and only the component which rotates in the same sense as the nuclear precession has a significant influence on the spins.

The vector model* introduced by Bloch (1) translates the NMR phenomenon into a problem of classical mechanics by considering the net macroscopic magnetization arising from the resultant of all nuclear magnetization vectors present in the sample. At Boltzmann equilibrium this is simply a vector M_0 aligned along the magnetic field direction Z. Spins are either aligned with or against the field B_0 and for the great majority, their magnetizations cancel; only the very small excess population in the lower energy state contributes to M_0. Since the precession phases of the individual spins are random there is no transverse magnetization at equilibrium.

The problem is to calculate how B_1 interacts with the nuclear magnetization vector M_0. In particular, what happens if a short, strong radiofrequency pulse is applied to a spin system at Boltzmann equilibrium? The trick is to transform the entire problem into a rotating coordinate frame in which B_1 is a static field, since then the resulting motion of M_0 is particularly simple, a rotation about the static field. If f_1 is the frequency of the B_1 field, the rotating frame is the usual Cartesian coordinate frame except that the X and Y axes are rotating about the Z axis at an angular frequency $\omega_1 = 2\pi f_1$ rad s^{-1} in the sense of the nuclear precession.

Nuclei placed in a field B_0 precess at a frequency γB_0 rad s^{-1}. Since nuclei appear to precess more slowly in a rotating reference frame, the magnetic field must be correspondingly reduced to $B_0 - \omega_1/\gamma$. Thus if B_0 is adjusted for exact resonance, the nuclei cease to precess in the rotating frame and appear to experience zero applied field. Note that the normal choice for the frequency of the rotating frame is the frequency of the transmitter, not the Larmor precession frequency of the nuclei, although of course the two are close.

When a radiofrequency pulse is applied, for a few microseconds there is an intense B_1 field aligned along the +X axis of the rotating frame. For nuclei that are off resonance by an amount ΔB, there are two fields at right angles, B_1 and ΔB, which have a resultant B_{eff} acting in a direction which makes an angle θ with respect to the X axis in the XZ plane with $\tan\theta = \Delta B/B_1$. The nuclear magnetization vector

thus rotates about B_{eff} through an angle $\gamma B_{eff} t_p$, where t_p is the width of the pulse. (See Radiofrequency pulses*.)

This explains why a strong pulse can excite a wide range of chemical shifts. If $B_1 >> \Delta B$ for the nuclei furthest from resonance, then θ is always very small and B_{eff} differs very little from B_1 so that all the different magnetization vectors rotate about the X axis through the same angle $\gamma B_1 t_p$ radians. In the fairly common case where $\gamma B_1 t_p = \pi/2$, all the individual magnetizations are left aligned along the +Y axis where the induced signal is maximum. Once the radiofrequency pulse is extinguished these magnetization vectors are free to precess at their characteristic frequencies ω_k, and since the receiver coil is rotating at an angular frequency ω_1 rad s^{-1} with respect to this frame, the induced signals are at $(\omega_k + \omega_1)/2\pi$ (hertz), in the radiofrequency region.

In a more mathematical sense, transformation into a rotating frame is a device for removing the time dependence from the problem. Essentially all of the vector pictures used in this book implicitly assume transformation into the rotating frame. The vector model is by far the simplest way to visualize the effects of multiple-pulse sequences; it is applicable to the majority of high-resolution NMR experiments with the exception of those that involve multiple-quantum coherence*. In the rotating frame the motion of the nuclear magnetization breaks down into rotation about B_{eff} (during a pulse) and free precession about ΔB in the intervals between pulses. It is permissible to consider one nuclear species (say, protons) in a frame rotating at the Larmor frequency of protons, while simultaneously considering another nuclear species (say carbon-13) in another frame rotating at the appropriate carbon-13 precession frequency. For the analysis of double-resonance experiments it is convenient to transform to a coordinate system rotating in synchronism which the *second* radiofrequency field B_2. The concept may be extended to visualizing energy-level diagrams in a rotating frame; such transformations have been used in discussing coherent decoupling* and spin tickling*.

Experiments which apply strong radiofrequency fields for relatively long periods cause continuous precession about the effective field B_{eff} in the rotating frame, sometimes described as *transient nutations** or 'Torrey oscillations' (2). In the simple case, B_{eff} is approximately the same as B_1 and nutation takes place about the X axis of the rotating frame. The macroscopic nuclear magnetization M_0 rotates in the ZY plane inducing a sinusoidally oscillating NMR signal of constant frequency $\gamma B_1/2\pi$ (Hz). This observed signal eventually decays owing to spatial inhomogeneity of the B_1 field, as magnetization isochromats from different regions of the sample get out of phase with one another. If the B_1 field is suddenly reversed in phase, this loss of phase coherence is refocused and the result is a *rotary echo* (3). As with conventional spin echoes*, multiple refocusing is possible and then the envelope of the rotary echoes decays with a time constant T given by

$$1/T = 0.5(1/T_1 + 1/T_2). \qquad [1]$$

Sometimes it may be necessary, while in the rotating frame, to make a further transformation into a second reference frame which rotates about B_{eff} at an angular frequency γB_{eff}. This provides a convenient picture for the 'rotating frame resonance' which occurs in the Hartmann–Hahn experiment* (4).

REFERENCES

1. F. Bloch, *Phys. Rev.* **102**, 104 (1956).
2. H. C. Torrey, *Phys. Rev.* **76**, 1059 (1949).
3. I. Solomon, *Phys. Rev. Lett.* **2**, 301 (1959).
4. S. R. Hartmann and E. L. Hahn, *Phys. Rev.* **128**, 2042 (1962).

Cross-references

Coherent decoupling
Hartmann–Hahn experiment
Multiple-quantum coherence
Radiofrequency pulses
Spin echoes
Spin tickling
Transient nutations
Vector model

Sample Spinning

When all precautions have been taken to obtain the most uniform applied magnetic field B_0, it is still possible to make a significant improvement in resolution by spinning the sample about a suitable axis, and essentially all high-resolution spectrometers employ this technique (1). It relies on the fact that if all the spins move through a range of local magnetic field intensities (due to inhomogeneity) at a rate that is fast compared with the linewidth of a stationary sample, then they behave as if they had experienced only the mean value of the field, averaged over the entire trajectory. Thus the B_0 field must be reasonably homogeneous if resolution is to be improved by spinning at a practicable rate. It also follows that only the effects of *transverse* field gradients are reduced, any gradients along the spinning axis retaining their broadening effect. In a superconducting solenoid it is usual to spin about the Z axis (the direction of the B_0 field). Occasionally a 'sideways-spinning probe' may be employed where the sample is spun about the radiofrequency coil axis (X), enabling a solenoid coil to be used instead of the usual saddle coil, thus providing a better filling factor and higher sensitivity.

A simple air-driven turbine is commonly used to spin the sample, usually supported on an air bearing. The availability of precision-bore sample tubes has alleviated some of the early difficulties with spinning samples, but variable temperature studies can still be troublesome because the mechanical clearances are critical. Monitoring the spinning speed with a tachometer is a useful guide; a light beam is reflected from a panel on the turbine rotor and generates a modulated signal on a photodiode. This frequency is then displayed on the monitor screen and is often used to stabilize the spinning rate through a servo loop controlling the air flow. Interruption of spinning may cause the internal field/frequency regulator to unlock.

Heroic attempts have been made to extend this simple idea to motion about more than one axis, without any notable success. However, several spectroscopists have noted an interesting effect with conventional sample spinning – while the spinner is accelerating from rest, the resolution appears to be significantly better than that observed for a constant spinning speed. This transient improvement in resolution appears to originate in a 'washing machine' motion of the liquid in the sample tube (Fig. 1(a)). During the acceleration phase, liquid near the tube wall is moving faster than liquid near the tube axis, and this induces a new kind of circulation that partially averages the effects of Z gradients, along with the expected averaging of

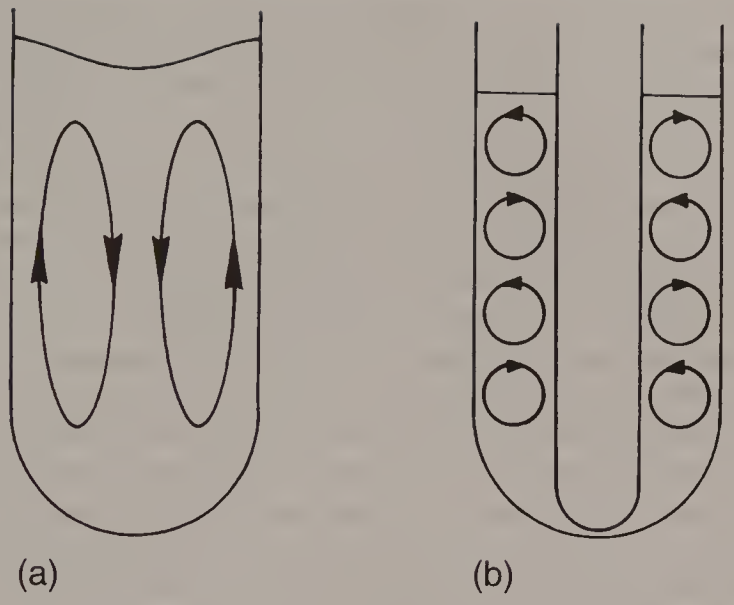

Fig. 1. (a) While the spinner is accelerating, the liquid may undergo a 'washing machine' motion, partially averaging the effect of the vertical field gradients and improving resolution. (b) In a stationary sample tube containing a central coaxial tube rotating at uniform speed, Taylor vortex flow is initiated in the annular region.

the transverse gradients. Some support for this explanation is provided by experiments in a stationary tube with an inner coaxial tube that is rotating (2). At a suitably high rotation rate, the liquid in the annular region breaks up into discrete cells in which the liquid circulates as indicated in Fig. 1(b). This is called Taylor vortex flow (3). Since similar shear forces would be expected in an ordinary sample tube accelerating from rest, the circulation proposed in Fig. 1(a) does not seem unreasonable.

SPINNING SIDEBANDS

The improvement in resolution by sample spinning is not obtained without some cost. As the sample rotates in a linear field gradient, a typical nuclear spin passes through a magnetic field that is modulated in intensity, $B_0 + B_m \cos \omega_m t$, and since this spin precesses at its *instantaneous* Larmor frequency, its resonance frequency is frequency modulated. Viewed in the frequency domain, this corresponds to the introduction of a set of *spinning sidebands* on each side of the main resonance, at distances equal to integral multiples of the spinner frequency. The general mathematical expressions for the amplitudes of these spinning sidebands involve Bessel functions, but for the practical cases of interest they can be greatly simplified because the modulation index is very low if the field gradients are only moderate. Under such conditions, all the sidebands are weak in comparison with

the intensity of the main 'parent' resonance, and only the first-order sidebands (at $\pm\omega_m$) have appreciable intensity. They may be further reduced either by improving the field homogeneity (by adjusting the currents in the correction coils) or by increasing the spinning rate. Both reduce the modulation index. However, there is a practical limit on the spinning rate because of the onset of vortexing of the liquid in the sample tube. If this vortex approaches the radiofrequency coil, the consequent discontinuity in magnetic susceptibility degrades the resolution. Plastic 'vortex plugs' are sometimes used to prevent this problem.

Spinning sidebands can interfere with the identification of weak signals, for example weak satellites arising from low-abundance isotopomers. In critical cases it is important to check the spectrum at two different spinning rates in order to identify the spinning sidebands. In multiscan averaging experiments, the spinning sidebands may be broadened (and diminished in intensity) by deliberately varying the spinner speed. In two-dimensional spectroscopy, the spurious modulation due to spinning can be 'chopped up' by the slightly non-uniform timing of successive scans as the evolution time t_1 is incremented. This converts a coherent modulation into an apparently noisy one, contributing to t_1 noise* (4).

While it is the inhomogeneity in the B_0 field that is the major contributor to spinning sidebands, other effects are also involved. These include the spatial inhomogeneity of the radiofrequency field B_1, the variation of the coupling of the nuclei to the receiver coil, and the influence of uneven wall thickness of the sample tube (a bulk magnetic susceptibility effect). A combination of these effects induces a contribution to the spinning sidebands whose intensity is independent of the spinning rate (5,6) whereas, normally, sidebands get weaker as the spinning rate is increased. An indication that more than one factor is at work is provided when the low-field and high-field sidebands are observed to have different phases. Such a complex interplay of contributions from different physical phenomena makes it difficult to devise the optimum strategy for adjusting the correction currents for minimum sideband intensities. For example, it is not necessarily best to optimize the shim coil currents with a stationary sample, since contributions from some transverse gradients may interfere with each other when the sample is spinning (6).

MAGIC-ANGLE SPINNING

Very rapid spinning of a solid sample at the magic angle (54.7°) is the common practice for solid-state NMR studies to average dipole–dipole interactions and chemical shift anisotropy (7). Solid-state NMR is outside the scope of this book, but a similar scheme has been introduced for liquid samples. It addresses the problem of obtaining high-resolution spectra from very small sample volumes. Discontinuities in magnetic susceptibility at the walls of the sample container seriously degrade the spatial homogeneity when very small sample tubes are used, because the ratio of wall thickness to inside diameter increases disproportionately. For this reason, scaling down the dimensions of the sample and its container

normally degrades resolution rather than improving it, and the signal-to-noise ratio suffers. An exception is a small transverse coil surrounded by a fluid with a magnetic susceptibility matched to that of copper; this has a small volume but a high filling factor (8).

These susceptibility effects become increasingly important in very high-field spectrometers, and present-day shimming systems are not able to compensate these inhomogeneities properly. The use of spherical sample cells or susceptibility-matched polymer plugs only partially solves this problem. Some success has been achieved by limiting the *effective* volume of a spherical sample by selective excitation in a Z gradient followed by acquisition after the gradient is removed (9).

The most promising solution takes a leaf out of the book of the solid-state NMR spectroscopist, with the discovery that spinning the sample about the magic angle averages all field gradients arising from the rotor and the sample. On the other hand, any inhomogeneous fields generated by the probe itself are only averaged perpendicular to the spinning axis, so it must be constructed with materials that minimize discontinuities in magnetic susceptibility. With these precautions, the residual field gradients are not too serious and the required spinning rates are not excessive (typically 2 kHz). The sample is confined inside a container approximating a rather squat cylinder with rounded ends, closed by a tight-fitting plastic plug, and entirely within the effective volume of the receiver coil, so the filling factor and sensitivity are high. High-resolution proton spectra with linewidths as low as 0.4 Hz can be obtained from as little as 400 *nanograms* of material in 40 *microlitres* of solution (10,11).

SPINNING SAMPLES AND SPIN ECHOES

Consider a sample that is spinning in a linear transverse magnetic field gradient. Immediately after excitation by a radiofrequency pulse, the signals from all volume elements (isochromats) are in phase, but they begin to lose phase coherence as they precess at the different frequencies imposed by the gradient. After one full revolution of the spinner, each isochromat at a given radius has passed through the same combination of local fields and the signal components are all in phase once more. This may be regarded as a *spinning echo*. As a result, the free induction decay is modulated at the spinning rate, and its Fourier transform contains spinning sidebands.

It is therefore not surprising that spinning can interfere with conventional spin-echo experiments, as the refocusing cycle and the spinning cycle move in and out of coincidence. One simple remedy is to use a non-spinning sample for spin-echo measurements, but this broadens the observed lines somewhat. Alternatively the problem can be circumvented by synchronizing the 180° refocusing pulses with the sample rotation, using a trigger signal from the spinner tachometer. Two complete revolutions of the spinner are allowed to occur between 180° pulses, so that each volume element passes through the same sequence of magnetic fields during the

defocusing and refocusing periods. This is equivalent to synchronizing the 180° pulses with the centres of the spinning echoes.

In the last few years there has been a noticeable trend towards the use of *non-spinning* samples for high-resolution work, encouraged by the tendency to study larger and larger molecules where the natural linewidths often outweigh the instrumental linewidths, even with a stationary sample. Furthermore, field shimming technology has made significant progress through field mapping and the use of higher-order correction coils. If the use of non-spinning samples ever becomes the normal practice, it should offer an appreciable gain in sensitivity, because the probe coil could be redesigned with a higher filling factor, the sample tube need no longer be a long cylinder, and all the sample could be enclosed within the effective volume of the coil.

REFERENCES

1. F. Bloch, *Phys, Rev.* **102**, 104 (1956).
2. M. Vera and J. B. Grutzner, *J. Am. Chem. Soc.* **108**, 1304 (1986).
3. G. I. Taylor, *Phil. Trans. R. Soc.* **A223**, 289 (1923).
4. A. F. Mehlkopf, D. Korbee, T. A. Tiggleman and R. Freeman, *J. Magn. Reson.* **58**, 315 (1984).
5. E. R. Malinowski and A. R. Pierpaoli, *J. Magn. Reson.* **1**, 509 (1969).
6. J. Dadok, unpublished report.
7. E. R. Andrew, *Prog. NMR Spectrosc.* **8**, 1 (1971).
8. D. L. Olson, T. L. Peck, A. G. Webb, R. L. Magin and J. V. Sweedler, *Science* **270**, 1967 (1995).
9. A. Bax and R. Freeman, *J. Magn. Reson.* **37**, 177 (1980).
10. T. A. Barbara, *J. Magn. Reson. A* **109**, 256 (1994).
11. P. A. Keifer, L. Baltusis, D. M. Rice, A. A. Tymiak and J. N. Shoolery, *J. Magn. Reson. A* **119**, 65 (1996).

Cross-references

Field/frequency regulation
Resolution enhancement
Sensitivity enhancement
Spin echoes
t_1 noise

Saturation Transfer

Most methods of chemical kinetics are only applicable to systems not at thermodynamic equilibrium, but NMR provides an opportunity to measure rates of chemical exchange* between components in a true equilibrium state. The method depends on being able to attach an innocuous label to an atom or group of atoms that is being carried to another site by chemical exchange. These techniques are particularly important in the limit of slow exchange (slow compared with the chemical shift difference between the two sites) when separate resonances are observed for the two exchanging sites. In the early experiments it was the phase of the nuclear precession which acted as the label, exchange causing a loss of phase coherence and a consequent broadening of the lines which increased as the rate of exchange increased. An extra damping term can be introduced into the Bloch equations to represent the effects of exchange. A more direct method was pioneered by Forsén and Hoffman using a population disturbance as the label (1). In the slow exchange limit, sudden saturation of resonance X causes a gradual loss of intensity of resonance A as saturated spins are transferred from site X to site A. This competes with the normal spin–lattice relaxation* acting to restore the thermal equilibrium populations, but if these relaxation times are measured, then the exchange rate can be deduced from the time evolution of the intensity of the A resonance. In this form, the technique raises some difficult questions about how fast a given resonance line can be saturated. Nowadays the Forsén–Hoffman experiment is much more conveniently initiated by a selective population inversion pulse, the progress of population transfer being followed by monitoring the free induction decays in a series of experiments with different delays τ between the inversion pulse and the observation pulse. Nevertheless, it is convenient to retain the original term 'saturation transfer' to cover all these experiments.

Consider the simple case of just two exchanging sites with equal populations, so that the forward and backward exchange rates are equal, represented by a rate constant k, and equal spin–lattice relaxation times at the two sites, T_1. Let the X spins be inverted by a selective 180° pulse, followed by a variable delay τ and a 90° monitoring pulse which is non-selective. When τ is infinite both signals reach their equilibrium values $M_\infty(A)$ and $M_\infty(X)$. The solution of the differential equations governing the longitudinal magnetizations gives

$$M_\infty(A) - M_Z(A) = M_\infty(A)[\exp(-\tau/T_1) - \exp(-\tau/T_1 - 2k\tau)] \qquad [1]$$

and

$$M_\infty(X) - M_Z(X) = M_\infty(X)[\exp(-\tau/T_1) + \exp(-\tau/T_1 - 2k\tau)] \quad [2]$$

It is easy to check that these equations have the right form by first setting $k = 0$ so that there is no exchange, and noting that $M_Z(A) = M_\infty(A)$ throughout, while

$$M_Z(X) = M_\infty(X)[1 - 2\exp(-\tau/T_1)]. \quad [3]$$

This is the expression describing the recovery of the X signal after a population inversion (Fig. 1(a)). Then the case of finite exchange but infinitely long relaxation time may be considered, where $\exp(-\tau/T_1) = 1$. The equations then reduce to

$$M_Z(A) = M_\infty(A)\exp(-2k\tau) \quad [4]$$

and

$$M_Z(X) = -M_\infty(X)\exp(-2k\tau). \quad [5]$$

These describe a situation where the A resonance decays to zero with a time constant $1/(2k)$, while the inverted X resonance grows back to zero with the same time constant (Fig. 1(b)). The factor 2 arises because each exchange 'event' involves the loss of a polarized spin and the gain of an inverted spin (or vice versa). Had this been a *saturation* transfer experiment the factor 2 would be absent.

When both exchange and relaxation occur together, the recovery curves are no longer simple exponentials (Fig. 1(c)). The A signal loses intensity and passes through a minimum before growing back to $M_\infty(A)$ as spin–lattice relaxation effects take over. The X resonance recovers from its initial inversion, quite quickly at first as exchange and relaxation effects reinforce, and then more slowly as the exchange becomes less effective because the transferred spins are less and less perturbed. An analysis of these two curves allows both the exchange rate and the spin–lattice relaxation time to be extracted.

Real examples of chemical exchange are seldom as simple as this. Even when the problem is limited to just two exchanging sites, the relative populations may differ, giving two rate constants k_A and k_X, and the spin–lattice relaxation times are in general different, T_{1A} and T_{1X}. The equations governing the time evolution after a selective population inversion of the X resonance are then (2)

$$M_Z(A)/M_\infty(A) = 1 - (2k_A/\beta)\{\exp[-\tfrac{1}{2}(\alpha - \beta)\tau] - \exp[-\tfrac{1}{2}(\alpha + \beta)\tau]\} \quad [6]$$

and

$$M_Z(X)/M_\infty(X) = 1 - (1/\beta)\{(\beta + R_X - R_A)\exp[-\tfrac{1}{2}(\alpha + \beta)\tau]$$

$$+ (\beta + R_A - R_X)\exp[-\tfrac{1}{2}(\alpha - \beta)\tau]\} \quad [7]$$

where

$$\alpha = R_A + R_X, \quad \beta = [(R_A - R_X)^2 + 4k_A k_X]^{1/2}$$

and

$$R_A = k_A + (1/T_{1A}), \quad R_X = k_X + (1/T_{1X}).$$

Further complications must be introduced if more than two exchanging sites are involved; these cases are usually treated by a full density matrix calculation.

An illustrative two-site exchange problem is shown in Fig. 2. The 1,2,6-trimethylpiperidinium ion exchanges slowly between two forms, one having the

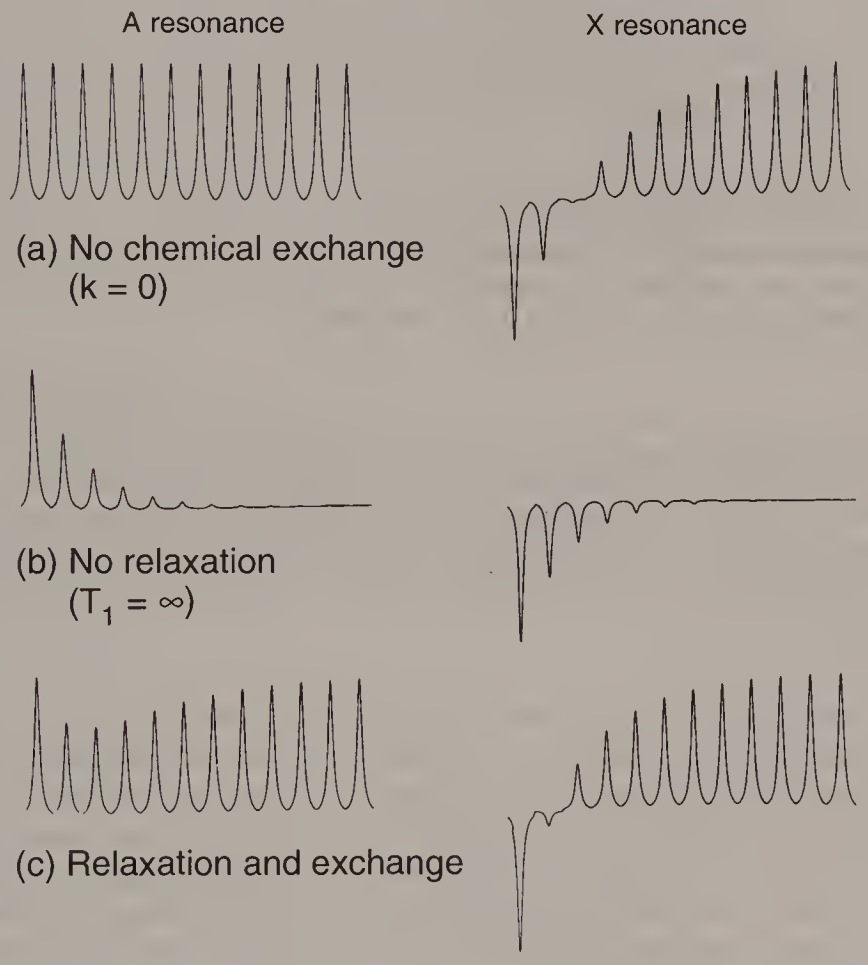

Fig. 1. Chemical exchange in a weakly coupled two-spin system after population inversion of the X resonance. (a) In the case of no chemical exchange (k = 0) there is no effect on the A spins, while the X spins recover by spin–lattice relaxation. (b) With chemical exchange but no relaxation ($T_1 = \infty$), transfer of inverted spins to site A causes an exponential decay of the A resonance. Both A and X approach a state of saturation. (c) With both relaxation and exchange, the A resonance loses intensity owing to transfer but then recovers owing to relaxation. The X resonance exhibits a biexponential recovery.

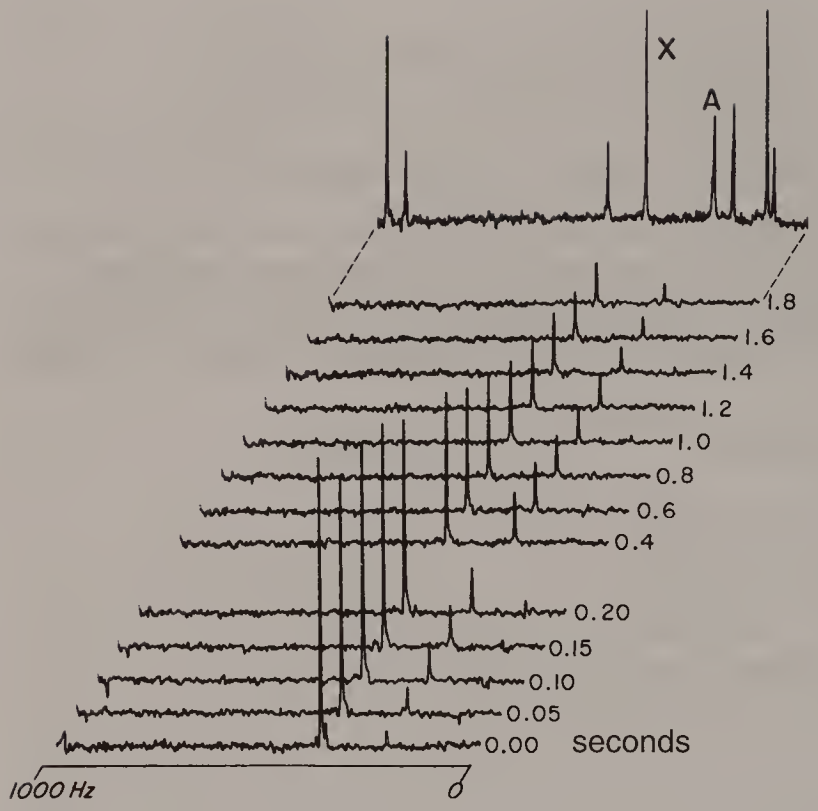

Fig. 2. Chemical exchange studied by difference spectroscopy. The experiment is initiated by a selective population inversion of resonance X (positive signals in the difference spectrum). Exchange carries inverted spins to site A, causing a population disturbance which increases with time and then dies away owing to spin–lattice relaxation. Note the break in the time scale where the increments change from 0.05 seconds to 0.20 seconds. The conventional spectrum (top trace) is from carbon-13 in the two stereoisomers of the 1,2,6-trimethylpiperidinium ion.

N-methyl group axial and the other equatorial. The experiment studies spin exchange between the 3,5 carbon-13 resonances of the two forms by applying a selective population inversion pulse to the low-field resonance (the equatorial N-methyl isomer). In practice, these experiments are conveniently performed in a difference mode, by subtracting the perturbed free induction decay from the unperturbed decay. All resonances that are unaffected by exchange then cancel, leaving a strong X resonance which decays monotonically to zero and an A resonance which grows from zero, passes through a maximum and then decays asymptotically to zero.

Recent developments in two-dimensional spectroscopy* exploit the same ideas in a different fashion (3). Suppose, for simplicity, that exchange occurs between just two sites A and X. First, the equilibrium longitudinal magnetizations are converted into transverse magnetizations by a 90° pulse, and labelled according to their precession frequencies ω_A and ω_X during a variable evolution period t_1. A part of

these vectors is then returned to the Z axis by another 90° pulse and a period of τ seconds is allowed for chemical exchange between the sites, residual transverse magnetization being dispersed by a field gradient *homospoil* pulse. At the end of this period, a third 90° pulse generates transverse magnetizations again, and the amount transferred from site X to site A is identified by the fact that it now has a new precession frequency ω_A. All the NMR signal components that retain the same precession frequencies throughout the experiment give rise to peaks on the principal diagonal of the two-dimensional spectrum, but those that have suffered a frequency jump due to exchange give rise to easily identifiable *cross-peaks* lying off the main diagonal. Information about the rate of exchange is contained in the relative intensities of these cross-peaks. The beauty of the method lies in the clear picture that it provides of the many possible exchange paths in a complicated system, each pair of cross-peaks identifying one of the paths. If the mixing time is short compared with the inverse of the exchange rate only single-step exchange events are observed. In the one-dimensional Forsén–Hoffman experiment each exchange pathway would have to be investigated separately, and the analysis becomes quite difficult for multisite exchange. Further refinements of this experiment (4) make τ a variable by incrementing it in step with the evolution time t_1 in some constant proportion – the 'accordion' experiment.

REFERENCES

1. S. Forsén and R. A. Hoffman, *J. Chem. Phys.* **39**, 2892 (1963).
2. G. A. Morris and R. Freeman, *J. Magn. Reson.* **29**, 433 (1978).
3. J. Jeener, B. H. Meier, P. Bachmann and R. R. Ernst, *J. Chem. Phys.* **71**, 4546 (1979).
4. G. Bodenhausen and R. R. Ernst, *J. Am. Chem. Soc.* **104**, 1304 (1982).

Cross-references

Chemical exchange
Difference spectroscopy
Selective excitation
Spin–lattice relaxation
Two-dimensional spectroscopy

Selective Decoupling

In the section on Coherent decoupling* a pictorial description of double resonance is presented where it is seen intuitively that the influence of the B_2 field extends over a frequency range of the order of magnitude $\gamma B_2/2\pi$ Hz. It is therefore feasible to use coherent irradiation to decouple one chemically shifted group of spins with a negligible influence on the others, provided the latter are well separated in frequency. This is called selective decoupling.

Consider the very simple case of two protons P and Q, with a chemical shift separation of Δ Hz, coupled with similar direct couplings $^1J_{CH}$ to carbon-13 spins P′ and Q′ respectively. Each proton resonance is a doublet of splitting $^1J_{CH}$, and we assume that P and Q are well separated so that $\Delta >> |^1J_{CH}|$. If proton P is irradiated at its chemical shift frequency with a decoupling field $\gamma_H B_2/2\pi$ comparable with $^1J_{CH}$, then the two proton transitions are acted on by equal effective radiofrequency fields (expressed in frequency units)

$$E_1 = E_2 = [(\tfrac{1}{2}J_{CH})^2 + (\gamma_H B_2/2\pi)^2]^{1/2}. \qquad [1]$$

The residual splitting on the P′ resonance is given by $(E_1 - E_2)$, so P′ is completely decoupled. However, the decoupler is Δ Hz off resonance for the Q proton, so the effective fields acting on the two Q transitions are

$$E_3 = [(\Delta + \tfrac{1}{2}J_{CH})^2 + (\gamma_H B_2/2\pi)^2]^{1/2} \qquad [2]$$

$$E_4 = [(\Delta - \tfrac{1}{2}J_{CH})^2 + (\gamma_H B_2/2\pi)^2]^{1/2}. \qquad [3]$$

Now, because $\Delta >> |^1J_{CH}|$ the residual splitting on the Q′ carbon-13 resonance is

$$E_3 - E_4 = \frac{J_{CH}\Delta}{\left[\Delta^2 + \left(\gamma_H B_2 / 2\pi\right)^2\right]^{1/2}}. \qquad [4]$$

Since $\Delta >> \gamma_H B_2/2\pi$, the residual splitting $E_3 - E_4$ is approximately equal to J_{CH}. Thus, while the P′ spin is decoupled, the Q′ spin is not.

This principle has been used for locating hidden resonances in homonuclear systems, and for determining which multiplets in a complicated spectrum are related by spin–spin coupling. It is not of course necessary to find the *exact* decoupling condition $\Delta = 0$, since the residual splitting will be small provided that $\gamma B_2/2\pi >> \Delta$. Selective decoupling can be applied to the task of correlating proton

shifts with carbon-13 shifts, although this is more usually accomplished by two-dimensional correlation spectroscopy*.

RELATIVE SIGNS OF COUPLING CONSTANTS

Suppose we have a system of three spins, A, M and X, all weakly coupled to each other with resolvable couplings. Let us take M to be the passive spin, the one not directly involved in our selective decoupling experiment. This passive spin merely creates effective chemical shifts for the A and X spins, $(\delta_A + \frac{1}{2}J_{AM})$ and $(\delta_A - \frac{1}{2}J_{AM})$ instead of δ_A, and $(\delta_X + \frac{1}{2}J_{MX})$ and $(\delta_X - \frac{1}{2}J_{MX})$ instead of δ_X. If we had the services of a Maxwell demon, we could separate the sample into two different flasks – one with all the M spins in α spin states, the other with M spins in β spin states. If we were able to run the NMR spectrum from one of these flasks, it would tell us the relative signs of J_{AM} and J_{MX} by identifying the effective chemical shifts. In effect, selective decoupling accomplishes the same result (1).

For simplicity, suppose that $|J_{MX}| >> |J_{AX}|$. This makes it feasible to irradiate the low-field doublet of the X resonance with $\gamma B_2/2\pi$ comparable with J_{AX}, without appreciably affecting the high-field X doublet, a distance J_{MX} away (Fig. 1). In this experiment J_{MX} takes on the function of Δ in eqns [2] and [3]. Only one of the A-spin doublets is decoupled. If it is the low-field doublet, then J_{AM} and J_{MX} have like signs; if it is the high-field doublet, they have opposite signs. We could work this out by writing α and β labels on the A and X transitions to indicate the spin state of M. This has been done in Fig. 1 for the case of opposite signs, which is the situation in the practical example of 2,3-dibromopropanoic acid, where the vicinal

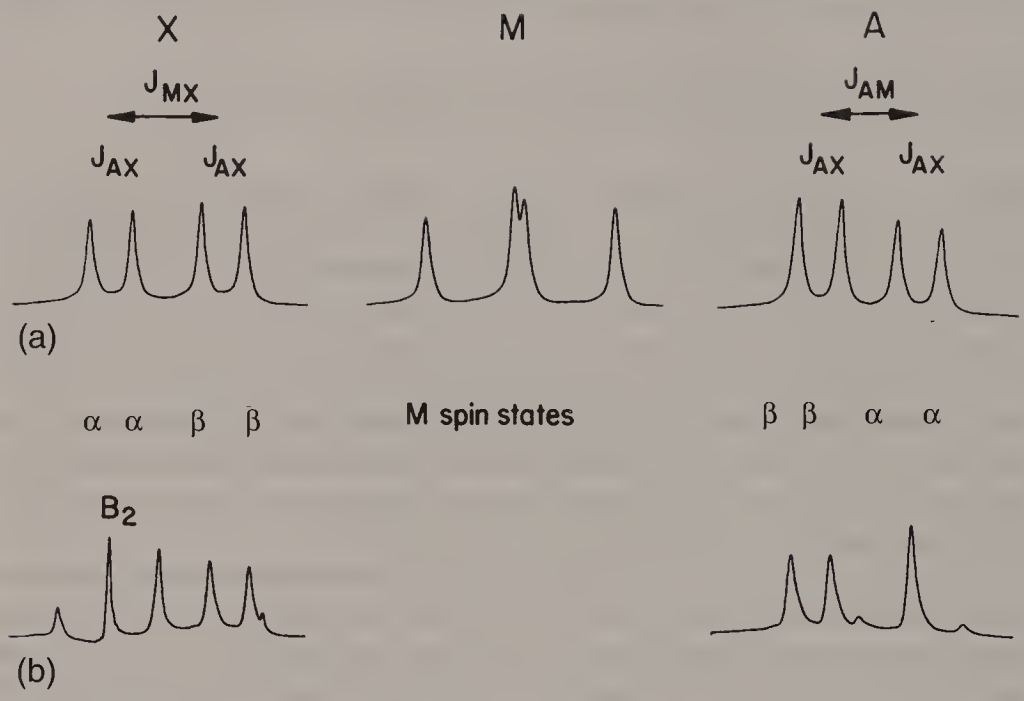

Fig. 1. Demonstration that the geminal (J_{AM}) and vicinal (J_{MX}) couplings in 2,3-dibromopropanoic acid have opposite signs (2). A selective decoupling field B_2 applied to the *low-field* X doublet causes the *high-field* A doublet to coalesce (b). The α and β labels represent the case of opposite signs, but since the absolute signs are unknown, α and β can be interchanged throughout. In addition to the decoupled line in the A spectrum, there are two weak satellites where both B_1 and B_2 contribute a quantum.

and geminal couplings have opposite signs (2). We see that irradiation of the *low-field* X doublet decouples the *high-field* A doublet. Of course we could have reversed all the α and β labels in Fig. 1, but the decoupling result is the same. This reminds us that absolute signs of coupling constants are not accessible by this technique.

For relative sign determinations in heteronuclear spin systems it should be noted that it is strictly the reduced coupling constants $J_{AM}/(\gamma_A\gamma_M)$ and $J_{MX}/(\gamma_M\gamma_X)$ that are being related, so that if one of the gyromagnetic ratios happens to be negative, then the argument above has to be reversed. This caveat applies to decoupling experiments between protons and nitrogen-15 or silicon-29, which both have negative gyromagnetic ratios.

Coupling constants from a wide variety of bond configurations and many different combinations of nuclear species have had their relative signs determined in this manner. Two-dimensional correlation spectroscopy* gives relative signs by inspection (3). More sophisticated experiments (4) have related the absolute sign of $^1J_{CH}$ to the sign of the chemical shift anisotropy of fluorine, so we now believe that $^1J_{CH}$ is positive, and the absolute signs of the other coupling constants can be related to this.

BAND-SELECTIVE DECOUPLING

The experiments described above are 'multiplet-selective'. There are, however, situations where decoupling is required to be effective over a range of chemical shifts, while having a negligible effect elsewhere. This may be the case in some heteronuclear systems, where carbon-13 chemical shifts of proteins tend to cluster in specific regions of the spectrum, separated by wide intervals. This suggests an application for *multiple* band-selective decoupling of carbon-13 while observing the proton spectrum. By concentrating the irradiation in regions occupied by carbon-13 shifts, this appreciably lowers the mean radiofrequency power dissipation compared with broadband decoupling.

In homonuclear selective decoupling experiments the requirements are more severe. The aim is to achieve vanishingly small residual splittings over a predefined spectral region with essentially full splittings elsewhere, apart from narrow transition regions. Band-selective decoupling of this kind has been performed by incorporating a band-selective spin inversion pulse, such as I-BURP-2 (5), into a broadband decoupling cycle, such as MLEV-4 (6). Unlike broadband decoupling with hard radiofrequency pulses, this ensures that the decoupler has a negligible effect outside the operating band; there is a clear and rather sharp distinction between fully coupled multiplets and decoupled singlets (7). A practical example is provided by the crowded 400 MHz proton spectrum of erythromycin (Fig. 2). It shows the effect of band-selective decoupling with repeated selective I-BURP-2 inversion pulses. The decoupler irradiates a group of methyl resonances lying

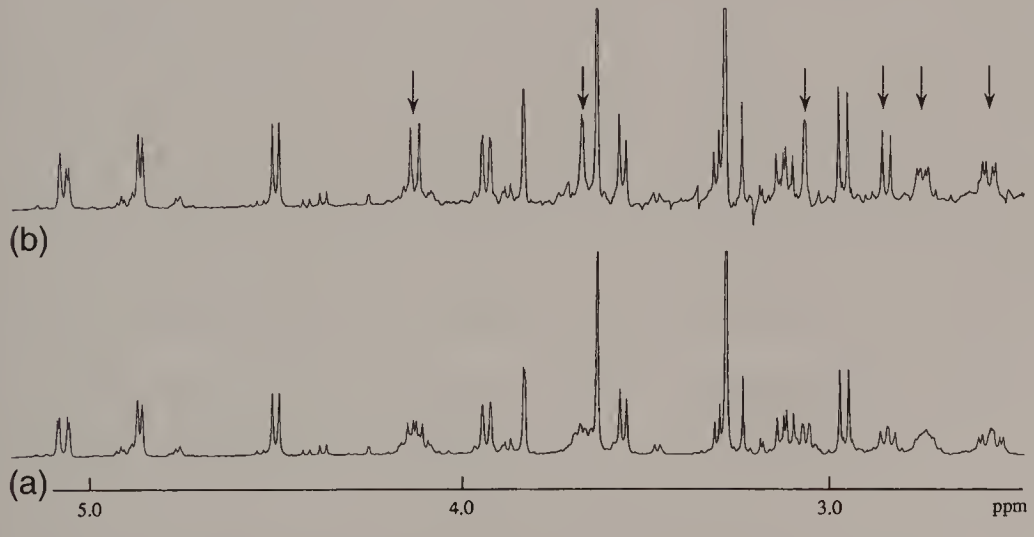

Fig. 2. Part of the 400 MHz proton spectrum of erythromycin (a) unperturbed and (b) with band-selective decoupling of methyl groups in the range 0.9 to 1.3 ppm. The six multiplets indicated by the arrows are simplified by the decoupling, while the remainder are unaffected.

between 1.9 and 2.3 ppm; the rest of the proton spectrum remains unaffected, except for six proton multiplets that are considerably simplified (7).

REFERENCES

1. D. F. Evans and J. P. Maher, *Proc. Chem. Soc.* 208 (1961).
2. R. Freeman, K. A. McLauchlan, J. I. Musher and K. G. R. Pachler, *Mol. Phys.* **5**, 321 (1962).
3. A. Bax and R. Freeman, *J. Magn. Reson.* **44,** 542 (1981).
4. E. L. Mackor and C. MacLean, *J. Chem. Phys.* **44**, 64 (1966).
5. H. Geen and R. Freeman, *J. Magn. Reson.* **93**, 93 (1991).
6. M. H. Levitt and R. Freeman, *J. Magn. Reson.* **43**, 502 (1981).
7. Ē. Kupče and R. Freeman, *J. Magn. Reson. A* **102**, 364 (1993).

Cross-references

Broadband decoupling
Coherent decoupling
Correlation spectroscopy
Selective excitation
Two-dimensional spectroscopy

Selective Excitation

When a conventional high-resolution spectrum has been recorded and the spectroscopist requires further information, for example correlations based on spin–spin coupling or the nuclear Overhauser effect, the usual procedure is to run a two-dimensional spectrum. This has the advantage that it explores all the correlations in a single experiment, and is readily implemented by standard software routines. Sometimes the problem can be solved with far less new information – for example, we might be interested in testing for proximity between just two protons, any other correlations being irrelevant to the task in hand. Then a nuclear Overhauser experiment initiated by a frequency-selective 180° pulse would suffice, and this would be quicker than the two-dimensional analogue if the sensitivity is already high.

It is convenient to label all such selective excitation schemes as 'soft-pulse' experiments, in contrast to 'hard-pulse' excitation, where all chemically shifted sites are affected essentially equally. There are various degrees of selectivity – line-selective, multiplet-selective and band-selective schemes are feasible. There are even 'hole-burning' experiments where the selectivity is so high that only a narrow slice of the instrumental linewidth is appreciably affected. Excitation may take place in the presence of a pulsed magnetic field gradient, as in the slice-selection stage of magnetic resonance imaging (1). A distinction should be made between a 90° excitation pulse, which takes magnetization from the Z axis to the XY plane, and a 'universal' 90° pulse which rotates a vector through 90° from an *arbitrary* initial position. Two further important categories of soft pulses are the 180° spin inversion pulse which takes vectors from +Z to –Z or vice versa, and the 180° refocusing pulse which takes a vector at an arbitrary position in the XY plane and rotates it into a mirror image configuration in that plane with a view to forming a spin echo at a later time.

The pulse flip angle α (usually 90° or 180°) is determined by the type of experiment to be performed; it is given by

$$\alpha = \gamma B_1 t_p \text{ radians}, \qquad [1]$$

where B_1 is the radiofrequency intensity and t_p is the pulse duration. Whereas a hard pulse employs an intense field B_1 and consequently a short pulse duration t_p, a soft pulse operates at a much lower level of B_1 and a proportionately longer duration t_p. As a rough rule of thumb, B_1 influences nuclear spins within a range of the order of

$\pm\gamma B_1/2\pi$ Hz from exact resonance. For example, a 10 ms soft 90° pulse has an effective 'range' of the order of ±25 Hz, whereas a typical hard 90° pulse might have a duration of 10 μs and cover a frequency range of the order of ±25 kHz.

For isolated nuclear spins (no spin–spin coupling) the Bloch equations can be used to calculate the form of the excitation profile in the frequency domain simply by following magnetization trajectories for a series of different offsets from resonance. This is an application of the vector model*. In fact, even the individual lines of a spin multiplet can be represented as independent magnetization vectors and their motion during a soft pulse calculated according to the Bloch equations, provided we are not applying simultaneous soft pulses to two coupled spins (2). At a given offset from resonance ΔB, the nuclear magnetization vector simply rotates about an effective field

$$B_{eff} = \left(\Delta B^2 + B_1^2\right)^{1/2} \qquad [2]$$

tilted in the XZ plane with respect to the +X axis through an angle

$$\theta = \arctan(\Delta B/B_1). \qquad [3]$$

In situations where $\alpha << 1$ radian, the NMR response is essentially linear with respect to the excitation field B_1 and then the excitation profile is the Fourier transform of the time-domain pulse envelope. Thus a rectangular pulse gives a sin x/x excitation profile in the frequency domain. For a 90° pulse, this is a poor approximation at resonance (Fig. 1) but becomes progressively more correct as the offset increases. The profile is actually a *distorted* sin x/x function. For a 180° pulse the linear approximation breaks down completely. In fact the non-linearity of the response is an important feature; without it, selective excitation in an applied field

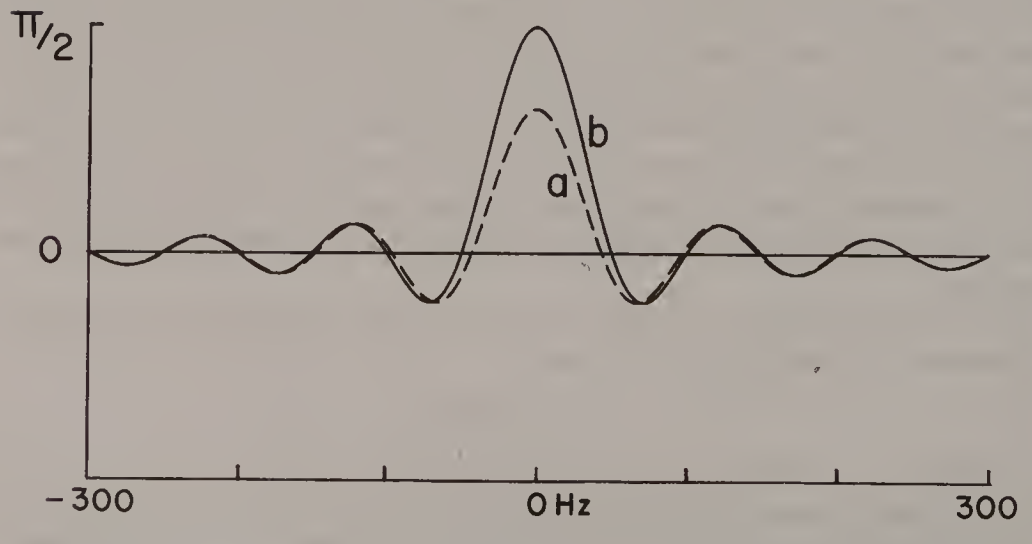

Fig. 1. Frequency-domain excitation profiles calculated for a 10 ms rectangular 90° pulse on the basis of the Bloch equations (curve a) and a Fourier transform relationship (curve b). The two curves become indistinguishable at large offsets.

gradient would give a null response after the soft pulse (3). The non-linearity is also essential for soft pulses designed to refocus magnetization trajectories so that they terminate along (say) the +Y axis of the rotating frame (4).

THE DANTE SEQUENCE

In older high-resolution spectrometers, switching from a high radiofrequency level (hard pulse) to a low level (soft pulse) was not always straightforward, and phase coherence was not always strictly maintained; furthermore the transmitter frequency was not tuneable in the very fine steps required by certain selective experiments. The DANTE sequence (5) was designed to circumvent these problems.

The operation is most easily visualized in terms of the vector model*. We apply a regular train of N short, hard radiofrequency pulses at a repetition rate $1/\tau$. At exact resonance the effect is cumulative; if each individual hard pulse has a flip angle β, a magnetization vector along +Z is carried in a continuous arc in the YZ plane through a total angle $\alpha = N\beta$ (a in Fig. 2). Now consider another vector representing spins at a small offset from resonance $\Delta\nu$. Between each hard pulse

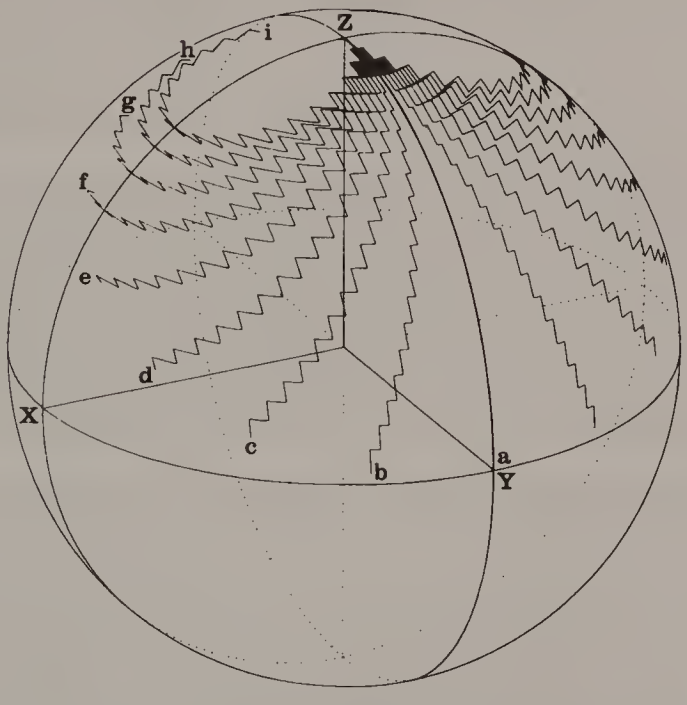

Fig. 2. Magnetization trajectories during a DANTE sequence. For exact resonance (a) the pulses have a cumulative effect, taking the magnetization to the +Y axis. For increasing offsets from resonance, (b) through (i), the vectors follow a zig-zag path that carries them further and further from the ZY plane. At very large offsets they execute small cyclic excursions close to the +Z axis.

this vector precesses about the Z axis through a small angle

$$\theta = 2\pi\Delta\nu\tau. \quad [4]$$

The trajectory consists of a zig-zag motion that carries this vector away from the ZY plane (b in Fig. 2). At appreciable offsets ($\theta > \beta$) the trajectory loops back towards the +Z axis and the detected signal can be very small (i in Fig. 2). This is the offset region where the detected signal follows the 'wiggles' characteristic of a sin x/x function, as the trajectories make cyclic excursions near the +Z axis. At still larger offsets the detected signal becomes negligible. In the limit of a large number N of constituent pulses, the zig-zag trajectories closely approximate the smooth curves obtained with a single soft pulse of the same overall duration. The only practical limitation is the lower limit on the pulse duration; for pulses much shorter than 1 microsecond there can be spurious phase shifts (6).

There is one important difference between a DANTE sequence and a single soft pulse. Had we written the precession angle as $(2k\pi + \theta)$, where k is an integer, the trajectories would have been essentially the same. There is therefore a set of sideband responses at offsets from exact resonance

$$\Delta\nu = \pm k/\tau. \quad [5]$$

That is to say, spins at these offsets accomplish a small number k of complete revolutions about the +Z axis in each interval τ. This is useful, since we can choose to work at (say) the first-sideband condition (k = 1) where the effective excitation frequency can be fine tuned by changing the interval τ, leaving the transmitter frequency at the setting used for a conventional spectrum. The centreband response and all the unused sideband responses can be kept well clear of the NMR spectrum by setting a high repetition rate $1/\tau$.

The free precession intervals of a DANTE sequence can be used to monitor the NMR signal, one data point at a time. This can provide direct evidence for the complex magnetization trajectories that evolve during the shaped soft pulses described below. Figure 3 shows experimental trajectories obtained during excitation by an E-BURP-2 pulse (4), implemented by a 128-pulse DANTE sequence. Only the X and Y components are detected; the Z component is deduced under the assumption that relaxation losses and radiation damping effects are negligible (7).

In Dante's Purgatory, souls progress toward Heaven by negotiating a series of seven circular ledges running around a mountain. Progress from one ledge to the next is only permitted after one complete circumnavigation. Apart from a trivial sign inversion, this complex trajectory clearly anticipates the motion of a nuclear magnetization vector in the rotating frame experiencing a sequence of seven pulses at the first sideband condition. This is the origin of the name DANTE (Delays Alternating with Nutation for Tailored Excitation).

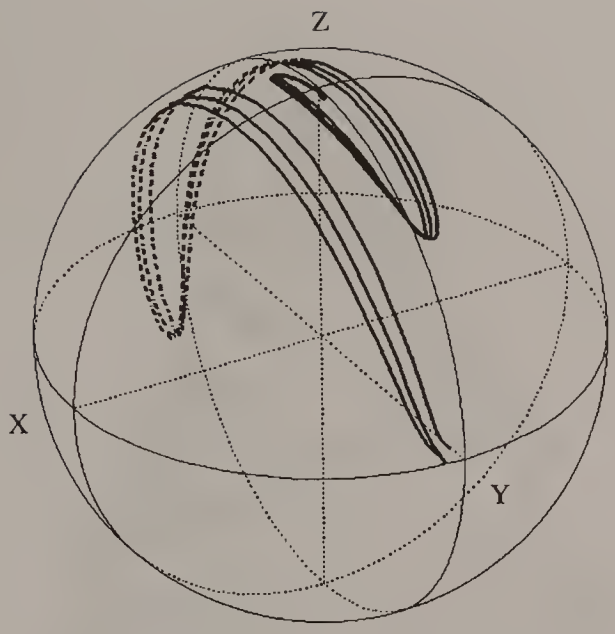

Fig. 3. Magnetization trajectories during a 45.7 ms E-BURP-2 selective excitation pulse with $\gamma B_1/2\pi$ = 3.6 kHz for resonance offsets of 6, 8 and 10 Hz. These were derived from direct experimental observation of the X and Y components of magnetization during the 128 'windows' of a shaped DANTE sequence. The Z component was deduced on the assumption of negligible relaxation losses. The sections of the trajectories at the rear of the unit sphere are shown dotted. Diagram courtesy of Helmut Sengstschmid.

PULSE SHAPING

A rectangular pulse is not ideal for selective excitation. It has sidelobe responses that extend to surprisingly large offsets from resonance, approximating the sin x/x frequency profile predicted for the Fourier transform of a rectangle. One of these distant sidelobes could induce an undesirable excitation of a neighbour resonance, thus undermining the intent of the selective excitation experiment. Smoothing the sharp leading and trailing edges of the pulse corrects this problem. One of the tenets of Fourier transform theory (8) is that if a time-domain function can be differentiated n times before the derivative exhibits a discontinuity, then the frequency-domain excitation falls off as $\Delta\nu^{-n}$ at large offsets $\Delta\nu$. Thus a rectangular pulse, which has a discontinuous first derivative, has an excitation that falls off as $\Delta\nu^{-1}$ in the tails.

This theorem suggests that a Gaussian pulse envelope (9) would be a good choice for a shaping function because all the derivatives of a Gaussian are continuous. The only practical problem is that the time-domain Gaussian function needs to be truncated in the tails; usually the cut-off point is where the amplitude has fallen below about 2 to 3% of the peak amplitude. Figure 4 compares the frequency-

Dante's Purgatory. The idea seems to be not so much to escape but to work one's way up to the more interesting vices.

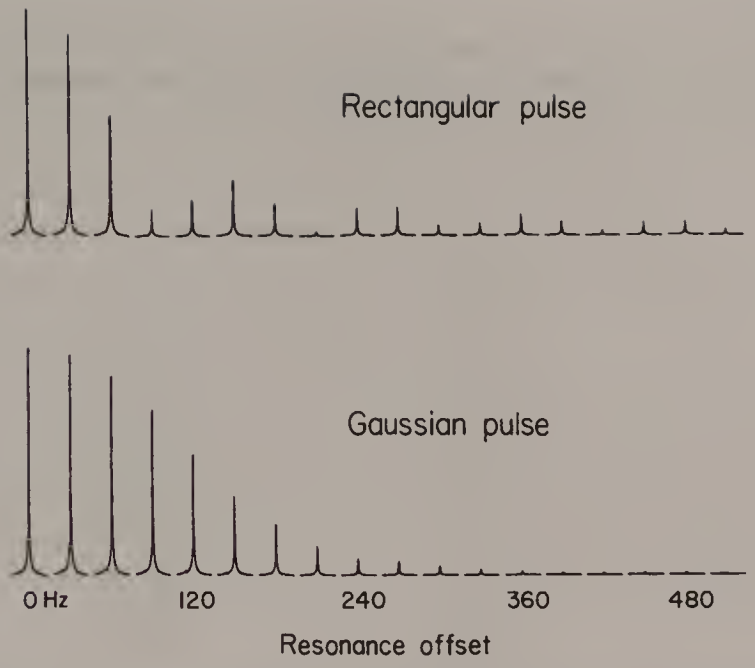

Fig. 4. The frequency-domain excitation profiles of rectangular and Gaussian soft pulses of the same duration (10 ms). At large offsets from resonance the rectangular pulse has sidelobes of appreciable intensity, whereas the excitation after the Gaussian pulse dies away monotonically.

domain excitation pattern of a rectangular pulse with that of a Gaussian pulse of the same duration (10 ms). The sidelobes from the rectangular pulse extend far beyond the point where the Gaussian excitation has fallen to a negligible level. The excitation band can be further narrowed by a more severe truncation of the Gaussian function, at the expense of introducing a slight sin x/x character.

In general, soft pulses introduce a frequency-dependent phase error into the excited spectrum. This can be appreciated by studying magnetization trajectories similar to those in Fig. 2; they spread out in the XY plane as a function of offset from resonance. The resulting phase gradient is an approximately linear function of offset, so we can think of the vectors as originating at a focus somewhere near the middle of the soft pulse, acquiring a significant spread at the time that signal acquisition begins. It is in fact possible to move this focus point to the end of the soft pulse (or even beyond) by suitably shaping the pulse envelope. By swinging the magnetization vectors back and forth between the +Y and –Y hemispheres of the rotating reference frame, these 'pure-phase' pulses balance divergence in the positive hemisphere by convergence in the negative hemisphere, bringing all the trajectories to a focus along +Y and the end of the pulse. (Where vectors have already been dispersed in the XY plane, a time-reversed pure-phase 90° pulse will rotate them all back to the +Z axis.) This complex design process is implemented by a simulated annealing algorithm that optimizes the Fourier coefficients used to define the pulse shape to match a predefined 'target' excitation profile in which all dispersion-mode components are set to zero (4). For experiments performed in an

Table 1. Fourier coefficients[a] used to define the shape of a band-selective 'pure-phase' excitation pulse designed to have a very flat excitation profile over a frequency band 4/T Hz (where T is the pulse duration) and very low excitation outside this band (11).

n	A_n	B_n
0	+0.250	—
1	+0.934	–0.197
2	+0.180	–1.772
3	–1.527	+0.204
4	+0.003	+0.619
5	+0.143	+0.076
6	+0.050	+0.039
7	+0.072	–0.025
8	–0.015	–0.060
9	–0.040	+0.005
10	–0.005	+0.017

[a]To be inserted in the expression for the pulse amplitude as a function of $\omega = 2\pi/T$:

$$\gamma B_1(t) = \omega\left\{A_0 + \sum_{n=1}^{10}\left[A_n \cos(n\omega t) + B_n \sin(n\omega t)\right]\right\}$$

applied magnetic field gradient there is the simpler expedient of reversing the gradient direction to refocus the divergent vectors.

Pure-phase pulses have been designed not only for excitation and spin inversion, but also as 'universal' 90° and 180° rotations where the initial orientation of the vector is arbitrary (4). They can be refined to give a particularly flat excitation profile within the operating range (10) or to generate 'quiet' baselines in the distant regions where the excitation would ideally be zero (11). Table 1 sets out the Fourier coefficients required to reproduce a band-selective pulse with both of these attributes. Where there is significant spin–spin or spin–lattice relaxation during the pulse, the pulse shape can be redesigned to minimize distortions of the excitation profile (12).

SIMULTANEOUS SOFT PULSES

There are now many experiments that require the application of two or more soft pulses at the same time. The soft pulses may have different frequencies, phases, flip angles, pulse envelopes and selectivities. Let us first of all address the simplest case of two simultaneous soft pulses. Suppose we interleave two DANTE sequences, A and B, each with the same pulse repetition rate $1/\tau$ Hz. Sequence A terminates at $\tau/2$ ms before the start of signal acquisition whereas sequence B ends immediately

prior to acquisition. All the hard pulses are at the same frequency, but those in sequence A have a constant phase whereas those in sequence B have a progressive phase incrementation of ϕ radians per step, giving an *effective* excitation frequency displaced from the carrier by $\Delta f = \phi/(2\pi\tau)$ Hz. To a good approximation, the two sequences do not interfere with each other, except when Δf is very small and the pulses of sequence B slightly distort the trajectories of magnetization excited by sequence A (and vice versa). The two flip angles and pulse shapes can be adjusted independently (13). The A and B sequences need not start at the same time, so the frequency selectivities (1/T) may be different.

We can readily imagine extensions of this scheme that interleave several DANTE sequences, but eventually the 'windows' get filled with pulses. Then it is more profitable to adopt a slightly different approach (14). The total pulse duration T is divided into N segments with no windows for free precession, just as if we were planning to digitize a single soft pulse. We define each individual soft pulse as a histogram of N segments, each with a specific phase and amplitude, and

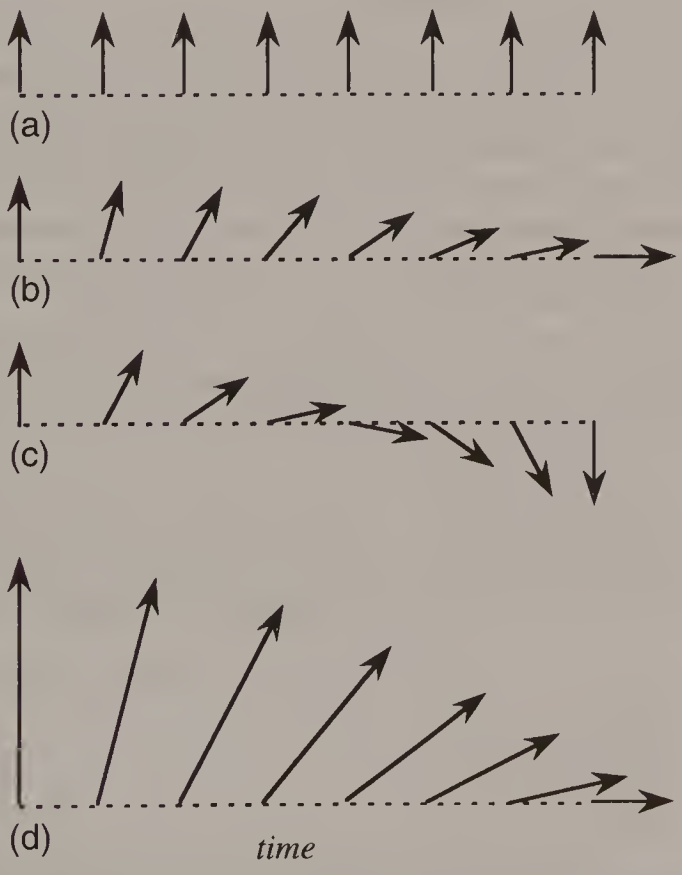

Fig. 5. Generation of three simultaneous soft pulses (a), (b) and (c) at different frequencies. Each pulse envelope is divided into segments of a given amplitude and phase (represented by vectors). The required frequency differences are implemented by advancing the phase at the appropriate rate. The resultant (d) is obtained by vector addition of (a), (b) and (c) at each segment.

represented by a vector (Fig. 5(a)). The effective frequency (with respect to the carrier) is determined by the rate of phase incrementation from one segment to the next (Fig. 5(b)). Pulse shaping is determined by the amplitude modulation. Several such pulses may be combined by vector addition at each segment (Fig. 5(d)). If all the individual hard-pulse flip angles are small, the various soft pulses act essentially independently.

If two rectangular soft pulses are separated in frequency by $\Delta f = 1/(2T)$, where T is the pulse duration, then the sin x/x wiggles of the individual frequency-domain responses tend to cancel, the peaks of one excitation pattern falling in the troughs of the other. This allows us to construct a large array of regularly spaced soft pulses so as to cover a wide frequency band with essentially uniform excitation and a linear phase gradient. The frequency-domain profile of such a 'polychromatic pulse' (15) can be tailored by hand by readjusting the individual pulse intensities. For example, it is a simple matter to design a rejection notch for solvent suppression* while retaining uniform excitation elsewhere.

PHASE ENCODING SCHEMES

A single soft-pulse spectrum affords roughly the same sensitivity as the corresponding two-dimensional spectrum run in the same total time. Consequently if we divide up the available time into N equal segments in order to perform N consecutive soft-pulse measurements, we sacrifice a factor of $N^{1/2}$ in sensitivity. This reflects the well-known multiplex advantage of two-dimensional spectroscopy; it gathers information equivalent to that obtained from an entire series of conventional NMR measurements made in a single dimension.

Fortunately there is a trick that will allow us to perform all N soft-pulse measurements *simultaneously* and then unravel the results later, thus restoring the multiplex advantage. The principle was elucidated by Hadamard (16). Take the simplest case of four measurements A, B, C and D. We set up an experiment in which four soft pulses are applied simultaneously, giving four separate pieces of correlation information. In order to be able to separate these four results later, each measurement is phase encoded, the simplest system using 180° phase inversions as the code. Four consecutive scans are made, each with a different encoding scheme:

	A	B	C	D
scan 1	+	+	+	+
scan 2	+	+	−	−
scan 3	+	−	+	−
scan 4	+	−	−	+

This is a Hadamard matrix of order 4 (there are larger Hadamard matrices of order 4k where k is an integer). If we add the results of all four scans, we obtain the result of measurement A, the spectra from B, C and D cancelling exactly. Result B is extracted by adding scans 1 and 2 and subtracting scans 3 and 4. This has the advantage that the overall measurement time can be quite short (if the signal-to-

noise is sufficiently high), and that it targets specific correlations instead of the unplanned blanket coverage of two-dimensional spectroscopy (17). More general types of phase encoding are possible (see Phase cycling*).

REFERENCES

1. P. C. Lauterbur, *Nature* **242**, 190 (1973).
2. Ē. Kupče, J. M. Nuzillard, V. S. Dimitrov and R. Freeman, *J. Magn. Reson. A* **107**, 246 (1994).
3. D. I. Hoult, *J. Magn. Reson.* **35**, 69 (1979).
4. H. Geen and R. Freeman, *J. Magn. Reson.* **93**, 93 (1991).
5. G. A. Morris and R. Freeman, *J. Magn. Reson.* **29**, 433 (1978).
6. M. Mehring and J. S. Waugh, *Rev. Sci. Instrum.* **43**, 649 (1972).
7. H. Sengstschmid and R. Freeman, *J. Magn. Reson. A* **121**, 212 (1996).
8. R. N. Bracewell, *The Fourier Transform and its Applications* McGraw-Hill: New York, 1978.
9. C. Bauer, R. Freeman, T. Frenkiel, J. Keeler and A. J. Shaka, *J. Magn. Reson.* **58**, 442 (1984).
10. J. M. Nuzillard and R. Freeman, *J. Magn. Reson. A* **110**, 252 (1994).
11. Ē. Kupče and R. Freeman, *J. Magn. Reson. A* **112,** 134 (1995).
12. J. M. Nuzillard and R. Freeman, *J. Magn. Reson. A* **107**, 113 (1994).
13. H. Geen, X. L. Wu, P. Xu, J. Friedrich and R. Freeman, *J. Magn. Reson.* **81**, 646 (1989).
14. Ē. Kupče and R. Freeman, *J. Magn. Reson. A* **105,** 234 (1993).
15. Ē. Kupče and R. Freeman, *J. Magn. Reson. A* **102,** 122 (1993).
16. J. Hadamard, *Bull. Sci. Math.* **17**, 240 (1893).
17. V. Blechta and R. Freeman, *Chem. Phys. Lett.* **215**, 341 (1993).

Cross-references

Fourier transformation
Phase cycling
Radiofrequency pulses
Rotating frame
Solvent suppression
Vector model

Sensitivity

NMR spectroscopy has always suffered from poor sensitivity, largely due to the low Boltzmann factors involved. It is therefore important to understand the various factors which limit the attainable signal-to-noise ratio, some of which are out of the control of the operator, while others may be optimized. Codrington *et al.* (1) have calculated the sensitivity of a Fourier transform spectrometer by modifying an earlier treatment applicable to continuous-wave spectroscopy (2). Fundamental to this calculation is the assumption that the output of the receiver is made up of two *independent* components, the signal voltage V_s and the noise voltage V_n. Since the Fourier transformation stage is a linear operation, signal and noise components remain independent.

The calculation involves the following parameters:

N	Number of nuclear spins per unit volume of the sample
B_0	Applied static magnetic field intensity
γ	Gyromagnetic ratio of the nucleus
I	Spin quantum number
T	Absolute temperature
$\hbar$	Planck's constant divided by 2π
k	Boltzmann's constant
μ_0	Permeability of free space (SI unit conversion factor)
ω_0	Larmor precession frequency ($\omega_0 = \gamma B_0$)
T_2^*	Decay constant of transverse magnetization
$\Delta\omega$	Offset from exact resonance (drops out)
α	Flip angle of the radiofrequency pulse
ξ	Filling factor of the receiver coil ($\xi < 1$)
ρ	Ratio of effective inductance to total inductance of coil
Q	Quality factor of the receiver coil (typical value 250)
V_c	Volume enclosed by the receiver coil
n	Number of turns on the receiver coil (cancels out)
a	Length of the receiver coil (cancels out)
F	Noise figure of the preamplifier ($F > 1$)
G	Overall gain of the receiver (cancels out)
B	Final bandwidth of the receiver (cancels out)
λ	Nagaoka's constant ($\lambda = 1$ for infinitely long solenoid).

THE SIGNAL

The equilibrium nuclear magnetization M_0 is given by

$$M_0 = NB_0\gamma^2\hbar^2I(I + 1)/3kT. \quad [1]$$

A radiofrequency pulse of flip angle α produces a Y component of magnetization

$$M_Y = M_0 \sin \alpha. \quad [2]$$

This is taken as the basis of the NMR signal calculation, relaxation and the attendant steady-state effects in a repeated pulse sequence being disregarded in this treatment. It is assumed that a crossed-coil probe is used and that the transmitter coil is sufficiently large compared with the receiver coil that the transmitter field may be regarded as uniform over the effective sample volume. The signal is only acquired for a limited time (the acquisition time), otherwise the noise would be unlimited. The free induction signal is weighted with a suitable sensitivity enhancement* function in order to de-emphasize the noise components in the tail of the decay. It is assumed that the optimum weighting function is used, having a time constant equal to T_2^*, the equivalent of a matched filter (3). The signal transformed into the frequency domain is

$$S(\omega) = \tfrac{1}{4}GKT_2^*(1 + i\Delta\omega T_2^*)/[1 + \tfrac{1}{4}\Delta\omega^2(T_2^*)^2] \quad [3]$$

where

$$K = n\rho\xi QM_0 \sin \alpha\ \omega_0 V_c/a.$$

This is the expression for a Lorentzian line of full width $2/(\pi T_2^*)$ Hz, twice the width of the line before sensitivity enhancement. The real part of this expression represents the absorption-mode signal, and the peak height is given by setting $\Delta\omega = 0$:

$$S_p(\omega) = \tfrac{1}{4}GKT_2^*. \quad [4]$$

THE NOISE

Most of the noise arises from the thermal agitation of the electrons in the receiver coil, the 'Johnson noise', and depends on kT. Noise from the transmitter (a potential problem in continuous-wave spectrometers) may be neglected in a pulse-modulated Fourier transform spectrometer. Noise introduced in the amplification stages, principally by the preamplifier, is accounted for through the noise figure F, a number greater than unity.

Plancherel's theorem states that the total noise energy is the same in the time and frequency domains (4). It is assumed that, within the bandwidth of interest, the noise is 'white', that is to say its distribution function is independent of frequency and time. This allows us to calculate the noise voltage in the frequency domain:

$$N(\omega) = G(\tfrac{1}{2}kT\omega_0\lambda\mu_0 V_c\rho QFT_2^*)^{1/2}(n/a). \quad [5]$$

SIGNAL-TO-NOISE RATIO

The quantity of interest is the ratio of the peak absorption-mode signal to twice the root-mean-square noise. This is the form adopted by the instrument manufacturers. Taking the peak signal amplitude as

$$S_p(\omega) = \tfrac{1}{4}Gn\rho\xi QM_0 \sin\alpha(V_c/a)\omega_0 T_2^*, \quad [6]$$

this gives

$$R(\omega) = S_p(\omega)/2N(\omega)$$

$$= \frac{1}{24}\left(\frac{2\rho QV_c T_2^*}{\mu_0 F\lambda}\right)^{1/2}\left(\frac{\omega_0}{kT}\right)^{3/2} N\xi\gamma\hbar^2 I(I+1)\sin\alpha. \quad [7]$$

(We shall see later that the peak-to-peak noise is five times the root-mean-square noise.) Note that the number of turns per centimetre on the receiver coil (n/a) has cancelled out of this expression, as has the receiver gain G and bandwidth B.

This expression may be rewritten in order to group the various factors into three categories: fundamental constants, properties of the NMR sample and receiver parameters.

$$R(\omega) = \left(\frac{\gamma\hbar^2 I(I+1)}{24k^{3/2}\mu_0^{1/2}}\right)\left(\frac{N\omega^{3/2}\left(T_2^*\right)^{1/2}}{T^{3/2}}\right)\left(\frac{2\xi^2\rho QV_c}{\lambda F}\right)^{1/2}\sin\alpha\,. \quad [8]$$

This is a convenient form for considering the optimization of sensitivity.

SENSITIVITY OPTIMIZATION

There is of course nothing to be done about the fundamental constants, except to recognize that a high gyromagnetic ratio γ is important, and to note in passing that nuclei with $I > 1$ have slightly stronger signals than $I = \frac{1}{2}$ nuclei, although they tend not to be too interesting for high-resolution studies.

The next group of parameters is under the control of the investigator. Every effort is made to increase N, the number of nuclei per unit volume. It is proportional to the molar concentration of the solution, the natural abundance of the nuclear species, and the number of equivalent spins contributing to a given resonance line. In certain circumstances there may be no alternative but to enrich a given isotope artificially in order to boost sensitivity.

The operating frequency may or may not be a parameter which the investigator can select. It is not simply a matter of designing magnets at the highest possible field, since there is the parallel requirement that a large enough volume of homogeneous field be accessible. Nevertheless this is one parameter that has seen the most consistent improvement over the years, with the almost universal adoption of superconducting solenoids for high-resolution NMR. The operating frequency enters the calculation in three separate ways: in the expression for the Boltzmann population difference; as the frequency at which the nuclear magnetization oscillates in the receiver coil; and in the frequency dependence of the noise $(\omega_0)^{1/2}$. The resulting dependence on $(\omega_0)^{3/2}$ is not maintained for high-γ nuclei such as protons, because at very high operating frequencies the Q factor degrades and the noise figure F increases, while the proportion of the inductance wasted in the receiver coil leads increases. Resonant cavities, similar to those used in electron spin resonance, have been used on a few very high-field spectrometers. For nuclei like carbon-13 which require efficient broadband decoupling from protons, higher operating frequencies put higher demands on the bandwidth covered by the decoupler if sensitivity is to be maintained.

Low temperatures favour sensitivity, since the Boltzmann population differences increase and the noise power falls off. The result is a predicted $T^{-3/2}$ dependence. Unfortunately, the temperature range accessible to the operator is limited by the liquid range of the available solvents, and in any case the proportional change in T is quite small. In fact, it may often be more profitable to work at higher temperature since the solubility usually increases (increasing N) and the spin–lattice relaxation time usually decreases, allowing faster repetition of the excitation pulses. Because of the difficulties of precise temperature regulation, most experiments are conducted at the ambient probe temperature (often several degrees above room temperature). However, it is feasible to cool the receiver coil while maintaining the sample near room temperature. This has the advantage of reducing the Johnson noise in the receiver coil and increasing the quality factor Q. Experiments have been carried out with the receiver coil cooled by liquid helium, using conventional (5) and high-temperature (6) superconductors. Although filling factor is sacrificed owing to the need for thermal isolation of the sample from the coil, a sensitivity improvement of a factor of about five has been achieved at the time of writing (6).

The decay rate of the sensitivity enhancement function affects both the signal intensity (by broadening the lines) and the noise energy (by filtering out rapidly fluctuating noise). Note that the calculation assumed the equivalent of matched filtration. Under these conditions the sensitivity is proportional to $(T_2^*)^{1/2}$. An improvement to the resolving power of the spectrometer is therefore reflected in stronger signals, provided that instrumental broadening still outweighs the natural linewidths. Imperfect heteronuclear decoupling or residual field/frequency instabilities may contribute to the linewidth $(T_2^*)^{-1}$ and therefore degrade the signal-to-noise ratio.

The operator has a rather restricted choice of the receiver coil parameters, essentially limited to the selection of the sample tube diameter. It is nevertheless

important to understand how these parameters influence the signal-to-noise ratio. The receiver coil filling factor ξ influences the signal strength directly. Under the assumption that the radiofrequency field of the transmitter coils is essentially uniform when measured over the effective volume of the receiver coil, the filling factor may be approximated by $(d_s/d_c)^2$, where d_s and d_c are the diameters of the sample and the coil respectively. The sample tube wall thickness, any Dewar vessels and the clearance required for a spinning sample tube all contribute to $d_c - d_s$, but the proportional effect on ξ falls off for larger sample diameters. Recently significant improvements in filling factor have been achieved by careful attention to the bulk magnetic susceptibility of the wire used for the receiver coil, making this close to zero by combining metals with susceptibilities of opposite signs. This picks up magnetization from sample regions very close to the coil, normally 'lost' because of distortions of the B_0 field.

The quality factor Q of the coil affects sensitivity as $Q^{1/2}$ since it improves the signal voltage proportional to Q and the noise as $Q^{1/2}$. It represents the ratio of the energy stored in the tuned circuit to the energy dissipated in the series resistance. Hence it is favoured by heavy-gauge wire, high-conductivity copper and low-loss capacitors. The Q factor tends to follow a broad maximum as a function of frequency. Samples which contain ions, for example aqueous solutions of some biological materials, can appreciable degrade the Q factor of the coil and reduce sensitivity. This can be thought of as a capacitive coupling of the tuned circuit to

Filling factor.

the random Brownian motion of the ions. For this reason, coils constructed of flat strips of copper foil, although they normally possess high quality factors, are not really suitable for the study of ionic solutions since they have a relatively large capacitive coupling; thin wire is preferable. The rate at which a radiofrequency pulse can be switched on or off depends on Q, so single-coil spectrometers may require a Q-spoiling device (e.g. crossed diodes) which operates during the pulse but not during signal acquisition.

The inductance of the leads to the receiver coil is largely wasted for the detection of NMR signals, and this loss of efficiency is reflected in the correction factor $\rho^{1/2}$. This can be quite important at high frequencies when the number of turns on the receiver coil is small (often unity). For a nucleus of intermediate frequency it is often found that increasing the number of turns on the receiver coil improves sensitivity, although this parameter n dropped out of the expression for signal-to-noise ratio; the effect is explained by the change in the ρ factor.

The simplest way of increasing sensitivity is to use a larger-volume sample coil, since the signal-to-noise ratio increases as $(V_c)^{1/2}$ while Q, ξ and ρ also tend to increase with V_c. Of course, this does not help if the absolute amount of sample is limited and the concentration has to be reduced, nor is it profitable to use a small-diameter sample tube in a large-diameter coil, since the filling factor would be very poor. Receiver coils have been specially designed to accept small (2 mm) samples for cases where the sample is limited. If the receiver coil is increased in size too much, problems arise with the homogeneity of the field and with broadband heteronuclear decoupling. A practical limit seems to be 20–25 mm diameter samples.

Nagaoka's constant λ reflects the receiver coil geometry, favouring short, fat coils, since $\lambda^{1/2}$ affects noise but not the signal. For a solenoid coil with length equal to its diameter, $\lambda = 0.69$. Note that quite different considerations apply to saddle-shaped receiver coils (7) commonly used in superconducting solenoids where the sample tube axis is along the field direction B_0 rather than at right angles. Some probes have been designed for superconducting solenoids which have a 'sideways-spinning sample' and a solenoid receiver coil in order to retrieve this loss of sensitivity.

The receiver noise figure enters the calculation as $F^{-3/2}$. With good preamplifier design F can be quite close to unity (within 10%), so there is little scope for improvement here for conventional samples in non-aqueous solvents. The picture changes dramatically for proton NMR in aqueous solution because of the dynamic range problem (see Digitization* and Solvent suppression*). Non-linear effects in the radiofrequency mixers, intermodulation distortion in the receiver and the limited vertical resolution of the analogue-to-digital converter all conspire to introduce spurious fluctuations which appear to the spectroscopist as 'noise' and which obscure very weak NMR signals. Note that the specifications for sensitivity quoted by the instrument manufacturers seldom (if ever) apply to biochemical samples in aqueous solution.

For carbon-13 spectroscopy, or for that matter any experiment involving broadband decoupling*, there is another type of 'noisy' artefact. The decoupler radiofrequency applied to the protons is periodically phase modulated and some spurious modulation is transmitted to the carbon-13 free induction decay. This appears in the spectrum as weak *cycling sidebands*. Under certain conditions the proliferation of these weak sidebands resembles true noise and degrades the spectrometer sensitivity.

It might seem rather surprising that the receiver bandwidth B dropped out of the expression for sensitivity, since it appears in the corresponding expression for a slow-passage continuous-wave spectrometer. In the Fourier transform experiment, the equivalent of the last stage of bandwidth reduction is the sensitivity enhancement weighting function applied to the free induction decay. In the present calculation it has been assumed that this weighting function is an exponential of time constant T_2^*. Hence the counterpart of the receiver bandwidth parameter is the factor $(T_2^*)^{1/2}$ which affects the noise level.

The factor $\sin \alpha$ has been deliberately left until last. For a single isolated pulse acting on a spin system at thermal equilibrium the condition $\alpha = 90°$ obviously gives the maximum detected signal, and for this setting, small deviations in the intensity of the B_1 field over the sample have little effect. Many applications of NMR, however, require that the sensitivity be improved by repetitive excitation, and steady-state effects must be considered. Usually it is the Z component of magnetization which exhibits appreciable steady-state effects*, and the effects of transverse magnetization can be disregarded. Then the optimum flip angle is the 'Ernst angle' α given by $\cos \alpha = \exp(-T/T_1)$, where T is the interval between pulses.

THE PRACTICAL MEASUREMENT OF SIGNAL-TO-NOISE RATIOS

The difficulty lies in measuring the noise level. First, a section of baseline must be selected which does not contain artefacts that might be mistaken for noise, such as weak spinning sidebands. If the noise is to be measured from a chart recording, the gain must be increased by a suitable known factor until the level of noise is sufficiently high.

The next step is to select a section of noise containing 100 zero crossings and to measure the peak-to-peak noise in this section; this is taken to be 5.0 times the root-mean-square noise voltage. For spectra that have been properly digitized and stored in the computer, a better method is to calculate the root-mean-square noise directly by means of a suitable computer routine. The 'signal-to-noise ratio' is then the peak signal height divided by *twice* the r.m.s. noise.

Finally, an important caveat. Strictly the term 'sensitivity' is defined in terms of the minimum concentration of test material required to produce a signal that is just detectable above the level of the noise. For most purposes, 'sensitivity' and 'signal-

to-noise ratio' may be used interchangeably, but only when all spectrometer operations are *linear.*

REFERENCES

1. R. S. Codrington, H. D. W. Hill and R. Freeman, Varian Research Report, Number 105 (1974).
2. H. D. W. Hill and R. E. Richards, *J. Phys. E: Sci. Instrum.* **1**, 977 (1968).
3. R. R. Ernst, *Adv. Magn. Reson.* **2**, 1 (1966).
4. D. I. Hoult and R. E. Richards, *Proc. R. Soc. A* **344**, 311 (1975).
5. P. Styles, N. F. Soffe, C. A. Scott, D. A. Cragg, F. Row, D. J. White and P. C. J. White, *J. Magn. Reson.* **60**, 397 (1984).
6. W. A. Anderson, W. W. Brey, A. L. Brooke. B. Cole, K. A. Delin, J. F. Fuks, H. D. W. Hill, M. E. Johanson, V. Y. Kotsubo, R. Nast, R. S. Withers and W. H.Wong, *Bull. Magn. Reson.* **17**, 98 (1995).
7. D. I. Hoult, *Prog. NMR Spectrosc.* **12**, 41 (1978).

Cross-references

Broadband decoupling
Digitization
Sensitivity enhancement
Solvent suppression
Steady-state effects

Sensitivity Enhancement

The sensitivity* of a particular NMR spectrometer is measured by the minimum amount of material needed to give a detectable signal. Provided that the system is linear, sensitivity is directly related to the signal-to-noise ratio. This section examines methods for enhancing this important parameter, assuming that all the normal precautions have already been taken to optimize the instrumental conditions. Enhancement techniques can be broken down into three categories – methods that increase the signal strength, those that reduce the noise level, and those that separate the two by some kind of data processing technique (1).

SIGNAL ENHANCEMENT

It is not always necessary to work with the equilibrium nuclear magnetization M_0. Prepolarization in a more intense magnetic field is one possibility, and this has been exploited for NMR spectroscopy in the Earth's magnetic field. Enhancement through the electron–nuclear Overhauser effect* is a second approach, promising improvements as high as two or three orders of magnitude for proton NMR. However, because of the practical difficulties imposed by the need for both microwave and radiofrequency irradiation, and the complications introduced by the addition of a paramagnetic reagent to the sample, this method has had little impact on high-resolution methodology. This leaves the much more modest enhancements achievable through the nuclear–nuclear Overhauser effect, essentially a routine technique for carbon-13 spectroscopy, where the maximum enhancement is a factor of three. The price paid for this improvement is a lack of uniformity in the relative signal intensities, attributable to variations in the Overhauser effect from one chemical site to another; this renders quantitative work unreliable.

Polarization transfer* offers an alternative that, unlike the Overhauser effect, is not based on a particular relaxation mechanism, and is therefore more generally applicable. In its simple form, the INEPT technique (2) offers an enhancement of γ_I/γ_S, where I is the source nucleus and S is the low-sensitivity species. This is already higher than the corresponding nuclear Overhauser enhancement, and it is further augmented if the I spins have a faster rate of spin–lattice relaxation, permitting more rapid recycling during signal accumulation. Coherence transfer through the Hartmann–Hahn experiment* affords a similar level of enhancement, albeit by a quite different mechanism (3). When the I spins are protons, their high

detection efficiency can be exploited in a 'round-trip' transfer of polarization of the type $I \rightarrow S \rightarrow I$, a procedure first introduced by Bodenhausen and Ruben (4) and now known as heteronuclear single-quantum correlation (HSQC). Together with the closely related coherence transfer experiment known as heteronuclear multiple-quantum correlation (HMQC), this technique has been widely applied to the proton spectroscopy of biomolecules (5,6). Considerable success has been achieved in simplifying two-dimensional proton spectra of proteins by isotopic enrichment in carbon-13 or nitrogen-15 based on round-trip polarization or coherence transfer.

Unusually high Boltzmann populations can be engineered in some rather special cases. Probably the most common is chemically induced nuclear polarization* (CIDNP) where a spin sorting process takes place during a free radical recombination reaction leading to enormously enhanced absorption or emission lines, albeit from species that are actually in rather low concentrations (7,8). Parahydrogen is another unique example. According to Fermi–Dirac statistics, the wavefunction of molecular hydrogen must be antisymmetric with respect to interchange of the two hydrogen atoms. There are thus two forms, orthohydrogen which has symmetrical spin states and odd rotational states, and parahydrogen which has antisymmetrical spin states and even rotational states. The latter form is the more stable at very low temperatures. When cooled in liquid nitrogen in the presence of charcoal, ordinary hydrogen gas largely converts into parahydrogen, in which only the $\alpha\beta$ and $\beta\alpha$ energy levels are populated while the $\alpha\alpha$ and $\beta\beta$ levels are empty. Although there is no enhanced NMR signal from parahydrogen itself, when it adds across a double or triple bond and the symmetry is thereby broken, very intense antiphase doublets are observed at the two sites, persisting until normal populations are restored by spin–lattice relaxation. This has been called the PASADENA technique (9). Optical pumping is another specialized technique for obtaining a high nuclear polarization. Laser pumping of rubidium vapour mixed with xenon gas creates spin populations for xenon-129 nuclei that are several orders of magnitude higher than those at Boltzmann equilibrium (10). Pines and co-workers (11) have exploited this effect to induce Hartmann–Hahn cross-polarization to protons on the surface of a polytriarylcarbinol polymer and has used this as a technique for studying surface properties by NMR.

NOISE REDUCTION

If the NMR spectrometer is properly designed, the dominant source of noise is the thermal agitation of the electrons in the wire of the receiver coil; later amplifiers should only contribute negligible amounts of noise. Since the NMR signal is inherently weak, it will always be in competition with this thermal noise, just as a radar set, working at extreme range, loses weak radar reflections in the background noise. Although high-resolution liquid-phase spectroscopy requires the sample to be at or near room temperature, it is possible to reduce the thermal noise by cooling the receiver coil (12). This entails thermally shielding the coil from the sample,

with the concomitant loss of filling factor. In principle the reduction in noise is proportional to the square root of the temperature ratio, suggesting an improvement of 8.4 for a reduction from 298 K to 4.2 K.

In fact there is another important factor at play here, because cooling decreases the series resistance of the coil, thereby increasing the quality factor Q which determines the signal-to-noise ratio. The technique has received a welcome boost in recent years by the discovery of high-temperature superconductors. Although the coil resistance is not zero for radiofrequencies, it is greatly reduced, leading to loaded Q factors of the order of 10 000 at 25 K. Liquid helium is presently used as the coolant, but we can anticipate that one day liquid nitrogen will suffice. To prevent additional noise being contributed by the preamplifier, it is usual to cool this in liquid nitrogen. At the time of writing, signal-to-noise enhancements of about five have been obtained in practice (13). The main drawback appears to be the reduction in Q factor when aqueous samples are used, particularly if ions are present.

NMR signals can be obscured by noise-like phenomena that are not strictly random and do not originate in the thermal noise from the receiver coil. One such artefact is 'digitization noise', which arises when the analogue-to-digital converter (ADC) has insufficient dynamic range. Conversion of the signal to digital form necessarily involves errors of the order of the least-significant bit of the ADC and the Fourier transform of these errors is called digitization noise (see Digitization*). The usual remedy is solvent suppression* to ensure that the incoming free induction signal does not contain extremely strong and extremely weak signals at the same time.

Another noise-like artefact that is widely observed in two-dimensional spectroscopy is 't_1 noise', caused by medium-term spectrometer instabilities that induce a noisy modulation, most easily seen on very intense signals. Even coherent modulation effects contribute to t_1 noise when the sampling occurs at irregular times. The remedy is to replace difference methods and phase cycling by pulsed field gradient methods, where medium-term instabilities are not important (14). Alternatively, reference deconvolution (15) may be used to correct these perturbations by monitoring their effects on a singlet reference line.

DISCRIMINATION BETWEEN SIGNALS AND NOISE

The signal-to-noise ratio can be improved if we can find some characteristic property that distinguishes true signal from random noise. Often the noise is fluctuating faster than the NMR signal – its Fourier spectrum contains high-frequency components. This is the case if the acquisition time is too long and we accept the noise in the tail of the free induction decay. This problem is routinely solved by applying a 'sensitivity enhancement function' that multiplies the raw free induction signal with a decaying function (often an exponential), thus de-emphasizing the noisy tail. If this imposed weighting function is too severe, the

NMR signal is broadened and eventually the signal-to-noise ratio is degraded, because the signal height is more strongly affected than the noise. The optimum condition is known as the matched filter, where the sensitivity enhancement function decays at the same rate as the incoming NMR signal. A matched filter broadens a Lorentzian line by a factor 2, and a Gaussian line by a factor $2^{1/2}$. In two-dimensional spectroscopy a Gaussian lineshape is probably preferable to a Lorentzian because the intensity contours are then circles or ellipses rather than a four-pointed star shape.

Multiplication by a decaying exponential in the time domain is equivalent to convolution* with a Lorentzian in the frequency domain (the two functions form a Fourier transform pair). Then we can think of the process as smoothing out the noise. Usually sensitivity enhancement is carried out in the time domain but there are occasions where frequency-domain convolution is more convenient. As we are normally dealing with digitized data, one very simple operation is the 1:2:1 convolution function, which is very fast, and can be repeated several times, approaching a Gaussian convolution in the limit of many passes.

A second, more fundamental property of noise that distinguishes it from the NMR signal, is its random character. If a free induction decay is recorded a second time, then at any chosen point the signal reproduces itself, whereas the noise fluctuates in amplitude and perhaps in polarity. Summation of successive measurements accumulates the signal components linearly as the number N of scans, whereas noise grows only as $N^{1/2}$ (16). It is important to remember that this time-averaging* method only works properly if the noise is truly random; coherent fluctuations are not averaged out. Because the signal-to-noise enhancement depends on the square root of the number of scans it offers diminishing returns; signal accumulation over an entire weekend only doubles the signal-to-noise compared with an overnight run.

LIMITED SAMPLES

There are many chemical applications where the total quantity of material is strictly limited, for example liquid chromatography, capillary electrophoresis, and a host of biological applications. Then the use of microcells can be essential. Nanogram quantities of proton samples can be studied in a small tube in a specially constructed high-resolution magic-angle spinning probe (17). Discontinuities in magnetic susceptibility between the sample and its container are averaged by spinning at this particular inclination to the applied field. Alternatively, Olson *et al.* (18) have used a tiny non-spinning capillary sample (77 μm inside diameter, 1 mm long) inside a very small radiofrequency coil. The problem created by differences of magnetic susceptibility was circumvented by surrounding the capillary tube and coil with a perfluorinated organic liquid of matched susceptibility. A sensitivity enhancement of about 30 is claimed with respect to the same weight of sample studied in a conventional 5 mm sample tube.

REFERENCES

1. R. R. Ernst, *Advances in Magnetic Resonance*, ed. J. S. Waugh. Academic Press: New York, Vol. 2, 1966.
2. G. A. Morris and R. Freeman, *J. Am. Chem. Soc.* **101**, 760 (1979).
3. S. R. Hartmann and E. L. Hahn, *Phys. Rev.* **128**, 2042 (1962).
4. G. Bodenhausen and D. J. Ruben, *Chem. Phys. Lett.* **69**, 185 (1980).
5. A. Bax, M. Ikura, L. E. Kay, D. E. Torchia and R. Tschudin, *J. Magn. Reson.* **86**, 304 (1990).
6. A. Bax, R. H. Griffey and B. L. Hawkins, *J. Am. Chem. Soc.* **105**, 7188 (1983).
7. G. L. Closs, *J. Am. Chem. Soc.* **91**, 4552 (1969).
8. R. Kaptein and L. J. Oosterhoff, *Chem. Phys. Lett.* **4**, 195, 214 (1969).
9. C. R. Bowers and D. P. Weitekamp, *Phys. Rev. Lett.* **57**, 2645 (1986).
10. N. D. Bhaskar, W. Happer and T. McClelland, *Phys. Rev. Lett.* **49**, 25 (1982).
11. H. W. Long, H. C. Gaede, J. Shore, L. Reven, C. R. Bowers, J. Kritzenberger, T. Pietrass, A. Pines, P. Tang and J. A. Reimer, *J. Am. Chem. Soc.* **115**, 8491 (1993).
12. P. Styles, N. F. Soffe, C. A. Scott, D. A. Cragg, F. Row, D. J. White and P. C. J. White, *J. Magn. Reson.* **60**, 397 (1984).
13. W. A. Anderson, W. W. Brey, A. L. Brooke, B. Cole, K. A. Delin, J. F. Fuks, H. D. W. Hill, M. E. Johanson, V. Y. Kotsubo, R. Nast, R. S. Withers and W. H. Wong, *Bull. Magn. Reson.* **17**, 98 (1995).
14. R. E. Hurd, *J. Magn. Reson.* **87**, 472 (1990).
15. A. Gibbs, G. A. Morris, A. G. Swanson and D. Cowburn, *J. Magn. Reson. A* **101**, 351 (1993).
16. M. P. Klein and G. W. Barton, *Rev. Sci. Instrum.* **34**, 754 (1963).
17. P. A. Keifer, L. Baltusis, D. M. Rice, A. A. Tymiak and J. N. Shoolery, *J. Magn. Reson. A* **119**, 65 (1996).
18. D. L. Olson, T. L. Peck, A. G. Webb, R. L. Magin and J. V. Sweedler, *Science* **270**, 1967 (1995).

Cross-references

Chemically induced nuclear polarization
Convolution
Digitization
Hartmann–Hahn experiment
Lineshapes in two-dimensional spectra
Nuclear Overhauser effect
Polarization transfer
Sensitivity
Solvent suppression
t_1 noise
Time averaging

Solvent Suppression

One of the main unsolved problems of Fourier transform NMR is its inability to deal properly with signals of high dynamic range, for example dilute aqueous solutions where it may be necessary to study millimolar amounts of solute in the presence of 110 molar water. The use of heavy water is often ruled out because it exchanges with the NH protons of peptides, proteins and nucleic acids.

The intense water signal causes several different problems. One is radiation damping* which can unduly broaden the water line and can interfere with pulse experiments by creating an additional torque on the magnetization (1). Another is the bulk nuclear susceptibility* effect which can cause small frequency shifts and may induce 'false' correlation peaks in two-dimensional spectra (2). A third problem is the introduction of additional weak resonance lines in the spectrum. Unless the receiver system is perfectly linear, there will be spurious harmonics of the solvent frequency and intermodulation distortion (sums and difference frequencies) wherever two or more strong signal components are present at the same time. In two-dimensional spectroscopy, the intense water resonance creates a new problem. In sequences that involve phase cycling, residual spectrometer instabilities create t_1 noise*, a band of noisy artefacts running parallel to the F_1 axis at the level of the water resonance. Pulsed field gradient techniques seek to circumvent this problem by performing the necessary spin manipulations in a single scan so that there are no subtraction errors to generate t_1 noise.

However, the most serious problem of all occurs in the analogue-to-digital converter (ADC). This device has a limited dynamic range, typically 15 bits (see Digitization*). Since no part of the incoming free induction signal may be allowed to overflow the most-significant bit, very weak solvent signals may be smaller than the least-significant bit of the converter. One might imagine that this means that these weak signal components are lost once and for all, but because they are riding on top of the intense solvent signal they survive the digitization process. Unfortunately the ADC necessarily makes a digitization error of the order of the least-significant bit at each sampling operation. The Fourier transform of these digitization errors introduces 'digitization noise' into the spectrum and this obscures the weak solute signals. Although this is not strictly random noise, in practice it resembles noise and is spread throughout the spectrum.

This problem has spawned an entire family of remedies aimed at solvent suppression – schemes to reduce the amplitude of the solvent signal while leaving the remainder of the spectrum with as little perturbation as possible. The methods

can be categorized into three main groups: (a) examination of the free induction decay while the solvent signal is passing through a null condition after population inversion; (b) selective presaturation of the solvent resonance; and (c) arranging not to excite the solvent peak.

SOLVENT SIGNAL PASSING THROUGH A NULL CONDITION

This is a modification of the classic inversion-recovery experiment for the measurement of spin–lattice relaxation times (3). Called 'water-eliminated Fourier transformation (WEFT)', it relies on the fact that, of all the components of the sample, water probably has the longest spin–lattice relaxation time. After population inversion of the entire spectrum, the signals of interest are well on their way towards their equilibrium condition when the water is passing through the null point on its recovery curve (4). This occurs at a time $T_1 \ln 2$ where T_1 is the relaxation time of water. The principal advantage of this technique is that it provides one of the best chances for observing solute signals that lie very close to the water frequency. The disadvantage is that relative intensities within the spectrum are distorted by differential relaxation effects. There is a modification of WEFT that employs a frequency-selective population inversion pulse, largely avoiding these intensity distortions, and no longer requiring differential relaxation between water and solute.

An experiment that is conceptually related to WEFT exploits differences in spin–spin relaxation times. A paramagnetic relaxation reagent is added to the solution at low concentration (< 0.2 millimolar). By penetrating the inner hydration sphere of the ion, the reagent relaxes the water protons but has a much weaker influence on the solute molecules. A spin-echo experiment is performed, the final half echo being acquired at a time when the water signal has a greatly diminished amplitude. Suppression ratios of 10^4 are claimed for this method (5). Echo modulation through spin–spin coupling is suppressed by using a high pulse repetition rate. Similar experiments have been performed in which chemical exchange is used to shorten the spin–spin relaxation time, by adding a high concentration (typically 0.5 molar) of ammonium chloride to the solution (6).

PRESATURATION OF THE WATER PEAK

This method has the great advantage of simplicity and is widely used. A soft radiofrequency pulse or a DANTE sequence is used to cause a high level of saturation of the water resonance, and then a hard 90° pulse is applied to elicit the free induction decay. In addition to true saturation, the mechanism may involve dispersal of isochromats in the spatially inhomogeneous radiofrequency (B_1) field, and it may be advantageous to shift the phase of B_1 during the preirradiation so as

to spread these isochromatic vectors in three spatial dimensions rather than two. High suppression ratios can be achieved through presaturation, but it is impossible to avoid some collateral saturation of neighbouring resonances. Since the water resonance is inhomogeneously broadened, it does not necessarily saturate uniformly across the line profile, leaving some baseline distortions. This problem can be alleviated by making small changes in the irradiation frequency.

One practical disadvantage of presaturation, particularly important if the duration of the saturating pulse is long, is the possibility of intensity distortions in the remainder of the spectrum through cross-relaxation or chemical exchange with other proton sites.

AVOIDING EXCITATION OF THE SOLVENT PEAK

Soft radiofrequency pulses can be designed to avoid excitation of the solvent peak and yet give a reasonably undistorted version of the rest of the spectrum. The idea was pioneered by Alexander (7) and refined by Redfield *et al.* (8) who designed a composite sandwich of five pulses of constant amplitude and relative widths $2\ \bar{1}\ 4\ \bar{1}\ 2$, where the overbars indicate inversion of the radiofrequency phase. This can be thought of as a single long pulse of duration τ and amplitude B_1, superimposed on a negative-going pulse pair with separation $\tau/2$ and amplitude $2B_1$. It generates a null in the excitation spectrum at about $0.97/\tau$ Hz. A relatively broad null is achieved by arranging that the first derivative with respect to resonance offset is also near a null condition. In practice the relative widths of the pulses are finely adjusted for the best solvent suppression; two orders of magnitude suppression is readily achieved. The phase shifts introduced into the spectrum follow a quite complicated function of offset, partially corrected by a computer-controlled correction scheme.

Plateau and Guéron (9) introduced the 'jump-and-return' sequence in which a hard 90°(+X) pulse is followed by a second hard 90°(–X) pulse after an interval τ for free precession. The transmitter frequency is set on resonance for the water peak, so the water signal undergoes no precession and is returned to the +Z axis, but all other signals in the spectrum are excited to some degree. They can be recorded in the pure absorption mode, but signals upfield from water have the opposite sign to downfield signals. The method has the advantage of simplicity but suffers from the fact that the null is rather too sharp for effective suppression of the rather broad water peak. It was soon realized that the jump-and-return sequence was the first member of an entire family of binomial pulse sequences; if it is written $1:\bar{1}$, then there are sequences $1:\bar{2}:1$ (10) and $1:\bar{3}:3:\bar{1}$ (11,12). These have progressively broader nulls at the water resonance because their Fourier transforms follow $\sin^2(\pi\Delta f\tau)$ and $\sin^3(\pi\Delta f\tau)$ respectively, where Δf (Hz) is the offset from the transmitter frequency. The $1:\bar{3}:3:\bar{1}$ binomial sequence, in particular, is rather insensitive to effects of the spatial inhomogeneity of the B_1 field, and tolerates a

small error in setting the 1:3 ratio of pulse widths (13). The induced phase gradient in the spectrum can be handled by the usual linear frequency-dependent phase correction, but with a 180° discontinuity at the transmitter frequency. Adequate time must be allowed for water spin–lattice relaxation so that no steady-state regime is established for longitudinal magnetization.

Improvements in modern spectrometers allow pulsed field gradients* to be used in a routine fashion, and a more effective version of the soft-pulse excitation scheme, called 'WATERGATE', is now widely used (14). This employs a hard 180° pulse applied at the same time as a soft 180° pulse on the water resonance, sandwiched between two equal field gradient pulses of the same polarity. Transverse magnetization components dispersed by the first gradient pulse are refocused by the combined effect of the hard 180° pulse and the second gradient, except for the water signal, which experiences no refocusing pulse. This offers a high degree of suppression, and can be used as a module for insertion into existing pulse sequences; however, there could be some signal loss through spin–spin relaxation and some modulation due to spin–spin coupling.

The preceding schemes have concentrated on the shape of the rejection notch, paying less attention to the problem of achieving uniform excitation across the rest of the spectrum. Polychromatic pulses (15) provide a solution to both problems. They are made up of a regular 'comb' of soft, rectangular radiofrequency pulse elements covering the entire spectral range under investigation. The intensities of these elements are independently adjustable, but for this application they are uniform, except for a rejection notch at the water frequency, and half-intensity pulses at the extremities of the range. The frequency separation between elements is set at $\Delta f = 1/(2T)$, where T is the soft-pulse duration; this ensures that the peaks of the sinc function oscillations generated by one rectangular pulse fall in the troughs of the sinc function from its neighbour, and largely cancel them. The resulting frequency-domain excitation profile is very uniform and can be tailored if necessary by fine adjustment of the relative intensities, while the induced phase gradient is essentially linear and can be readily corrected. The form of the rejection notch can be reshaped at will, and the degree of suppression can be optimized by fine adjustments of the soft-pulse intensities in this region. Present-day digitally controlled waveform generators can be readily programmed to provide a large array of soft pulses of this kind.

THE ANALOGUE-TO-DIGITAL CONVERTER

All these complex manipulations of the spins might prove unnecessary if the ADC could be designed with a much higher dynamic range. Unfortunately NMR spectroscopy demands faster and faster sampling rates in order to cover wider spectral widths and to satisfy the needs of digital filters. Because the ADC operates by a method of successive approximations, the time required for each conversion

increases in proportion to the number of bits. At the time of writing it seems unlikely that we can have both high dynamic range and very fast sampling.

Another approach is to compress the dynamic range of the incoming NMR signal by some suitable trick. One possibility is to examine only the *change* in signal intensity between one sampling operation and the next (16). The first data point would be stored in a sample-and-hold device and used as a reference to measure the change in voltage for the second sample point, using a differential amplifier. The second ordinate would be used as a reference for the third sample, and so on. With the water resonance set close to the transmitter frequency, and a sufficiently high sampling rate, the differential water signal would be much weaker than the actual signal, and this would allow a much higher gain to be used before imminent overflow of the ADC. Once the free induction decay has been digitized in this differential mode, dynamic range is no longer a problem and the original free induction decay can be reconstructed by adding ordinates cumulatively.

An alternative strategy is to sample the signal appreciably faster than the rate decreed by the Nyquist condition (two samples per period of the highest frequency component). This 'oversampling' technique has been proposed by Delsuc and Lallemand (17) as a method for improving the effective dynamic range of the ADC. For example, with four-fold oversampling we could time average groups of four successive conversions to give a result that still satisfies the Nyquist criterion but which comprises a more faithful record of the weak signal components.

Neither of these methods has gained any general acceptance and we are forced to the conclusion that solvent suppression techniques will be required for some time yet.

REFERENCES

1. N. V. Bloembergen and R. V. Pound, *Phys. Rev.* **95**, 8 (1954).
2. M. H. Levitt, *Concepts Magn. Reson.* **8**, 77 (1996).
3. R. L. Vold, J. S. Waugh, M. P. Klein and D. E. Phelps, *J. Chem. Phys.* **48**, 3831 (1968).
4. S. L. Patt and B. D. Sykes, *J. Chem. Phys.* **56**, 3182 (1972).
5. R. G. Bryant and T. M. Eads, *J. Magn. Reson.* **64**, 312 (1985).
6. D. L. Rabenstein, S. Fan and T. T. Nakashima, *J. Magn. Reson.* **64**, 541 (1985).
7. S. Alexander, *Rev. Sci. Instrum.* **32**, 1066 (1961).
8. A. G. Redfield, S. D. Kunz and E. K. Ralph, *J. Magn. Reson.* **19**, 114 (1975).
9. P. Plateau and M. Guéron, *J. Am. Chem. Soc.* **104**, 7310 (1982).
10. V. Sklenář and Z. Starčuk, *J. Magn. Reson.* **50**, 495 (1982).
11. D. L. Turner, *J. Magn. Reson.* **54**, 146 (1983).
12. P. J. Hore, *J. Magn. Reson.* **54**, 539 (1983).
13. P. J. Hore, *J. Magn. Reson.* **55**, 283 (1983).
14. M. Piotto, V. Saudek and V. Sklenář, *J. Biomed. NMR* **2**, 661 (1992).
15. Ē. Kupče and R. Freeman, *J. Magn. Reson. A* **103**, 358 (1993).
16. S. Davies, C. Bauer, P. Barker and R. Freeman, *J. Magn. Reson.* **64**, 155 (1985).
17. M. A. Delsuc and J. Y. Lallemand, *J. Magn. Reson.* **69**, 504 (1986).

Cross-references

Digitization
Nuclear susceptibility
Pulsed field gradients
Radiation damping
Selective excitation
Spin–lattice relaxation
Spin–spin relaxation
Steady-state effects
t_1 noise

Spin Echoes

When the sample is in an inhomogeneous applied magnetic field B_0, it is convenient to visualize it as a three-dimensional mosaic of small volume elements, each small enough that field gradients across that element can be neglected, but with each element in a slightly different applied field. The macroscopic nuclear magnetization from one such element is called an *isochromat* since it has a fixed precession frequency (provided that diffusion and convection can be neglected). The magnetization from each isochromat may be represented by a small vector, the resultant of all such vectors giving the total macroscopic magnetization M_0. When excited by a strong radiofrequency pulse, all these isochromatic vectors are aligned along the Y axis of the rotating frame* of reference, that is to say they all start their free precession in phase. As they evolve with time they fan out in the XY plane and their resultant decays monotonically, accounting for the decay of the observed free precession signal. For simplicity, this is often represented by the decay constant T_2^* although this should not be confused with a true relaxation time. For smallish molecules in non-viscous media, T_2 will normally be much longer than T_2^* and this will be the situation we consider in what follows.

After a delay of (say) $3T_2^*$ the observed NMR signal has decayed to a negligible level. Yet if it were possible to confine the observation to only a small region of the sample, the spins there would still be precessing in a concerted fashion and there would be a significant macroscopic NMR signal which would persist for a time of the order of the spin–spin relaxation* time T_2. The T_2^* decay is thus a spurious instrumental effect. Hahn (1) was the first to realize that this 'lost' signal could be retrieved in a two-pulse experiment. After the initial free induction signal had disappeared, a second pulse at time τ induced a new response which peaked at time 2τ. By analogy with the reflection of sound waves, this new response was called a 'spin echo'.

Hahn's experiment used a 90° pulse followed by another 90° pulse, but the picture is much clearer in the method devised by Carr and Purcell (2), where the second pulse rotates all vectors by 180°. Consider a simplified case where the array of isochromats is represented by just three vectors a, b, and c, with c the furthest from resonance, and thus the fastest vector in the frame rotating at the transmitter frequency. All three vectors are aligned along the +Y axis by the first 90° pulse (Fig. 1(a)) and after a time τ disperse into a fan of vectors in the XY plane. A 180° pulse about the X axis turns these vectors into mirror image positions with respect to the X axis, so arranged with the fast vectors behind the slow vectors that all move

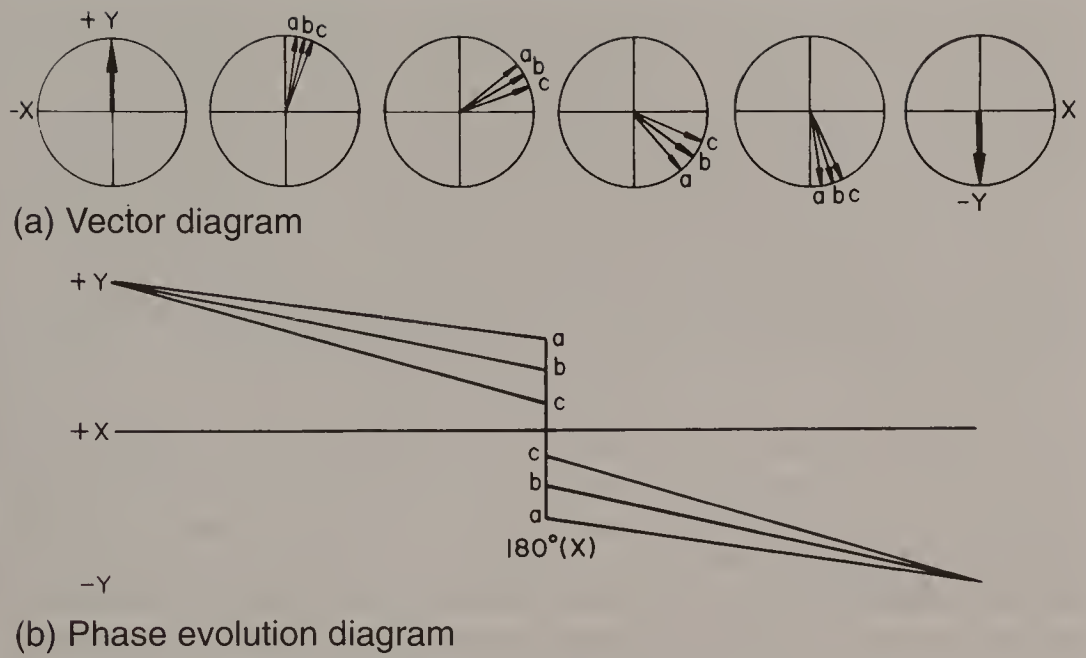

Fig. 1. (a) Vector diagram illustrating the refocusing of isochromats in a spin-echo experiment, together with (b) the corresponding phase evolution diagram.

into coincidence along the –Y axis after a further period τ of free precession. In terms of a 'phase evolution diagram' (Fig. 1(b)) it is clear that the 180° pulse has a refocusing effect.

If the echo peak amplitude is monitored as a function of 2τ in a series of experiments, it is observed to decay with a time constant T_2 which may be much longer than T_2^* for the type of sample we are considering here. In spectra with many lines, Fourier transformation of the echoes allows the individual spin–spin relaxation times to be determined. It is as if the linewidths had been measured in a perfectly uniform applied magnetic field B_0. This, however, presupposes that all isochromats retain the same precession frequency throughout the experiment. In practice, some diffusion across the field gradients occurs. Carr and Purcell showed that this effect could be minimized by keeping 2τ short and by following the time evolution by repeatedly refocusing with 180° pulses, giving a 'train' of spin echoes. Only the diffusion between refocusing pulses matters, and this can be kept to a negligible level. Multiple refocusing introduces the possibility of cumulative errors if the 180° pulses are imperfect, but by applying these pulses about the Y axis rather than the X axis, these errors are compensated for the even-numbered echoes, provided there is no modulation on the echo. This modification, suggested by Meiboom and Gill (3), is widely used in spin-echo work. An alternative is to use a composite 180° pulse (4) designed to be self-compensating.

Spin-echo experiments provide the most direct method of measuring spin–spin relaxation times in the common situation where the natural linewidths are obscured by field inhomogeneity broadening. Figure 2 shows a sketch of a typical spin-echo train.

When a Carr–Purcell spin-echo train with multiple refocusing is used to study the effect of chemical exchange on spin–spin relaxation times, an interesting new phenomenon is observed (5). A chemical exchange 'event' shortens the phase memory of the spins by replacing a precessing spin that has good phase coherence with another spin of random phase. If the exchange rate is fast compared with the rate of application of refocusing pulses, then exchange causes fast decay of the observed echoes. In contrast, if the exchange rate is slow compared with the pulse repetition rate, the probability of an event occurring between refocusing pulses is negligibly small, and the echo delay becomes essentially independent of chemical exchange effects.

Spin echoes can be used to monitor molecular diffusion. Usually, this is carried out by applying a known intense field gradient during one of the τ delays, thus interfering with the refocusing if molecular motion occurs. A variation of this experiment can be used to study concerted flow of the sample along an applied magnetic field gradient. Needless to say, these experiments are carried out on a non-spinning sample. For high-resolution spectroscopy involving spin echoes, a spinning sample is normally used since this provides narrower lines in the observed spectrum and a narrow deuterium signal for field/frequency regulation*. Occasionally, there can be serious interactions between the spinning and spin-echo formation. It may then be necessary to adopt a scheme where the pulse repetition rate is synchronized with the sample spinning rate, or to switch the spinner off altogether.

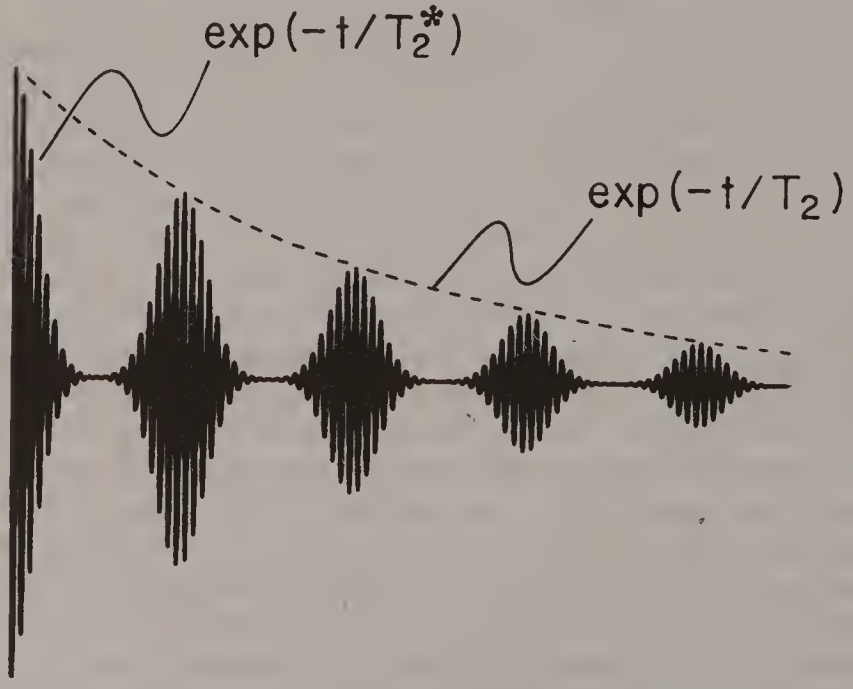

Fig. 2. Simulation of a train of spin echoes showing the rapid signal decay due to instrumental effects (T_2^*) and the slower decay of the echo envelope due to spin–spin relaxation (T_2).

It is possible to engineer gross differences in spin–spin relaxation times of solvent water and dissolved macromolecules by the addition of low concentrations (~0.2 millimolar) of paramagnetic ions. Each ion is surrounded by a hydration sphere which inhibits access by the macromolecules but which is in rapid exchange with bulk water thus shortening its spin–spin relaxation time. This has been made the basis of several techniques for solvent suppression* in which a spin-echo experiment is used to discriminate between water and the slowly relaxing solute.

If we neglect spin–spin relaxation on this time scale, a spin echo is exactly symmetrical with respect to its mid-point. Thus the Fourier transform of an entire spin echo can contain no antisymmetrical components (dispersion-mode signals) but only symmetrical components (absorption-mode).

ECHO MODULATION

In a spin-echo experiment on a homonuclear spin system, chemical shifts have the same effect as an offset from the transmitter frequency, being refocused at the time of the echo. In contrast, spin–spin coupling is not refocused but modulates the echoes at a frequency of $\frac{1}{2}$J Hz (6). (We consider here only the simple case where the coupling is first order.) The echo modulation arises because the 180° refocusing pulse of the spin-echo experiment flips both coupled spins I and S, leaving the coupling term JI_ZS_Z unchanged.

The origin of this J-modulation of the echo is readily visualized on a simple vector picture, taking the case of a two-spin IS system as an example. The I-spin resonance is made up of two lines corresponding to the α and β states of the S spin, and may be represented by two magnetization vectors, f (fast) and s (slow), which have natural precession frequencies in the rotating frame of $\Delta f \pm \frac{1}{2}$J Hz, where Δf is the offset of the I shift from the transmitter frequency. The initial 90° pulse aligns both vectors along the +Y axis (Fig. 3(a)) and they then precess freely, building up a relative phase difference of $2\pi J\tau$ rad by the end of the first interval τ seconds. (At the same time field inhomogeneity spreads out each vector into a fan of isochromats, but since this is reversed in the second τ interval, it may be disregarded for the purposes of this discussion.) At this point the 180° pulse is applied and has two quite distinct effects. First, it rotates f and s into mirror image positions with respect to the Y axis of the rotating frame. Had this been the only effect, f and s would come to an exact focus at time 2τ (Fig. 3(d)). However, the 180° pulse also flips the S spin, interchanging the α and β spin states and thus interchanging the labels f and s in the diagram. Now f is further from the transmitter and precesses faster than s in the first τ interval, but becomes the slower vector in the second τ interval. The divergence between the two vectors does not therefore cancel but is cumulative, building up into a phase difference $4\pi J\tau$ rad at the time of the echo (Fig. 3(f)). The echo is thus made up of two components. If the experiment is repeated for a series of different settings of 2τ, or if an echo train is generated by multiple refocusing, the echo peaks are observed to be amplitude modulated according to $M_0 \cos(\pi Jt) \exp(-t/T_2)$.

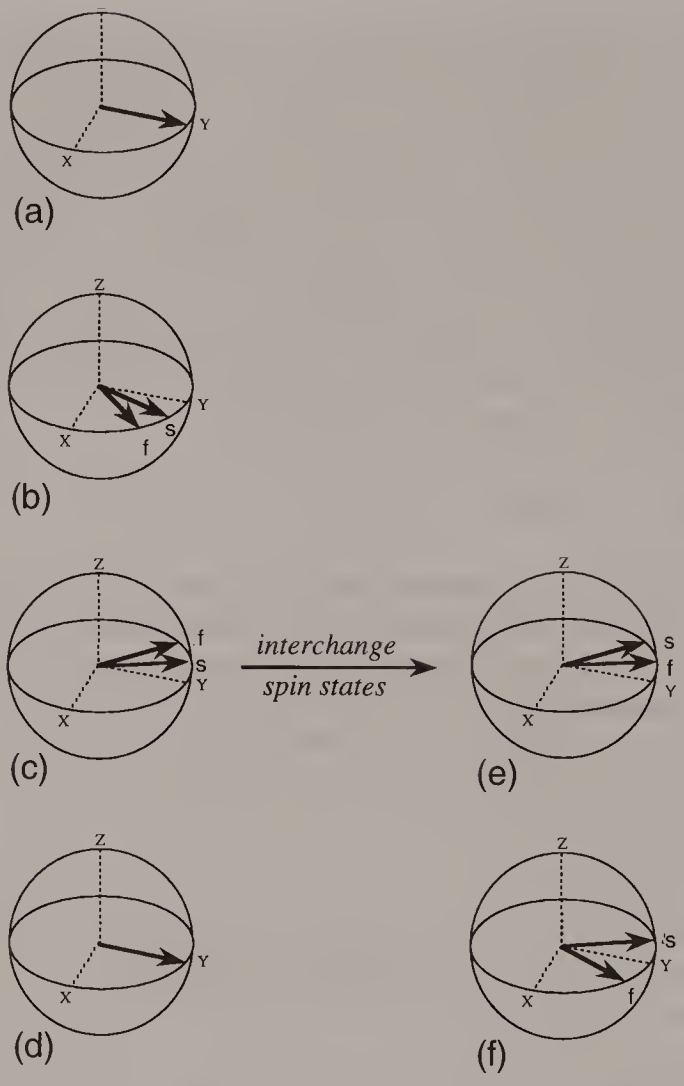

Fig. 3. Vector diagram illustrating the origin of echo modulation. In the sequence (a)–(b)–(c)–(d), both chemical shift and spin coupling effects are refocused and there is no echo modulation. By contrast, in the sequence (a)–(b)–(c)–(e)–(f), where the spin-state labels (f and s) are interchanged, the two vectors continue to diverge owing to spin coupling and the echo therefore carries J-modulation.

Inversion of *both* coupled spins is thus the key to echo modulation. For a heteronuclear spin system, the I-spin echoes are not normally modulated by the coupling J_{IS}, and it is only if another 180° pulse is deliberately applied to the S spins that the modulation is observed. In homonuclear spin systems the 180° is normally non-selective and affects both the I and the S spins, generating modulated echoes, but if the 180° pulse is made frequency selective so that it flips the I spins without influencing the S spins, then the I-spin echoes remain unmodulated. More complicated rules apply in the case of strong coupling or situations where the second pulse is not exactly 180°. For very high pulse repetition rates (comparable

with chemical shift differences) the echo modulation disappears. This can be important when using spin echoes to suppress broad lines in a J-coupled spectrum.

Echo modulation can be exploited for all kinds of applications in high-resolution spectroscopy. Suppose we are interested in detecting the weak satellites which appear in proton spectra owing to the presence of low-abundance carbon-13 or nitrogen-15 spins. Under normal circumstances, these weak signals are swamped by the much larger proton signals from molecules containing carbon-12 or nitrogen-14 spins. If a spin-echo experiment is performed on the proton system, using a relatively short timing interval 2τ, the Fourier transform of the second part of the echo has the same form as the Fourier transform of the free induction decay*; there is only a small loss of intensity due to spin–spin relaxation. By contrast, if the same experiment is repeated with a 180° pulse applied to carbon-13 (or nitrogen-15) simultaneous with the proton 180° refocusing pulse, then the proton echo is changed in amplitude by a factor $\cos(2\pi J_{IS}\tau)$, where J_{IS} is the coupling constant to the heteronucleus. By setting $\tau = 1/(2J_{IS})$ the echo is simply inverted. Difference spectroscopy* then eliminates the 'parent' proton spectrum, leaving only the satellites (7). Suppression ratios can be quite high, particularly for the nitrogen-15 experiment because the protons on nitrogen-14 are preferentially broadened, giving a cleaner difference spectrum. Related techniques are used for multiplicity determination* in carbon-13 spectroscopy; the form of the echo modulation for the various groups (methine, methylene and methyl) is shown in Fig. 4.

In the general case where several spin–spin couplings are involved, the corresponding echo modulation can be quite complicated and then it proves convenient to analyse it by Fourier transformation. This is J-spectroscopy*. A

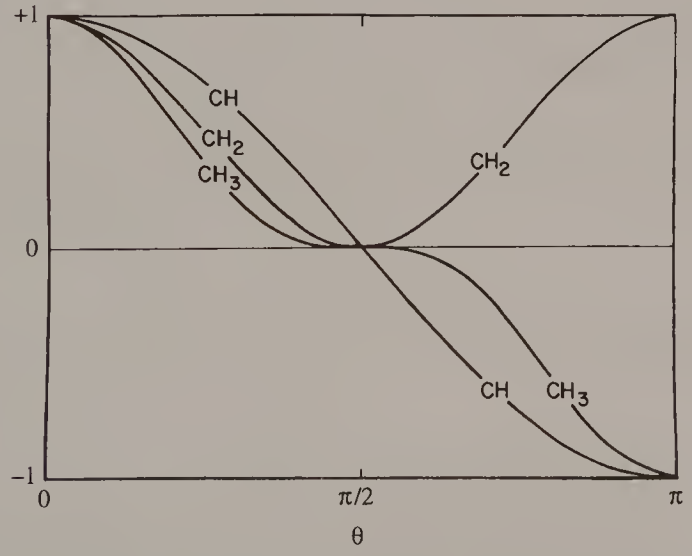

Fig. 4. Echo-modulation patterns for CH, CH_2 and CH_3 groups as a function of $\theta = 2\pi J_{CH}\tau$. This can be used as a technique for 'editing' carbon-13 spectra. Quaternary sites have such small CH couplings as to give virtually no modulation on this time scale.

J-spectrum may be thought of as a conventional high-resolution spectrum that has been collapsed by removing all chemical shift effects, leaving only J-couplings.

REFERENCES

1. E. L. Hahn, *Phys. Rev.* **80**, 580 (1950).
2. H. Y. Carr and E. M. Purcell, *Phys. Rev.* **94**, 630 (1954).
3. S. Meiboom and D. Gill, *Rev. Sci. Instrum.* **29**, 688 (1958).
4. M. H. Levitt and R. Freeman, *J. Magn. Reson.* **43**, 65 (1981).
5. Z. Luz and S. Meiboom, *J. Chem. Phys.* **39**, 366 (1963).
6. E. L. Hahn and D. E. Maxwell, *Phys. Rev.* **84**, 1246 (1951).
7. R. Freeman, T. H. Mareci and G. A. Morris, *J. Magn. Reson.* **42**, 341 (1981).

Cross-references

Chemical exchange
Composite pulses
Difference spectroscopy
Field/frequency regulation
Free induction decay
J-spectroscopy
Multiplicity determination
Rotating frame
Solvent suppression
Spin–spin relaxation
Two-dimensional spectroscopy

Spin–Lattice Relaxation

Suppose it were possible to drop the NMR sample into the probe instantaneously and then to apply an excitation pulse immediately. Would we observe an NMR signal? The simple answer is no. The nuclear polarization would be negligibly small in such an experiment for the nuclei were only polarized in the very weak Earth's field, giving a negligible population difference between the lower and upper energy levels. When the field is suddenly changed to the intense field B_0 of the spectrometer, the process of building up the appropriate Boltzmann population distribution can be quite slow. Initially, the nuclear spins are 'hot' (essentially equal populations in both states) and they cool down by transferring some magnetic energy to their surroundings, a process called relaxation. If we were to plot the variation of the population difference (Z magnetization) as a function of time, we would find an exponential curve starting near zero and rising asymptotically towards the Boltzmann equilibrium condition. It would have a time constant T_1, the spin–lattice relaxation time. 'Lattice' here is used as a general term for the nuclear environment, dating from the early theories of spin–lattice relaxation which were all concerned with the solid state.

In practice, the high-resolution NMR spectroscopist is seldom concerned with the delay which ensues after the insertion of the sample and before the detection of the first free induction signal (although this is a problem for studies on nuclei like silicon-29 in solids). Spin–lattice relaxation is involved in a much more fundamental way. The Boltzmann equilibrium nuclear magnetization is usually represented by M_0. Any deviation of the actual longitudinal magnetization M_Z away from its equilibrium value M_0 is followed by an exponential recovery according to the equation

$$(M_Z - M_0)_t = (M_Z - M_0)_0 \exp(-t/T_1). \qquad [1]$$

This expression is simply derived from one of the Bloch equations in the rotating frame, and in the absence of any B_1 field

$$dM_Z/dt = -(M_Z - M_0)/T_1, \qquad [2]$$

which defines T_1 phenomenologically as a *longitudinal* relaxation time.

In continuous-wave spectroscopy, irradiation with too high a level of the radiofrequency field B_1 causes 'saturation' of the spins by pumping them from a lower to an upper level at a rate so fast that spin–lattice relaxation cannot compete effectively. The detected signal M_Y becomes weak and may disappear in the limit.

This is reflected in the expression for the steady-state solution of the Bloch equations

$$M_Y = M_0\gamma B_1 T_2/[1 + (\Delta\omega T_2)^2 + \gamma^2 B_1^2 T_1 T_2]. \quad [3]$$

At exact resonance ($\Delta\omega = 0$) this expression shows that M_Y increases with B_1 provided that $\gamma^2 B_1^2 T_1 T_2 < 1$, reaches a maximum where this term is unity and then decreases when $\gamma^2 B_1^2 T_1 T_2 > 1$. This saturation behaviour is given a geometrical interpretation in the section on Continuous-wave spectroscopy*. Since the wings of the line profile saturate less readily than the peak, saturation also broadens the line in a slow-passage continuous-wave spectrum.

A process equivalent to saturation can occur in pulsed NMR if a train of pulses is applied. Suppose that perfect 90° pulses are employed, converting M_Z into M_Y, which corresponds to an equalization of the spin populations of the two energy levels, that is to say saturation. If the interval between pulses is comparable with the spin–lattice relaxation time T_1, then the recovery of M_Z towards M_0 is incomplete. A steady-state* regime is set up where the observed signal amplitude M_Y is a function of T_1:

$$M_Y = M_0[1 - \exp(-t/T_1)]. \quad [4]$$

This is an important consideration when setting up a pulsed NMR experiment for optimum sensitivity. There are two schools of thought. One advocates the use of 90° pulses with suitable delays (t_d) after signal acquisition (t_a) so that the pulse interval ($t_d + t_a$) allows adequate spin–lattice relaxation. The recommended ratio is $(t_d + t_a) \simeq 1.3\ T_1$ (1). The second school sets $t_d = 0$ and balances the effects of saturation by reducing the flip angle α of the pulses. Provided that there is no transverse magnetization just before the pulse (a difficult condition to fulfil in practice) the optimum flip angle can be shown to be given by

$$\cos \alpha_{OPT} = \exp(-t_a/T_1) \quad [5]$$

where t_a is now the interval between pulses (2).

These relaxation phenomena can also be used to measure spin–lattice relaxation times by monitoring the recovery of the Z magnetization after a suitable perturbation, using eqn [1]. Through Fourier transformation this permits the determination of the T_1 values of individual lines in spectra of many resonances. These *inversion-recovery*, *saturation-recovery* and *progressive saturation* techniques are examined in detail in a later section.

MECHANISMS FOR SPIN–LATTICE RELAXATION

Nuclei are almost completely isolated from the violent rotations of the molecular framework. Just like gyroscopes mounted on perfectly frictionless bearings, they align themselves with the direction of the magnetic field whatever the orientation of the molecule. They cannot exchange their magnetic energy with their

surroundings by direct mechanical coupling but only indirectly, by magnetic dipole or electric quadrupole interactions. For nuclei with $I = \frac{1}{2}$ the only interactions with the lattice are magnetic in origin. Transfer of energy from the spins to the lattice requires that there be a magnetic field at the nucleus fluctuating at the Larmor precession frequency in order to induce an NMR transition. This field originates from magnetic dipoles, and since the frequency spectrum of these motions is very wide, the component actually in tune with the Larmor frequency is very weak. This is why NMR spin–lattice relaxation is a slow process compared with the rates at which populations come to equilibrium in, say, infrared or optical spectroscopy.

Compared with the frequencies of molecular motion in a liquid (translation, rotation and vibration), nuclear precession frequencies are slow, so it is only the slowest molecular motions (rotation) that are even approximately matched to the Larmor frequency. The distribution function or *spectral density* function for reorientational motion is not known in detail, but it is usually taken to be a

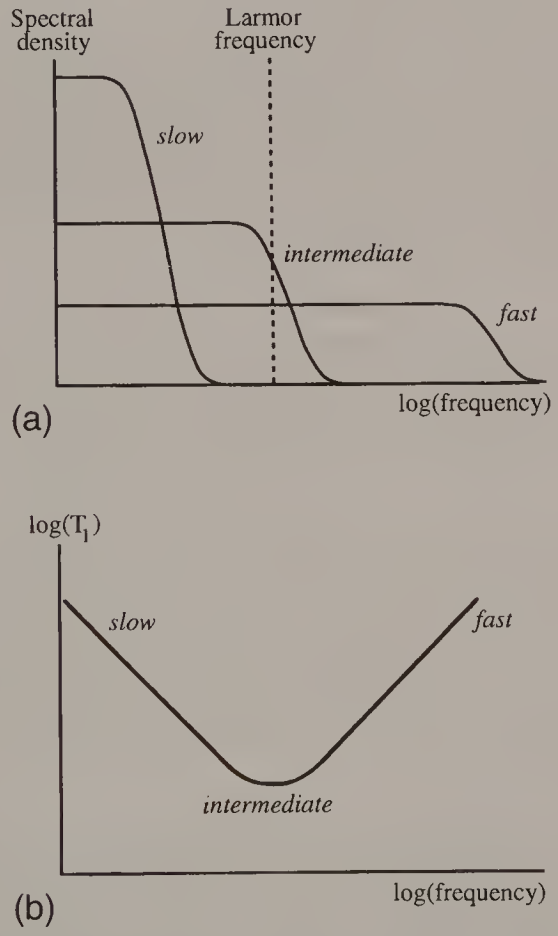

Fig. 1. Spectral density functions for slow, intermediate and fast molecular reorientation (the curves are Lorentzian, distorted by the logarithmic frequency scale). Molecular motion at an intermediate rate generates the largest component at the Larmor frequency, giving a minimum in the curve of T_1 against frequency (lower graph).

Lorentzian function of frequency, since the time-domain correlation function is assumed to be exponential. It is customary to plot the spectral density function on a logarithmic frequency scale, giving it the appearance of a rather flat curve which falls off as it approaches the critical frequency $1/\tau_c$, where τ_c is the *correlation time* for reorientation. Inertial and viscosity effects tend to determine τ_c.

Figure 1(a) sketches typical spectral density functions for fast, intermediate and slow molecular tumbling, the area under these curves remaining constant. In the fast limit the component at the Larmor frequency is small, but increases as the molecular reorientation rate is slowed down. Most small organic molecules in non-viscous solvents are in this category. This means that any factor which slows the molecular motion shortens the spin–lattice relaxation time. A minimum is reached near the condition sketched for intermediate molecular tumbling rates, and any further slowing of the motion reduces the component at the Larmor frequency and therefore increases the relaxation time (Fig. 1(b)). Large biological molecules fall into this category. For high-resolution NMR spectroscopy, a short T_1 favours sensitivity but too short a T_1 begins to broaden the lines and degrades resolution (since T_2 cannot be longer than T_1).

There are three principal types of magnetic interaction which contribute to spin–lattice relaxation of $I = \frac{1}{2}$ nuclei. The most important is the *dipole–dipole interaction*, where the nucleus experiences a fluctuating field due to the motion of neighbouring magnetic dipoles (unpaired electrons or other nuclei). The field due to a dipole of strength μ at a distance r and subtending an angle θ with respect to the B_0 direction is given by the simple formula

$$B_{DD} = \pm(\mu_0/4\pi)\mu(3\cos^2\theta - 1)/r^3. \qquad [6]$$

(The term $(\mu_0/4\pi)$ is the conversion factor for SI units.) The sign of this field depends on the orientation of the dipole (with or against the magnetic field). Unpaired electrons have much stronger magnetic dipoles than nuclei, and samples intended for high-resolution work usually exclude paramagnetic transition metal compounds, free radicals and triplet molecules in order to avoid excessive spin–lattice relaxation. Even paramagnetic oxygen gas dissolved in the solvent can have a significant effect on long spin–lattice relaxation times (of the order of 1–10 seconds) and is usually removed by several freeze–pump–thaw cycles for very high-resolution work or for determinations of long spin–lattice relaxation times. The remaining dipolar fields originate from other nuclear spins in the immediate environment and can therefore provide information about molecular structure or molecular motion.

A second type of magnetic interaction arises because the chemical shielding of the nucleus depends on the orientation of the molecule with respect to the B_0 field direction. It is therefore known as the *chemical shift anisotropy* mechanism. Shielding can be represented as a weak secondary magnetic field set up when the electrons surrounding the nucleus precess in the applied field B_0. This field is thus proportional to B_0 and fluctuates as the molecule tumbles. For protons, which have small chemical shifts, this relaxation mechanism is not important, but it is often

significant for nuclei with large chemical shift ranges, for example flourine-19, carbon-13 and many metals. Since the relaxation rate depends on the square of the appropriate field at the nucleus, the rate of spin–lattice relaxation by chemical shift anisotropy increases as the square of the applied field strength B_0. There is an ingenious test for this mechanism if the spin–lattice relaxation time is sufficiently long – the sample is temporarily removed from the B_0 field during an inversion recovery experiment, thus eliminating the shift anisotropy effect for this period (3). Relaxation by chemical shift anisotropy becomes relatively more important as spectrometers are constructed at higher and higher fields. It may then dominate all other mechanisms and there is some concern that this may set an upper limit on the resolving power and sensitivity of phosphorus-31 spectroscopy at high fields by broadening the lines faster than the increase in chemical shifts.

The third mechanism is known as *spin–rotation interaction*. As a molecule rotates, the moving charges of electrons and nuclei create small electric currents which in turn induce a small magnetic field at the nucleus. Although the charges of electrons and nuclei balance, the resulting fields do not quite cancel because in general the 'centre of gravity' of the electron charge does not coincide with that of the corresponding nucleus. This leaves a net field at the nucleus which fluctuates because the reorientational motion is not uniform but proceeds by a series of random jumps. This mechanism increases in effectiveness as the tumbling motion speeds up, so that, unlike the dipolar mechanism, spin–rotational relaxation is more effective for small molecules in low-viscosity solutions at high temperature. This opposite temperature dependence may be used to distinguish the two mechanisms.

A fourth, extremely rare, relaxation mechanism relies on the weak magnetic field induced at the site of a spin I by spin–spin coupling J_{IS} to a neighbouring spin S. This is only an effective relaxation mechanism if the induced field is rapidly fluctuating because S is a rapidly relaxing quadrupolar nucleus, and also has a Larmor frequency very close to the Larmor frequency of nucleus I. This occurs for carbon-13 coupled to bromine-81, which has such a broad resonance that its tail overlaps the carbon-13 resonance (4).

If the nucleus possesses a quadrupole moment there is a much more effective mechanism coupling the spin to the motions of the environment. The distribution of the nuclear charge is no longer spherical, but is of the form of an ellipsoid, and this can interact strongly with an electrostatic field gradient. Most chemical bonds generate such a gradient of the electrostatic field at the nucleus and the interaction fluctuates as the molecule reorients in solution. Spin–lattice relaxation thus tends to be rapid and the spin–spin relaxation* time is similarly shortened, giving broad lines and making these nuclei unsuitable for high-resolution work, since any small chemical shift effects are swamped by the excessive line broadening. At sufficiently high fields, chemical shifts may nevertheless be measurable. In special cases, notably the deuterium nucleus (I = 1) in small molecules, the quadrupole moment is so small that high-resolution spectra may be recorded with only rather slight line broadening. In general, however, nuclei which do not have $I = \frac{1}{2}$ prove of little interest for high-resolution work. This includes all the isotopes of the halogens of significant natural abundance.

Rapid relaxation of quadrupolar nuclei also has a beneficial effect in that it leads to some simplification of the spectra of protons and carbon-13. Although quadrupolar nuclei such as chlorine-35 have significant coupling to protons and carbon-13, spin–lattice relaxation washes out the splitting if the relaxation rate is fast compared with the coupling constant J. Thus it is possible for most purposes to ignore the presence of halogen atoms in the molecule, much as we ignore non-magnetic nuclei like oxygen-16. Nitrogen-14 may split protons into a 1:1:1 triplet under conditions of slow spin–lattice relaxation. It is, however, important to remember that coupling to a quadrupolar nucleus may shorten the spin–spin relaxation time of the observed nucleus (which may or may not result in a detectable broadening), and that the quadrupolar nucleus may have a significant magnetic dipole moment and thus contribute to spin–lattice relaxation of near neighbours.

The time dependence of the nuclear magnetization during spin–lattice relaxation is not necessarily a simple exponential curve. In a coupled spin system, for example, cross-relaxation causes multiexponential behaviour, and in the case of chemical exchange* where the experiment is initiated with a selective inversion pulse, some lines will first lose intensity and then recover.

DETERMINATION OF SPIN–LATTICE RELAXATION TIMES

Nowadays spin–lattice relaxation measurements are usually carried out by pulse methods (5), and the T_1 values of individual lines in a multiline spectrum are readily extracted by separating the appropriate frequency components by Fourier transformation (6). The decay time constant for transverse magnetization (T_2) can often be shorter than T_1, so in all these experiments it is important to eliminate transverse components of magnetization while the longitudinal magnetization is being monitored.

The most widely used technique is that of *inversion recovery* (7). This requires a preparation period long compared with T_1 for the spins to reach thermal equilibrium before the pulse sequence is applied. A 180° pulse then inverts the Z component of magnetization and after a variable delay t during which the inverted spin population recovers back towards equilibrium, the component M_Z is examined by applying a 90° pulse. If S_t is the amplitude of the detected NMR signal, and S_∞ is the corresponding asymptotic signal observed when $t >> T_1$, then if perfect inversion can be assumed

$$S_\infty - S_t = 2S_\infty \exp(-t/T_1). \qquad [7]$$

Figure 2 shows a typical inversion-recovery experiment on the carbon-13 spectrum of *meta*-xylene. The spin–lattice relaxation time is then evaluated either by making a graphical plot on semilogarithmic paper or through a suitable computer routine which accepts digital peak height data. Since timing errors are usually negligible in computer-controlled spectrometers, the errors are essentially only in the

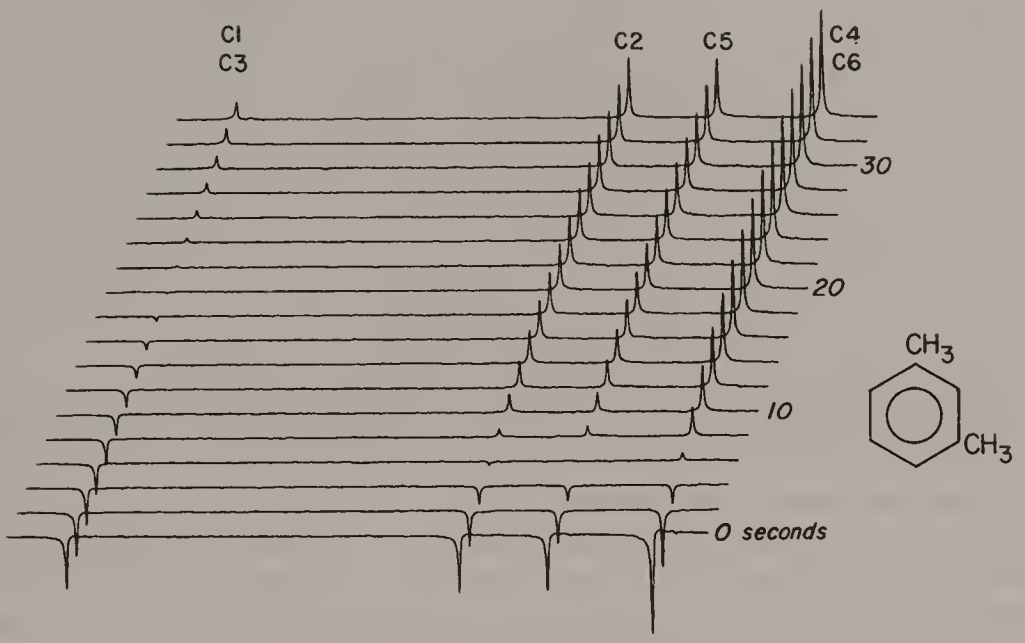

Fig. 2. A typical inversion–recovery experiment to determine individual spin–lattice relaxation times. Carbon-13 nuclei 1 and 3, having no close proton neighbours, have a very long relaxation time. The slightly different relaxation rates of carbons 2 and 5 compared with carbons 4 and 6 suggest that the molecular reorientation is slightly anisotropic.

measurement of intensity. Note that the statistical errors on S_∞ are really just as significant as those on S_t, so that it can be argued that an equal number of measurements of S_∞ and S_t should be made. If the spectrometer resolution is not reproducible, then the normalized intensity difference $(S_\infty - S_t)/S_\infty$ should be computed. If the initial inversion pulse is imperfect, the residual transverse magnetization should be cancelled by phase alternation of the monitoring pulse (8) or eliminated by means of a strong field gradient *homospoil* pulse. The recovery is *still* exponential:

$$S_\infty - S_t = S_\infty(1 - k)\exp(-t/T_1) \qquad [8]$$

where k measures the efficiency of the inversion (ideally $k = -1$), depending on the error in the flip angle and the extent of any resonance offset effects. An alternative is to employ a composite 180° pulse* such that offset effects or flip-angle errors are compensated (9).

Most relaxation experiments are time consuming, and this may be the critical consideration for low-sensitivity nuclei which require extensive time averaging. One problem is that the determination of S_∞ requires a rough estimate of the longest T_1 to be measured, so that an interval of 4–5 times T_1 can be programmed. Some workers leave the unknown value of S_∞ as a variable parameter in a non-linear least-squares computer program, along with the time constant T_1. It should,

however, be remembered that a two-parameter fit seriously reduces the significance of a given piece of experimental data compared with a single-parameter fit, and there are objections in principle against deriving a quantity by a fitting procedure when it can in fact be measured directly. If the measurement of S_∞ is abandoned, the experiment may be further accelerated by reducing the number of different values of t employed, and in the limit, approximate values of the relaxation times may be obtained with just two settings of t (10). This procedure requires estimates of the relaxation times in order to choose suitable values of t, so it would be applicable to situations where T_1 is measured in a series of closely related compounds, or for a given molecule under different physical conditions.

The other time-consuming aspect of the inversion-recovery method is the waiting period 4–5 T_1 required to allow the establishment of thermal equilibrium before each pulse sequence is initiated. Two alternative techniques, *progressive saturation* and *saturation recovery*, have been devised to circumvent this problem. Progressive saturation is the analogue in pulsed spectroscopy of the method used in continuous-wave instruments, where the spectrum is examined at different levels of the B_1 field and the degree of saturation monitored. A regular sequence of 90° pulses is applied at a rate fast compared with the rate of spin–lattice relaxation so that a steady-state regime is established for the longitudinal magnetization. Immediately after each 90° pulse the spin populations in the upper and lower energy levels are equal ($M_Z = 0$) and in the short interval before the next pulse, spin–lattice processes return some spins to the lower level and M_Z grows towards M_0. The observed NMR signal is thus proportional to the growth in M_Z, and if the experiment is repeated for several different pulse intervals t, one of which is long compared with all spin–lattice relaxation times, then

$$S_\infty - S_t = S_\infty \exp(-t/T_1). \qquad [9]$$

Instead of a waiting period of 4–5 T_1, this experiment requires only one or two pulse intervals to settle into a steady state. Free induction decays are therefore acquired more rapidly, giving improved signal-to-noise in a given time; however, each ordinate on the final graph ($S_\infty - S_t$) is only one-half that of the inversion-recovery method, as can be seen by comparing eqn [7] with eqn [9]. Progressive saturation measurements presuppose that some technique is used to prevent the establishment of steady-state components of transverse magnetization immediately before each pulse (11). Systematic errors can be introduced by imperfections in the 90° pulse, particularly errors in the pulse length.

The saturation-recovery technique is related to progressive saturation but has the advantage that the minimum setting of the relaxation interval t is not limited by the acquisition time. Again there is no preparation period required, the spins are simply saturated by a sequence of radiofrequency pulses* and any transverse magnetization is dispersed by a field gradient pulse (12). After a variable interval t (which allows partial recovery of Z magnetization), this is monitored by a 90° pulse. The time evolution of the signal intensity is again described by eqn [9].

In all these experiments there remains the difficulty of estimating an approximate value for the spin–lattice relaxation time in order to set up the experimental parameters. In multiline spectra this difficulty is compounded because there is usually a distribution of T_1 values. The most satisfactory remedy to this problem has been suggested by Canet *et al.* (13) and called the *fast inversion-recovery* method. It recognizes that sensitivity requirements will not permit a sufficiently long preparation period for the slowly relaxing spins and therefore accepts a compromise setting of this interval. For the rapidly relaxing resonances the experiment is thus a conventional inversion-recovery sequence, but for the slowly relaxing resonances the Z magnetization just before the 180° pulse is considerably less than M_0, and in the limit the experiment resembles a saturation-recovery sequence. Spin–lattice relaxation times can be extracted for all the resonance lines, the only penalty being that the sensitivity is reduced for the slowly relaxing species.

REFERENCES

1. J. S. Waugh, *J. Mol. Spectrosc.* **35**, 298 (1970).
2. R. R. Ernst, Sensitivity Enhancement in Magnetic Resonance. In *Advances in Magnetic Resonance*, ed. J. S. Waugh. Academic Press: New York, Vol. 2, 1966.
3. G. C. Levy, D. M. White and F. A. L. Anet, *J. Magn. Reson.* **6**, 453 (1972).
4. J. R. Lyerla, D. M. Grant and G. D. Bertrand, *J. Phys Chem.* **75**, 3967 (1971).
5. H. Y. Carr and E. M. Purcell, *Phys. Rev.* **94**, 630 (1954).
6. R. L. Vold, J. S. Waugh, M. P. Klein and D. E. Phelps, *J. Chem. Phys.* **48**, 3831 (1968).
7. E. L. Hahn, *Phys. Rev.* **76**, 145 (1949).
8. D. E. Demco, P. van Hecke and J. S. Waugh, *J. Magn. Reson.* **16**, 467 (1974).
9. M. H. Levitt and R. Freeman, *J. Magn. Reson.* **33**, 473 (1979).
10. R. Freeeman, H. D. W. Hill and R. Kaptein, *J. Magn. Reson.* **7**, 82 (1972).
11. R. Freeman and H. D. W. Hill, *J. Chem. Phys.* **54**, 3367 (1971).
12. J. L. Markley, W. H. Horsley and M. P. Klein, *J. Chem. Phys.* **55**, 3604 (1971).
13. D. Canet, G. C. Levy and I. R. Peat, *J. Magn. Reson.* **18**, 199 (1975).

Cross-references

Chemical exchange
Composite pulses
Continuous-wave spectroscopy
Radiofrequency pulses
Spin–spin relaxation
Steady-state effects

Spin Locking

In a spin-echo* experiment, the amplitude of the echo observed at time t is given by $M_0 \exp(-t/T_2)$. where T_2 is the spin–spin relaxation* time. Certain other factors may influence this amplitude, for example diffusion of the spins in a B_0 gradient, slow chemical exchange* or echo modulation by homonuclear spin–spin coupling. When a repeated train of 180° refocusing pulses is used, all three effects get weaker and finally disappear as the pulse repetition rate is increased. In this limit the refocusing pulses are applied in such rapid succession that the amount of free precession is negligible and all magnetization vectors remain essentially 'locked' along the Y axis of the rotating frame.

The same effect is achieved if a continuous B_1 field is applied along the Y axis in lieu of the sequence of 180° pulses. The experiment consists of a 90° pulse about the X axis followed by a rapid 90° phase shift of the radiofrequency field, which is then left on for a time of the order of milliseconds to seconds. This is called *spin locking* or *forced transitory precession* (1). Alternatively, the same condition can be reached with an adiabatic rapid passage* interrupted when the sweep reaches the exact resonance condition, but with the radiofrequency field B_1 left on.

If we are dealing with a single-line spectrum, B_1 will normally be so intense compared with off-resonance effects attributable to static field inhomogeneity that the latter may be neglected. Each small volume element of the sample (*isochromat*) experiences almost exactly the same effective field B_{eff}, essentially equal to B_1 and aligned along the Y axis of the rotating frame. The NMR signal consequently decays only by spin–spin relaxation and not by field inhomogeneity effects (as in a free induction decay). Since this relaxation takes place longitudinal to the effective field, the decay time constant is more correctly called the *spin–lattice relaxation time in the rotating frame**, $T_{1\rho}$, but for a liquid sample this is essentially the spin–spin relaxation time T_2.

In certain practical situations the spin-locking experiment might be preferred over the better-known spin-echo method for determining spin–spin relaxation times in liquids. For example, it neatly avoids the problem of cumulative errors in the 180° refocusing pulses. As mentioned above, it also avoids the complications associated with echo modulation in coupled spin systems. Furthermore, when it is feasible to perform a selective spin-locking experiment (where B_1 influences an entire spin multiplet but leaves adjacent spin multiplets essentially unaffected) the individual spin–spin relaxation times can be measured one at a time. In practice, limitations imposed by the electronics, and sample heating effects often preclude the use of a

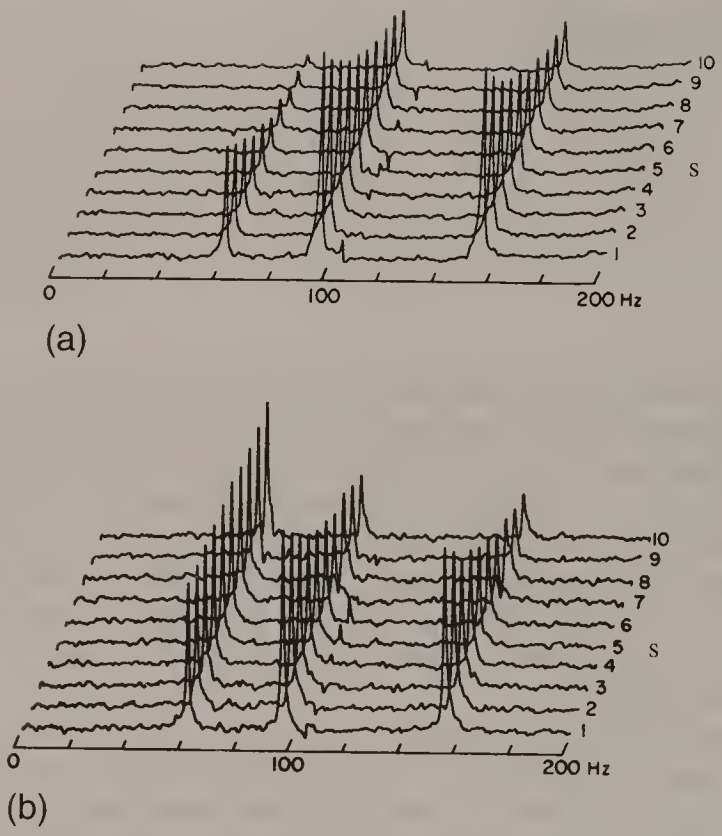

Fig. 1. (a) Spin–spin relaxation of the carbon-13 nuclei in orthodichlorobenzene studied in a spin-locking experiment. The quadrupolar chlorine nuclei cause a shortening of T_2 for the low-field line (T_2 = 4.2 s). (b) Spin–lattice relaxation curves for comparison. Now the chlorine-bearing sites are seen to have a long T_1 since there are no nearby protons (T_1 = 66 s). Otherwise T_1 and T_2 are essentially equal.

B_1 field so intense as to cover the entire spectral width. Selective spin locking, with a much reduced B_1 intensity, would therefore be the preferred approach.

A spin–spin relaxation study simply involves a series of experiments with different lengths of the spin-locking time t_L, the free induction decay being acquired after the extinction of the B_1 field. Intensities of individual resonance lines are then followed as they decay as a function of t_L. Figure 1 shows the example of the carbon-13 resonances of orthodichlorobenzene, where the carbon-13 chemical shifts are sufficiently small that the entire spectrum could be covered by a relatively weak spin-locking field $\gamma B_1/2\pi = 2.6$ kHz. It illustrates (2) that the carbon sites with directly attached chlorine atoms exhibit a short spin–spin relaxation time attributable to scalar coupling to chlorine-35 and chlorine-37 nuclei. These experiments employed coherent proton decoupling and could only be carried out successfully by specifically avoiding the Hartmann–Hahn* condition

$$\gamma_H B_2/2\pi = \gamma_C B_1/2\pi, \qquad [1]$$

otherwise spurious decay rates were observed (3). Spin–lattice relaxation measurements on the same sample are shown for comparison; in these, the carbon site directly attached to chlorine showed an extremely *long* spin–lattice relaxation time because there were no close proton spins.

While spin locked, the nuclei possess a very large magnetization ($\approx M_0$) while experiencing only a weak effective field B_{eff}, much less intense than the polarizing field B_0 initially used to create M_0. The spins may therefore be thought of as very 'cold' and they return to thermal equilibrium by losing magnetization. This explains why the relaxation, although *longitudinal*, nevertheless corresponds to a decay rather than a recovery.

Whereas the spin–spin relaxation time is sensitive to components of the spectral density of molecular motions near to zero frequency, spin-locking experiments probe motions around the frequency $\gamma B_1/2\pi$. For the majority of situations in liquids, the spectral density function does not change significantly between these two frequencies, but occasionally there might be very slow motions that influence T_2 more than $T_{1\rho}$. Spin locking is thus a more versatile method for examining slow molecular motion than the spin-echo experiment, since B_1 becomes a useful variable parameter.

REFERENCES

1. I. Solomon, *CR Acad. Sci. Paris* **248**, 92 (1959).
2. R. Freeman and H. D. W. Hill, *J. Chem Phys.* **55**, 1985 (1971).
3. R. Freeman and H. D. W. Hill, *Dynamic Nuclear Magnetic Resonance Spectroscopy*, ed. L. M. Jackman and F. A Cotton. Academic Press: New York, Ch. 5, 1975.

Cross-references

Adiabatic rapid passage
Chemical exchange
Hartmann–Hahn experiment
Rotating frame
Selective excitation
Spin echoes
Spin–spin relaxation

Spin–Spin Relaxation

A client was trying to negotiate a loan from a pawnbroker and offered him a wristwatch as security. The pawnbroker declined, saying that he had an entire drawer full of wristwatches already. 'Well', said the client. 'What time is it?' Now even if we suppose that the pawnbroker had very carefully set all the watches to the correct time at 9 a.m. on Monday morning, there would of course be some difficulty in deciding the exact time some days later; in fact we might anticipate some kind of Gaussian distribution function of the readings over the large ensemble of watches in the drawer. A related problem arises with the time keeping of precessing nuclear spins because of weak magnetic interactions between the nuclei which perturb the

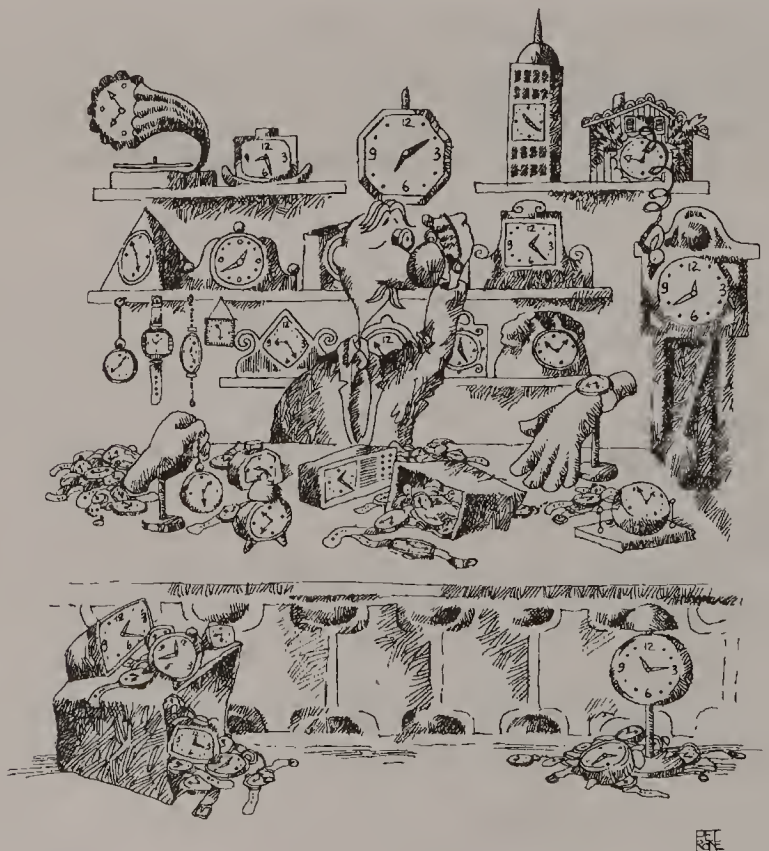

exact nuclear precession frequencies. If the spins are all set to precess in phase at time zero (by the application of a hard radiofrequency pulse) this phase coherence is gradually lost, with a time constant called the spin–spin relaxation time T_2. In order to observe this dephasing effect in practice, we would need to have a perfectly stable spectrometer and a perfectly uniform magnetic field B_0; then the free precession signal would decay exponentially with a time constant T_2. This relaxation time is defined phenomenologically by the Bloch equations as the decay constant of transverse nuclear magnetization, neglecting instrumental shortcomings. In the steady-state solutions of the Bloch equations, $1/(\pi T_2)$ may be identified with the natural linewidth, and this could be measured in a slow-passage continuous-wave spectrometer with a perfectly stable and uniform magnetic field.

It is important to make a clear distinction between the spin–spin relaxation time T_2 and the lifetime of the spins in a given energy state, the spin–lattice relaxation time T_1. In many high-resolution NMR situations with liquid samples, the same physical mechanisms determine both T_1 and T_2, and they are consequently equal. The cases of interest are those where there are *additional* mechanisms for spin–spin relaxation such that T_2 is shorter than T_1. We can define a *phase memory time*, accepting that certain interactions between spins may destroy their phase coherence faster than the spin-state lifetime (T_1). According to the vector model* this means that transverse (XY) magnetization decays faster than the regrowth of longitudinal (Z) magnetization. In what follows we shall focus attention on these additional mechanisms for spin–spin relaxation, taking the spin–lattice relaxation processes for granted.

The two relaxation times can be distinguished in another way. The spin–lattice relaxation time measures the time constant for the transfer of energy from the spin system to its environment (the lattice). We could say that it represents the time taken for 'hot' spins to cool down. On the other hand, there is no energy change in the spin system due to spin–spin relaxation. In solids, where there are strong dipole–dipole interactions between spins ($T_2 \ll T_1$), these serve to establish a true thermal equilibrium within the spin system, and we can then define a 'spin temperature' which may be quite different from the lattice temperature. Indeed there is the interesting concept of a *negative* spin temperature (a population inversion). In liquids, however, the interactions between spins are relatively weak and it is not correct to talk about spin temperature in this context.

In practical spectrometers, the transverse nuclear magnetization usually decays with a time constant T_2^* which, for small molecules, can be significantly shorter than T_2 as isochromats from different regions of the sample interfere destructively because of the spatial inhomogeneity of B_0. For this reason we cannot observe the T_2 decay directly but must resort to a spin-echo* experiment in which field inhomogeneity effects are periodically refocused. In a multiple-echo train, the envelope of the echo peaks decays exponentially with a time constant T_2, provided that molecular diffusion effects can be neglected. Spin locking* can also be used.

In the frequency domain it is possible to distinguish the broadening by B_0 inhomogeneity from the broadening by spin–spin relaxation by the fact that in the

former case it is possible to 'burn a hole' in the line by frequency-selective irradiation just prior to a hard read pulse. The saturating radiation affects only a restricted volume of the sample where the B_0 field is very close to exact resonance. By contrast, when the linewidth is determined purely by spin–spin relaxation, irradiation of any part of the line (even the distant tail) saturates the entire profile. The line is said to be *homogeneously broadened.*

THE SPECTRAL DENSITY FUNCTION

Relaxation is caused by local magnetic fields modulated by the random reorientational motion of the molecules. The frequency spectrum of these fluctuations is described by the spectral density function, already discussed in the section on Spin–lattice relaxation*. The component of the spectral density function at the Larmor frequency determines the spin–lattice relaxation time. Spin–spin relaxation is affected by fields fluctuating at the Larmor frequency, but it is also

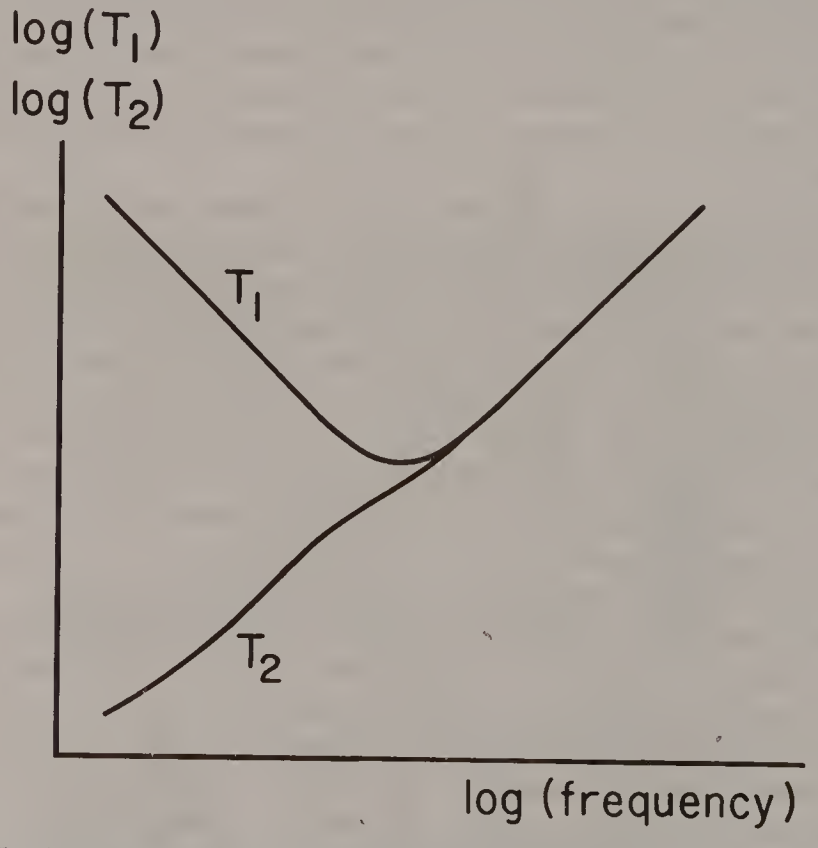

Fig. 1. The dependence of the spin–spin and spin–lattice relaxation times on the correlation frequency for molecular reorientation. For motion fast with respect to the Larmor frequency the two relaxation times are essentially equal, but for slow motion the spin–spin relaxation time T_2 continues to decrease whereas the spin–lattice relaxation time T_1 passes through a minimum and then increases.

sensitive to low-frequency fluctuations. If molecular tumbling is fast compared with the Larmor frequency, the spectral density function is very flat over the appropriate range of frequencies, so both T_1 and T_2 are influenced in the same manner and they are approximately equal.

If there are interactions that fluctuate more slowly, T_2 becomes shorter than T_1 (Fig. 1). When T_1 passes through its minimum value, it is about $1.6T_2$. For still slower molecular tumbling T_1 starts to increase, but T_2 continues to fall, and spin–spin relaxation is now dominated by the very low-frequency motions. Polymers and biological macromolecules usually fall into this category because the molecules move very sluggishly. The observed linewidths are then determined by spin–spin relaxation rather than by instrumental broadening, and the nuclear Overhauser effect* becomes negative. The spectra of such molecules exhibit broad lines, hardly affected by magnet shimming, and the power to resolve chemically shifted resonances can only be improved by increasing the intensity of the applied magnetic field.

MECHANISMS OF SPIN–SPIN RELAXATION

Spin–lattice relaxation limits the lifetime of spins in the upper energy state, introducing a Heisenberg broadening of the NMR resonance lines. We can think of this as the hard core of the natural linewidth. Any low-frequency fluctuations of the local magnetic field introduce *additional* broadening effects. In NMR parlance they are then loosely referred to as T_2 mechanisms. Chemical exchange* is probably the most important of these. An atom that moves from one chemically distinct site to another carries with it a nuclear spin, and when this spin arrives at the new site there is an essentially random jump in the precession phase. The phase memory time is therefore shortened. The details of what is observed depend on whether the exchange rate is slow, intermediate or fast compared with the chemical shift difference between the two sites. Slow chemical exchange broadens both resonances, fast exchange collapses them to a singlet at the weighted mean frequency. As the exchange rate is further increased, this collapsed line gets narrower.

One of the most common manifestations of slow chemical exchange is when an OH or NH resonance shows an appreciably broad resonance line in a high-resolution proton spectrum where all the other lines are narrow. In such cases, the rate of chemical exchange may be determined from the excess broadening of those particular lines. When no extra broadening is observable, evidence for chemical exchange may still be derived from spin-echo experiments (1,2). In some solvent suppression experiments the T_2 of water is deliberately shortened by chemical exchange so that its signal decays much more rapidly than the remaining signals; acquisition of a spin echo then suppresses the water signal selectively (3).

Another T_2 mechanism originates in the spin–spin interaction J_{IS} with another nucleus (I) that has a short spin-state lifetime. The I spin exerts a weak magnetic

field at the S-spin site due to the J-coupling, and this field fluctuates if the I spin state is changed, either by chemical exchange (as described above) or through relatively rapid spin–lattice relaxation (this is a common occurrence if I is a quadrupolar nucleus, such as nitrogen-14, chlorine-35 or chlorine-37). These two mechanisms have been called, respectively, scalar relaxation of the first and second kinds (4). If the rate of fluctuation is fast compared with J_{IS}, the S spin shows only a singlet resonance; its multiplet structure has been 'washed out'.

REFERENCES

1. E. L. Hahn, *Phys. Rev.* **80**, 580 (1950).
2. H. Y. Carr and E. M. Purcell, *Phys. Rev.* **94**, 630 (1954).
3. D. L. Rabenstein, S. Fan and T. T. Nakashima, *J. Magn. Reson.* **64**, 541 (1985).
4. A. Abragam, *The Principles of Nuclear Magnetism.* Oxford University Press, 1961.

Cross-references

Chemical exchange
Nuclear Overhauser effect
Selective excitation
Spin echoes
Spin–lattice relaxation
Spin locking
Vector model

Spin Tickling

While decoupling effects require irradiation fields $\gamma B_2/2\pi$ comparable with the coupling constant J_{IS}, certain double-resonance effects persist at much lower levels of irradiation. The phenomenon is based on a non-crossing rule for energy levels transformed into the rotating frame* so it is to be expected intuitively that the maximum displacement of resonance lines would be of the order of $\gamma B_2/2\pi$ Hz. Observable changes in the spectrum occur provided that $\gamma B_2/2\pi$ is comparable with the linewidth, and provided that the frequency f_2 of this irradiation is located close to exact resonance of one of the lines of a spin multiplet (not necessarily the chemical shift frequency). The two requirements – precise location and weak perturbation – have given rise to the term 'spin tickling' for this kind of double-resonance experiment (1).

In order to observe tickling effects in an NMR spectrum, two nuclei must be spin coupled, but the magnitude of the coupling is irrelevant provided it is large enough to give a resolved splitting so that one line of the multiplet can be irradiated without significantly perturbing the others. In fact, the method is most useful for complicated networks of spin coupling between large numbers of spins, as often encountered in proton NMR systems. Suppose we isolate just three energy levels p, q and r from the complex network of energy levels appropriate to such a system, and focus attention on the allowed transition at frequencies f_{pq} and f_{qr}. Consider what would happen if f_{qr} were to be irradiated with a weak field B_2 exactly at resonance, $f_2 = f_{qr}$. In order to remove the time dependence of the problem, the energy-level diagram is transformed into a rotating reference frame at the frequency f_2, where B_2 becomes a static field (Fig. 1(a)). In the first step of this process, levels q and r become degenerate (Fig. 1(b)) and then as B_2 is introduced, their degeneracy is lifted and they are forced apart by an amount $\gamma B_2/2\pi$ Hz.

The selection rules are now changed so that there are two transitions from level p to the perturbed levels q' and r'. After transformation back from the rotating frame to the laboratory frame, the transition f_{pq} becomes a doublet $f_{pq} \pm \frac{1}{2}\gamma B_2/2\pi$. Thus in this simple case, tickling has given rise to a doublet where only a single line existed initially. We can see that the irradiated line and the split line are related by the fact that they share an energy level in common (q). They are said to be *connected* transitions. Irradiation of a connected transition at exact resonance gives a doublet of splitting $\gamma B_2/2\pi$ Hz.

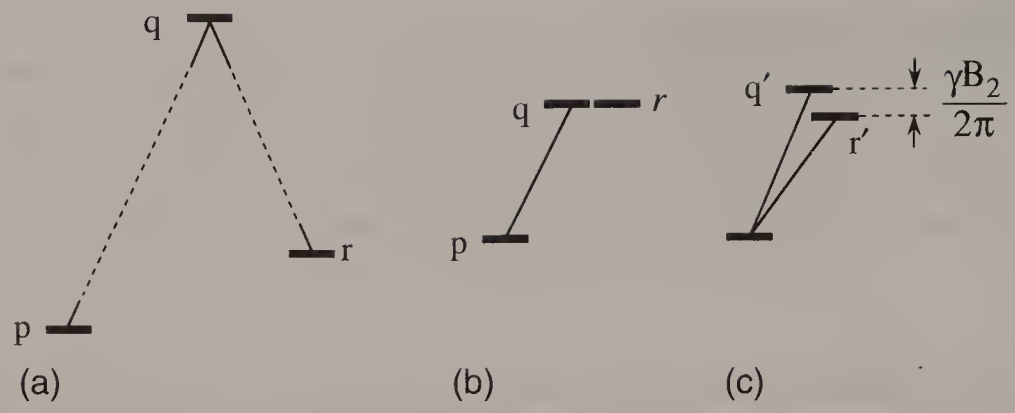

Fig. 1. Transformation of the laboratory frame energy-level diagram (a) into a frame (b) rotating at the frequency of the transition q–r (not drawn to scale). When a B_2 field is applied (c) at this frequency it lifts the degeneracy of levels q and r, introducing a splitting $\gamma B_2/2\pi$ Hz and making the transitions pq′ and pr′ equally allowed.

Consider now the more general case where f_2 is not at exact resonance for f_{qr} but is offset a small amount Δf_2 Hz. Transformation to the rotating frame at frequency f_2 leaves levels q and r not quite degenerate, separated by Δf_2 Hz, and the introduction of the static field B_2 increases this splitting to S Hz, where

$$S = [(\Delta f_2)^2 + (\gamma B_2/2\pi)^2]^{1/2}. \qquad [1]$$

One of the new transitions (say $f_{pq'}$) takes on more the character of an allowed transition and gains intensity at the expense of $f_{pr'}$, which can now be said to take on the character of a forbidden transition. In the limit where Δf_2 becomes large compared with $\gamma B_2/2\pi$, one component of the doublet is fully allowed and falls at the unperturbed frequency f_{pq}, while the other is forbidden and has vanishing intensity. By monitoring the imbalance in the intensities of the two doublet components, it is possible to search for the exact resonance condition $f_2 = f_{qr}$ and thus locate a hidden or unobservable line with high precision. Figure 2 shows a heteronuclear spin-tickling experiment to determine the frequency of a carbon-13 transition indirectly by observation of the splitting of a satellite line in the proton spectrum. At the exact tickling condition the two lines of the observed doublet have equal intensity; as the B_2 frequency goes off resonance the doublet intensities become asymmetrical. The frequency of the carbon-13 transition can be determined with an accuracy that is better than ±0.1 Hz.

The treatment has so far considered only a simple AX system of coupled spins. For an AX_2 system where one of the X lines is irradiated, three levels become degenerate in the rotating frame and the introduction of the B_2 field splits this degeneracy, leaving a subtriplet for each A resonance. Similarly, for the AX_3 system, the A lines become 1:3:3:1 subquartets because of the tickling condition.

While spin tickling gives more precise information about the frequencies of hidden transitions, it is more tedious to carry out than coherent decoupling since the

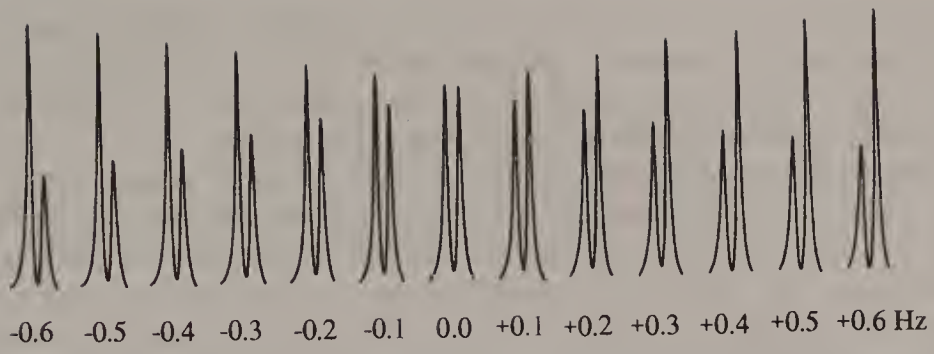

Fig. 2. Illustration of the frequency dependence of the spin-tickling experiment. The low-field carbon-13 satellite in the proton spectrum of formic acid is monitored while the B_2 field irradiates close to the high-field carbon-13 transition. At exact resonance (0 Hz) the observed line is a symmetrical doublet.

experiment must be repeated many times with quite small increments of f_2. For complicated spectra, Fourier transform difference spectroscopy* may be used to clarify the results.

In continuous-wave spectroscopy*, the arrangement of the spin-tickling experiment can be reversed with the B_1 field monitoring the peak of one resonance line while the frequency f_2 is swept through the rest of the spectrum to locate connected transitions. This is called the 'INDOR' experiment (2) by analogy with electron–nuclear double resonance (ENDOR). Unfortunately, two physical processes contribute to the observed effect – the splitting of the monitored line due to spin tickling, and a population disturbance caused by saturation effects of the B_2 field. For very weak levels of irradiation, the population rearrangement effects appear to predominate. In order to understand the *direction* of the intensity changes, we must make a distinction between two kinds of connected transitions – the *progressive* configuration and the *regressive* configuration (Fig. 3). In the

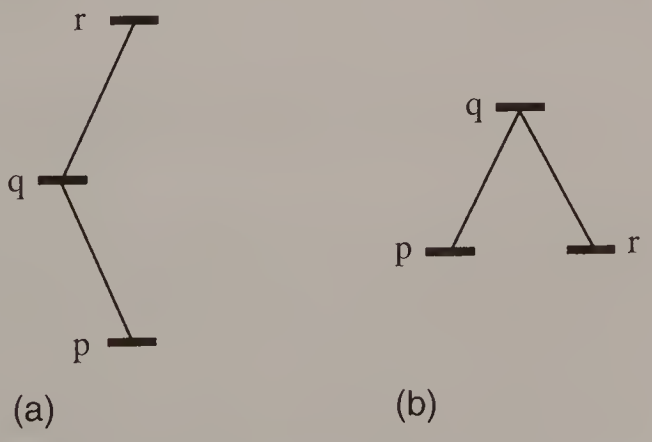

Fig. 3. Two transitions which share a common energy level are said to be *connected.* They may have (a) the *progressive* configuration or (b) the *regressive* configuration.

progressive case the monitored line increases in intensity as spins are pumped into the lower level or alternatively pumped out of the upper level. By contrast, the regressive configuration always shows a decrease in intensity of the monitored line because the population disturbances have the opposite sense.

The progressive and regressive cases are distinguishable in another interesting way when spin tickling occurs. In the progressive case the action of the B_2 field mixes in some of the double-quantum transition, rendering the doublet *more* sensitive to static field inhomogeneity effects, whereas in the regressive case it mixes in some of the zero-quantum transition and the observed doublet is unusually well resolved (1). This is a situation where we cannot simply work out the allowed transition frequencies and then convolute with a field broadening function to obtain the observed lineshapes. Tickling takes place within a molecule, over such a short distance that field inhomogeneity may be completely neglected. If that molecule is situated in a region where the B_0 field is (say) slightly higher than the mean, then the resonance offsets for both the B_1 and B_2 fields must be in the same sense. For the progressive case this makes inhomogeneity broadening worse, but for the regressive case it is reduced. Similar effects occur, of course, in experiments with multiple-quantum coherence*.

REFERENCES

1. R. Freeman and W. A. Anderson, *J. Chem Phys.* **37**, 2053 (1962).
2. E. B. Baker, *J. Chem Phys.* **37**, 911 (1962).

Cross-references

Continuous-wave spectroscopy
Difference spectroscopy
Multiple-quantum coherence
Rotating frame

Steady-state Effects

It is tempting to analyse an NMR experiment in terms of a single radiofrequency pulse followed by a free induction decay, for this avoids a host of complicating factors that arise when using a sequence of pulses and acquisitions. Unfortunately the demands imposed by time averaging* and the desire for optimal sensitivity compel us to repeat the excitation–detection cycle quite rapidly, consistent with the resolution requirement, which determines the acquisition time t_a. In general the interval between radiofrequency pulses is $t_a + t_d$, where t_d is a waiting period that allows for relaxation. The choice of t_a is determined by the instrumental decay constant T_2^*; if t_a is less than T_2^* the free induction decay is prematurely truncated, whereas if t_a is very much greater than T_2^*, time is wasted gathering negligible signals in the tail. In many applications the decay rate is accelerated by imposition of a sensitivity enhancement function, often the equivalent of a matched filter.

These practical considerations mean that many experiments are conducted under conditions where spin–lattice or even spin–spin relaxation is incomplete:

$$t_a + t_d < T_1, T_2. \qquad [1]$$

As a result, the radiofrequency pulses are not applied to nuclear magnetization at Boltzmann equilibrium, represented by a vector M_0 along the +Z axis, but to a spin system still suffering the effects of previous pulses. A steady-state regime is established where there is a partially saturated longitudinal component M_Z^- and (possibly) transverse components M_X^- and M_Y^- immediately before the radiofrequency pulse.

STEADY-STATE REGIME FOR LONGITUDINAL MAGNETIZATION

Consider, first of all, the simpler (and more common) case where spin–spin relaxation is essentially complete during the interval $t_a + t_d$ but where there is still incomplete spin–lattice relaxation between consecutive pulses. (We shall see below that other practical matters, such as spectrometer instabilities, also conspire to render transverse relaxation effects unimportant in many cases.) If we write the longitudinal magnetization component immediately before the pulse as M_Z^- and that after the pulse as M_Z^+, the steady-state condition can easily be calculated (1–4)

by evaluating the effect of longitudinal relaxation on M_Z^+, putting the result equal to M_Z^-:

$$M_Z^+(1 - E_1) = M_Z^- \quad [2]$$

where

$$E_1 = \exp[-(t_a + t_d)/T_1]. \quad [3]$$

The effect on longitudinal magnetization of a pulse of flip angle α is simply

$$M_Z^+ = M_Z^- \cos \alpha. \quad [4]$$

So we see that the flip angle for optimum sensitivity is the 'Ernst angle' α_E, given by

$$\cos \alpha_E = E_1 = \exp[-(t_a + t_d)/T_1]. \quad [5]$$

Unless $t_a + t_d$ is very long in comparison with T_1, the Ernst angle is less than 90°. One way to operate would be to set the flip angle to α_E, based on some knowledge or estimate of the spin–lattice relaxation time. Since these T_1 values vary between different resonances in the same spectrum, a more pragmatic approach is normally taken, setting the flip angle to 90° and choosing a suitable value of t_d to give near-optimum intensities; this may mean $t_d = 0$.

Steady-state effects can be quite a nuisance in multidimensional spectroscopy, where time constraints usually demand that the scans be repeated before there is complete spin–lattice relaxation. One result is the introduction of a ridge in the F_1 dimension wherever there is a strong NMR response, thus enhancing the effect of t_1 noise*. It can be explained by the fact that the very first t_1 increment excites a signal from an initial state at Boltzmann equilibrium, giving a strong response, whereas subsequent signals are partly saturated. The usual remedy is to run a few dummy scans before signal acquisition is started. Phase cycles must be designed to circumvent the effects of longitudinal steady-state effects, otherwise there may be appreciable artefacts attributable to imperfect subtraction of strong signal components (5).

THE GENERAL STEADY-STATE REGIME

The situation is a great deal more complicated when transverse magnetization must be taken into account, because the angle of precession between pulses (θ) has an important influence on the result. When there is transverse magnetization, the effect of a radiofrequency pulse depends on the azimuthal angle ϕ, which in the steady state depends on the precession angle θ (Fig. 1). This angle θ is determined by the offset from resonance $\Delta\omega$ and the interval between pulses

$$\theta = \Delta\omega(t_a + t_d). \quad [6]$$

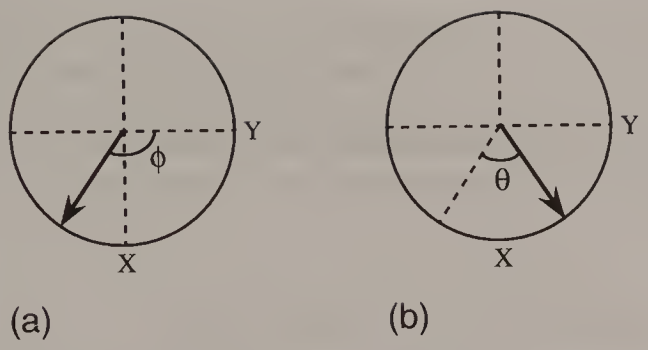

Fig. 1. (a) In the steady-state regime, just prior to a radiofrequency pulse, a general magnetization vector subtends an azimuthal angle ϕ with respect to the +Y axis. (b) The pulse rotates this vector about the +X axis, changing the azimuthal angle by $-\theta$. Subsequent free precession during the interval $t_a + t_d$ carries the vector through $+\theta$ back to the position shown in (a).

We are only interested in the value of θ modulo 2π. If the pulses are applied about the +X axis, and if we define

$$E_2 = \exp\left[-\left(t_a + t_d\right)/T_2\right] \qquad [7]$$

then the steady-state solutions are

$$M_X^- = M_0\left(1 - E_1\right)\left(E_2 \sin\alpha \sin\theta\right)/D \qquad [8]$$

$$M_X^+ = M_X^- \qquad [9]$$

$$M_Y^- = M_0\left(1 - E_1\right)\left(E_2 \sin\alpha \cos\theta - E_2^2 \sin\alpha\right)/D \qquad [10]$$

$$M_Y^+ = M_0\left(1 - E_1\right)\left[\left(1 - E_2 \cos\theta\right)\sin\alpha\right]/D \qquad [11]$$

$$M_Z^- = M_0\left(1 - E_1\right)\left[1 - E_2 \cos\theta - E_2 \cos\alpha\left(\cos\theta - E_2\right)\right]/D \qquad [12]$$

$$g(\tau) = \left\langle R(t)\, R(t+\tau)\right\rangle, \qquad [13]$$

where the denominator D is given by

$$D = \left(1 - E_1 \cos\alpha\right)\left(1 - E_2 \cos\theta\right) - \left(E_1 - \cos\alpha\right)\left(E_2 - \cos\theta\right)E_2. \qquad [14]$$

For small to medium-sized molecules of interest to the organic chemist, T_2 is not very different from T_1, and the establishment of a steady-state regime for transverse magnetization cannot be neglected.

The question then arises why these effects are not eliminated altogether by static field inhomogeneity (T_2^*) effects that normally damp the transverse magnetization in the relatively long interval $t_a + t_d$. The answer is that there is a refocusing effect analogous to that which occurs in a Hahn spin-echo experiment (6). However, in this case it is a steady-state refocusing effect because another radiofrequency pulse

is applied at the centre of each Hahn echo. A steady-state regime is established for each individual isochromat in the sample; if the isochromats are in phase just after the pulse, in a steady-state regime they must also be in phase just before the pulse. The envelope of the free precession signal does decay owing to T_2^* effects, but then grows again with time before the next pulse as the various isochromats are brought back into focus.

PHASE AND INTENSITY ANOMALIES

The first conclusion to be drawn from eqns [8] through [13] is that the steady-state effects of transverse relaxation are quite complex and that they affect different resonance lines in different fashions, depending on the offset from resonance $\Delta\omega$. The relative intensities are 'perturbed' in the sense that they are not the same as those predicted by eqn [2] for the case of complete transverse relaxation between pulses. If the flip angle α is set equal to the Ernst angle α_E, then eqn [11] is considerably simplified to

$$M_Y^+ = M_0 \sin\alpha_E / (1 + E_1). \qquad [15]$$

Rather surprisingly, in this special case, the intensities are then independent of θ.

In the general case, the individual resonances also have differing degrees of dispersion character (depending on the local value of ϕ, which depends on θ), making it impossible to set the entire spectrum into pure absorption with the usual phase controls. These phase and intensity anomalies are more easily observed in a very stable, homogeneous magnetic field. Strong instrumental broadening ($T_2^* << T_2$) tends to obscure them by summing over a large set of isochromats with different values of ϕ.

Another important result emerges for the condition $T_2^* << T_2$; the curve relating the signal-to-noise ratio to the pulse flip angle has a broad flat maximum that is virtually independent of the precession angle θ. The optimum flip angle is near to 70° and is not at all critical; a variation between 60° and 90° only changes the signal intensity by a few per cent. In this respect a sensitivity enhancement function applied to the free induction decay has an effect similar to a reduction in T_2^*.

This is one of those rare occasions where instrumental shortcomings actually *improve* the situation, at least from the point of view of routine spectroscopy. Instabilities in the field/frequency ratio, even with the usual deuterium lock, upset the establishment of a steady state for transverse magnetization. Small variations in the timing of t_a or t_d also inhibit steady-state effects. This suggests a simple and effective solution to the problem – the deliberate introduction of a short pseudo-random timing jitter (of the order of 10 ms) into the relaxation delay t_d, thus randomizing the phase angle ϕ at the time of the radiofrequency pulses (4).

REFERENCES

1. H. Y. Carr, *Phys. Rev.* **112**, 1693 (1958).
2. R. R. Ernst and W. A. Anderson, *Rev. Sci. Instrum.* **37**, 93 (1966).
3. R. R. Ernst, *Advances in Magnetic Resonance*, ed. J. S. Waugh. Academic Press: New York, Vol. 2, 1966.
4. R. Freeman and H. D. W. Hill, *J. Magn. Reson.* **4**, 366 (1971).
5. C. J. Turner, *J. Magn. Reson.* **96**, 551 (1992).
6. E. L. Hahn, *Phys. Rev.* **80**, 580 (1950).

Cross-references

Field/frequency regulation
Phase cycling
Spin echoes
Spin–lattice relaxation
Spin–spin relaxation
t_1 noise
Time averaging

Stochastic Excitation

One of the concerns of an automobile designer is to eliminate rattles and squeaks from a new creation. In an attempt to track them down, the designer might subject the car to a sinusoidal oscillation of gradually increasing frequency until all the resonances were located, or let the car fall from a height onto a concrete floor and analyse the sound of the resulting crunch by Fourier transformation. We have all been schooled in these alternative 'slow-passage' and 'impulse response' modes of excitation of magnetic resonance spectra, represented by the steady-state and transient solutions of the Bloch equations. But there is also a third way. Drive the car over a very bumpy road, all the time listening carefully to its reaction to this particular kind of continuous random agitation. Stochastic excitation (1–6) seeks to examine the possibilities of this largely overlooked procedure for NMR spectroscopy. There is a certain elegance in the use of random noise to interrogate the spin system, once we have satisfied ourselves that this should not in itself contribute additional noise to our final spectrum.

Strictly speaking, the stochastic resonance experiment should be carried out with white noise excitation, where the root-mean-square noise level is independent of frequency, and with a Gaussian distribution of amplitudes. White noise applied to a spin system acquires a 'colour' – information about the spin system that will eventually be converted into the familiar high-resolution NMR spectrum. In practice it is quite acceptable to employ pseudo-random binary noise generated by a shift register. This controls the pulse phase (0° or 180°) of a regular sequence of radiofrequency pulses, with a typical duty cycle of about 1%. Once a steady-state response to the initial pulses has been established, the NMR response is sampled (once) in each interval between pulses. The pulse repetition rate is therefore the sampling rate, and must be adjusted so as to satisfy the Nyquist condition (see Digitization*). Alongside the NMR response we retain a record of the pseudo-random code used to excite that particular section of the NMR signal. This is essential, because we shall later unscramble the coding of the NMR information by computing the cross-correlation between the excitation function and the signal response.

DATA PROCESSING

Data reduction is considerably more complicated than in conventional Fourier transform NMR, and only an outline will be presented here. The detected signal is a very long string of apparently random ordinates, but it actually contains both NMR information and the imposed pseudo-random noise. Our task is to separate the two, keeping the genuine NMR data (and genuine thermal noise) but removing the imposed excitation noise. At any given point in time, the NMR signal represents the response to all the previous radiofrequency pulses, extending backwards in time for T_2^*, the decay time constant due to instrumental imperfections, mainly the inhomogeneity of the applied magnetic field. If we assume for the moment that the excitation is weak, and that only the linear (first-order) response term is appreciable, the detected signal y(t) can be represented as the convolution of the stochastic excitation function x(t) with the NMR system impulse response $k_1(t)$

$$y(t) = \int_0^\infty k_1(\tau)\, x(t-\tau)d\tau. \qquad [1]$$

In this context, $k_1(t)$ is equivalent to the familiar free induction decay.

In order to extract $k_1(t)$ we have to deconvolute x(t) from y(t) by a process of cross-correlation. This can be performed either in the time domain or in the frequency domain, but for practical reasons of speed and data storage, it is usually carried out in the frequency domain. This has the important advantage that it is possible to examine just those selected regions of frequency space that contain the NMR lines of interest.

Typically a record containing of the order of 10^6 time-domain samples would be acquired. This is first subdivided into M equal sections, each with a duration of T seconds, where 1/T will determine the attainable resolution. Each section is Fourier transformed, the NMR response y(t) becoming a spectrum y(f) which contains recognizable resonance lines grossly distorted by the excitation noise. The excitation function x(t) is transformed into x(f).

First x(f) and y(f) are cross-correlated (by complex multiplication and averaging) and then the results are averaged with those from the remaining M – 1 sections of the initial record. Since each of the M sections is statistically independent of the rest (a very long pseudo-random sequence is used), both the systematic and thermal noise are reduced by this process. An even higher degree of suppression of systematic noise can be achieved by oversampling the NMR data (7), imposing a much finer time grid than required by the Nyquist condition. With these precautions, systematic noise from the excitation is reduced well below the thermal noise level, and the sensitivity should match that of conventional Fourier transform NMR.

Operated in this simple mode, stochastic excitation has one important attribute – it achieves excitation over a wide frequency band with low radiofrequency power, essentially combining the advantage of continuous-wave excitation (low power)

with that of hard-pulse excitation (rapid data acquisition). This could prove useful in very-high-field spectrometers, particularly where high radiofrequency power or peak voltage must be limited. One application might be in cryogenic probes designed with superconducting radiofrequency coils (8).

HIGHER-ORDER RESPONSES

In practice, stochastic excitation is normally operated in a non-linear regime where the NMR response is partly saturated; this improves the sensitivity at the expense of a certain amount of line broadening. It also opens up some exciting possibilities, such as coherence transfer schemes equivalent to the well-known two-dimensional correlation experiments. This involves the calculation of the *three-dimensional* cross-correlation between y(f) and x(f), instead of the one-dimensional cross-

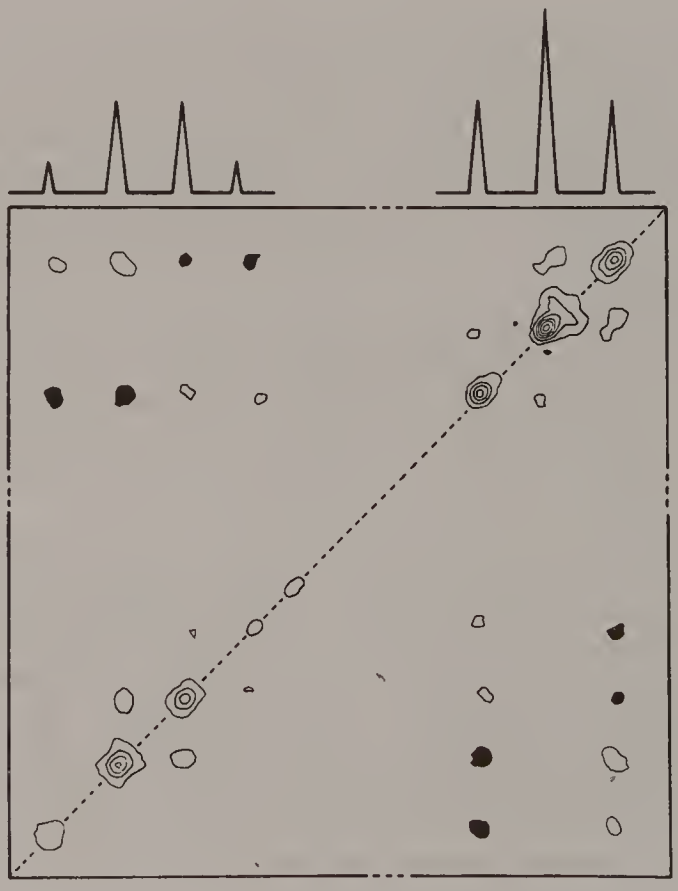

Fig. 1. A two-dimensional correlation spectrum of protons in ethanol obtained by stochastic excitation. This contour map represents selected regions from a section through the stochastic excitation data. Negative contours are indicated in black. Reproduced by permission from B. Blümich and R. Kaiser (9).

correlation described above. A particular section through the resulting three-dimensional spectrum yields a contour map very similar to a COSY spectrum. An example is shown in Fig. 1 for the two-dimensional correlation spectrum of the protons in ethanol, where the usual cross-peaks are evident, made up of the familiar antiphase square patterns of lines (9). Unfortunately one region of this spectrum is obscured by strong noisy ridges passing through the intense diagonal peaks, attributable to cross-talk from the one-dimensional cross-correlation spectrum; this section of the record is not displayed. Clearly there is scope for technical improvements in the stochastic resonance methodology.

Chemical exchange can be studied by stochastic excitation and (with special precautions) nuclear Overhauser effects can also be investigated. Of course, years of intensive development have perfected hard-pulse multidimensional methods that now solve these problems with ease, so the motivation for investigating stochastic methods is low, and only very slow progress has been made. It is claimed (but not yet demonstrated) that the method offers an exciting new *modus operandi* for high-resolution NMR. Excite the spins in a strongly non-linear fashion and store the data. Extract all the different types of information (one-dimensional spectrum, correlations of various kinds) *off-line from the spectrometer* simply by processing the experimental data in different ways. This complete separation of data gathering from the usual spin gymnastics would allow the harassed chemist to return to a problem at some later date in order to extract further information, without the need to run any new experiments.

REFERENCES

1. R. R. Ernst, *J. Magn. Reson.* **3**, 10 (1970).
2. R. Kaiser, *J. Magn. Reson.* **3**, 28 (1970).
3. B. Blümich and D. Ziessow, *J. Magn. Reson.* **52**, 42 (1983).
4. B. Blümich and D. Ziessow, *J. Chem. Phys.* **78**, 1059 (1983).
5. B. Blümich and R. Kaiser, *J. Magn. Reson.* **54**, 486 (1983).
6. B. Blümich, *Prog. NMR Spectrosc.* **19**, 331 (1987).
7. J. Paff, R. Freeman and B. Blümich, *J. Magn. Reson. A* **102**, 332 (1993).
8. W. A. Anderson, W. W. Brey, A. L. Brooke, B. Cole, K. A. Delin, J. F. Fuks, H. D. W. Hill, M. E. Johanson, V. Y. Kotsubo, R. Nast, R. S. Withers and W. H. Wong, *Bull. Magn. Reson.* **17**, 98 (1995).
9. B. Blümich and R. Kaiser, *J. Magn. Reson.* **58**, 149 (1984).

Cross-references

Correlation spectroscopy
Digitization
Fourier transformation
Free induction decay
Steady-state effects

t_1 Noise

Two-dimensional NMR spectra suffer from a persistent artefact usually known as *t_1 noise*. This is a band of noisy fluctuations that runs parallel to the F_1 axis wherever there is a strong resonance peak in the two-dimensional spectrum. The problem is particularly serious for aqueous solutions since the t_1 noise may remain, even though the parent water line has been largely cancelled by difference spectroscopy. The artefact is actually made up of two parts – an apparently random fluctuation, significantly larger than the true thermal noise, and a net displacement of the baseline that is too large to be accounted for by the tails of the intense resonance line, even allowing for aliasing at the edges of the spectrum. The presence of this 'F_1 ridge' tends to make the noisy component more obtrusive by raising the mean level of the t_1 noise.

We consider first of all the F_1 ridge. Although it is difficult to disentangle this from the t_1 noise itself, it is often clear that a d.c. component is present. This implies that the first data point on that particular t_1 interferogram has an anomalously high intensity due to the presence of a strong NMR response at that F_2 frequency. One possible explanation is that the repetition rate in the t_1 domain is too high to allow adequate spin–lattice relaxation, leading to the establishment of steady-state longitudinal magnetization (partial saturation) rather than Boltzmann equilibrium. Since the experiment is usually initiated with $t_1 = 0$, the first point acquired on the t_1 interferogram corresponds to a spin system at thermal equilibrium, and therefore has higher intensity than the rest. The usual remedy is to program a few 'dummy runs' through the pulse sequence before data acquisitions are initiated. Another expedient is to run the t_1 evolution in reverse, starting with the longest value, t_1(max), and ending with zero.

With some computer software there could be a more insidious problem arising from improper sampling of data fed to the Fourier transform program. A smooth analogue signal is digitized by slicing it up into a sequence of trapezia, representing the area of each trapezium as a number. Ideally, the time registration of this data point should be the centre of the corresponding slice, not the beginning nor the end. However, if the first data point is taken at time zero, it should be halved in intensity because it represents only half a slice (the first half is missing). See Baseline correction*. A similar problem arises in the conversion of a soft radiofrequency

pulse into the equivalent DANTE sequence (1). The resulting slight baseline offset usually goes unnoticed in one-dimensional spectroscopy, but in two-dimensional spectra it can contribute to the F_1 ridge.

The t_1 noise should be clearly distinguished from true thermal noise originating in the receiver coil and associated amplifiers. It arises because various types of instrumental instabilities cause fluctuations in the amplitude of the free induction decay between one increment of t_1 and the next (2). These instabilities have no effect unless there is a strong NMR signal at that particular F_2 frequency. These are exactly the same types of longer-term perturbations that cause problems in difference spectroscopy*, for example in studies of the nuclear Overhauser effect.

A common and often serious source of instability arises in the field/frequency regulation scheme if the deuterium reference signal has an inadequate signal-to-noise ratio. In one-dimensional spectra this shows up as a line broadening and noisy fluctuations in the skirts of the resonance line, because the bandwidth of these fluctuations tends to be quite narrow. By contrast, in two-dimensional spectroscopy* the t_1 noise is distributed along the entire F_1 frequency dimension. The remedy is to employ a sufficiently strong deuterium reference material and careful field shimming.

Another source of t_1 noise arises if the phase or amplitude of the transmitter pulses are not properly reproducible. This type of fluctuation has little impact on one-dimensional spectra, because several free induction decays subject to slight changes in phase or amplitude can be accumulated without any noticeable degradation in the resulting spectrum. In two-dimensional spectroscopy, on the other hand, this can make an important noisy contribution to F_1 traces if they include an intense resonance line. Similar longer-term fluctuations in signal intensity (and linewidth) also come about through variations in the spatial inhomogeneity of the magnetic field. Changes in line position and linewidth often occur through room temperature variations, for example the cycling of an air-conditioning unit. These fluctuations are sampled at a very low repetition rate as t_1 is incremented, and thus appear as noisy contributions over the entire F_1 dimension (through aliasing). Instabilities in the receiver gain or in the receiver phase-shifting circuitry are usually so small over the short term that they can be safely neglected in one-dimensional spectroscopy, but could be appreciable over the much longer t_1 time scale appropriate to multidimensional experiments or difference spectroscopy.

In conventional NMR spectroscopy it is usually a good approximation to assume that the sampling of the free induction decay is perfectly regular in the time domain. This is not necessarily the case for the evolution dimensions of multidimensional spectroscopy because of poor programming or variable delays due to disc transfers. Although these are strictly deterministic errors they appear to be random after Fourier transformation. The signal $S(t_1)$ actually recorded may be thought of as the sum of an ideal signal $S_0(t_1)$ and a superimposed error signal $S_N(t_1)$ that is only present when $S_0(t_1)$ is also present. It is the Fourier transform of $S_N(t_1)$ that constitutes the t_1 noise.

A further insidious consequence of slightly irregular timing of the sampling operations in the t_1 domain is that even a *coherent* perturbation such as a sinusoidal modulation of the magnetic field may generate apparently random fluctuations in the baseline in the F_1 dimension if a strong signal is present. This is because the sampling rate is both irregular and very slow in comparison with most modulation frequencies; the latter get 'chopped up' before being fed into the Fourier transform 'machine'. We can all think of possible sources of spurious coherent modulation – sample spinning, decoupler cycling, mains frequencies, cross-talk from other frequency channels, oscillations in the helium dewar vessel, etc.

Spectra recorded with small spectral widths in the F_1 dimension are particularly susceptible to t_1 noise. In conventional spectroscopy, precautions are taken to avoid aliasing of high-frequency noise by filtration of the signals before analogue-to-digital conversion. It is not feasible to carry out the equivalent operation in the t_1 dimension, with the result that noisy artefacts may be aliased several times from a much wider frequency band, thus increasing the t_1 noise. A particularly serious case occurs in two-dimensional J-spectroscopy* where the spectral width in the F_1 dimension is very small.

In situations where multiscan averaging is used to enhance the signal-to-noise ratio, it can be advantageous to employ *oversampling* in the t_1 dimension (3), that is to say, sampling at a rate several times higher than that required by the Nyquist condition. Since oversampling followed by Fourier transformation performs a signal-averaging role, we can increase the total number of t_1 increments while decreasing the number of t_2 scans in proportion, retaining the same total instrument time and yielding the same signal-to-noise ratio. However, a large fraction of the new F_1 spectral width is now devoid of NMR signals and can be discarded, *along with its associated t_1 noise*. In this manner we avoid unnecessary aliasing of t_1 noise.

REDUCTION OF t_1 NOISE

Since t_1 noise is not true random noise it may be feasible to suppress it by data processing techniques without harming genuine NMR signals. For example, in homonuclear correlation spectroscopy* (COSY) the spectrum is known to be symmetrical about the principal diagonal $F_1 = F_2$; when there is a cross-peak with coordinates (a, b) there must also be another equal cross-peak with coordinates (b, a). By comparing symmetrically related points in the data matrix $S(F_1, F_2)$ and replacing both ordinates with their arithmetic or geometric mean, we can attenuate the bands of t_1 noise because they fail to fulfil the symmetry criterion. A more drastic operation replaces the two symmetrically related ordinates by the lower value, largely eliminating the t_1 noise but barely affecting genuine signals (4). Such non-linear processes should not be applied where there are cross-peaks comparable in intensity with the baseplane noise.

The most promising remedy for t_1 noise is to attack the problem right at the source. The gradual conversion of modern pulse experiments from phase-cycling to

pulsed field gradient methods (5) permits the design of pulse sequences in which the abundant water protons remain dephased throughout, so that not only is the water signal suppressed, but also it no longer contributes to t_1 noise. Hurd (6) has demonstrated a remarkable degree of reduction of such artefacts in the gradient-enhanced double-quantum filtered COSY spectrum of an aqueous sample of angiotensin.

A second powerful attack on the source of the t_1 noise is through reference deconvolution (7). We can represent an experimental NMR resonance lineshape E(f) as an ideal lineshape T(f) distorted by spectrometer instabilities. This ideal lineshape T(f) can be defined by the operator, for example as a pure Lorentzian line of the appropriate width. It may also be expressed as the experimental lineshape E(f) convoluted by a correction function C(f) representing the effects of the instabilities that give rise to t_1 noise. If these perturbations affect all the lines in the spectrum in the same manner, they can be corrected, in principle, by examining their effect on a reference line R(f) that is known to be a singlet. This is formally a deconvolution process if viewed in the frequency domain, but processing is simpler in the time domain, because there only multiplications are involved. A well-isolated reference line is excised from the rest of the spectrum, properly phased, and back-transformed into the time domain, $R(f) \rightarrow R(t)$. The corrected experimental time-domain reference signal C(t)R(t) is equivalent to T(t), the Fourier transform of the ideal lineshape function T(f). Consequently the required time-domain correction function, the transform of C(f), is given by

$$C(t) = T(t)/R(t). \qquad [1]$$

The experimental free induction signal E(t) is then corrected in phase and amplitude at each point by multiplication by the (complex) correction function C(t). In a two-dimensional spectrum we expect the longer-term instabilities to affect all the free induction decays in the same manner, so the t_1 noise is highly correlated from one F_1 trace to the next. Reference deconvolution in the F_1 dimension corrects these imperfections. Deconvolution in both frequency dimensions is also feasible, but may not be necessary.

REFERENCES

1. X. L. Wu, P. Xu and R. Freeman, *J. Magn. Reson.* **81**, 206 (1989).
2. A. F. Mehlkopf, D. Korbee, T. A. Tiggleman and R. Freeman, *J. Magn. Reson.* **58**, 315 (1984).
3. J. M. Nuzillard and R. Freeman, *J. Magn. Reson. A* **110**, 252 (1994).
4. R. Baumann, A. Kumar, R. R. Ernst and K. Wüthrich, *J. Magn. Reson.* **44**, 76 (1981).
5. P. Barker and R. Freeman, *J. Magn. Reson.* **65**, 535 (1985).
6. R. E. Hurd, *J. Magn. Reson.* **87**, 422 (1990).
7. A. Gibbs, G. A. Morris, A. G. Swanson and D. Cowburn, *J. Magn. Reson. A* **101**, 351 (1993).

Cross-references

Baseline correction
Correlation spectroscopy
Difference spectroscopy
Field/frequency regulation
J-spectroscopy
Solvent suppression
Steady-state effects
Two-dimensional spectroscopy

Time Averaging

The NMR phenomenon is such a tiny effect that the thermal fluctuations of the electrons in the receiver coil compete with it. This is called *Johnson noise*. This irreducible minimum of thermal noise masks the weaker NMR signals and thus limits the sensitivity* of the technique. Proper design of the preamplifier and receiver avoids the introduction of additional noise components from the electronic amplifiers and normally ensures that Johnson noise remains the dominant source of noise in the final NMR spectrum.

It then seems natural to enquire whether there is any characteristic property that might distinguish noise from true NMR signals when they both have comparable intensities. The first such criterion is that the noise commonly includes higher-frequency fluctuations than the signals; viewed in the form of a free induction decay, the NMR signals are seen to decay with a time constant T_2^*, whereas the noise remains at a constant level. Sensitivity is therefore improved by the application of a suitable weighting function which de-emphasizes the tail of the free induction decay, usually by multiplying with a decaying exponential, the optimum being the *matched filter* which falls off at the same rate as the NMR signals. Any more drastic filtration reduces the signals faster than the noise and there is no further advantage to be gained.

The second criterion is that signals are reproducible if the experiment is repeated, whereas noise should be uncorrelated from one measurement to the next. (Certain other undesirable artefacts may be reproducible, for example some of the effects responsible for 't_1 noise'* in two-dimensional spectroscopy*.) In the early 1960s it was realized that this could be made the basis of an important new method of sensitivity improvement known as *time averaging*. The instrumentation was developed from the multichannel analyser used in nuclear physics. Klein (1,2) seems to have been the first to bring this important technique to the attention of NMR spectroscopists. That was in the days of continuous-wave spectroscopy* but the same principles apply to Fourier transform methods. Indeed time averaging is essential if the Fourier method is to have any sensitivity advantage.

The spectrum or the free induction decay is sampled at regular intervals and the voltage converted into digital form for storage in a computer. At any given sampling point one expects the same intensity signal each time the experiment is repeated, so the total signal builds up linearly with the number of passes. Noise, being a random phenomenon, fluctuates in sign and intensity and builds up only as

the square root of the number of passes. Consequently the signal-to-noise ratio improves as the square root of the number of free induction decays that are time averaged.

Clearly the method presupposes that the spectrometer has good field/frequency regulation* otherwise the signal component at a given sampling point would also fluctuate and thus the signal-to-noise ratio would not improve as rapidly as expected. As the number of accumulations increases, the dynamic range of the stored signal increases and the number of bits of data storage (the computer word length) eventually becomes a limitation, and double-precision arithmetic may be required. Care must be taken with the round-off errors made by the Fourier transform algorithm since, although these may give the appearance of noise, they are to some extent reproducible and therefore not reduced by time averaging.

Ernst (3) has pointed out that the principle of time averaging still applies if the NMR signal, instead of being identical in each experiment, varies in a periodic manner, for example if it is amplitude modulated as in certain two-dimensional spectroscopy experiments. Consequently, the necessary repetition of the measurements for a large number of different values of the evolution period (t_1) gives rise to a sensitivity improvement similar to that enjoyed by one-dimensional spectroscopy. This accounts for the surprisingly low sensitivity penalty paid by two-dimensional NMR.

The dependence on the square root of the number of recorded free induction decays imposes practical limitations on the extent of time averaging. For many laboratories the operational maximum is the overnight accumulation ($\approx$ 15 hours); a weekend run only improves the sensitivity by another factor of two. Beyond this, sensitivity improvements must be sought, not through noise reduction, but through sensitivity enhancement* or more efficient spin–lattice relaxation*.

REFERENCES

1. M. P. Klein, *American Chemical Society Meeting in Miniature*, University of California at Berkeley, 1962.
2. M. P. Klein and G. W. Barton, *Rev. Sci. Instrum.* **34**, 754 (1963).
3. R. R. Ernst, Sensitivity Enhancement in Magnetic Resonance. In *Advances in Magnetic Resonance*, ed. J. S. Waugh. Academic Press: New York, Vol. 2, 1966.

Cross-references

Continuous-wave spectroscopy
Field/frequency regulation
Fourier transformation
Sensitivity
Sensitivity enhancement
Spin–lattice relaxation
t_1 noise
Two-dimensional spectroscopy

Transient Nutations

The Earth spins about its axis and this axis itself moves on the surface of a cone, that is, it *precesses*. In addition, the angle of this cone is not constant; there is an additional wobbling of the precession axis, called a *nutation*. Nuclei have the same types of motion – spin, precession and nutation, the latter being taken now to mean any periodic variation of the precession axis. In order to stay with classical (as opposed to quantum-mechanical) motion we must consider the net macroscopic magnetization vector M, the resultant of all the individual nuclear magnetizations in the sample. The motion takes on its simplest form in the rotating frame* of reference.

At thermal equilibrium M is aligned along the +Z axis and not much of interest is happening. Suppose we suddenly apply a radiofrequency field B_1 along the X axis, with B_1 strong compared with any resonance offset ΔB. The subsequent motion of M is called a *transient nutation*. In this simple case M describes a circular path in the ZY plane; in the laboratory frame this would appear as a rather drastic nutational motion. This induces a sinusoidally modulated NMR response in the receiver, peak signals being observed as M passes through the +Y and –Y axes.

Torrey (1) has analysed this experiment and has shown that the magnetization decays with a time constant T given by

$$\frac{1}{T} = \frac{1}{2}\left(\frac{1}{T_1} + \frac{1}{T_2}\right). \qquad [1]$$

That is to say, both spin–spin and spin–lattice relaxation influence the decay of the observed NMR signal. In the majority of NMR experiments B_1 is switched off after a very short time and we have (say) a 90° or 180° pulse; during such short intervals relaxation is usually neglected.

In situations where the transient nutations are allowed to continue for many rotations, it is observed in practice that the signal decays appreciably faster than predicted by eqn [1]. This is a result of the spatial inhomogeneity of the radiofrequency field B_1, magnetization vectors from different volume elements of the sample (*isochromats*) nutating at different rates and fanning out in the YZ plane. Solomon (2) discovered that this effect could be refocused by suddenly reversing the phase of the radiofrequency field B_1 giving a *rotary echo* analogous to the spin echoes* generated by refocusing the effect of B_0 inhomogeneities.

Transient nutations are also observed if the radiofrequency field B_1 is applied continuously but the nuclear magnetization is generated abruptly, and this is sometimes a useful mode of detection because the constant frequency nutation signal provides a characteristic, easily recognized, pattern. For example, transient nutations are observed in pulse-modulated double-resonance experiments (3) and in chemically induced electron spin polarization (4) where magnetization is suddenly created by a laser pulse. The method provides a convenient practical scheme for monitoring polarization transfer* effects. Instead of sitting on the peak of a line with a very weak B_1 field, subjected to the vicissitudes of poor field/frequency regulation*, a strong (saturating) B_1 field may be used since it is not the natural NMR signal that is of interest but the sudden polarization transfer from another site.

Figure 1 illustrates the transient nutations observed for the three-spin ABC system of protons in 2-chlorothiophene (5). This is a continuous-wave experiment

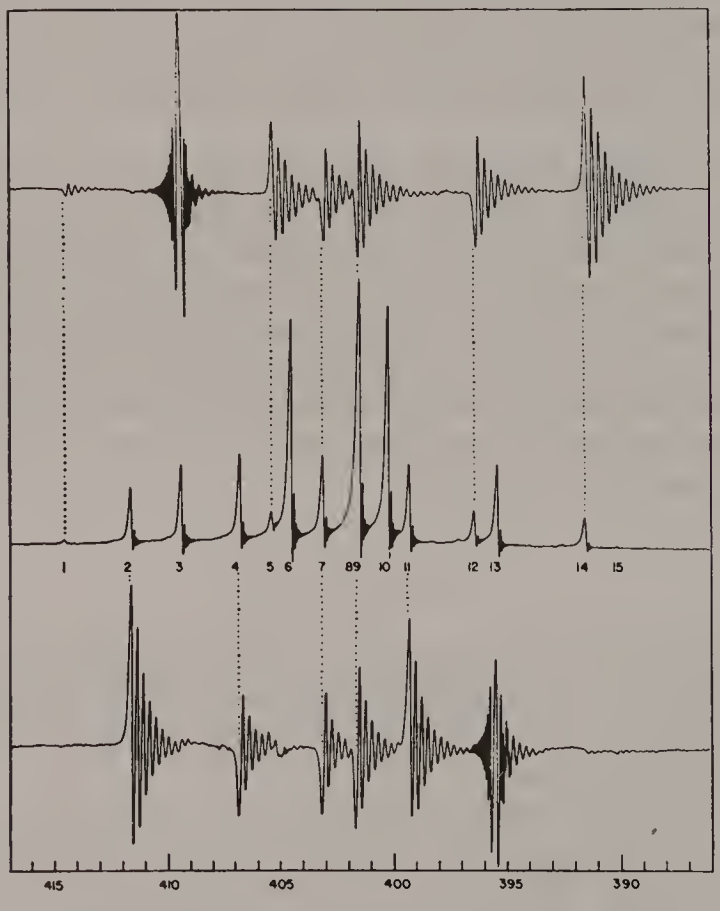

Fig. 1. Transient nutations excited by monitoring one of the lines of the proton spectrum of 2-chlorothiophene (centre) with a saturating continuous-wave field B_1 while sweeping a strong perturbing field B_2 through the entire spectrum. Line 3 is monitored in the upper trace and line 13 in the lower trace. A progressively connected transition gives a positive-going response and a regressively connected transition a negative-going response. The nutation frequency is $\gamma B_1/2\pi$ multiplied by the transition probability of the monitored line.

where the B_1 field is adjusted to exact resonance for a chosen line and has sufficient intensity to saturate that line. The second radiofrequency field B_2 is swept through the same spectrum under conditions of adiabatic rapid passage*. Whenever B_2 passes through a transition it inverts the appropriate spin population; if this transition has an energy level in common with the transition monitored by B_1, a transient nutation is excited. Progressively connected transitions show a positive-going nutation whereas regressively connected transitions show a negative-going nutation.

REFERENCES

1. H. C. Torrey, *Phys. Rev.* **76**, 1059 (1949).
2. I. Solomon, *Phys. Rev. Lett.* **2**, 301 (1959).
3. R. Freeman, *J. Chem. Phys.* **43**, 3087 (1965).
4. P. J. Hore and K. A. McLauchlan, *Mol. Phys.* **42**, 533 (1981).
5. J. A. Ferretti and R. Freeman, *J. Chem. Phys.* **44**, 2054 (1966).

Cross-references

Adiabatic rapid passage
Field/frequency regulation
Polarization transfer
Rotating frame
Spin echoes

Two-dimensional Spectroscopy

The advent of Fourier transform methods in NMR (1) achieved two important advantages that were immediately exploited. The first was the dramatic improvement in sensitivity brought about by monitoring all the resonances in the spectrum simultaneously rather than one at a time – the so-called multiplex advantage. The second was the possibility of studying time-dependent phenomena such as spin–spin and spin–lattice relaxation, chemical exchange, and transient nuclear Overhauser effects. Prior to the Fourier transform revolution, the techniques available for following these transient phenomena had been very cumbersome. Imagine having to sweep through a spectrum under slow-passage conditions when the phenomenon under investigation is changing the intensities on a time scale of seconds.

A third development, of comparable importance with the other two, passed almost unnoticed at the time. At a summer school in the former Yugoslavia, Jeener (2) described a novel experiment in which a coupled spin system was excited by a sequence of two 90° pulses separated by a variable time interval t_1. Jeener realized that if t_1 were to be varied in small steps in a series of experiments, this would introduce a new time dimension, and that the signal could be Fourier transformed as a function of t_1. This variable period is now known as the *evolution time*. The other independent time dimension (t_2) is the running variable for sampling the free induction decay, but no signal acquisition takes place during the evolution time. Information about the behaviour of the nuclear spins during t_1 is only derived indirectly by detecting its influence on the set of free induction decays. This relies on the fact that the spins possess a memory of what happened to them in the past, a memory with a time constant T_2, the spin–spin relaxation time. The evolution of the spins is mapped out point by point by incrementing t_1 in suitable small steps while detecting the free induction decays.

Although Jeener obtained experimental spectra by this new two-dimensional method, the equipment available at the time was quite unstable and the spectra were consequently very noisy. He decided not to publish them for fear that they might jeopardize the acceptance of the two-dimensional concept. Much of the credit for demonstrating the generality of the idea and for extending it to many more applications is due to Ernst (3). Close parallels can be traced with the development of double-resonance methods in the previous decade; indeed most two-dimensional

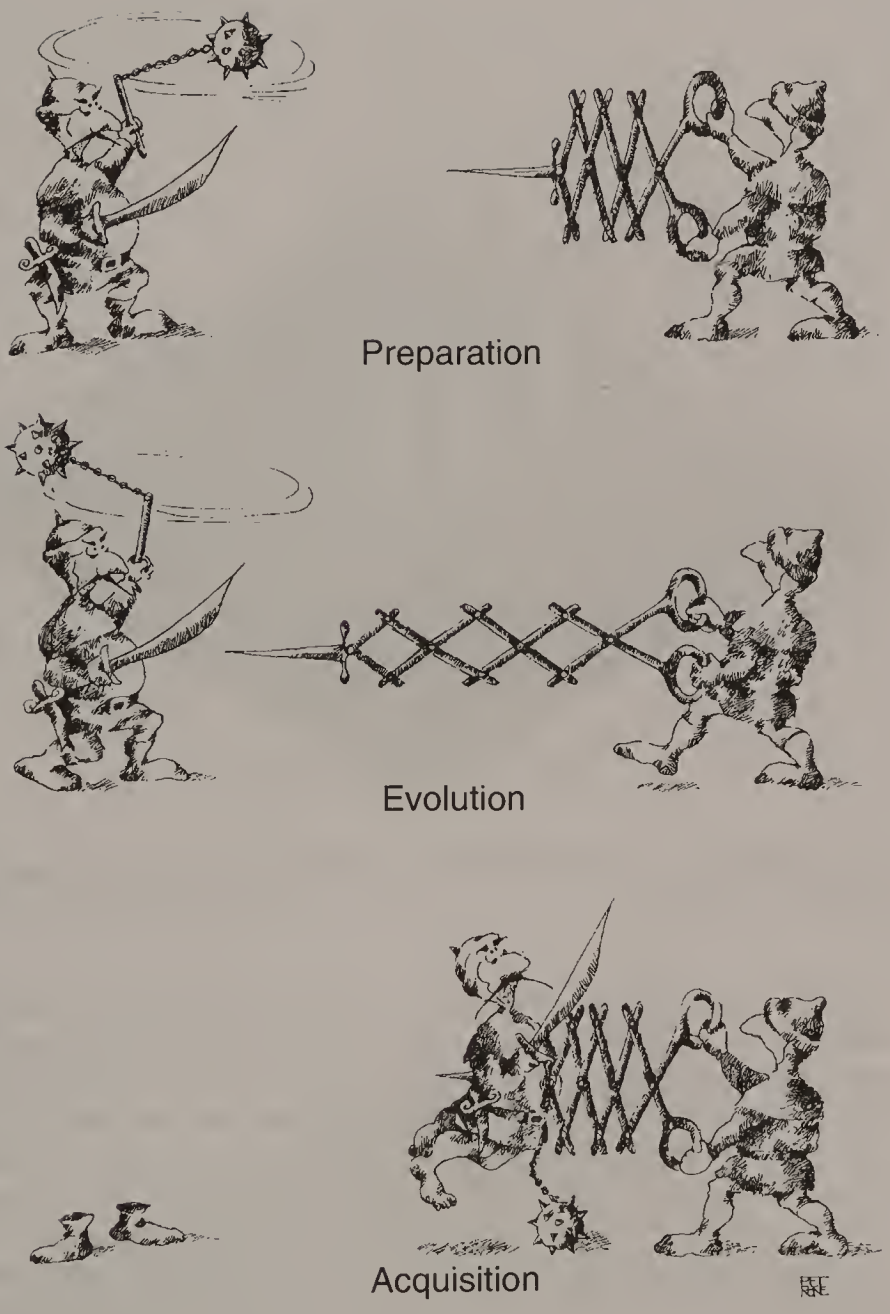

experiments can be thought of as the translation of double-resonance techniques into the time domain.

It is convenient to think of the experimental data (3–6) as a two-dimensional array $S(t_1, t_2)$. In the simplest case where there is only one frequency present, this array might look like Fig. 1. The signal follows a decaying cosine wave in both time dimensions. We could imagine converting this array directly into a two-dimensional spectrum $S(F_1, F_2)$ through two-dimensional Fourier transformation, but in practice this operation is carried out in two stages. First of all, each free

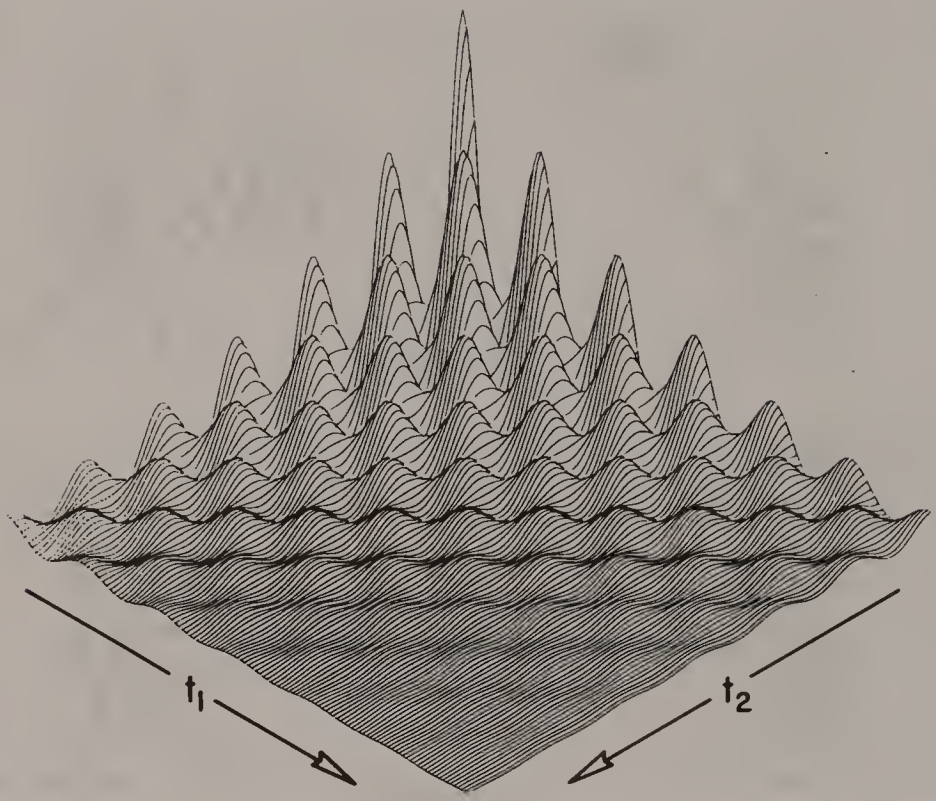

Fig. 1. Schematic diagram of the data array $S(t_1, t_2)$ when there is a single decaying cosine wave in both time dimensions.

induction decay $S(t_2)$ is Fourier transformed, one for every increment t_1, creating a new array $S(t_1, F_2)$ which has spectra in one dimension and an oscillatory signal, sometimes called an *interferogram*, in the other (Fig. 2). It is now necessary to read this array in the other sense, that is to say, to follow the modulation in the t_1 dimension for each and every point in the spectrum $S(F_2)$. Because the array $S(t_1, F_2)$ is usually quite large, it is often stored in a linear fashion on a disc, so it may be necessary to rearrange the data set $[S(t_1, F_2) \rightarrow S(F_2, t_1)]$ so that it can be read in the form of interferograms (Fig. 3). Then the second Fourier transformation can be carried out as a function of t_1 to give the two-dimensional spectrum $S(F_1, F_2)$. For this very simple example, the spectrum is only a single peak (Fig. 4) which happens to have the characteristic shape of a two-dimensional Lorentzian because we assumed that the signal decayed exponentially in both time dimensions.

An important factor that has contributed to the general acceptance of two-dimensional spectroscopy has been its inherently high sensitivity – comparable with that of a one-dimensional experiment accumulated for the same total time. As far as the signal-to-noise ratio is concerned, there is little to choose between time averaging an amplitude-modulated time-domain signal, and time averaging an equal set of identical signals. Looked at from a different viewpoint, this multiplex advantage comes about because two-dimensional spectroscopy spreads the noise

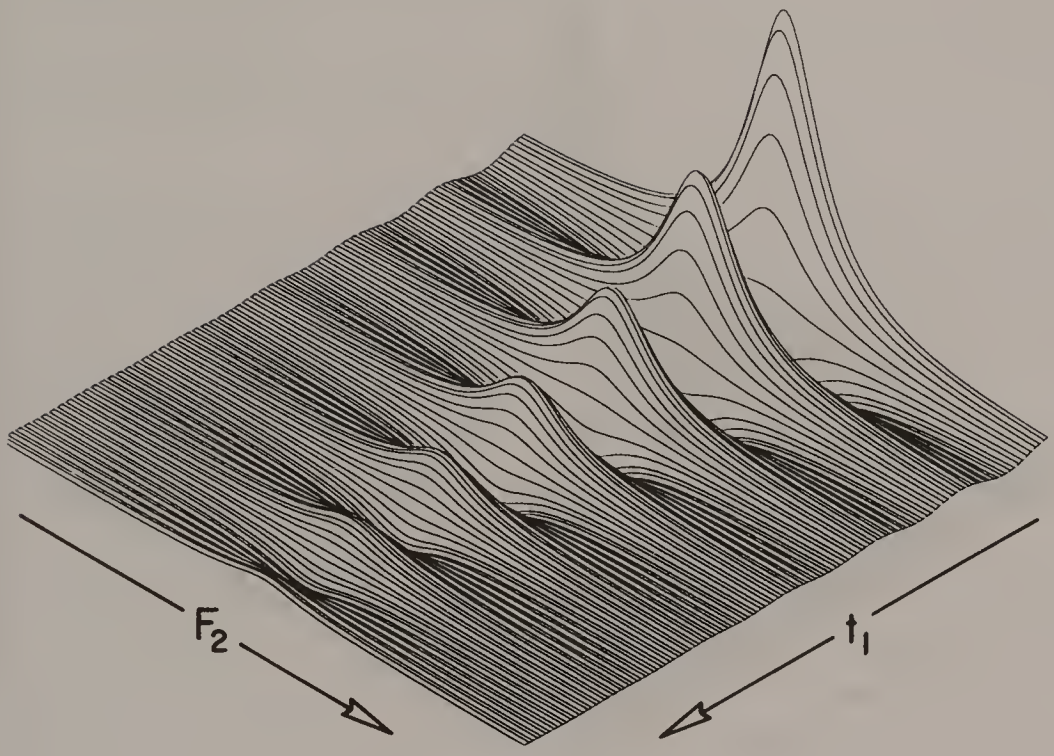

Fig. 2. The intermediate data array $S(t_1, F_2)$ obtained from Fig. 1 by Fourier transformation with respect to t_2.

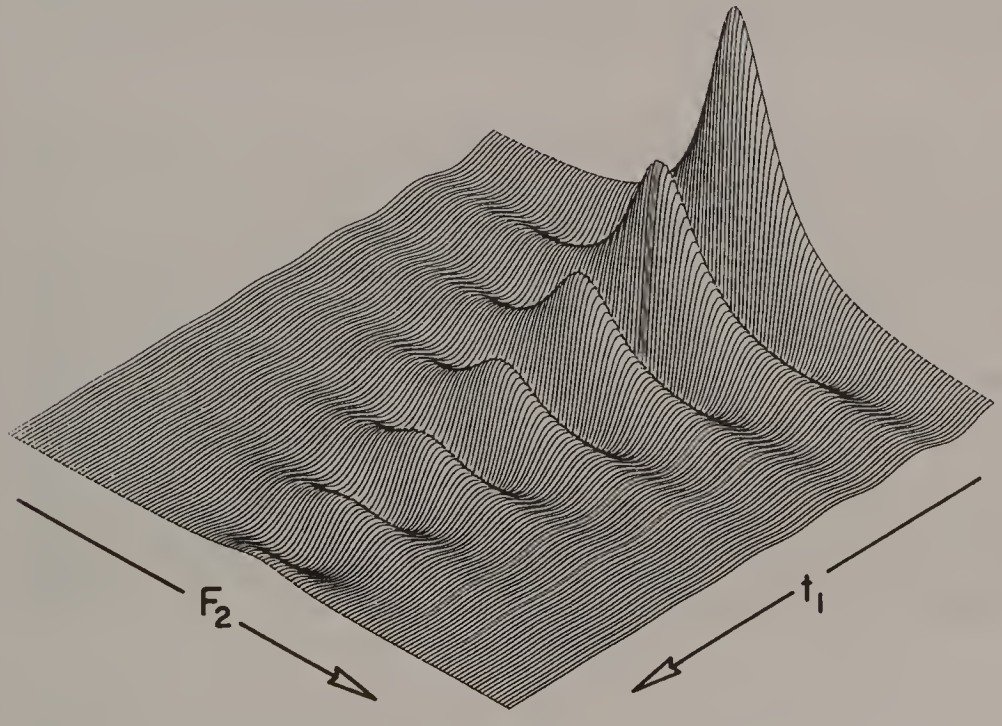

Fig. 3. Transposition of the data array shown in Fig. 2 so as to provide rapid access to t_1 traces in preparation for the second stage of Fourier transformation.

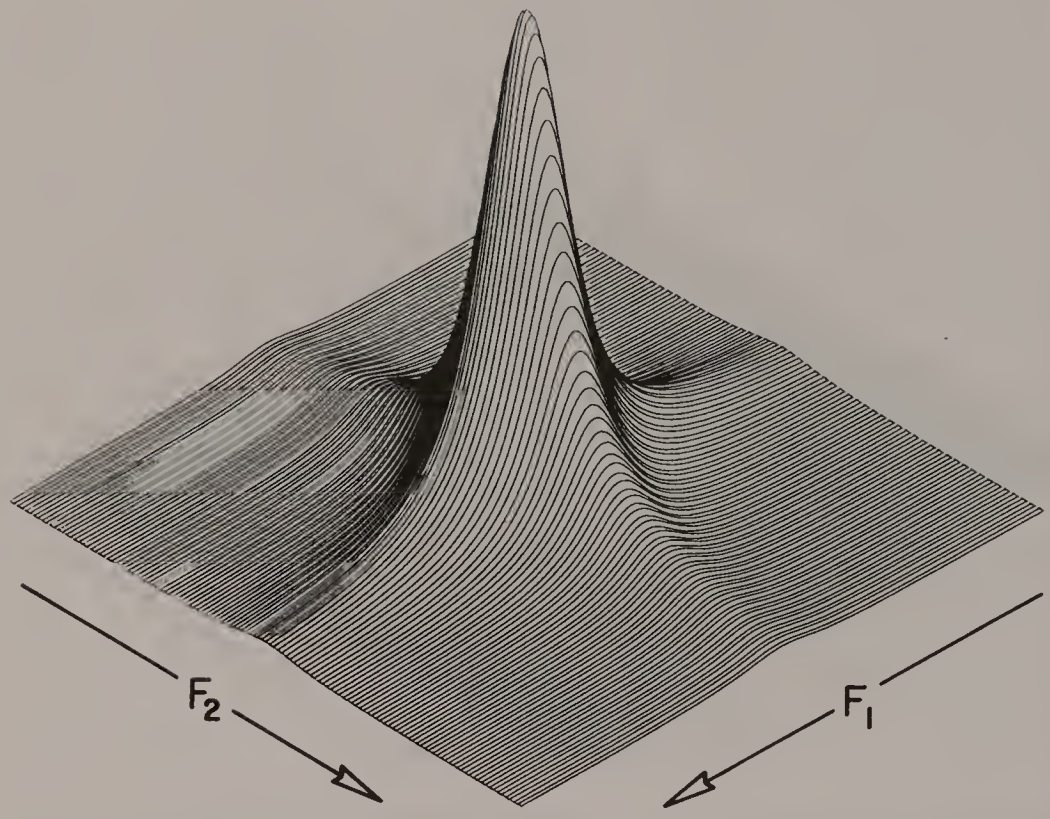

Fig. 4. A two-dimensional Lorentzian line obtained by Fourier transformation of the data array in Fig. 3 with respect to t_1. The Lorentzian shape originates in the assumption that the signal in Fig. 1 decayed exponentially in both time dimensions.

out over a plane, without reducing the signal amplitudes. Jeener in fact anticipated this key feature in the abstract of his summer school presentation (2).

So far this is not too exciting. The importance of Jeener's idea stems from the fact that the conditions governing the motion of the spins during the evolution period may be different from those prevailing during the detection period; indeed we must arrange for this to be so. Furthermore, the precession occurring during t_1 may represent a formally forbidden transition, since we only detect it indirectly. Consequently there are very many possible two-dimensional experiments, limited mainly by the spectroscopist's ingenuity. They may be divided into three broad categories, although it can be dangerously unproductive to insist on hard-and-fast rules about two-dimensional spectroscopy. It makes surprising leaps into quite new fields, for example Fourier zeugmatography (7), one of the most powerful methods for magnetic resonance imaging.

SEPARATION OF PARAMETERS

Chemical shifts can be separated from spin–spin coupling effects by performing a spin-echo experiment during the evolution time t_1:

$$90° - \tfrac{1}{2}t_1 - 180° - \tfrac{1}{2}t_1 - \text{acquisition } (t_2). \qquad [1]$$

The chemical shifts are refocused by the 180° pulse but the divergence due to spin coupling persists, because the term $J_{IS}I_ZS_Z$ remains unaffected by the 180° pulse. The resulting 'J-spectrum' has spin multiplets displayed in the F_1 dimension and the conventional (coupled) spectrum in the F_2 dimension. This technique is treated in detail under J-spectroscopy*. It can be used to obtain high-resolution proton spectra without spin–spin splittings (8).

CORRELATION EXPERIMENTS

If the polarization or coherence that exists at a given chemical site during the evolution period is transferred to another site before detection, then this is said to be a *correlation* experiment, because it identifies the two sites as having a spin–spin interaction. This is the ubiquitous COSY experiment (3), treated in detail under Correlation spectroscopy*. It provides, in a single spectrum, all the information that would be obtained from a large number of selective decoupling experiments, and presents it in the convenient form of a contour diagram (9) in which pairs of cross-peaks indicate spin–spin interactions.

We might be tempted to generalize correlation experiments to include two-dimensional nuclear Overhauser spectroscopy (NOESY) (10) and chemical exchange spectroscopy (EXSY) (11) where, although the interactions are different, the basic principle is the same. These two-dimensional experiments include a 'mixing period' t_m between evolution and detection to allow time for cross-relaxation or chemical exchange. The nuclear Overhauser effect* has proved to be of enormous importance for the structure determination of biological macromolecules in solution, where information about internuclear distances is invaluable.

FORBIDDEN TRANSITIONS

Multiple-quantum coherence* is said to be 'invisible' in the sense that it does not induce any voltage in the receiver coil. We might think of it as two diametrically opposed vectors, rotating in the XY plane at the same rate, and always having a zero resultant. Multiple-quantum coherence must be detected indirectly, by allowing it to precess during the evolution period of a two-dimensional experiment. Just before the detection stage, a radiofrequency pulse converts it into observable transverse magnetization. Multiple-quantum spectra can offer some important

simplifications compared with conventional high-resolution spectra of complex spin systems. There are fewer transitions, and the spin multiplet structure is simpler because the active spin–spin splittings do not appear in these spectra (12). Furthermore, multiple-quantum spectra can be separated according to the order of coherence, either through the excitation scheme or by the use of the appropriate multiple-quantum filters (13).

One useful application is to detect pairs of directly bound carbon-13 spins in molecules of samples with the natural isotopic abundance, in spite of the fact that molecules with isolated carbon-13 nuclei outnumber them by two orders of magnitude. The experiment relies on the fact that only pairs of coupled spins can support double-quantum coherence, so a suitable phase cycle, or pulsed field gradient sequence, can be employed to filter out the desired response, even though it is very weak. This is the two-dimensional 'INADEQUATE' experiment (14) which has proved to be a powerful tool for determining the structure of the carbon 'skeleton' of an organic molecule by building up a picture of the carbon–carbon connectivity one bond at a time. Its main drawback is the inadequate sensitivity.

MULTIDIMENSIONAL SPECTROSCOPY

It was some time before anyone ventured to tack two two-dimensional pulse sequences together to implement a three-dimensional experiment (15,16). But, as larger and more complex molecules come under investigation, the ability to spread the information into yet another frequency dimension seems more and more attractive. We might write a three-dimensional experiment schematically as

$$\text{preparation} - \text{evolution } (t_1) - \text{mixing} - \text{evolution } (t_2) - \text{mixing} - \text{detection } (t_3). \quad [2]$$

The basic building blocks are often the popular two-dimensional techniques such as COSY, NOESY or TOCSY (17). The duration of the experiment is primarily determined by the product of the number of increments in t_1 and t_2, and by any phase cycling that is used.

It is not really feasible to make useful measurements from cross-peaks distributed in three frequency dimensions, so plane sections are normally displayed. Consider the case of a three-dimensional correlation experiment performed on a coupled three-spin (ISR) system. We might investigate transfers of the type $I \rightarrow S \rightarrow S$, which give rise to peaks on the first mixing plane (Fig. 5(a)), or transfers of the type $S \rightarrow S \rightarrow R$, which give rise to peaks in the second mixing plane (Fig. 5(b)), or back-transfers of the type $I \rightarrow S \rightarrow I$, giving peaks in the back-transfer plane (Fig. 5(c)). The true three-dimensional cross-peaks, generated by two consecutive transfers of the type $I \rightarrow S \rightarrow R$, are not located on any of these planes.

Three-dimensional spectroscopy really comes into its own when biosynthetic isotopic enrichment is used to simplify two-dimensional spectra, for example the

NOESY spectra of protons in macromolecules such as proteins. These experiments rely on a 'round-trip' coherence transfer (18) of the kind

$$\text{protons} \rightarrow \text{carbon-13} \rightarrow \text{protons}$$

or

$$\text{protons} \rightarrow \text{nitrogen-15} \rightarrow \text{protons}.$$

(See Polarization transfer*.) The third dimension serves to separate a set of proton NOESY subspectra, one for each chemical shift of the heteronuclear species.

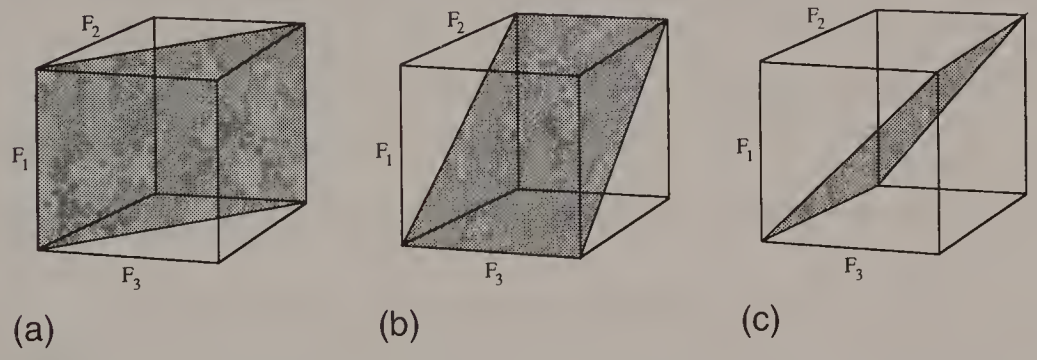

Fig. 5. Selection of particular sections through a three-dimensional spectrum representing two stages of coherence transfer. (a) The first mixing plane, showing transfers of the type $I \rightarrow S \rightarrow S$. (b) The second mixing plane, showing transfers of the type $S \rightarrow S \rightarrow R$. (c) The back-transfer plane showing transfers of the type $I \rightarrow S \rightarrow I$.

IMPACT ON CONVENTIONAL NMR

The ramifications of Jeener's original idea are not limited to multidimensional spectroscopy. It stimulated the new science of 'spin choreography' in which spin systems were manipulated in the most ingenious ways in order to extract useful information. The polarization transfer experiment INEPT (19) is a direct descendant of heteronuclear correlation schemes. Multiplicity determinations in carbon-13 spectroscopy employing spin-echo modulation can be thought of as a projection of the corresponding two-dimensional J-spectrum onto the F_2 axis (20). Many two-dimensional experiments have been converted into one-dimensional counterparts by employing selective radiofrequency pulses (21,22). Even the concept of broadband decoupling* with 180° pulses can be traced back to ideas first advanced in the context of two-dimensional correlation spectroscopy (23). It seems that Jeener's idea, rather tentatively proposed in 1971, has proved one of the most important stimuli for innovation in high-resolution NMR spectroscopy.

REFERENCES

1. R. R. Ernst and W. A. Anderson, *Rev. Sci. Instrum.* **37**, 93 (1966).
2. J. Jeener, *Ampere International Summer School,* Basko Polje, Yugoslavia, 1971, reported in *NMR and More. In Honour of Anatole Abragam,* ed. M. Goldman and M. Porneuf. Les Editions de Physique: Les Ulis, France, 1994.
3. W. P. Aue, E. Bartholdi and R. R. Ernst, *J. Chem. Phys.* **64**, 2229 (1976).
4. R. Freeman and G. A. Morris, *Bull. Magn. Reson.* **1**, 5 (1979).
5. R. Freeman, *Proc. R. Soc. A* **373**, 149 (1980).
6. A. Bax, *Bull. Magn. Reson.* **7**, 167 (1985).
7. A. Kumar, D. Welti and R. R. Ernst, *J. Magn. Reson.* **18**, 69 (1975).
8. W. P. Aue, J. Karhan and R. R. Ernst, *J. Chem. Phys.* **64**, 4226 (1976).
9. A. Bax and R. Freeman, *J. Magn. Reson.* **44**, 542 (1981).
10. K. Wüthrich, *NMR of Proteins and Nucleic Acids.* John Wiley: New York, 1986.
11. J. Jeener, B. H. Meier, P. Bachmann and R. R. Ernst, *J. Chem. Phys.* **71**, 4546 (1979).
12. X. L. Wu, P. Xu and R. Freeman, *J. Magn. Reson.* **88**, 417 (1990).
13. U. Piantini, O. W. Sørensen and R. R. Ernst, *J. Am. Chem. Soc.* **104**, 6800 (1982).
14. A. Bax, R. Freeman and S. P. Kempsell, *J. Am. Chem. Soc.* **102**, 4849 (1980).
15. G. W. Vuister and R. Boelens, *J. Magn. Reson.* **73**, 328 (1987).
16. C. Griesinger, O. W. Sørensen and R. R. Ernst, *J. Magn. Reson.* **73**, 574 (1987).
17. L. Braunschweiler and R. R. Ernst, *J. Magn. Reson.* **53**, 521 (1983).
18. D. Marion, L. E. Kay, S. W. Sparks, D. A. Torchia and A. Bax, *J. Am. Chem. Soc.* **111**, 1515 (1989).
19. G. A. Morris and R. Freeman, *J. Am. Chem. Soc.* **101**, 760 (1979).
20. M. H. Levitt and R. Freeman, *J. Magn. Reson.* **39**, 533 (1980).
21. H. Kessler, S. Mronga and G. Gemmecker, *Magn. Reson. Chem.* **29**, 527 (1991).
22. R. Freeman, *Chem. Rev.* **91**, 1397 (1991).
23. A. A. Maudsley, A. Wokaun and R. R. Ernst, *Chem. Phys. Lett.* **55**, 9 (1978).

Cross-references

Broadband decoupling
Chemical exchange
Correlation spectroscopy
J-spectroscopy
Lineshapes in two-dimensional spectra
Multiple-quantum coherence
Nuclear Overhauser effect
Polarization transfer
Selective excitation

Vector Model

Spin choreography is becoming more and more intricate. Many modern NMR experiments involve complex manipulations of nuclear magnetizations – enhancement, decoupling, correlation, refocusing, scaling, filtration, editing or purging. A simple scheme for visualizing these operations is therefore essential. The density operator theory is generally too cumbersome for the task, so many spectroscopists adopt the shorthand product operator formalism*, usually reduced to the bare minimum. Otherwise any intuitive insight is quickly lost if there are several coupled spins or if the manipulations become too complex. The vector model fills an important gap here, by permitting a ready visualization of possible spin manipulations, thus facilitating the task of devising new pulse sequences.

The vector picture is a natural extension of the classic treatment of magnetic resonance by Bloch (1,2) embodying the transient solutions of the Bloch equations. Although nuclear spins obey quantum laws, the ensemble average, taken over the very large number of spins in a typical sample, behaves just like a classical system, obeying the familiar laws of classical mechanics. We consider (initially) an isolated set of spin-$\frac{1}{2}$ nuclei in an intense field B_0 and represented by a single vector M, the resultant of all the individual nuclear magnetizations within the active volume of the sample. The motion is considered in a rotating frame* of reference, chosen such that the applied radiofrequency field $2B_1 \cos(\omega_0 t)$ can be represented as a static field B_1 aligned along the +X axis of this frame. The counter-rotating component of the radiofrequency field is ignored. In this frame the applied static magnetic field B_0 is reduced to a residual field

$$\Delta B = B_0 - \omega_0/\gamma \qquad [1]$$

so as to retain the Larmor precession condition.

At Boltzmann equilibrium, and in the absence of any recent radiofrequency excitation, the precession phases of individual spins are random and there is no resultant transverse magnetization ($M_{XY} = 0$). The longitudinal magnetization component M_0 reflects the slight excess of spins aligned along the field B_0 compared with those opposed to B_0. Most experiments start from this initial condition. In their simplest form, the Bloch equations tell us how the macroscopic magnetization vector reacts to the presence of the applied magnetic field and the temporary imposition of a radiofrequency field. At this stage we neglect relaxation effects.

$$dM_X/dt = \gamma(M_Y B_Z - M_Z B_Y) \quad [2]$$

$$dM_Y/dt = \gamma(M_Z B_X - M_X B_Z) \quad [3]$$

$$dM_Z/dt = \gamma(M_X B_Y - M_Y B_X). \quad [4]$$

This resolves the magnetization vector into its X, Y and Z components and considers their motion in the presence of magnetic fields B_X, B_Y or B_Z. If there is any magnetic field in the rotating frame, the nuclear magnetization vector M precesses around the field direction until that field is extinguished. For example, the familiar 90° excitation pulse is represented as a field B_X applied for such a duration that a vector M_0 along +Z is turned through 90° to the +Y axis of the rotating frame. Normally we are dealing with a hard pulse ($B_X = B_1 >> \Delta B$) so the residual field ΔB is neglected during the pulse. After the pulse the transverse nuclear magnetization vector precesses in the XY plane at a rate $\gamma\Delta B$ rad s^{-1}. In this case ΔB represents the chemical shift measured with respect to the transmitter frequency (the rotating frame frequency). A vector rotating in the XY plane intersects the receiver coil and induces a voltage which we call the free induction signal. The coil is, of course, in the laboratory frame, so we must add the frequency of the rotating frame, giving a result measured in hundreds of MHz, but the spectrometer reconverts this to an audiofrequency signal by subtracting the transmitter frequency (heterodyne action) so we are again dealing with the precession frequency in the rotating frame of reference.

In the more general case, the radiofrequency pulse may not satisfy the condition $B_1 >> \Delta B$, and we must consider an effective field

$$B_{eff} = (\Delta B^2 + B_1^2)^{1/2} \quad [5]$$

which is tilted in the XZ plane away from the +X axis through an angle θ given by

$$\tan \theta = \Delta B/B_1. \quad [6]$$

A radiofrequency pulse applied to an equilibrium magnetization vector then rotates the latter about the tilted effective field (see Radiofrequency pulses*).

Extensions of these simple manipulations can be represented by arcs on the surface of a unit sphere. In the presence of relaxation effects these magnetization trajectories must also include changes in length of the magnetization vector with time. This is achieved by treating relaxation *phenomenologically*, simply adding extra terms in the Bloch equations

$$dM_X/dt = \gamma(M_Y B_Z - M_Z B_Y) - M_X/T_2 \quad [7]$$

$$dM_Y/dt = \gamma(M_Z B_X - M_X B_Z) - M_Y/T_2 \quad [8]$$

$$dM_Z/dt = \gamma(M_X B_Y - M_Y B_X) + (M_0 - M_Z)/T_1. \quad [9]$$

This asks no questions about the nature of relaxation; T_1 is merely the time constant for the recovery of longitudinal magnetization, while T_2 is the time constant for the decay of transverse magnetization. Thus we see how thermal equilibrium is established when a sample is first placed in the magnetic field (eqn [9]), longitudinal relaxation carrying the instantaneous magnetization M_Z back to its equilibrium value M_0. It also describes how the transverse magnetization decays with time (eqns [7] and [8]), giving rise to a *free induction decay*.

We recognize, of course, that free induction signals usually decay much faster than predicted by the spin–spin relaxation rate. We now need another extension of the model, dividing up the sample into a mosaic of tiny volume elements called *isochromats* (2). These are large enough that they still contain a very large number of spins, but small enough that any gradients of the applied magnetic field can be neglected within an isochromat. The inhomogeneity of the applied field is thereby 'digitized', being represented by the slightly different Larmor frequencies of the different isochromats. Each isochromat is assigned a small vector m; their resultant is the macroscopic vector M. After a hard 90° pulse all the isochromatic vectors are in phase along the +Y axis, but they precess at different rates, fanning out in the XY plane and causing a decay of the detected NMR response. We normally represent this decay by a time constant T_2^*, the *instrumental* decay constant; this should not be confused with T_2. This picture clearly highlights the difference between the irreversible loss of magnetization through spin–spin relaxation and the dispersal of local isochromats, which can be reversed in a spin-echo* experiment.

EXTENSIONS OF THE BLOCH PICTURE

The Bloch equations were formulated at a time when high-resolution spectra with many different resonance lines were far in the future. Yet it can be very useful to extend these concepts to encompass several groups of chemically shifted nuclei, represented by independent vectors M_A, M_B,..., having the appropriate resonance offsets and relative intensities. Furthermore, the individual lines of a spin multiplet may also be assigned vectors, and they precess at frequencies which differ by the relevant spin–spin coupling constant. They can be labelled according to the spin states of the coupling partner, for example α and β for a doublet. We must therefore recognize that if this neighbour spin is inverted by a 180° pulse, the α and β labels are interchanged, and divergence becomes convergence (or vice versa).

This extension immediately suggests the concept of a selective (soft) radiofrequency pulse, one designed with a low-intensity B_1 (and correspondingly longer duration) so that it affects only one line (or close group of lines) without significantly perturbing the rest. We are then implicitly relying on the tilt of the effective field to discriminate between 'resonant' and 'non-resonant' situations: an effective field near the XY plane implies excitation, an effective field near the Z axis has little effect. We see that this can only be a relatively slow function of offset;

hence the need for shaped soft pulses with a more sharply defined transition between 'resonant' and 'non-resonant'. See Selective excitation*.

Such a picture has a reassuring parallel with the actual frequency-domain spectrum obtained by Fourier transformation. A vector M_A precessing at a frequency f_A in the XY plane during a free induction decay corresponds to a resonance at the frequency f_A Hz in the high-resolution spectrum and has an intensity proportional to M_A. If that particular vector decays with a time constant T_2 or T_2^* in the time domain, the corresponding resonance has a full linewidth of $1/(\pi T_2)$ or $1/(\pi T_2^*)$ Hz in the frequency domain. If we rotate the vector M_A through 180° (e.g. by a population inversion), the corresponding resonance line appears inverted. Note that we are implicitly assuming that each individual vector obeys the Bloch equations.

As new phenomena were discovered, the Bloch picture was adapted to include them. Slow chemical exchange carries spins from one site (A) to another site (B) with a different chemical shift. A population inversion of the spins at A therefore diminishes the length of the vector M_B as the inverted spins arrive at that site, but eventually M_B recovers its original length through spin–lattice relaxation. During exchange, spins departing from site A are replaced by B spins that have an essentially random phase. This can be reflected by introducing a new decay term into the relevant Bloch equation, for example

$$dM_Y/dt = \gamma(M_Z B_X - M_X B_Z) - M_Y/T_2 - M_Y/\tau \qquad [10]$$

where $1/\tau$ is the rate of chemical exchange. Analogous considerations apply to the nuclear Overhauser effect*; a rearrangement of spin populations brought about by cross-relaxation increases the length of a vector M_B when site A is saturated.

MAGNETIZATION TRAJECTORIES

Several important innovations in NMR methodology owe their inspiration to the intuitive application of the vector model. Tracing out the trajectory of a magnetization vector helps us understand certain types of pulse imperfection, for example the tilt effect of an off-resonance pulse. Levitt and Freeman (3) showed by drawing the appropriate magnetization trajectories that the error due to a tilt of the effective radiofrequency field could be largely compensated by combining three radiofrequency pulses into a composite pulse*

$$R = 90°(X)\ 180°(Y)\ 90°(X). \qquad [11]$$

This became the precursor of an entire family of self-compensating pulses that have enjoyed considerable success in many applications, for example broadband decoupling*.

In a similar manner, it is hard to imagine the discovery of the DANTE sequence (4) without being able to visualize the 'zig-zag' trajectories followed by an off-resonance spin, and the existence of multiple sideband responses follows neatly

from the vector picture. (See Selective excitation.) While it may now be common practice to rely on computer optimization techniques to design shaped soft radiofrequency pulses for (say) pure phase excitation (5), it will always be more satisfying to visualize the complex defocusing and refocusing effects by displaying families of magnetization vectors on the unit sphere.

At the heart of many modern spin manipulation schemes is some trick to separate interesting signal components from undesirable responses. Often this is achieved by phase cycling* or by the application of pulsed field gradients*. The former method discriminates between desirable and undesirable responses by distributing the corresponding vectors differently in phase space (usually along the four orthogonal directions in the XY plane), retrieving the interesting signals by cycling the receiver reference phase. The latter method spreads the various signal components in geometrical space through the application of a pulsed magnetic field gradient. Individual isochromatic vectors would then find themselves arranged in the form of a helix whose axis is the field gradient direction. The required signals are then collected by a suitable recall gradient that leaves the unwanted components still widely dispersed in space. The vector model is crucial to the understanding of both of these methods.

LIMITATIONS OF THE VECTOR MODEL

Not all experiments can be adequately treated by the vector model. One of the important cases where it breaks down (or at best involves too many *ad hoc* assumptions) is in the treatment of multiple-quantum coherence. The initial stage of this experiment is readily formulated as the preparation of two vectors α and β

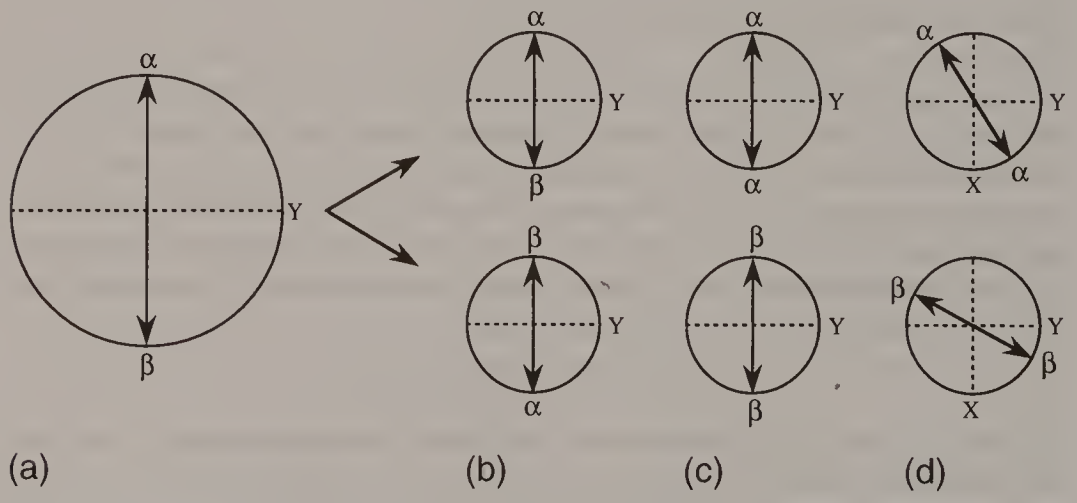

Fig. 1. Preparation and evolution of double-quantum coherence couched in terms of vectors. (a) The initial antiphase configuration of α and β vectors. (b) A 90° pulse applied to the coupling partner interchanges α and β labels for half of the spins. (c) Rearrangement of these vectors. (d) Evolution of double-quantum coherence by free precession of 'locked' vectors.

from a J-doublet in an arrangement where they are diametrically opposed along the ±X axes of the rotating frame. A 90° pulse on the coupling partner interchanges the α and β labels for just one-half of the spins, leaving two sets of antiphase vectors 'locked' into a configuration from which they cannot escape by free precession alone (Fig. 1). During this period no signal can be induced in the receiver coil but some *entity* ('double-quantum coherence') certainly evolves with time and can eventually be reconverted into observable magnetization by a radiofrequency pulse. This is where the product operator formalism comes into its own; we forsake geometrical pictures for an algebraic notation, a sure sign that we have a less intimate understanding of the problem.

REFERENCES

1. F. Bloch, *Phys. Rev.* **102**, 104 (1956).
2. A. Abragam, *The Principles of Nuclear Magnetism.* Oxford University Press, 1961.
3. M. H. Levitt and R. Freeman, *J. Magn. Reson.* **33**, 473 (1979).
4. G. A. Morris and R. Freeman, *J. Magn. Reson.* **29**, 433 (1978).
5 H. Geen and R. Freeman, *J. Magn. Reson.* **93**, 93 (1991).

Cross-references

Broadband decoupling
Composite pulses
Free induction decay
Multiple-quantum coherence
Nuclear Overhauser effect
Phase cycling
Product operator formalism
Pulsed field gradients
Radiofrequency pulses
Rotating frame
Selective excitation
Spin echoes
Spin–lattice relaxation
Spin–spin relaxation

Zero Filling

Fourier transformation of the free induction decay* is normally carried out digitally, so that it is necessary to sample the free induction signal at discrete, evenly spaced intervals between t = 0 and the maximum value t = T, the acquisition time. The fast Fourier transform* program requires that the size of the data table to be transformed be an integral power of 2, say $N = 2^n$. Now, in practical cases the free induction signal often decays to a low level before all N samples have been acquired, and to avoid significant contributions from noise in the tail of this signal, a weighting function is commonly used which reduces both signal and noise to a negligible level at the end of the free induction decay. It is therefore natural to complete the data table to the next power of 2 by adding zeros.

In some other experiments, data acquisition may have to be curtailed before the free precession signal has properly decayed. This is particularly unfortunate in cases where there are two or more lines in the spectrum that are not quite resolved, because we realize that the resolving power has been unnecessarily impaired, just as in optical spectroscopy when the slit width is too large. It turns out that doubling the data table by adding an equal number of ordinates of zero intensity does in fact improve the resolution in this situation, allowing the peaks in question to be recognized as separate entities (Fig. 1). But how can adding zeros possibly improve the quality of the information in the final spectrum? Surely, by comparison with a free induction decay followed for 2T seconds, a transient signal zero filled from T to 2T must contain *false* information? The key to this apparent paradox is that under normal conditions significant information is actually discarded and zero filling allows it to be retrieved (1).

Suppose that a free induction decay S(t) is sampled with N real coefficients from time t = 0 to t = T. In the programs normally used, Fourier transformation gives N/2 absorption-mode data points and N/2 dispersion-mode data points, which are independent data sets. Normally, only the absorption-mode part would be retained and the dispersion-mode information would be lost. Zero filling provides a method of retrieving this information and thus improving the definition and resolution of the frequency-domain spectrum. Since the function to be transformed is periodic in time (period 2T), appending N zeros to the tail is entirely equivalent to putting N zeros immediately in front of the free induction decay, giving a signal which runs from –T to +T, designated Z(t). By specifically defining the signal to be zero at all times prior to the radiofrequency pulse, this is said to impose *causality*.

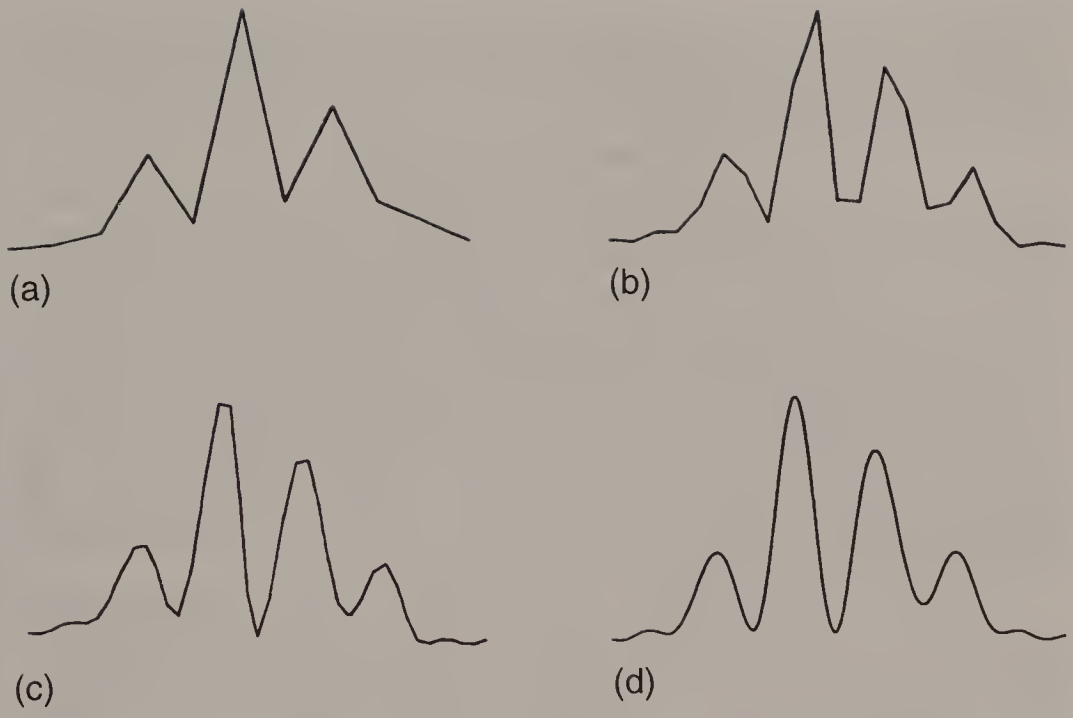

Fig. 1. Spectrum of the methylene protons of ethanol obtained by transforming a truncated free induction decay. (a) No zero filling, 11 data points defining the multiplet. (b) Zero-filled to give 21 data points. (c) Zero-filled to give 41 data points. (d) Zero-filled to give 2561 data points. Resolution is appreciably improved by the first stage of zero filling but further extension of the free induction signal simply improves the *digital* resolution.

Two spectroscopists exchanging views about zero filling.

The signal Z(t) may be decomposed (1,2) into an even part $Z_{even}(t)$ and an odd part $Z_{odd}(t)$ as illustrated in Fig. 2:

$$Z(t) = 0.5[Z_{even}(t) + Z_{odd}(t)]. \quad [1]$$

Since the Fourier transform of an even function must itself be even, $Z_{even}(t)$ transforms into a pure absorption-mode spectrum, whereas $Z_{odd}(t)$ gives a dispersion-mode spectrum. Each spectrum now contains N data points and each has an identical information content, having shared the information in S(t) equally. It is *as if* there had been a transfer from dispersion to absorption (and vice versa) by way of a Hilbert transform. The end result is an absorption-mode spectrum with N coefficients, twice as many as the Fourier transform of the original free induction decay S(t). The 'new' values lie interleaved between the 'old' values. The absorption-mode and dispersion-mode spectra now contain the same information and the latter may now be abandoned without regret.

The paradox is now resolved. The processing of a raw experimental free induction decay without zero filling does not use all the available information; zero filling retrieves the 'lost' data. The interesting point is that it does so automatically, achieving in one step what we might have expected to do by way of a Hilbert

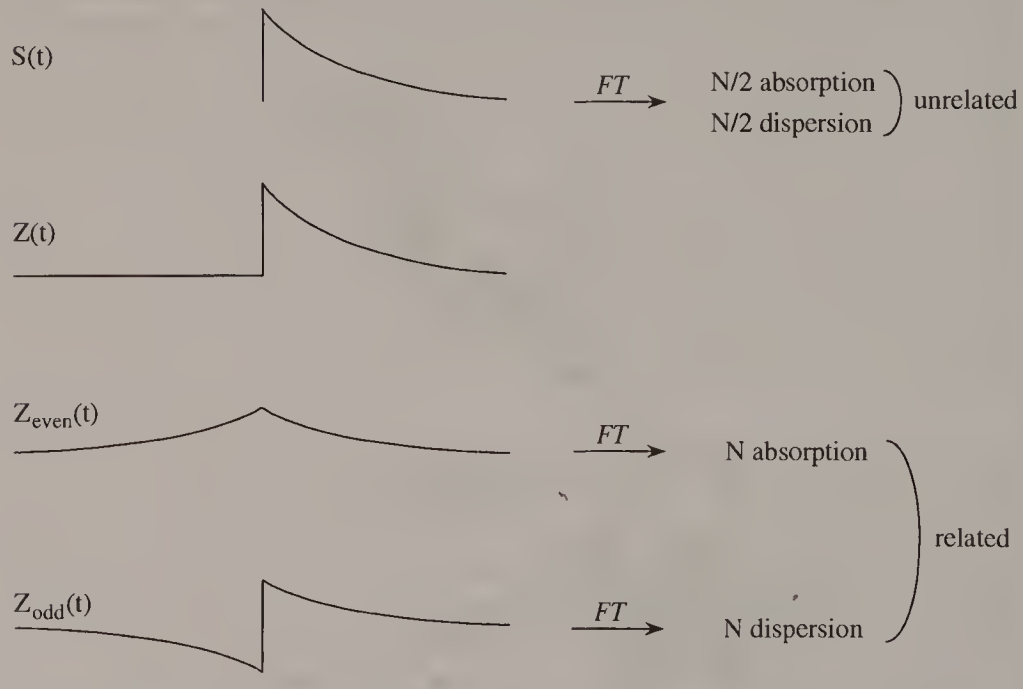

Fig. 2. With the commonly used Fourier transform algorithm, a free induction decay S(t) defined by N data points generates an 'absorption' spectrum of N/2 points while the 'dispersion' spectrum is discarded. If S(t) is zero-filled, Z(t) may be considered as the superposition of an even signal and an odd signal. Fourier transformation of $Z_{even}(t)$ gives an absorption spectrum defined by N data points, an appreciable improvement in resolution.

transform of the unused dispersion-mode spectrum. Spectroscopic resolution is improved and in marginal cases an unresolved multiplet can become resolved. It also affords a small sensitivity improvement ($2^{1/2}$) through a doubling of the number of measurements of the signal, each carrying uncorrelated noise. However, in the usual case where a sensitivity enhancement* function has been imposed on the free induction decay, these noise components have already been correlated and any sensitivity improvement anticipated.

Once the period has been extended from T to 2T by zero filling, no new information can be retrieved by adding more zeros. This would only improve the *digital* resolution of the spectrum interpolating between 'true' data points and giving better definition to the lineshape. In practice, it can often be important to improve the digitization* in this way, for example when fitting the lineshape or when using a computer routine to find the frequency and intensity of a given peak in the spectrum. It may, however, prove more convenient to perform the equivalent process of interpolation in the frequency domain, since this operation would be carried out only on the actual peaks, not on the entire data table.

We may summarize the conditions under which zero filling can be advantageous:

(1) in order to complete the data table up to 2^n words for the purposes of the Cooley–Tukey algorithm*;
(2) in order to enhance the resolution* of fine structure from a truncated free induction decay by doubling the length of the time-domain data table;
(3) in order to improve the fineness of digitization in the frequency domain by zero filling beyond the criterion of (2).

REFERENCES

1. E. Bartholdi and R. R. Ernst, *J. Magn. Reson.* **11**, 9 (1973).
2. E. Oran Brigham, *The Fast Fourier Transform*. Prentice Hall: Englewood Cliffs, New Jersey, 1974.

Cross-references

Cooley–Tukey algorithm
Digitization
Fourier transformation
Free induction decay
Resolution enhancement
Sensitivity enhancement

Index

Bold entries refer to main sections of the book.

New Nuclear Magnetic Resonance (NMR) te
being introduced, and it is often difficult for p
spectroscopy to keep pace with the many ne
involved.

The second edition of *A Handbook of Nuclear*
incorporates a radical revision of more than
particularly the topics that are related to the
multidimensional spectroscopy. The subject m
format that provides rapid access to the mos
concepts, with approximately 60 sections arr
Every effort has been made to keep the expl
and to avoid technical jargon.

Features of the Second Edition:

- material on multidimensional spectroscopy
  expanded, this includes sections on correlat
  multiple-quantum coherence, the Nuclear O
  polarisation transfer, t_1 noise, and general tv
  methodology
- new sections on coherence, bilinear rotatio
  measurement of coupling constants, nuclear
  field gradients
- considerably expanded and updated literatu
- includes over 120 diagrams illustrating spectr
  vector diagrams and magnetisation trajectories.

A Handbook of Nuclear Magnetic Resonance is written for advanced undergraduates, postgraduates and research workers in organic, physical, analytical and pharmaceutical chemistry.

Ray Freeman is the John Humphrey Plummer Professor of Magnetic Resonance at the University of Cambridge, and a Fellow of the Royal Society.

ISBN 0-582-25184-2
9 780582 251847 >

LONGMAN